UNIVERSIDAD DE GRANADA

FACULTAD DE CIENCIAS

Departamento de Química Analítica

Grupo de investigación FQM-297 "*Control Analítico, Ambiental, Bioquímico y Alimentario*"

Programa Oficial de Doctorado en Química

DESARROLLO DE BIOSENSORES PARA EL CONTROL DE PARÁMETROS BIOQUÍMICOS

Memoria de Tesis para optar al grado de Doctor Internacional en Química presentada por

María Teresa Ramón Márquez

Tesis dirigida por

Dr. D. Alberto Fernández Gutiérrez
Dr. D. Jorge Fernando Fernández Sánchez

Granada, Junio de 2017

Editor: Universidad de Granada. Tesis Doctorales
Autora: María Teresa Ramón Márquez
ISBN: 978-84-9163-487-4
URI: http://hdl.handle.net/10481/48237

UNIVERSIDAD DE GRANADA

La doctoranda *Dña. María Teresa Ramón Márquez*, y los Directores de la Tesis *Dr. D. Alberto Fernández Gutiérrez*, Catedrático Emérito del Departamento de Química Analítica, y *Dr. D. Jorge Fernando Fernández Sánchez,* Profesor Titular del Departamento de Química Analítica, todos pertenecientes al Grupo de investigación FQM-297, *Control Analítico, Ambiental, Bioquímico y Alimentario*, de la Universidad de Granada:

Garantizamos, al firmar esta Tesis Doctoral, que el trabajo ha sido realizado por la doctoranda bajo la dirección de los directores de la Tesis y hasta donde nuestro conocimiento alcanza, en la realización del trabajo, se han respetado los derechos de otros autores a ser citados, cuando se han utilizado sus resultados o publicaciones.

Granada, 19 de Junio de 2017

Directores de la tesis

Dr. D. Alberto Fernández Gutiérrez *Dr. D. Jorge F. Fernández Sánchez*

Doctoranda

Dña. María Teresa Ramón Márquez

UNIVERSIDAD DE GRANADA

D. Alberto Fernández Gutiérrez, Catedrático Emérito del Departamento de Química Analítica de la Facultad de Ciencias de la Universidad de Granada, y Director del Grupo de Investigación FQM-297, *Control Analítico, Ambiental, Bioquímico y Alimentario*,

CERTIFICA QUE:

El trabajo que se presenta en esta Tesis Doctoral con el título *Desarrollo de biosensores para el control de parámetros bioquímicos*, que ha sido realizado bajo mi dirección, reúne todos los requisitos legales, académicos y científicos para hacer que la doctoranda *Dña. María Teresa Ramón Márquez* pueda optar al grado de Doctor Internacional en Química.

Esta Tesis ha sido realizada en los laboratorios del grupo de investigación FQM-297 en el Departamento de Química Analítica de la Universidad de Granada, y también, parcialmente, en el laboratorio de NanoMyP®, Nanomateriales y Polímeros S.L., empresa spin-off de la Universidad de Granada, en el Instituto de Catálisis y Petroleoquímica del Consejo Superior de Investigaciones Científicas en Madrid, y en el CEMIS-Oulu Measurement Technology Unit de la Universidad de Oulu en Kajaani (Finlandia).

Y para que así conste, expido y firmo el presente certificado en Granada a 19 de Junio de 2017:

UNIVERSIDAD DE GRANADA

D. Jorge Fernando Fernández Sánchez, Profesor Titular del Departamento de Química Analítica de la Facultad de Ciencias de la Universidad de Granada,

CERTIFICA QUE:

El trabajo que se presenta en esta Tesis Doctoral con el título *Desarrollo de biosensores para el control de parámetros bioquímicos*, que ha sido realizado bajo mi dirección, reúne todos los requisitos legales, académicos y científicos para hacer que la doctoranda *Dña. María Teresa Ramón Márquez* pueda optar al grado de Doctor Internacional en Química.

Esta Tesis ha sido realizada en los laboratorios del grupo de investigación FQM-297 en el Departamento de Química Analítica de la Universidad de Granada, y también, parcialmente, en el laboratorio de NanoMyP®, Nanomateriales y Polímeros S.L., empresa spin-off de la Universidad de Granada, en el Instituto de Catálisis y Petroleoquímica del Consejo Superior de Investigaciones Científicas en Madrid, y en el CEMIS-Oulu Measurement Technology Unit de la Universidad de Oulu en Kajaani (Finlandia).

Y para que así conste, expido y firmo el presente certificado en Granada a 19 de Junio de 2017:

La presente Tesis Doctoral ha sido realizada con la financiación recibida a través de una beca predoctoral del Subprograma de Formación de Profesorado Universitario (FPU) dentro del Programa Estatal de Promoción del Talento y su Empleabilidad, procedente del Ministerio de Educación, Cultura y Deporte, y de referencia AP2012-0944.

AGRADECIMIENTOS

En primer lugar quisiera dar mi más profundo agradecimiento a mis directores de tesis, D. Alberto Fernández Gutiérrez y D. Jorge Fernando Fernández Sánchez, por su dedicación y paciencia, por todo el conocimiento que me han transmitido a lo largo de estos años, y por el inestimable esfuerzo invertido en la realización de esta Tesis Doctoral, sin ellos este trabajo nunca hubiese sido posible.

En segundo lugar quiero agradecer a D. Antonio Luis Medina Castillo el tiempo que ha dedicado a ayudarme y a guiarme en la elaboración de los experimentos. Gracias por tu entrega y entusiasmo, de los que me he contagiado siempre, para mí has sido como un tercer director de tesis.

Igualmente quiero dar las gracias a mis compañeros y amigos del grupo de investigación FQM-297 del Departamento de Química Analítica, a los que están y a los que ya no están: Alegría, Lucía, Adil, Marta, Elena, Pachi y Santi, gracias por acompañarme en el día a día, por animarme siempre, por esas charlas y esos ratos de risas, ha sido un placer compartir con vosotros el laboratorio y la becaría durante estos años.

Quisiera dar las gracias también a los compañeros del laboratorio de NanoMyP, Antonio, Jose y Mari Carmen, por todos esos momentos que hemos compartido en el laboratorio y fuera de él, por vuestros consejos y por hacerme un hueco en un laboratorio tan pequeño.

Además, también quiero agradecer a Carmen, Romina, Doris y Carlos, los momentos compartidos, especialmente fuera del laboratorio.

No quisiera olvidarme de dar las gracias a la gente del centro CEMIS-Oulu en Kajaani, por su recibimiento y acogida. En especial a Adama, por su paciencia, preocupación e interés, y a Peter y Hanna Liisa por su simpatía y por hacerme tan amena la estancia en un centro extranjero tan alejado de mi familia.

También quiero acordarme de mi amiga de toda la vida, gracias Luz por todos esos momentos y experiencias que hemos vivido juntas a largo de tantos años.

Quisiera dar mi más cariñoso agradecimiento a mi amigo, compañero y querido Víctor. Gracias por estar siempre dispuesto a escucharme y ayudarme, por esas largas conversaciones a veces científicas a veces filosóficas, y por valorarme tanto. Eres un rayo de luz en mi vida.

Finalmente, quiero dar las gracias a mi familia, por acompañarme siempre en los buenos y en los malos momentos, y por ser el apoyo más valioso en mi vida. En especial quiero dar las gracias a mis padres por su inmensa dedicación, su comprensión, por sus sabios consejos y por anteponer mi bienestar por encima de cualquier cosa, el mérito de este trabajo es tanto mío como vuestro; a mis hermanos, Manu, Alberto y Bea, gracias por llenar mi vida de felicidad, por vuestra complicidad y vuestro cariño, en especial a mi hermana, eres la mejor, te adoro; a Ismael, que ya lo considero parte de mi familia, le quisiera agradecer su ánimo y apoyo constante; y a mi tita Montse, que no por última menos importante, gracias por toda tu generosidad y por estar siempre dispuesta a acompañarme, os quiero a todos.

A mi familia,

por su apoyo incondicional

ÍNDICE

OBJETIVOS DE LA TESIS

El objetivo principal de esta memoria de tesis es el diseño y desarrollo de nuevos biosensores ópticos para el control y la determinación de parámetros bioquímicos tales como glucosa, ácido úrico y aminas biógenas, mediante el empleo tanto de micropartículas con diferentes grupos funcionales como de tejidos de nanofibras poliméricas producidos por electrospinning, que presenten interacción biocatalítica y que se puedan implementar fácilmente en dispositivos robustos, miniaturizables y de fácil manejo.

Para lograr este objetivo principal se propone cumplir una serie de objetivos específicos que se detallan a continuación:

En primer lugar, se va a realizar un estudio teórico y experimental sobre cómo afectan factores como temperatura, pH, tiempo reacción y tipo de funcionalización de un soporte sólido, entre otros, al grado de inmovilización de ciertas biomoléculas, así como, a la retención de sus propiedades biológicas, características fundamentales para el desarrollo de fases sensoras con posibles aplicaciones en el análisis de muestras biológicas. Para ello se llevará a cabo la inmovilización de glucosa oxidasa (GOx) en varias micropartículas con diferentes grupos funcionales y, posteriormente, se evaluará su utilización en el desarrollo de biosensores capaces de detectar glucosa por transducción óptica de oxígeno.

El segundo objetivo específico de esta memoria consiste en efectuar trabajos de inmovilización de una serie de biomoléculas en tejidos no tejidos de nanofibras poliméricas producidos por electrospinning y con diferentes funcionalizaciones químicas, para, a continuación, estudiar la capacidad e idoneidad de dicho soporte para inmovilizar biomoléculas.

Una vez realizado este estudio, el siguiente objetivo se centrará en aplicar los resultados obtenidos en el desarrollo de fases sensoras basadas en tejidos de nanofibras poliméricas para la detección y determinación óptica, ya sea mediante medidas de fluorescencia o de fosforescencia, de determinadas aminas biógenas presentes tanto en fluidos biológicos como en muestras alimentarias.

El cuarto objetivo de esta tesis se dirigirá al estudio de los complejos de iridio(III) empleados en el desarrollo de sensores ópticos. Para lo cual, se realizará una revisión bibliográfica de los sensores ópticos diseñados hasta la fecha, con especial interés en los empleados en la determinación y análisis de parámetros bioquímicos.

El siguiente de los objetivos específicos se enfocará en la optimización de las condiciones de inmovilización de uricasa en el soporte sólido de nanofibras poliméricas mencionado

anteriormente, atendiendo tanto a grado de inmovilización como a actividad catalítica de la enzima inmovilizada, para poder llegar a un compromiso entre ambas propiedades y así obtener un material con las cualidades óptimas. Posteriormente, se evaluará la incorporación de complejos organometálicos sensibles a oxígeno en el material nanoestructurado con la enzima inmovilizada, para así poder diseñar una fase sensora sensible a ácido úrico con transducción óptica de oxígeno, que pueda ser aplicada al análisis de muestras reales y sea capaz de proporcionar una mejora en sensibilidad, selectividad y tiempo de respuesta, a la vez que se pueda conseguir una simplificación del método de análisis y/o una reducción de los costes del mismo.

Como objetivo final se pretende incorporar las fases sensoras obtenidas en dispositivos de microfluídica con el propósito de automatizar y miniaturizar el sistema de detección diseñado. Esto permitirá ampliar enormemente la versatilidad y la aplicabilidad de las fases sensoras desarrolladas, así como reducir costes y tiempos de análisis, y establecer un entorno controlado donde llevar a cabo la determinación de analitos procedentes de muestras complejas.

RESUMEN

La memoria aquí presentada expone y detalla los resultados obtenidos durante la realización del trabajo que ha conducido a la elaboración de la Tesis Doctoral titulada *Desarrollo de biosensores para el control de parámetros bioquímicos*.

La memoria está dividida en dos partes fundamentales, introducción y parte experimental, cuyos contenidos principales se describen a continuación:

La **introducción** engloba los aspectos más generales e importantes a considerar durante el proceso de diseño y desarrollo de un biosensor, incluyendo la clasificación y definición de las diferentes metodologías existentes para llevar a cabo la inmovilización de biomoléculas sobre soportes sólidos para la fabricación de biosensores, con las ventajas e inconvenientes que conlleva cada una de ellas. Asimismo, también se incluye una clasificación de los distintos soportes empleados en el diseño de biosensores, en función tanto de su naturaleza como de sus propiedades físicas, y una enumeración de los distintos factores y condicionantes a tener en cuenta para conseguir una integración óptima de los distintos elementos que componen un biosensor. En la última parte de la introducción se detallan los sistemas de transducción ópticos más ampliamente utilizados en el desarrollo de biosensores, haciendo especial hincapié en las técnicas luminiscentes; se recogen las características de los sistemas de microfluídica y las ventajas e inconvenientes que dichos sistemas aportan cuando se combinan con las fases sensoras; y, finalmente, se ofrece una visión global sobre las aplicaciones de los biosensores ópticos, así como sobre las expectativas de futuro de los mismos.

La parte **experimental** incluye los procedimientos llevados a cabo para alcanzar los objetivos propuestos, los resultados obtenidos durante la consecución de cada uno de ellos y una discusión detallada de los mismos. Esta parte ha sido dividida en cinco bloques en función de la temática abordada en cada uno de ellos.

En el *bloque I* se realiza el estudio de cómo influye la distinta funcionalización de la superficie de varios soportes en la inmovilización de biomoléculas, con el fin de desarrollar biosensores con las mejores prestaciones analíticas.

El capítulo 1, incluido en este bloque, se centra en la comparación de las características obtenidas tras llevar a cabo la inmovilización de una enzima modelo, glucosa oxidasa, en una serie de micropartículas poliméricas con las mismas propiedades pero distinta funcionalización química en su superficie. Los grupos funcionales estudiados son: cloruro, epóxido, ácido carboxílico y vinil

sulfona, los cuales permiten poder realizar la unión covalente de la enzima a las partículas de manera directa o a través de un agente activante que favorezca la reacción.

Además, en este capítulo también se realiza la identificación de los factores y condicionantes que afectan al proceso de inmovilización, incluyendo temperatura, pH, tiempo de reacción, concentración, fuerza iónica, porosidad del material, reactividad, entre otros, para establecer las condiciones óptimas de inmovilización de la enzima seleccionada como modelo para cada una de las partículas estudiadas. Asimismo, se presentan las ventajas e inconvenientes de cada una de las funcionalizaciones estudiadas, con el fin de determinar el grupo funcional con la mayor aplicabilidad en el diseño de biosensores ópticos.

La otra parte del trabajo recogido en este bloque fue desarrollada en colaboración con investigadores del *Instituto de Catálisis y Petroleoquímica* del *Consejo Superior de Investigaciones Científicas* en Madrid y se detalla en el capítulo 2. En él se pormenoriza acerca de las ventajas que ofrece la activación de soportes con divinil sulfona para la posterior inmovilización de biomoléculas con un elevado rendimiento de inmovilización y una alta capacidad de retención de actividad biológica.

En el *bloque II* se lleva a cabo la investigación sobre la posibilidad de aplicar tejidos de nanofibras poliméricas producidos por electrospinning como soportes para realizar procesos de inmovilización de biomoléculas de muestras complejas, y la evaluación de la capacidad para determinar algunas de las biomoléculas inmovilizadas gracias a sus propiedades ópticas intrínsecas, sin la necesidad de incorporar indicadores luminiscentes.

Este bloque está dividido en dos capítulos en los que se describen los procedimientos aplicados para diseñar fases sensoras para la detección y determinación mediante medidas de luminiscencia en fase sólida de triptamina presente en muestras de cerveza y de serotonina existente en muestras de suero. Las fases sensoras diseñadas en estos trabajos permitieron determinar los analitos de interés de una manera rápida y directa, sin prácticamente etapas previas de tratamiento de las muestras, y con una elevada correlación con los resultados obtenidos por laboratorios certificados externos.

El *bloque III* está compuesto por el capítulo 5, en el cual se establece una clasificación de los complejos de iridio(III) empleados en la fabricación de sensores ópticos, y se describe detalladamente la aplicación de los mismos en la determinación de una gran variedad de analitos, tanto en aquellos sistemas en los que los complejos de iridio se encuentran inmovilizados sobre

soportes sólidos como en los casos en los que están sin inmovilizar, incluyendo, además, las características estructurales de una gran variedad de ellos y sus mecanismos de detección.

En el *bloque IV* se plantea el estudio de las condiciones óptimas de inmovilización de uricasa en tejidos de nanofibras poliméricas y coaxiales producidas por co-electrospinning, y funcionalizados con diferentes grupos químicos superficiales, así como la evaluación y optimización del proceso de incorporación de indicadores luminiscentes sensibles a oxígeno a dichos tejidos. En este estudio también se lleva a cabo la identificación de las variables que influyen sobre el procedimiento de inmovilización y se realiza la variación controlada de cada una de ellas independientemente, manteniendo el resto inalteradas, con el fin de determinar cualitativa y cuantitativamente el grado de influencia de todas ellas en el proceso global de inmovilización, y de optimizar dicho proceso para obtener la mejor respuesta analítica y los mejores resultados.

Este bloque se compone de dos capítulos que detallan las diferentes metodologías seguidas para realizar la inmovilización de uricasa y permiten hacer una comparación de los resultados de retención de actividad biológica y rendimiento de inmovilización obtenidos al aplicar distintas técnicas de inmovilización sobre un mismo soporte y con una misma biomolécula. Además, en el primero de estos capítulos se incluye el procedimiento utilizado para la obtención de las nanofibras coaxiales y un estudio sobre cómo se ven afectadas las propiedades ópticas de varios indicadores luminiscentes cuando son incorporados en estas nanofibras.

Por último, el *bloque V* está constituido por el capítulo 8 y en él se estudia la posibilidad de incluir los tejidos de nanofibras poliméricas en dispositivos de microfluídica. En este capítulo se detalla en primer lugar el procedimiento de inmovilización de la enzima modelo glucosa oxidasa en los tejidos de nanofibras coaxiales con un indicador sensible a oxígeno incorporado en su estructura interna, y a continuación, se realiza la inclusión de las fases sensoras obtenidas en chips de microfluídica. Las respuestas de estas fases sensoras en el interior de entornos más controlados fueron comparadas con las obtenidas para las mismas fases situadas fuera de los chips de microfluídica, consiguiendo una gran mejora en la sensibilidad de las medidas. El trabajo incluido en este bloque fue desarrollado en colaboración con el *CEMIS-Oulu Measurement Technology Unit* de la *University of Oulu* en Kajaani (Finlandia).

SUMMARY

This manuscript shows and explains the results obtained during the work that has led to the elaboration of the doctoral thesis entitled *Development of biosensors for the control of biochemical parameters*.

The report is divided in two fundamental parts, introduction and experimental part:

The **introduction** describes the most important and general issues to be considered for designing and developing a biosensor, including: the classification and definition of different methodologies to carry out the immobilization of biomolecules on solid supports; the advantages and disadvantages of the tested immobilization methods; a classification of different supports used in the design of biosensors, based on both their nature and their physical properties; and a list of several factors to take into account in order to achieve an optimal integration of the different elements which take part of a biosensor. The last section of the introduction details the optical transduction systems most widely used in the development of biosensors, with special emphasis on luminescent techniques; the characteristics of the microfluidic systems, with the advantages and disadvantages provides by the combination of these systems with sensing phases; and, finally, an overview of the applications of optical biosensors, as well as of the future expectations of them.

The **experimental** part includes the procedures carried out to achieve the proposed objectives, the results obtained during their realization, and a detailed discussion about these results. This part has been divided in five sections.

The *section I* contains a study of the influence of different chemical groups on the surface of several supports over the immobilization of biomolecules. This study was carried out in order to develop biosensors with the best analytical parameters. This section is divided in two chapters:

Chapter 1 focuses on the comparison of the features obtained after immobilizing a model enzyme, glucose oxidase, on a series of polymeric microparticles with different chemical functionalization on their surface. The studied functional groups are: chloride, epoxide, carboxylic acid and vinyl sulfone, which allow the covalent attachment of the enzyme to the particles directly or through an activating agent.

In addition, in this first chapter, the factors and conditions that affect the immobilization process, such as temperature, pH, reaction time, concentration, ionic strength, porosity of the material, reactivity, among others, are studied in order to establish the optimal conditions for immobilizing the enzyme selected as model for every tested particle. Moreover, the advantages and

disadvantages of each studied chemical functionalization are presented with the aim of determining the functional group with the greatest applicability in the design of optical biosensors.

The other part of the work included in this section was developed in collaboration with the *Institute of Catalysis and Petrochemistry* of the *Spanish National Research Council* (CSIC), Madrid, and it is detailed in chapter 2. This chapter shows the advantages of activating supports with divinyl sulfone for the subsequent immobilization with high immobilization yield and great retention of biological activity.

The *section II* incorporates the investigation carried out to determine the possibility of using polymeric nanofibres membranes made by electrospinning as supports to immobilize biomolecules of complex samples, and the evaluation of the capacity to determine some of the immobilized biomolecules by their intrinsic optical properties, without the need to add any luminescent dye.

This second section is divided in two chapters that describe the procedures applied for designing sensing phases for carrying out the detection and determination by solid surface luminescence measurements of tryptamine in beer samples and serotonin in serum samples. The sensing phases design in these works allowed determining the analytes of interest in a fast and direct way, without practically previous sample treatment steps, and obtaining results with a high correlation with those obtained by external certified laboratories.

The *section III* is composed by chapter 5, in which a classification of the iridium(III) complexes used in the fabrication of optical sensors is detailed, including the application of these complexes in the determination of a wide variety of analytes, both in systems with iridium immobilized on solid supports and examples without immobilizing. In addition, this chapter also includes the structural characteristics of a variety of iridium(III) complexes and their detection mechanisms.

Section IV contains a study of the optimal conditions for immobilizing uricase on polymeric coaxial nanofibres membranes made by co-electrospinning, and functionalized with different chemical groups, as well as, the evaluation and optimization of the process carried out to incorporate oxygen-sensitive luminescent indicators into these membranes.

In this study, the variables that influence over the immobilization procedure are identified, and independently and controllably modified in order to determine qualitatively and quantitatively the influence of all of them over the process of immobilization, and to optimize this process with the aim of obtaining the best analytical response and results.

This section contains two chapters that detail the different methodologies used to carry out the immobilization of uricase, including a comparison of the results of biological activity and immobilization yield obtained after immobilizing the enzyme by applying different immobilization techniques on the same support and with the same biomolecule. In addition, the first of these chapters includes the procedure used to obtain the coaxial nanofibres and a study about the optical properties of several luminescent indicators before and after their incorporation into these nanofibres.

Finally, *section V* is composed of chapter 8, where the possibility of including the polymeric nanofibres membranes into microfluidic devices is studied. This chapter details the immobilization procedure of the model enzyme glucose oxidase on the coaxial membranes containing an oxygen-sensitive dye inside its internal structure, and the incorporation of the sensing membranes into chips of microfluidic. The responses of these sensing membranes inside the controlled environment provides by the chip were compared with those obtained for the same membranes outside the microfluidic chips, achieving a significant improvement in the sensitivity of the measurements. The work included in this section was developed in collaboration with the *CEMIS-Oulu Measurement Technology Unit* of the *University of Oulu* in Kajaani (Finland).

INTRODUCCIÓN

La ciencia es más que un simple conjunto de conocimientos:

es una manera de pensar.

Carl Sagan

1. BIOSENSORES

1.1. Definición de biosensor

Desde que en el año 1962 Clark y Lyons desarrollaran el primer biosensor para la detección de glucosa en sangre, han sido muchos los biosensores diseñados con el fin de determinar una enorme cantidad de analitos en variedad de muestras.

El término biosensor es definido por la IUPAC como un *dispositivo que utiliza reacciones bioquímicas específicas mediadas por enzimas aisladas, inmunosistemas, tejidos, orgánulos o células completas para detectar compuestos químicos normalmente mediante señales eléctricas, térmicas u ópticas.* Por lo tanto, en general, un biosensor estará formado por un **componente biológico** que actúa como elemento de reconocimiento interaccionando específicamente con una sustancia determinada, y un **componente transductor** que es capaz de interpretar dicha interacción y transformarla en una señal medible, a partir de la cual se podrá obtener información analítica específica y cuantitativa o semi-cuantitativa. La integración de ambos componentes en un único dispositivo es lo que le confiere las extraordinarias características de selectividad y sensibilidad a los biosensores.

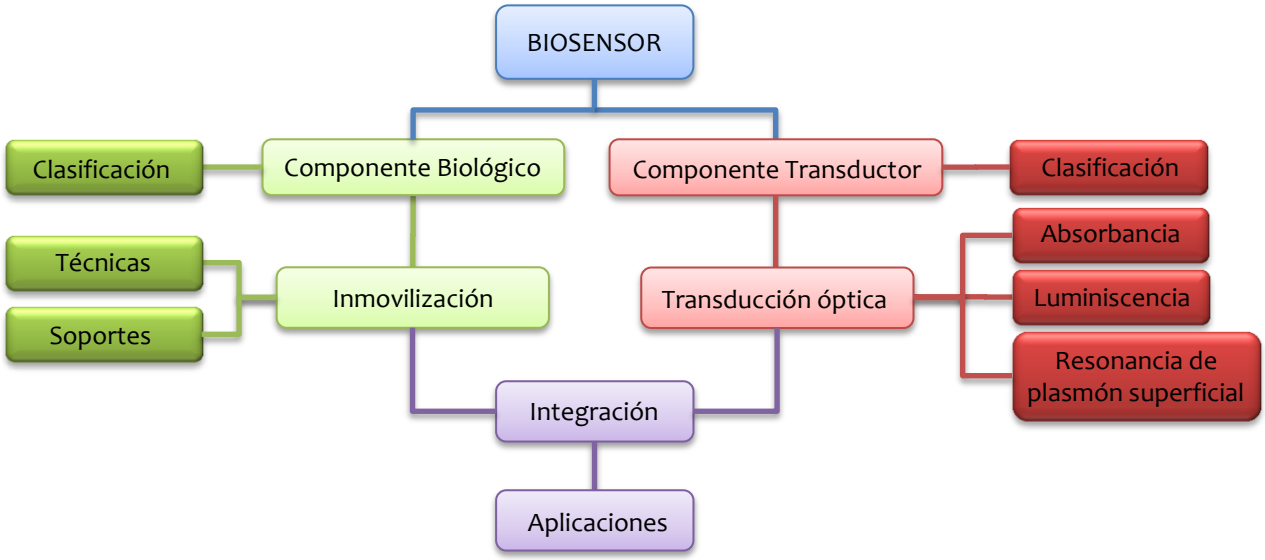

Figura 1. Esquema resumen de los distintos aspectos relacionados con el diseño y la fabricación de un biosensor tratados en esta introducción.

1.2. Componente biológico

El componente de reconocimiento biológico de los biosensores suele estar constituido por biomoléculas como enzimas, anticuerpos o ácidos nucleicos, o por sistemas biológicos más complejos como células, tejidos, orgánulos, etc.

Estos elementos se caracterizan por presentar un elevado grado de selectividad hacia un sustrato o analito determinado, permitiendo que los biosensores puedan ser utilizados en matrices complejas sin necesidad de etapas de purificación de la muestra, que sí suelen ser indispensables en la mayoría de técnicas analíticas convencionales. Sin embargo, dichos elementos biológicos también son altamente sensibles a las condiciones de temperatura, pH, fuerza iónica del medio y a la presencia de agentes desnaturalizantes. Es por ello que la integridad del componente biológico así como la preservación de sus características biológicas constituyen factores clave en el desarrollo de un biosensor.

1.3. Componente transductor

El componente de transducción tiene que ser seleccionado de manera que no interfiera en la reacción de reconocimiento biológico y su respuesta a los cambios producidos por esta reacción tiene que ser lo más rápida posible. Además, es necesario que responda específicamente a dicha reacción de reconocimiento, ya que de lo contrario haría disminuir la selectividad del biosensor y sería obligatorio incluir etapas de tratamiento y purificación de las muestras. Por otra parte, es esencial que el componente transductor y el componente biológico se encuentren en contacto directo o situados muy próximos entre sí para facilitar la respuesta de transducción.

Los elementos de transducción que se pueden utilizar en la fabricación de un biosensor abarcan una enorme variedad de materiales, sustancias y compuestos; así por ejemplo, se emplean electrodos modificados o no con especies electroquímicamente activas en biosensores electroquímicos, semiconductores en biosensores térmicos, cristales de cuarzo y turmalina en biosensores piezoeléctricos, y colorantes y complejos metálicos luminiscentes en biosensores ópticos.

1.4. Clasificación de los biosensores

Los biosensores se pueden clasificar considerando distintos criterios tanto del componente biológico como del componente transductor. En general, existen dos tipos de clasificaciones: una en función de la naturaleza de la interacción del componente biológico con su sustrato, distinguiendo entre biosensores catalíticos y biosensores de afinidad; y otra en función del tipo de sistema de transducción, que engloba a los biosensores en cuatro grandes grupos: ópticos, electroquímicos, térmicos y piezoeléctricos (Figura 2).

1.4.1. Clasificación en función del componente biológico

Biosensores catalíticos: el mecanismo de reconocimiento se basa en la unión y posterior reacción de catálisis del sustrato específico de cada componente biológico. El seguimiento de la reacción se puede realizar mediante la detección de la formación de uno de los productos o de la desaparición de uno de los reactivos de partida. Dentro de esta categoría se encuentran los biosensores enzimáticos[1], los celulares[2] y los tisulares[3]; siendo las enzimas el componente biológico más ampliamente utilizado para el desarrollo de biosensores catalíticos.

Las enzimas son biocatalizadores que se caracterizan por su elevada selectividad, siendo muy específicas tanto para el tipo de reacción que catalizan como para el sustrato involucrado en dicha reacción. Entre las enzimas empleadas con mayor frecuencia se encuentran la glucosa oxidasa (GOx)[4], la lactato oxidasa (LOx)[5], la colesterol oxidasa (ChOx)[6] y la acetilcolinesterasa (AChE)[7], las cuales han sido utilizadas en la fabricación de biosensores para la determinación de glucosa, lactato, colesterol y acetilcolina, respectivamente, en análisis clínicos y alimentarios.

Biosensores de afinidad: se basan en la unión específica del analito al elemento de reconocimiento biológico mediante interacciones de afinidad; además, dicha unión permite la separación selectiva de determinados componentes de muestras complejas de biomoléculas. El seguimiento de las interacciones de afinidad se lleva a cabo mediante la medida de los cambios en las propiedades ópticas o eléctricas asociados a dichas interacciones. Este grupo está formado por los inmunosensores[8], cuyo componente biológico son los anticuerpos y están basados en las interacciones antígeno-anticuerpo, los genosensores[9], constituidos por secuencias de ADN o ARN y basados en su interacción con secuencias diana complementarias, y biosensores fabricados con determinados receptores hormonales[10]. De entre todos ellos, destacan los inmunosensores, extensamente utilizados en la determinación de toxinas, pesticidas, drogas, bacterias, etc.[11, 12]

1.4.2. Clasificación en función del componente transductor

Ópticos: se basan en la medida de la interacción entre la radiación electromagnética y la materia, la cual puede originar variaciones en intensidad, amplitud, polarización, frecuencia, velocidad de la radiación, etc.; lo que implica que estos biosensores pueden medir por ejemplo cambios en absorbancia, luminiscencia (fluorescencia o fosforescencia), difracción o refracción de la radiación. A causa de esta gran variedad de propiedades medibles por los biosensores ópticos, son muy numerosas y diversas las aplicaciones desarrolladas para este tipo de biosensores, destacando la monitorización clínica[13], el análisis de contaminantes medioambientales[14, 15], y la determinación de compuestos de interés alimentario[16, 17].

Electroquímicos: el sistema de transducción mide el cambio en las propiedades eléctricas del medio (corriente, potencial, conductividad, etc.) producido como consecuencia de la reacción de reconocimiento entre el componente biológico y su sustrato. Estos biosensores se pueden clasificar a su vez en amperométricos, potenciométricos, conductimétricos y sensibles a iones, en función de la propiedad eléctrica medida por el transductor. Constituyen los tipos de biosensores más ampliamente utilizados, con aplicaciones en campos como la biomedicina[18-20], la agroalimentación, el control de calidad de los alimentos[21] y el control medioambiental[22, 23].

Térmicos: su principio básico consiste en medir los cambios de temperatura que tienen lugar durante las reacciones, los cuales son proporcionales a la entalpía molar y a la concentración de las especias implicadas en dichas reacciones. Debido a que la mayoría de reacciones bioquímicas conllevan cambios en la temperatura, es posible utilizar el calor generado o absorbido en estas reacciones para determinar sustratos y productos. Este tipo de biosensores son sensibles a los cambios en la temperatura, pero no responden a cambios en las propiedades ópticas o electroquímicas del medio, por lo que no sufren de este tipo de interferencias. Entre las aplicaciones de los biosensores térmicos se encuentran la determinación de parámetros clínicos[24], el análisis de alimentos[25, 26] y cosméticos[27], y la monitorización de fermentaciones y otros procesos[28].

Piezoeléctricos: están basados en el cambio de la frecuencia de resonancia característica de un cristal piezoeléctrico, como por ejemplo, cuarzo, turmalina o tantalato de litio, cuando tiene lugar una variación de masa en su superficie. Estos cristales pueden vibrar a una determinada frecuencia cuando son sometidos a una señal eléctrica de frecuencia específica, por lo que, la frecuencia de resonancia del cristal depende tanto de la frecuencia de la señal eléctrica aplicada

como de la masa del cristal. Así, si se produce un cambio de masa en el cristal como consecuencia de la unión o separación de moléculas, también se originará un cambio en la frecuencia de resonancia del cristal que podrá ser medido eléctricamente y utilizado para determinar la variación en la masa, tanto incremento como disminución. Estos biosensores han sido aplicados en análisis ambiental[29], clínico[30, 31] y alimentario[32, 33].

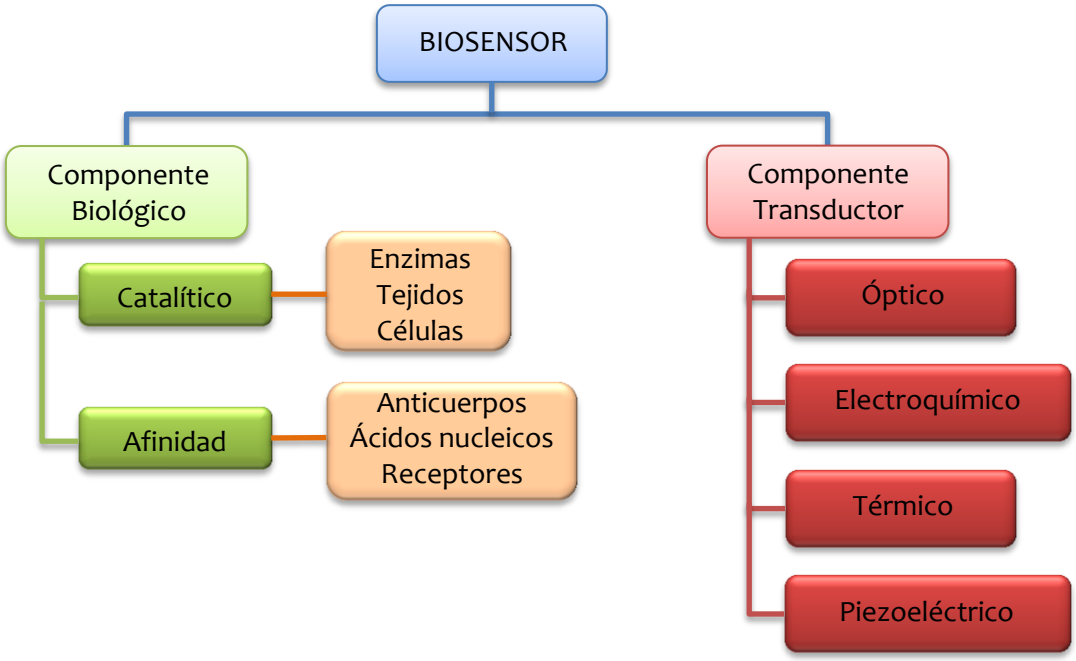

Figura 2. Clasificación de los biosensores.

1.5. Integración de los componentes biológicos y transductores en la fabricación de un biosensor

Para poder realizar la integración del componente biológico y del componente transductor en un solo dispositivo y así obtener un biosensor, es necesario llevar a cabo la inmovilización del componente biológico en un soporte sólido. Este proceso de inmovilización de biomoléculas en soportes sólidos les confiere además la capacidad de poder ser reutilizadas con la menor pérdida de actividad biológica posible, así como poder ser separadas más fácilmente del resto de reactivos y productos de la reacción. Por lo tanto, es necesario que el procedimiento de inmovilización le confiera estabilidad a la biomolécula a la vez que le permite retener su actividad biológica, ya que la sensibilidad y la selectividad del biosensor están directamente relacionadas con la actividad de las biomoléculas inmovilizadas.

Uno de los requisitos imprescindibles para conseguir una inmovilización eficiente es el hecho de que el centro activo de la biomolécula debe permanecer intacto o lo más inalterado posible tras el proceso de inmovilización. Una de las formas de conseguir este objetivo se basa en llevar a

cabo una *inmovilización dirigida*, es decir, realizar la unión entre el soporte y la biomolécula a través de grupos funcionales de la biomolécula que no estén presentes en su centro activo, siendo necesario para ello conocer la estructura de la biomolécula y la parte de la misma implicada en su actividad biológica.

Existen dos alternativas a este método para evitar afectar el centro activo durante la inmovilización: una consiste en realizar la unión en presencia del sustrato o de un inhibidor competitivo que proteja el centro activo durante la reacción con el soporte, y la otra se basa en hacer reaccionar previamente el centro activo con algún grupo protector que pueda ser eliminado tras la unión de la biomolécula al soporte sin causar la pérdida de su actividad. Sin embargo, aun llevando a cabo la inmovilización de cualquiera de estas formas, es posible que la orientación de la biomolécula unida al soporte no sea la adecuada y su centro activo no quede lo suficientemente expuesto y accesible para el sustrato, con lo cual la biomolécula perdería su actividad biológica, parcial o completamente, a pesar de permanecer con su centro activo intacto.

Por lo tanto, es muy importante considerar además de la invariabilidad del centro activo, otros factores como orientación, conformación espacial y microambiente en las proximidades de la biomolécula a la hora de realizar la inmovilización en el soporte sólido seleccionado. Así, por ejemplo, una de las estrategias para establecer un microambiente adecuado para la biomolécula consiste en colocar espaciadores entre el soporte y la biomolécula y controlar la distancia entre ambos; esto se ha comprobado que le confiere a la biomolécula, además de flexibilidad conformacional, una mejor retención de su actividad biológica.

Muchos de los procedimientos de inmovilización no controlan activamente ninguno de estos factores, por lo que las biomoléculas sufren cambios sustanciales después de ser inmovilizadas y el resultado final es la pérdida de actividad y estabilidad de la biomolécula, observado con frecuencia cuando se usan estos procedimientos.

Por otra parte, la naturaleza física y química del soporte sólido donde se realiza la inmovilización también influye en las propiedades de estabilidad y actividad final de la biomolécula, afectando especialmente al microambiente que la rodea. De esta forma, es muy conveniente tener en cuenta cualidades del soporte como el carácter hidrofílico o hidrofóbico, la carga, los grupos funcionales, el tipo de interacción a la que da lugar y la porosidad para poder realizar una inmovilización óptima en la que la biomolécula sea compatible con el soporte.

Además, parámetros relacionados con el procedimiento de inmovilización, tales como temperatura, disolvente, pH y tiempo de reacción, así como la técnica escogida para realizar la inmovilización, también condicionan la actividad de la biomolécula inmovilizada, por lo cual es fundamental tener un control estricto sobre los mismos.

Finalmente, existen una serie de condiciones, incluyendo coste, tiempo de procesado, simplicidad y reproducibilidad del proceso de inmovilización, que obviamente no afectan a la actividad de la biomolécula, pero que igualmente se consideran a la hora de fabricar un biosensor.

Resumiendo, la inmovilización eficiente del componente biológico en un soporte sólido para llevar a cabo la fabricación de un biosensor no es un proceso trivial, ya que son muchos los factores relacionados con dicho proceso los que afectan a la actividad del componente biológico, la cual en última instancia determina las características analíticas del biosensor (Figura 3).

Figura 3. Esquema resumen de los distintos factores a considerar durante la fabricación de un biosensor.

2. TÉCNICAS DE INMOVILIZACIÓN DE BIOMOLÉCULAS EMPLEADAS EN LA FABRICACIÓN DE BIOSENSORES

Existen varias formas de clasificar las técnicas de inmovilización, ya sea en función del tipo de interacción (física o química) entre la biomolécula y el soporte, de la naturaleza del soporte empleado (polímeros naturales o sintéticos, o materiales inorgánicos) o de las características del conjunto resultante.

Considerando esta última categoría, las técnicas de inmovilización se pueden clasificar básicamente en dos grandes grupos: **técnicas reversibles**, que permiten la liberación de las biomoléculas del soporte bajo condiciones suaves que no dañan su actividad biológica haciendo posible la reutilización tanto del soporte como de la biomolécula, y **técnicas irreversibles**, que implican la formación de un enlace mucho más fuerte entre el soporte y la biomolécula o la inclusión de la misma en el interior de cavidades**,** siendo imposible llevar a cabo la liberación de la biomolécula sin modificar su actividad biológica y/o sin modificar el soporte sólido[34, 35].

Cada estrategia de inmovilización presenta sus características propias con una serie de aspectos positivos y negativos que la hacen más o menos adecuada para una aplicación determinada. Es por ello que seleccionar uno u otro método de inmovilización dependerá de las características finales que se le quieran dar al biosensor y constituirá un factor clave en la utilidad del mismo; así, por ejemplo, en ocasiones se combinan diferentes estrategias de inmovilización para lograr resultados óptimos.

En la Tabla 1 se resumen las ventajas e inconvenientes de las distintas técnicas de inmovilización, así como los soportes más ampliamente utilizados para cada una de ellas; mientras que en la Figura 4 se muestra una representación esquemática de las diferentes técnicas de inmovilización de biomoléculas.

Tabla 1. Ventajas, inconvenientes y tipos de soportes más empleados para cada una de las diferentes técnicas de inmovilización de biomoléculas.

Técnica	Ventajas	Inconvenientes	Soportes
Adsorción física	Elevada simplicidad y bajo coste Baja o nula alteración de la actividad biológica Reutilización del soporte	Desorción Adsorción inespecífica de interferentes Orientación aleatoria	Celulosa, colágeno, vidrio, compuestos basados en sílice y una gran variedad de polímeros
Adsorción iónica	Escasa modificación de la conformación de las biomoléculas Reutilización del soporte	Muy sensible a cambios en el pH o en la fuerza iónica del medio Baja especificidad Desprendimiento de las biomoléculas inmovilizadas	Polielectrolitos como los ácidos poliacrílico y polimetacrílico, la polialilamina, la polietilenimina, etc.
Afinidad	Inmovilización orientada y dirigida Baja alteración de la conformación de las biomoléculas Mayor disposición y accesibilidad de las zonas activas de las biomoléculas Resistencia a condiciones variables de temperatura, pH y fuerza iónica	Requiere la presencia de grupos específicos en la biomolécula, que en la mayoría de los casos no se encuentran de forma natural y deben ser incorporados a través de etapas previas de funcionalización	Multitud de polímeros sintéticos y naturales
Puentes disulfuro	Elevada especificidad de la reacción entre grupos tiol Posibilidad de controlar la orientación de las biomoléculas Liberación de las biomoléculas y reutilización del soporte	Necesidad, en la mayoría de los casos, de incluir etapas de funcionalización con grupos tiol libres y accesibles tanto en el soporte como en la biomolécula	Agarosa activada con 2-piridil-disulfuros y geles funcionalizados con tiosulfonato y tiosulfinato

Enlaces covalentes	Unión fuerte con el soporte Elevada disponibilidad de reactivos químicos con diferentes propiedades de solubilidad, reactividad y estabilidad Posibilidad de incluir espaciadores entre la biomolécula y el soporte	Pérdida de actividad biológica si no se controlan los grupos de la biomolécula que reaccionan con el soporte En muchos casos son necesarios etapas previas de activación del soporte Utilización de reactivos tóxicos	Multitud de polímeros sintéticos y naturales
Entrecruzamiento	Sencillez No es necesario un soporte	Sensible a las condiciones de pH y temperatura Los agregados pueden originar la distorsión de la conformación de las biomoléculas	No es necesario
Atrapamiento	Formación de un microentorno favorable para la biomolécula Reducida alteración de la actividad biológica Inmovilización simultánea de diferentes biomoléculas	Dificultad para controlar el tamaño de los poros y cavidades Baja capacidad de carga	Agarosa, almidón, alginato, albúmina, caseína, colágeno
Encapsulación	Formación de las cápsulas a través de procesos sencillos y en condiciones suaves Protección de la biomolécula de agentes externos desnaturalizantes Inmovilización simultánea de diferentes biomoléculas	Limitada a sustratos y reactivos de pequeño tamaño Dificultad para controlar el espesor y la permeabilidad de las membranas	Surfactantes y polímeros como el quitosano o el ácido poliacrílico

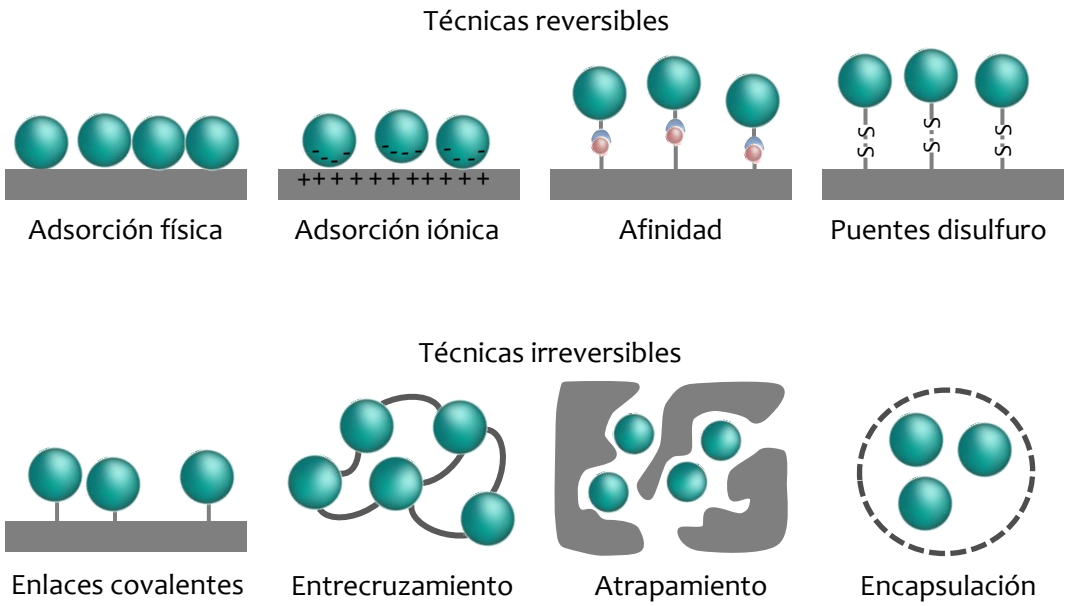

Figura 4. Representación esquemática de las distintas técnicas de inmovilización de biomoléculas.

2.1. Técnicas de inmovilización reversible

Este tipo de técnicas se caracterizan en general por su simplicidad y presentan la ventaja de que cuando se produce la disminución o pérdida de la actividad de la enzima inmovilizada, es posible reemplazarla por nueva enzima sin afectar a las propiedades del soporte, permitiendo así su regeneración y prolongando su vida útil.

Las técnicas reversibles engloban una amplia variedad de interacciones entre la biomolécula y el soporte (enlaces de hidrógeno, interacciones hidrofóbicas, fuerzas de Van der Waals, interacciones electrostáticas, interacciones de afinidad, etc.) y se pueden clasificar en las siguientes 4 modalidades:

2.1.1. Adsorción física

La inmovilización mediante adsorción física constituye el método más simple de inmovilización. El procedimiento consiste en depositar directamente una disolución de la biomolécula sobre el soporte donde se quiere realizar la inmovilización, retirando a continuación el exceso de biomolécula que no ha sido adsorbida. De esta manera, la biomolécula queda retenida en el soporte a través de interacciones débiles y no específicas como enlaces de hidrógeno, fuerzas de Van der Waals o interacciones hidrofóbicas[36, 37].

Esta técnica no requiere ningún tipo de funcionalización del soporte y generalmente no afecta a la actividad biológica de la biomolécula. Sin embargo, las débiles interacciones producidas entre el soporte y la biomolécula originan que la retención de la misma no sea duradera, de forma que, cambios en el pH, en la temperatura o en la fuerza iónica del medio pueden originar la desorción de la biomolécula, constituyendo el principal inconveniente de esta técnica[37]. Además, debido a la poca especificidad del tipo de interacciones que tienen lugar, también existe la posibilidad de que se produzca la adsorción indeseada de otras biomoléculas y sustancias. Con el fin de resolver estos inconvenientes, en los últimos años se han desarrollado una serie de variantes de esta técnica en combinación con otros métodos de inmovilización, como por ejemplo con el entrecruzamiento o la unión mediante enlaces covalentes. Una descripción más detallada de éstas y otras técnicas combinadas será descrita más adelante (Sección 2.3).

Entre los materiales más empleados para llevar a cabo este tipo de inmovilización se encuentran polímeros naturales como la celulosa y el colágeno, polímeros sintéticos derivados del poliestireno, y materiales inorgánicos como el vidrio y otros compuestos basados en sílice[38]. La mayoría de estos materiales son macroporosos y pueden adsorber las biomoléculas en el interior de sus poros, por lo que, el tamaño de los poros afectará al grado de inmovilización, y en muchos casos también influirá sobre la retención de la actividad biológica de la biomolécula una vez inmovilizada.

2.1.2. Adsorción iónica

Este tipo de unión tiene lugar a través de interacciones electrostáticas y se lleva a cabo sobre soportes que posean cierta carga, de manera que los grupos cargados del soporte interaccionan con residuos de aminoácidos cargados de las biomoléculas (por ejemplo, grupos amino de lisinas y grupos ácido carboxílico de los ácidos glutámico y aspártico)[34, 39]. En general, los soportes empleados pueden ser modificados mediante la introducción de grupos cargados que favorezcan el establecimiento de las interacciones electrostáticas y con ello la inmovilización, y además pueden ser regenerados fácilmente para su reutilización.

El pH del medio en el que se encuentra disuelta la biomolécula inicialmente es un factor muy importante en este tipo de inmovilización, ya que si el punto isoeléctrico de la misma es menor que el pH del medio, la biomolécula se encontrará cargada negativamente, permitiendo así el establecimiento de interacciones iónicas con soportes cargados positivamente. Es por ello que la

cantidad de biomolécula inmovilizada así como la retención de su actividad biológica dependerán de la carga que posea la biomolécula.

Esta técnica presenta la ventaja de que normalmente la conformación de la biomolécula permanece inalterada tras la inmovilización en el soporte y el conjugado es más estable que el obtenido mediante adsorción física. Sin embargo, el principal inconveniente es que la alteración del pH del medio o de la fuerza iónica del mismo puede producir la separación de la enzima[40, 41].

Se distinguen dos tipos de metodologías:

a) *Deposición layer-by-layer*: se basa en alternar capas de polielectrolito y de biomolécula con cargas opuestas. En primer lugar, el soporte se sumerge en una disolución de un policatión o un polianión para formar la primera capa con carga. A continuación, la biomolécula con carga opuesta es depositada sobre el soporte siendo inmovilizada a través de interacciones electrostáticas. Posteriormente, una nueva capa de policatión o polianión es depositada sobre la capa de biomolécula. Este proceso se repite hasta alcanzar el número de capas deseado.

   Entre los polianiones más empleados se encuentran el sulfonato de poliestireno (PSS), la poliacrilamida, y los ácidos poliacrílico (PAA) y polimetacrílico (PMAA). Por otra parte, los policationes más usados son la polialilamina, la polietilenimina y el cloruro de polidialildimetilamonio (poliDADMAC), entre otros[34].

b) *Dopado electroquímico*: consiste en la deposición de la biomolécula sobre un soporte conductor durante su oxidación o reducción[34]. Así, por ejemplo, durante la oxidación el soporte se carga positivamente y la biomolécula disuelta en el medio a un valor dado de pH se encuentra cargada negativamente, por lo que puede establecer interacciones de tipo iónico con el soporte, y así ser incorporada al mismo.

2.1.3. Afinidad

El fundamento de la inmovilización por interacciones de afinidad se basa en la alta selectividad y capacidad de reconocimiento existentes entre ciertos tipos de biomoléculas, como por ejemplo, entre biotina y (estrept)avidina, entre carbohidratos y lectinas, y iones metálicos e histidina[42-45].

La complementariedad entre estos tipos de moléculas permite llevar a cabo la inmovilización de una manera más orientada estructuralmente y más dirigida a un sitio en concreto del soporte, afectando así en pequeña medida a la conformación de las moléculas implicadas y evitando el bloqueo de las zonas más activas de la biomolécula. Estos hechos favorecen que la biomolécula conserve un mayor grado de actividad después de su inmovilización.

La estrategia empleada para realizar este tipo de inmovilizaciones consiste en activar el soporte con una de las moléculas implicadas en la interacción de afinidad (por ejemplo, avidina), y unir su par específico (biotina) a la biomolécula que se quiere inmovilizar. En ocasiones este grupo específico se encuentra de forma natural en la biomolécula y no es imprescindible su introducción; sin embargo, en la mayoría de los casos es necesario realizar la unión, ya sea mediante reacciones covalentes con grupos funcionales de la biomolécula no implicados en su actividad biológica, o a través de métodos de ingeniería genética que permitan su introducción en secuencias específicas de la biomolécula que no interfieran con su actividad. En cualquier caso, la introducción del grupo específico no debe alterar su interacción de afinidad con su molécula complementaria en el soporte activado.

Entre los tipos de interacciones de afinidad mencionados destaca la que tiene lugar entre las moléculas de biotina y las proteínas avidina o estreptavidina. La interacción no covalente que se establece entre ellas es realmente fuerte y específica, originando complejos de una alta afinidad con una constante de disociación K_d de aproximadamente 10^{-15} M[43, 46]. De esta forma, la bioespecificidad existente en esta interacción es similar a la que ocurre en el reconocimiento de un antígeno por su anticuerpo o en la interacción ligando-receptor, sin embargo, la afinidad es mucho mayor en el caso de la interacción biotina-(estrept)avidina (por ejemplo, las interacciones antígeno-anticuerpo tienen valores de K_d en el rango de 10^{-6} hasta 10^{-12} M)[46, 47].

Además, la interacción biotina-(estrept)avidina se produce de forma rápida y se puede dar en condiciones extremas de pH, temperatura y fuerza iónica, siendo incluso resistente a la presencia de ciertos agentes desnaturalizantes, detergentes y determinados disolventes orgánicos[42].

Por otra parte, la molécula de biotina puede ser fácilmente acoplada a muchas moléculas y biomoléculas (en un proceso que se conoce por el nombre de biotinilación) mediante el grupo carboxilo de su cadena lateral, el cual puede ser derivatizado para mejorar su reactividad y favorecer dicho acoplamiento, y además, la unión por esta cadena lateral no limita la interacción de afinidad con la avidina o la estreptavidina. Asimismo, su pequeño tamaño la convierte en una

candidata ideal para ser incorporada a las biomoléculas, ya que en la mayoría de los casos no afecta a la actividad biológica de las mismas[42, 48].

Como consecuencia de las excelentes características que presenta la interacción biotina-(estrept)avidina, ha sido y es ampliamente utilizada como estrategia para inmovilización de biomoléculas y como técnica de bioconjugación.

Otro tipo de interacciones de afinidad empleadas para la inmovilización de biomoléculas son las que tienen lugar entre determinados iones metálicos y los residuos de histidina de las biomoléculas[45, 49]. Para llevar a cabo este tipo de inmovilización es necesario en primer lugar dopar la superficie del soporte con alguna sal o hidróxido de un ion metálico adecuado, siendo los más empleados los de níquel y cobalto. Para ello, la sal o hidróxido metálico se precipita sobre el soporte mediante calentamiento o neutralización, produciéndose la coordinación del metal con los grupos nucleófilos del soporte. Sin embargo, y debido a factores estéricos, no todas las posiciones de coordinación del metal pueden ser ocupadas por los grupos del soporte, pudiendo ser empleadas por tanto para la coordinación con grupos de la biomolécula a inmovilizar.

Por otro lado, debido a que la presencia de residuos de histidina en las biomoléculas es relativamente escasa, en la mayoría de los casos es necesario llevar a cabo procedimientos de modificación sobre las biomoléculas para incorporarles cadenas de histidina en posiciones de su estructura que no afecten ni a su conformación espacial ni a su actividad biológica.

Con este método se puede lograr cierto control de los sitios para la inmovilización de biomoléculas si en primer lugar se lleva a cabo la unión de agentes quelantes a la superficie del soporte, a continuación, se realiza el acoplamiento del ion metálico por algunas de sus posiciones de coordinación, y, posteriormente, se añaden las biomoléculas que se unirán al metal por sus posiciones de coordinación restantes. Finalmente, las biomoléculas unidas pueden ser fácilmente eluidas mediante competición con ligandos metálicos o mediante cambios en el pH del medio; mientras que el soporte puede ser regenerado usando quelatos fuertes como por ejemplo el ácido etilendiaminotetraacético (EDTA)[34].

Las interacciones de afinidad específicas que tienen lugar entre carbohidratos y lectinas también se utilizan para realizar la inmovilización de biomoléculas[44, 50, 51]. Las lectinas son un grupo heterogéneo de proteínas con una elevada capacidad para reconocer e interaccionar de manera altamente específica con determinados carbohidratos o glicoconjugados[52]. Entre la variedad de lectinas existentes, la concanavalina A (Con A) es la más ampliamente utilizada para

la inmovilización de biomoléculas debido a su habilidad para reconocer selectivamente glucosa y manosa[44, 51].

El procedimiento de inmovilización mediante interacciones de afinidad con lectinas requiere una etapa previa de unión de estas proteínas al soporte y, en muchos casos, en los que las biomoléculas no contengan de manera natural carbohidratos en su estructura, también es necesario realizar la incorporación de cadenas azucaradas a las biomoléculas que se desean inmovilizar.

Por último, los soportes empleados para realizar las inmovilizaciones a través de interacciones de afinidad (ya sea mediante interacciones biotina-(estrept)avidina, iones metálicos-histidina o carbohidratos-lectinas) son muy diversos, incluyendo multitud de polímeros naturales, como la celulosa y el alginato, y una gran variedad de polímeros sintéticos, como la poliacrilamida y el poliestireno.

2.1.4. Puentes disulfuro

Esta técnica de inmovilización se clasifica dentro de las técnicas reversibles a pesar de que el procedimiento de unión está basado en la formación de enlaces de tipo disulfuro covalentes y estables entre la biomolécula y el soporte[53-55]. Este tipo de clasificación es posible gracias a que los puentes disulfuro tienen la característica de ser fácilmente rompibles en condiciones suaves de reacción con agentes adecuados como el ditiotreitol (DTT)[56].

Para llevar a cabo este tipo de inmovilización las biomoléculas, con grupos tioles libres y accesibles, se hacen reaccionar en condiciones suaves con soportes activados con grupos disulfuro o con óxidos de disulfuro. Estos grupos activantes pueden ser introducidos en una amplia variedad de soportes con diferentes grados de porosidad y diversas propiedades físicas y mecánicas. Por otra parte, aunque las biomoléculas no posean grupos tioles libres, también es posible realizar la introducción de dichos grupos químicamente (a través de un proceso de tiolación usando reactivos heterobifuncionales como el *N*-succinimidil 3-(2-piridilditiopropionato) (SPDP))[56], o mediante técnicas de ingeniería genética, lo que incrementa aún más la aplicabilidad de esta técnica, no quedando así restringida a biomoléculas con grupos tioles reactivos de forma natural[57].

Entre las ventajas de esta técnica de inmovilización destacan la reutilización del soporte gracias al carácter reversible de los enlaces disulfuro, la alta especificidad de la reacción entre los

grupos tiol, y la posibilidad de controlar la orientación de las biomoléculas debido a que los grupos tioles de las mismas se localizan en regiones muy concretas.

Ejemplos de materiales empleados para la inmovilización mediante esta técnica son la agarosa activada con 2-piridil-disulfuros y geles funcionalizados con tiosulfonato y tiosulfinato[54].

2.2. Técnicas de inmovilización irreversible

En estas técnicas las biomoléculas quedan unidas al soporte de manera que es prácticamente imposible liberarlas sin producir la pérdida de su actividad biológica o la alteración del propio soporte. Este tipo de técnicas presentan la ventaja de que la retención de la biomolécula en el soporte no se ve afectada por cambios en el pH o la fuerza iónica del medio. Se pueden clasificar en 4 grandes grupos: formación de enlaces covalentes, entrecruzamiento, atrapamiento y encapsulación.

2.2.1. Formación de enlaces covalentes

La inmovilización de biomoléculas mediante enlaces covalentes es uno de los métodos de inmovilización más utilizados debido a que los enlaces covalentes generalmente proporcionan la unión más fuerte entre el soporte y la biomolécula, reduciendo considerablemente el desprendimiento de la misma, y además, esta técnica presenta una enorme versatilidad gracias a la gran cantidad de reactivos disponibles con distintas propiedades de solubilidad, reactividad y estabilidad, que pueden dar lugar a la formación de dichos enlaces covalentes.

Entre la gran variedad de reacciones que se han empleado para generar este tipo de enlaces entre una biomolécula y un soporte, las más utilizadas son las que implican grupos amino, carboxilo, hidroxilo o tiol pertenecientes a la cadena lateral de aminoácidos como lisina, ácido aspártico, ácido glutámico, serina o cisteína de la biomolécula[36, 58]. Así, los enlaces covalentes que se forman entre biomolécula y soporte son principalmente de tipo amida, éter o tioéter[59].

Debido a que los grupos funcionales mencionados pueden también estar involucrados en la actividad biológica de la biomolécula, por ejemplo, pueden estar localizados en el centro activo de una enzima o muy próximos a él, es muy conveniente conocer previamente el mecanismo por el cual la biomolécula desarrolla su actividad, puesto que la implicación en el proceso de

inmovilización de estos grupos clave para la actividad conduce a la pérdida parcial o total de la misma.

Para realizar este tipo de inmovilizaciones es necesario además que el soporte presente algún grupo funcional disponible y accesible para reaccionar con los grupos de las biomoléculas mencionados. La presencia de estos grupos funcionales en el soporte puede deberse al propio proceso de fabricación del soporte, de manera que se obtiene un material directamente activado, con grupos funcionales reactivos, y listo para reaccionar con la biomolécula, o a procesos de activación superficial llevados a cabo después de la producción del material. Por cualquiera de estos dos métodos, los grupos funcionales que generalmente presentan las superficies de los soportes son aldehídos, epóxidos, ácidos carboxílicos, aminas, maleimidas e hidroxilos[57, 60-62]. En la Figura 5 se muestra un esquema de los reactivos más empleados para activar los soportes con los grupos funcionales mencionados, así como los tipos de enlaces covalentes que se forman tras la reacción con las biomoléculas; mientras que en la Tabla 2 se resumen los grupos funcionales tanto del soporte como de la biomolécula que reaccionan entre sí, el tipo de enlace covalente que originan y algunos ejemplos de utilización de las reactividades mencionadas en la fabricación de biosensores.

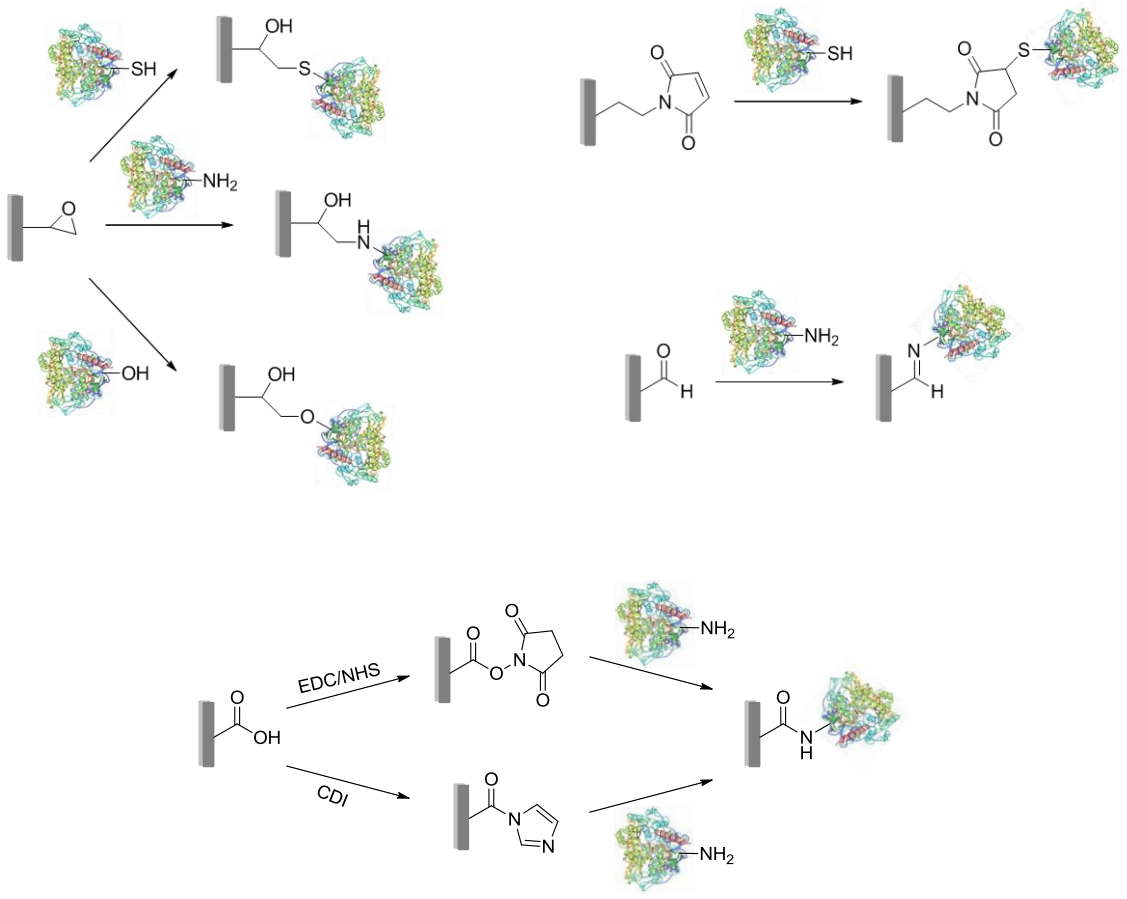

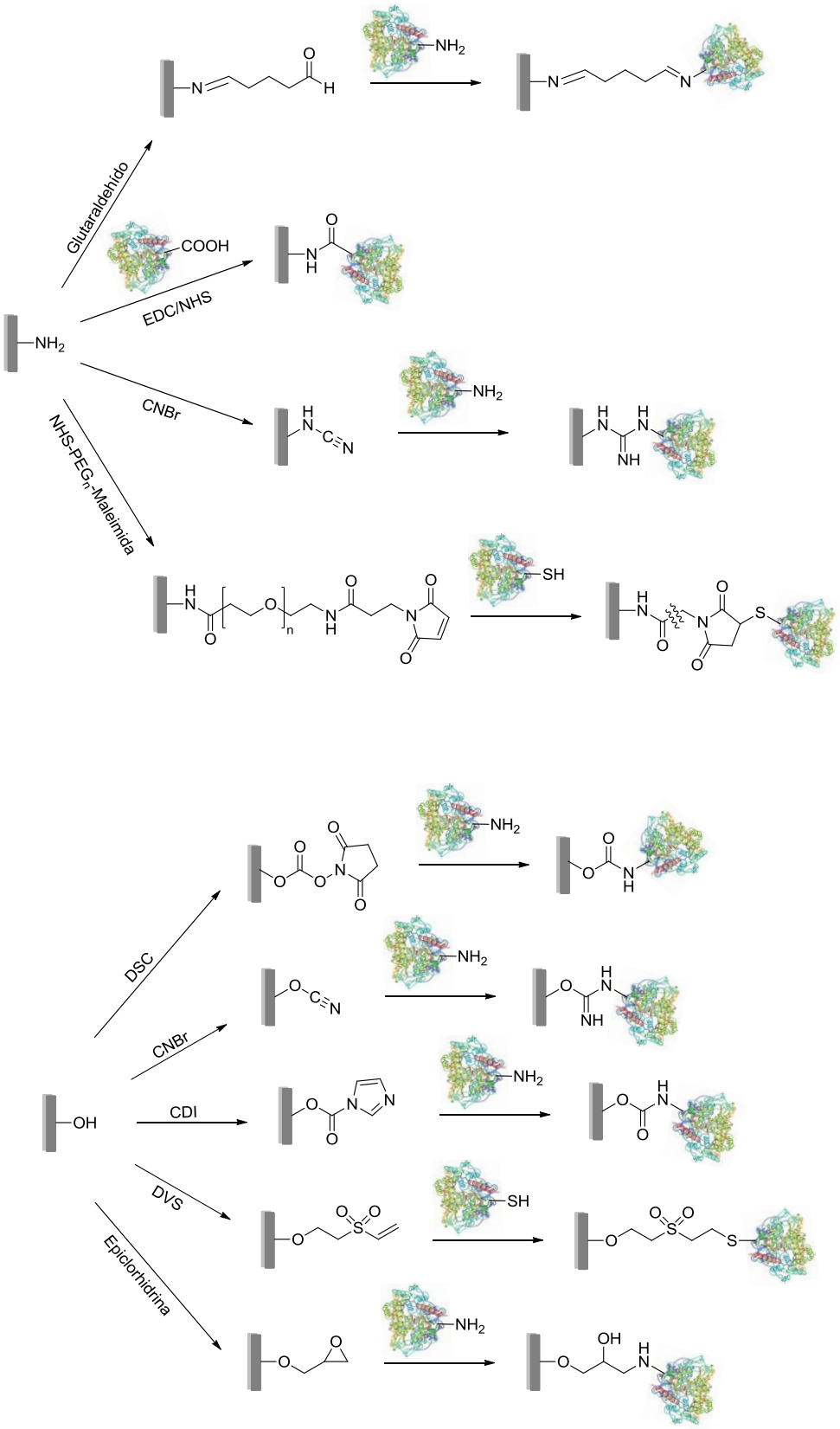

Figura 5. Representación esquemática de los distintos tipos de reactividades más empleados en la inmovilización de biomoléculas a través de la formación de enlaces covalentes.

Tabla 2. Grupos funcionales de soporte y biomolécula implicados en la formación de enlaces covalentes.

Grupo funcional del soporte	**Reactivos utilizados para llevar a cabo la inmovilización**	**Grupo funcional de la biomolécula con el que reacciona mayoritariamente (aminoácidos a los que pertenece el grupo funcional)**	**Tipo de enlace covalente formado entre el soporte y la biomolécula**	**Referencia**
Aldehído	-	Amina primaria (Lys)	Imina	63-65
Epóxido	-	Tiol (Cys)	Tioéter	66-68
	-	Amina primaria (Lys)	Amina	
	-	Hidroxilo (Ser y Thr)	Éter	
Ácido carboxílico	EDC/NHS CDI	Amina primaria (Lys)	Amida	69-73
Amina	EDC/NHS	Ácido carboxílico (Asp y Glu)	Amida	74-77
	CNBr	Amina primaria (Lys)	Imido-carbonato	
	Glutaraldehído	Amina primaria (Lys)	Imina	
	NHS-PEG_n-Maleimida	Tiol (Cys)	Tioéter	
Maleimida	-	Tiol (Cys)	Tioéter	59, 78
Hidroxilo	DSC CNBr Epiclorhidrina CDI	Amina primaria (Lys)	Carbamato Isourea Amina Carbamato	79, 80
	DVS	Tiol (Cys), amina primaria (Lys), hidroxilo (Ser y Thr)	Tioéter, amina secundaria, éter	59, 81, 82

Lys: lisina; Cys: cisteína; Ser: serina; Thr: treonina; Asp: ácido aspártico; Glu: ácido glutámico

Cada tipo de unión covalente requiere una funcionalización específica tanto en el soporte como en la biomolécula implicada. En general, es complicado predecir el grupo funcional con el que se debe activar un determinado soporte de manera que sea el más adecuado para la biomolécula deseada, debido a que son muchos factores, relacionados con la naturaleza tanto del soporte (forma, porosidad de la superficie o composición química) como de la biomolécula, así como con las condiciones específicas en las que tiene lugar la reacción de inmovilización, los que

influyen en la retención de la actividad biológica de la biomolécula una vez inmovilizada. Es por ello que las condiciones óptimas para inmovilizar biomoléculas difieren de una biomolécula a otra en función del soporte, de la biomolécula y del tipo de funcionalización disponible.

Entre los grupos reactivos de las biomoléculas, los grupos tiol, pertenecientes a residuos de cisteína, presentan la ventaja de ser más nucleófilos, y por tanto, más reactivos, que los grupos amino a valores de pH por debajo de 9, en los que la mayoría de biomoléculas son más estables[83, 84]. Además, los residuos de cisteína libres son relativamente poco abundantes de manera natural en las proteínas, ya que frecuentemente se encuentran formando enlaces disulfuro, y, por ello, es posible utilizarlos para realizar inmovilizaciones más orientadas y dirigidas a zonas de la biomolécula que no estén involucradas en el desarrollo de su actividad biológica[85]. En los casos en los que las proteínas no presenten estos residuos de cisteína libres también es posible añadirlos mediante reacción con algún reactivo o, más específicamente, a través de métodos de ingeniería genética[45, 83].

Por otra parte, en este tipo de inmovilizaciones se suelen emplear espaciadores entre el soporte y la biomolécula para mantener una distancia apropiada entre ambos, ya que dicha distancia constituye otro factor que también afecta a las características finales de estabilidad y actividad de la biomolécula inmovilizada[86, 87]. Así, la influencia de la distancia viene determinada principalmente por los siguientes efectos:

- *Impedimento estérico*: si la distancia entre el soporte y la biomolécula es insuficiente, el soporte puede limitar la aproximación del sustrato a la biomolécula.

- *Microambiente en las proximidades de la biomolécula*: la naturaleza del soporte (por ejemplo, el carácter hidrofílico o hidrofóbico) puede modificar negativamente el microambiente de la biomolécula si ésta se encuentra demasiado cerca del soporte.

- *Interacciones indeseadas* de tipo no covalente e inespecíficas entre la biomolécula y el soporte si se hallan demasiado próximos entre sí.

- *Movilidad y flexibilidad conformacional*: si la distancia con el soporte es adecuada, la biomolécula tendrá cierta libertad de movimiento y podrá adoptar la orientación y la conformación espacial adecuadas para desarrollar su actividad biológica.

En general, las moléculas empleadas como espaciadores se caracterizan por su longitud, su estructura lineal o ramificada, su carácter hidrofílico o hidrofóbico y la presencia o no de cargas

positivas o negativas. Así, una gran variedad de compuestos, incluyendo moléculas bifuncionales como el glutaraldehído y el glioxal, polímeros lineales como el polietilenglicol o ramificados como el dextrano, y biomoléculas como la albúmina de suero bovino o cadenas de ADN, han sido empleados como agentes espaciadores en multitud de ocasiones con diferentes soportes y biomoléculas[86-90].

Otros factores a considerar a la hora de llevar a cabo la inmovilización covalente son la densidad de unión y la unión multipuntual[45, 91, 92]. El primero de ellos viene dado por el número de biomoléculas inmovilizadas por unidad de superficie del soporte, el cual será óptimo para cada biomolécula en función de su tamaño, de su orientación, de su conformación espacial, y de la disponibilidad de los grupos funcionales reactivos. Así, generalmente, al aumentar la densidad de unión también aumenta la actividad global, hasta alcanzar un máximo a partir del cual, una mayor inmovilización implica una disminución o, en el mejor de los casos, no variación de la actividad, debido sobre todo al impedimento estérico que una biomolécula ejerce sobre las contiguas y a la mayor limitación en la aproximación del sustrato a la biomolécula.

En el caso de la unión multipuntual, es decir, la unión por varios grupos de la biomolécula al soporte, se suele producir una mayor estabilización de la biomolécula inmovilizada; sin embargo, es necesario controlar el grado de unión multipuntual para que los efectos no sean negativos y contrarios a los deseados, ya que dicha unión conduce a una mayor rigidez de la conformación de la biomolécula, la cual generalmente hace disminuir su actividad. Una forma de controlar la unión multipuntual consiste en llevar a cabo la inmovilización a través de grupos funcionales que sean más o menos abundantes en la biomolécula en función del grado de unión que se quiera. Así por ejemplo, si la inmovilización se realiza a través de grupos tiol de residuos de cisteína, que generalmente son poco abundantes, la unión tendrá lugar mediante uno o dos enlaces, pero si se utilizan residuos de lisina, presentes en mucha mayor medida, la unión se dará por muchos puntos de la biomolécula.

Teniendo en mente todos los factores mencionados y todas las variables implicadas en el proceso de inmovilización y retención de la actividad biológica, se han desarrollado una serie de estrategias de modificación de la superficie del soporte y, en menor medida, también de modificación de la superficie de la biomolécula, para mejorar tanto la retención de la actividad como la estabilidad de la biomolécula inmovilizada. Algunas de estas estrategias se aplican previamente a la inmovilización y otras son posteriores a la misma. Entre dichas metodologías destacan la introducción de grupos polares o apolares, pertenecientes o no a un determinado

espaciador, para adecuar el microambiente a las necesidades de la biomolécula, la modificación de los grupos funcionales de la biomolécula para incrementar o disminuir su reactividad, y la utilización de agentes de bloqueo de la superficie del soporte que disminuyen el grado de unión multipuntual y a la vez pueden alterar el microambiente, ajustándolo a cada biomolécula.

Finalmente, los soportes más comúnmente empleados para realizar la inmovilización mediante enlaces covalentes abarcan polímeros sintéticos como el nylon, materiales inorgánicos como el vidrio, o polímeros naturales como la celulosa, la agarosa y el almidón. Algunos de los cuales poseen grupos funcionales superficiales que pueden reaccionar directamente con las biomoléculas, mientras que otros requieren de un proceso de activación previo[60].

2.2.2. Entrecruzamiento

Este método de inmovilización no requiere del uso de un soporte sólido sino que son las propias biomoléculas las que se enlazan entre sí o con otras proteínas inertes, como por ejemplo la albúmina de suero bovino, mediante el uso de agentes de entrecruzamiento multifuncionales, originando así agregados proteicos[93-95].

El glutaraldehído es uno de los reactivos más utilizados para realizar el entrecruzamiento de biomoléculas[96, 97], generalmente por medio de dos tipos de reacciones: por un lado y mayoritariamente, mediante la formación de bases de Schiff entre los grupos amino libres de residuos de lisina o arginina de las biomoléculas y los grupos aldehído de oligómeros o polímeros de glutaraldehído, y por otro, a través de adiciones 1,4 de tipo Michael entre dichos grupos amino y restos de aldehídos α,β-insaturados. Otros reactivos empleados para llevar a cabo el entrecruzamiento de biomoléculas son el glioxal, los diisocianatos de tolueno y hexametileno, y diiminoésteres[98].

La gran ventaja de este método es su sencillez, sin embargo, la formación de los agregados por entrecruzamiento es muy sensible a las condiciones de reacción, tales como pH y temperatura, y pueden producirse pérdidas en la actividad biológica de la biomolécula debido a la posible modificación del centro activo durante la reacción y a la distorsión de la conformación. Asimismo, también es necesario controlar la forma y el tamaño de los agregados para maximizar la retención de actividad.

Esta técnica ha sido empleada fundamentalmente para el entrecruzamiento de enzimas, distinguiéndose dos tipos de metodologías en función del estado cristalino de la enzima:

a) *CLECs (cristales de enzimas entrecruzadas)*: se preparan mediante la cristalización de las enzimas en medio acuoso en presencia del reactivo de entrecruzamiento que dará lugar a la unión entre los cristales de enzima. El conjunto resultante mantiene una alta actividad enzimática y su tamaño puede variar desde 1 a 100 µm en función de la cantidad de agente de entrecruzamiento y del tiempo de reacción. Sin embargo, el principal inconveniente de esta metodología es que la cristalización enzimática es un proceso laborioso que requiere enzimas de alta pureza, lo que hace que sea un procedimiento realmente costoso[93, 99, 100].

b) *CLEAs (agregados de enzimas entrecruzadas)*: preparados a partir de la precipitación de las enzimas en medio acuoso como consecuencia de la adición de sales, disolventes orgánicos miscibles con el agua, o polímeros no iónicos, lo que origina agregados físicos que se mantienen unidos mediante enlaces no covalentes. Posteriormente con la incorporación del reactivo de entrecruzamiento tiene lugar la unión covalente de estos agregados que conservan su estructura pre-organizada y con ello su actividad catalítica. Además, esta técnica presenta la ventaja de que algunos de los reactivos usados para provocar la precipitación de las enzimas también se utilizan en la purificación de las mismas, por lo que no se requieren enzimas de una alta pureza. En este caso, los agregados resultantes pueden tener un tamaño entre los 5 y los 50 µm variando también la cantidad de agente entrecruzante y el tiempo de reacción[101-103].

2.2.3. Atrapamiento

La inmovilización mediante atrapamiento se basa en la retención física o química de la biomolécula en el entramado interno de una matriz porosa, cuyos espacios intersticiales son lo suficientemente grandes como para permitir el paso de sustrato y productos, pero no para permitir el movimiento de la biomolécula[36, 104, 105].

Se trata de un método de inmovilización sencillo en el que la biomolécula es suspendida con una mezcla de monómeros, los cuales posteriormente son sometidos a procesos de gelificación física o de polimerización (normalmente mediante adición de un iniciador y/o un agente entrecruzante o por modificaciones en la temperatura), originando una estructura tipo gel o en forma de fibras, membranas o esferas, en cuyas cavidades la biomolécula queda retenida[106-108]. Por tanto, generalmente, la matriz donde queda atrapada la biomolécula se forma durante el

proceso de inmovilización, lo que hace necesario que todos los reactivos implicados en la formación de la misma sean compatibles con la biomolécula a inmovilizar.

Una de las ventajas que presenta este método es la posibilidad de inmovilizar la biomolécula en un microentorno totalmente favorable con unas condiciones óptimas de pH, hidrofobicidad y polaridad para desarrollar su actividad biológica. Esto se puede conseguir mediante la selección del material que originará las cavidades donde quedará ocluida la biomolécula, de manera que sus propiedades físico-químicas sean las más adecuadas para cada biomolécula en particular. Hoy en día gracias al gran avance en la Ciencia de Materiales es posible disponer de multitud de polímeros, compuestos precursores de procesos sol-gel y otros materiales inorgánicos con variedad de propiedades que pueden ser utilizados para llevar a cabo este tipo de inmovilización.

En muchos casos, además, la actividad de la biomolécula inmovilizada se puede controlar mediante la incorporación de aditivos durante el proceso de formación de la matriz porosa, los cuales también condicionarán el microambiente donde finalmente quedará recluida la biomolécula. Estos aditivos pueden ayudar a modular la porosidad de la matriz y la difusión a través de la misma, así como condicionar la orientación y la conformación espacial de la biomolécula inmovilizada en el interior de las cavidades. Entre los aditivos más empleados se encuentran el polietilenglicol y ciertos tipos de surfactantes, polisacáridos y éteres corona[105].

Otra de las ventajas de esta técnica es que se puede utilizar para inmovilizar varias biomoléculas diferentes simultáneamente, simplemente mediante adición de las mismas a la mezcla de monómeros.

El caso de la inmovilización por gelificación presenta además la ventaja de que al tratarse de una inmovilización mediante un proceso de retención física, la biomolécula no sufre ningún tipo de reacción química con el soporte, por lo que es posible evitar la desnaturalización y pérdida de actividad biológica derivada de los procesos químicos[106, 107]. Sin embargo, para ello es necesario que a la hora de seleccionar el material no solamente se tenga en cuenta el microentorno al que dará lugar y donde se ubicará la biomolécula, sino que también hay que considerar su reactividad, así como la de todos los reactivos implicados en el proceso de polimerización, para evitar cualquier tipo de interacción química con la biomolécula.

Por otro lado, el mayor inconveniente de este tipo de inmovilizaciones es la dificultad en muchos casos para controlar el tamaño de los poros y cavidades, un factor muy importante, ya que poros demasiado pequeños originan limitaciones en el movimiento de sustrato y productos a

través del material, y por el contrario cavidades demasiado grandes pueden causar la pérdida de la biomolécula. Otra desventaja de esta técnica es la baja capacidad de carga que tienen algunos de los materiales empleados, y que, en algunos casos, un aumento de la cantidad de biomolécula inmovilizada no conlleva un aumento de actividad debido a limitaciones de difusión a través del soporte.

Entre la gran variedad de materiales que se pueden emplear como matrices, tanto de origen natural como sintético, se encuentran polisacáridos como la agarosa, el almidón y el alginato, polipéptidos como la albúmina, la caseína y el colágeno, y polímeros sintéticos como la poliacrilamida, el polieuretano, etc. Entre ellos destaca el uso de los alginatos debido su inocuidad y a su propiedad de producir geles en condiciones suaves.

2.2.4. Encapsulación

Esta técnica de inmovilización es similar a la de atrapamiento, pero en este caso la biomolécula queda confinada en el interior de membranas o microcápsulas esféricas cuyas paredes son semipermeables y permiten el paso de las moléculas de sustrato y producto pero no de biomolécula, de manera que la membrana que rodea a la biomolécula actúa como una barrera física sólo para ella[104, 109]; es por ello que el control del tamaño de los poros no supone tanta limitación para esta técnica como para la de atrapamiento, sino que la eficiencia de la técnica de encapsulación depende en gran medida de la estabilidad de la biomolécula situada en el interior de la microcápsula.

Las microcápsulas empleadas en esta técnica pueden ser generalmente de dos tipos:

a) *Permanentes*: originadas por procesos de polimerización interfacial o de inversión de fase. En el primer caso, la biomolécula a inmovilizar y uno de los reactivos que intervendrá en la polimerización se encuentran disueltos en medio acuoso, mientras que el otro reactivo implicado en la polimerización se disuelve en un disolvente orgánico inmiscible con el agua, como por ejemplo ciclohexano. De esta manera, la polimerización que da lugar a la formación de la membrana ocurre en la interfase entre ambos disolventes y la biomolécula, aún en disolución, queda atrapada en el interior de la membrana. Como reactivos solubles en agua se suelen utilizar piperidina, polifenoles o polímeros como el quitosano o el ácido poliacrílico; mientras que los reactivos solubles en fase orgánica suelen ser compuestos dihalogenados como el cloruro de sebacoilo o el cloruro de tereftaloilo[110].

En el método por inversión de fase, la fase líquida que rodea a la disolución de biomolécula solidifica como consecuencia de un cambio en su solubilidad debido a la evaporación o a la difusión de los disolventes que la componen, dando lugar a la formación de la membrana alrededor de la biomolécula.

b) No permanentes: generadas por surfactantes que se someten a un proceso de agitación para formar micelas en cuyo interior quedan atrapadas las biomoléculas. El diámetro de las micelas puede variar de los 100 a los 250 nm dependiendo del tipo de surfactante utilizado. Los surfactantes más empleados para producir este tipo de micelas son CTAB, SDS, AOT, TOMAC y DDAB entre otros[110].

Entre las ventajas de esta técnica destacan su simplicidad, la capacidad para mantener a la biomolécula protegida de agentes externos que pueden originar su desnaturalización, la posibilidad de inmovilizar diferentes tipos de biomoléculas simultáneamente y que, generalmente, las microcápsulas se forman en condiciones muy suaves. Además, en muchos casos, la inocuidad de los reactivos utilizados para generar las microcápsulas permite que puedan ser usadas con fines farmacológicos.

Por otro lado, la principal desventaja de este método de inmovilización radica en que solamente los sustratos y productos pequeños son capaces de atravesar la membrana de las microcápsulas, limitando su utilidad a un tamaño determinado de moléculas. Asimismo, la dificultad para controlar el espesor y la permeabilidad de dichas membranas condiciona aún más el uso de esta técnica.

2.3. Combinación de diferentes técnicas de inmovilización

En muchos casos la utilización de los métodos de inmovilización descritos hasta ahora no conduce a resultados satisfactorios de actividad y/o estabilidad de la biomolécula inmovilizada, o proporciona niveles insuficientes de inmovilización. Es por ello que se han desarrollado una serie de técnicas en las que se combinan diferentes aproximaciones de inmovilización para resolver estos y otros problemas que no pueden ser solucionados con los métodos convencionales[111]. Así, por ejemplo, se ha utilizado la combinación de la inmovilización mediante adsorción con la técnica de entrecruzamiento o con la inmovilización covalente, e incluso se han desarrollado

nuevos métodos de inmovilización mediante el acoplamiento de la encapsulación con el entrecruzamiento.

2.3.1. Adsorción-entrecruzamiento

La combinación de la técnica de adsorción con el entrecruzamiento constituye una de las formas más simples y sencillas de solventar los problemas derivados de la inmovilización reversible mediante adsorción física[112]. Así, esta combinación permite incrementar la fortaleza de las interacciones, evitando así los desprendimientos producidos como consecuencia de las débiles interacciones originadas durante los procesos de adsorción física. Estos procedimientos, a su vez, mejoran en algunos casos la estabilidad de la biomolécula inmovilizada, pero suelen afectar negativamente a la actividad biológica.

2.3.2. Adsorción-inmovilización covalente

La conjunción de la adsorción física o iónica con la inmovilización covalente es una de las metodologías combinadas más empleadas debido a las ventajas que aporta un primer paso de retención mediante adsorción sobre la inmovilización covalente posterior[113]. Así, gracias a que los procesos de adsorción física o iónica son muchos más rápidos que el establecimiento de enlaces covalentes, es posible prevenir o minimizar el grado de precipitación o proteólisis de determinadas biomoléculas mediante una primera etapa de adsorción consiguiendo que las biomoléculas pasen menor tiempo en disolución antes de ser inmovilizadas covalentemente. Además, este proceso de adsorción previo puede tener en algunos casos un efecto positivo sobre la estabilidad de la biomolécula retenida, permitiendo la disminución del grado de inactivación causada por la distorsión de su estructura.

Posteriormente al proceso de adsorción tiene lugar la formación de los enlaces covalentes con una mayor rapidez gracias a la mayor proximidad espacial entre la biomolécula y el soporte, conseguida tras la adsorción. En esta segunda etapa de inmovilización, el grado de activación del soporte y el tipo de grupo funcional del mismo juegan un papel fundamental en el proceso de inmovilización.

Por otra parte, con la combinación de estas dos técnicas también es posible lograr la inmovilización de las biomoléculas con una orientación controlada. Para ello es necesario seleccionar los grupos del soporte que originan la adsorción de la biomolécula, de manera que los grupos de la biomolécula implicados en este proceso de adsorción quedan más próximos al

soporte y son los que formarán principalmente los enlaces covalentes con el mismo. De esta forma es posible establecer la zona de la biomolécula que reacciona con el soporte, y con ello, la orientación espacial de la misma tras su inmovilización[113].

El inconveniente de realizar una etapa de inmovilización covalente tras la adsorción física o iónica es que, en muchos casos, no existe garantía de que la biomolécula establezca finalmente los enlaces covalentes con el soporte.

2.3.3. Encapsulación-entrecruzamiento

Una de las principales desventajas de la técnica de encapsulación convencional consiste en la dificultad para controlar el espesor y la permeabilidad de las membranas, de manera que se consiga retener la biomolécula en el interior de las microcápsulas y a la vez se permita el paso de sustratos y productos.

Con el fin de resolver este y otros inconvenientes asociados a la inmovilización por encapsulación, se ha propuesto su combinación con la técnica de entrecruzamiento; con lo cual se ha conseguido mejorar la estabilidad de las biomoléculas y aumentar la retención de las mismas en el interior de las microcápsulas.

El procedimiento consiste en formar los agregados de biomoléculas entrecruzadas en el interior de las microcápsulas, de manera que es posible controlar el tamaño de dichos agregados mediante la selección del tamaño y geometría de las cápsulas[110]. Con esto se consigue además, que no sea necesario el uso de una membrana semipermeable con un tamaño de poro controlado, ya que el tamaño del agregado en el interior de las cápsulas es mucho mayor que la biomolécula individual, y se pueden utilizar membranas con poros de mayores tamaños, facilitando el paso de sustratos y productos. Asimismo, se consiguen solventar algunos de los problemas asociados con la técnica de entrecruzamiento como, por ejemplo, el control de la forma y el tamaño de los agregados para mejorar la actividad biológica y el aislamiento de las biomoléculas en un microentorno más favorable.

3. SOPORTES EMPLEADOS EN EL DISEÑO DE BIOSENSORES

El avance en las técnicas de inmovilización de biomoléculas ha venido de la mano de la fabricación de nuevos soportes, lo que combinado con el rápido desarrollo de la nanotecnología y su implicación en la Ciencia de Materiales, ha conducido hacia un amplio abanico de posibilidades en el diseño y la producción de nuevos materiales. Así, hoy en día existen en el mercado numerosos soportes con diferentes propiedades físicas, químicas y mecánicas, y con una gran diversidad de formas y tamaños, desde partículas, hasta láminas, membranas, fibras o cápsulas.

Debido a que el material elegido para llevar a cabo la inmovilización de una determinada biomolécula afecta en gran medida a las características que tendrá la biomolécula una vez inmovilizada, la elección del material deberá realizarse teniendo en cuenta una serie de factores, entre los que destacan los siguientes:

- Funcionalización de su superficie con los grupos químicos adecuados que permitan realizar la inmovilización en condiciones suaves de reacción.
- Microambiente apropiado para la biomolécula inmovilizada.
- Carácter hidrofílico o hidrofóbico en función del tipo de biomolécula que se desea inmovilizar (en general, se minimiza el carácter hidrofóbico porque muchas biomoléculas son hidrofílicas, evitando así su desnaturalización y además, disminuyendo la adsorción de otras sustancias; sin embargo, en el caso de la inmovilización de biomoléculas hidrofóbicas como las lipasas, sí que es necesario seleccionar soportes hidrofóbicos).
- Bajo alcance de las interacciones inespecíficas para minimizar la inmovilización de sustancias interferentes.
- Inerte bajo las condiciones de operación de la biomolécula inmovilizada para no interferir con su reacción bioquímica específica.
- Alta capacidad de inmovilización de biomoléculas.
- Elevada área superficial, porosidad y adecuado tamaño y distribución de poro o de partícula.
- Resistencia mecánica, térmica y microbiana.

- Bajo impacto ambiental y bajo coste.

Los soportes empleados para inmovilización de biomoléculas se pueden clasificar en función de la naturaleza del material, distinguiendo 3 grandes categorías (materiales inorgánicos, polímeros naturales y polímeros sintéticos), o en función de sus propiedades físicas, incluyendo forma, tamaño y estructura interna (grado de porosidad, tamaño y distribución de los poros).

3.1. Clasificación de los soportes en función de su naturaleza

La naturaleza de los soportes utilizados para la inmovilización de biomoléculas puede influir tanto en la capacidad de inmovilización como en la disposición espacial de la biomolécula unida y en la retención de su actividad biológica. Es por ello que mediante la adecuada selección de la naturaleza del soporte empleado en la fabricación de un biosensor se puede lograr mantener e incluso mejorar la actividad biológica de la biomolécula inmovilizada, así como conseguir una elevada capacidad de unión. En la Tabla 3 se muestra una clasificación en función de la naturaleza de los materiales más ampliamente utilizados como soportes para la inmovilización de biomoléculas, y algunos ejemplos de aplicaciones de los mismos en el diseño de biosensores.

Tabla 3. Materiales empleados en la inmovilización de biomoléculas.

Naturaleza del soporte			Aplicaciones
Inorgánico	Minerales naturales	Corindón (Al_2O_3), baddeleyita (ZrO_2), rutilo (TiO_2), casiterita (SnO_2), zeolitas, etc.	114-116
	Materiales procesados	Vidrios, óxidos metálicos con tamaño de poro controlado, metales con elementos dopantes, materiales derivados del carbono, etc.	117-121
Orgánico	Polímeros naturales	Polisacáridos: celulosa, almidón, dextrano, quitosano, alginato, agarosa, carragenanos Proteínas: colágeno, queratina, fibroína	122-130
	Polímeros sintéticos	Poliestireno, poliacrilamida, poliamidas, derivados del metacrilato (HEMA, PMMA, GMA, BMA), derivados del alcohol de polivinilo, poliuretano, polianilina, polipirrol, poliacetileno, etc.	131-138

3.1.1. Materiales inorgánicos

En general, los materiales inorgánicos están disponibles en una amplia variedad de formas con porosidades muy variables, que abarcan desde zeolitas y carbones con porosidades nanométricas, hasta materiales cerámicos con tamaños de poros micrométricos, y con un gran rango de áreas superficiales, desde los 40 m^2/g hasta más de 3500 m^2/g [139]. Además, la superficie de estos materiales puede ser sometida a distintos procesos químicos para obtener la funcionalización adecuada (por ejemplo, mediante la introducción de grupos amino, ácido carboxílico o tiol) que favorezca el rendimiento de la inmovilización de biomoléculas[61]. Al mismo tiempo, varios de estos métodos de activación de la superficie permiten también minimizar algunos de los inconvenientes observados durante la inmovilización, como pueden ser la pérdida de actividad biológica o la modificación de la conformación espacial de la biomolécula al ser inmovilizada.

Por otra parte, la mayoría de estos materiales se caracterizan por poseer una elevada resistencia mecánica, térmica y microbiana, ya que, debido a su naturaleza inorgánica, no constituyen medios adecuados para el desarrollo de bacterias y hongos.

Dentro de esta categoría de materiales se pueden encontrar óxidos metálicos como por ejemplo, alúmina (Al_2O_3), zirconia (ZrO_2) y los dióxidos de titanio y estaño, materiales basados en sílice como zeolitas, silicatos mesoporosos y vidrios no porosos o de tamaño de poro controlado, y materiales derivados del carbono, como carbón activado y carbón vegetal[61, 98].

Gracias a la amplia variedad de áreas superficiales y porosidades, así como a la capacidad para funcionalizar sus superficies con diversos grupos reactivos, los materiales inorgánicos han sido utilizados en numerosas aplicaciones como biosensores para multitud de analitos[115, 117, 118]. Así, por ejemplo, se han desarrollado sendos biosensores para la determinación de glucosa y acetilcolina mediante la inmovilización de glucosa oxidasa y acetilcolinesterasa, respectivamente, en zeolitas nanoporosas[116]. Por otra parte, también se han diseñado biosensores basados en superficies carbonadas para la detección de pesticidas organofosforados[119], neurotransmisores[120], peróxido de hidrógeno[114, 121], etc.

3.1.2. Polímeros naturales

Los polímeros naturales han sido los materiales más ampliamente utilizados para llevar a cabo la inmovilización de biomoléculas debido principalmente a su elevada disponibilidad y a su

escasa toxicidad[140]. Entre ellos destacan fundamentalmente polisacáridos como la celulosa, el almidón, el dextrano, el quitosano, el alginato, la agarosa y los carragenanos[140-142] (Figura 6). Los cuales han sido empleados en numerosas aplicaciones incluyendo la fabricación de biosensores para la detección de parámetros clínicos[122-126]. En general, gracias a su estructura formada por azúcares con grupos hidroxilo disponibles, es posible realizar la inmovilización de biomoléculas mediante la formación de enlaces covalentes con algunos de sus grupos funcionales disponibles.

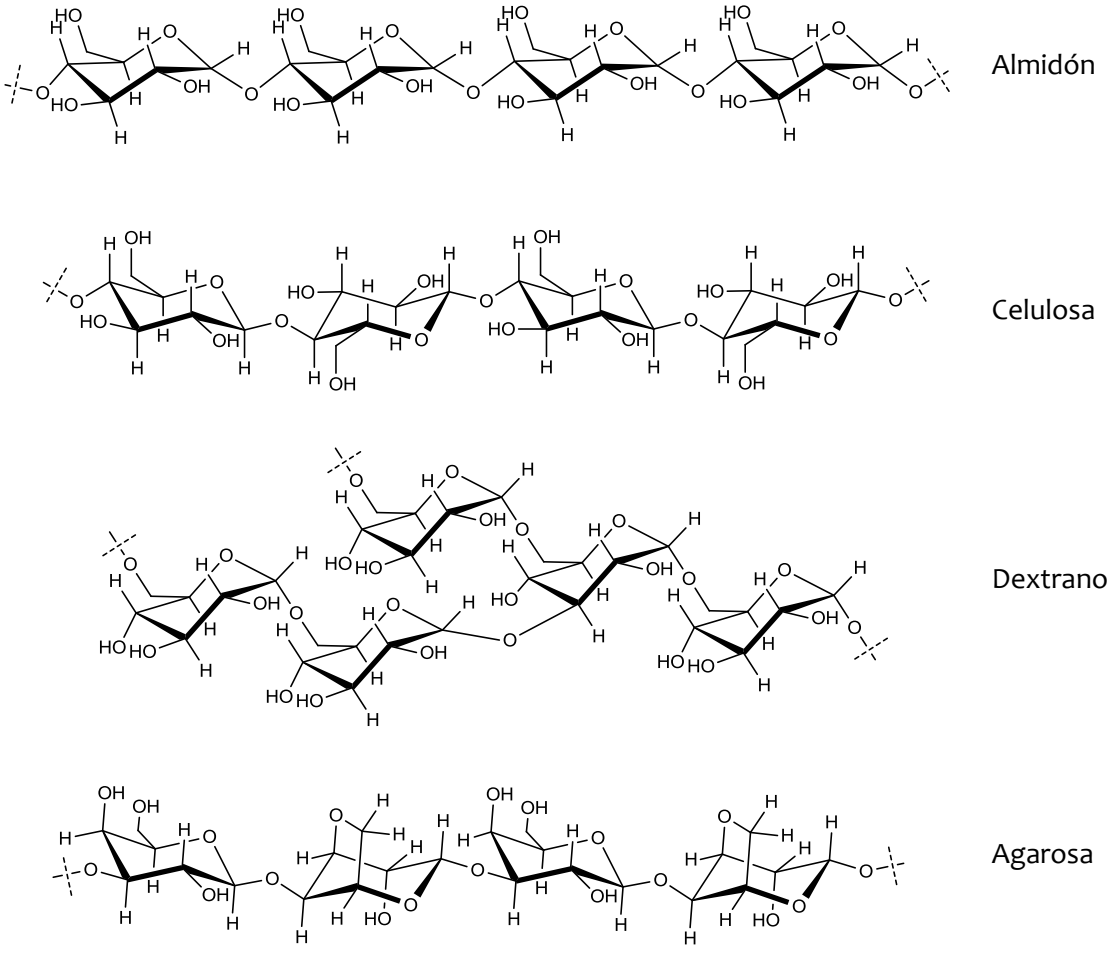

Figura 6. Estructuras de algunos de los polisacáridos más ampliamente utilizados para la inmovilización de biomoléculas.

De entre todos los polisacáridos, el almidón y la celulosa son los más económicos y con una química y una estructura más conocidas, razones por las que tradicionalmente han sido los más usados para todo tipo de aplicaciones[143, 144]. Sin embargo, poseen una inadecuada estructura porosa, con cadenas muy compactas que dificultan el paso de los reactivos, requiriendo en muchos casos tratamientos drásticos para obtener derivados con espacios más accesibles. Además, debido a su naturaleza orgánica, tienen muy pobre resistencia microbiana, siendo muy

susceptibles de sufrir daños en su estructura y propiedades, y una baja resistencia mecánica. Debido a estos inconvenientes, la celulosa y el almidón son cada vez menos utilizados para llevar a cabo la inmovilización de biomoléculas.

Otros de los polisacáridos más utilizados son el dextrano y sus derivados entrecruzados gracias a que no presentan algunos de los inconvenientes de la celulosa y el almidón[140, 143]. Así por ejemplo, ciertos derivados del dextrano son mucho más resistentes al deterioro microbiano y poseen mayores áreas superficiales y poros de mayor tamaño. No obstante, su resistencia mecánica sigue siendo baja y al tratarse de derivados obtenidos artificialmente su coste es mayor.

Por su parte, las excelentes propiedades de la agarosa la han convertido en una alternativa interesante para realizar la inmovilización de biomoléculas[143]. La estructura de la agarosa es bastante estable a diferentes pHs, temperaturas y en presencia de varios disolventes y agentes reductores. Además presenta una elevada resistencia bacteriana, comparable a la de algunos polímeros sintéticos, y está disponible con una amplia variedad de tamaños de poros. Otra de las propiedades de la agarosa que la hacen interesante para la inmovilización de biomoléculas es su capacidad para formar geles estables, los cuales han sido muy utilizados para realizar inmovilizaciones por atrapamiento[145-147].

Por otro lado, otro tipo de polímeros naturales empleados en inmovilización de biomoléculas son las proteínas fibrosas como el colágeno, la queratina y la fibroína[130, 140, 148] (Figura 7). Estos materiales se caracterizan por sus fantásticas propiedades mecánicas (elasticidad y resistencia mecánica), una elevada área superficial, elevada estabilidad térmica, biocompatibilidad y baja toxicidad. Además, son muy poco solubles en agua como consecuencia de la presencia de residuos de aminoácidos hidrofóbicos en su esqueleto. Aunque su uso en el desarrollo de biosensores está mucho menos extendido que el de los polisacáridos mencionados anteriormente, es posible encontrar ciertas aplicaciones con enzimas inmovilizadas mediante atrapamiento o a través de enlaces covalentes[127-130].

Actualmente y con el fin de mejorar las propiedades y características de los polímeros naturales, estos han sido sometidos tanto a procedimientos de transformación física mediante tratamientos con rayos gamma o radiación ultravioleta, como a procesos de alteración química de sus cadenas laterales. De esta forma, se han obtenido polímeros naturales modificados tales como amino-celulosa[149], TiO_2-celulosa[150], Fe_3O_4-quitosano[151] y Au-colágeno[152], entre muchos otros.

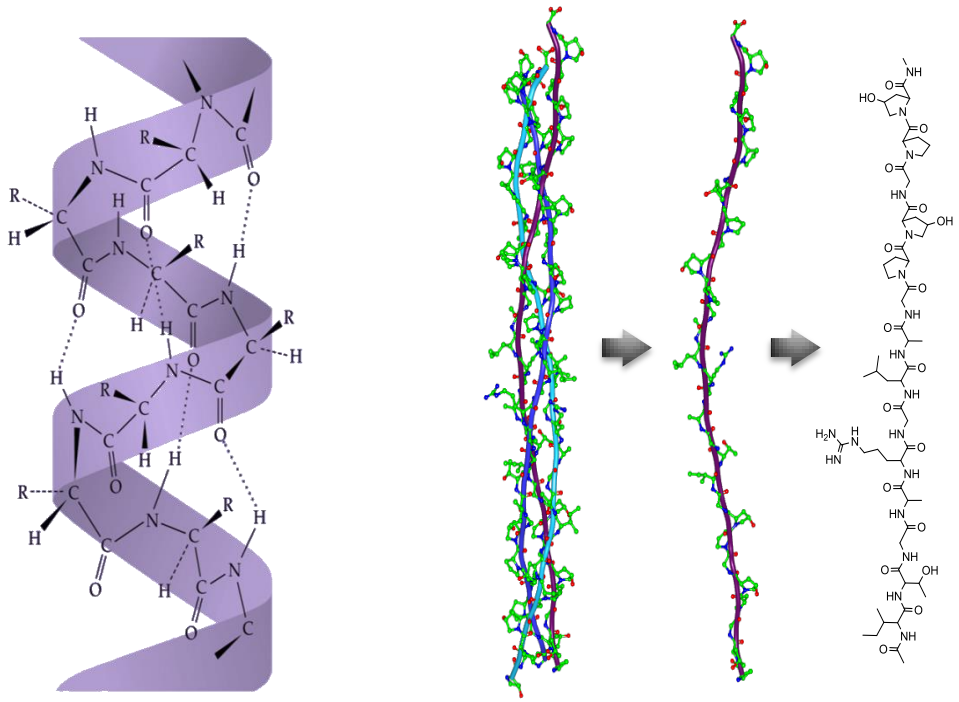

Figura 7. Estructuras de algunas proteínas fibrosas empleadas en la inmovilización de biomoléculas.

3.1.3. Polímeros sintéticos

Este tipo de materiales han sido diseñados en su mayoría para mejorar ciertas características que no se alcanzan con los polímeros naturales, como por ejemplo, activación de su superficie para favorecer determinados tipos de interacciones, ya sea covalente, iónica o por afinidad, aumento de la porosidad y del área superficial para incrementar la capacidad de carga, y mejora de la estabilidad y resistencia química, mecánica y térmica, entre otras muchas propiedades.

Ejemplos de materiales pertenecientes a esta categoría son el poliestireno, la poliacrilamida, las poliamidas como el nylon, los derivados del ácido metacrílico y del alcohol de polivinilo, el poliuretano, la polianilina, etc., además de una amplia variedad de copolímeros formados por combinación de varios de ellos en proporciones variables[35, 85, 153, 154].

De entre todos ellos destacan los polímeros basados en metacrilato con multitud de aplicaciones en biomedicina y biotecnología[133-135]. Estos materiales presentan una estructura tridimensional formada por cadenas lineales poliméricas interconectadas a través de agentes de entrecruzamiento, y generalmente se fabrican combinando dos monómeros diferentes derivados del metacrilato, de forma que se obtienen copolímeros con propiedades variables en función de la naturaleza y concentración de los monómeros, de las condiciones y el grado de polimerización, y

de la reactividad de los grupos funcionales implicados en la polimerización[155]. Los monómeros del metacrilato más comúnmente utilizados son el 2-hidroxietil metacrilato (HEMA), el poli(metil metacrilato) (PMMA), el glicidil metacrilato (GMA) y el butil metacrilato (BMA) (Figura 8). Estos presentan diferentes reactividades y diversos grados de hidrofilicidad, siendo el HEMA el más empleado para la inmovilización de biomoléculas debido a su elevado carácter hidrofílico, proporcionado por la presencia de los grupos hidroxietilo, y a su alta biocompatibilidad.

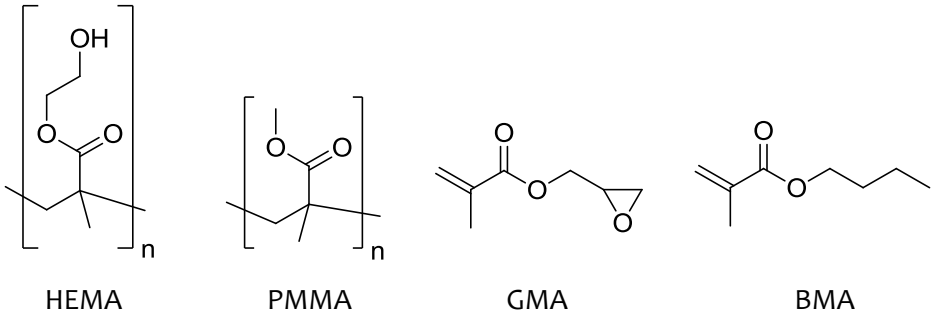

Figura 8. Estructuras de algunos monómeros del metacrilato.

Adicionalmente, dentro de los polímeros sintéticos se encuentran también los denominados polímeros conductores, los cuales incluyen compuestos como la polianilina (PANI), el polipirrol (PPY), el politiofeno (PTH), el poliacetileno (PA), el poli(*p*-fenileno) (PPP), el poli(*p*-fenilenvinileno) (PPV), el poli(*p*-fenilenetileno) (PPE) y el polifluoreno (PF) (Figura 9). La capacidad de estos polímeros para conducir la corriente se debe a la presencia de dobles enlaces conjugados o alternos en sus estructuras, los cuales permiten la deslocalización y movilidad de los electrones a lo largo de toda la cadena de polímero[156, 157]. Esta capacidad conductora se ve incrementada con el dopaje o la adición de otras sustancias.

Los polímeros conductores se han utilizado como soportes conductores para la inmovilización de biomoléculas a través de dos procedimientos principalmente: por un lado, mediante adsorción o unión covalente de la biomolécula al polímero después de su polimerización; y por otro lado, llevando a cabo el proceso de electro-polimerización del polímero en presencia de las biomoléculas a inmovilizar, de manera que a medida que se va formando el polímero, las biomoléculas van quedando retenidas en su matriz polimérica[136]. Este procedimiento sólo es posible realizarlo con polímeros conductores que puedan polimerizar en condiciones suaves de reacción y en medio acuoso para evitar la desnaturalización de las biomoléculas. Este es el caso de los polipirroles, las polianilinas, y algunos politiofenos dopados con grupos funcionales polares.

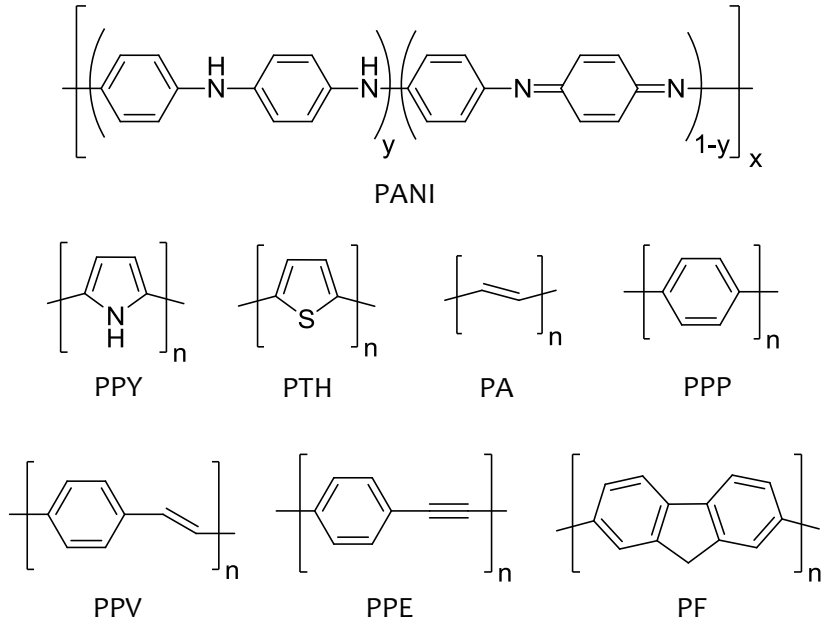

Figura 9. Estructuras de los polímeros conductores más comunes.

Debido a las propiedades conductoras de estos polímeros, son capaces de actuar como mediadores en las transferencias de electrones de las reacciones redox o de las reacciones biológicas en las que participan las biomoléculas inmovilizadas. Muchos de ellos poseen también buena resistencia térmica, biocompatibilidad, estabilidad en el tiempo y se pueden obtener en forma de láminas con diferentes espesores y grados de polimerización, pudiendo controlar fácilmente sus dimensiones.

Por otra parte, la posibilidad de combinar estos polímeros con otros componentes tales como, nanopartículas metálicas, bimetálicas o de óxidos metálicos, materiales derivados del carbono como el grafeno o los nanotubos de carbono, calcogenuros, etc., permite mejorar las características de estos polímeros y, en ocasiones, obtener materiales con nuevas propiedades térmicas, eléctricas, ópticas o magnéticas. Es por ello que las aplicaciones de los polímeros conductores en el campo de los biosensores son muy abundantes y variadas[136-138, 156, 157].

3.1.4. Materiales híbridos y de última generación

En la actualidad además de estas 3 categorías, se han desarrollado nuevos soportes híbridos como los denominados *metal-organic frameworks* (MOFs), formados por la unión de cationes metálicos y ligandos orgánicos multidentados, otros materiales conocidos como *polímeros inteligentes*, tales como la poli(*N*-isopropilacrilamida) (PNIPAM) y sus copolímeros con derivados de acrilamida, que son capaces de responder a estímulos externos, modificando su

conformación en respuesta a cambios en la temperatura, el pH o la fuerza iónica del medio que los rodea, e incluso polímeros con capacidad para reconocer específicamente determinadas moléculas diana como son los denominados *polímeros de impronta molecular* (MIPs).

a) Metal-organic frameworks

Los MOFs son materiales cristalinos altamente porosos, cuya estructura tridimensional y propiedades dependen de las características geométricas de los cationes y de los ligandos orgánicos que los componen[158-161]. Las distintas combinaciones posibles en las que se pueden coordinar dichos componentes originan multitud de estructuras con diferentes cavidades y tamaños de poro, lo que hace posible seleccionar y diseñar la morfología de estos materiales más adecuada para cada aplicación.

Entre los cationes metálicos más empleados se encuentran los metales de transición, los metales alcalinos y los actínidos, los cuales pueden presentar diferentes geometrías en función de su número de coordinación[160, 162]. Dichas geometrías abarcan desde las más sencillas como la lineal o la de forma de T o Y, hasta disposiciones espaciales más complejas como la bipirámide trigonal o la pentagonal, entre otras muchas (Figura 10). Por otra parte, los ligandos orgánicos más utilizados suelen ser aminas, fosfatos, nitratos, sulfonatos y carboxilatos[161].

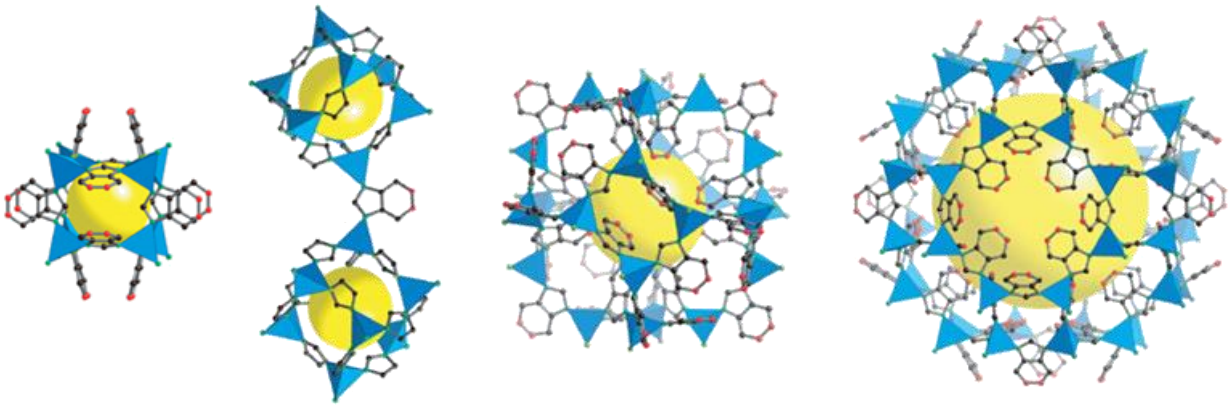

Figura 10. Estructuras de algunos metal-organic frameworks.

Estos materiales presentan además, una elevada área superficial (en algunos casos alcanzan los 6000 m^2/g), lo que les confiere una gran capacidad de carga, una alta estabilidad térmica y mecánica, diferentes funcionalidades superficiales, y en ocasiones exhiben cambios detectables en sus propiedades ópticas o magnéticas como consecuencia de la inclusión de moléculas en sus cavidades[162, 163].

Algunos ejemplos de MOFs utilizados para el desarrollo de biosensores están constituidos por zinc[164], aluminio[165, 166] o hierro[167, 168] como cationes metálicos, mientras que las metodologías de inmovilización de biomoléculas en los MOFs abarcan desde la adsorción y la encapsulación, hasta la unión covalente[163, 169].

b) Polímeros inteligentes

La inmovilización covalente de biomoléculas en los denominados polímeros inteligentes constituye otra de las aproximaciones más novedosas en el diseño de biosensores. Entre dichos polímeros el más representativo y utilizado es el PNIPAM, altamente sensible a cambios en la temperatura y biocompatible[170-173]. El PNIPAM se caracteriza por tener una transición crítica a bajas temperaturas (LCST), alrededor de los 32 ºC, por lo que, por debajo de esta temperatura el polímero se encuentra disuelto en agua, pero a temperaturas superiores se vuelve insoluble expulsando las moléculas de agua del interior de su estructura polimérica[173, 174]. En la Figura 11 se muestra una representación esquemática del cambio estructural que ocurre cuando se alcanza la temperatura de transición.

Este tipo de transiciones LCST se deben al cambio en el balance entre los distintos tipos de interacciones que se dan en el seno de estos polímeros, fundamentalmente interacciones hidrofóbicas y enlaces de hidrógeno[174, 175]. En muchos casos, además, existe la posibilidad de modificar la temperatura de transición y seleccionar una temperatura determinada, e incluso en ocasiones es posible producir polímeros con varias temperaturas de transición, mediante la variación de la composición y la densidad de entrecruzamiento de los polímeros.

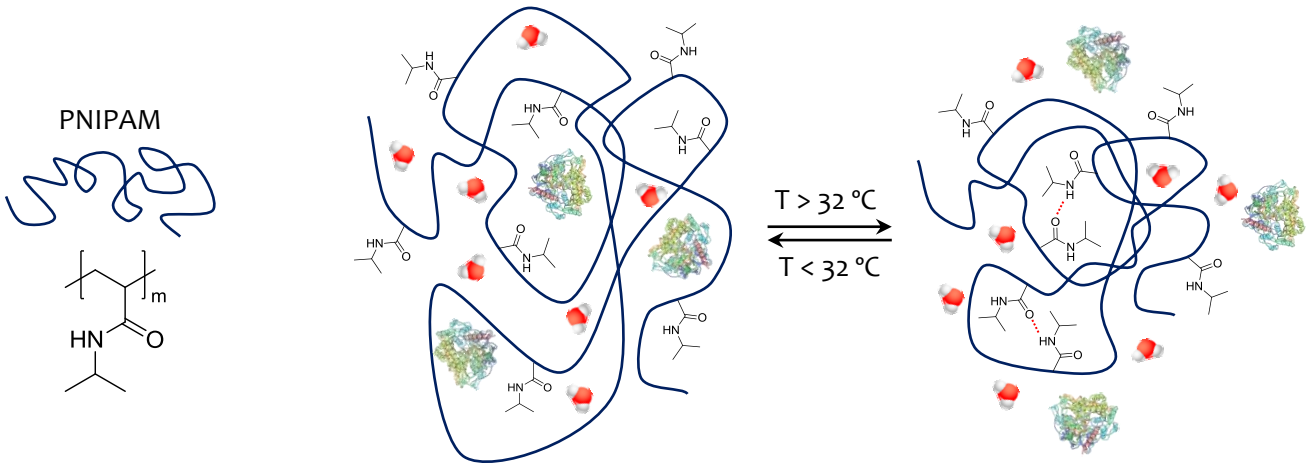

Figura 11. Representación esquemática del cambio estructural sufrido por el PNIPAM cuando se alcanza la temperatura de transición crítica.

Con la inmovilización en estos polímeros inteligentes se puede conseguir la regulación de la actividad de una biomolécula mediante el control de la temperatura, de forma que a temperaturas por debajo de la temperatura de transición, el polímero se encuentra disuelto permitiendo la libre circulación de sustratos y productos que podrán entrar en contacto con la biomolécula. Sin embargo, a temperaturas cercanas a la de transición, el polímero se contrae, disminuyendo el tamaño de los poros y limitando el paso de las moléculas de mayor tamaño. Finalmente, si se sobrepasa la temperatura de transición, el polímero colapsa produciendo la liberación de la biomolécula inmovilizada y, en algunos casos, su precipitación con la consecuente paralización de la reacción biológica. Este procedimiento tiene la ventaja además de que en muchos casos las biomoléculas precipitadas pueden ser recuperadas y reutilizadas[176, 177].

Así, por ejemplo, se han utilizado PNIPAM y copolímeros del mismo con derivados de acrilamida para la fabricación de biosensores capaces de determinar peróxido de hidrógeno[178, 179], hormonas[180] y ADN[181].

c) Polímeros de impronta molecular

Los MIPs se caracterizan por poseer cavidades con formas, tamaños y distribuciones espaciales determinados que pueden actuar como sitios de reconocimiento específico de las moléculas de interés[182-185]. La especificidad de este reconocimiento molecular es posible gracias a la complementariedad existente entre las cavidades de los MIPs y las estructuras tridimensionales de las moléculas, lo que a su vez permite poder llevar a cabo la determinación de dichas moléculas en muestras complejas. Así, este tipo de polímeros han sido empleados para el reconocimiento de una amplia variedad de moléculas de diferentes tamaños, desde moléculas pequeñas como azúcares o aminoácidos hasta moléculas más complejas como péptidos y proteínas[184, 186].

Este tipo de materiales se sintetizan mediante un proceso de polimerización en el que la propia molécula de interés o una molécula estructuralmente análoga, se utilizan como plantilla para crear las cavidades que posteriormente servirán como sitios de reconocimiento. Dicho procedimiento de polimerización tiene lugar básicamente a partir de una mezcla de monómero, agente entrecruzante, iniciador y molécula plantilla en un determinado disolvente[182, 185, 187]. En la Tabla 4 se muestran algunos de los compuestos más usualmente utilizados en este proceso de polimerización.

Una vez que la polimerización comienza, las moléculas de monómero se van situando y entrecruzando alrededor de las moléculas plantilla originando una estructura tridimensional porosa con las moléculas plantilla alojadas en su interior. Cuando la polimerización termina, las moléculas plantilla son retiradas lavando con un disolvente (por lo general metanol o acetona acidificados) dejando así cavidades disponibles y complementarias, tanto en forma y tamaño como en posicionamiento de los grupos químicos, a dichas moléculas plantilla. Estas cavidades poseerán diferentes disposiciones espaciales y distintas características en función de las interacciones establecidas entre monómero y plantilla durante el proceso de polimerización. Dichas interacciones suelen ser de tipo iónico, dipolo-dipolo o por enlaces de hidrógeno, y constituyen las principales impulsoras del fenómeno de reconocimiento molecular[188]. En la Figura 12 se muestra una representación esquemática del procedimiento de fabricación y funcionamiento de un MIP.

Tabla 4. Compuestos y disolventes más comúnmente empleados en la fabricación de MIPs.

Monómero	**Agente entrecruzante**	**Iniciador**	**Disolvente**
Ácido metacrílico (MAA)	Divinilbenceno (DVB)	Azobisisobutironitrilo (AIBN)	Acetonitrilo
4-vinilpiridina (4-VPY)	Dimetilacrilato de etilenglicol (EGDMA)	Persulfato amónico (APS)	Tolueno
Acrilamida (AAm)	Pentaeritritol triacrilato (PETRA)	Persulfato potásico (KPS)	DMF
Ácido acrílico (AAc)	Trimetilpropano trimetacrilato (TRIM)		DMSO
Ácido 2-(trifluorometil)acrílico (TFMAA)			
2-hidroxietil metacrilato (HEMA)			

Dos propiedades importantes que debe cumplir el MIP obtenido son que debe ser lo suficientemente rígido como para retener permanentemente la forma, el tamaño y la distribución espacial de las cavidades originadas en su interior, y, a la vez, debe ser lo bastante poroso como para permitir la circulación de las moléculas de interés tanto hacia el interior de las cavidades como hacia el exterior de las mismas, posibilitando así el reconocimiento molecular y la posterior reutilización.

Entre las ventajas de estos polímeros destacan su elevada afinidad y selectividad por la molécula diana previamente utilizada como plantilla, y su alta estabilidad térmica, química y mecánica, que variará en función del monómero seleccionado y que les confiere resistencia a elevadas temperaturas y presiones, y a la presencia de ácidos, bases y disolventes orgánicos.

Gracias a estas ventajas de selectividad y estabilidad, los MIPs están siendo cada vez más empleados para la determinación de variedad de analitos en muestras reales, incluyendo fluidos biológicos[189-193] y muestras alimentarias[194-197].

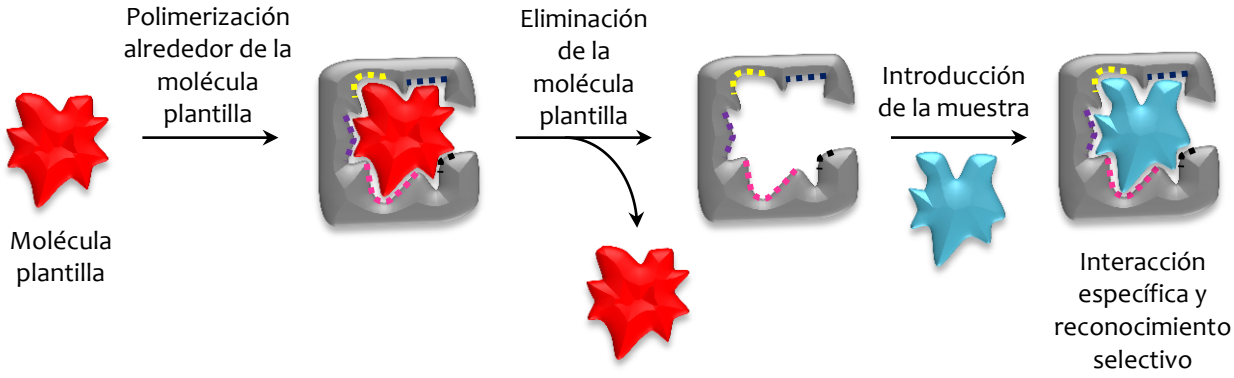

Figura 12. Representación esquemática de las diferentes etapas implicadas en la fabricación y funcionamiento de un MIP.

3.2. Clasificación de los soportes en función de sus propiedades físicas

Las propiedades físicas de los soportes empleados en la inmovilización de biomoléculas ejercen una gran influencia sobre las características finales del biosensor, tanto en lo que respecta a su aplicabilidad y estabilidad, como a sus propiedades analíticas de selectividad y sensibilidad. Es por ello que la selección del diseño más adecuado para cada biosensor en relación a forma, tamaño, porosidad del material y distribución de los poros, constituye una etapa crucial previa a la realización de la inmovilización.

De esta forma, la correcta selección de las propiedades físicas de un soporte puede y debe satisfacer las necesidades geométricas de la aplicación final, así como mantener un nivel adecuado de estabilidad, actividad y selectividad de las biomoléculas inmovilizadas, las cuales se ven altamente influenciadas por el tamaño y la distribución de los poros, la densidad de unión, la superficie disponible para la inmovilización y las limitaciones en la difusión a través del material.

Siendo necesario, por tanto, seleccionar el soporte con las propiedades físicas más adecuadas para cada tipo de aplicación concreta y para cada biomolécula, considerando además, sustratos, productos y naturaleza de la reacción biológica.

3.2.1. Forma de los soportes

La forma de los materiales utilizados para la inmovilización puede abarcar desde partículas compactas o huecas, hasta membranas, cápsulas o fibras[198]. En la Figura 13 se muestra una representación de las formas más comunes. Cada una de estas geometrías se obtiene a través del empleo de diferentes materiales, técnicas y condiciones de preparación, y afectan en mayor o menor medida al proceso de inmovilización. Es por ello que la selección de la configuración geométrica del material se realiza en función de la aplicación deseada siguiendo una serie de criterios:

- Carga de biomolécula deseada.
- Limitaciones en la difusión a través del material.
- Condiciones de temperatura y presión en las que va a ser utilizado el soporte.
- Método de inmovilización empleado.
- Facilidad de preparación del material.

Figura 13. Formas más comunes de los materiales empleados para inmovilización de biomoléculas.

3.2.2. Tamaño de los soportes

El tamaño de los soportes determina el área superficial en la que puede tener lugar la inmovilización de las biomoléculas, por lo que influye de manera crítica sobre la capacidad de unión que presenta cada material. Los soportes empleados para inmovilización de biomoléculas abarcan desde materiales voluminosos hasta otros micro y nanométricos, siendo las propiedades

físicas y químicas de los materiales de escala nanométrica significativamente diferentes de aquellas de los materiales voluminosos.

En la actualidad, gracias al avance en la nanotecnología se han desarrollado una enorme variedad de materiales nanodimensionales, tales como nanopartículas, nanofibras o nanotubos (Figura 14), entre otros[199], los cuales han pasado a ser los materiales más ampliamente utilizados en el desarrollo de biosensores, siendo incorporados en multitud de biosensores enzimáticos, inmunosensores y genosensores[200-207].

Estos nanomateriales se caracterizan por su elevada área superficial y sus reducidas limitaciones difusionales, lo que permite incrementar la eficiencia y la capacidad de inmovilización de biomoléculas. Además, poseen una gran versatilidad tanto para ser funcionalizados con una gran variedad de grupos reactivos como para ser obtenidos con diferentes tamaños de poro en función de las necesidades de cada aplicación.

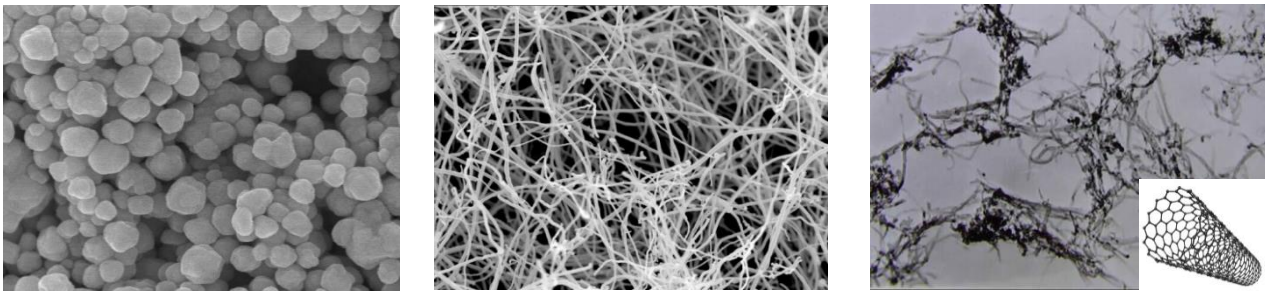

Figura 14. Imágenes de microscopía de nanopartículas, nanofibras poliméricas y nanotubos de carbono.

a) Nanopartículas

Las nanopartículas, generalmente obtenidas con tamaños comprendidos entre los 10 y los 1000 nm, constituyen uno de los nanomateriales más extensamente utilizados y con mayor número de aplicaciones, las cuales se han visto enormemente incrementadas gracias a la incorporación de propiedades ópticas, eléctricas o magnéticas, mediante tratamientos pre- o post-procesado[199, 208-210].

Los tipos nanopartículas con aplicaciones en el campo de los biosensores han sido tradicionalmente no porosos y con formas esféricas. Sin embargo, en la actualidad, se han diseñado nanopartículas con multitud de formas y tamaños, incluyendo geometrías elaboradas como cubos, triángulos y conos, y otras estructuras amorfas o formadas por agregación de partículas.

La naturaleza de las nanopartículas empleadas en la fabricación de biosensores abarca desde metales (Au, Ag) y óxidos metálicos (Fe_3O_4, Fe_2O_3, ZnO) hasta polímeros sintéticos como poliésteres, poliacrilamidas, poliacrilatos, poliestireno y copolímeros de todos ellos, entre otros muchos[115, 209, 211, 212].

Las nanopartículas de metales nobles, obtenidas normalmente con tamaños entre 5 y 100 nm, poseen unas excelentes propiedades físicas, químicas, ópticas y electrónicas, caracterizándose por su capacidad para responder óptica o electroquímicamente a estímulos externos o cambios en las condiciones del medio que las rodea. Además, presentan una baja toxicidad y pueden ser fácilmente funcionalizadas con diferentes grupos reactivos, incrementando así su habilidad para la bioconjugación.

De entre todas las nanopartículas metálicas, destaca el uso más generalizado de las nanopartículas de oro gracias a su extraordinaria biocompatibilidad y a la facilidad con la que pueden producir la inmovilización de biomoléculas mediante la interacción de los grupos amino y tiol de las proteínas con el oro[213, 214]. De esta manera, es posible inmovilizar directamente proteínas y aminoácidos en las nanopartículas de oro sin necesidad de ningún tratamiento de funcionalización con otros grupos químicos.

Por otro lado, la utilización de nanopartículas poliméricas ha sufrido una gran expansión en las últimas dos décadas debido a la posibilidad de optimizar sus propiedades y adaptarlas a cada aplicación particular, lo que les ha otorgado una enorme versatilidad, pudiendo ser utilizadas en áreas que abarcan desde la biomedicina, la biotecnología o el diseño de biosensores, hasta el control de la polución y la monitorización clínica y medioambiental[215-220].

La técnica de fabricación empleada en la obtención de las nanopartículas poliméricas juega un papel fundamental en las propiedades, características y geometrías finales que poseerán las partículas. Es por ello que se han ideado multitud de técnicas de producción con el fin de adaptar dichas propiedades a las aplicaciones deseadas. Dichas técnicas se pueden dividir en dos grandes subgrupos en función de si se parte de una dispersión de los polímeros preformados o de si la polimerización tiene lugar directamente a partir de los monómeros. Dentro del primer subgrupo se encuentran metodologías como la emulsificación-evaporación, la nano-precipitación o el *salting out*; mientras que el segundo subgrupo abarca técnicas como la microemulsión y la miniemulsión, la emulsión sin surfactantes y la polimerización interfacial[212, 218, 221, 222].

Durante el proceso de síntesis de las nanopartículas poliméricas es posible incorporar a la mezcla de reacción otros componentes tales como colorantes, indicadores luminiscentes o incluso partículas magnéticas (como por ejemplo, magnetita, Fe_3O_4), consiguiendo en muchos casos que dichos componentes queden retenidos en el interior de las nanopartículas. De esta forma es posible obtener nanopartículas con propiedades ópticas y/o magnéticas, mejorando así su utilidad y ampliando su aplicabilidad, especialmente en el diseño de biosensores con transducción óptica[223, 224].

Además de la técnica empleada para la fabricación de las nanopartículas, el tipo y la naturaleza del polímero utilizado también afectan de manera importante a las propiedades y a la estructura de las partículas obtenidas. Asimismo, la concentración y el peso molecular del polímero influyen directamente sobre el tamaño de las nanopartículas obtenidas.

Es por todo ello que, tanto la técnica de fabricación como el tipo de polímero o mezcla de polímeros empleados, deben ser seleccionados considerando detenidamente las características necesarias para cada aplicación en concreto.

b) Tejidos de nanofibras

Este tipo de materiales están constituidos por nanoestructuras fibrosas y no presentan ciertos inconvenientes que sí sufren algunas nanopartículas, como son las dificultades a la hora de obtener dispersiones homogéneas de las partículas en el medio de reacción más adecuado para realizar la inmovilización de las biomoléculas, de manera que el medio afecte en la menor medida posible a la actividad biológica. Normalmente, las reacciones de inmovilización se realizan en medio acuoso que es donde las biomoléculas de naturaleza hidrofílica mantienen una más alta actividad, sin embargo, muchos tipos de nanopartículas son difícilmente dispersables en estos medios acuosos[208]. Otro de los inconvenientes que presentan las nanopartículas es la necesidad de incluir etapas de centrifugación para la purificación y recuperación de las mismas, que no son requeridas en el caso de los tejidos de nanofibras.

Las nanofibras presentan además las ventajas de poder ser obtenidas con multitud de dimensiones y diámetros (que pueden abarcar desde 1 nm hasta los 1000 nm) formando membranas altamente porosas y flexibles con diferentes espesores, de poseer una elevada área superficial que les confiere una gran capacidad para la inmovilización, y de presentar unas excelentes propiedades mecánicas que facilitan su manipulación[217, 225, 226]. Estos materiales también pueden ser funcionalizados con diferentes grupos reactivos o dopados con partículas de

diversa naturaleza, lo que les permite tanto mejorar su reactividad como modificar sus propiedades físico-químicas para adaptarlas a las necesidades de cada aplicación.

Dentro de este tipo de estructuras nanométricas, las de naturaleza polimérica con propiedades de biocompatibilidad y biodegradabilidad han atraído especial atención para el desarrollo de una gran variedad de aplicaciones que incluyen tanto la fabricación de biosensores, como la elaboración de sistemas de liberación controlada de fármacos, entre otras muchas aplicaciones biotecnológicas[200, 227, 228].

Una de las técnicas más empleadas para la obtención de nanofibras poliméricas es el electrospinning o electrohilado[229-231], debido a que permite la rápida preparación de estos materiales con una morfología controlable a partir de una gran variedad de polímeros o mezclas poliméricas, tanto de origen natural como sintético. Entre los polímeros de origen natural más utilizados se encuentran el acetato de celulosa, el quitosano, el colágeno y la fibroína; mientras que como polímeros sintéticos se han empleado poliamidas, poliestireno, poliuretano y polímeros basados en metacrilato como el HEMA y el PMMA[229, 232]. Sin embargo, la combinación de algunos de estos y otros polímeros ha permitido obtener fibras copoliméricas con propiedades mecánicas, estructurales y físicas mejoradas, ofreciendo una mayor versatilidad a la técnica.

La tecnología de electrospinning se basa fundamentalmente en la aplicación de un campo eléctrico con la suficiente intensidad como para superar las fuerzas de tensión superficial de las disoluciones de polímeros, que a su vez también son sometidas a extrusión mecánica. En la Figura 15 se muestra uno de los montajes más comunes para llevar a cabo el procesado de fibras mediante electrospinning.

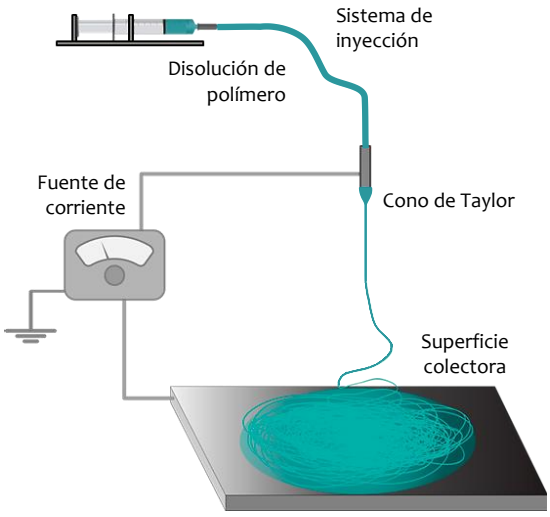

Figura 15. Representación esquemática de un equipo de electrospinning.

El equipo consta de un sistema de inyección con una o varias agujas, a través de las cuales es expulsada la disolución polimérica, una superficie colectora donde se depositan las fibras, y una fuente de corriente con dos electrodos, uno de los cuales se encuentra conectado a la salida del sistema de inyección y el otro a la superficie colectora.

En un principio, las disoluciones de polímeros caen por extrusión mecánica en forma de gotas desde la aguja, conectada al sistema de inyección donde se encuentran almacenadas, hasta la superficie colectora, pero a medida que se va incrementando el voltaje aplicado, dichas gotas comienzan a estirarse en la punta de la aguja, creando una forma cónica conocida como cono de Taylor[233]. De esta manera, cuando se alcanza un voltaje determinado, la intensidad del campo eléctrico supera las fuerzas de cohesión de la disolución polimérica, en su mayoría fuerzas de tensión superficial, y la disolución fluye en forma de finos chorros desde el sistema de inyección donde se encuentra hasta la superficie colectora. Estos chorros fluctúan en la dirección del campo eléctrico, alargándose y estirándose en hilos, al mismo tiempo que se va evaporando el disolvente donde se encontraban los polímeros, hasta originar las membranas de fibras no tejidas sobre la superficie colectora. La disposición de las fibras sobre el colector puede producirse de manera alineada o aleatoria en función de si el colector se encuentra en movimiento rotatorio o en estado estacionario, respectivamente. Por otra parte, los polímeros seleccionados deben ser completamente solubles en los disolventes empleados, los cuales a su vez deben presentar una volatilidad adecuada.

Las condiciones de operación del proceso de electrospinning como son la velocidad de flujo de las disoluciones poliméricas, el voltaje aplicado, la distancia entre el colector y el sistema de inyección, afectan directamente a las propiedades de las fibras obtenidas. Adicionalmente, las propiedades reológicas, como viscosidad, plasticidad y elasticidad, de las disoluciones de los polímeros iniciales también condicionan el proceso de formación de las fibras, mientras que otras características como peso molecular de los polímeros, concentración y conductividad influyen directamente en las peculiaridades de las fibras obtenidas[233-235]. Asimismo, las condiciones ambientales como temperatura y humedad pueden influir igualmente en la morfología final de las fibras.

Es por todo ello que mediante la variación y el control de los parámetros del procedimiento de electrospinning y de las propiedades de los polímeros de partida, se pueden originar fibras con diferentes y establecidas morfologías, orientaciones y características superficiales, con variedad de porosidades y sin defectos estructurales.

Finalmente, las membranas de fibras obtenidas pueden ser sometidas a tratamientos de post-procesado, tanto térmicos como físicos y químicos, con la finalidad de modificar algunas de sus características de hidrofilicidad, permeabilidad, conductividad y reactividad, entre otras.

Una de las innovaciones más recientes de la técnica de electrospinning consiste en la fabricación de fibras coaxiales con estructuras tipo *core-shell* formadas por una fibra interna y otra externa con diferentes propiedades y naturaleza[236-238]. Este tipo de metodología se conoce por el nombre de co-electrospinning y, en este caso, para la obtención de las fibras, el sistema de inyección cuenta con dos agujas, una insertada en el interior de la otra, por las cuales fluyen simultáneamente las diferentes disoluciones de polímeros que originarán la estructura coaxial. Esta aproximación permite obtener en un solo paso nuevas membranas de fibras coaxiales con propiedades difícilmente alcanzables mediante la técnica de electrospinning simple, ya que es posible originar conjuntamente diferentes ambientes muy próximos en una misma fibra, al tiempo que se controla su estructura *core-shell*.

La aplicación de estas fibras coaxiales en el desarrollo de biosensores ópticos supone un novedoso avance, ya que permite obtener materiales multifuncionales con diferentes ambientes químicos, en los que poder llevar a cabo la inmovilización de biomoléculas a la vez que se retienen indicadores ópticos, que por lo general requieren condiciones diferentes para su funcionamiento óptimo[239, 240]. Así, por ejemplo, las fibras coaxiales pueden aportar por un lado un entorno hidrofílico, donde realizar las reacciones de inmovilización de las biomoléculas, por lo general hidrofílicas, manteniendo un elevado grado de retención de su actividad biológica; y por otro lado, aportan un entorno hidrofóbico más apropiado para los colorantes y los indicadores luminiscentes, muchos de los cuales sufren pérdida de su señal óptica en contacto con medios acuosos. De esta manera, tanto el compuesto biológico como el indicador se pueden encontrar retenidos en el entorno más favorable para cada uno de ellos, y al mismo tiempo, situados muy próximos entre sí, permitiendo que los cambios originados por uno sean detectados por el otro.

c) Nanotubos y nanohilos

Los nanotubos de carbono (CNTs) constituyen el ejemplo más representativo de este tipo de nanomateriales. Los CNTs son materiales con estructuras tubulares huecas formadas a partir de láminas de grafeno enrolladas sobre sí mismas, que presentan excelentes propiedades mecánicas y electrónicas y una elevada estabilidad química[207, 241-243]. Sus paredes laterales pueden ser sometidas tanto a procesos de oxidación sin afectar ni destruir su estructura, como a reacciones de

funcionalización covalente con diferentes tipos de partículas o cadenas poliméricas[244]. Además, poseen la capacidad para inmovilizar biomoléculas con un relativamente alto nivel de retención sin formación de enlaces covalentes a lo largo de su estructura en forma de tubo[245].

En función del grado de enrollamiento y del número de láminas de grafeno empleadas, los nanotubos de carbono pueden ser obtenidos con distintos diámetros, longitudes, espesores y geometrías internas, distinguiéndose así dos subgrupos de CNTs: por un lado, los denominados nanotubos de carbono de pared simple (SWCNTs), formados por una única lámina de grafeno que se encuentra enrollada sobre sí misma creando cilindros con diámetros internos de 0.4 o 2 nm; y por otro lado, los nanotubos de carbono de pared múltiple (MWCNTs), en los que se emplean multitud de láminas de grafeno que se disponen concéntricamente creando cilindros con diámetros de entre 2 y 100 nm[241].

Este tipo de materiales han sido utilizados para el desarrollo de biosensores principalmente con transducción electroquímica, ya que poseen unas extraordinarias propiedades eléctricas que pueden ser modificadas mediante tratamientos con ácidos, presentan además la capacidad de mediar en las reacciones de transferencia de electrones con especies electroactivas cuando se utilizan como electrodos, y por último, también se pueden comportar como metales o semiconductores dependiendo del diámetro y la forma helicoidal de su estructura tubular. La combinación de todas estas propiedades hace que sean unos magníficos candidatos para la fabricación de biosensores electroquímicos con aplicaciones en biomedicina y biotecnología[206, 207, 245].

3.2.3. Porosidad y distribución de los poros

Las propiedades de los soportes relacionadas con su porosidad (tamaño y forma de los poros y distribución de los mismos) influyen enormemente en su capacidad de inmovilización.

En general, los materiales no porosos presentan muy escasas o nulas limitaciones en la difusión a través del propio material, pero por el contrario se caracterizan por poseer una capacidad de carga excesivamente baja en comparación con los materiales porosos[36, 246]. Es por ello que el número de aplicaciones en las que se emplean materiales no porosos es muy inferior a la elevada cantidad de aplicaciones llevadas a cabo con materiales porosos. Sin embargo, esto no implica que los materiales porosos no presenten también ciertos inconvenientes, tales como las restricciones difusionales causadas por la lentitud de los procesos de difusión a través de los poros, y las dificultades en muchos casos para controlar el tamaño y la distribución de los poros.

Así, es necesario que los materiales porosos sean obtenidos con una porosidad lo más controlada posible con el fin de optimizar la capacidad de inmovilización, minimizar las limitaciones de difusión y mejorar la retención de la actividad biológica de la biomolécula inmovilizada[36].

Los procesos de inmovilización en los materiales porosos tienen lugar en un primer momento en la superficie más accesible de los mismos, y posteriormente, a medida que se va reduciendo el número de sitios de unión superficiales disponibles empiezan a tener lugar los procesos de difusión hacia el interior de los poros y cavidades del material. No obstante, estos procesos de difusión solamente tienen lugar si el tamaño de los poros es lo suficientemente grande como para albergar a las biomoléculas. Así, por lo general, aquellos soportes que poseen tamaños de poros más grandes presentan una mayor capacidad de inmovilización, con la ventaja además de que disminuyen las limitaciones difusionales de los productos y sustratos, los cuales podrán alcanzar más fácilmente a la biomolécula inmovilizada permitiendo retener su actividad biológica.

Consecuentemente, para llevar a cabo la inmovilización de una biomolécula concreta en un soporte sólido se puede elegir entre una variedad de técnicas (adsorción, afinidad, unión covalente, encapsulación, combinación de varias de ellas, etc.), de soportes (polímeros naturales o sintéticos, orgánicos o inorgánicos, porosos o no porosos, en forma de partículas, láminas, fibras, etc.) y en diferentes condiciones de reacción (temperatura, pH, fuerza iónica, medio acuoso o disolvente orgánico, etc.), que afectarán a cada biomolécula de una manera determinada. Es por ello que la selección de cada uno de estos parámetros se debe hacer considerando detenidamente la biomolécula a inmovilizar y la aplicación específica en la que se empleará, y aunque en un principio esta enorme cantidad de métodos y materiales disponibles para realizar la inmovilización de biomoléculas puede resultar abrumadora, también otorga la posibilidad de lograr una óptima inmovilización seleccionando las condiciones para cada biomolécula en particular.

4. BIOSENSORES ÓPTICOS

Los biosensores con sistemas de transducción ópticos combinan la selectividad de las biomoléculas con el potencial de las técnicas ópticas. Al contrario de lo que ocurre con los sensores electroquímicos, los sensores ópticos pueden ser aplicados a sistemas *in vivo* sin riesgos de producirse descargas eléctricas y no requieren de sistemas de referencia, además, al no depender de electrodos, carecen de los inconvenientes derivados de su utilización, como pueden ser el deterioro de sus superficies, con la consecuente pérdida de sensibilidad, y los problemas asociados a la difusión de los analitos hacia los electrodos.

La superación de estos inconvenientes junto con ventajas como la facilidad de uso, la capacidad para detectar analitos en matrices complejas, en muchos casos con mínimos tratamientos de muestra, la posibilidad de realizar las mediciones en tiempo real y a distancia, la baja relación señal-ruido, la selectividad, la rapidez y el reducido coste, ha favorecido el auge de los sensores y biosensores ópticos.

4.1. Sistemas de transducción ópticos

Los sistemas de transducción ópticos más extendidamente utilizados en el diseño de biosensores se basan en técnicas como la absorción UV-visible, la luminiscencia y la resonancia de plasmón superficial (SPR).

4.1.1. Absorción UV-visible

La absorción UV-visible es una de las técnicas espectroscópicas más sencillas empleadas para la detección de analitos. Este tipo de técnica se utiliza generalmente en análisis colorimétricos, los cuales permiten la determinación tanto cualitativa como cuantitativa de multitud de analitos. En muchos casos, un simple cambio de color es suficiente para realizar la detección de determinados analitos, por lo que la instrumentación para realizar las medidas de absorbancia suele ser mucho más simple que la necesitada para otro tipo de técnicas.

Las técnicas de absorción se basan en hacer incidir un haz de radiación sobre la muestra, de manera que, tras la interacción que tiene lugar entre ambas, parte de esa radiación incidente es absorbida por la muestra haciendo que la intensidad de la radiación transmitida sea diferente[247]. De esta manera, la cantidad de radiación absorbida permite establecer la relación entre la

intensidad de la radiación incidente y la intensidad de la radiación transmitida (Ecuación 1). Además, esta variación en la intensidad de la radiación puede ser detectada y utilizada para determinar cualitativamente y en muchos casos cuantitativamente la concentración de las especies con capacidad para absorber la radiación.

$$A = log\frac{I_0}{I} \qquad \text{Ecuaci n 1}$$

donde A es la cantidad de radiación absorbida o absorbancia, I_0 es la intensidad de la radiación incidente e I es la intensidad de la radiación transmitida.

Por otra parte, dicha absorbancia puede ser relacionada con otra serie de parámetros mediante la que se conoce como ley de Lambert-Beer (Ecuación 2), en la cual está basado el principio de detección de las técnicas de absorción y que puede ser utilizada para determinar la concentración de la especie de interés con capacidad para absorber radiación[247, 248]. Asimismo, debido a que la absorción depende de la longitud de onda, es posible determinar diferentes especies de una misma muestra, siempre y cuando posean espectros de absorción diferentes.

$$A = \varepsilon \cdot l \cdot C \qquad \text{Ecuaci n 2}$$

donde A es absorbancia, ε es el coeficiente de absortividad molar del analito a una determinada longitud de onda, l es el paso de luz a través de la muestra y C es la concentración de analito.

Esta técnica ha sido utilizada tanto para la determinación directa de especies absorbentes como para la determinación indirecta de especies sin capacidad de absorción, pero que pueden ser transformadas en otras sustancias que sí son capaces de absorber la radiación[248]. Así, por ejemplo, se han desarrollo métodos de absorción para la determinación indirecta de sustratos de enzimas oxidasas, como glucosa oxidasa o uricasa. Las reacciones catalíticas de dichas enzimas implican la oxidación del sustrato correspondiente (glucosa y ácido úrico, respectivamente) con la consiguiente formación del producto oxidado y la liberación de H_2O_2, de manera que ninguno de los compuestos implicados en dichas reacciones presenta una absorción de radiación suficiente como para poder llevar a cabo su análisis de manera directa. Es por ello que dichas reacciones catalíticas se acoplan con una segunda reacción, en la que participa una especie que sí es capaz de absorber la radiación, como la quinoneimina. Las reacciones que tienen lugar para la formación de este indicador colorimétrico a partir de ácido úrico y uricasa se indican en la Figura 16 y sus espectros de absorción característicos a distintas concentraciones se muestran en la Figura 17.

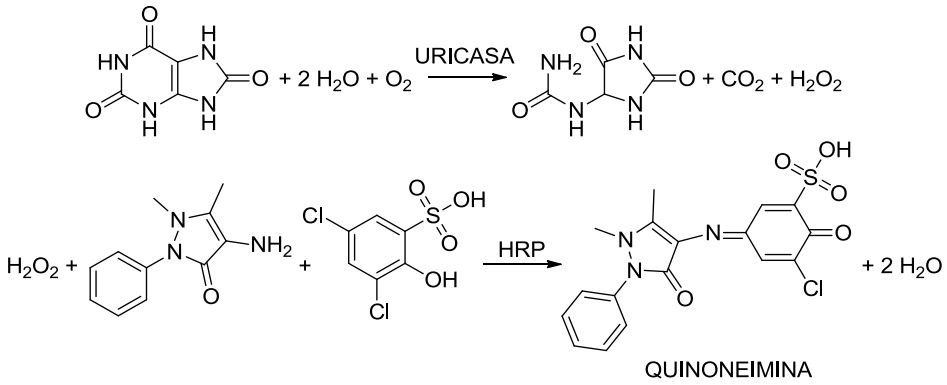

Figura 16. Reacción catalítica de la uricasa y posterior reacción de formación de quinoneimina.

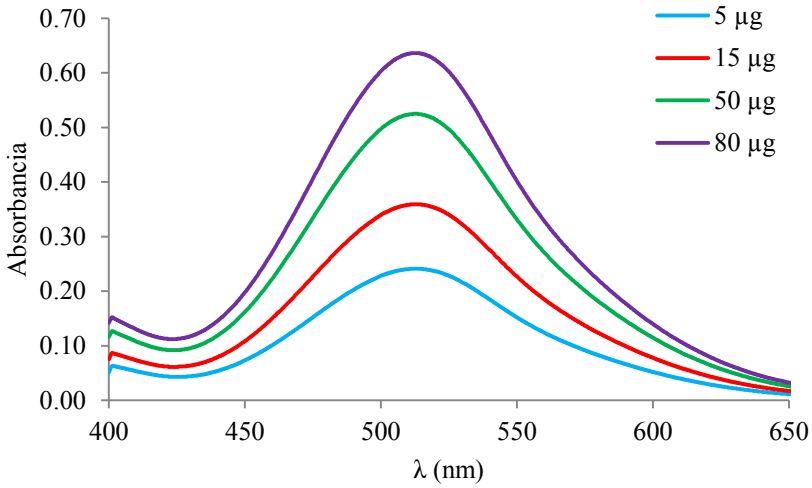

Figura 17. Espectros de absorción de quinoneimina utilizados en la determinación de la actividad de uricasa. La leyenda indica las distintas concentraciones de uricasa a las cuales han sido obtenidos los espectros.

Las principales ventajas de los biosensores basados en medidas de absorción UV-visible son su simplicidad, su fácil utilización y su bajo coste. Sin embargo, presentan baja sensibilidad, selectividad y pueden sufrir interacciones de especies interferentes en muestras complejas. Debido a estos inconvenientes los biosensores de absorción UV-visible están siendo sustituidos por otros como los basados en medidas de luminiscencia[249, 250].

4.1.2. Luminiscencia

Los fenómenos de luminiscencia, tanto de emisión como de atenuación o *quenching*, han sido ampliamente utilizados en la determinación de numerosas sustancias gracias a su elevada selectividad y sensibilidad, con límites de detección del orden de las partes por billón (muy inferiores a los encontrados en la absorción UV-visible), y a su amplio intervalo lineal, también

significativamente mayor que en las técnicas de absorción, convirtiéndose en una de las principales aproximaciones en el desarrollo de biosensores con transducción óptica[249, 251]. Además, la disponibilidad de un gran número de fluoróforos y de indicadores luminiscentes junto con la síntesis y aparición de nuevos de estos compuestos, han hecho posible ampliar la versatilidad y aplicabilidad de las técnicas luminiscentes.

Entre los fenómenos luminiscentes más ampliamente utilizados se encuentran la fluorescencia y la fosforescencia, siendo las medidas de parámetros como intensidad y tiempo de vida las más utilizadas en los biosensores ópticos para la determinación cualitativa y cuantitativa.

La fluorescencia y la fosforescencia son procesos de emisión que tienen lugar cuando las moléculas absorben energía procedente de una radiación incidente a una determinada longitud de onda y posteriormente, tras una serie de procesos electrónicos, emiten radiación a una longitud de onda mayor. Los mecanismos por los que ocurren dichos procesos de emisión se pueden representar mediante el denominado diagrama de Jablonski (Figura 18), donde se muestran los distintos niveles electrónicos de una molécula y las posibles transiciones electrónicas que pueden tener lugar entre dichos niveles[252, 253].

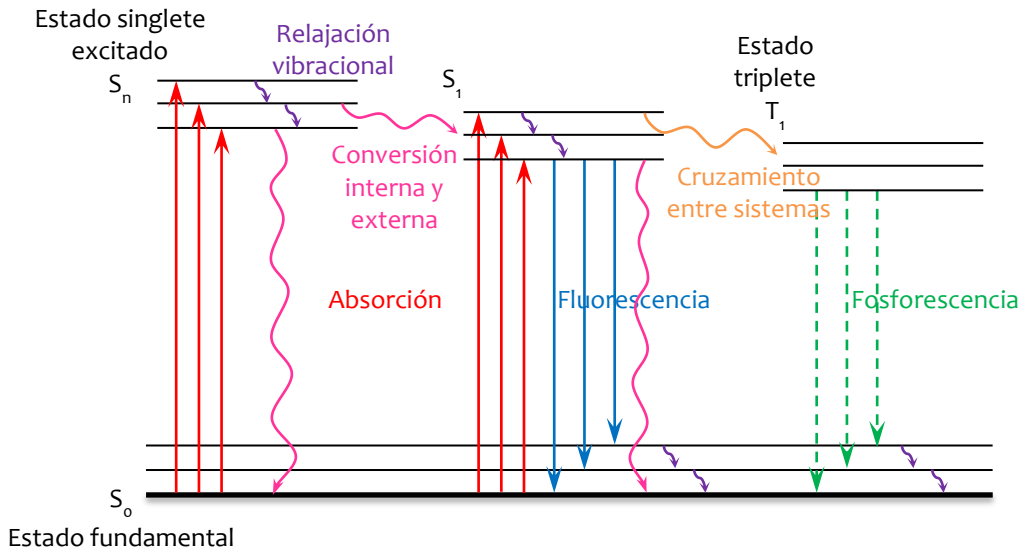

Figura 18. Diagrama de Jablonski.

La absorción de radiación por parte de las moléculas produce la excitación de algunos de sus electrones, promoviéndolos desde el estado fundamental S_0 hasta niveles electrónicos de mayor energía S_n ($S_0 \rightarrow S_n$). Posteriormente dichos electrones excitados pueden regresar al estado fundamental o a niveles electrónicos de menor energía mediante procesos de desactivación no

radiantes o mediante procesos radiantes, los cuales se suelen dar de manera combinada. En la Tabla 5 se muestran las distintas transiciones electrónicas que tienen lugar durante estos procesos, así como sus tiempos de vida medios.

Entre los procesos de desactivación no radiantes se encuentran la relajación vibracional, las conversiones interna y externa, y el cruzamiento entre sistemas. La *relajación vibracional* se produce como consecuencia de las colisiones entre moléculas excitadas y moléculas del disolvente, de manera que durante dichas colisiones el exceso de energía vibracional de las moléculas excitadas se transfiere a las moléculas del disolvente, produciéndose transiciones a niveles vibracionales de menor energía dentro de un mismo nivel electrónico ($S_{1,\,v=n} \rightarrow S_{1,\,v=n-1}$). Este incremento en la energía vibracional del disolvente se traduce en un ligero aumento de su temperatura. La relajación vibracional es un proceso altamente eficiente que implica que el tiempo de vida medio de los estados excitados vibracionalmente sea del orden de 10^{-12} segundos o inferior.

Conjuntamente con la relajación vibracional también pueden ocurrir procesos de *conversión interna*, los cuales involucran transiciones intermoleculares por las cuales las moléculas pasan desde un estado electrónico de mayor energía a otro de energía inferior sin emisión de radiación ($S_n \rightarrow S_{n-1}$; $T_n \rightarrow T_{n-1}$). Estos procesos son más eficaces cuanto más próximos se encuentran entre sí los distintos niveles de energía y ocurren en una escala de tiempo de entre 10^{-14} y 10^{-11} segundos.

Por su parte, la *conversión externa* engloba los procesos de desactivación producidos por la interacción y transferencia de energía entre las moléculas excitadas y el disolvente u otras sustancias presentes en el medio ($S_1 \rightarrow S_0$). El efecto de este procedimiento de desactivación sobre la emisión se puede reducir mediante la modificación de las condiciones del medio que afectan directamente al número de colisiones que tienen lugar entre las partículas, como son por ejemplo temperatura y viscosidad. Así, mediante una disminución de la temperatura y un incremento de la viscosidad del medio es posible minimizar la desactivación por conversión externa, consiguiendo un incremento de la emisión.

Por otra parte, dentro de los procesos radiantes se incluyen la emisión de fluorescencia y de fosforescencia. El mecanismo de la *fluorescencia* está basado por tanto en la transición de los electrones desde estados excitados al estado fundamental con emisión directa de radiación ($S_1 \rightarrow S_0$), mientras que el mecanismo por el cual ocurre la *fosforescencia* implica un cambio en el espín

de dichos electrones excitados a través de un proceso conocido como *cruzamiento entre sistemas*. Este cruce entre sistemas implica un cambio en la multiplicidad de la molécula con una transición entre el estado singlete excitado S_1 y el estado triplete excitado T_1 ($S_1 \rightarrow T_1$; $S_n \rightarrow T_n$), que tiene lugar en una escala de tiempo de entre 10^{-11} y 10^{-6} segundos. Posteriormente, la transición desde el estado triplete excitado hasta el estado fundamental es la que origina la emisión de fosforescencia ($T_1 \rightarrow S_0$) con un tiempo del orden de 10^{-3} hasta 10^4 segundos.

Debido a estas diferencias en los mecanismos de las transiciones electrónicas, la emisión de fluorescencia sucede más rápidamente que la emisión fosforescente y generalmente finaliza unos 10^{-6} segundos después del inicio de la excitación. Por el contario, la emisión de fosforescencia se origina durante períodos de tiempo mayores de 10^{-6} segundos, pudiendo continuar en algunos casos durante minutos después de que la radiación incidente haya terminado. Los procesos de cruzamiento entre sistemas que originan la emisión de fosforescencia requieren de la presencia de átomos pesados como bromo o yodo que favorezcan el cambio en el espín entre los electrones excitados. Además de la diferencia temporal, por lo general, existe una mayor separación entre las longitudes de onda de emisión y excitación en los procesos fosforescentes que en los fluorescentes debido a la menor energía del estado triplete[254]. Por otra parte, es posible conseguir una mayor selectividad con los procesos fosforescentes que con los fluorescentes, debido a que el número de compuestos que emiten fosforescencia es mucho menor que el número de compuestos fluorescentes[255].

Tabla 5. Transiciones electrónicas y tiempos de vida de los distintos procesos radiantes y no radiantes.

Proceso	Transición	Tiempo de vida (s)
Absorción de radiación (excitación)	$S_0 \rightarrow S_n$	$\approx 10^{-15}$ (instantáneo)
Relajación vibracional	$S_{1,\, v=n} \rightarrow S_{1,\, v=n-1}$	$10^{-12} - 10^{-10}$
Conversión interna	$S_n \rightarrow S_{n-1}$; $T_n \rightarrow T_{n-1}$	$10^{-14} - 10^{-11}$
Conversión externa	$S_1 \rightarrow S_0$	$10^{-7} - 10^{-6}$
Fluorescencia	$S_1 \rightarrow S_0$	$10^{-9} - 10^{-6}$
Cruzamiento entre sistemas	$S_1 \rightarrow T_1$; $S_n \rightarrow T_n$	$10^{-11} - 10^{-6}$
Fosforescencia	$T_1 \rightarrow S_0$	$10^{-3} - 10^4$

Finalmente, todos estos procesos, tanto de desactivación no radiante como de emisión de radiación compiten entre sí, de forma que el mecanismo de vuelta hacia el estado fundamental que ocurrirá con mayor probabilidad será aquel que minimice el tiempo de vida medio del estado excitado. Es por ello que, si por ejemplo, la emisión de fluorescencia tiene lugar de manera más rápida que el resto de procesos de desactivación, se observará emisión fluorescente, y en el caso contrario, en el que los procesos no radiantes estén favorecidos, la emisión de fluorescencia no tendrá lugar o será menos intensa. Por otra parte, cualquier factor que haga aumentar la probabilidad de que suceda el cruzamiento entre sistemas hacia el estado triplete, hará que se favorezca la emisión fosforescente en detrimento de la fluorescente.

Así, la competición entre los procesos radiantes y no radiantes hace que la emisión de luminiscencia esté limitada a determinadas moléculas que cumplen ciertas características estructurales que, combinadas con unas condiciones ambientales adecuadas, hacen que la velocidad con la cual transcurren los procesos de desactivación no radiante se minimice hasta el punto en el que la emisión luminiscente puede competir cinéticamente con ellos.

Entre los factores que afectan a la emisión luminiscente se encuentran la estructura y rigidez estructural de las moléculas, el tipo de disolvente, la temperatura, el pH y la presencia de oxígeno disuelto[256]:

- *Estructura*: la presencia de grupos aromáticos, de grupos carbonilos o de dobles enlaces altamente conjugados favorece la emisión luminiscente. Además, por lo general, el incremento en el número de anillos aromáticos y en el grado de condensación origina mayores rendimientos cuánticos, es decir, hace incrementar la relación entre el número de moléculas que emiten luminiscencia y el número total de moléculas excitadas.
- *Rigidez estructural*: las estructuras rígidas incrementan la emisión de luminiscencia, probablemente debido a que la rigidez estructural provoca una disminución en la velocidad a la que se producen los procesos de conversión interna, y por tanto, se consigue disminuir la probabilidad de que ocurra este tipo de desactivación no radiante.
- *Disolvente*: la viscosidad del disolvente en el que se encuentran disueltas las moléculas excitadas juega un papel importante en la emisión luminiscente, ya que viscosidades bajas permiten una mayor movilidad a las moléculas aumentando la probabilidad de colisiones entre ellas y con las moléculas del disolvente. Dichas colisiones originan procesos de desactivación no radiante y desfavorecen por tanto la emisión de luminiscencia. Por otra

parte, si el disolvente contiene átomos pesados o estos son incorporados al medio, se favorece la emisión fosforescente sobre la fluorescente.

- *Temperatura*: las temperaturas elevadas favorecen las colisiones entre las moléculas y por consiguiente aumentan la probabilidad de que se produzcan procesos de desactivación no radiante.
- *pH*: los compuestos con sustituyentes con carácter ácido o básico sufren generalmente cambios en su emisión luminiscente en función del pH. Esto sucede cuando las formas ionizada y no ionizada de dichos compuestos presentan diferentes intensidades de emisión, longitudes de onda de emisión o ambas.
- *Oxígeno disuelto*: la presencia de oxígeno disuelto suele tener un efecto negativo sobre la emisión luminiscente. Este efecto puede deberse a la oxidación de las especies luminiscentes o, en la mayoría de los casos, a la atenuación de los estados excitados, tanto singlete como triplete, implicados en la emisión luminiscente. Dicha atenuación se produce como consecuencia de la transferencia de la energía de excitación desde las moléculas excitadas a las moléculas de oxígeno, generando el primer estado excitado de la molécula de oxígeno, conocido como oxígeno singlete, y disminuyendo la emisión luminiscente.

4.1.2.1. Técnicas basadas en la atenuación de la luminiscencia

Los biosensores luminiscentes pueden estar basados tanto en medidas de la emisión luminiscente como en medidas de atenuación o *quenching* de la misma. En el primer caso, la emisión luminiscente medida puede ser relacionada directamente con la concentración de especie emisora (Ecuación 3), por lo que puede ser utilizada para determinar de manera directa especies luminiscentes. En el caso de las medidas de atenuación de la emisión luminiscente, la variación en la intensidad de luminiscencia medida puede ser utilizada para determinar de manera directa la concentración de especie atenuadora o de manera indirecta la concentración de sustancias que afecten a la concentración de dicha especie atenuadora.

$$I_f = k\ I_0\ \phi\ [\varepsilon\ l\ C] \qquad \text{Ecuaci n 3}$$

donde I_f es la intensidad de radiación luminiscente medida, I_0 es la intensidad de la radiación incidente, k es una constante de proporcionalidad que depende de parámetros instrumentales (eficacia del sistema detector y geometría), ϕ es el rendimiento cuántico de luminiscencia, ε es el coeficiente de absortividad molar, l es el paso de luz y C es la concentración de especie emisora.

Los fenómenos de atenuación o desactivación de luminiscencia hacen referencia a los procesos que originan disminución de la intensidad de la emisión de luminiscencia de una especie emisora o luminóforo. Estos fenómenos suelen dar información sobre la existencia de interacciones moleculares en el medio donde se encuentra el luminóforo[257].

Dichos procesos de atenuación de la luminiscencia se pueden describir mediante la ecuación de Stern-Volmer (Ecuación 4), la cual relaciona los cambios producidos en la intensidad de la emisión luminiscente con la concentración de especie atenuadora o *quencher*.

$$\frac{I_0}{I} = 1 + K_{SV}[Q] \qquad \text{Ecuaci n 4}$$

donde I_0 es la intensidad de luminiscencia en ausencia de *quencher*, I es la intensidad de luminiscencia en presencia de *quencher*, K_{SV} es la constante de Stern-Volmer y $[Q]$ es la concentración de *quencher*. La K_{SV} está relacionada con la accesibilidad del *quencher* a la especie luminiscente.

Dicha ecuación puede ser adaptada y aplicada también a medidas de tiempos de vida (Ecuación 5), relacionando así el tiempo de vida medio de los estados excitados de las especies emisoras con la concentración de *quencher*.

$$\frac{\tau_0}{\tau} = 1 + K_{SV}[Q] \qquad \text{Ecuaci n 5}$$

donde τ_0 es el tiempo de vida del estado excitado en ausencia de *quencher*, τ es la intensidad de luminiscencia en presencia de *quencher*.

Así, mediante la aplicación de dichas ecuaciones de Stern-Volmer es posible determinar la concentración de un determinado *quencher* siempre que la especie cuya emisión se ve atenuada se encuentre aislada de otras sustancias capaces de actuar también como atenuadores de su luminiscencia, tales como surfactantes, iones cloruro y yoduro, oxígeno molecular e iones metálicos, entre otros[252, 257]. En la Figura 19 se muestra el efecto de una especie atenuadora típica (oxígeno) sobre la intensidad de luminiscencia de dos indicadores ópticos.

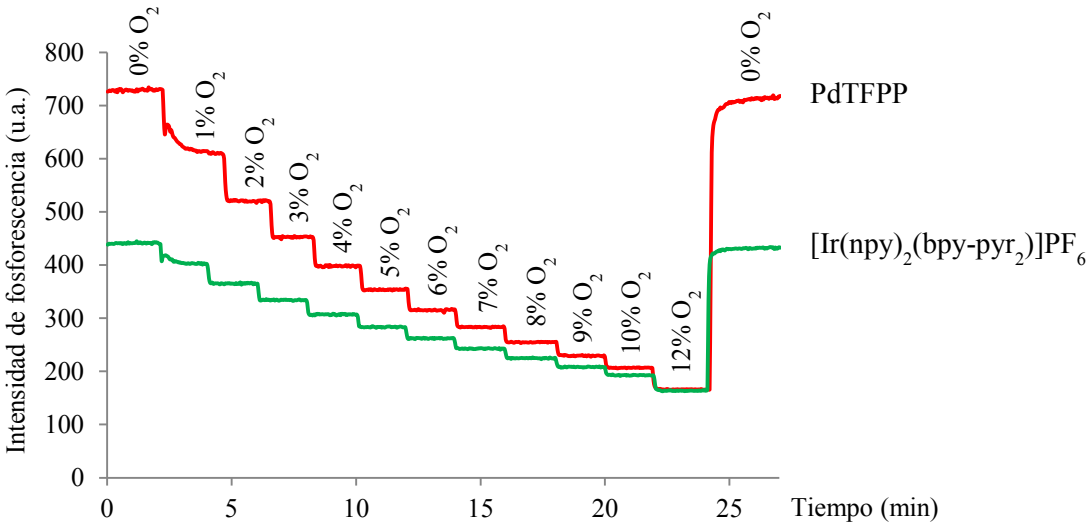

Figura 19. Variación de la intensidad de luminiscencia de dos indicadores diferentes en función de la concentración de oxígeno.

Por otra parte, la atenuación o *quenching* de la luminiscencia puede ser debida a varios mecanismos que incluyen transferencias de energía por resonancia, formación de complejos y desactivación por colisiones. Todos estos tipos de desactivaciones requieren que se produzca contacto molecular entre las moléculas luminiscentes o luminóforos y las moléculas de atenuador o *quencher*, siendo fenómenos especialmente importantes en disolución donde las colisiones son más frecuentes, y generando en todos los casos disipación de energía en forma de calor y no en forma de emisión radiante[257]. La diferencia fundamental entre uno y otro tipo de desactivación depende de la manera en que se produce el contacto entre las moléculas implicadas.

- *Transferencia de energía por resonancia (Fluorescence Resonance Energy Transfer, FRET)*: el mecanismo de este proceso implica la transferencia no radiante de la energía de excitación desde la molécula emisora hasta el atenuador mediante interacciones dipolo-dipolo de larga distancia. Este mecanismo se explica en base al concepto de que las moléculas emisoras se pueden comportar como dipolos oscilantes capaces de originar intercambios de energía con otros dipolos con la misma frecuencia de resonancia. Este tipo de transferencia de energía es altamente dependiente de la distancia entre las moléculas implicadas, y puede ser utilizada para medir distancias de escala nanométrica y cambios en las distancias, así como para analizar cambios estructurales en proteínas, ácidos nucleicos y otras biomoléculas.
- *Formación de complejos o quenching estático*: implica la atenuación de la luminiscencia como consecuencia de la formación de un complejo no luminiscente entre la molécula emisora y la molécula *quencher*. Este tipo de atenuación depende de la concentración de

molécula *quencher*, pero no está regido por la difusión del *quencher* en el medio. Se caracteriza por generar un comportamiento lineal en las gráficas de Stern-Volmer.

- *Desactivación por colisiones o quenching colisional o dinámico*: la desactivación de la luminiscencia es debida a los choques producidos entre la molécula luminiscente y el *quencher*, por lo que este proceso sí depende de la difusión del *quencher* en el medio. Dichas colisiones provocan la transferencia de energía desde la molécula emisora excitada hacia la molécula *quencher*. En este caso se observa que el rendimiento cuántico de la especie emisora disminuye proporcionalmente con la concentración de *quencher*, por lo que la desactivación colisional también genera una relación lineal en las gráficas de Stern-Volmer.

Asimismo, también es posible que se originen otro tipo de fenómenos que conlleven atenuación de la luminiscencia sin la presencia de moléculas de atenuador[253]. Estos fenómenos pueden ser de dos tipos fundamentalmente: *auto quenching*, producido como consecuencia de las colisiones entre moléculas excitadas de la propia especie emisora, originando una desactivación en forma de energía no radiante que puede ser minimizada mediante la disminución de la concentración de especie emisora. Y *auto absorción*, debida a que la luminiscencia emitida por moléculas excitadas de la especie emisora puede ser absorbida por parte de moléculas no excitadas de la misma especie. La probabilidad de que se produzca auto absorción también puede ser minimizada disminuyendo la concentración de especie emisora.

4.1.2.2. Indicadores luminiscentes

En general, los biosensores basados en fenómenos de luminiscencia están constituidos básicamente por un componente biológico acoplado a un componente transductor, de manera que la reacción de reconocimiento específica llevada a cabo por el componente biológico es detectada por el componente transductor, el cual es capaz de generar una señal fluorescente o fosforescente medible, en respuesta a los cambios producidos por dicha reacción de reconocimiento.

La funcionalidad de un biosensor óptico luminiscente viene determinada, en gran medida, por el tipo de componente transductor empleado. Dicho componente suele ser un indicador luminiscente, cuya idoneidad para formar parte de un biosensor depende generalmente de una serie de propiedades espectroscópicas y físico-químicas[252], entre las que destacan:

- *Longitudes de onda de excitación y de emisión*: debido a que los procesos luminiscentes implican tanto una etapa de absorción de radiación por parte de las especies luminiscentes,

como la posterior emisión de la radiación absorbida, dichas especies presentan dos espectros característicos (excitación y emisión), con longitudes de onda máximas y formas determinadas. Por lo general, estos espectros son simétricos entre sí, debido a que las transiciones y los niveles de energía vibracional implicados en los procesos de absorción y emisión son los mismos. Asimismo, en general, la forma del espectro de emisión es independiente de la longitud de onda de excitación, la cual sí que influye directamente sobre la intensidad de la señal fluorescente.

- *Tiempo de vida*: determinado por el tiempo que la especie luminiscente pasa en estado excitado antes de regresar al estado fundamental. Los tiempos de vida prolongados permiten obtener una mayor sensibilidad, debido a que posibilitan la eliminación de la interferencia producida por la auto-fluorescencia de la propia muestra, generalmente emitida a tiempos cortos.
- *Desplazamiento de Stokes*: dado por la diferencia de longitud de onda o de frecuencia existente entre los máximos de excitación y de emisión, la cual a su vez se origina como consecuencia de la existencia de los procesos de desactivación no radiantes. Dichos procesos hacen que no toda la radiación absorbida sea emitida nuevamente en forma de radiación. De esta manera, cuanto mayor sea el desplazamiento de Stokes mayor será la facilidad para discriminar entre la longitud de onda de excitación y la de emisión, y menor será la probabilidad de que se produzcan fenómenos de *auto quenching*.
- *Rendimiento cuántico*: definido como la relación existente entre el número de moléculas que emiten luminiscencia y el número total de moléculas que se encuentran en estado excitado, es decir, el rendimiento cuántico proporciona una idea sobre la probabilidad de que el estado excitado sea desactivado por emisión de luminiscencia en lugar de por otros procesos no radiantes, dando así una medida de la eficiencia del proceso luminiscente. Por lo tanto, rendimientos cuánticos elevados originan señales luminiscentes más intensas y proporcionan una mayor sensibilidad.
- *Fotoestabilidad*: resistencia a tiempos largos de irradiación.
- *Sensibilidad y selectividad*.
- *Compatibilidad con disolventes orgánicos*.
- *Respuesta rápida* a los cambios en el entorno.

Por otra parte, existen ejemplos en los que no es necesario incluir un indicador luminiscente externo en el biosensor, ya que el propio elemento biológico es capaz de generar una señal luminiscente medible que puede ser utilizada para llevar a cabo la determinación de su

concentración. Sin embargo, en la mayoría de los casos, el componente biológico no presenta propiedades intrínsecas de luminiscencia y es necesario acoplarlo a moléculas luminiscentes o indicadores, los cuales responden a la aparición o desaparición de determinadas sustancias implicadas en la reacción de reconocimiento biológico. Así, es posible diferenciar entre dos tipos de indicadores luminiscentes o luminóforos: *intrínsecos* o luminóforos naturales y *extrínsecos*.

a) Luminóforos intrínsecos

Son compuestos luminiscentes presentes en las biomoléculas de forma natural. Entre ellos destacan fundamentalmente aminoácidos aromáticos, como la fenilalanina, la tirosina y el triptófano, y cofactores enzimáticos como el NADH (nicotinamida adenina dinucleótido) y el FAD (flavina adenina dinucleótido)[258-260]. En la Figura 20 se muestran las estructuras de cada uno de estos compuestos.

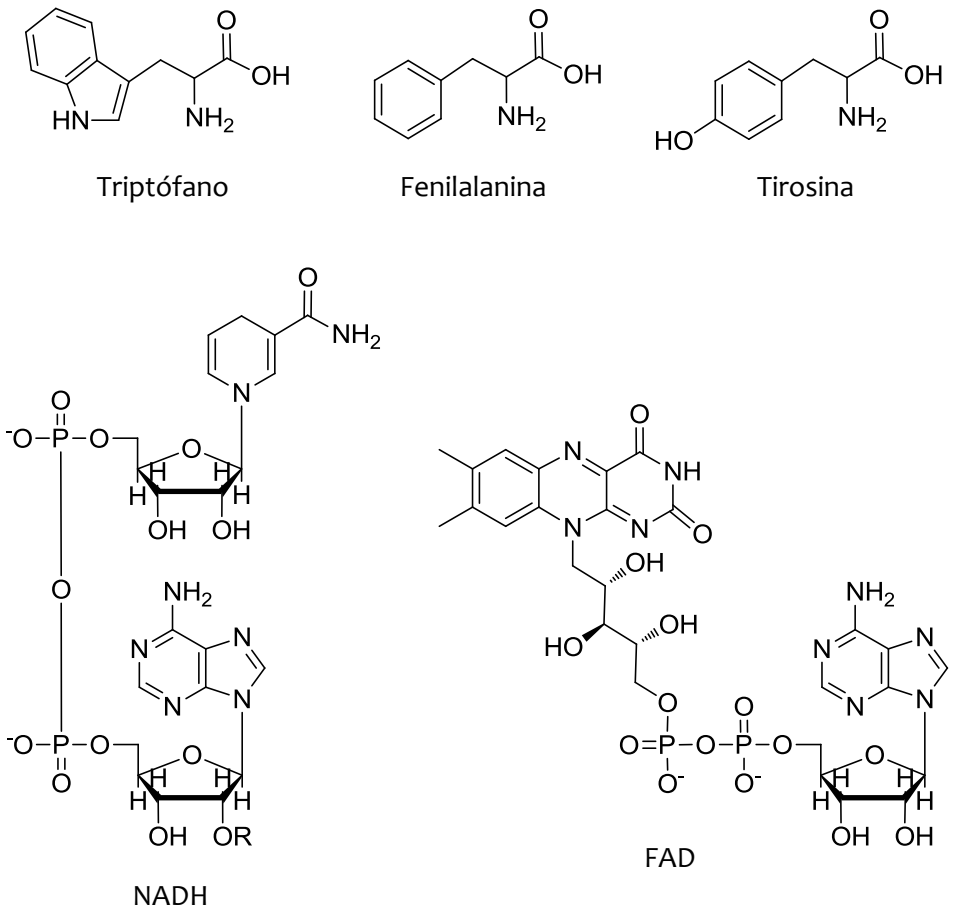

Figura 20. Aminoácidos y cofactores enzimáticos con luminiscencia intrínseca.

De entre los aminoácidos mencionados, la emisión del triptófano es la más representativa y mayoritaria en las proteínas. Esto se debe principalmente a que presenta la mayor diferencia entre la longitud de onda del máximo de excitación y la del máximo de emisión, por lo que se minimizan los fenómenos de *auto quenching*, y a que posee un buen rendimiento cuántico comparado con el resto de aminoácidos (ver Tabla 6). La tirosina presenta un rendimiento cuántico ligeramente inferior y su emisión se ve atenuada con frecuencia como consecuencia de su interacción con el resto de aminoácidos de la proteína[258]. Por su parte, la emisión de la fenilalanina, con un rendimiento cuántico bastante inferior, sólo se observa cuando la proteína carece de residuos de tirosina y de triptófano, algo totalmente inusual[258, 261].

Tabla 6. Propiedades ópticas de los aminoácidos y cofactores enzimáticos con luminiscencia intrínseca en agua a pH neutro[259, 260, 262].

Aminoácido o cofactor	**λ_{exc} (nm)**	**λ_{em} (nm)**	**Rendimiento cuántico**	**Tiempo de vida (ns)**
Triptófano	280	348	0.2	3.1
Tirosina	274	303	0.14	3.6
Fenilalanina	257	282	0.04	6.4
NADH	340	460	0.019	0.4
FAD	450	525	0.033	2.3

La emisión del triptófano se caracteriza por ser altamente sensible a su microentorno, por lo que es común utilizarla para analizar y seguir los cambios conformacionales sufridos por las proteínas. Así por ejemplo, se observan desplazamientos en la longitud de onda de emisión del triptófano a causa de fenómenos como la unión de ligandos a la proteína o la interacción proteína-proteína, entre otros.

En la Figura 21 se muestra una serie de espectros de emisión de una enzima (glucosa oxidasa), donde se puede apreciar que su máximo de emisión se corresponde mayoritariamente con la emisión del triptófano.

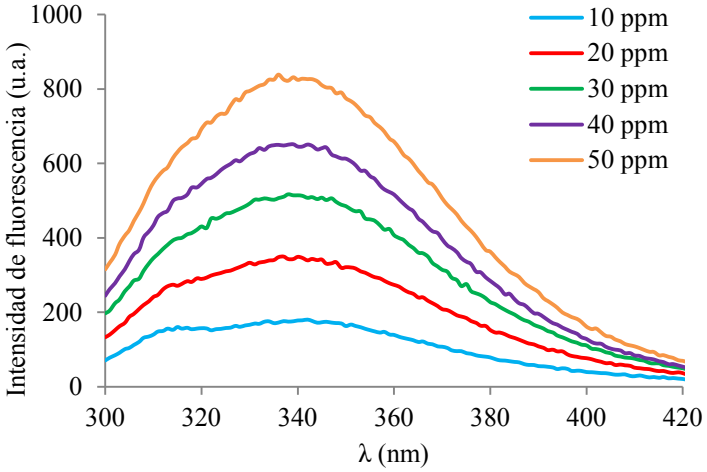

Figura 21. Espectros de emisión luminiscente de glucosa oxidasa a diferentes concentraciones en tampón fosfato pH 7.

Por otro lado, el NADH libre presenta una relativamente elevada intensidad de emisión fluorescente, con un tiempo de vida de 0.4 ns y un rendimiento cuántico de 0.019 en disolución acuosa, con una longitud de onda de excitación de 340 nm y una longitud de onda de emisión de 460 nm. Por lo general, cuando el NADH se une a las proteínas, su rendimiento cuántico experimenta un incremento, al igual que el tiempo de vida, sin embargo, la intensidad de la emisión puede incrementar o disminuir en función del tipo de proteína a la que se una[258, 259]. En el caso del FAD, su tiempo de vida es de aproximadamente 2.3 ns, sus longitudes de onda de excitación y emisión son 450 nm y 525 nm, respectivamente, y siempre sufre atenuación de su luminiscencia cuando se une a las proteínas[260]. Estas variaciones en las intensidades de luminiscencia como consecuencia de la unión a proteínas, tanto para el NADH como para el FAD, se utilizan para determinar cambios conformacionales en las proteínas, y debido a que ambos cofactores presentan diferentes longitudes de onda de emisión y excitación, es posible obtener información complementaria mediante las medidas de luminiscencia de ambos.

Asimismo, ambos cofactores están implicados también en una amplia variedad de reacciones celulares de oxidación-reducción y en procesos metabólicos, por lo cual, las medidas de su emisión luminiscente constituyen una alternativa para realizar el seguimiento de la actividad celular.

Especial mención merece la denominada proteína verde fluorescente (GFP). Esta proteína presenta una estructura con una hélice central en cuya cadena incorpora una secuencia de 3 aminoácidos consecutivos (Ser-Tyr-Gly) que forman un luminóforo natural (Figura 22), de manera que, cuando la GFP es iluminada con luz UV, dicho luminóforo es capaz de absorber

radiación y emitir fluorescencia de color verde[263, 264]. Así, la GFP presenta un máximo de emisión a aproximadamente 508 nm y un máximo de excitación alrededor de los 395 nm (Figura 23).

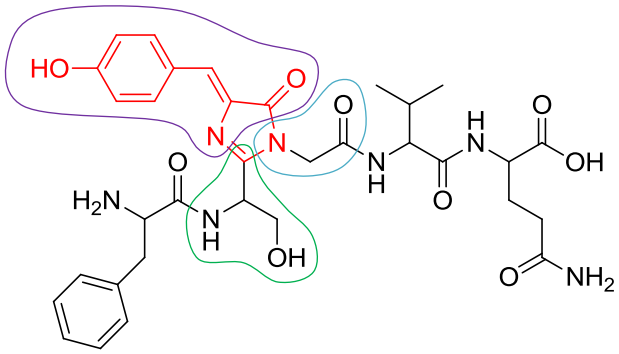

Figura 22. Luminóforo natural de la GFP formado por serina, tirosina y glicina.

Una de las ventajas de este luminóforo natural es que puede ser incorporado mediante técnicas de ingeniería genética a otras proteínas que no lo presenten de forma natural, haciendo posible el diseño de proteínas fluorescentes, cuyos movimientos, actividades y localizaciones pueden ser monitorizados *in vivo*, además de poder cuantificar la cantidad de proteína presente en un momento dado[265-268].

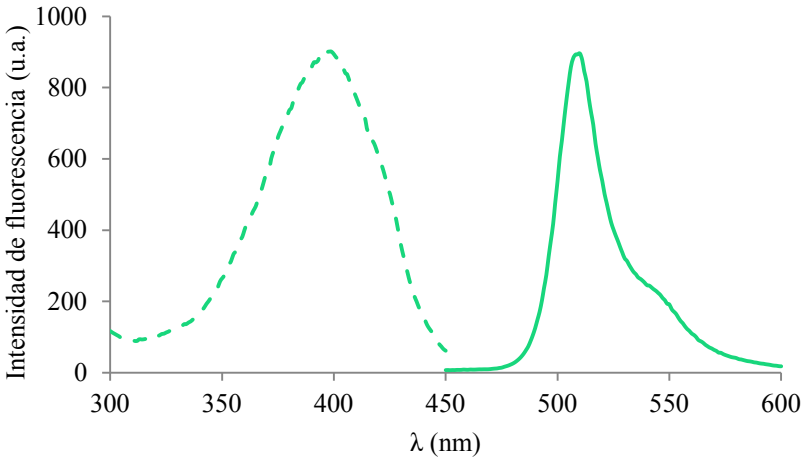

Figura 23. Espectros de excitación y emisión característicos de la GFP.

b) Luminóforos extrínsecos

Son compuestos sintéticos, u obtenidos a partir de modificaciones de compuestos de origen natural, con propiedades luminiscentes por lo general mejoradas (elevados rendimientos cuánticos y tiempos de vida, y mayores longitudes de onda de emisión y excitación, que permiten minimizar los problemas ocasionados por la emisión fluorescente de fondo de la mayoría de las muestras biológicas).

Dentro de esta categoría es posible distinguir entre una gran variedad de especies en función de su naturaleza: indicadores orgánicos (fluoresceínas, rodaminas, BODIPYs, cumarinas, cianinas, ftalocianinas, etc.), complejos organometálicos (basados en Pt(II), Pd(II), Ru(II), Re(I), Eu(III), Ir(III), Cu(I)), nanocristales semiconductores o puntos cuánticos (*quantum dots*, QDs), y polímeros luminiscentes[269-272].

Generalmente, los indicadores de naturaleza orgánica (Figura 24) presentan unas propiedades ópticas menos ventajosas que el resto de luminóforos extrínsecos, caracterizándose por poseer tiempos de vida y rendimientos cuánticos inferiores, ser más susceptibles de sufrir atenuación de su luminiscencia y mostrar una menor fotoestabilidad[273-275]. Es por ello que este tipo de indicadores están siendo reemplazados cada vez más por los luminóforos inorgánicos, los cuales presentan numerosas ventajas en sus propiedades espectroscópicas.

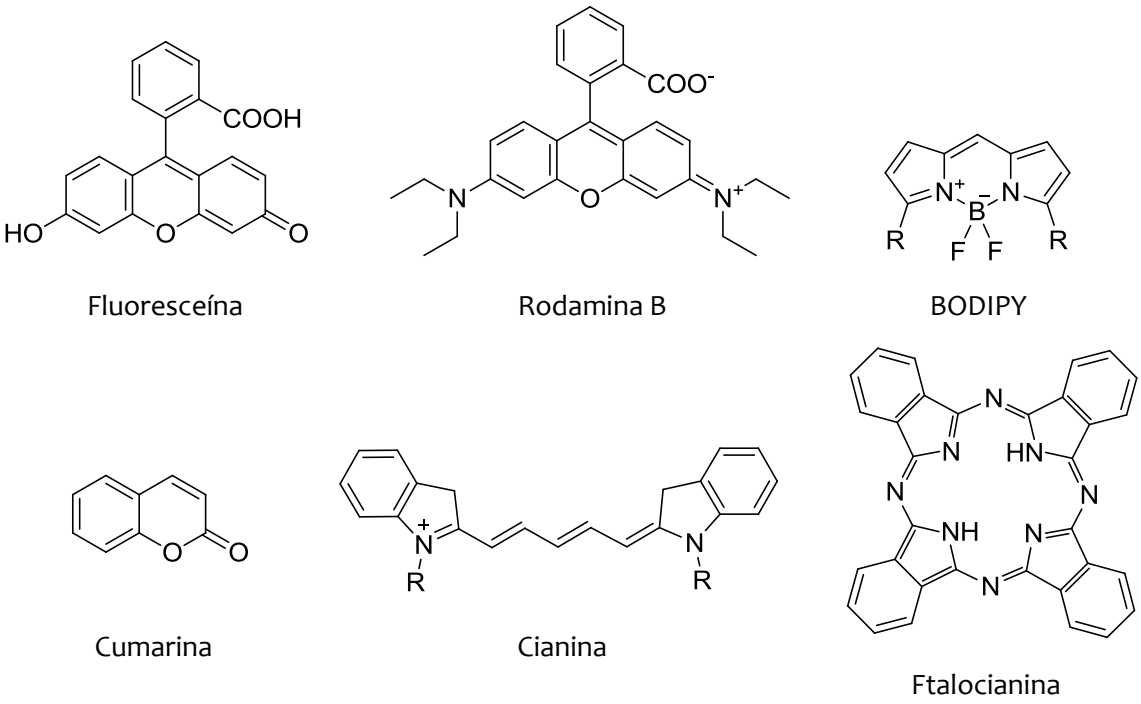

Figura 24. Estructuras de algunos de los indicadores orgánicos más característicos.

Los complejos organometálicos (OMCs) se caracterizan por contener un metal de transición coordinado con uno o más ligandos orgánicos. En comparación con los indicadores orgánicos, los OMCs son térmica y fotoquímicamente más estables, y presentan una mayor versatilidad, ya que sus propiedades ópticas (rendimiento cuántico, tiempo de vida, longitudes de onda de excitación y de emisión) y sus características físico-químicas (forma, carga, reactividad, solubilidad) pueden ser fácilmente modificadas y ajustadas aplicando cambios en su estructura, ya sea mediante

variaciones de los ligandos o del metal de transición[276, 277]. En la Figura 25 se muestran los espectros característicos de dos OMCs con distinto catión metálico.

La mayoría de las propiedades espectroscópicas tan favorables de los OMCs vienen determinadas por las características de sus estados electrónicos y por las transferencias de electrones que tienen lugar entre los ligandos y el metal. Estas transferencias entre ambos pueden ser de dos tipos fundamentalmente, transferencias de carga del metal al ligando (MLCT) o transferencias desde el ligando al metal (LMCT), y se caracterizan por ser muy sensibles al microentorno y a cambios en el pH, la temperatura, la humedad y el disolvente[278]. Dichas transferencias de electrones originan estados excitados conocidos por el mismo nombre, cuya desactivación al estado fundamental es la responsable de la emisión luminiscente característica de estos complejos.

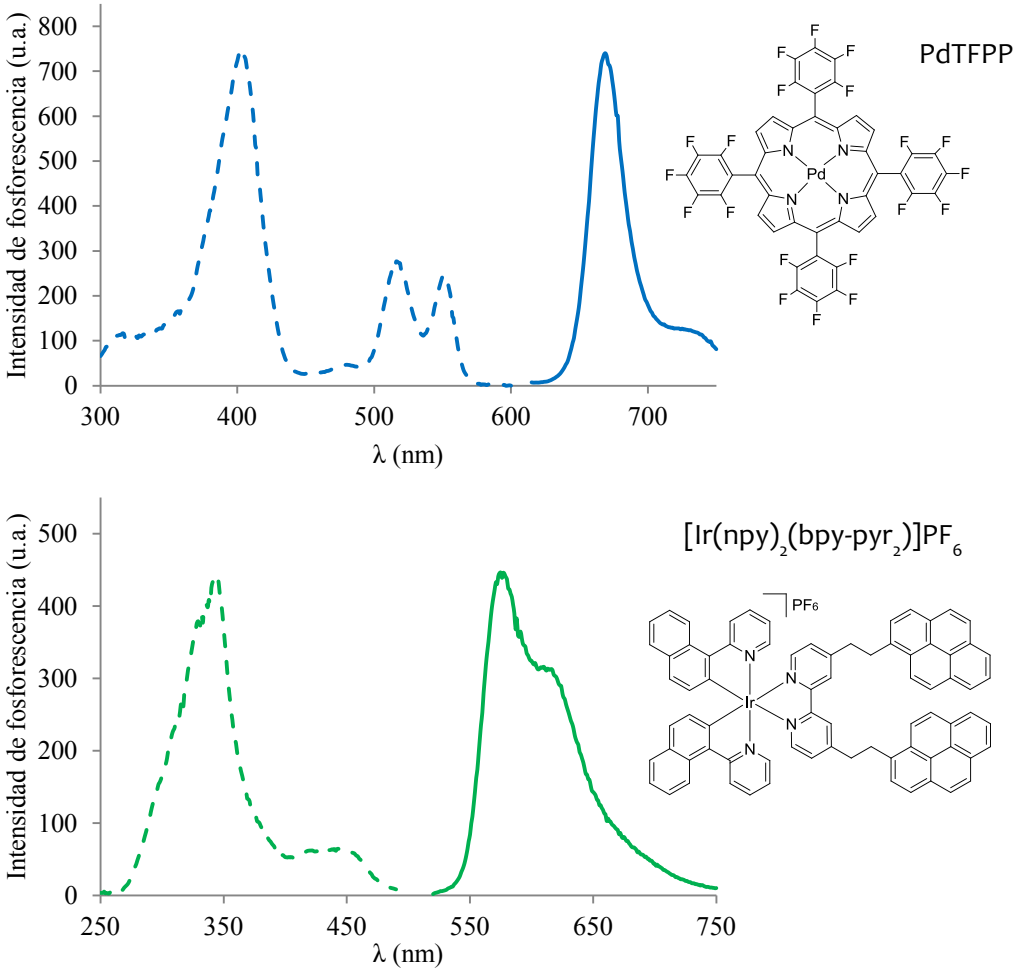

Figura 25. Espectros de excitación y emisión, y estructuras de dos complejos organometálicos.

Resumidamente, las principales ventajas de los OMCs en su utilización como luminóforos extrínsecos son[270]:

- Largos tiempos de vida (con valores entre 0.1 y 100 μs) y elevados rendimientos cuánticos (alcanzando en algunos casos valores de 0.7), pudiendo ser empleados en muestras con elevada fluorescencia de fondo.
- Emisión luminiscente altamente sensible a los cambios en el entorno o en la estructura.
- Estabilidad química y fotoquímica.
- Posibilidad de ajustar sus propiedades ópticas y electrónicas mediante el empleo de diferentes ligandos.
- Capacidad para modificar su tamaño y geometría en función del metal y los ligandos empleados.
- Elevada diversidad de ligandos con diferentes químicas, estructuras y propiedades de coordinación, que permiten obtener una enorme variedad de complejos con selectividad hacia un gran número de compuestos.

Gracias a estas características, el empleo de OMCs en el desarrollo de biosensores es una estrategia en auge en la actualidad, con aplicaciones de muy diversa índole, entre las que se incluyen la determinación de aminoácidos, proteínas, ácidos nucleicos, azúcares y otras biomoléculas implicadas en el metabolismo celular[279-282].

Otro tipo de luminóforos extrínsecos inorgánicos son los denominados *quantum dots*[283-285]. El estudio y desarrollo de estos materiales ha experimentado un gran avance en los últimos años, lo que a su vez ha impulsado una gran mejora en sus propiedades, permitiendo así, entre otras cosas, incrementar su estabilidad química y fotoquímica, mejorar sus rendimientos cuánticos, y obtener una distribución de tamaños mucho más controlada. Además, en muchos casos, la superficie de estos nanocristales se diseña con el fin de que sean dispersables en agua y compatibles con moléculas biológicas como proteínas y anticuerpos. Todo ello, junto con su elevada intensidad de luminiscencia y su fotoestabilidad, ha permitido aumentar considerablemente sus aplicaciones en campos como la biomedicina y el análisis medioambiental[271, 286-289].

Estos nanocristales están fabricados con materiales semiconductores, entre los que destacan compuestos de cadmio como CdSe, CdS y CdTe, y otros compuestos como el ZnS y el PbS, los cuales presentan características electrónicas adecuadas para originar *quantum dots* fluorescentes con diferentes propiedades ópticas, químicas y estructurales (Figura 26). Además, en muchos casos, con el fin de mejorar su estabilidad, su biocompatibilidad y su resistencia química, estas nanopartículas se fabrican con una estructura tipo *core-shell*, en la que tanto el núcleo como la corteza están constituidos por materiales semiconductores de distinta naturaleza[288].

En este tipo de partículas el movimiento de los electrones de los elementos que las forman está restringido, ya que estos solamente pueden moverse por la pequeña región que forma la partícula, normalmente con un diámetro comprendido entre 2 y 10 nm[290, 291]. Esta característica hace que sea posible diseñar *quantum dots* con una gran variedad de propiedades ópticas y electrónicas que varían en función del tamaño de la partícula y de su composición química. Así, por ejemplo, la utilización de distintos *quantum dots* permite detectar simultáneamente diferentes biomarcadores por la diferencia de color en su emisión.

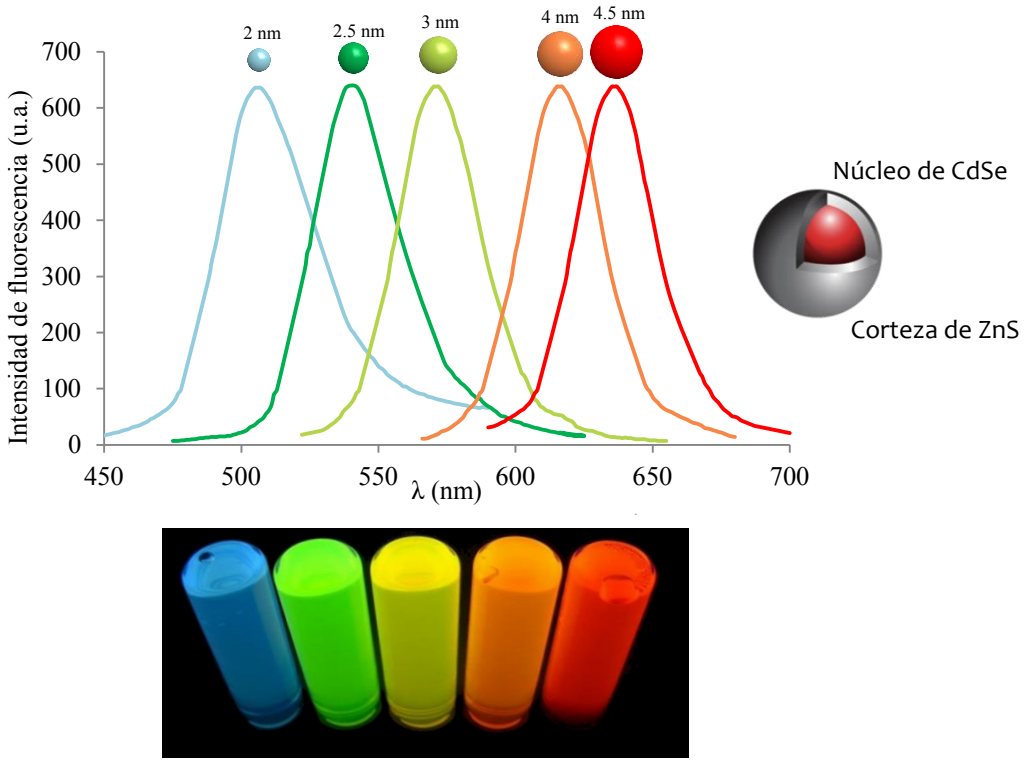

Figura 26. Espectros de emisión de nanocristales de CdSe/ZnS.

Por último, los polímeros luminiscentes constituyen otra clase de luminóforos extrínsecos de naturaleza orgánica. Estos materiales presentan una estructura con electrones deslocalizados que le confieren propiedades semiconductoras, las cuales han sido ampliamente aprovechadas en aplicaciones optoelectrónicas como, por ejemplo, la fabricación de diodos orgánicos emisores de luz (OLEDs) o transistores orgánicos de efecto campo (OFETs)[272, 292, 293]. Sin embargo, las aplicaciones en el campo de los sensores son menos conocidas pero igualmente interesantes. Así, estos polímeros han sido empleados para la determinación de una variedad de analitos que abarcan desde pequeñas moléculas e iones hasta macromoléculas como proteínas, basándose para ello en la medida de los cambios sufridos en sus propiedades optoelectrónicas (absorción, emisión, conductividad o potencial electroquímico)[294-297].

Las aplicaciones de los polímeros luminiscentes en el ámbito de los biosensores ópticos están basadas principalmente en la atenuación de su emisión luminiscente como consecuencia de la interacción con un analito determinado, debido sobre todo a procesos de transferencia de carga o energía. Dicha interacción entre el polímero y el analito no solamente afecta a la zona de contacto directo entre ambos, sino que también las unidades cercanas de la cadena polimérica se ven influenciadas debido a transferencias de los electrones deslocalizados, amplificando de esta manera la perturbación ocasionada por la molécula de analito. Es por ello que incluso cantidades muy pequeñas de analito son capaces de generar variaciones medibles en la señal luminiscente del polímero[295].

Entre algunos de los ejemplos más representativos de este tipo de polímeros luminiscentes se encuentran el poli(*p*-fenilenetileno) (PPE), el poli(*p*-fenilenvinileno) (PPV) y el polifluoreno (PF), los cuales han sido empleados en la fabricación de biosensores basados en medidas de FRET, en análisis de la agregación inducida por el analito o en cambios conformacionales[298, 299].

En la actualidad, y gracias al avance en las técnicas de síntesis, es posible encontrar multitud de indicadores luminiscentes extrínsecos, muchos de los cuales se encuentran disponibles comercialmente. La variedad estructural y de naturaleza química de estos compuestos es realmente amplia, y su comportamiento puede estar basado en diferentes aproximaciones de transducción, ya sea emisión o *quenching* de luminiscencia, anisotropía luminiscente, medidas de tiempo de vida de luminiscencia o medidas de FRET. Estos compuestos presentan además la ventaja de que sus propiedades estructurales, ópticas y físico-químicas pueden ser controladas y modificadas a través de la estrategia y el proceso de síntesis, permitiendo así obtener indicadores específicos para cada tipo de aplicación. Es por todo ello que la selección del indicador luminiscente más adecuado para la fabricación de un determinado biosensor debe hacerse en función de cada aplicación específica y considerando factores como sensibilidad, selectividad y estabilidad.

4.1.2.3. Medidas de luminiscencia en fase sólida

Comúnmente, las medidas de luminiscencia se realizan en disolución, sin embargo, también es posible llevar a cabo medidas de fluorescencia y fosforescencia en fase sólida. Este tipo de medidas presentan ciertas ventajas con respecto a las realizadas en disolución, entre las que se incluyen:

- Disminución de los procesos de *quenching* debido a que se reduce la probabilidad de que se produzcan colisiones entre las moléculas de luminóforo y otras moléculas presentes en la muestra.
- En muchos casos se consigue aumentar la intensidad de la emisión luminiscente como consecuencia del incremento de la rigidez del medio donde se encuentra el luminóforo.
- Consumo de un menor volumen de muestra y de reactivos.
- Reducción de los interferentes de la matriz de la muestra.
- Mejora de la sensibilidad y de la selectividad de la determinación analítica.

Por otro lado, para realizar las medidas en fase sólida es imprescindible depositar la muestra en un soporte sólido cuya emisión luminiscente no interfiera con la de la propia muestra. Este hecho constituye en ocasiones un procedimiento complejo en el que es necesario seleccionar y optimizar una serie de parámetros, tales como, tipo y naturaleza del soporte sólido, longitudes de onda de emisión y excitación, tiempo de retardo o *delay time* (tiempo transcurrido desde que se inicia la excitación hasta que se recoge la señal de emisión), condiciones ambientales como temperatura y humedad, entre otros, con el fin de obtener la mayor sensibilidad y selectividad posibles.

En las últimas décadas, la combinación de las medidas en fase sólida con la técnica de fosforescencia a temperatura ambiente (SS-RTP) ha experimentado una gran evolución y, en la actualidad, se presenta como una estrategia eficaz para la detección y la determinación de concentraciones muy pequeñas de compuestos en muestras con matrices complejas, como por ejemplo, muestras biológicas o muestras alimentarias[300-305].

Para llevar a cabo las mediciones de SS-RTP es necesario tener en cuenta una serie de factores que condicionan, en mayor o menor medida, la señal de fosforescencia[306, 307]. Entre dichos factores destacan:

- La presencia de sales de *átomos pesados*: este tipo de compuestos favorecen los procedimientos de cruzamiento entre sistemas, permitiendo obtener una elevada población de electrones en estado triplete excitado, lo que se traduce en un incremento de la emisión fosforescente. Estos compuestos posibilitan en muchos casos conseguir una elevada señal de fosforescencia de compuestos con rendimientos cuánticos bajos.

  Entre las sales de átomos pesados más frecuentemente utilizadas se encuentran el KI, el NaI, el $AgNO_3$ y el $TlNO_3$.

- La presencia de *oxígeno*: al igual que ocurre con las medidas de luminiscencia en disolución, la presencia de oxígeno en el medio afecta negativamente a la señal de emisión fosforescente en fase sólida debido a la atenuación de los estados excitados. Es por ello que para la realización de las medidas de SS-RTP es necesario pasar una corriente de un gas inerte, por lo general nitrógeno, para eliminar el oxígeno presente en la muestra y obtener así la máxima señal de emisión fosforescente.
- Las condiciones de *humedad*: la existencia de moléculas de agua o de cualquier otro disolvente en el soporte sólido fomenta los procesos de atenuación de los estados excitados, por lo que es necesario llevar a cabo su completa eliminación para mejorar la emisión de fosforescencia; lo cual también se consigue mediante el paso de una corriente de un gas.
- La *temperatura*: es necesario llevar a cabo las medidas bajo un estricto control de la temperatura, ya que variaciones en la misma producen cambios en la señal de emisión fosforescente.
- Las *interacciones* con el soporte sólido: los tipos de interacciones que se pueden dar entre la muestra (incluidos los analitos, los posibles interferentes, el disolvente y el resto de moléculas que pueden estar presentes en la muestra) y el soporte sólido condicionan de manera significativa la señal de fosforescencia obtenida.

Entre los soportes sólidos más ampliamente utilizados para realizar las medidas tanto de fluorescencia como de fosforescencia en fase sólida se encuentran la celulosa y algunos de sus derivados como la nitro-celulosa y la acetil-celulosa, ciertos tipos de poliamidas y algunas resinas de copolímeros, tales como las formadas por estireno y divinilbenceno[308, 309]. Sin embargo, en los últimos años el progreso de la nanotecnología ha impulsado el diseño de nuevos materiales con aplicaciones en las técnicas de luminiscencia en fase sólida, entre los que destacan soportes de micro y nanofibras con base polimérica.

En general, las técnicas de luminiscencia en fase sólida están basadas en medidas de la emisión luminiscente y su relación directa con la concentración de especie emisora, siendo, por ello, necesario eliminar o minimizar cualquier tipo de factor o condicionante que provoque la atenuación de dicha emisión. Sin embargo, también es posible llevar a cabo medidas de *quenching* de la emisión luminiscente en fase sólida y relacionarlas tanto con la concentración de atenuador como con la concentración de otras especies que modifiquen la concentración de dicha sustancia atenuadora.

Al igual que ocurre con las medidas de atenuación de la emisión luminiscente en disolución, los procesos de *quenching* en fase sólida pueden ser descritos mediante la ecuación de Stern-Volmer (Ecuación 3). No obstante, en la mayoría de los casos, cuando se aplica dicha ecuación a los sistemas sólidos se producen ciertas desviaciones que la apartan de la linealidad como consecuencia de la heterogeneidad aportada por la presencia del soporte sólido. Esta heterogeneidad propicia que se formen varios ambientes diferentes en el sistema donde se encuentra la especie emisora, y en los cuales dicha especie presenta distinto comportamiento hacia la presencia de la sustancia atenuadora. La formación de los diferentes ambientes en el soporte sólido suele venir determinada por procesos de difusión no homogéneos de las diferentes especies presentes en el soporte[276, 310].

Debido a estas desviaciones de la ecuación de Stern-Volmer en sistemas sólidos, es imprescindible introducir determinadas modificaciones en la ecuación para conseguir un mejor ajuste matemático. Dichas modificaciones conducen a modelos matemáticos más complejos, tales como los modelos multiestado de Demas o Lehrer, en los que se considera cada uno de los diferentes ambientes de manera separada y con una constante de Stern-Volmer (K_{SV}) distinta. La ecuación general para los modelos multiestado es la siguiente (Ecuación 6):

$$\frac{I_0}{I} = \left[\sum_{i=1}^{m} \frac{f_i}{1 + K_{SVi}[Q]}\right]^{-1} \qquad \text{Ecuaci n 6}$$

donde I_0 es la intensidad de luminiscencia en ausencia de sustancia atenuadora, I es la intensidad de luminiscencia en presencia de sustancia atenuadora, m es el número de ambientes diferentes, f_i es la contribución fraccionada de cada uno de los ambientes (de manera que, $\sum_{i=1}^{m} f_i = 1$), K_{SVi} es la constante de Stern-Volmer para cada uno de los distintos ambientes, y $[Q]$ es la concentración de sustancia atenuadora.

En los modelos mencionados de Demas y Lehrer[311, 312], se supone la existencia de dos ambientes diferentes, por lo que el valor de m en estos casos sería igual a dos. Más detalladamente, por una parte, en el modelo de Demas (Ecuación 7) se parte de la suposición de que en dichos dos ambientes la señal luminiscente de la especie emisora se ve afectada de manera diferente por la presencia de la sustancia atenuadora, por lo que se originan dos constantes de Stern-Volmer con valores diferentes y mayores de cero. Por otra parte, según el modelo de Lehrer (Ecuación 8), se presupone también la existencia de dos ambientes diferentes, pero, en este caso, la señal de luminiscencia de la especie emisora se ve atenuada solamente en uno de los ambientes

(con un valor de K_{SV1} mayor de cero), mientras que en el segundo ambiente la presencia de la sustancia atenuadora no afecta a la emisión luminiscente, obteniendo un valor de cero para la constante de Stern-Volmer ($K_{SV2} = 0$).

$$\frac{I_0}{I} = \left[\frac{f_1}{1 + K_{SV1}[Q]} + \frac{f_2}{1 + K_{SV2}[Q]}\right]^{-1} \qquad \text{Ecuaci n 7}$$

$$\frac{I_0}{I} = \left[\frac{f_1}{1 + K_{SV1}[Q]} + (1-f_1)\right]^{-1} \qquad \text{Ecuaci n 8}$$

Con la aplicación de estos y otros modelos más complejos derivados de la ecuación de Stern-Volmer a las medidas de atenuación de la luminiscencia en fase sólida es posible obtener buenos ajustes matemáticos de los datos experimentales, permitiendo así emplear este tipo de medidas para la determinación de una gran cantidad de sustancias atenuadoras.

4.1.3. Resonancia de plasmón superficial

Los biosensores de resonancia de plasmón superficial (SPR) se basan en las medidas de los cambios que se producen en el índice de refracción de un haz de radiación cuando es dirigido hacia una superficie metálica[313, 314]. Dichos cambios se originan como consecuencia de la interacción entre dicha superficie y las moléculas localizadas en sus proximidades.

En general, la instrumentación de los biosensores basados en SPR consta de los siguientes componentes: una lámpara, un prisma acoplado a una superficie donde tiene lugar la interacción con el analito (normalmente una superficie de vidrio recubierta con una fina lámina de oro de entre 50 y 100 nm), un sistema de flujo y un detector. La Figura 27 muestra un esquema básico de la disposición de dichos componentes.

Otros metales tales como plata, cobre y aluminio también se pueden utilizar en los dispositivos de SPR. Sin embargo, la utilización del oro es la más generalizada debido a su estabilidad química[314].

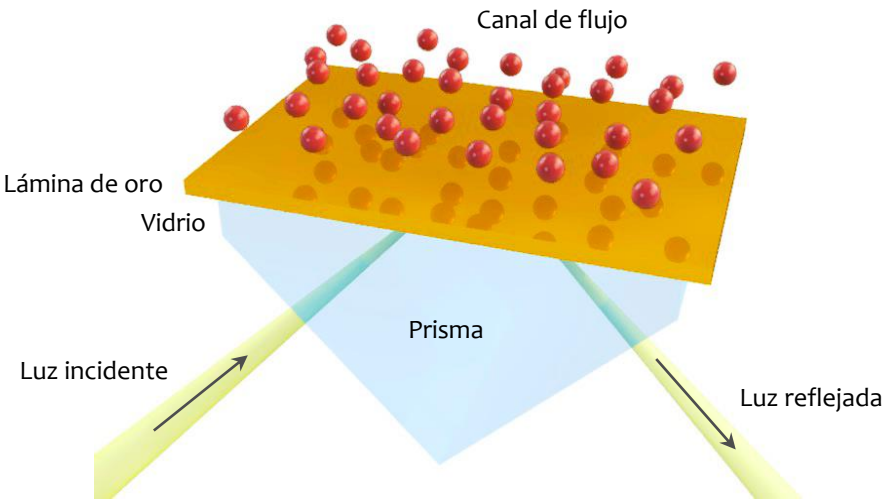

Figura 27. Representación esquemática de los componentes de un sistema de SPR.

El funcionamiento básico de un dispositivo de SPR consiste en hacer circular la disolución de la muestra sobre la superficie metálica mientras que se hace incidir radiación, con un ángulo y una longitud de onda determinados, sobre el prisma situado en la parte inferior. Una vez que la radiación atraviesa el prisma y llega a la superficie metálica, se produce la interacción con los electrones libres del metal y, si el ángulo y la longitud de onda incidentes son los adecuados, se origina una resonancia del plasmón superficial que interacciona con las sustancias presentes en la superficie metálica y, además, causa que la energía de la radiación incidente se pierda en la película metálica, ocasionando como resultado una disminución en la intensidad de la luz reflejada. Este fenómeno de resonancia ocurre exclusivamente para un ángulo concreto denominado ángulo de resonancia, el cual depende del índice de refracción del medio contiguo a la superficie metálica, de la longitud de onda de la radiación incidente, y del tipo de metal empleado, entre otros factores[315]. De esta manera, cualquier cambio producido en la superficie metálica o en sus proximidades (por ejemplo, la inmovilización de alguna molécula), originará la modificación del índice de refracción superficial que puede ser detectado como un desplazamiento en el ángulo de resonancia (Figura 28).

Así, midiendo la variación en el ángulo de resonancia es posible determinar información sobre la concentración de moléculas adsorbidas en la superficie metálica, las características de las interacciones moleculares entre las especies adsorbidas y otras sustancias presentes en la disolución (constantes de afinidad y cinéticas de unión) e incluso sobre ciertos cambios conformacionales sufridos por las moléculas adsorbidas.

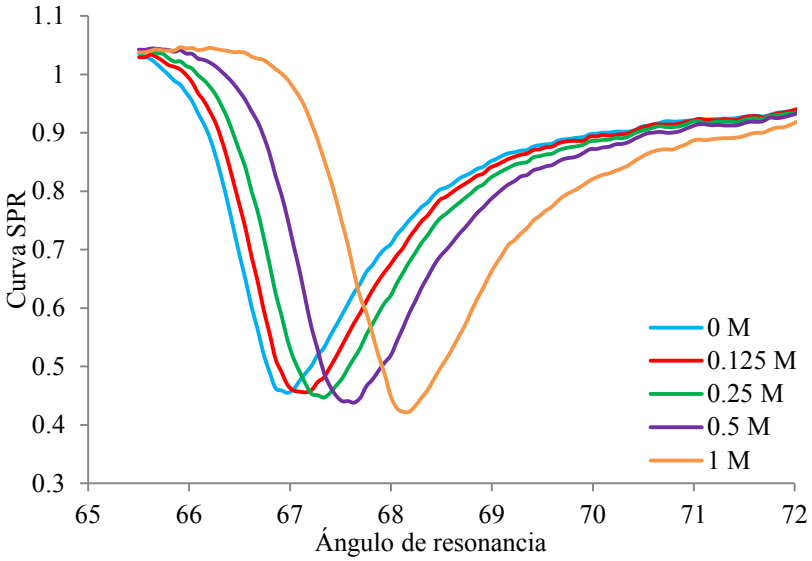

Figura 28. Curvas de SPR obtenidas para distintas concentraciones de NaOH en buffer fosfato.

Uno de los inconvenientes de esta técnica es su dificultad para detectar compuestos de bajo peso molecular (por debajo de los 500 Da) dado que las moléculas pequeñas originan cambios en el ángulo de resonancia demasiado pequeños y difícilmente detectables. Sin embargo, en los últimos años, este tipo de inconvenientes están siendo superados gracias a la mejora en los sistemas de detección y al incremento en la relación señal-ruido[316].

Entre las ventajas de los sistemas de SPR destacan su capacidad para medir en continuo y en tiempo real las interacciones que tienen lugar entre las biomoléculas y la superficie, la posibilidad de regenerar la superficie metálica tras cada uso mediante el lavado con determinados disolventes, siendo posible además monitorizar dicho procedimiento de regeneración, y su facilidad para ser miniaturizados e incluidos en la fabricación de biosensores portátiles para la detección *in situ* de, por ejemplo, compuestos de interés clínico y alimentario, y contaminantes medioambientales[317-319].

4.2. Integración del componente transductor en un biosensor

Para llevar a cabo la fabricación de un biosensor es necesario realizar la integración del componente biológico y del componente transductor en un único dispositivo. En la Sección 2 se detallan las técnicas empleadas para la inmovilización del componente biológico, siendo algunas de esas mismas técnicas las utilizadas también para la retención del elemento transductor.

En el caso de los biosensores electroquímicos, el propio electrodo es el que actúa como sistema de transducción, por lo que no es necesario realizar ningún tipo de operación para la integración del componente transductor en el biosensor. Pero en el caso de los biosensores ópticos sí que suele ser imprescindible, por lo general, efectuar la inmovilización del componente transductor en una localización en estrecho contacto con el componente biológico, excepto para los biosensores basados en resonancia de plasmón superficial en los que la propia superficie metálica es utilizada como elemento transductor.

Así, para la obtención de los biosensores ópticos basados en técnicas de absorción y luminiscencia se requiere de una etapa de inmovilización o retención de un determinado indicador colorimétrico o luminiscente, respectivamente, en un soporte adecuado. Este procedimiento de inmovilización constituye otra de las etapas clave en la fabricación de un biosensor, ya que tanto el tipo y la naturaleza del soporte, su composición química y su reactividad, así como el procedimiento de retención llevado a cabo, influyen de manera determinante en las propiedades del indicador inmovilizado.

Es por ello que los materiales empleados para la inmovilización de indicadores deben cumplir una serie de requisitos fundamentales[320, 321], entre los que destacan:

- Permeabilidad selectiva para permitir el paso de los analitos, evitando o minimizando el paso del resto de sustancias interferentes.
- Estabilidad estructural suficiente como para soportar esfuerzos mecánicos y resistencia a la degradación.
- Evitar la migración y el desprendimiento o lixiviación del indicador inmovilizado, así como prevenir su agregación.
- Mantener o mejorar la fotoestabilidad del indicador y su rendimiento cuántico.
- Proporcionar el entorno adecuado para incrementar la sensibilidad y la selectividad del indicador.

Las metodologías empleadas para llevar a cabo la inmovilización de los indicadores colorimétricos y luminiscentes en los soportes sólidos son muy variadas y abarcan desde la formación de enlaces covalentes o de afinidad, la adsorción física, la encapsulación y el atrapamiento, hasta técnicas como la deposición electroforética y el establecimiento de interacciones electrostáticas, o una combinación de varias ellas[321, 322].

Las metodologías de adsorción física, encapsulación y atrapamiento de los indicadores en soportes sólidos son técnicas ampliamente utilizadas en la fabricación de biosensores debido a su sencillez y a que suelen afectar en pequeña medida a las propiedades ópticas de los indicadores[323]. Los soportes más ampliamente utilizados para llevar a cabo este tipo de inmovilizaciones suelen ser materiales tipo sol-gel (los alcóxidos metálicos como el tetraetoxisilano (TEOS) y el tetrametoxisilano (TMOS) son los más utilizados para la preparación de este tipo de geles) y membranas y cápsulas poliméricas (formadas principalmente por polímeros como poliestireno, poli(metil metacrilato) y tereftalato de polietileno)[240, 324-327]. Sin embargo, en los últimos años se han desarrollado nuevos tipos de materiales micro y nanométricos que están aportando nuevas vías para realizar este tipo de inmovilizaciones. Así, por ejemplo, destaca el empleo de nanopartículas y nanofibras poliméricas con una alta capacidad de retención de indicadores en su interior, manteniendo además intactas sus propiedades ópticas y consiguiendo, en muchos casos, incrementar su sensibilidad, su selectividad y su tiempo de vida.

La inmovilización a través de la formación de enlaces covalentes constituye otra de las técnicas más comúnmente empleadas gracias, sobre todo, a que el establecimiento de enlaces covalentes con el soporte garantiza la retención del indicador y evita los procesos de lixiviación y desprendimiento del mismo[323, 328]. No obstante, durante la reacción o reacciones de inmovilización se puede producir la modificación química del indicador, con la consecuente alteración de sus propiedades ópticas.

La formación de este tipo de enlaces se puede originar fundamentalmente a través de dos metodologías: por un lado, mediante reacciones entre grupos reactivos presentes tanto en el soporte como en el indicador, como por ejemplo, grupos hidroxilo, haluros, tioles y éteres, entre otros, los cuales pueden formar parte de su composición o ser introducidos mediante procesos de funcionalización y activación previos; y por otro lado, mediante reacciones radicalarias inducidas térmica o fotoquímicamente[329-334].

Otra de las técnicas empleadas para llevar a cabo la inmovilización de indicadores es la conocida como deposición electroforética (EPD). Esta técnica consiste básicamente en un procedimiento de formación de láminas mediante la aplicación de una diferencia de potencial a una disolución o suspensión con especies cargadas[335-337]. Dicho procedimiento se suele llevar a cabo en una celda con dos electrodos como la representada en la Figura 29.

El mecanismo de la EPD implica dos etapas sucesivas. En primer lugar se aplica una diferencia de potencial entre los dos electrodos de la celda, de manera que las especies cargadas, ya sea en suspensión o disueltas, se desplazan hacia el electrodo de carga opuesta, en un proceso denominado electroforesis. En una segunda etapa conocida como deposición, las especies cargadas se acumulan en el electrodo y crean una lámina relativamente compacta y homogénea[336].

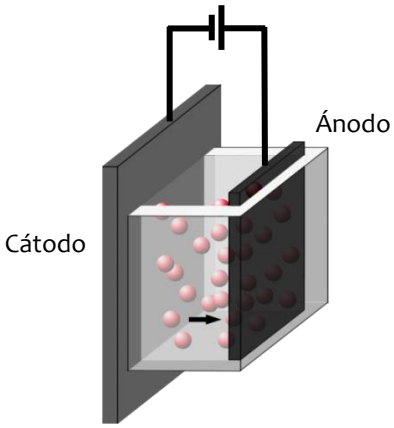

Figura 29. Celda con dos electrodos empleada para realizar la deposición electroforética.

Para poder aplicar esta técnica es necesario que las especies cargadas se encuentren distribuidas de manera homogénea en la disolución o la suspensión, con una alta estabilidad y con libertad para moverse cuando el campo eléctrico externo es aplicado. Así, es posible aplicar la EPD a sólidos en suspensión, tales como ciertos tipos de polímeros y compuestos metálicos, que cumplan esos requisitos.

Las características de las láminas obtenidas con esta técnica dependen de una serie de parámetros relacionados tanto con la naturaleza de la suspensión y las propiedades de los electrodos, como con las condiciones de procesado tales como voltaje aplicado y tiempo de deposición. Así, es posible controlar la morfología y el espesor de las láminas mediante la variación y selección de los tiempos de deposición y a través del control de los voltajes aplicados, los cuales pueden ser constantes o variables en el tiempo[335].

La selección del procedimiento de retención más adecuado para cada indicador depende de la aplicación final, del tipo de soporte sólido y de las características de permeabilidad, grado y tipo de retención y estabilidad que se le quieran dar al indicador inmovilizado. Es por ello que, al igual que ocurre con los procesos de inmovilización empleados para la retención del componente biológico, los procedimientos de retención del componente transductor deben ser seleccionados y optimizados durante la fabricación del biosensor, con el fin de alcanzar las mejores propiedades analíticas posibles para cada biosensor.

4.3. Microfluídica

El imparable avance de las nuevas tecnologías ligado a la fabricación de nuevos materiales ha propiciado la aparición de novedosos sistemas integrados que aportan innovadoras utilidades en el campo de los biosensores ópticos. Así, el desarrollo de la microfluídica, definida como la ciencia y tecnología de sistemas que operan con cantidades de fluidos del orden de los nanolitros e incluso inferiores, utilizando para ello canales y cámaras con dimensiones que no superan los centenares de micrómetros, ha favorecido la miniaturización de muchos procedimientos que anteriormente requerían cantidades relativamente grandes de reactivos y muestras y las instalaciones de laboratorios especializados[338, 339].

Estos sistemas de canales integrados se conocen como chips microfluídicos (Figura 30) y su principal utilidad se fundamenta en la capacidad para incorporar y aunar las etapas de tratamiento de las muestras, como purificación, separación y concentración de las mismas, las operaciones de ensayo y el proceso de detección en un único chip.

Los chips microfluídicos pueden a su vez integrar elementos químicos y bioquímicos junto con otros componentes como nanopartículas y nanofibras, o incluso con elementos ópticos o electrónicos[339-342]. Lo cual los convierte en una poderosa herramienta posibilitando enormemente su aplicación en ámbitos como la monitorización clínica, el análisis medioambiental y la biomedicina.

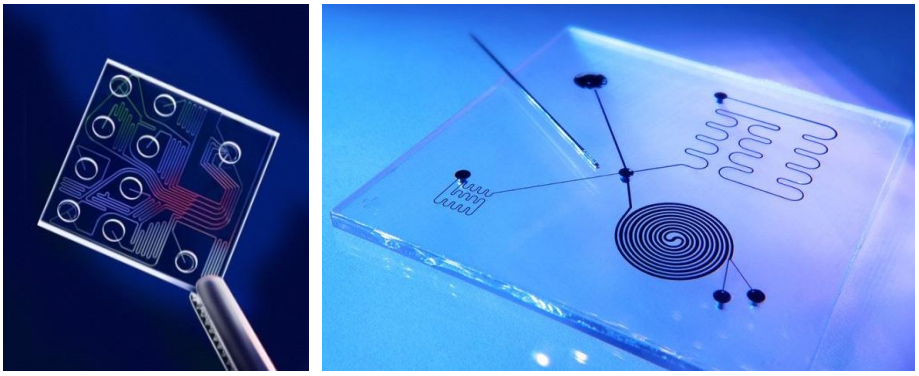

Figura 30. Chips de microfluídica donde se aprecian los canales integrados.

En comparación con las técnicas de análisis convencionales, la microfluídica y el empleo de estos sistemas de canales y cámaras integrados presentan numerosas ventajas, entre las que destacan un consumo reducido de muestras y reactivos, el establecimiento de un entorno controlado donde manipular fluidos, moléculas y partículas, la posibilidad de realizar análisis múltiples en paralelo en un mismo chip con un alto rendimiento, sensibilidad y rapidez, la facilidad de automatización, y la reducción de los costes de cada análisis[343, 344]. Además, las

reducidas dimensiones de estos chips hacen posible que puedan ser utilizados para la fabricación de dispositivos como los denominados *Point-of-Care* (POC), que permiten la realización de tests de diagnóstico rápidos fuera de los laboratorios especializados[343].

Otra de las características fundamentales de los chips de microfluídica es que las propiedades del material empleado para la fabricación del chip determinan su función y aplicación, y cada tipo de material requiere por lo general una estrategia de fabricación específica.

Entre los materiales más ampliamente utilizados para la fabricación de los chips predominan el vidrio, el silicio y los polímeros tanto plásticos como elastómeros[345-347]. De entre ellos, el vidrio y el silicio fueron los primeros en ser utilizados gracias a su resistencia a los disolventes orgánicos, a su alta conductividad térmica y a su capacidad para producir una movilidad estable de los fluidos. Sin embargo, debido al alto coste de procesado y fabricación de los chips, estos materiales han sido reemplazados en la mayoría de las aplicaciones por polímeros sintéticos, con un mucho menor coste y una mayor rapidez de fabricación.

Como polímeros plásticos se han utilizado comúnmente poliestireno (PS), poli(metil metacrilato) (PMMA) y tereftalato de polietileno (PET); mientras que como materiales elastómeros destacan el polidimetilsiloxano (PDMS), los perfluoropoliéteres (PFPEs) y los elastómeros termoplásticos estirénicos (TPEs)[344, 347]. Estos materiales poliméricos presentan diferentes propiedades de permeabilidad, biocompatibilidad, flexibilidad y estabilidad frente a disolventes orgánicos, por lo que generalmente la elección del material depende del tipo de aplicación en la cual va a ser utilizado. Es necesario mencionar además, que los materiales poliméricos presentan la ventaja de poder ser modificados y combinados para ajustar sus propiedades, haciéndolas más adecuadas para cada aplicación particular.

4.4. Aplicaciones y expectativas de futuro de los biosensores ópticos

A lo largo de esta introducción se han dado pequeñas pinceladas del enorme y variado campo que abarcan los biosensores ópticos y de su gran versatilidad y aplicabilidad, contando con numerosos diseños y utilidades.

En los últimos años, el estudio sobre el desarrollo, el diseño y las aplicaciones de nuevos biosensores ópticos ha sido abordado en una cantidad ingente de publicaciones científicas, incluyendo multitud de revisiones y libros de diversa índole. Así, por ejemplo, es posible

encontrar una gran variedad de publicaciones recientes sobre la aplicación de biosensores ópticos en el ámbito alimentario[348-351], biomédico y clínico[352-356], y medioambiental[357-359]. Asimismo, también se pueden encontrar publicaciones sobre biosensores ópticos en función del tipo de material sobre el que se depositan e inmovilizan los elementos biológicos[360-364].

El conjunto de toda esta cantidad de aplicaciones demuestra el potencial de los biosensores ópticos y constituye un claro ejemplo de la importancia que el diseño y desarrollo de nuevos biosensores está teniendo en la actualidad. Parte de ese potencial es debido principalmente a determinadas ventajas que presentan los biosensores ópticos sobre el resto de métodos analíticos de detección convencionales, entre las que destacan: tiempos reducidos de análisis, elevada especificidad (aportada por la reacción de reconocimiento biológico entre la biomolécula y la especie de interés), amplio rango dinámico y, en muchos casos, bajos límites de detección y cuantificación. Todas estas ventajas unidas a la posibilidad de integrar los biosensores en sistemas nanotecnológicos, abren un enorme abanico de oportunidades con nuevos diseños, estrategias y aplicaciones en la detección de una gran variedad de analitos en multitud de muestras de distinta naturaleza y complejidad.

Así, es posible identificar algunos de los factores que son y serán claves en el futuro de los biosensores ópticos, destacando: la disponibilidad de nuevas metodologías de inmovilización que mejoren las propiedades de las biomoléculas inmovilizadas, fundamentalmente en lo que se refiere a su estabilidad y retención de actividad biológica; el desarrollo de nuevos materiales para la inmovilización de biomoléculas, así como, de nuevos indicadores ópticos con mejores propiedades de estabilidad, tiempo de vida y sensibilidad; el perfeccionamiento de las técnicas de medida, de manera que sea posible obtener una amplificación y mejora de las señales analíticas, que se traduzca en una mayor sensibilidad de detección y análisis; y el diseño de nuevos sistemas miniaturizados, portátiles y automáticos, que permitan minimizar el tiempo de análisis y realizar las mediciones fuera del laboratorio. La consecución de todas estas características está haciendo y hará aún más en el futuro, que los biosensores ópticos se conviertan en unas eficientes y potentes herramientas en la determinación de multitud de analitos con elevada selectividad y sensibilidad.

REFERENCIAS

1. Ispas, C. R.; Crivat, G.; Andreescu, S., Review: Recent Developments in Enzyme-Based Biosensors for Biomedical Analysis. Analytical Letters 2012, 45, (2-3), 168-186.
2. D'Souza, S. F., Microbial biosensors. Biosensors and Bioelectronics 2001, 16, (6), 337-353.
3. Wu, C.; Lillehoj, P. B.; Wang, P., Bioanalytical and chemical sensors using living taste, olfactory, and neural cells and tissues: a short review. Analyst 2015, 140, (21), 7048-7061.
4. Wong, C. M.; Wong, K. H.; Chen, X. D., Glucose oxidase: natural occurrence, function, properties and industrial applications. Applied Microbiology and Biotechnology 2008, 78, (6), 927-938.
5. Rassaei, L.; Olthuis, W.; Tsujimura, S.; Sudhölter, E. J. R.; van den Berg, A., Lactate biosensors: current status and outlook. Analytical and Bioanalytical Chemistry 2014, 406, (1), 123-137.
6. Arya, S. K.; Datta, M.; Malhotra, B. D., Recent advances in cholesterol biosensor. Biosensors and Bioelectronics 2008, 23, (7), 1083-1100.
7. Pohanka, M., Cholinesterases in Biorecognition and Biosensors Construction: A Review. Analytical Letters 2013, 46, (12), 1849-1868.
8. Menti, C.; Henriques, J. A. P.; Missell, F. P.; Roesch-Ely, M., Antibody-based magneto-elastic biosensors: potential devices for detection of pathogens and associated toxins. Applied Microbiology and Biotechnology 2016, 100, (14), 6149-6163.
9. Manzanares-Palenzuela, C. L.; Martín-Fernández, B.; Sánchez-Paniagua López, M.; López-Ruiz, B., Electrochemical genosensors as innovative tools for detection of genetically modified organisms. TrAC Trends in Analytical Chemistry 2015, 66, 19-31.
10. McLachlan, M. J.; Katzenellenbogen, J. A.; Zhao, H., A new fluorescence complementation biosensor for detection of estrogenic compounds. Biotechnology and Bioengineering 2011, 108, (12), 2794-2803.
11. Ricci, F.; Volpe, G.; Micheli, L.; Palleschi, G., A review on novel developments and applications of immunosensors in food analysis. Analytica Chimica Acta 2007, 605, (2), 111-129.
12. Catanante, G.; Rhouati, A.; Hayat, A.; Marty, J. L., An Overview of Recent Electrochemical Immunosensing Strategies for Mycotoxins Detection. Electroanalysis 2016, 28, (8), 1750-1763.
13. Yoo, S. M.; Lee, S. Y., Optical Biosensors for the Detection of Pathogenic Microorganisms. Trends in Biotechnology 2016, 34, (1), 7-25.
14. Benito-Peña, E.; Valdés, M. G.; Glahn-Martínez, B.; Moreno-Bondi, M. C., Fluorescence based fiber optic and planar waveguide biosensors. A review. Analytica Chimica Acta 2016, 943, 17-40.
15. Tereshchenko, A.; Bechelany, M.; Viter, R.; Khranovskyy, V.; Smyntyna, V.; Starodub, N.; Yakimova, R., Optical biosensors based on ZnO nanostructures: advantages and perspectives. A review. Sensors and Actuators B: Chemical 2016, 229, 664-677.
16. Homola, J., Surface Plasmon Resonance Sensors for Detection of Chemical and Biological Species. Chemical Reviews 2008, 108, (2), 462-493.

17. Sharma, H.; Mutharasan, R., Review of biosensors for foodborne pathogens and toxins. Sensors and Actuators B: Chemical 2013, 183, 535-549.
18. Hasanzadeh, M.; Shadjou, N., Electrochemical nanobiosensing in whole blood: Recent advances. TrAC Trends in Analytical Chemistry 2016, 80, 167-176.
19. Weltin, A.; Kieninger, J.; Urban, G. A., Microfabricated, amperometric, enzyme-based biosensors for in vivo applications. Analytical and Bioanalytical Chemistry 2016, 408, (17), 4503-4521.
20. Laocharoensuk, R., Development of Electrochemical Immunosensors towards Point-of-care Cancer Diagnostics: Clinically Relevant Studies. Electroanalysis 2016, 28, (8), 1716-1729.
21. Vasilescu, A.; Nunes, G.; Hayat, A.; Latif, U.; Marty, J.-L., Electrochemical Affinity Biosensors Based on Disposable Screen-Printed Electrodes for Detection of Food Allergens. Sensors 2016, 16, (11), 1863.
22. Nigam, V. K.; Shukla, P., Enzyme based biosensors for detection of environmental pollutants-A review. Journal of Microbiology and Biotechnology 2015, 25, (11), 1773-1781.
23. Liu, S.; Zheng, Z.; Li, X., Advances in pesticide biosensors: current status, challenges, and future perspectives. Analytical and Bioanalytical Chemistry 2013, 405, (1), 63-90.
24. Gaddes, D. E.; Tadigadapa, S. In A calorimetric biosensing system for clinical diagnostic applications, 2015 IEEE SENSORS - Proceedings, 2015; 2015.
25. Bhand, S. G.; Soundararajan, S.; Surugiu-Wärnmark, I.; Milea, J. S.; Dey, E. S.; Yakovleva, M.; Danielsson, B., Fructose-selective calorimetric biosensor in flow injection analysis. Analytica Chimica Acta 2010, 668, (1), 13-18.
26. Ramanathan, K.; Jönsson, B. R.; Danielsson, B., Sol–gel based thermal biosensor for glucose. Analytica Chimica Acta 2001, 427, (1), 1-10.
27. Antonelli, M. L.; Spadaro, C.; Tornelli, R. F., A microcalorimetric sensor for food and cosmetic analyses: l-Malic acid determination. Talanta 2008, 74, (5), 1450-1454.
28. Ramanathan, K.; Rank, M.; Svitel, J.; Dzgoev, A.; Danielsson, B., The development and applications of thermal biosensors for bioprocess monitoring. Trends in Biotechnology 1999, 17, (12), 499-505.
29. Halámek, J.; Teller, C.; Žeravík, J.; Fournier, D.; Makower, A.; Scheller, F. W., Characterization of Binding of Cholinesterases to Surface Immobilized Ligands. Analytical Letters 2006, 39, (8), 1491-1502.
30. Skládal, P.; Riccardi, C. d. S.; Yamanaka, H.; da Costa, P. I., Piezoelectric biosensors for real-time monitoring of hybridization and detection of hepatitis C virus. Journal of Virological Methods 2004, 117, (2), 145-151.
31. Minunni, M.; Tombelli, S.; Scielzi, R.; Mannelli, I.; Mascini, M.; Gaudiano, C., Detection of β-thalassemia by a DNA piezoelectric biosensor coupled with polymerase chain reaction. Analytica Chimica Acta 2003, 481, (1), 55-64.

32. Wong, Y. Y.; Ng, S. P.; Ng, M. H.; Si, S. H.; Yao, S. Z.; Fung, Y. S., Immunosensor for the differentiation and detection of Salmonella species based on a quartz crystal microbalance. Biosensors and Bioelectronics 2002, 17, (8), 676-684.
33. Mannelli, I.; Minunni, M.; Tombelli, S.; Mascini, M., Quartz crystal microbalance (QCM) affinity biosensor for genetically modified organisms (GMOs) detection. Biosensors and Bioelectronics 2003, 18, (2–3), 129-140.
34. Sassolas, A.; Blum, L. J.; Leca-Bouvier, B. D., Immobilization strategies to develop enzymatic biosensors. Biotechnology Advances 2012, 30, (3), 489-511.
35. Homaei, A. A.; Sariri, R.; Vianello, F.; Stevanato, R., Enzyme immobilization: an update. Journal of Chemical Biology 2013, 6, (4), 185-205.
36. Mohamad, N. R.; Marzuki, N. H. C.; Buang, N. A.; Huyop, F.; Wahab, R. A., An overview of technologies for immobilization of enzymes and surface analysis techniques for immobilized enzymes. Biotechnology & Biotechnological Equipment 2015, 29, (2), 205-220.
37. van de Velde, F.; Lourenço, N. D.; Pinheiro, H. M.; Bakker, M., Carrageenan: A Food-Grade and Biocompatible Support for Immobilisation Techniques. Advanced Synthesis & Catalysis 2002, 344, (8), 815-835.
38. Jesionowski, T.; Zdarta, J.; Krajewska, B., Enzyme immobilization by adsorption: a review. Adsorption 2014, 20, (5), 801-821.
39. Putzbach, W.; Ronkainen, N., Immobilization Techniques in the Fabrication of Nanomaterial-Based Electrochemical Biosensors: A Review. Sensors 2013, 13, (4), 4811.
40. Hanefeld, U.; Gardossi, L.; Magner, E., Understanding enzyme immobilisation. Chemical Society Reviews 2009, 38, (2), 453-468.
41. Costa, S. A.; Azevedo, H.; Reis, R., Enzyme Immobilization in Biodegradable Polymers for Biomedical Applications. In Biodegradable Systems in Tissue Engineering and Regenerative Medicine, CRC Press: 2004.
42. Hermanson, G. T., Chapter 11 - (Strept)avidin–Biotin Systems. In Bioconjugate Techniques (Third edition), Academic Press: Boston, 2013; pp 465-505.
43. Wilchek, M.; Bayer, E. A.; Livnah, O., Essentials of biorecognition: The (strept)avidin–biotin system as a model for protein–protein and protein–ligand interaction. Immunology Letters 2006, 103, (1), 27-32.
44. Wang, B.; Anzai, J.-i., Recent Progress in Lectin-Based Biosensors. Materials 2015, 8, (12), 5478.
45. Hernandez, K.; Fernandez-Lafuente, R., Control of protein immobilization: Coupling immobilization and site-directed mutagenesis to improve biocatalyst or biosensor performance. Enzyme and Microbial Technology 2011, 48, (2), 107-122.
46. Smith, C. L.; Milea, J. S.; Nguyen, G. H., Immobilization of Nucleic Acids Using Biotin-Strept(avidin) Systems. In Immobilisation of DNA on Chips II, Wittmann, C., Ed. Springer Berlin Heidelberg: Berlin, Heidelberg, 2005; pp 63-90.

47. Ferenčík, M., Immunochemical methods. In Handbook of Immunochemistry, Springer Netherlands: Dordrecht, 1993; pp 309-386.
48. Elia, G., Protein Biotinylation. In Current Protocols in Protein Science, John Wiley & Sons, Inc.: 2001.
49. Hall, E. A. H.; Chen, S.; Chun, J.; Du, Y.; Zhao, Z., A molecular biology approach to protein coupling at a biosensor interface. TrAC Trends in Analytical Chemistry 2016, 79, 247-256.
50. Miura, Y.; Hoshino, Y.; Seto, H., Glycopolymer nanobiotechnology. Chemical Reviews 2016, 116, (4), 1673-1692.
51. Bojarova, P.; Kren, V., Sugared biomaterial binding lectins: achievements and perspectives. Biomaterials Science 2016, 4, (8), 1142-1160.
52. Arnaud, J.; Audfray, A.; Imberty, A., Binding sugars: from natural lectins to synthetic receptors and engineered neolectins. Chemical Society Reviews 2013, 42, (11), 4798-4813.
53. Ovsejevi, K.; Manta, C.; Batista-Viera, F., Reversible Covalent Immobilization of Enzymes via Disulfide Bonds. In Immobilization of Enzymes and Cells: Third Edition, Guisan, J. M., Ed. Humana Press: Totowa, NJ, 2013; pp 89-116.
54. Mihailović, M.; Trbojević-Ivić, J.; Banjanac, K.; Milosavić, N.; Velicković, D.; Carević, M.; Bezbradica, D., Immobilization of maltase from Saccharomyces cerevisiae on thiosulfonate supports. Journal of the Serbian Chemical Society 2016, 81, (12), 1371-1382.
55. Alemán, E. A.; Pedini, H. S.; Rueda, D., Covalent-bond-based immobilization approaches for single-molecule fluorescence. ChemBioChem 2009, 10, (18), 2862-2866.
56. Hermanson, G. T., Chapter 2 - Functional Targets for Bioconjugation. In Bioconjugate Techniques (Third edition), Academic Press: Boston, 2013; pp 127-228.
57. Mateo, C.; Grazu, V.; Guisan, J. M., Immobilization of Enzymes on Monofunctional and Heterofunctional Epoxy-Activated Supports. In Immobilization of Enzymes and Cells: Third Edition, Guisan, J. M., Ed. Humana Press: Totowa, NJ, 2013; pp 43-57.
58. Brena, B.; González-Pombo, P.; Batista-Viera, F., Immobilization of Enzymes: A Literature Survey. In Immobilization of Enzymes and Cells: Third Edition, Guisan, J. M., Ed. Humana Press: Totowa, NJ, 2013; pp 15-31.
59. Hermanson, G. T., Chapter 3 - The Reactions of Bioconjugation. In Bioconjugate Techniques (Third edition), Academic Press: Boston, 2013; pp 229-258.
60. Hermanson, G. T., Chapter 14 - Microparticles and Nanoparticles. In Bioconjugate Techniques (Third edition), Academic Press: Boston, 2013; pp 549-587.
61. Zucca, P.; Sanjust, E., Inorganic Materials as Supports for Covalent Enzyme Immobilization: Methods and Mechanisms. Molecules 2014, 19, (9), 14139.
62. Yu, Q.; Wang, Q.; Li, B.; Lin, Q.; Duan, Y., Technological Development of Antibody Immobilization for Optical Immunoassays: Progress and Prospects. Critical Reviews in Analytical Chemistry 2015, 45, (1), 62-75.

63. Demirci Uzun, S.; Kayaci, F.; Uyar, T.; Timur, S.; Toppare, L., Bioactive Surface Design Based on Functional Composite Electrospun Nanofibers for Biomolecule Immobilization and Biosensor Applications. ACS Applied Materials & Interfaces 2014, 6, (7), 5235-5243.
64. Mashhadizadeh, M. H.; Pourtaghavi Talemi, R., A highly sensitive and selective hepatitis B DNA biosensor using gold nanoparticle electrodeposition on an Au electrode and mercaptobenzaldehyde. Analytical Methods 2014, 6, (22), 8956-8964.
65. Twala, B. V.; Sewell, B. T.; Jordaan, J., Immobilisation and characterisation of biocatalytic co-factor recycling enzymes, glucose dehydrogenase and NADH oxidase, on aldehyde functional ReSyn™ polymer microspheres. Enzyme and Microbial Technology 2012, 50, (6–7), 331-336.
66. Vasylieva, N.; Barnych, B.; Meiller, A.; Maucler, C.; Pollegioni, L.; Lin, J.-S.; Barbier, D.; Marinesco, S., Covalent enzyme immobilization by poly(ethylene glycol) diglycidyl ether (PEGDE) for microelectrode biosensor preparation. Biosensors and Bioelectronics 2011, 26, (10), 3993-4000.
67. Mateo, C.; Torres, R.; Fernández-Lorente, G.; Ortiz, C.; Fuentes, M.; Hidalgo, A.; López-Gallego, F.; Abian, O.; Palomo, J. M.; Betancor, L.; Pessela, B. C. C.; Guisan, J. M.; Fernández-Lafuente, R., Epoxy-Amino Groups: A New Tool for Improved Immobilization of Proteins by the Epoxy Method. Biomacromolecules 2003, 4, (3), 772-777.
68. Arora, J.; Nandwani, S.; Bhambi, M.; Pundir, C. S., Fabrication of dissolved O2 metric uric acid biosensor using uricase epoxy resin biocomposite membrane. Analytica Chimica Acta 2009, 647, (2), 195-201.
69. Dagar, K.; Pundir, C. S., An improved amperometric L-lactate biosensor based on covalent immobilization of microbial lactate oxidase onto carboxylated multiwalled carbon nanotubes/copper nanoparticles/polyaniline modified pencil graphite electrode. Enzyme and Microbial Technology 2017, 96, 177-186.
70. Kumar, V.; Misra, N.; Paul, J.; Dhanawade, B. R.; Varshney, L., Uricase-immobilization on radiation grafted polymer support for detection of uric acid using Ag-nanoparticle based optical biosensor. Polymer 2014, 55, (11), 2652-2660.
71. Stolarow, J.; Heinzelmann, M.; Yeremchuk, W.; Syldatk, C.; Hausmann, R., Immobilization of trypsin in organic and aqueous media for enzymatic peptide synthesis and hydrolysis reactions. BMC Biotechnology 2015, 15, (1), 77.
72. Mahmoudifard, M.; Soudi, S.; Soleimani, M.; Hosseinzadeh, S.; Esmaeili, E.; Vossoughi, M., Efficient protein immobilization on polyethersolfone electrospun nanofibrous membrane via covalent binding for biosensing applications. Materials Science and Engineering: C 2016, 58, 586-594.
73. Hermanson, G. T., Chapter 4 - Zero-Length Crosslinkers. In Bioconjugate Techniques (Third edition), Academic Press: Boston, 2013; pp 259-273.
74. Delvaux, M.; Demoustier-Champagne, S., Immobilisation of glucose oxidase within metallic nanotubes arrays for application to enzyme biosensors. Biosensors and Bioelectronics 2003, 18, (7), 943-951.

75. Mohiuddin, M.; Arbain, D.; Islam, A. K. M. S.; Ahmad, M. S.; Ahmad, M. N., Alpha-Glucosidase Enzyme Biosensor for the Electrochemical Measurement of Antidiabetic Potential of Medicinal Plants. Nanoscale Research Letters 2016, 11, (1), 95.
76. Boujakhrout, A.; Jimenez-Falcao, S.; Martinez-Ruiz, P.; Sanchez, A.; Diez, P.; Pingarron, J. M.; Villalonga, R., Novel reduced graphene oxide-glycol chitosan nanohybrid for the assembly of an amperometric enzyme biosensor for phenols. Analyst 2016, 141, (13), 4162-4169.
77. Torrance, L.; Ziegler, A.; Pittman, H.; Paterson, M.; Toth, R.; Eggleston, I., Oriented immobilisation of engineered single-chain antibodies to develop biosensors for virus detection. Journal of Virological Methods 2006, 134, (1–2), 164-170.
78. Yang, H.-M.; Bao, R.-M.; Cheng, Y.-Z.; Tang, J.-B., Site-specific covalent attachment of an engineered Z-domain onto a solid matrix: An efficient platform for 3D IgG immobilization. Analytica Chimica Acta 2015, 872, 1-6.
79. Yucel, D.; Ozer, N.; Hasirci, V., Construction of a choline biosensor through enzyme immobilization on a poly(2-hydroxyethyl methacrylate)-grafted teflon film. Journal of Applied Polymer Science 2007, 104, (5), 3469-3477.
80. Böcking, T.; Kilian, K. A.; Hanley, T.; Ilyas, S.; Gaus, K.; Gal, M.; Gooding, J. J., Formation of Tetra(ethylene oxide) Terminated Si−C Linked Monolayers and Their Derivatization with Glycine: An Example of a Generic Strategy for the Immobilization of Biomolecules on Silicon. Langmuir 2005, 21, (23), 10522-10529.
81. Medina-Castillo, A. L.; Morales-Sanfrutos, J.; Megia-Fernandez, A.; Fernandez-Sanchez, J. F.; Santoyo-Gonzalez, F.; Fernandez-Gutierrez, A., Novel synthetic route for covalent coupling of biomolecules on super-paramagnetic hybrid nanoparticles. Journal of Polymer Science Part A: Polymer Chemistry 2012, 50, (19), 3944-3953.
82. Morales-Sanfrutos, J.; Lopez-Jaramillo, J.; Ortega-Munoz, M.; Megia-Fernandez, A.; Perez-Balderas, F.; Hernandez-Mateo, F.; Santoyo-Gonzalez, F., Vinyl sulfone: a versatile function for simple bioconjugation and immobilization. Organic & Biomolecular Chemistry 2010, 8, (3), 667-675.
83. Baslé, E.; Joubert, N.; Pucheault, M., Protein Chemical Modification on Endogenous Amino Acids. Chemistry & Biology 2010, 17, (3), 213-227.
84. Talley, K.; Alexov, E., On the pH-optimum of activity and stability of proteins. Proteins 2010, 78, (12), 2699-2706.
85. Liu, Y.; Yu, J., Oriented immobilization of proteins on solid supports for use in biosensors and biochips: a review. Microchimica Acta 2016, 183, (1), 1-19.
86. Cao, L., Covalent Enzyme Immobilization. In Carrier-bound Immobilized Enzymes, Wiley-VCH Verlag GmbH & Co. KGaA: 2006; pp 169-316.
87. Jiang, H.; Xu, F.-J., Biomolecule-functionalized polymer brushes. Chemical Society Reviews 2013, 42, (8), 3394-3426.

88. Costa, F.; Carvalho, I. F.; Montelaro, R. C.; Gomes, P.; Martins, M. C. L., Covalent immobilization of antimicrobial peptides (AMPs) onto biomaterial surfaces. Acta Biomaterialia 2011, 7, (4), 1431-1440.
89. Singh, P.; Morris, H.; Tivanski, A. V.; Kohen, A., Determination of concentration and activity of immobilized enzymes. Analytical Biochemistry 2015, 484, 169-172.
90. Goda, T.; Higashi, D.; Matsumoto, A.; Hoshi, T.; Sawaguchi, T.; Miyahara, Y., Dual aptamer-immobilized surfaces for improved affinity through multiple target binding in potentiometric thrombin biosensing. Biosensors and Bioelectronics 2015, 73, 174-180.
91. López-Gallego, F.; Fernandez-Lorente, G.; Rocha-Martin, J.; Bolivar, J. M.; Mateo, C.; Guisan, J. M., Stabilization of Enzymes by Multipoint Covalent Immobilization on Supports Activated with Glyoxyl Groups. In Immobilization of Enzymes and Cells: Third Edition, Guisan, J. M., Ed. Humana Press: Totowa, NJ, 2013; pp 59-71.
92. Balcão, V. M.; Vila, M. M. D. C., Structural and functional stabilization of protein entities: state-of-the-art. Advanced Drug Delivery Reviews 2015, 93, 25-41.
93. Yan, E.-K.; Cao, H.-L.; Zhang, C.-Y.; Lu, Q.-Q.; Ye, Y.-J.; He, J.; Huang, L.-J.; Yin, D.-C., Cross-linked protein crystals by glutaraldehyde and their applications. RSC Advances 2015, 5, (33), 26163-26174.
94. Talekar, S.; Joshi, A.; Joshi, G.; Kamat, P.; Haripurkar, R.; Kambale, S., Parameters in preparation and characterization of cross linked enzyme aggregates (CLEAs). RSC Advances 2013, 3, (31), 12485-12511.
95. Cui, J. D.; Jia, S. R., Optimization protocols and improved strategies of cross-linked enzyme aggregates technology: current development and future challenges. Critical Reviews in Biotechnology 2015, 35, (1), 15-28.
96. Sheldon, R. A., Characteristic features and biotechnological applications of cross-linked enzyme aggregates (CLEAs). Applied Microbiology and Biotechnology 2011, 92, (3), 467-477.
97. Sheldon, R. A.; van Pelt, S., Enzyme immobilisation in biocatalysis: why, what and how. Chemical Society Reviews 2013, 42, (15), 6223-6235.
98. Basak, S.; Punetha, V. D.; Bisht, G.; Bisht, S. S.; Sahoo, N. G.; Cho, J. W., Recent Trends of Polymer-Protein Conjugate Application in Biocatalysis: A Review. Polymer Reviews 2015, 55, (1), 163-198.
99. Vaghjiani, J. D.; Lee, T. S.; Lye, G. J.; Turner, M. K., Production and Characterisation of Cross-Linked Enzyme Crystals (Clecs®) for Application as Process Scale Biocatalysts. Biocatalysis and Biotransformation 2000, 18, (2), 151-175.
100. Jegan Roy, J.; Emilia Abraham, T., Strategies in Making Cross-Linked Enzyme Crystals. Chemical Reviews 2004, 104, (9), 3705-3722.
101. Sheldon, R. A., Cross-Linked Enzyme Aggregates as Industrial Biocatalysts. Organic Process Research & Development 2011, 15, (1), 213-223.

102. Sheldon, R. A.; Schoevaart, R.; Van Langen, L. M., Cross-linked enzyme aggregates (CLEAs): A novel and versatile method for enzyme immobilization (a review). Biocatalysis and Biotransformation 2005, 23, (3-4), 141-147.
103. Sheldon, R. A., Enzyme Immobilization: The Quest for Optimum Performance. Advanced Synthesis & Catalysis 2007, 349, (8-9), 1289-1307.
104. Brady, D.; Jordaan, J., Advances in enzyme immobilisation. Biotechnology Letters 2009, 31, (11), 1639.
105. Cao, L., Enzyme Entrapment. In Carrier-bound Immobilized Enzymes, Wiley-VCH Verlag GmbH & Co. KGaA: 2006; pp 317-395.
106. Jin, W.; Brennan, J. D., Properties and applications of proteins encapsulated within sol–gel derived materials. Analytica Chimica Acta 2002, 461, (1), 1-36.
107. Gupta, R.; Chaudhury, N. K., Entrapment of biomolecules in sol–gel matrix for applications in biosensors: Problems and future prospects. Biosensors and Bioelectronics 2007, 22, (11), 2387-2399.
108. Avnir, D.; Coradin, T.; Lev, O.; Livage, J., Recent bio-applications of sol-gel materials. Journal of Materials Chemistry 2006, 16, (11), 1013-1030.
109. Park, B.-W.; Yoon, D.-Y.; Kim, D.-S., Recent progress in bio-sensing techniques with encapsulated enzymes. Biosensors and Bioelectronics 2010, 26, (1), 1-10.
110. Cao, L., Enzyme Encapsulation. In Carrier-bound Immobilized Enzymes, Wiley-VCH Verlag GmbH & Co. KGaA: 2006; pp 397-448.
111. Cao, L., Unconventional Enzyme Immobilization. In Carrier-bound Immobilized Enzymes, Wiley-VCH Verlag GmbH & Co. KGaA: 2006; pp 449-549.
112. Cao, L., Adsorption-based Immobilization. In Carrier-bound Immobilized Enzymes, Wiley-VCH Verlag GmbH & Co. KGaA: 2006; pp 53-168.
113. Barbosa, O.; Torres, R.; Ortiz, C.; Berenguer-Murcia, Á.; Rodrigues, R. C.; Fernandez-Lafuente, R., Heterofunctional Supports in Enzyme Immobilization: From Traditional Immobilization Protocols to Opportunities in Tuning Enzyme Properties. Biomacromolecules 2013, 14, (8), 2433-2462.
114. Lavanya, N.; Radhakrishnan, S.; Sekar, C., Fabrication of hydrogen peroxide biosensor based on Ni doped SnO2 nanoparticles. Biosensors and Bioelectronics 2012, 36, (1), 41-47.
115. Shi, X.; Gu, W.; Li, B.; Chen, N.; Zhao, K.; Xian, Y., Enzymatic biosensors based on the use of metal oxide nanoparticles. Microchimica Acta 2014, 181, (1), 1-22.
116. Kucherenko, I.; Soldatkin, O.; Kasap, B. O.; Kirdeciler, S. K.; Kurc, B. A.; Jaffrezic-Renault, N.; Soldatkin, A.; Lagarde, F.; Dzyadevych, S., Nanosized zeolites as a perspective material for conductometric biosensors creation. Nanoscale Research Letters 2015, 10, (1).
117. Hasanzadeh, M.; Shadjou, N.; Eskandani, M.; Guardia, M. d. l., Mesoporous silica-based materials for use in electrochemical enzyme nanobiosensors. TrAC Trends in Analytical Chemistry 2012, 40, 106-118.

118. Bahadır, E. B.; Sezgintürk, M. K., Applications of graphene in electrochemical sensing and biosensing. TrAC Trends in Analytical Chemistry 2016, 76, 1-14.
119. Gong, N. C.; Li, Y. L.; Jiang, X.; Zheng, X. F.; Wang, Y. Y.; Huan, S. Y., Fluorescence resonance energy transfer-based biosensor composed of nitrogen-doped carbon dots and gold nanoparticles for the highly sensitive detection of organophosphorus pesticides. Analytical Sciences 2016, 32, (9), 951-956.
120. Kaivosoja, E.; Tujunen, N.; Jokinen, V.; Protopopova, V.; Heinilehto, S.; Koskinen, J.; Laurila, T., Glutamate detection by amino functionalized tetrahedral amorphous carbon surfaces. Talanta 2015, 141, 175-181.
121. Fan, Z.; Lin, Q.; Gong, P.; Liu, B.; Wang, J.; Yang, S., A new enzymatic immobilization carrier based on graphene capsule for hydrogen peroxide biosensors. Electrochimica Acta 2015, 151, 186-194.
122. Luo, Z.; Fu, X., Immobilization of urease on dialdehyde porous starch. Starch - Stärke 2010, 62, (12), 652-657.
123. Pohanka, M.; Vlcek, V., Preparation and performance of a colorimetric biosensor using acetylcholinesterase and indoxylacetate for assay of nerve agents and drugs. In Interdisciplinary Toxicology, 2014; Vol. 7, p 215.
124. Chandra Sekar, N.; Mousavi Shaegh, S. A.; Ng, S. H.; Ge, L.; Tan, S. N., A paper-based amperometric glucose biosensor developed with Prussian Blue-modified screen-printed electrodes. Sensors and Actuators B: Chemical 2014, 204, 414-420.
125. Shin, H. J., Agarose-gel-immobilized recombinant bacterial biosensors for simple and disposable on-site detection of phenolic compounds. Applied Microbiology and Biotechnology 2012, 93, (5), 1895-1904.
126. Fatoni, A.; Anggraeni, M. D.; Dwiasi, D. W. In Simple colorimetric glucose biosensor using chitosan cryogel supporting material, AIP Conference Proceedings, 2016; 2016.
127. Lu, Q.; Wang, X.; Zhu, H.; Kaplan, D. L., Surface immobilization of antibody on silk fibroin through conformational transition. Acta Biomaterialia 2011, 7, (7), 2782-2786.
128. Mohamed, S. A.; Darwish, A. A.; El-Shishtawy, R. M., Immobilization of horseradish peroxidase on activated wool. Process Biochemistry 2013, 48, (4), 649-655.
129. Xue, R.; Kang, T.-F.; Lu, L.-P.; Cheng, S.-Y., Immobilization of acetylcholinesterase via biocompatible interface of silk fibroin for detection of organophosphate and carbamate pesticides. Applied Surface Science 2012, 258, (16), 6040-6045.
130. Hanachi, P.; jafary, f.; Jafary, F.; Motamedi, S., Immobilization of the Alkaline Phosphatase on Collagen Surface via Cross-Linking Method. Iranian Journal of Biotechnology 2015, 13, (3), 32-38.
131. Wang, X.; Hagiwara, T.; Uchiyama, S., Immobilization of uricase within polystyrene using polymaleimidostyrene as a stabilizer and its application to uric acid sensor. Analytica Chimica Acta 2007, 587, (1), 41-46.

132. Farahmand, E.; Ibrahim, F.; Hosseini, S.; Rothan, H. A.; Yusof, R.; Koole, L. H.; Djordjevic, I., A novel approach for application of nylon membranes in the biosensing domain. Applied Surface Science 2015, 353, 1310-1319.
133. Pérez, J. P. H.; López-Cabarcos, E.; López-Ruiz, B., The application of methacrylate-based polymers to enzyme biosensors. Biomolecular Engineering 2006, 23, (5), 233-245.
134. Hervás Pérez, J. P.; López-Cabarcos, E.; López-Ruiz, B., Encapsulation of glucose oxidase within poly(ethylene glycol) methyl ether methacrylate microparticles for developing an amperometric glucose biosensor. Talanta 2008, 75, (5), 1151-1157.
135. Hosseini, S.; Azari, P.; Farahmand, E.; Gan, S. N.; Rothan, H. A.; Yusof, R.; Koole, L. H.; Djordjevic, I.; Ibrahim, F., Polymethacrylate coated electrospun PHB fibers: An exquisite outlook for fabrication of paper-based biosensors. Biosensors and Bioelectronics 2015, 69, 257-264.
136. Ahuja, T.; Mir, I. A.; Kumar, D.; Rajesh, Biomolecular immobilization on conducting polymers for biosensing applications. Biomaterials 2007, 28, (5), 791-805.
137. Sen, T.; Mishra, S.; Shimpi, N. G., Synthesis and sensing applications of polyaniline nanocomposites: a review. RSC Advances 2016, 6, (48), 42196-42222.
138. Ates, M., A review study of (bio)sensor systems based on conducting polymers. Materials Science and Engineering: C 2013, 33, (4), 1853-1859.
139. Valdés-Solís, T.; Fuertes, A. B., High-surface area inorganic compounds prepared by nanocasting techniques. Materials Research Bulletin 2006, 41, (12), 2187-2197.
140. Bezerra, C. S.; de Farias Lemos, C. M. G.; de Sousa, M.; Gonçalves, L. R. B., Enzyme immobilization onto renewable polymeric matrixes: Past, present, and future trends. Journal of Applied Polymer Science 2015, 132, (26), n/a-n/a.
141. Datta, S.; Christena, L. R.; Rajaram, Y. R. S., Enzyme immobilization: an overview on techniques and support materials. 3 Biotech 2013, 3, (1), 1-9.
142. Krajewska, B., Application of chitin- and chitosan-based materials for enzyme immobilizations: a review. Enzyme and Microbial Technology 2004, 35, (2–3), 126-139.
143. Zucca, P.; Fernandez-Lafuente, R.; Sanjust, E., Agarose and Its Derivatives as Supports for Enzyme Immobilization. Molecules 2016, 21, (11), 1577.
144. Franssen, M. C. R.; Steunenberg, P.; Scott, E. L.; Zuilhof, H.; Sanders, J. P. M., Immobilised enzymes in biorenewables production. Chemical Society Reviews 2013, 42, (15), 6491-6533.
145. Tembe, S.; Inamdar, S.; Haram, S.; Karve, M.; D'Souza, S. F., Electrochemical biosensor for catechol using agarose–guar gum entrapped tyrosinase. Journal of Biotechnology 2007, 128, (1), 80-85.
146. Nawaz, M. A.; Karim, A.; Bibi, Z.; Rehman, H. U.; Aman, A.; Hussain, D.; Ullah, M.; Qader, S. A. U., Maltase entrapment approach as an efficient alternative to increase the stability and recycling efficiency of free enzyme within agarose matrix. Journal of the Taiwan Institute of Chemical Engineers 2016.

147. Prakash, O.; Puliga, S.; Bachan Upadhyay, L. S., Immobilization of watermelon (Citrullus vulgaris) urease in agarose gel for urea estimation. Biotechnology and Bioprocess Engineering 2007, 12, (2), 131-135.
148. Pritchard, E. M.; Dennis, P. B.; Omenetto, F.; Naik, R. R.; Kaplan, D. L., Review: Physical and chemical aspects of stabilization of compounds in silk. Biopolymers 2012, 97, (6), 479-498.
149. Heinze, T.; Siebert, M.; Berlin, P.; Koschella, A., Biofunctional Materials Based on Amino Cellulose Derivatives - A Nanobiotechnological Concept. Macromolecular Bioscience 2016, 16, (1), 10-42.
150. Maniruzzaman, M.; Jang, S.-D.; Kim, J., Titanium dioxide–cellulose hybrid nanocomposite and its glucose biosensor application. Materials Science and Engineering: B 2012, 177, (11), 844-848.
151. Prabhakar, N.; Thakur, H.; Bharti, A.; Kaur, N., Chitosan-iron oxide nanocomposite based electrochemical aptasensor for determination of malathion. Analytica Chimica Acta 2016, 939, 108-116.
152. Unser, S.; Holcomb, S.; Cary, R.; Sagle, L., Collagen-Gold Nanoparticle Conjugates for Versatile Biosensing. Sensors 2017, 17, (2), 378.
153. Cipolatti, E. P.; Valerio, A.; Henriques, R. O.; Moritz, D. E.; Ninow, J. L.; Freire, D. M. G.; Manoel, E. A.; Fernandez-Lafuente, R.; de Oliveira, D., Nanomaterials for biocatalyst immobilization - state of the art and future trends. RSC Advances 2016, 6, (106), 104675-104692.
154. Cao, S.; Xu, P.; Ma, Y.; Yao, X.; Yao, Y.; Zong, M.; Li, X.; Lou, W., Recent advances in immobilized enzymes on nanocarriers. Chinese Journal of Catalysis 2016, 37, (11), 1814-1823.
155. Hosseini, S.; Ibrahim, F.; Djordjevic, I.; Koole, L. H., Recent advances in surface functionalization techniques on polymethacrylate materials for optical biosensor applications. Analyst 2014, 139, (12), 2933-2943.
156. Malhotra, B. D.; Chaubey, A.; Singh, S. P., Prospects of conducting polymers in biosensors. Analytica Chimica Acta 2006, 578, (1), 59-74.
157. Gerard, M.; Chaubey, A.; Malhotra, B. D., Application of conducting polymers to biosensors. Biosensors and Bioelectronics 2002, 17, (5), 345-359.
158. Mehta, J.; Bhardwaj, N.; Bhardwaj, S. K.; Kim, K.-H.; Deep, A., Recent advances in enzyme immobilization techniques: Metal-organic frameworks as novel substrates. Coordination Chemistry Reviews 2016, 322, 30-40.
159. Rowsell, J. L. C.; Yaghi, O. M., Metal–organic frameworks: a new class of porous materials. Microporous and Mesoporous Materials 2004, 73, (1–2), 3-14.
160. Luo, X.-L.; Yin, Z.; Zeng, M.-H.; Kurmoo, M., The construction, structures, and functions of pillared layer metal-organic frameworks. Inorganic Chemistry Frontiers 2016, 3, (10), 1208-1226.
161. Rosseinsky, M. J., Recent developments in metal–organic framework chemistry: design, discovery, permanent porosity and flexibility. Microporous and Mesoporous Materials 2004, 73, (1–2), 15-30.
162. Roy, S.; Chakraborty, A.; Maji, T. K., Lanthanide–organic frameworks for gas storage and as magneto-luminescent materials. Coordination Chemistry Reviews 2014, 273–274, 139-164.

163. Gkaniatsou, E.; Sicard, C.; Ricoux, R.; Mahy, J.-P.; Steunou, N.; Serre, C., Metal-organic frameworks: a novel host platform for enzymatic catalysis and detection. Materials Horizons 2017, 4, (1), 55-63.
164. Ma, W.; Jiang, Q.; Yu, P.; Yang, L.; Mao, L., Zeolitic Imidazolate Framework-Based Electrochemical Biosensor for in Vivo Electrochemical Measurements. Analytical Chemistry 2013, 85, (15), 7550-7557.
165. Liu, C.-S.; Sun, C.-X.; Tian, J.-Y.; Wang, Z.-W.; Ji, H.-F.; Song, Y.-P.; Zhang, S.; Zhang, Z.-H.; He, L.-H.; Du, M., Highly stable aluminum-based metal-organic frameworks as biosensing platforms for assessment of food safety. Biosensors and Bioelectronics 2017, 91, 804-810.
166. Wang, L.; Gong, C.; Shen, Y.; Ye, W.; Xu, M.; Song, Y., A novel ratiometric electrochemical biosensor for sensitive detection of ascorbic acid. Sensors and Actuators B: Chemical 2017, 242, 625-631.
167. Lu, J.; Xiong, Y.; Liao, C.; Ye, F., Colorimetric detection of uric acid in human urine and serum based on peroxidase mimetic activity of MIL-53(Fe). Analytical Methods 2015, 7, (23), 9894-9899.
168. Xie, S.; Ye, J.; Yuan, Y.; Chai, Y.; Yuan, R., A multifunctional hemin@metal-organic framework and its application to construct an electrochemical aptasensor for thrombin detection. Nanoscale 2015, 7, (43), 18232-18238.
169. Wu, X.; Hou, M.; Ge, J., Metal-organic frameworks and inorganic nanoflowers: a type of emerging inorganic crystal nanocarrier for enzyme immobilization. Catalysis Science & Technology 2015, 5, (12), 5077-5085.
170. Islam, M.; Ahiabu, A.; Li, X.; Serpe, M., Poly (N-isopropylacrylamide) Microgel-Based Optical Devices for Sensing and Biosensing. Sensors 2014, 14, (5), 8984.
171. Gandhi, A.; Paul, A.; Sen, S. O.; Sen, K. K., Studies on thermoresponsive polymers: Phase behaviour, drug delivery and biomedical applications. Asian Journal of Pharmaceutical Sciences 2015, 10, (2), 99-107.
172. Guan, Y.; Zhang, Y., PNIPAM microgels for biomedical applications: from dispersed particles to 3D assemblies. Soft Matter 2011, 7, (14), 6375-6384.
173. Schmaljohann, D., Thermo- and pH-responsive polymers in drug delivery. Advanced Drug Delivery Reviews 2006, 58, (15), 1655-1670.
174. Haq, M. A.; Su, Y.; Wang, D., Mechanical properties of PNIPAM based hydrogels: A review. Materials Science and Engineering: C 2017, 70, Part 1, 842-855.
175. Ashraf, S.; Park, H.-K.; Park, H.; Lee, S.-H., Snapshot of phase transition in thermoresponsive hydrogel PNIPAM: Role in drug delivery and tissue engineering. Macromolecular Research 2016, 24, (4), 297-304.
176. Alarcon, C. d. l. H.; Pennadam, S.; Alexander, C., Stimuli responsive polymers for biomedical applications. Chemical Society Reviews 2005, 34, (3), 276-285.

177. Roy, D.; Brooks, W. L. A.; Sumerlin, B. S., New directions in thermoresponsive polymers. Chemical Society Reviews 2013, 42, (17), 7214-7243.
178. Zhang, G.; Yang, N.; Ni, Y.; Shen, J.; Zhao, W.; Huang, X., A H2O2 electrochemical biosensor based on biocompatible PNIPAM-g-P (NIPAM-co-St) nanoparticles and multi-walled carbon nanotubes modified glass carbon electrode. Sensors and Actuators B: Chemical 2011, 158, (1), 130-137.
179. Zhou, Y.; Cao, J.; Zhao, J.; Xie, Y.; Fei, J.; Cai, Y., Temperature-responsive amperometric H2O2 biosensor using a composite film consisting of poly(N-isopropylacrylamide)-b-poly (2-acrylamidoethyl benzoate), graphene oxide and hemoglobin. Microchimica Acta 2016, 183, (9), 2501-2508.
180. Jiang, Y.; Colazo, M. G.; Serpe, M. J., Poly(N-isopropylacrylamide) microgel-based sensor for progesterone in aqueous samples. Colloid and Polymer Science 2016, 294, (11), 1733-1741.
181. Islam, M. R.; Serpe, M. J., A novel label-free colorimetric assay for DNA concentration in solution. Analytica Chimica Acta 2014, 843, 83-88.
182. Alexander, C.; Andersson, H. S.; Andersson, L. I.; Ansell, R. J.; Kirsch, N.; Nicholls, I. A.; O'Mahony, J.; Whitcombe, M. J., Molecular imprinting science and technology: a survey of the literature for the years up to and including 2003. Journal of Molecular Recognition 2006, 19, (2), 106-180.
183. Sharma, P. S.; Dabrowski, M.; D'Souza, F.; Kutner, W., Surface development of molecularly imprinted polymer films to enhance sensing signals. TrAC Trends in Analytical Chemistry 2013, 51, 146-157.
184. Van Dorst, B.; Mehta, J.; Bekaert, K.; Rouah-Martin, E.; De Coen, W.; Dubruel, P.; Blust, R.; Robbens, J., Recent advances in recognition elements of food and environmental biosensors: A review. Biosensors and Bioelectronics 2010, 26, (4), 1178-1194.
185. Whitcombe, M. J.; Chianella, I.; Larcombe, L.; Piletsky, S. A.; Noble, J.; Porter, R.; Horgan, A., The rational development of molecularly imprinted polymer-based sensors for protein detection. Chemical Society Reviews 2011, 40, (3), 1547-1571.
186. Shimizu, K. D.; Stephenson, C. J., Molecularly imprinted polymer sensor arrays. Current Opinion in Chemical Biology 2010, 14, (6), 743-750.
187. Wackerlig, J.; Lieberzeit, P. A., Molecularly imprinted polymer nanoparticles in chemical sensing – Synthesis, characterisation and application. Sensors and Actuators B: Chemical 2015, 207, Part A, 144-157.
188. Vasapollo, G.; Sole, R. D.; Mergola, L.; Lazzoi, M. R.; Scardino, A.; Scorrano, S.; Mele, G., Molecularly Imprinted Polymers: Present and Future Prospective. International Journal of Molecular Sciences 2011, 12, (9), 5908-5945.

189. Sun, Y.; Du, H.; Lan, Y.; Wang, W.; Liang, Y.; Feng, C.; Yang, M., Preparation of hemoglobin (Hb) imprinted polymer by Hb catalyzed eATRP and its application in biosensor. Biosensors and Bioelectronics 2016, 77, 894-900.
190. Diouf, A.; Motia, S.; El Alami El Hassani, N.; El Bari, N.; Bouchikhi, B., Development and characterization of an electrochemical biosensor for creatinine detection in human urine based on functional molecularly imprinted polymer. Journal of Electroanalytical Chemistry 2017, 788, 44-53.
191. Javanbakht, M.; Fard, S. E.; Mohammadi, A.; Abdouss, M.; Ganjali, M. R.; Norouzi, P.; Safaraliee, L., Molecularly imprinted polymer based potentiometric sensor for the determination of hydroxyzine in tablets and biological fluids. Analytica Chimica Acta 2008, 612, (1), 65-74.
192. He, Y.; Lu, J.; Liu, M.; Du, J., Molecular imprinting-chemiluminescence determination of trimethoprim using trimethoprim-imprinted polymer as recognition material. Analyst 2005, 130, (7), 1032-1037.
193. Alexander, S.; Baraneedharan, P.; Balasubrahmanyan, S.; Ramaprabhu, S., Modified graphene based molecular imprinted polymer for electrochemical non-enzymatic cholesterol biosensor. European Polymer Journal 2017, 86, 106-116.
194. Shafiqul Islam, A. K. M.; Krishnan, H.; Singh, H.; Ahmad, M. N., A noble molecular imprint polymer biosensor for caffeic acid detection in orthosiphon Stamineus extracts. Jurnal Teknologi 2015, 77, (7), 97-101.
195. Quesada-Molina, C.; Claude, B.; García-Campaña, A. M.; Del Olmo-Iruela, M.; Morin, P., Convenient solid phase extraction of cephalosporins in milk using a molecularly imprinted polymer. Food Chemistry 2012, 135, (2), 775-779.
196. Liu, H.; Fang, G.; Wang, S., Molecularly imprinted optosensing material based on hydrophobic CdSe quantum dots via a reverse microemulsion for specific recognition of ractopamine. Biosensors and Bioelectronics 2014, 55, 127-132.
197. Hu, Y.; Feng, S.; Gao, F.; Li-Chan, E. C. Y.; Grant, E.; Lu, X., Detection of melamine in milk using molecularly imprinted polymers-surface enhanced Raman spectroscopy. Food Chemistry 2015, 176, 123-129.
198. Cao, L.; Langen, L. v.; Sheldon, R. A., Immobilised enzymes: carrier-bound or carrier-free? Current Opinion in Biotechnology 2003, 14, (4), 387-394.
199. Buzea, C.; Pacheco, I., Nanomaterials and their classification. In Advanced Structured Materials, 2017; Vol. 62, pp 3-45.
200. Chen, Z.; Chen, Z.; Zhang, A.; Hu, J.; Wang, X.; Yang, Z., Electrospun nanofibers for cancer diagnosis and therapy. Biomaterials Science 2016, 4, (6), 922-932.
201. Taguchi, M.; Ptitsyn, A.; McLamore, E. S.; Claussen, J. C., Nanomaterial-mediated Biosensors for Monitoring Glucose. Journal of Diabetes Science and Technology 2014, 8, (2), 403-411.
202. Matlock-Colangelo, L.; Baeumner, A. J., Recent progress in the design of nanofiber-based biosensing devices. Lab on a Chip 2012, 12, (15), 2612-2620.

203. Othman, A.; Karimi, A.; Andreescu, S., Functional nanostructures for enzyme based biosensors: properties, fabrication and applications. Journal of Materials Chemistry B 2016, 4, (45), 7178-7203.
204. Zhu, X.; Li, J.; He, H.; Huang, M.; Zhang, X.; Wang, S., Application of nanomaterials in the bioanalytical detection of disease-related genes. Biosensors and Bioelectronics 2015, 74, 113-133.
205. Quesada-González, D.; Merkoçi, A., Nanoparticle-based lateral flow biosensors. Biosensors and Bioelectronics 2015, 73, 47-63.
206. Kruss, S.; Hilmer, A. J.; Zhang, J.; Reuel, N. F.; Mu, B.; Strano, M. S., Carbon nanotubes as optical biomedical sensors. Advanced Drug Delivery Reviews 2013, 65, (15), 1933-1950.
207. Liu, Z.; Tabakman, S.; Welsher, K.; Dai, H., Carbon nanotubes in biology and medicine: In vitro and in vivo detection, imaging and drug delivery. Nano Research 2009, 2, (2), 85-120.
208. Kim, J.; Grate, J. W.; Wang, P., Nanostructures for enzyme stabilization. Chemical Engineering Science 2006, 61, (3), 1017-1026.
209. Ansari, S. A.; Husain, Q., Potential applications of enzymes immobilized on/in nano materials: A review. Biotechnology Advances 2012, 30, (3), 512-523.
210. Bohara, R. A.; Thorat, N. D.; Pawar, S. H., Role of functionalization: strategies to explore potential nano-bio applications of magnetic nanoparticles. RSC Advances 2016, 6, (50), 43989-44012.
211. Cipolatti, E. P.; Silva, M. J. A.; Klein, M.; Feddern, V.; Feltes, M. M. C.; Oliveira, J. V.; Ninow, J. L.; de Oliveira, D., Current status and trends in enzymatic nanoimmobilization. Journal of Molecular Catalysis B: Enzymatic 2014, 99, 56-67.
212. Rao, J. P.; Geckeler, K. E., Polymer nanoparticles: Preparation techniques and size-control parameters. Progress in Polymer Science 2011, 36, (7), 887-913.
213. Ronkainen, N.; Okon, S., Nanomaterial-Based Electrochemical Immunosensors for Clinically Significant Biomarkers. Materials 2014, 7, (6), 4669.
214. Lim, M. C.; Kim, Y. R., Analytical Applications of Nanomaterials in Monitoring Biological and Chemical Contaminants in Food. J Microbiol Biotechnol 2016, 26, (9), 1505-16.
215. Vrignaud, S.; Benoit, J.-P.; Saulnier, P., Strategies for the nanoencapsulation of hydrophilic molecules in polymer-based nanoparticles. Biomaterials 2011, 32, (33), 8593-8604.
216. Faridi Esfanjani, A.; Jafari, S. M., Biopolymer nano-particles and natural nano-carriers for nano-encapsulation of phenolic compounds. Colloids and Surfaces B: Biointerfaces 2016, 146, 532-543.
217. Tang, Z.; He, C.; Tian, H.; Ding, J.; Hsiao, B. S.; Chu, B.; Chen, X., Polymeric nanostructured materials for biomedical applications. Progress in Polymer Science 2016, 60, 86-128.
218. Reisch, A.; Klymchenko, A. S., Fluorescent Polymer Nanoparticles Based on Dyes: Seeking Brighter Tools for Bioimaging. Small 2016, 12, (15), 1968-1992.
219. Meyer, R. A.; Green, J. J., Shaping the future of nanomedicine: Anisotropy in polymeric nanoparticle design. Wiley Interdisciplinary Reviews: Nanomedicine and Nanobiotechnology 2016, 8, (2), 191-207.

220. Banik, B. L.; Fattahi, P.; Brown, J. L., Polymeric nanoparticles: The future of nanomedicine. Wiley Interdisciplinary Reviews: Nanomedicine and Nanobiotechnology 2016, 8, (2), 271-299.
221. Nagavarma, B. V. N.; Yadav, H. K. S.; Ayaz, A.; Vasudha, L. S.; Shivakumar, H. G., Different techniques for preparation of polymeric nanoparticles- A review. Asian Journal of Pharmaceutical and Clinical Research 2012, 5, (SUPPL. 3), 16-23.
222. Hans, M. L.; Lowman, A. M., Biodegradable nanoparticles for drug delivery and targeting. Current Opinion in Solid State and Materials Science 2002, 6, (4), 319-327.
223. Wang, X.; Niessner, R.; Tang, D.; Knopp, D., Nanoparticle-based immunosensors and immunoassays for aflatoxins. Analytica Chimica Acta 2016, 912, 10-23.
224. Kim, Y. P.; Kim, H. S., Nanoparticles for Use in Enzyme Assays. ChemBioChem 2016, 17, (4), 275-282.
225. Wang, Z.-G.; Wan, L.-S.; Liu, Z.-M.; Huang, X.-J.; Xu, Z.-K., Enzyme immobilization on electrospun polymer nanofibers: An overview. Journal of Molecular Catalysis B: Enzymatic 2009, 56, (4), 189-195.
226. Semnani, D., 7 - Geometrical characterization of electrospun nanofibers A2 - Afshari, Mehdi. In Electrospun Nanofibers, Woodhead Publishing: 2017; pp 151-180.
227. Thenmozhi, S.; Dharmaraj, N.; Kadirvelu, K.; Kim, H. Y., Electrospun nanofibers: New generation materials for advanced applications. Materials Science and Engineering: B 2017, 217, 36-48.
228. Mondal, K.; Sharma, A., Recent advances in electrospun metal-oxide nanofiber based interfaces for electrochemical biosensing. RSC Advances 2016, 6, (97), 94595-94616.
229. Bhardwaj, N.; Kundu, S. C., Electrospinning: A fascinating fiber fabrication technique. Biotechnology Advances 2010, 28, (3), 325-347.
230. Wang, X.; Hsiao, B. S., Electrospun nanofiber membranes. Current Opinion in Chemical Engineering 2016, 12, 62-81.
231. Salas, C., 4 - Solution electrospinning of nanofibers A2 - Afshari, Mehdi. In Electrospun Nanofibers, Woodhead Publishing: 2017; pp 73-108.
232. Cheng, J.; Jun, Y.; Qin, J.; Lee, S.-H., Electrospinning versus microfluidic spinning of functional fibers for biomedical applications. Biomaterials 2017, 114, 121-143.
233. Ahmed, F. E.; Lalia, B. S.; Hashaikeh, R., A review on electrospinning for membrane fabrication: Challenges and applications. Desalination 2015, 356, 15-30.
234. Abdul Khalil, H. P.; Davoudpour, Y.; Bhat, A. H.; Rosamah, E.; Tahir, P. M., Electrospun cellulose composite nanofibers. In Handbook of Polymer Nanocomposites. Processing, Performance and Application: Volume C: Polymer Nanocomposites of Cellulose Nanoparticles, 2015; pp 191-228.
235. Khajavi, R.; Abbasipour, M., 5 - Controlling nanofiber morphology by the electrospinning process A2 - Afshari, Mehdi. In Electrospun Nanofibers, Woodhead Publishing: 2017; pp 109-123.

236. Lu, Y.; Huang, J.; Yu, G.; Cardenas, R.; Wei, S.; Wujcik, E. K.; Guo, Z., Coaxial electrospun fibers: applications in drug delivery and tissue engineering. Wiley Interdisciplinary Reviews: Nanomedicine and Nanobiotechnology 2016, 8, (5), 654-677.
237. Qin, X., 3 - Coaxial electrospinning of nanofibers A2 - Afshari, Mehdi. In Electrospun Nanofibers, Woodhead Publishing: 2017; pp 41-71.
238. Medina-Castillo, A. L.; Fernández-Sánchez, J. F.; Fernández-Gutiérrez, A., One-Step Fabrication of Multifunctional Core-Shell Fibres by Co-Electrospinning. Advanced Functional Materials 2011, 21, (18), 3488-3495.
239. Talbert, J. N.; Goddard, J. M., Enzymes on material surfaces. Colloids and Surfaces B: Biointerfaces 2012, 93, 8-19.
240. Borisov, S. M.; Mayr, T.; Klimant, I., Poly(styrene-block-vinylpyrrolidone) Beads as a Versatile Material for Simple Fabrication of Optical Nanosensors. Analytical Chemistry 2008, 80, (3), 573-582.
241. Yang, W.; Ratinac, K. R.; Ringer, S. P.; Thordarson, P.; Gooding, J. J.; Braet, F., Carbon Nanomaterials in Biosensors: Should You Use Nanotubes or Graphene? Angewandte Chemie International Edition 2010, 49, (12), 2114-2138.
242. Dasgupta, A.; Rajukumar, L. P.; Rotella, C.; Lei, Y.; Terrones, M., Covalent three-dimensional networks of graphene and carbon nanotubes: synthesis and environmental applications. Nano Today 2017, 12, 116-135.
243. Mehra, N. K.; Jain, N. K., Multifunctional hybrid-carbon nanotubes: new horizon in drug delivery and targeting. Journal of Drug Targeting 2016, 24, (4), 294-308.
244. Rabti, A.; Raouafi, N.; Merkoçi, A., Bio(Sensing) devices based on ferrocene–functionalized graphene and carbon nanotubes. Carbon 2016, 108, 481-514.
245. Zhu, Z., An Overview of Carbon Nanotubes and Graphene for Biosensing Applications. Nano-Micro Letters 2017, 9, (3), 25.
246. Bayne, L.; Ulijn, R. V.; Halling, P. J., Effect of pore size on the performance of immobilised enzymes. Chemical Society Reviews 2013, 42, (23), 9000-9010.
247. Braeuer, A., Chapter 2 - Interaction of Matter and Electromagnetic Radiation. In Supercritical Fluid Science and Technology, Andreas, B., Ed. Elsevier: 2015; Vol. Volume 7, pp 41-192.
248. Leca-Bouvier, B. D.; Blum, L. J., Enzyme for biosensing applications. In Recognition Receptors in Biosensors, 2010; pp 177-220.
249. Choi, M. M. F., Progress in Enzyme-Based Biosensors Using Optical Transducers. Microchimica Acta 2004, 148, (3), 107-132.
250. Jenie, S. N. A.; Plush, S. E.; Voelcker, N. H., Recent Advances on Luminescent Enhancement-Based Porous Silicon Biosensors. Pharmaceutical Research 2016, 33, (10), 2314-2336.
251. Lakowicz, J. R., Fluorescence Sensing. In Principles of Fluorescence Spectroscopy, Lakowicz, J. R., Ed. Springer US: Boston, MA, 2006; pp 623-673.

252. Lakowicz, J. R., Introduction to Fluorescence. In Principles of Fluorescence Spectroscopy, Lakowicz, J. R., Ed. Springer US: Boston, MA, 2006; pp 1-26.
253. Hof, M.; Fidler, V.; Hutterer, R., Basics of Fluorescence Spectroscopy in Biosciences. In Fluorescence Spectroscopy in Biology: Advanced Methods and their Applications to Membranes, Proteins, DNA, and Cells, Hof, M.; Hutterer, R.; Fidler, V., Eds. Springer Berlin Heidelberg: Berlin, Heidelberg, 2005; pp 3-29.
254. So, P. T. C.; Dong, C. Y., Fluorescence Spectrophotometry. In eLS, John Wiley & Sons, Ltd: 2001.
255. Sauer, M.; Hofkens, J.; Enderlein, J., Basic Principles of Fluorescence Spectroscopy. In Handbook of Fluorescence Spectroscopy and Imaging, Wiley-VCH Verlag GmbH & Co. KGaA: 2011; pp 1-30.
256. Skoog, D. A.; Holler, F. J.; Crouch, S. R., Principles of instrumental analysis. 5th ed.; Belmont, CA : Thomson, Brooks/Cole: 2007.
257. Lakowicz, J. R., Quenching of Fluorescence. In Principles of Fluorescence Spectroscopy, Lakowicz, J. R., Ed. Springer US: Boston, MA, 2006; pp 277-330.
258. Lakowicz, J. R., Fluorophores. In Principles of Fluorescence Spectroscopy, Lakowicz, J. R., Ed. Springer US: Boston, MA, 2006; pp 63-95.
259. Baici, A.; Joppich-Kuhn, R.; Luisi, P. L.; Olomucki, A.; Monneuse-Doublet, M.-O.; ThomÉ-Beau, F., Fluorescence Properties of Reduced Thionicotinamide - Adenine Dinucleotide and of Its Complex with Octopine Dehydrogenase. European Journal of Biochemistry 1978, 83, (2), 601-607.
260. Islam, S. D. M.; Susdorf, T.; Penzkofer, A.; Hegemann, P., Fluorescence quenching of flavin adenine dinucleotide in aqueous solution by pH dependent isomerisation and photo-induced electron transfer. Chemical Physics 2003, 295, (2), 137-149.
261. Smith, M. H., The amino acid composition of proteins. Journal of Theoretical Biology 1966, 13, 261-282.
262. Ghisaidoobe, A. B. T.; Chung, S. J., Intrinsic Tryptophan Fluorescence in the Detection and Analysis of Proteins: A Focus on Förster Resonance Energy Transfer Techniques. International Journal of Molecular Sciences 2014, 15, (12), 22518-22538.
263. Rajbongshi, B. K.; Ramanathan, G., Dominant π…π interaction in the self assemblies of 4-benzylidene imidazolin-5-one analogues. Journal of Chemical Sciences 2009, 121, (6), 973.
264. Pakhomov, A. A.; Martynov, V. I., GFP Family: Structural Insights into Spectral Tuning. Chemistry & Biology 2008, 15, (8), 755-764.
265. Walker, C. L.; Lukyanov, K. A.; Yampolsky, I. V.; Mishin, A. S.; Bommarius, A. S.; Duraj-Thatte, A. M.; Azizi, B.; Tolbert, L. M.; Solntsev, K. M., Fluorescence imaging using synthetic GFP chromophores. Current Opinion in Chemical Biology 2015, 27, 64-74.
266. Ashby, M. C.; Ibaraki, K.; Henley, J. M., It's green outside: tracking cell surface proteins with pH-sensitive GFP. Trends in Neurosciences 2004, 27, (5), 257-261.
267. Levitan, E. S., Using GFP to image peptide hormone and neuropeptide release in vitro and in vivo. Methods 2004, 33, (4), 281-286.

268. Ehrhardt, D., GFP technology for live cell imaging. Current Opinion in Plant Biology 2003, 6, (6), 622-628.
269. Gonçalves, M. S. T., Fluorescent Labeling of Biomolecules with Organic Probes. Chemical Reviews 2009, 109, (1), 190-212.
270. Ma, D.-L.; Ma, V. P.-Y.; Chan, D. S.-H.; Leung, K.-H.; He, H.-Z.; Leung, C.-H., Recent advances in luminescent heavy metal complexes for sensing. Coordination Chemistry Reviews 2012, 256, (23–24), 3087-3113.
271. Stanisavljevic, M.; Krizkova, S.; Vaculovicova, M.; Kizek, R.; Adam, V., Quantum dots-fluorescence resonance energy transfer-based nanosensors and their application. Biosensors and Bioelectronics 2015, 74, 562-574.
272. AlSalhi, M. S.; Alam, J.; Dass, L. A.; Raja, M., Recent Advances in Conjugated Polymers for Light Emitting Devices. International Journal of Molecular Sciences 2011, 12, (3), 2036.
273. Terai, T.; Nagano, T., Small-molecule fluorophores and fluorescent probes for bioimaging. Pflügers Archiv - European Journal of Physiology 2013, 465, (3), 347-359.
274. Chan, J.; Dodani, S. C.; Chang, C. J., Reaction-based small-molecule fluorescent probes for chemoselective bioimaging. Nature chemistry 2012, 4, (12), 973-984.
275. Wang, R.; Yu, C.; Yu, F.; Chen, L., Molecular fluorescent probes for monitoring pH changes in living cells. TrAC Trends in Analytical Chemistry 2010, 29, (9), 1004-1013.
276. Demas, J. N.; DeGraff, B. A., Applications of luminescent transition platinum group metal complexes to sensor technology and molecular probes. Coordination Chemistry Reviews 2001, 211, (1), 317-351.
277. Guerchais, V.; Ordronneau, L.; Le Bozec, H., Recent developments in the field of metal complexes containing photochromic ligands: Modulation of linear and nonlinear optical properties. Coordination Chemistry Reviews 2010, 254, (21–22), 2533-2545.
278. Lakowicz, J. R., Novel Fluorophores. In Principles of Fluorescence Spectroscopy, Lakowicz, J. R., Ed. Springer US: Boston, MA, 2006; pp 675-703.
279. Lo, K. K.-W.; Choi, A. W.-T.; Law, W. H.-T., Applications of luminescent inorganic and organometallic transition metal complexes as biomolecular and cellular probes. Dalton Transactions 2012, 41, (20), 6021-6047.
280. Lo, K. K.-W.; Louie, M.-W.; Zhang, K. Y., Design of luminescent iridium(III) and rhenium(I) polypyridine complexes as in vitro and in vivo ion, molecular and biological probes. Coordination Chemistry Reviews 2010, 254, (21–22), 2603-2622.
281. Thorp-Greenwood, F. L.; Balasingham, R. G.; Coogan, M. P., Organometallic complexes of transition metals in luminescent cell imaging applications. Journal of Organometallic Chemistry 2012, 714, 12-21.
282. Zhao, Q.; Li, F.; Huang, C., Phosphorescent chemosensors based on heavy-metal complexes. Chemical Society Reviews 2010, 39, (8), 3007-3030.

283. Fu, A.; Gu, W.; Larabell, C.; Alivisatos, A. P., Semiconductor nanocrystals for biological imaging. Current Opinion in Neurobiology 2005, 15, (5), 568-575.
284. Alivisatos, A. P.; Gu, W.; Larabell, C., Quantum dots as cellular probes. In Annual Review of Biomedical Engineering, 2005; Vol. 7, pp 55-76.
285. Li, J.; Zhu, J.-J., Quantum dots for fluorescent biosensing and bio-imaging applications. Analyst 2013, 138, (9), 2506-2515.
286. Xu, S.; Cui, J.; Wang, L., Recent developments of low-toxicity NIR II quantum dots for sensing and bioimaging. TrAC Trends in Analytical Chemistry 2016, 80, 149-155.
287. Miao, Y.; Lv, J.; Li, Y.; Yan, G., Construction of biomolecular sensors based on quantum dots. RSC Advances 2016, 6, (110), 109009-109022.
288. Hildebrandt, N.; Spillmann, C. M.; Algar, W. R.; Pons, T.; Stewart, M. H.; Oh, E.; Susumu, K.; Díaz, S. A.; Delehanty, J. B.; Medintz, I. L., Energy Transfer with Semiconductor Quantum Dot Bioconjugates: A Versatile Platform for Biosensing, Energy Harvesting, and Other Developing Applications. Chemical Reviews 2017, 117, (2), 536-711.
289. Sanvicens, N.; Pascual, N.; Fernández-Argüelles, M. T.; Adrián, J.; Costa-Fernández, J. M.; Sánchez-Baeza, F.; Sanz-Medel, A.; Marco, M.-P., Quantum dot-based array for sensitive detection of Escherichia coli. Analytical and Bioanalytical Chemistry 2011, 399, (8), 2755-2762.
290. Walling, M.; Novak, J.; Shepard, J. R. E., Quantum Dots for Live Cell and In Vivo Imaging. International Journal of Molecular Sciences 2009, 10, (2), 441.
291. Zrazhevskiy, P.; Sena, M.; Gao, X., Designing multifunctional quantum dots for bioimaging, detection, and drug delivery. Chemical Society Reviews 2010, 39, (11), 4326-4354.
292. Guo, X.; Baumgarten, M.; Müllen, K., Designing π-conjugated polymers for organic electronics. Progress in Polymer Science 2013, 38, (12), 1832-1908.
293. Xie, L.-H.; Yin, C.-R.; Lai, W.-Y.; Fan, Q.-L.; Huang, W., Polyfluorene-based semiconductors combined with various periodic table elements for organic electronics. Progress in Polymer Science 2012, 37, (9), 1192-1264.
294. Sun, X.; Wang, Y.; Lei, Y., Fluorescence based explosive detection: from mechanisms to sensory materials. Chemical Society Reviews 2015, 44, (22), 8019-8061.
295. Li, K.; Liu, B., Water-soluble conjugated polymers as the platform for protein sensors. Polymer Chemistry 2010, 1, (3), 252-259.
296. Liu, Y.; Ogawa, K.; Schanze, K. S., Conjugated polyelectrolytes as fluorescent sensors. Journal of Photochemistry and Photobiology C: Photochemistry Reviews 2009, 10, (4), 173-190.
297. Rajesh; Ahuja, T.; Kumar, D., Recent progress in the development of nano-structured conducting polymers/nanocomposites for sensor applications. Sensors and Actuators B: Chemical 2009, 136, (1), 275-286.
298. Feng, F.; He, F.; An, L.; Wang, S.; Li, Y.; Zhu, D., Fluorescent Conjugated Polyelectrolytes for Biomacromolecule Detection. Advanced Materials 2008, 20, (15), 2959-2964.

299. Feng, F.; Liu, L.; Yang, Q.; Wang, S., Water-Soluble Conjugated Polymers for Fluorescent-Enzyme Assays. Macromolecular Rapid Communications 2010, 31, (16), 1405-1421.
300. Liu, J.-M.; Gao, F.; Gao, W.-Y.; Zeng, L.-Q.; Huang, X.-M.; Li, Z.-M.; Huang, X.-C.; Lin, W.-N.; Wang, F.-M.; Nie, C.-L., Solid Substrate–Room Temperature Phosphorimetry for the Determination of Trace Terbutaline Sulfate Based on Its Inhibition Oxidation of Rhodamine 6G by Sodium Periodate. Journal of Fluorescence 2008, 18, (2), 573-579.
301. Liu, J.; Yang, T.; Zhu, G.; Chen, H.; Li, P.; Lin, X.; Huang, X., Determination of trace formaldehyde by solid substrate-room temperature phosphorescence quenching method based on the rose bengal–potassium bromate–Tween-80 system. Spectrochimica Acta Part A: Molecular and Biomolecular Spectroscopy 2008, 69, (3), 1004-1009.
302. Liu, J. M.; Liu, Z. B.; Li, X. N.; Li, Z. M.; Huang, X. M.; Hong, F. S.; Lin, W. N.; Chen, F., Determination of trace α-fetoprotein variant by affinity adsorption solid substrate-room temperature phosphorimetry. Luminescence 2009, 24, (1), 15-22.
303. Liu, J.; Zeng, L.; Li, Z.; Gao, F.; Huang, X.; Li, F.; Lin, H., Solid substrate-room temperature phosphorimetry for the determination of residual clenbuterol hydrochloride based on the catalysis of sodium periodate oxidizing eosine Y. Analytica Chimica Acta 2009, 638, (1), 69-74.
304. Liu, J. M.; Lin, S. Q.; Lin, X.; Zeng, L. Q.; Huang, X. M., Determination of trace carvedilol by solid substrate-room temperature phosphorimetry, based on its activating effect on hypochlorite-oxidizing amaranth using sodium dodecyl benzene sulphonate as sensitizer. Luminescence 2011, 26, (6), 734-740.
305. Marques, F. F. d. C.; Figueiredo, F. d. S.; Aucelio, R. Q., Heavy atom enhanced room-temperature phosphorimetry for ultratrace determination of harmane. Química Nova 2008, 31, 204-208.
306. Matsuoka, S.; Yoshimura, K., Recent trends in solid phase spectrometry: 2003–2009. A Review. Analytica Chimica Acta 2010, 664, (1), 1-18.
307. Hurtubise, R. J., Solid-matrix luminescence analysis: photophysics, physicochemical interactions and applications. Analytica Chimica Acta 1997, 351, (1), 1-22.
308. Sanz-Medel, A., Solid surface photoluminescence and flow analysis: a happy marriage. Analytica Chimica Acta 1993, 283, (1), 367-378.
309. Miller, J. N., Luminescence measurements on surfaces. Pure and Applied Chemistry 1985, 57, (3), 515-522.
310. Carraway, E. R.; Demas, J. N.; DeGraff, B. A.; Bacon, J. R., Photophysics and photochemistry of oxygen sensors based on luminescent transition-metal complexes. Analytical Chemistry 1991, 63, (4), 337-342.
311. Demas, J. N.; DeGraff, B. A.; Xu, W., Modeling of Luminescence Quenching-Based Sensors: Comparison of Multisite and Nonlinear Gas Solubility Models. Analytical Chemistry 1995, 67, (8), 1377-1380.

312. Lehrer, S., Solute perturbation of protein fluorescence. Quenching of the tryptophyl fluorescence of model compounds and of lysozyme by iodide ion. Biochemistry 1971, 10, (17), 3254-3263.
313. Pilolli, R.; Monaci, L.; Visconti, A., Advances in biosensor development based on integrating nanotechnology and applied to food-allergen management. TrAC Trends in Analytical Chemistry 2013, 47, 12-26.
314. Nguyen, H.; Park, J.; Kang, S.; Kim, M., Surface Plasmon Resonance: A Versatile Technique for Biosensor Applications. Sensors 2015, 15, (5), 10481.
315. Arima, Y.; Toda, M.; Iwata, H., Surface plasmon resonance in monitoring of complement activation on biomaterials. Advanced Drug Delivery Reviews 2011, 63, (12), 988-999.
316. Ouyang, Q.; Zeng, S.; Jiang, L.; Hong, L.; Xu, G.; Dinh, X.-Q.; Qian, J.; He, S.; Qu, J.; Coquet, P.; Yong, K.-T., Sensitivity Enhancement of Transition Metal Dichalcogenides/Silicon Nanostructure-based Surface Plasmon Resonance Biosensor. Scientific Reports 2016, 6, 28190.
317. Singh, P., SPR Biosensors: Historical Perspectives and Current Challenges. Sensors and Actuators B: Chemical 2016, 229, 110-130.
318. Zeng, S.; Baillargeat, D.; Ho, H.-P.; Yong, K.-T., Nanomaterials enhanced surface plasmon resonance for biological and chemical sensing applications. Chemical Society Reviews 2014, 43, (10), 3426-3452.
319. Shankaran, D. R.; Gobi, K. V.; Miura, N., Recent advancements in surface plasmon resonance immunosensors for detection of small molecules of biomedical, food and environmental interest. Sensors and Actuators B: Chemical 2007, 121, (1), 158-177.
320. Fernández-Sánchez, J. F.; Cannas, R.; Spichiger, S.; Steiger, R.; Spichiger-Keller, U. E., Novel nanostructured materials to develop oxygen-sensitive films for optical sensors. Analytica Chimica Acta 2006, 566, (2), 271-282.
321. Oehme, I.; Prattes, S.; Wolfbeis, O. S.; Mohr, G. J., The effect of polymeric supports and methods of immobilization on the performance of an optical copper(II)-sensitive membrane based on the colourimetric reagent Zincon. Talanta 1998, 47, (3), 595-604.
322. Wolfbeis, O. S., Materials for fluorescence-based optical chemical sensors. Journal of Materials Chemistry 2005, 15, (27-28), 2657-2669.
323. Lin, J.; Brown, C. W., Sol-gel glass as a matrix for chemical and biochemical sensing. TrAC Trends in Analytical Chemistry 1997, 16, (4), 200-211.
324. Amao, Y., Probes and Polymers for Optical Sensing of Oxygen. Microchimica Acta 2003, 143, (1), 1-12.
325. Jerónimo, P. C. A.; Araújo, A. N.; Conceição B.S.M. Montenegro, M., Optical sensors and biosensors based on sol–gel films. Talanta 2007, 72, (1), 13-27.
326. Borisov, S. M.; Wolfbeis, O. S., Optical Biosensors. Chemical Reviews 2008, 108, (2), 423-461.

327. Sotelo-Gonzalez, E.; Coto-Garcia, A. M.; Fernandez-Argüelles, M. T.; Costa-Fernandez, J. M.; Sanz-Medel, A., Immobilization of phosphorescent quantum dots in a sol–gel matrix for acetone sensing. Sensors and Actuators B: Chemical 2012, 174, 102-108.
328. Koren, K.; Borisov, S. M.; Klimant, I., Stable optical oxygen sensing materials based on click-coupling of fluorinated platinum(II) and palladium(II) porphyrins—A convenient way to eliminate dye migration and leaching. Sensors and Actuators B: Chemical 2012, 169, 173-181.
329. Ganesh, A. B.; Radhakrishnan, T. K., Fiber-Optic pH Sensor. Fiber and Integrated Optics 2006, 25, (6), 403-409.
330. Niu, C.-G.; Guan, A.-L.; Zeng, G.-M.; Liu, Y.-G.; Huang, G.-H.; Gao, P.-F.; Gui, X.-Q., A ratiometric fluorescence halide sensor based on covalently immobilization of quinine and benzothioxanthene. Analytica Chimica Acta 2005, 547, (2), 221-228.
331. Tan, S.-z.; Long, S.; Xia, J.-y.; Cao, Z.; Zhang, L.; Gong, F.-c., Novel fluorescence sensor based on covalent immobilization of 3-amino-9-ethylcarbazole via electrostatically assembled gold nanoparticle layer. Journal of Central South University of Technology 2009, 16, (2), 212-217.
332. Niu, C.-G.; Zeng, G.-M.; Chen, L.-X.; Shen, G.-L.; Yu, R.-Q., Proton "off-on" behaviour of methylpiperazinyl derivative of naphthalimide: a pH sensor based on fluorescence enhancement. Analyst 2004, 129, (1), 20-24.
333. Niu, C.-G.; Li, Z.-Z.; Zhang, X.-B.; Lin, W.-Q.; Shen, G.-L.; Yu, R.-Q., Covalently immobilized aminonaphthalimide as fluorescent carrier for the preparation of optical sensors. Analytical and Bioanalytical Chemistry 2002, 372, (4), 519-524.
334. Tan, S. Z.; Zeng, P. N.; Cao, Z.; Xia, J. Y.; Li, W., A novel technique for preparation of the fluorescence sensor based on covalent immobilization of 1-Aminopyrene. In Advanced Materials Research, 2011; Vol. 239-242, pp 1442-1447.
335. Besra, L.; Liu, M., A review on fundamentals and applications of electrophoretic deposition (EPD). Progress in Materials Science 2007, 52, (1), 1-61.
336. Corni, I.; Ryan, M. P.; Boccaccini, A. R., Electrophoretic deposition: From traditional ceramics to nanotechnology. Journal of the European Ceramic Society 2008, 28, (7), 1353-1367.
337. Marin-Suarez, M.; Medina-Rodriguez, S.; Ergeneman, O.; Pane, S.; Fernandez-Sanchez, J. F.; Nelson, B. J.; Fernandez-Gutierrez, A., Electrophoretic deposition as a new approach to produce optical sensing films adaptable to microdevices. Nanoscale 2014, 6, (1), 263-271.
338. Hansen, C.; Quake, S. R., Microfluidics in structural biology: smaller, faster em leader better. Current opinion in structural biology 2003, 13, (5), 538-544.
339. Liang, W.; Lin, H.; Chen, J.; Chen, C., Utilization of nanoparticles in microfluidic systems for optical detection. Microsystem Technologies 2016, 22, (10), 2363-2370.
340. Lee, K. H.; Lee, J.; Choi, H.; Lee, D.; Park, Y.; Lee, S. H., Integration of microfluidic chip with biomimetic hydrogel for 3D controlling and monitoring of cell alignment and migration. Journal of Biomedical Materials Research - Part A 2014, 102, (4), 1164-1172.

341. Cho, D.; Matlock-Colangelo, L.; Xiang, C.; Asiello, P. J.; Baeumner, A. J.; Frey, M. W., Electrospun nanofibers for microfluidic analytical systems. Polymer 2011, 52, (15), 3413-3421.
342. Jin, S.; Dai, M.; Ye, B.-c.; Nugen, S. R., Development of a capillary flow microfluidic Escherichia coli biosensor with on-chip reagent delivery using water-soluble nanofibers. Microsystem Technologies 2013, 19, (12), 2011-2015.
343. Yeo, L. Y.; Chang, H. C.; Chan, P. P. Y.; Friend, J. R., Microfluidic devices for bioapplications. Small 2011, 7, (1), 12-48.
344. Rodrigues, R. O.; Lima, R.; Gomes, H. T.; Silva, A. M. T., Polymer microfluidic devices: an overview of fabrication methods. U.Porto Journal of Engineering 2015, 1, (1), 67-79.
345. Iliescu, C.; Taylor, H.; Avram, M.; Miao, J.; Franssila, S., A practical guide for the fabrication of microfluidic devices using glass and silicon. Biomicrofluidics 2012, 6, (1), 016505-016505-16.
346. Lei, K. F., Chapter 1 Materials and Fabrication Techniques for Nano- and Microfluidic Devices. In Microfluidics in Detection Science: Lab-on-a-chip Technologies, The Royal Society of Chemistry: 2015; pp 1-28.
347. Becker, H.; Locascio, L. E., Polymer microfluidic devices. Talanta 2002, 56, (2), 267-287.
348. Gaudin, V., Advances in biosensor development for the screening of antibiotic residues in food products of animal origin – A comprehensive review. Biosensors and Bioelectronics 2017, 90, 363-377.
349. Eivazzadeh-Keihan, R.; Pashazadeh, P.; Hejazi, M.; de la Guardia, M.; Mokhtarzadeh, A., Recent advances in Nanomaterial-mediated Bio and immune sensors for detection of aflatoxin in food products. TrAC Trends in Analytical Chemistry 2017, 87, 112-128.
350. Teng, J.; Yuan, F.; Ye, Y.; Zheng, L.; Yao, L.; Xue, F.; Chen, W.; Li, B., Aptamer-Based Technologies in Foodborne Pathogen Detection. Frontiers in Microbiology 2016, 7, (1426).
351. Lin, X.; Guo, X., Advances in Biosensors, Chemosensors and Assays for the Determination of Fusarium Mycotoxins. Toxins 2016, 8, (6), 161.
352. Valizadeh, A., Nanomaterials and Optical Diagnosis of HIV. Artificial Cells, Nanomedicine, and Biotechnology 2016, 44, (6), 1383-1390.
353. Lan, L.; Yao, Y.; Ping, J.; Ying, Y., Recent advances in nanomaterial-based biosensors for antibiotics detection. Biosensors and Bioelectronics 2017, 91, 504-514.
354. Jayanthi, V. S. P. K. Sankara A.; Das, A. B.; Saxena, U., Recent advances in biosensor development for the detection of cancer biomarkers. Biosensors and Bioelectronics 2017, 91, 15-23.
355. Mo, L.; Li, J.; Liu, Q.; Qiu, L.; Tan, W., Nucleic acid-functionalized transition metal nanosheets for biosensing applications. Biosensors and Bioelectronics 2017, 89, Part 1, 201-211.
356. Carrascosa, L. G.; Huertas, C. S.; Lechuga, L. M., Prospects of optical biosensors for emerging label-free RNA analysis. TrAC Trends in Analytical Chemistry 2016, 80, 177-189.
357. Raul, R. G.; Irineo, T. P.; Guevara-González, R. G.; Miguel, C. M. L., Biosensors Used for Quantification of Nitrates in Plants. Journal of Sensors 2016, 2016.

358. Xia, N.; Wang, Q.; Liu, L., Nanomaterials-Based Optical Techniques for the Detection of Acetylcholinesterase and Pesticides. Sensors 2015, 15, (1), 499.
359. Kumar, P.; Kim, K.-H.; Deep, A., Recent advancements in sensing techniques based on functional materials for organophosphate pesticides. Biosensors and Bioelectronics 2015, 70, 469-481.
360. Kim, J. E.; Choi, J. H.; Colas, M.; Kim, D. H.; Lee, H., Gold-based hybrid nanomaterials for biosensing and molecular diagnostic applications. Biosensors and Bioelectronics 2016, 80, 543-559.
361. Gavela, A. F.; García, D. G.; Ramirez, J. C.; Lechuga, L. M., Last advances in silicon-based optical biosensors. Sensors (Switzerland) 2016, 16, (3).
362. Zhang, H.; Zhang, H.; Aldalbahi, A.; Zuo, X.; Fan, C.; Mi, X., Fluorescent biosensors enabled by graphene and graphene oxide. Biosensors and Bioelectronics 2017, 89, Part 1, 96-106.
363. Kumar, P.; Deep, A.; Kim, K.-H., Metal organic frameworks for sensing applications. TrAC Trends in Analytical Chemistry 2015, 73, 39-53.
364. Rocha-Santos, T. A. P., Sensors and biosensors based on magnetic nanoparticles. TrAC Trends in Analytical Chemistry 2014, 62, 28-36.

EXPERIMENTAL

No fracasé, sólo descubrí 999 maneras de cómo no hacer una bombilla.

Thomas Alva Edison

Bloque I

Uno de los aspectos fundamentales a considerar durante el proceso de diseño de un biosensor lo constituye la selección del soporte sólido donde se llevará a cabo la inmovilización del componente biológico o biomolécula.

Este soporte debe reunir una serie de características determinadas, tanto estructurales y morfológicas, como de naturaleza y reactividad, para permitir la retención de la biomolécula en unas condiciones óptimas que conduzcan a la conservación de su actividad biológica en la mayor medida posible.

Los soportes sólidos disponibles para realizar trabajos de inmovilización de biomoléculas son muy diversos y pueden estar fabricados con una gran variedad de funcionalidades químicas superficiales. Es por ello que, en la mayoría de los casos, es imprescindible realizar un estudio sobre los efectos que tiene la química superficial de estos soportes sobre los procedimientos de inmovilización de biomoléculas llevados a cabo sobre los mismos.

Así, el trabajo desarrollado en este bloque trata de aportar datos sobre la influencia del grupo funcional reactivo presente en el soporte sólido sobre el proceso de inmovilización y sobre la retención de la actividad biológica de la biomolécula tras ser inmovilizada.

Capítulo 1

Evaluation of different functional groups for covalent immobilization of enzymes in the development of biosensors with oxygen optical transduction

Teresa Ramon-Marquez[a], *Antonio L. Medina-Castillo*[b], *Jorge F. Fernandez-Sanchez*[a], *Alberto Fernández-Gutiérrez*[a]

[a] Department of Analytical Chemistry, University of Granada, Avda. Fuentenueva s/n, 18071 Granada, Spain

[b] NanoMyP®, Nanomateriales y Polimeros S.L., Spin-Off company of the UGR, BIC Building, Avd. Innovacion 1, E-18016, Granada, Spain

Published in *Analytical Methods*, 2015, **7**, 2943-2949

ABSTRACT

Four different types of polymeric particles with different functional groups on their surface have been evaluated to develop biosensors using glucose oxidase as a model enzyme. Direct covalent immobilization was achieved on particles functionalized with chloride, epoxy and vinyl groups via the reactive functional groups on the surface, whereas particles functionalized with carboxylic groups, used as reference materials, were pre-activated with carbodiimide. Immobilization was successfully performed under very mild conditions (20 ºC, pH 8.0). In order to determine the advantages and disadvantages of each functional group, both the amounts of immobilized enzymes and their relative activities were fully investigated. In order to demonstrate their applicability on the design of biosensor with oxygen optical transduction, the functionalized particles were co-immobilized in gold chips with oxygen sensing particles (PSMA–PtTFPP) using electrophoretic deposition and characterised for glucose determination in solution.

1. Introduction

To develop a biosensing film with optical oxygen transduction, two elements, at least, are necessary (Steiner et al. 2011): (1) the biochemical recognition element (i.e. oxidase enzyme) which can oxidise the analyte and change the concentration of oxygen in the media, and (2) an oxygen transduction element which provides the analytical signal.

Immobilization of biomolecules and the preservation of their biological activities have proven to be particularly valuable and have been exploited to enhance the biomolecules properties for their successful utilization in the development of biosensors (Susanto et al. 2013). The vast amount of coupling chemistry and the diversity of carrier structure are also powerful assets for modulating the catalytic properties of the enzyme. Thus, selection or preparation of the carrier is of crucial importance with regard to the performance of the immobilized enzymes (Cao 2006; Hermanson 2008). Herein, four different types of spherical polymeric particles with different functional groups on their surface were tested for covalent immobilization of GOx, which was used as a model enzyme: chloride groups (PolymP®-Cl), epoxy groups (PolymP®-Epoxy), particles with a pre-activated vinyl surface (PolymP®-Link) and classical particles functionalized with carboxyl groups (PolymP®-H) which were used as referenced material. Optimum immobilization conditions of GOx for each type of particle were investigated.

The oxygen sensitive transducer should consist of an oxygen sensitive dye incorporated into an oxygen permeable, inert support. Pt(II) meso-tetra(pentafluorophenyl)porphyrin (PtTFPP) is one of the most widely used dyes for the preparation of optical oxygen sensing films due to its good photostability (Amao et al. 2001b), long luminescence lifetime, wide excitation range, and large Stokes shift, which simplifies the measurement system (Medina-Rodríguez et al. 2013a; Trettnak et al. 1996). On the other side, polymeric materials have demonstrated good properties in terms of solubility of the dye and permeability to oxygen (Amao 2003; Wang and Wolfbeis 2014). It has been proved that poly(styrene-*co*-maleic anhydride) provides nanoparticles with good stability and high zeta potential (Marin-Suarez et al. 2014; Mistlberger et al. 2010). Thus, PSMA-PtTFPP was used as optical oxygen transducers in this work.

Finally, these two elements have been deposited on an inert support in order to demonstrate their applicability in the determination of the analyte in solution. There are several strategies to deposit polymeric nanoparticles on a solid support. Electrophoretic deposition (EPD) is considered a suitable technique for the fabrication of devices with biotechnological applications

(Marin-Suarez et al. 2014). In traditional EPD, a dc voltage is applied across the cell, thereby creating an electric field that transports charged particles to the electrodes where they are deposited to form a cast film. The thickness and structure of coatings obtained by EPD can be easily adjusted by the processing parameters like deposition time, electric field and concentration of the suspension (Dickerson and Boccaccini 2012; Marin-Suarez et al. 2014; Seuss and Boccaccini 2013).

2. Experimental

2.1. Reagents and materials

Four different polymeric particles were kindly supplied by nanoMyP® (http://www.nanomyp.com). PolymP®-H are polymeric particles functionalized with carboxyl groups, PolymP®-Cl are functionalized with chloride groups, PolymP®-Epoxy are functionalized with epoxy groups and PolymP®-Link are functionalized with a pre-activated surface containing vinyl groups.

For the immobilization of glucose oxidase on their surface, glucose oxidase (GOx) from *Aspergillus niger* (EC 1.1.3.4), *N*-ethyl-*N'*-(3-dimethylaminopropyl) carbodiimide hydrochloride (EDC), *N*-hydroxysuccinimide (NHS), potassium dihydrogen phosphate (KH_2PO_4), potassium monohydrogen phosphate (K_2HPO_4) and *N*,*N*-dimethylformamide (DMF) were all purchased from Sigma Aldrich.

To test the activity of GOx, horseradish peroxidase (HRP) from horseradish (E.C.1.11.1.7), D-glucose, 4-aminoantipyrine (4-AAP) and phenol were purchased from Sigma Aldrich.

For the synthesis of the oxygen sensitive particles, the following chemicals were used: poly(styrene-*co*-maleic anhydride) polymer (PSMA, 7% maleic anhydride, M_w = 224000 g mol^{-1}) and tetrahydrofuran (THF) from Sigma Aldrich, and Pt(II) meso-tetra(pentafluorophenyl) porphyrin (PtTFPP) from Frontier Scientific.

All chemicals were of analytical grade and used without further purification. All the solutions were prepared using doubly distilled water.

2.2. Apparatus and measurements

The UV-visible absorption spectra were recorded on a Varian Cary 50 UV–Vis spectrophotometer. All luminescence measurements were carried out on a Varian Cary-Eclipse fluorescence spectrophotometer.

The average size of the particles, size distribution and zeta potential were determined with a particle size analyser Zetananosizer (Malvern Instrument, model Zetasizer Nano ZS, http://www.malvern.com).

The pH of the buffer solutions was controlled using a digital pH meter (Crison micropH 2000) calibrated at 20 ± 2°C.

2.3. Immobilization of the enzyme

The enzyme was immobilized on four different polymeric particles involving several covalent immobilization methods (Cao 2006; Hermanson 2008). PolymP®-H (functionalized with carboxyl groups), PolymP®-Cl (functionalized with chloride groups), PolymP®-Epoxy (functionalized with epoxy groups) and PolymP®-Link (functionalized with activated vinyl groups) were used as supports. The principle of coupling the enzyme with each support surface is illustrated in Fig 1.1. The following variables were optimized for all the immobilizations: temperature, enzyme concentration, reaction time and pH.

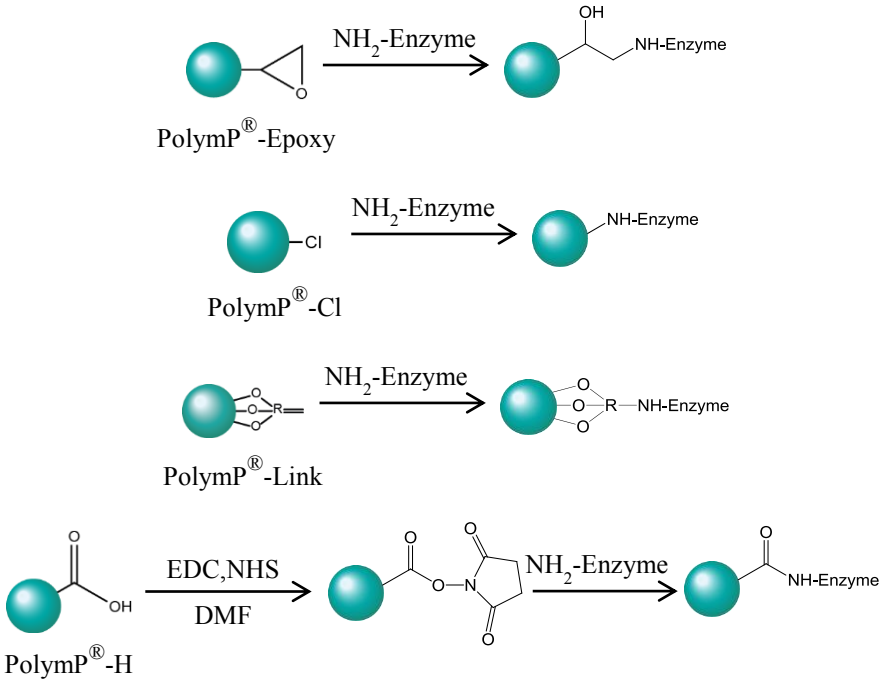

Fig. 1.1. Schematic representation of the four different protocols used for immobilizing enzymes.

In detail, immobilization on PolymP®-Cl and PolymP®-Epoxy particles was carried out by incubating 100 µL of 10 mg mL^{-1} enzyme solution in 100 mM potassium phosphate buffer pH 8 containing 1.2 mL of particle suspension (0.17 % w/v H_2O:MeOH (5:1)). This amount corresponds with 2 mg of particles instead of 5 mg used for the rest of particles. It is due to the lack of dispersion of these kinds of particles in the immobilization media.

Immobilization on PolymP®-Link particles was carried out by incubating 400 µL of 2.5 mg mL^{-1} enzyme solution in 100 mM potassium phosphate buffer pH 8, in 100 µL of particle suspension (5 % w/v); 5 mg of particles.

For the immobilization on PolymP®-H, the carboxylic acid groups of the particles were first preactivated (Gao and Kyratzis 2008; Hermanson 2008). Briefly, 100 µL of particle suspension (5 % w/v; equivalent to 5 mg of particles) were immersed in 400 µL of DMF containing 3.1 mg EDC and 46 mg NHS for 1 h. After that, the particles were washed with phosphate buffer solution (100 mM, pH 8.0) three times, and transferred to 400 µL of the same buffer solution containing 2.5 mg mL^{-1} of enzyme. The immobilization was allowed to proceed at room temperature for 20 min under rotational stirring.

Thereafter, all immobilized derivatives were separated from the solution by centrifugation, decantation, and washing with fresh buffer solution and with ionic strength (NaCl 1 M) until no enzyme signal was detected in the washing solvent. The separated particles loaded with immobilized enzymes were resuspended in 0.5 mL of phosphate buffer at pH 8 and stored at 4 ºC. The collected supernatants were preserved for further testing.

All the experiments were replicated three times in order to evaluate the error $\left({}^{st}/_{\sqrt{n}}\right)$, where *s* is the standard deviation, *t* the Student t and *n* the number of replicas.

2.4. Characterization of functionalized particles

The amount of enzyme immobilized on particles was calculated by measuring the concentration of enzyme in the supernatant and then subtracting from the total free enzyme amount, assuming that the loss of enzyme in each experiment could be negligible. The enzyme concentration in the supernatant solutions was measured by the spectrophotometric method at 348 nm (Shao et al. 2012). For each sample, the experiments were replicated three times to estimate the error.

The relative activity (%) of the immobilized enzyme was determined using the colorimetric method based on Trinder‘s reaction (Hou et al. 2007; Lott and Turner 1975; Rauf et al. 2006). GOx catalyses the oxidation of D-glucose to gluconic acid with the concurrent release of hydrogen peroxide. In the presence of peroxidase (horseradish peroxidase (HRP)), the produced hydrogen peroxide reacts with 4-aminoantipyrine (4-AAP) and phenol to form a red coloured quinoneimine dye, which has an absorption maxima at 510 nm. Based on this, the relative activity was calculated as a percentage of the immobilized GOx and free GOx absorbances.

In detail, to test the relative activity (%) of the immobilized GOx, 2.5 mL phosphate buffer (100 mM, pH 8.0) containing 2 µg free or immobilized GOx and 0.04 mmol glucose, were mixed with 1 mL of 4-aminoantipyrine (200 mM), 1 mL of phenol (200 mM), and 0.5 mL HRP (20 U mL^{-1}) and incubated at 37 ºC and stirred for 30 min. Afterward, the testing solution was analysed using a UV-Vis spectrophotometer at a wavelength of 510 nm (Hou et al. 2007).

2.5. Preparation and characterization of the oxygen sensitive particles

The PtTFPP-PSMA particles were prepared following the procedure described elsewhere (Borisov et al. 2009; Marin-Suarez et al. 2014). Briefly, 100 mg of PSMA (0.1 % w/v) and 1.5 mg of PtTFPP (1.5 % w/w respect to the polymer) were dissolved in 100 mL of THF. Then, 5 mL of the cocktail were added dropwise, with stirring, to 8 mL of deionized water. Finally, THF was evaporated under a stream of air.

The resulting polymeric particles with the embedded dye formed stable dispersions and presented an average particle diameter of 151.3 nm, a PdI of 0.088, a zeta potential of -32.9 mV and a conductivity of 0.0330 mS cm^{-1}.

2.6. Electrophoretic deposition

For the preparation of the biosensing film, oxygen sensitive particles and GOx functionalized particles were both deposited on the surface of a gold chip by EPD. The homemade electrophoretic cell previously described by our research group (Marin-Suarez et al. 2014) was used to carry out the electrophoretic deposition and several deposition strategies were tested. The chips were rinsed with deionized water and dried with nitrogen to remove all non-attached particles after each deposition.

To improve the adherence to the substrate material and to increase the density of the coating different potentials and deposition times were also tested.

3. Results and discussion

3.1. Determination of optimal conditions for enzyme immobilization

Four different methods for the covalent immobilization of enzymes were evaluated using GOx as a model enzyme. Two essential requirements must be met to achieve efficient covalent binding between the enzyme and the carrier: a suitable reactivity of the functional groups of the selected carrier and sterically accessible functional groups to each other under the selected immobilization conditions before binding. Based on this, GOx was directly covalently immobilized on PolymP®-Cl (functionalized with chloride groups), PolymP®-Epoxy (functionalized with epoxy groups) and PolymP®-Link (functionalized with a pre-activated surface containing vinyl groups). These functional groups may be used for covalent immobilization without any previous surface activation treatment. Whereas, the binding of the enzyme to PolymP®-H (functionalized with carboxyl groups) was carried out by initial activation of the surface using carbodiimide, followed by enzyme coupling to the activated support (Sassolas et al. 2012). The mechanisms of coupling the enzyme with these support surfaces are presented in Fig.1.1.

3.1.1. Optimization of the immobilization of the enzyme on carboxyl functionalized particles

The first step was to optimise the activation of the carboxyl groups on PolymP®-H particles. To do this, the amount of EDC, the amount of NHS and the reaction time were evaluated. Table 1.1 shows the optimal conditions for activating the carboxyl groups.

Table 1.1. Optimal conditions for immobilizing GOx on the four particles under study.

Particle	Activation	GOx immobilization			
		[GOx] (mg mL^{-1})	Media	Time (min)	Amount of GOx per mass of particles (mg g^{-1})
PolymP®-H	[EDC] = 40 mM, [NHS] = 0.8 M in DMF during 1 h	1.0	100 mM phosphate buffer pH 8	20	51
PolymP®-Link	Not needed			20	12
PolymP®-Cl	Not needed			30	35
PolymP®-Epoxy	Not needed			60	45

To investigate the optimum pH for immobilizing GOx, 5 mg of activated carboxylated particles were added to 400 µL of 2.5 mg mL^{-1} GOx prepared in 100 mM buffer solution at different pH values (6, 7, 8 and 9). The immobilization mixture was kept at room temperature for one hour and then was washed with the same buffer solution until no protein was detected in the washing solvent. As can be seen in Fig. 1.2a, the pH of the immobilization medium significantly affects both the amount of immobilized enzyme and the activity. The maximum amount of immobilized enzyme (0.051 mg enzyme per mg support) and the maximum relative activity (%) were both found at pH 8.0. Therefore, it was selected as optimum pH for further experiments.

To determine the effect of the temperature, the immobilization was carried out at different temperatures (4, 10, 20 and 40 ºC). Fig 1.2b shows the experimental results. It is known that temperature is an important parameter which determines the three-dimensional structures or conformational states of enzymes, and therefore, as expected, it affects both immobilization and activity (Arica and Hasirci 1993; Bulmuş et al. 1997). The amount of immobilized enzyme increases with the temperature, while the relative activity (%) drops significantly. Based on this result, the temperature selected for immobilizing GOx was 20 ºC. Under these conditions, the immobilized enzyme retained approximately 20 % of the native enzymatic activity.

The effect of the enzyme concentration was also investigated. GOx solutions at four different concentrations (0.625, 1.25, 2.5 and 5 mg mL^{-1}) were prepared with a buffer solution at pH 8.0. Then, 400 µL of each solution was added onto 5 mg of activated particles during 20 min at 20 ºC. Fig. 1.2c shows that the amount of immobilized enzyme increases when the initial amount of enzyme is increased. However, there is a pronounced decrease in the relative activity of the immobilized enzyme when the initial concentration of GOx is higher than 1 mg mL^{-1}. This phenomenon could be attributed to the aggregation of enzyme on the surface of particles that might cause the blockage of enzyme active sites, resulting in a drop in immobilized enzyme activity. These results clearly showed that a higher degree of immobilization of GOx on the support does not mean that it will exhibit higher activity. These effects were previously observed in the literature (Ye et al. 2009).

Table 1.1 shows an overview of the optimal conditions for the effective immobilization of GOx on PolymP®-H attending not only to the amount of immobilized enzyme but also to its activity after immobilization.

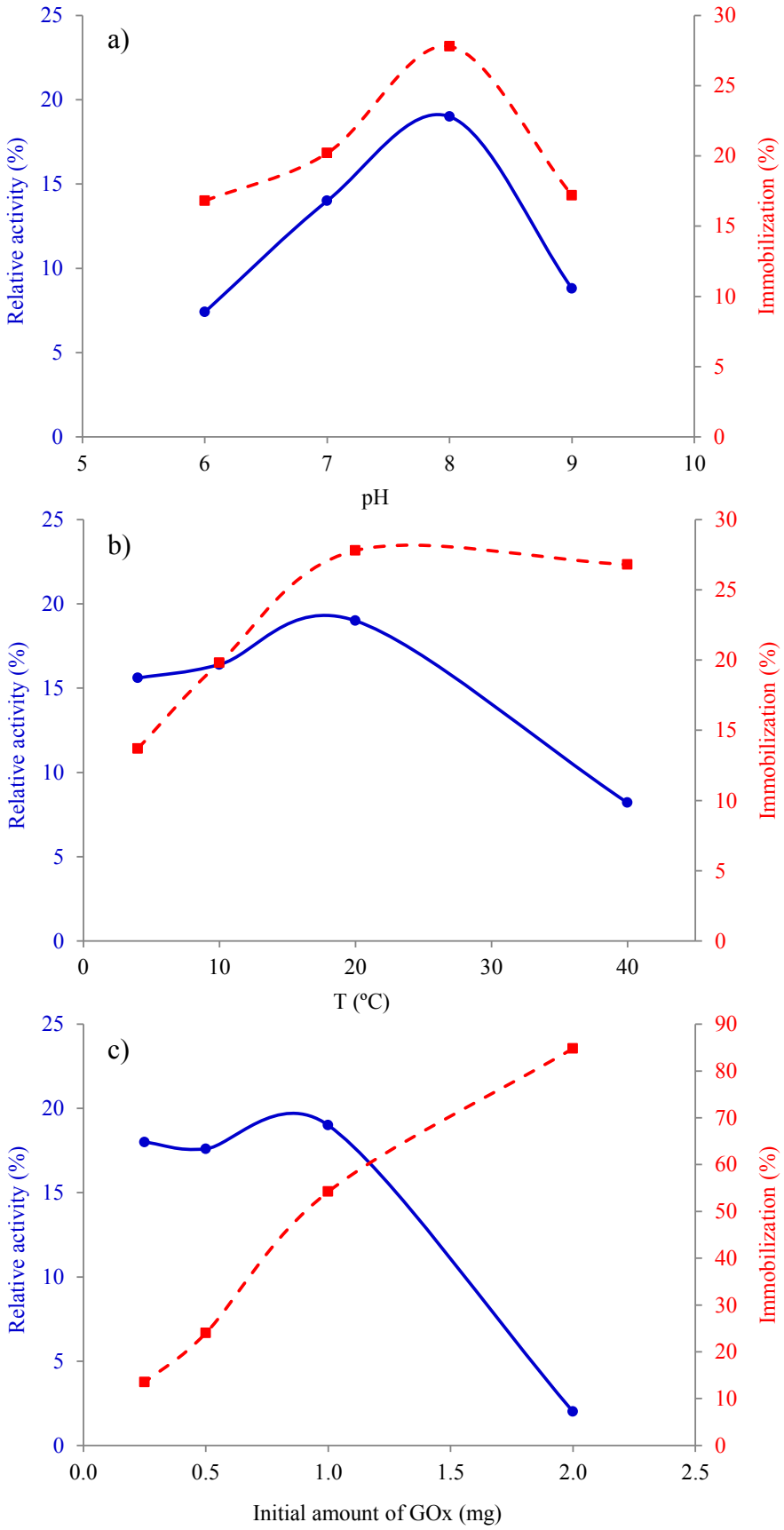

Fig. 1.2. Effect of the a) pH, b) temperature and c) initial amount of enzyme *versus* the amount of immobilized enzyme (--■--) and its relative activity (%) after immobilization (—●—).

3.1.2. Optimization of the immobilization of enzyme on chloride, epoxy and active vinyl functionalized particles

Having the optimal conditions for immobilizing the enzyme into PolymP®-H as starting point, pH, incubation temperature and concentration of the enzyme were also evaluated for the rest of polymeric particles (PolymP®-Cl, PolymP®-Epoxy and PolymP®-Link). In this case, the immobilization of the enzyme was carried out directly; no preactivation stage was necessary. Similar results than whose for PolymP®-H were obtained. The results have been summarized in Table 1.1.

3.2. Comparison of the immobilizing behaviours using different functional groups

To compare the immobilizing behaviours on different supports with different superficial chemistry, we investigated the variation of the immobilized amount of the enzyme and its activity under the optimum conditions *versus* time between 20 min and 48 h (see Fig. 1.3).

An increase in the incubation time provides an increase in the amount of immobilized enzyme for all the particles, but this increase is more effective for PolymP®-Link and PolymP®-H than for the others (see Fig. 1.3a). Thus, it is possible to immobilize more amount of enzyme in a shorter time using PolymP®-Link and PolymP®-H.

Fig. 1.3b shows that the relative activity (%) of immobilized enzyme decreases when the incubation time increases, but the highest activity is exhibited by the enzyme immobilized on PolymP®-Link particles at all the incubation times followed by carboxylic PolymP®-H particles. The relative activity (%) of the enzyme immobilized on PolymP®-Link was 26 % of the free enzyme while it was 19 % when it was immobilized on PolymP®-H for 30 min.

It is possible to conclude that PolymP®-Link particles show a similar or better superficial chemistry for the immobilization of enzymes than classical particles based on carboxyl groups. In addition, Table 1.1 summarises the amount of enzyme immobilised per mass of particles under the optimum conditions. It is possible to conclude that PolymP®-Link particles need the lowest amount of enzyme (only 12 mg per gram of particles) for providing the highest activity. Thus, its use provides a considerable reduction in the cost of the final biosensor.

The active vinyl functionalised particles show the best results even when they have the lowest amount of immobilized enzyme because the active centre of the biomolecule after its immobilisation in PolymP®-Link might be more available in this kind of particle than in the rest

of the tested supports. Or it might be due to a better stabilization of the quaternary structure of the enzyme after its attachment to an active vinyl group than to any of the other ones.

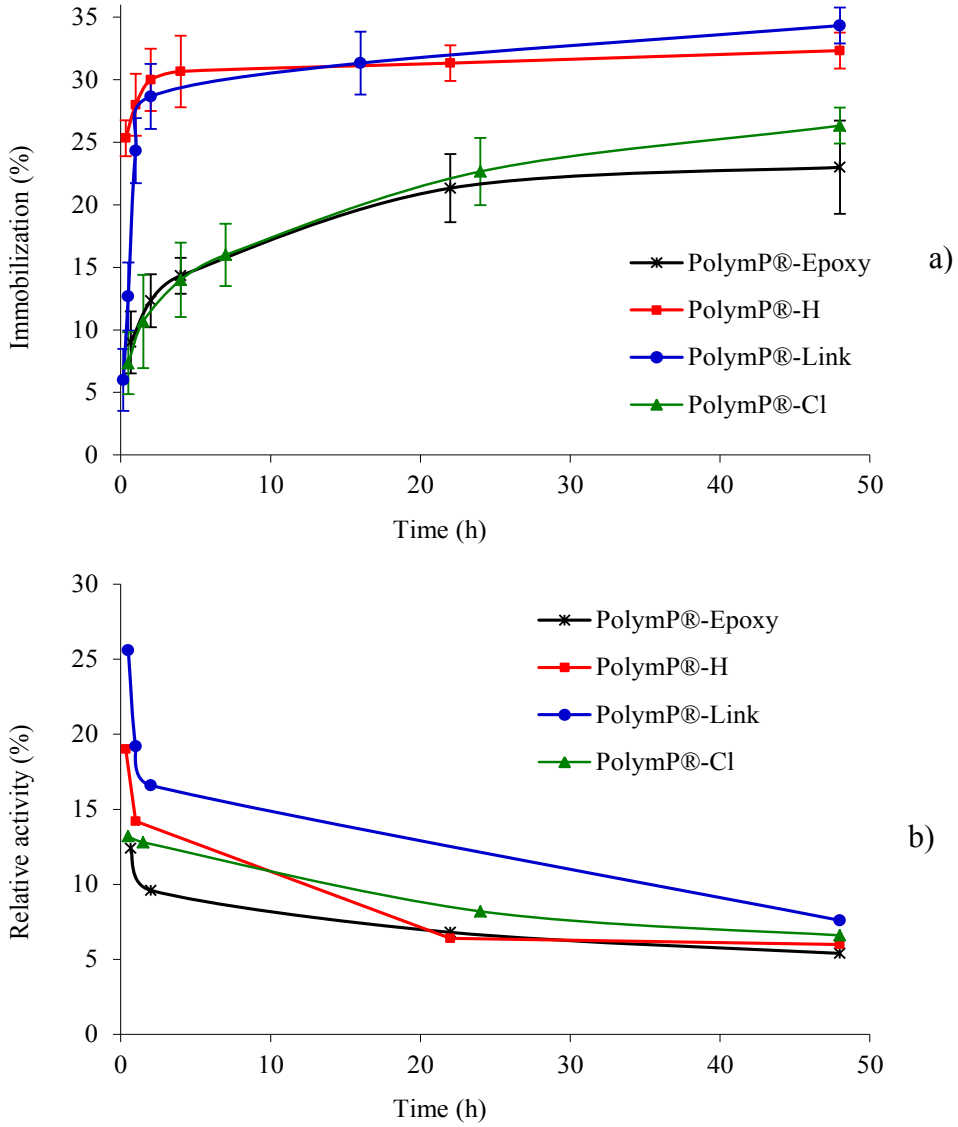

Fig. 1.3. Change of the a) amount of immobilized enzyme and b) the relative activity (%) *versus* the incubation time at RT.

3.3. Optimization of the EPD experimental conditions and applications

Different approaches were accessed for depositing both oxygen sensitive and enzyme-functionalized particles. However, deposition of both at the same time did not provide good results, probably due to the difference of charge between them. Therefore, deposition protocols consisting of alternating layers of oxygen sensitive and GOx-functionalized particles were evaluated. The optimal response was found by depositing a layer of oxygen sensitive particles first and then a layer of enzyme-functionalized particles.

The electrodeposition of oxygen sensitive particles was evaluated by applying constant potentials (2, 4 and 6 V cm^{-1}) and deposition times between 10 and 120 min, at a constant concentration of suspended particles and measuring the differences in luminescence intensity (I_x - I_0) where I_x corresponds with the relative luminescence intensity at 8 ppm of oxygen and I_0 is the relative luminescence intensity in the absence of oxygen. Electronic Supporting Information (ESI) shows the experimental results (see ESI, Fig. ESI-1.1).

The response signal (I_x - I_0) is proportional to the amount of deposited particles therefore it is possible to conclude that an increase in the deposition time provides an increase in the amount of deposited particle up to a certain deposition time in which the amount of particles remains constant. This is expected in a constant voltage EPD because at the initial period of EPD there is generally a linear relationship between deposition mass and time during (Dickerson and Boccaccini 2012; Zhitomirsky and Gal-Or 1997) and when deposition time increases, the electric field influencing electrophoresis decreases because of the formation of an insulating layer of deposited particles on the electrode surface. The maximum response to oxygen concentration was achieved at 6 V cm^{-1} and a deposition time of 30 min.

In addition, luminescence spectra were recorded to evaluate possible changes in the spectroscopic behaviour of the oxygen sensitive particles once the particles were deposited. No changes in the spectroscopic properties of deposited particles compared to particles in suspension were observed.

The effect of applied potential and deposition time on the electrophoretic deposition of immobilized GOx was evaluated by measuring the sensing response to 100 mg mL^{-1} glucose when constant potentials between 2 and 8 V cm^{-1} and deposition time between 10 and 60 min were applied at a constant concentration of particles. ESI shows the experimental results (Fig. ESI-1.2). Deposition times longer than 50 min and potentials higher than 6 V cm^{-1} led to the darkening of the deposit. Moreover, high potentials caused electrolysis of water and evolution of hydrogen and oxygen gases at the electrodes on application of an electric field. The incorporation of these gas bubbles in the deposit led to decrease the quality of the coating. The optimal parameters were found to be potential of 6 V cm^{-1} and deposition time of 30 min.

In addition, the number of alternating layers was also tested but the response was the same as for 1 layer of each kind of particle.

In order to determine the applicability of each functional group under study in the field of biosensing, the response of each chip was evaluated with different glucose concentrations (2, 5 and 10 mg mL^{-1}), in 100 mM phosphate buffer solution at pH 7.0. The activity of the enzyme remained constant during all the measurement and no dye photobleaching or leaching of the particles from the chip surface was detected. Fig. 1.4 and ESI (Fig. ESI-1.3) show the experimental results. They show that GOx immobilized on PolymP®-Link provided the best response, which was 50 times higher than the response showed by the classical carboxylated particles.

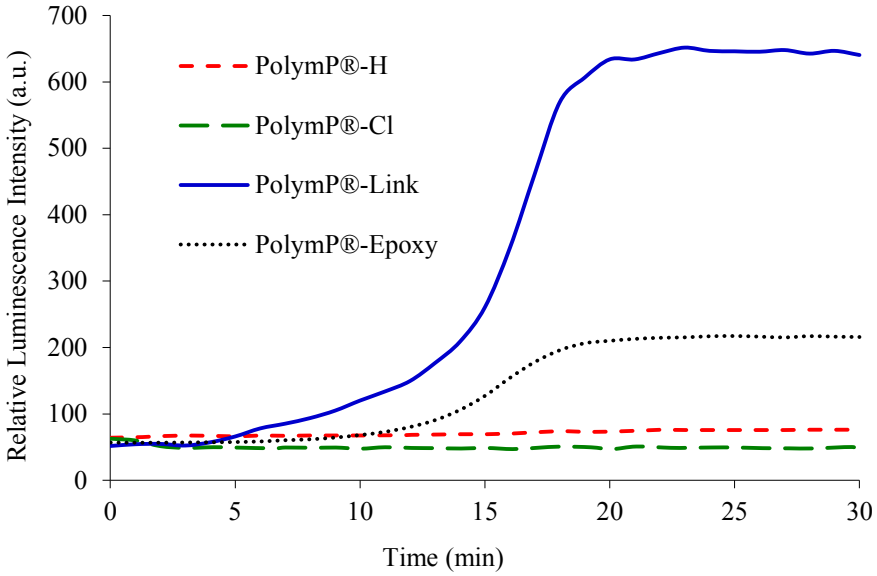

Fig. 1.4. Responses of the four glucose sensing films at a concentration level of 2 mg mL^{-1}. Detector voltage of 600 V, $\lambda_{exc/em}$ = 395/650 nm, monochromator slits $width_{exc/em}$ = 20/20 nm.

4. Conclusions

Four different types of polymeric particles with different superficial chemistry have been tested with the aim to determine the effect of the superficial functional group on chemical immobilization of the enzyme in the field of optical biosensing, using GOx as a model enzyme. In fact the immobilization of the enzyme has been optimised on chloride-functionalized (PolymP®-Cl), epoxy-functionalized (PolymP®-Epoxy), pre-activated surface containing vinyl groups (PolymP®-Link), and classical carboxyl-functionalized (PolymP®-H) particles; PolymP®-H were also used as a reference material.

The results showed that the enzyme immobilization is hardly influenced by the chemistry of

the carrier, pH, temperature, enzyme concentration, and immobilization time. Combining the results of activity and enzyme immobilization, it was determined that the particle with a pre-activated surface containing vinyl groups (PolymP®-Link) provides higher activity with a smaller amount of enzyme than the classical carboxyl-functionalized (PolymP®-H) particles, which are widely used for immobilizing biomolecules.

To demonstrate their applicability in the field of biosensing, the four enzyme-functionalized particles were deposited with oxygen sensitive particles in gold chips using EPD. The chip obtained using enzyme-functionalized PolymP®-Link showed the highest sensitivity to glucose, providing a sensing response 50 times higher than when classical carboxyl functionalized particles were used.

It is possible to conclude that particles with a pre-activated surface containing vinyl groups (PolymP®-Link) are a serious alternative to classical polymeric particles for effective immobilisation of biomolecules in the development of biosensing films.

Other interesting parameters to be considered are kinetic parameters (K_m and V_{max}) and the reusability and stability of immobilized enzymes. In this work they have not been included because these are not only related to the functional groups but also with the selected biomolecule. Thus, they should be evaluated when the aim of the research is the development of a sensor.

Acknowledgments

The authors gratefully acknowledge the financial support of the Spanish Ministry of Economy and Competitiveness (CTQ2011-25316, Ramon-Marquez‘s grant reference AP2012-0944 and Medina-Castillo‘s Torres Quevedo contract reference PTQ-11-04904) and the People Programme (Marie Curie Actions, Multi-ITN) of the European Union‘s Seventh Framework Programme (project EUROMBR grant agreement no. 608104).

References

Amao, Y., 2003. Probes and Polymers for Optical Sensing of Oxygen. Microchimica Acta 143(1), 1-12.

Amao, Y., Miyashita, T., Okura, I., 2001. Platinum tetrakis(pentafluorophenyl)porphyrin immobilized in polytrifluoroethylmethacrylate film as a photostable optical oxygen detection material. Journal of Fluorine Chemistry 107(1), 101-106.

Arica, M.Y., Hasirci, V., 1993. Immobilization of glucose oxidase: A comparison of entrapment and covalent bonding. Journal of Chemical Technology & Biotechnology 58(3), 287-292.

Borisov, S.M., Mayr, T., Mistlberger, G.n., Waich, K., Koren, K., Chojnacki, P., Klimant, I., 2009. Precipitation as a simple and versatile method for preparation of optical nanochemosensors. Talanta 79(5), 1322-1330.

Bulmuş, V., Ayhan, H., Pişkin, E., 1997. Modified PMMA monosize microbeads for glucose oxidase immobilization. The Chemical Engineering Journal and the Biochemical Engineering Journal 65(1), 71-76.

Cao, L. (Ed.), 2006. Carrier-bound Immobilized Enzymes: Principles, Applications and Design. WILEY-VCH.

Dickerson, J.H., Boccaccini, A.R. (Eds.), 2012. Electrophoretic Deposition of Nanomaterials.

Gao, Y., Kyratzis, I., 2008. Covalent Immobilization of Proteins on Carbon Nanotubes Using the Cross-Linker 1-Ethyl-3-(3-dimethylaminopropyl)carbodiimide—a Critical Assessment. Bioconjugate Chemistry 19(10), 1945-1950.

Hermanson, G.T. (Ed.), 2008. Bioconjugate Techniques, 2nd Edition ed. Academic Press.

Hou, X., Liu, B., Deng, X., Zhang, B., Chen, H., Luo, R., 2007. Covalent immobilization of glucose oxidase onto poly(styrene-co-glycidyl methacrylate) monodisperse fluorescent microspheres synthesized by dispersion polymerization. Analytical Biochemistry 368(1), 100-110.

Lott, J.A., Turner, K., 1975. Evaluation of Trinder's Glucose Oxidase Method for Measuring Glucose in Serum and Urine. Clinical Chemistry 21(12), 1754-1760.

Marin-Suarez, M., Medina-Rodriguez, S., Ergeneman, O., Pane, S., Fernandez-Sanchez, J.F., Nelson, B.J., Fernandez-Gutierrez, A., 2014. Electrophoretic deposition as a new approach to produce optical sensing films adaptable to microdevices. Nanoscale 6(1), 263-271.

Medina-Rodríguez, S., de la Torre-Vega, A., Fernández-Sánchez, J.F., Fernández-Gutiérrez, A., 2013a. An open and low-cost optical-fiber measurement system for the optical detection of oxygen using a multifrequency phase-resolved method. Sensors and Actuators B: Chemical 176(0), 1110-1120.

Mistlberger, G., Koren, K., Scheucher, E., Aigner, D., Borisov, S.M., Zankel, A., Pölt, P., Klimant, I., 2010. Multifunctional Magnetic Optical Sensor Particles with Tunable Sizes for Monitoring Metabolic Parameters and as a Basis for Nanotherapeutics. Advanced Functional Materials 20(11), 1842-1851.

Rauf, S., Ihsan, A., Akhtar, K., Ghauri, M.A., Rahman, M., Anwar, M.A., Khalid, A.M., 2006. Glucose oxidase immobilization on a novel cellulose acetate-polymethylmethacrylate membrane. Journal of Biotechnology 121(3), 351-360.

Sassolas, A., Blum, L.J., Leca-Bouvier, B.D., 2012. Immobilization strategies to develop enzymatic biosensors. Biotechnology Advances 30(3), 489-511.

Seuss, S., Boccaccini, A.R., 2013. Electrophoretic Deposition of Biological Macromolecules, Drugs, And Cells. Biomacromolecules 14(10), 3355-3369.

Shao, Q., Wu, P., Xu, X., Zhang, H., Cai, C., 2012. Insight into the effects of graphene oxide sheets on the conformation and activity of glucose oxidase: towards developing a nanomaterial-based protein conformation assay. Physical Chemistry Chemical Physics 14(25), 9076-9085.

Steiner, M.-S., Duerkop, A., Wolfbeis, O.S., 2011. Optical methods for sensing glucose. Chemical Society Reviews 40(9), 4805-4839.

Susanto, H., Samsudin, A.M., Rokhati, N., Widiasa, I.N., 2013. Immobilization of glucose oxidase on chitosan-based porous composite membranes and their potential use in biosensors. Enzyme and Microbial Technology 52(6-7), 386-392.

Trettnak, W., Kolle, C., Reininger, F., Dolezal, C., O'Leary, P., 1996. Miniaturized luminescence lifetime-based oxygen sensor instrumentation utilizing a phase modulation technique. Sensors and Actuators B: Chemical 36(1–3), 506-512.

Wang, X.-d., Wolfbeis, O.S., 2014. Optical methods for sensing and imaging oxygen: materials, spectroscopies and applications. Chemical Society Reviews 43(10), 3666-3761.

Ye, P., Wan, R.B., Wang, X.P., 2009. Quantitative enzyme immobilization: Control of the carboxyl group density on support surface. Journal of Molecular Catalysis B: Enzymatic 61(3-4), 296-302.

Zhitomirsky, I., Gal-Or, L., 1997. Electrophoretic deposition of hydroxyapatite. Journal of Materials Science: Materials in Medicine 8(4), 213-219.

Appendix. Electronic Supporting Material (ESI)

Content:

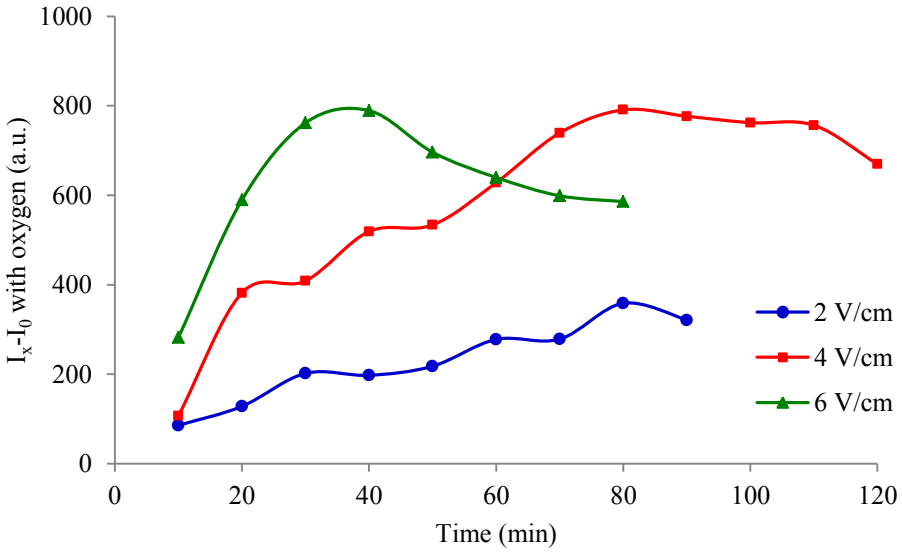

Fig. ESI-1.1. Variation of the signal response of the oxygen sensitive particles onto a golden chip *versus* deposition time at different deposition voltages in the determination of 8 ppm O_2 solubilized in water at RT. $\lambda_{exc/em}$ = 395/650 nm, slits width$_{exc/em}$ = 20/20 nm, t_d = 200 µs, t_g = 5 ms, detector voltage of 600 V.

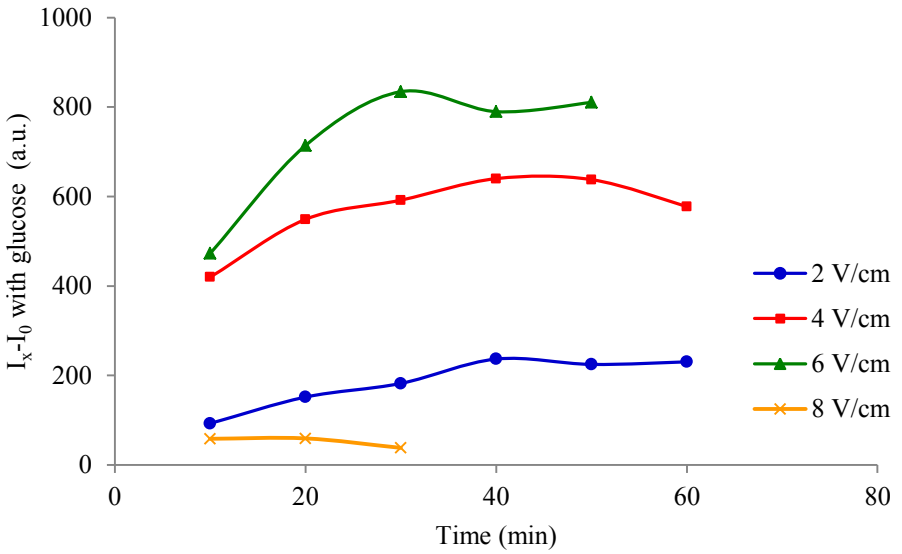

Fig. ESI-1.2. Variation of the signal response of the GOx functionalized particles onto oxygen-sensitive functionalized gold chip *versus* deposition time at different deposition voltages. [Glucose] = 100 mg mL^{-1}, $\lambda_{exc/em}$ = 395/650 nm, slits width$_{exc/em}$ = 20/20 nm, t_d = 200 µs, t_g = 5 ms, detector voltage of 600 V.

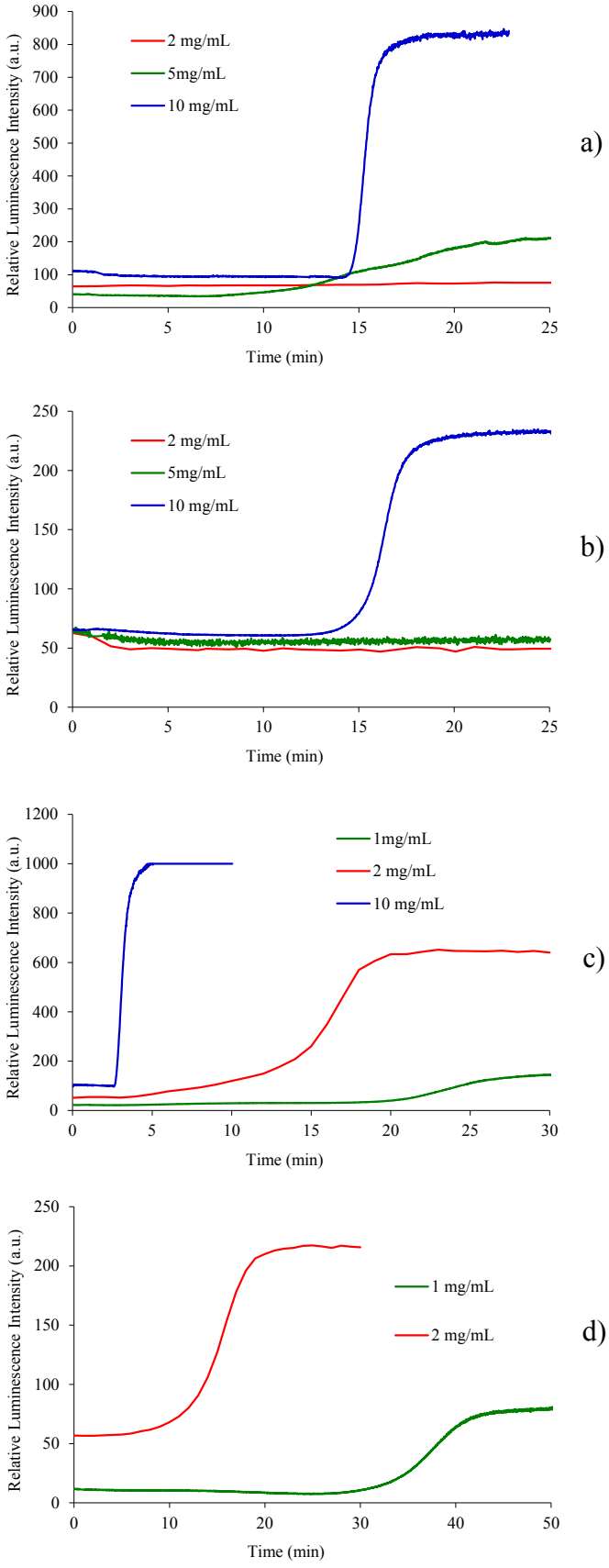

Fig. ESI-1.3. Response of the chips functionalized with a) PolymP®-H, b) PolymP®-Cl, c) PolymP®-Link and d) PolymP®-Epoxy and oxygen-sensitive particles in the determination of glucose.

Capítulo 2

Characterization of supports activated with divinyl sulfone as a tool to immobilize and stabilize enzymes via multipoint covalent attachment. Application to chymotrypsin

Jose C. S. dos Santos[a,b], Nazzoly Rueda[a,c], Oveimar Barbosa[d], Jorge F. Fernández-Sánchez[e], Antonio L. Medina-Castillo[f], Teresa Ramón-Márquez[e], María C. Arias-Martos[f], Mª Carmen Millán-Linares[g], Justo Pedroche[g], María del Mar Yust[g], Luciana R. B. Gonçalves[b] and Roberto Fernandez-Lafuente[a]

[a] ICP-CSIC, Departamento de Biocatálisis, Instituto de Catálisis-CSIC, 28049 Madrid, Spain

[b] Departamento de Engenharia Química, Universidade Federal do Ceara, Campus do Pici, CEP 60455-760, Fortaleza, CE, Brazil

[c] Escuela de Química, Universidad Industrial de Santander, Bucaramanga, Colombia

[d] Facultad de Ciencias, Departamento de Química, Universidad del Tolima, Ibague, Colombia

[e] Department of Analytical Chemistry, University of Granada, Avd. Fuentenueva s/n, 18071 Granada, Spain

[f] NanoMyP®, Nanomateriales y Polimeros S.L., Spin-Off company of the UGR, BIC Building, Avd. Innovacion 1, E-18016, Granada, Spain

[g] Instituto de la Grasa-CSIC, Av Padre García Tejero 4, 41012 Sevilla, Spain

Published in *RSC Advances*, 2015, **5**, 20639-20649

ABSTRACT

Divinyl sulfone (DVS) has been used to activate agarose beads. The DVS activated agarose resulted quite stable in the pH range 5-10 at 25 ºC under wet conditions, and can react rapidly with α-amides of Cys and His, at pH 5-10, with Lys mainly at pH 10 and with Tyr in a much slower fashion. After blocking with different nucleophiles, the support lost all reactivity, confirming that this protocol could be useful as an enzyme–support reaction end point. Then, chymotrypsin was immobilized on this support at pH 5, 7 and 10. Even though the enzyme was immobilized at all pH values, the immobilization rate decreased with the pH value. The effect of the immobilization on the activity depended on the immobilization pH, at pH 7 the activity decreased (to 50%) more than at pH 10 (by a 25%), while at pH 5 the immobilization has no effect. Then, the effect of blocking with different reagents was analysed. It was found that blocking with ethylenediamine improved the enzyme activity by 70% and gave the best stability. The stability of all enzyme preparations improved when 24 h incubation was performed at pH 10, but the qualitative stabilization depended on the inactivation conditions. The analysis of the amino acids of the preparation immobilized at pH 10 showed that Lys, Tyr and Cys residues were involved in the immobilization, involving a minimum of 10 residues (glyoxyl agarose gave 4 Lys involved in the immobilization). The new preparation was 4-5 fold more stable than glyoxyl agarose preparation, considered a very stable one, and in some instances was more active than the free enzyme (170% for the enzyme immobilized at pH 10). Thus, DVS activated supports are very promising to permit the multipoint covalent attachment of enzymes, and that way to improve their stability.

1. Introduction

Immobilization is in many instances a compulsory step in the design of a biocatalyst, as it is the simplest solution to the problems generated by the solubility of the proteins in aqueous media, enabling the enzyme recovery and its separation from the reaction medium (Brady and Jordaan 2009; Chibata et al. 1986; Hartmeier 1985; Katchalski-Katzir 1993; Kennedy et al. 1990; Klibanov 1983). Immobilization also simplifies bioreactor design and control over the reaction (Adlercreutz 2013; Cao 2011; Petkar et al. 2006; Singh et al. 2013).

Thus, many researchers have focused their efforts on the use of the "compulsory" immobilization step to improve other enzymes properties, mainly the enzyme stability (Fernandez-Lafuente 2009; Mateo et al. 2007; Petkar et al. 2006), but also activity, specificity or selectivity (Guzik et al. 2014; Hernandez and Fernandez-Lafuente 2011; Rodrigues et al. 2013).

Enzyme stabilization *via* immobilization may be achieved *via* different phenomena (Illanes 2011; Rodrigues et al. 2011). Any enzyme molecule that is immobilized and dispersed in the surface of a porous support cannot suffer any intermolecular inactivation process (precipitation, proteolysis, interaction with external hydrophobic interfaces) (Illanes 2011; Rodrigues et al. 2011). Moreover, a proper immobilization system may permit to improve the enzyme stability by generating a favourable enzyme environment (Hernandez et al. 2012; Mateo et al. 2006a; Rodrigues et al. 2011), by avoiding the subunit dissociation of multimeric proteins (Fernandez-Lafuente 2009) or by increasing the enzyme rigidity *via* multipoint covalent attachment (Brady and Jordaan 2009; Garcia-Galan et al. 2011; Gianfreda and Scarfi 1991; Hernandez and Fernandez-Lafuente 2011; Klibanov 1979; Mateo et al. 2007; Singh et al. 2013).

Multipoint covalent attachment has revealed itself as one of the most potent tools to improve enzyme stability (Garcia-Galan et al. 2011; Hernandez and Fernandez-Lafuente 2011; Klibanov 1979; Mateo et al. 2007). The selection of the support, the immobilization conditions and the reactive groups on enzyme and support are key points in the preparation of enzyme biocatalysts stabilized *via* multipoint covalent attachment (Blanco et al. 1989; Pedroche et al. 2007).

The support must offer flat surfaces to the reaction with the enzyme (*e.g.*, agarose) and must present many reactive groups on that surface (Mateo et al. 2007). The immobilization conditions must favour the enzyme mobility and the reactivity of the supports and enzyme groups (moderate temperatures, alkaline pH values, long reaction times) (Blanco et al. 1989; Pedroche et al. 2007). Finally, the reactive group on the support needs to be able to react with enzyme moieties that are

generally abundant in the enzyme surface (Mateo et al. 2007). Moreover, it must offer low steric hindrances to the reaction with the enzyme groups, good stability under immobilization conditions and be placed at a moderate distance from the support surface to really transmit the rigidity of the support to the enzyme (Mateo et al. 2007). The number of support groups suitable for producing very intense multipoint covalent attachment is not very high. The supports activated with glyoxyl (Mateo et al. 2005; Mateo et al. 2006b), epoxide (Boller et al. 2002; Hilterhaus et al. 2008; Katchalski-Katzir and Kraemer 2000) and the versatile glutaraldehyde (Barbosa et al. 2014; Barbosa et al. 2012) have offered good results in this topic and some industrial enzymatic biocatalysts have been prepared using these chemistries. However, each of these active groups has some problems which avoid their universal use, making very interesting to find some new protocols.

Glyoxyl supports have been described as very suitable to get an intense multipoint covalent attachment (Mateo et al. 2006b). This good result occurs even though the immobilization on this support only involves the primary amino groups of the protein (Mateo et al. 2006b). However, immobilization needs to be performed at alkaline pH value, even proteins with low density of Lys cannot be immobilized (Mateo et al. 2005) and the end point of the reaction requires the use of borohydride (Blanco and Guisán 1989). Epoxy-supports may react with a wide range of protein groups (amino, thiol, phenol, imidazole, carboxy) (Turková et al. 1978), but they have very low reactivity, even making a first adsorption of the enzyme on the support necessary to get a first covalent immobilization (Melander et al. 1984; Smalla et al. 1988; Wheatley and Schmidt 1993; Wheatley and Schmidt Jr 1999) (this has been useful to develop epoxy heterofunctional supports) (Barbosa et al. 2013). Due to this low reactivity, a very intense multipoint covalent attachment is hard to achieve compared to glyoxyl supports (Bolivar et al. 2010). Glutaraldehyde activated supports have low stability, and very low stability at alkaline pH (Barbosa et al. 2012), usually the best results are achieved by modifying anionically exchanged enzymes on amino supports (and that is not always positive for the enzyme activity because it means a global enzyme surface modification) (Barbosa et al. 2014). Thus, the search of new reactive groups on the support potentially useful to stabilize enzymes *via* multipoint covalent attachment is still a demand in the biocatalyst design.

In this regard, supports activated with divinyl sulfone (DVS) have been successfully used to immobilize some enzymes (Bale Oenick et al. 1990; Bryjak et al. 2008; Labus et al. 2011; Lopez-Jaramillo et al. 2012; Medina-Castillo et al. 2012; Morales-Sanfrutos et al. 2010; Ortega-Munoz

et al. 2010; Prikryl et al. 2012), but its potential use to stabilize the immobilized proteins and some of the relevant features to determine their prospects as a support for industrial immobilization of enzymes have not been even analysed.

Activation with DVS may be achieved in supports bearing in its surface a very wide range of groups, like amino, thiol or hydroxyl groups (Morales-Sanfrutos et al. 2010; Ortega-Munoz et al. 2010; Porath and Axén 1976). The reactive vinyl sulfone groups placed in the support can react with amino, phenol, imidazol or thiol groups of the proteins (Ilan et al. 1993; Morales-Sanfrutos et al. 2010), moieties that are frequently placed in its surface, therefore useful to get many enzyme-supports linkages (Srere and Uyeda 1976).

In this paper, we have analysed the prospects of DVS-agarose beads as support not just to immobilize enzyme, but to stabilize enzymes via multipoint covalent attachment. In literature there is a lack of information on some key features of a support to be considered a good support to produce an intense multipoint covalent attachment. For example, the reactivity of the different moieties of the proteins at different pH values and the stability of the groups under immobilization conditions are very important characteristic and have been analysed for first time in this paper, also some alternatives as enzyme-support reaction end-point have been compared. Then, a model enzyme, bovine alpha-chymotrypsin, has been immobilized on the DVS support and the variables that determine the final stabilization have been studied. This enzyme has been selected because it may be highly stabilized *via* multipoint covalent attachment; in fact it has been highly stabilized after immobilization on glyoxyl agarose beads (Guisán et al. 1991). The protocol of enzyme immobilization is usually critical to take the maximum profit of the characteristics of the support to achieve an intense multipoint covalent attachment, it may be stated that good results may be achieved only if a good support and a good immobilization protocol are utilized.

2. Materials and methods

2.1. Materials

Divinyl sulfone, α-chymotrypsin from bovine pancreas, benzoyl-L-tyrosine-*p*-nitroanilide (BTNA), ethylenediamine, ethanolamine, glycine, aspartic acid, cysteine and 2-mercaptoethanol were purchased from Sigma Chemical Co. (St. Louis, MO). The α-amides of Lys, His, Tyr and

Cys were purchased from Bachem. Agarose beads 6% (w/v) were purchase from Agarose Bead Technologies (ABT, Spain). All other reagents were of analytical grade.

2.2. Methods

All experiments were performed by triplicate and the results are reported as the mean of this value and the standard deviation (under 10%).

2.2.1. Enzymatic assays

The activity of the soluble or immobilized enzyme (30 mg mL^{-1}) was assayed by determination of the increase in absorbance at 405 nm which accompanies the hydrolysis of the synthetic substrate BTNA (100 or 200 µL of soluble or suspended enzyme were added to 2.5 mL 50 mM sodium phosphate 40 % ethanol, pH 7.0, containing 30 µL of 40 mM BTNA in hexane:dioxane 1:1 (v/v) at room temperature) (Pedroche et al. 2007).

In the determination of the effects of the pH value on the enzyme activity, the followed protocol was similar but the buffer in the measurements was changed according to the pH value studied: 100 mM of sodium acetate at pH 5–0, sodium phosphate at pH 6.0–8.0 and sodium borate at pH 9–0 and pH 10.0. At 25 ºC, all the preparations remained fully stable after incubation for several hours at any of these pH values. The ε values suffered very slight variations with the change in the pH value.

2.2.2. Preparation of glyoxyl-agarose-support

The activation of agarose gels was done according to the procedure previously described (Mateo et al. 2005; Mateo et al. 2006b). The agarose beads were suspended in 1 M NaOH and 0.5 M $NaBH_4$ (3 mL of solution per g of support). This suspension was maintained in an ice bucket under mechanical stirring, and glycidol was added drop wise in order to reach a 2 M final concentration. The resulting suspension was gently stirred overnight at room temperature. The activated gel was then washed with abundant distilled water.

Them, the glycidol activated support was incubated in a solution of water containing 80 µmol of $NaIO_4$ per wet gram of beads (10 mL of oxidation solution per g of wet support). This oxidative reaction was allowed to proceed for 2 h under mild stirring at room temperature (Nevell and Whistler 1963). Then, the glyoxyl support was washed with an excess of distilled water and stored at 4 ºC under wet conditions.

2.2.3. Preparation of divinyl sulfone-agarose-support

A volume of 7.5 mL divinyl sulfone was added to 200 mL of 333 mM sodium carbonate buffer at pH 12.5 and vigorously stirred until the solution became homogeneous, then 10 g of agarose beads was added and left under gentle agitation for 35 minutes. Then, the support was washed with an excess of distilled water and stored at 4 ºC.

2.2.4. Determination of the reaction rates between DVS support and different amino acids

The pH of 10 mL of 2 mM of amides with the α-amino acid of the amino acids His, Tyr, Lys and Cys, was adjusted at pH 5.0 (100 mM, sodium acetate), pH 7.0 (100 mM, sodium phosphate) or pH 10.0 (100 mM, sodium bicarbonate). Then, 1 g of DVS-support was added. Inert agarose was used as a reference. The remaining amide in the supernatant was measured periodically using an UV spectra (wavelength was 220 nm) (Jasco V-630) and in some cases the concentration was confirmed by HPLC (Spectra Physic SP 100) coupled to an UV detector (Spectra Physic SP 8450).

2.2.5. Immobilization of the enzymes

2.2.5.1. Immobilization on glyoxyl-support

The immobilization was performed suspending 10 g of wet support in 100 mL of chymotrypsin solution (maximum protein concentration was 1 mg mL^{-1}), prepared in 50 mM sodium carbonate at pH 10.0-10.1 at 25 ºC for 3 h under continuous stirring (Guisán et al. 1991). As a reaction end point, derivatives were reduced by addition of solid $NaBH_4$ (to reach a concentration of 1 mg mL^{-1}). After gentle stirring for 30 min at room temperature, the resulting derivatives were washed with abundant distilled water to eliminate residual sodium borohydride.

2.2.5.2. Immobilization on divinyl sulfone-support

The immobilization was performed suspending 10 g of wet support in 100 mL of proteins solutions (maximum protein concentration was 1 mg mL^{-1}), prepared in 50 mM sodium acetate at pH 5.0, sodium phosphate at pH 7.0 or sodium carbonate at pH 10.0, always at 25 ºC. In some cases, the immobilized enzyme preparations were incubated in 100 mL of 100 mM bicarbonate at pH 10.0 and 25 ºC for different times before stopping the enzyme–support reaction by blocking the support. As a reaction end point, all the immobilized biocatalysts were incubated for 24 hours at room temperature in 1 M of different nucleophiles (ethylenediamine, ethanolamine, glycine,

aspartic acid, cysteine or mercaptoethanol) dissolved in 100 mM sodium carbonate at pH 10.0. Finally, the immobilized enzyme preparations were washed with an excess of distilled water and stored at 4 ºC.

2.2.6. Thermal inactivations

To check the stability of the enzyme derivatives, 1 g of immobilized enzyme was suspended in 5 mL of 50 mM sodium acetate at pH 5.0, sodium phosphate at pH 7.0 or sodium carbonate at pH 9.0 at different temperatures. Periodically, samples were withdrawn and the activity was measured using BTNA. Half-lives were calculated from the observed inactivation courses.

2.2.7. Determination of the amino acids involved on the enzyme–support multipoint covalent attachment

The bonds formed by the enzymes and the glyoxyl (after reduction), or the DVS supports (after blocking) are highly stable and may stand acid hydrolysis of proteins. This strategy has been used previously with very good results on different glyoxyl-immobilized enzymes (Blanco et al. 1989; Pedroche et al. 2007). The number of free amino acids of the different biocatalysts was obtained by determining the amino acids of each biocatalyst that could be released to the medium by the method previously described by Alaiz *et al* (Alaiz et al. 1992). Briefly, samples of each derivative, containing 2-4 mg of enzyme, were hydrolysed with 6 N HCl at 120 ºC and subsequently analysed by high performance liquid chromatography (HPLC) after derivatization with ethoxymethylenmalonate, using D,L-α-aminobutyric acid as internal standard, and a 300 × 3.9 mm i.d. reverse-phase column (Novapack C18, 4 µm; waters). Likewise, amino acid composition of soluble chymotrypsin was also determined, in the presence and absence of blocked DVS support to ensure the lack of artefacts caused by the support. Concentrations (mol per g protein) of each amino acid were determined and the number of residues was calculated as followed:

Number of amino acid/molecule of chymotrypsin × amino acid concentration in sample/amino acid concentration in chymotrypsin.

2.2.8. Studies of enzyme structure and amino acid accessibility

Protein structures were modelled using PyMol software version 0.99rc6 (DeLano 2002). Surface accessibility (ASA) values of residues from 1TCA were calculated by the web-based program ASA-view (Ahmad et al. 2004). Solvent accessibility was divided into three classes:

buried, partially exposed and exposed, indicating, respectively, the least, moderate and high accessibility of the amino acid residues to the solvent (Gilis and Rooman 1996, 1997).

3. Results

3.1. Characterization of the DVS-agarose as a matrix to immobilize proteins and stabilize them via multipoint covalent attachment

3.1.1. DVS reactivity versus different amino acids under different pH values

The scheme of the reaction between the DVS and the agarose is shown in Scheme 2.1. A support to be used in immobilization and stabilization of enzymes *via* multipoint covalent attachment must have a good reactivity with groups frequently placed in the enzyme surface. DVS has been reported to react with hydroxyl, imidazol, amino or thiol groups (Bale Oenick et al. 1990; Begara-Morales et al. 2013; Bryjak et al. 2008; Labus et al. 2011; Lopez-Jaramillo et al. 2012; Medina-Castillo et al. 2012; Morales-Sanfrutos et al. 2010; Ortega-Munoz et al. 2010; Prikryl et al. 2012). Thus, Lys, Tyr, His and Cys are the amino acids that can exhibit a higher reactivity with the DVS-support.

Moreover, it may be expected that the reactivity of the different amino acids with DVS may differ at different pH value. This may open the opportunity to control the enzyme orientation by using conditions that can favour the reactivity of the support with one group kind or another, changing the amino acids involved in the first covalent attachment.

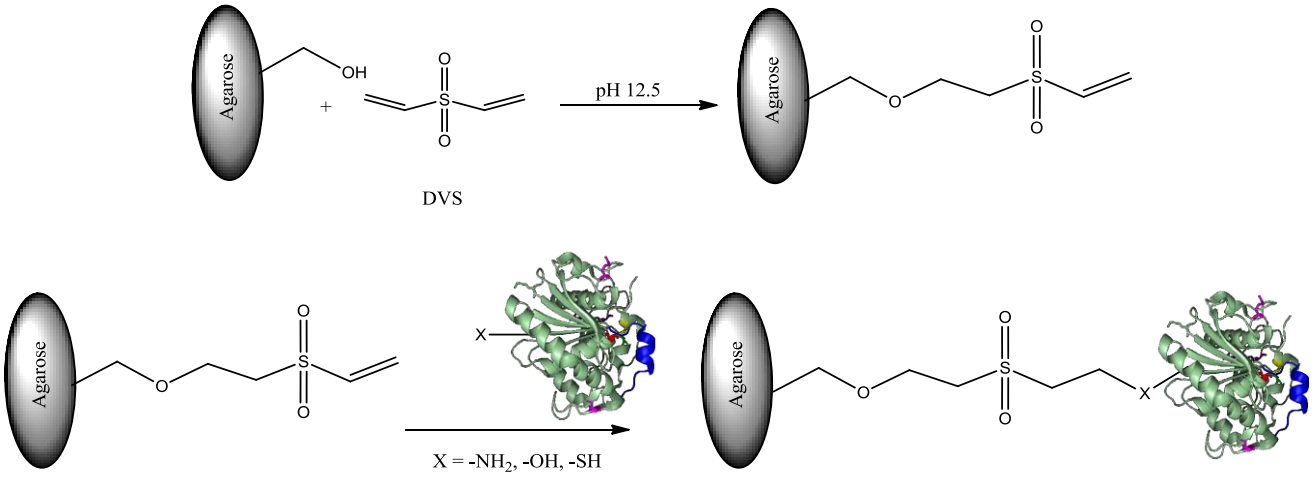

Scheme 2.1. Activation of agarose with DVS and reaction of DVS activated supports with proteins.

To this purpose, the amides (to eliminate the reactivity of the amino acid alpha-amino group) of Lys, Cys, His and Tyr were offered to DVS-activated supports at pH 5.0, 7.0 and 10.0. Table 2.1 shows the results. As expected, the highest immobilization rates for all amino acids were observed at pH 10.0 and the lowest at pH 5.0.

Table 2.1. Reaction rates of the α-amides of different amino acids. The experiments have been performed as described in Section 2. The immobilization rates are given as μmol of immobilized amide per h per g.

	Immobilization rates		
Amino acid	**pH 10**	**pH 7**	**pH 5**
Lysine	14.20 ± 0.5	1.09 ± 0.2	0.04 ± 0.01
Cysteine	24.80 ± 1	5.60 ± 0.4	2.60 ± 0.1
Tyrosine	0.73 ± 0.1	0.40 ± 0.1	0.27 ± 0.05
Histidine	21.00 ± 1	7.33 ± 0.8	1.67 ± 0.2

Lys, the most abundant residues among the studied ones had a good reactivity at pH 10.0, which drastically decreased at pH 7.0 and even more at pH 5.0. Cys and His are the most reactive groups at all studied pH values, decreasing the reactivity when the pH value was lowered in a slower fashion than Lys, while Tyr is the less reactive group, except at pH 5.0 where it is more reactive than Lys. Thus, it seems that at pH 5.0 the Lys residues will play an irrelevant role in the first immobilization of an enzyme on DVS activated supports even being the most abundant group, because the ionization degree of its amino group. At lower pH value, it is expected that the terminal amino group may be more relevant in the immobilization of the enzyme. The terminal amino group should have a pK value 2-3 units below that of the Lys (10.7), thus its reactivity at low pH value should be much more significant than that of the Lys residues, mainly at pH 5.0.

3.1.2. DVS stability under different experimental conditions

The usefulness of a support to immobilize enzymes at industrial level may be marked by the stability of the active groups under different conditions. This may affect the storage (*i.e.*, it is simpler if the support may be stored under wet conditions at 25 ºC that if it requires to be conserved under dry conditions at -20 ºC). Stability of the support groups also determines the range of conditions where the support can be used in the enzyme immobilization. Another point to be considered is that only if the support reactive groups are stable enough, the support surface

may be fully covered of enzyme molecules because this may require a relative long time. On the contrary, if the support groups are instable, it is possible that they become inactivated before the full support surface is coated with enzyme. Multipoint covalent attachment usually requires a quite long time, as the support and the enzyme are quite rigid structures that need to get the correct alignment to get an intense multipoint covalent attachment under conditions where the support and enzyme have a good reactivity attachment (Blanco et al. 1989; Pedroche et al. 2007). This makes that only supports having good stability may be used in the long term incubation necessary to get an intense multipoint covalent.

In order to check the stability of the DVS groups under different conditions that could be useful to immobilize different enzymes, the supports were incubated at pH values ranging from pH 4.0 to pH 10.5 at 25 ºC.

Periodically, samples were extracted and their reactivity *versus* *N*-alpha-amide-Lys at pH 10.0 was evaluated. After 24 h of incubations at 25 ºC, there was no difference in the reaction rate between the Lys-amide and the DVS support in all conditions, which means that the support remained fully reactive in this range of pH values. At pH 7.0 and 25 ºC, after 60 days, the reactivity of the support did not suffer any relevant decrement (less than 5%). The stability was really high even at 36 ºC, over 90 % of the reaction rate *versus* Lys was observed after 60 days of incubation at pH 7.

Thus, storage seems to be possible even under wet conditions at pH 7.0. Moreover, DVS supports seem to be useful to immobilize enzymes at 25 ºC in a broad range of pH values, also useful to get multipoint covalent attachment (even at pH 10.0 in 24 h the reactivity of the support is maintained).

3.1.3. Reaction end point

The usefulness of a support to immobilize enzymes, and more if the final goal is to have a highly stabilized biocatalyst, is favoured if there is some simple protocol to eliminate the chemical reactivity of the support with the enzyme when the desired degree of enzyme-support reaction has been achieved. This will permit the full control of the enzyme-support reaction, otherwise during operation the enzyme and the support can produce new covalent bonds that can drive to the inactivation of the enzyme by stabilizing inactive enzyme structures. To this goal, the DVS support was blocked by incubation in the presence of different compounds for 24 h, and also was reduced with 1 mg mL^{-1} sodium borohydride (compatible with many enzymes stability)

(Blanco and Guisán 1989), or submitted to incubation overnight in 1 M NaOH at 40 ºC to destroy the support reactivity. The incubation in NaOH left a support fully unreactive with the α-amide of Lys. Similar results were obtained by the blocking with all the studied compounds. However, using $NaBH_4$, the reactivity of the support decreased to 20%, but we were not able to fully eliminate the support reactivity even using 5 mg mL^{-1} $NaBH_4$, although this very high concentration was not compatible with the stability of many enzymes (Blanco and Guisán 1989). Thus, as in the case of the epoxide-activated supports, the proposed end point to the enzyme support reaction is the blocking of the support with different nucleophiles (Mateo et al. 2002). The selection of the blocking reagent will depend on the specific enzyme properties, and may be used also as a tool to further tuning the enzyme properties (Bonomi et al. 2013).

3.2. Immobilization of chymotrypsin in DVS supports at different pH values

From the previous results, the DVS-support seems very adequate to immobilize enzymes at industrial level. It may be handled or stored even in wet conditions and room temperature for weeks without decreasing its reactivity, and it permits its use at pH values from 5.0 to 10.0 for 24 h without any significant decrease in support reactivity. Coupling this stability results with the data on reactivity *versus* different amino acids, and the possibility of blocking by incubation with different nucleophiles, DVS supports seemed to have very good prospects to immobilize proteins under a broad range of pH values and to produce an intense support/enzyme multi-reaction.

Next, the immobilization of chymotrypsin has been tried in DVS-agarose at pH ranging from 5.0 to 10.0.

3.2.1. Analysis of the accessibility of the different amino acids to the medium

First of all, the number of reactive groups of the enzyme and their accessibilities in the enzyme surface (ASA) were studied. Table 2.2 shows the amount of likely reactive groups of chymotrypsin and their medium exposition degree. From Table 2.2, the 14 Lys residues that this enzyme has, are reasonably exposed to the medium, while from the 4 Tyr, only Tyr-171 have good exposition, while Tyr-228 is not exposed. Both His have a very low exposition. Regarding the 10 Cys all of them are involved in disulphide bridges (1-122; 42-58; 136-201; 168-182; 191-220) and therefore with low reactivity *via* the thiol group. Moreover, the amino terminal Cys has a very high exposition (and can react *via* its amino group), while the other have moderate or even null exposition to the medium.

Table 2.2. List of reactive groups of chymotrypsin and their medium accessibilities (ASA). Calculations have been performed as described in Section 2. Surface accessibility (ASA) values of residues from 1TCA were calculated by the web-based program ASA-view.

Amino acid	Tyr-94	Tyr-146	Tyr-171	Tyr-228	Lys-36	Lys-79	Lys-82	Lys-84
% ASA	24.3	15.9	59	0.5	74.4	99.2	73.4	73.4
Amino acid	Lys-87	Lys-90	Lys-93	Lys-107	Lys-169	Lys-170	Lys-175	Lys-177
% ASA	55.9	62.7	70	19.9	43.3	89.9	46.7	37.4
Amino acid	Lys-202	Lys-203	His-40	His-57	Ile-16	Ala-149	Cys-1	Cys-42
% ASA	62.2	37.9	12.1	2.7	0.5	27.2	77	2.8
Amino acid	Cys-58	Cys-122	Cys-136	Cys-168	Cys-182	Cys-191	Cys-201	Cys-220
% ASA	11.1	7.6	0	0	0	4.9	0.7	16

The terminal amino groups Ile-16 and Ala-149 have a moderate or very low exposition respectively. The requirement for the medium exposition is higher when we intend to achieve the reaction between the enzyme and a flat surface (*e.g.*, groups inside pockets will hardly react with the support, at least in a first step, before the enzyme is distorted by the enzyme-support interactions). However, the enzyme may suffer some distortions during immobilization involving some new groups in the immobilization. Moreover, once the enzyme is immobilized, only groups located in that face of the protein can react with the support. To better visualize this, Fig. 2.1 shows the structure of the chymotrypsin with the reactive groups marked, it seems that many groups on the enzyme may take part on the immobilization step and on the further multipoint covalent attachment, mainly in the upper area to the active centre, while in the other face the number of reactive groups decreased. The possibilities of getting an intense multipoint attachment seems to be not limited by the number and distribution of groups located on the enzyme surface.

3.2.2. Chymotrypsin immobilization

As expected from the data on amino acids reactivity, immobilization proceeded far more rapid at pH 10.0 than at pH 7.0 or 5.0 (Fig. 2.2). In fact, at pH 10.0 immobilization in DVS-agarose (90% enzyme immobilized in 2 h) is even more rapid than the immobilization in the same support activated with glyoxyl groups (80% immobilization after 2 h), a support described as very suitable for the immobilization/stabilization of this enzyme (Guisán et al. 1991). At pH 7.0, the

enzyme immobilization was slower, with a yield of 75 % after 24 h, and at pH 5.0 was even slower, with immobilization yield of only 10 % after 24 h.

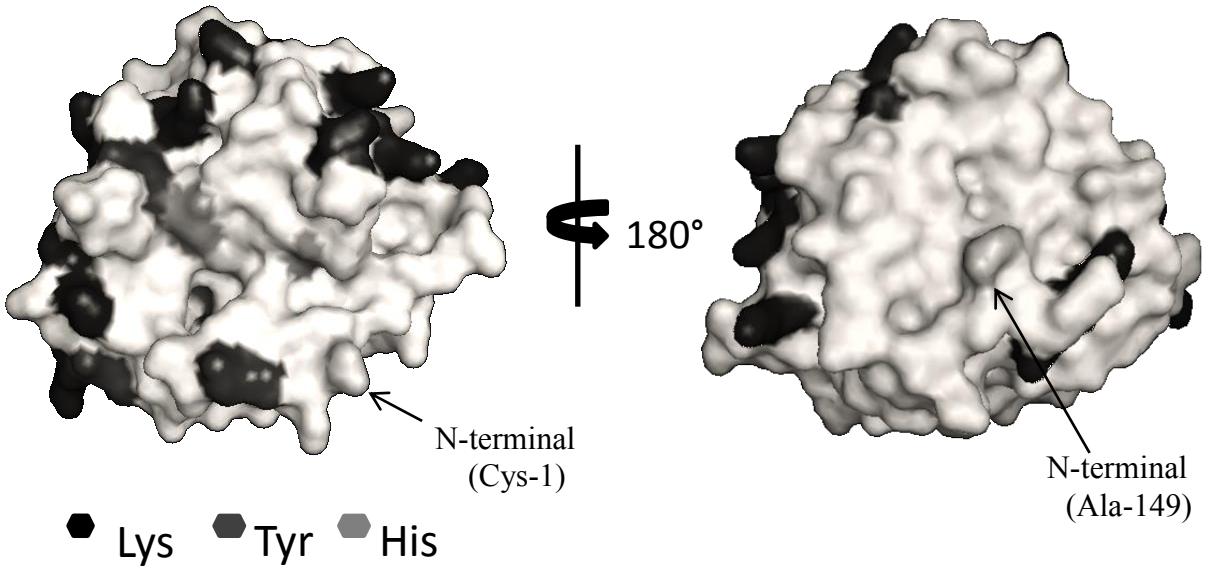

Fig. 2.1. 3D surface structure model of chymotrypsin. The 3D surface structure model of chymotrypsin indicates lysine, tyrosine and histidine residues and the *N*-terminal amino acids. (a) *N*-terminal face, (b) back face. The 3D surface structure was obtained using PyMol *versus* 0.99. The 3D structure of chymotrypsin was obtained from the Protein Data Bank (PDB). For chymotrypsin pdb code is 5CHA.

Regarding the activity (Fig. 2.2), the immobilization on DVS at pH 10.0 produced a decrease in enzyme activity of 25 % after 24 h. At pH 7.0, the decrease in activity is more significant, the expressed activity of the immobilized enzyme is around 50 % of that of the free enzyme. At pH 5.0, there are no significant changes in enzyme activity. The more drastic decrease in activity after immobilization at pH 7.0 cannot be related to a more intense reaction between enzyme and support, as show in the analysis of the reactivity of the different amino acids with this support showed in point 3.1.1, but may be explained if a different orientation of the enzyme in the support is produced. Fig. 2.1 shows that many of the groups relevant for enzyme immobilization are quite close to the active centre of the enzyme.

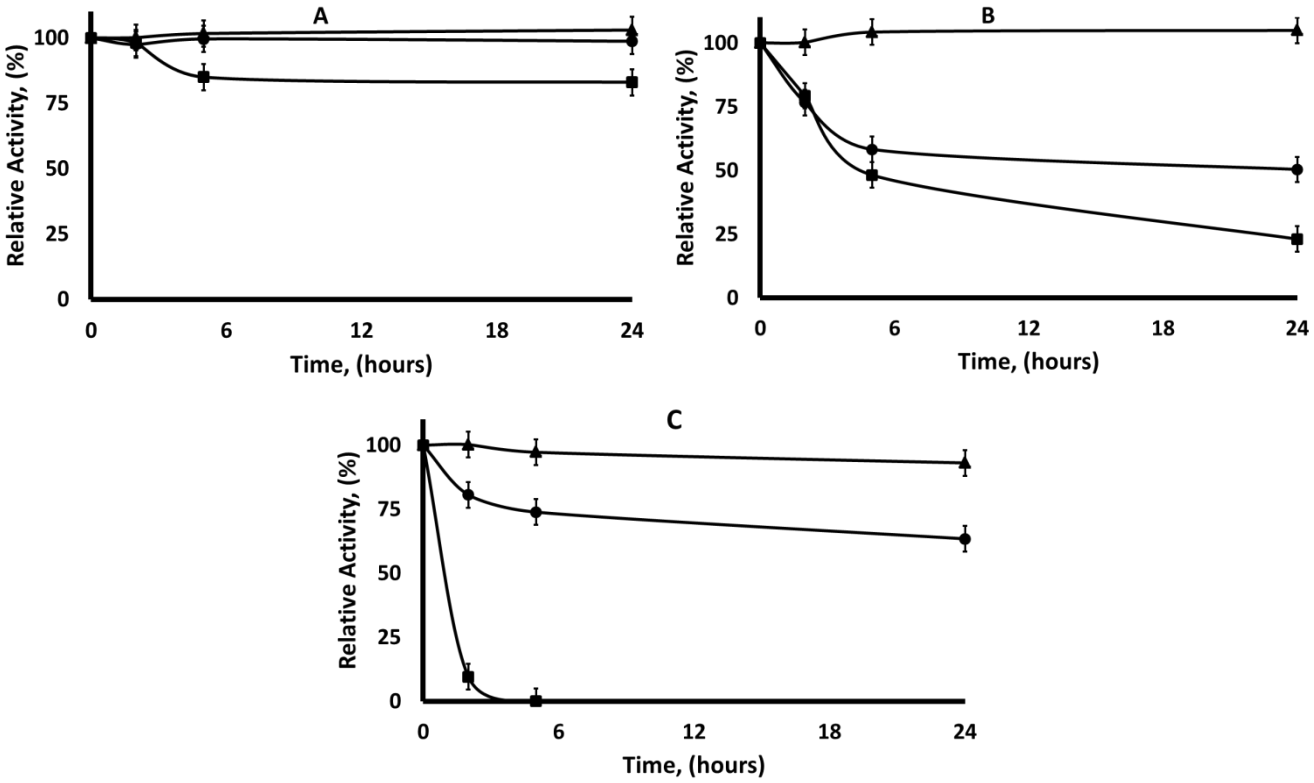

Fig. 2.2. Immobilization courses of chymotrypsin on DVS activated agarose at different pH values. Experiments have been performed at 25 ºC, other specifications are described in Section 2. Panel A: (pH 5.0), Panel B: (pH 7.0), Panel C: (pH 10.0): circles (suspension), square (supernatant), triangle (soluble enzyme).

3.3. Effect of the blocking step in the stability of chymotrypsin immobilized on DVS supports

Next, the enzyme that had been immobilized at pH 10.0 was subject to incubation in the presence of different nucleophiles to check the effects on enzyme activity and stability of the blocking of the reactive groups on the support. Fig. 2.3 shows that the incubation of the enzyme that had been immobilized at pH 10.0 in the presence of EDA permitted to increase the enzyme activity by a 75 % that decreases to 70 % after 24 h.

In opposition, the blocking with Cys produced a severe decrease of the enzyme activity, perhaps by their effect on the disulphide bonds that have chymotrypsin, while the incubation in the presence of the other blocking reagents did not produce a significant effect on enzyme activity. The biocatalyst blocked with EDA presented an activity slight higher than the activity of the free enzyme, reverting the slight decrease on enzyme activity observed during the immobilization step.

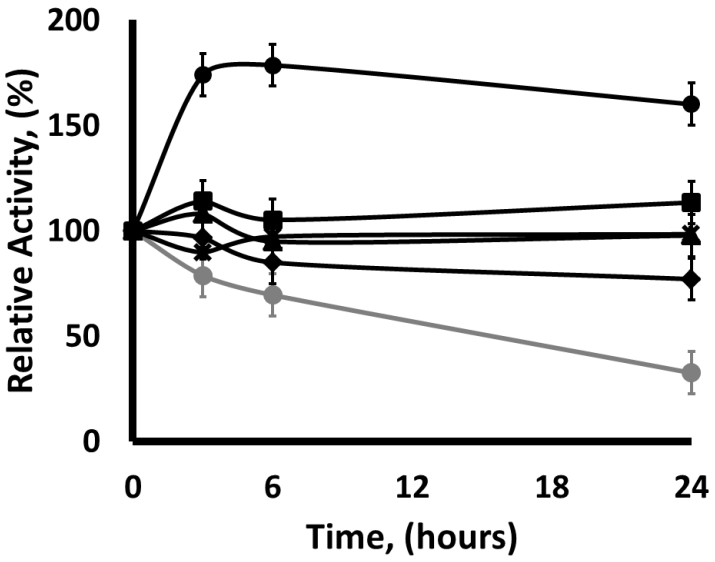

Fig. 2.3. Effect on enzyme activity of the incubation of the immobilized enzyme in the presence of different blocking agents. Experiments have been carried out at 25 ºC and at pH 10.0 using the enzyme immobilized at pH 10.0. Other specifications are described in Section 2. Circles, solid black line: (EDA); squares, solid black line: (ethanolamine); triangles, solid black line: (Gly); rhombus, solid black line: (Asp); stars, solid black line: (Cys); grey circles, solid grey line: (mercaptoethanol).

The less stable preparation was that unblocked, as the support still has the possibility to react with the distorted enzyme structure induced by heat. The most stable one was that blocked with EDA, while the less stable ones were those blocked with Gly or Asp, suggesting that the ionic nature of the support surface plays an important role on the stability of the immobilized chymotrypsin. Considering the high isoelectric point of chymotrypsin (9.2), the support with EDA may produce a lower number of ionic bridges with the enzyme than the Asp.

Thus, the EDA was selected as blocking reagent in further experiments.

Fig. 2.4 shows the thermal inactivation courses of the enzyme blocked with the different reagents.

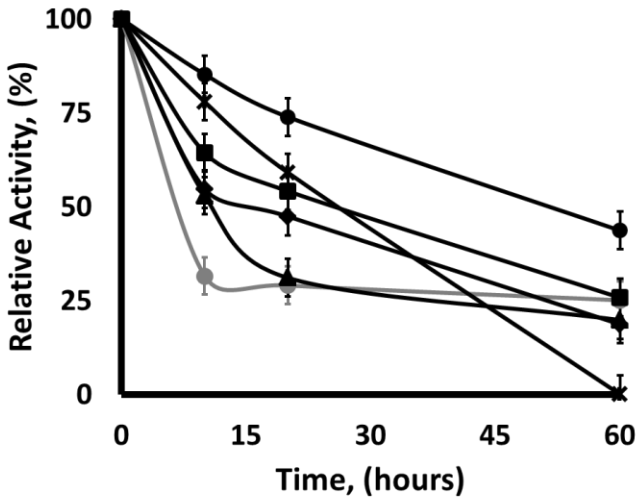

Fig. 2.4. Thermal inactivation courses of the enzyme blocked with the different blocking agents. Experiments have been performed at 60 ºC and pH 8.0, using the enzyme immobilized at pH 10.0. Other specifications as described in Section 2. Circles, solid black line: (EDA); squares, solid black line: (ethanolamine); triangles, solid black line: (glycine); rhombus, solid black line: (aspartic acid); stars, solid black line: (cysteine); grey circles, solid grey line: (pH 10.0).

3.4. Effect of the long term alkaline incubation on the activity/stability of DVS-chymotrypsin biocatalysts

In order to improve the enzyme stability, the enzyme that had been immobilized at pH 10.0 was further incubated at pH 10.0 for different times before the EDA blocking step. It should be considered that is not possible to ensure that during the blocking step there is not some enzyme-support reaction, and that can somehow minimize the effect of the long term incubation.

In this experiment, the biocatalyst was blocked with EDA just after immobilization (2 h), after 24 h, and after 72 h. The effect of this treatment on enzyme activity and stability has been analysed (Fig. 2.5). The long term incubation produced a certain decrement in enzyme activity (near to 50 % activity was lost after 72 h, Fig. 2.5a), while improving the enzyme stability, more clearly for the comparison between 2 and 24 h and in an almost negligible way if the incubation was prolonged from 24 to 72 h (Fig. 2.5b). Thus, incubation for 24 h at pH 10.0 seemed adequate to get optimal activity/stability parameters.

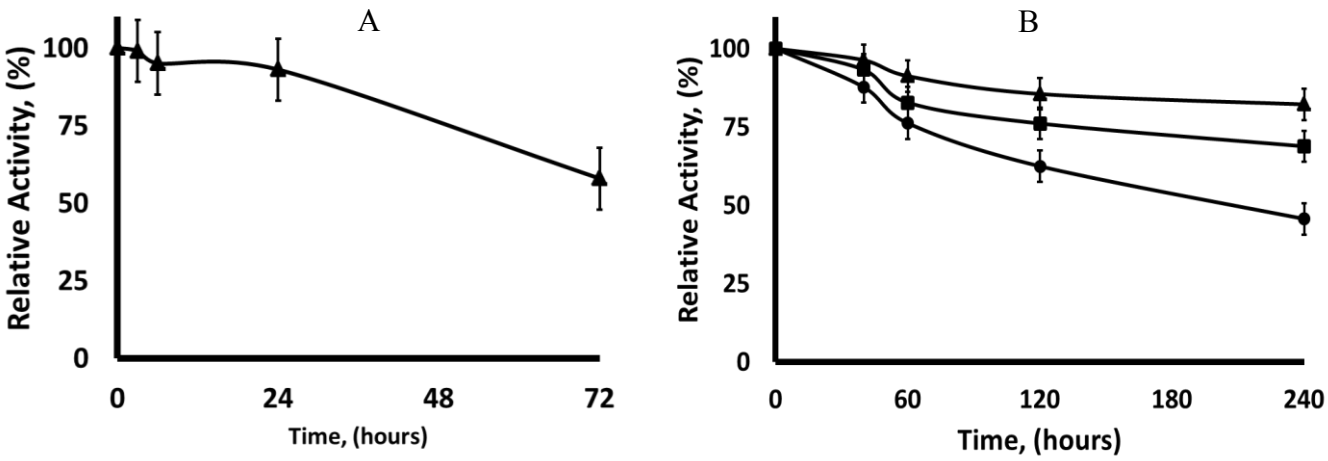

Fig. 2.5. Effect of the long incubation time on the activity/stability of DVS-chymotrypsin biocatalysts. Panel A: evolution of the activity of the chymotrypsin immobilized at pH 10.0 and 25 ºC. Other features are described in Section 2. Panel B: inactivation course of the different enzyme preparation at pH 10.0 and 25 ºC. Other features are described in Section 2. Circles, solid black line: DVS-chymotrypsin-6 h; squares, solid black line: DVS-chymotrypsin-24 h; triangles, solid black line: DVS-chymotrypsin-72 h.

3.5. Effect of the immobilization pH on the final activity/stability of the DVS-chymotrypsin preparation

As previously discussed, the immobilization pH value may alter the orientation of the enzyme on the support, and that way this may alter the final enzyme stability. This may be caused by the different amount of protein nucleophiles in each area (giving more or less possibilities of establishing many enzyme-support linkages) or by the relative importance of a specific area on enzyme stability. Thus, the activities and stabilities of enzymes immobilized at pH 5.0, 7.0 and 10.0 and blocked directly after immobilization have been compared to that of all these immobilized enzymes incubated for 24 h at pH 10.0 before the blocking step, giving similar possibilities at all enzyme preparations of producing an intense multipoint covalent attachment. Again, it must be considered that during the blocking step at alkaline pH, that may favour the enzyme-support reactivity, it is likely that some enzyme-support reaction may occur, and that may reduce the impact of the long term alkaline incubation. Table 2.3 shows the recovered activities of the different preparations and the half-lives obtained in thermal inactivations performed at pH 5.0, 7.0 and 9.0.

Regarding the activity, in many instances the positive effects of the blocking with EDA compensated the decrease of activity produced by immobilization. In fact, all preparations were

finally more active than the free enzyme. The positive effect of the blocking was similar in all preparations, and also the decrease caused by the alkaline pH incubation (even though the immobilization presented a higher negative effect on the enzyme activity at pH 7.0).

Table 2.3. Thermal stability of the different enzyme preparations is given as half-lives in minutes. Temperatures were 55 ºC at pH 5.0, 65 ºC at pH 7.0 and 60 ºC at pH 9.0. Other specifications are described in Section 2.

Biocatalysts	Recovered activity[a] (%)	Half-lives		
Soluble	100	pH 5	pH 7	pH 9
pH 5 (24 h)	170 ± 10	38 ± 3	17 ± 2	60 ± 4
pH 5 (24 h) + pH 10 (24 h)	140 ± 15	150 ± 10	60 ± 4	125 ± 8
pH 7 (24 h)	148 ± 14	47 ± 3	11 ± 2	23 ± 2
pH 7 (24 h) + pH 10 (24 h)	110 ± 14	180 ± 12	90 ± 4	87 ± 5
pH 10 (24 h)	175 ± 12	60 ± 3	120 ± 7	33 ± 4
pH 10 (24 h) + pH 10 (24h)	140 ± 13	195 ± 8	200 ± 9	117 ± 8
Glyoxyl	80 ± 5	31 ± 3	10 ± 2	11 ± 1

[a] 100 is the activity of the soluble enzyme activity recovered after the blocking step.

Regarding the effect on stability, the results offer a complex picture. At all three pH values of inactivation and immobilization, the enzymes incubated at pH 10.0 for 24 h showed an improved stability when compared to the enzyme blocked just after immobilization, the stabilization caused by the incubation ranged from less than 2 to more than 4 folds depending on the biocatalyst pH immobilization value and inactivation pH value. As the only possible difference between the enzymes just immobilized and those incubated for long-time at alkaline pH value is an increase in the number of enzyme-support linkages, it seems that the alkaline incubation favoured the enzyme-support reaction.

In inactivations at pH 5.0 of the just immobilized biocatalysts, the most stable one was that immobilized at pH 10.0 and the least stable was that immobilized at pH 5.0. After alkaline incubation, stability of all preparations increased, and the least stable preparations are the most stabilized. Thus, finally the stabilities of all of them became quite similar (half-lives from 150 min for preparation immobilized at pH 5.0 to 195 minutes when immobilized at pH 10.0).

When the inactivations were performed at pH 7.0, the enzyme immobilized at pH 10 is again clearly the most stable one just after immobilization (120 minutes *versus* half-live of 17 minutes for the biocatalyst prepared at pH 5.0 or 11 minutes if the biocatalyst is prepared at pH 7.0), and remains in this relative position after alkaline incubation even though it is the less stabilized by this treatment (half-live of 200 minutes *versus* 90 for the derivative immobilized at pH 7.0 or 60 if the immobilization is at pH 5.0).

However, in inactivations at pH 9.0, the most stable preparation just after immobilization is that immobilized at pH 5.0 (half-live of 60 minutes), doubling the stability of the other preparations. After incubation at pH 10.0, stability of the enzyme immobilized at pH 5.0 and 10.0 become similar, while that of the enzyme immobilized at pH 7.0 is clearly inferior. These qualitative differences on the stabilities of the different preparations suggest that the relevance of the different areas involved in the immobilization is not identical under any inactivation cause (Grazú et al. 2010; Mansfeld and Ulbrich-Hofmann 2000; Mansfeld et al. 1999).

Thus, the immobilization pH seems to really alter the enzyme orientation on the support, as that should be the only relevant difference between the immobilized enzymes after incubation at pH 10.0 for 24 h.

3.6. Comparison of glyoxyl-agarose, BrCN-agarose and DVS-agarose

Fig. 2.6 shows an inactivation course of the enzyme immobilized on DVS-agarose at pH 10.0 and incubated for 24 h before the blocking step and the chymotrypsin immobilized on glyoxyl under optimal conditions (Guisán et al. 1991) or BrCN agarose. BrCN-agarose-chymotrypsin is by far the least stable preparation, with full inactivation in the first measure in all the inactivation pH values. Glyoxyl-agarose-chymotrypsin was a much more stable preparation, as has been previously reported. Nevertheless, DVS-agarose-chymotrypsin is more stable than the very stable glyoxyl preparation at all studied pH values. In fact, even the biocatalysts prepared without the alkaline long term incubation were quite more stable than the glyoxyl support. This result suggested the good prospects of this support to give an important stabilization of enzymes *via* immobilization.

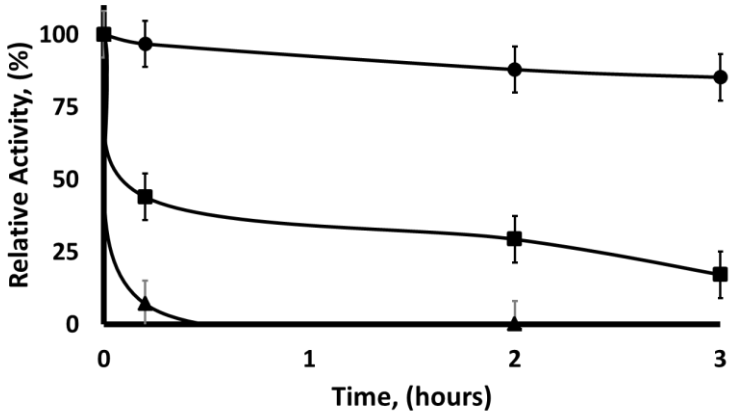

Fig. 2.6. Inactivation courses of the chymotrypsin immobilized on DVS-agarose, glyoxyl-agarose or BrCN-agarose. Experiments have been performed at 60 ºC and pH 8.0. Other features are described in Section 2. Triangles, solid black line: CNBr; square, solid black line: glyoxyl; circles, solid black line: DVS.

3.7. Determination of the number of enzyme-support linkages

To confirm that the enzyme was attached to the support *via* several attachments, the number of amino acids that can be released from the DVS and glyoxyl supports had been compared (Table 2.4). As reference, Arg, Ala and Pro were selected. The implication of the Ile-16 and Ala-149 (amino terminal groups) in the immobilization was not evaluated, as just one amino acid is not detected by this method.

Table 2.4. Free amino acids of different immobilized chymotrypsin preparations. Experiments have been performed as described in Section 2 (CT is chymotrypsin).

	CT	CT experimental	DVS-CT	DVS-CT (pH 10.0)	Glyoxyl-CT
His	2	2.1 ± 0.3	1.8 ± 0.2	1.5 ± 0.3	1.8 ± 0.3
Arg	3	3.9 ± 0.1	3.6 ± 0.1	2.6 ± 0.1	3.3 ± 0.6
Ala	22	22.3 ± 1.5	18.7 ± 1	14.4 ± 1	17.9 ± 1
Pro	9	9.3 ± 0.5	8.9 ± 0.8	9.8 ± 0.7	9.0 ± 0.3
Tyr	4	4.0 ± 0.3	3.9 ± 0.2	2.1 ± 0.2	3.3 ± 0.2
Cys	10	9.8 ± 0.5	10.3 ± 0.9	6.5 ± 0.3	9.5 ± 0.5
Lys	14	14.2 ± 0.6	13.6 ± 0.6	8.0 ± 0.4	10.6 ± 0.5

The amounts of the target groups in the presence or absence of blocked DVS were quite coincident; suggesting that the support did not alter the results (that is, can not react with any amino acid). Glyoxyl support involved in the immobilization around 4 Lys groups, while DVS involved at least 6 Lys, 1-2 Tyr and even several Cys (3-4) seemed to be involved in the immobilization that means that the disulphide bridge has been broken, as only the Cys 1 (that is the amino terminal) can react by its amino group, suggesting some enzyme distortion while multipoint covalent attachment was established. There were no clear indications on the involvement of any of the His on the immobilization. These results show two points: first, a very intense multipoint covalent attachment has been achieved (at least 10-12 groups involved), and second, the implication of at least Tyr, Lys and Cys on the multipoint covalent attachment has been shown. This occurred even though the reactivity of the free Tyr seemed to be very low even at pH 10.0, perhaps because the reaction is now ~~–i~~ntramolecular". Thus, it is evident that DVS-supports are very efficient to produce an intense multipoint covalent attachment, even using the only moderately favourable agarose 4BCL, that is an agarose with not very thick agarose fibres (Pedroche et al. 2007).

3.8. Activity/pH profile of different immobilized chymotrypsin preparations

Fig. 2.7 shows the pH/activity curve. The free enzyme had a clear optimum at pH 8.0, and the activity decrease is relatively marked around this optimum value. All immobilized preparations presented a different optimum pH value, and the curve is less narrow than using the free enzyme. The pH of immobilization on the DVS-support produced significant changes on the activity/pH curve, while the enzyme immobilized at pH 5.0 had the highest activity at pH 9.0, the other two preparations have the highest activity at pH 10.0, the maximum value used in this study to prevent chemical hydrolysis of the substrate.

The 24 h incubation at alkaline pH produced also changes. The enzyme immobilized at pH 5.0 is the one that suffered the greatest alterations in the pH/activity curve, changing a clear optimal at pH 9.0 to a flat plateau in the range 7-10. The enzyme immobilized at pH 7 also improved the percentage of activity at pH values from 7.0 to 9.0, while the enzyme immobilized at pH 10.0 almost did not suffer any change after the long term alkaline incubation.

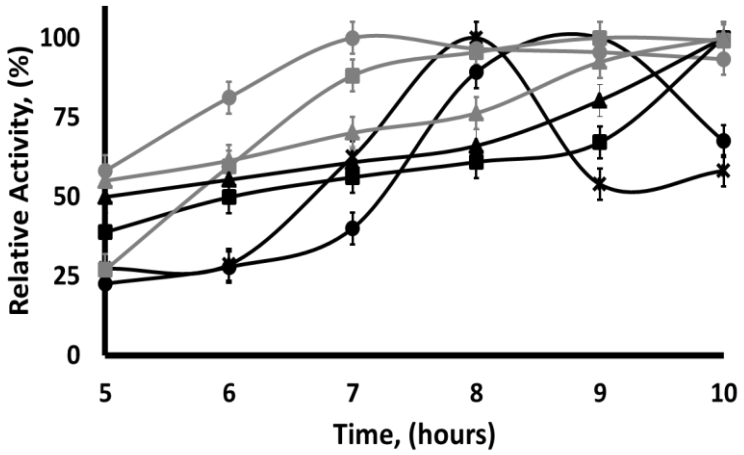

Fig. 2.7. Effect of the pH on the activity *versus* BTNA of the different α-chymotrypsin preparations. Experiments have been performed as described in Section 2. Circles, solid black line: (pH 5.0); circles, solid grey line: (pH 5.0 + pH 10.0); square, solid black line: (pH 7.0); square, solid grey line: (pH 7.0 + 10.0); triangle, solid black line: (pH 10.0); triangle, solid grey line: (pH 10.0 + pH 10.0); stars, solid black line: (soluble).

4. Conclusions

This paper shows the great potential of DVS-activated agarose not to immobilize enzymes, but to stabilize them *via* multipoint covalent attachment. First, the main features of the active groups to this goal have been analysed. The support is very stable, maintaining its reactivity after storage for two months even at 36 ºC in wet condition, also retained full reactivity after 24 h of incubation at pH 4.0 to 10.5 at 25 ºC. This support is able to react with Lys, His, Cys and Tyr, with a rate that depends on the pH value. Regarding reactivity with groups of proteins, DVS and epoxide are capable to react with different nucleophiles (Ortega-Munoz et al. 2010) while glyoxyl only can react with primary amino groups (Mateo et al. 2006b). However, DVS is much more reactive than epoxy groups, being able to covalently immobilize enzymes without requiring the previous adsorption of the enzyme. Moreover, DVS supports can be used in a wide range of pH values, in opposition to glyoxyl agarose that generally require the immobilization at alkaline pH value (Mateo et al. 2005). DVS can directly yield stable enzyme-support linkages, being no necessary any treatment to stabilize these bonds (*e.g.*, imine bonds obtained using glyoxyl require reduction). However, to avoid uncontrolled enzyme-support reaction, the support may be blocked using different nucleophiles. This may become a tool to further tailoring immobilized enzyme features (Bonomi et al. 2013).

Using it as a support to obtain a stabilized preparation of chymotrypsin, the results have been really good. To take advantages of the support properties, a proper immobilization protocol needs to be utilized, as multipoint covalent attachment is a quite complex process. The first enzyme immobilization may be performed at different pH values, obtaining preparations with different activity/stability properties, but still multipoint covalent attachment has not been maximized. Further incubation at pH 10.0 produced an increase in enzyme stability with some costs in terms of activity. The blocking of the remaining sulfone groups is another critical variable, as show in this paper and expected from the higher stability of DVS groups. In this case, the blocking with EDA permitted to avoid undesired covalent enzyme-support reactions, and improved the enzyme activity, that become even slightly higher than that of the free enzyme (175 % measured at pH 7.0) and stability. The results after the long term incubation at alkaline pH are different depending on the immobilization pH, considering that the support is full stable in the used conditions, and that the blocking is identical, the only likely explanation is that the enzyme orientation may be different depending on the immobilization pH value and that determine the number of enzyme groups that can react with the support, or affecting regions of the enzyme with different relevance for the enzyme stability.

Thus, the immobilization protocol to have an optimized enzyme stabilization *via* an intense multipoint covalent attachment is a first immobilization of the enzyme on DVS-agarose at different pH values (to involve different areas of the enzyme in the immobilization), an incubation under alkaline conditions to improve the enzyme reactivity and have an intense multipoint covalent attachment, and an optimization of the blocking step (assaying different blocking reagents) to have the best activity/stability features.

Acknowledgements

We gratefully recognize the support from the Spanish Government, grant CTQ2013-41507-R. The predoctoral fellowships for Mr dos Santos (CNPq, Brazil) and Ms Rueda (Colciencias, Colombia) are also recognized. The authors wish to thank Mr Ramiro Martínez (Novozymes, Spain) for kindly supplying the enzymes used in this research. The help and comments from Dr Ángel Berenguer (Instituto de Materiales, Universidad de Alicante) are kindly acknowledged.

References

Adlercreutz, P., 2013. Immobilisation and application of lipases in organic media. Chemical Society Reviews 42(15), 6406-6436.

Ahmad, S., Gromiha, M., Fawareh, H., Sarai, A., 2004. ASAView: Database and tool for solvent accessibility representation in proteins. BMC Bioinformatics 5(1), 51.

Alaiz, M., Navarro, J.L., Girón, J., Vioque, E., 1992. Amino acid analysis by high-performance liquid chromatography after derivatization with diethyl ethoxymethylenemalonate. Journal of Chromatography A 591(1–2), 181-186.

Bale Oenick, M.D., Danielson, S.J., Daiss, J.L., Sunderberg, M.W., Sutton, R.C., 1990. Antigen-binding activity of antibodies immobilized on styrene copolymer beads. Annales de Biologie Clinique 48(9), 651-654.

Barbosa, O., Ortiz, C., Berenguer-Murcia, A., Torres, R., Rodrigues, R.C., Fernandez-Lafuente, R., 2014. Glutaraldehyde in bio-catalysts design: a useful crosslinker and a versatile tool in enzyme immobilization. RSC Advances 4(4), 1583-1600.

Barbosa, O., Torres, R., Ortiz, C., Berenguer-Murcia, Á., Rodrigues, R.C., Fernandez-Lafuente, R., 2013. Heterofunctional Supports in Enzyme Immobilization: From Traditional Immobilization Protocols to Opportunities in Tuning Enzyme Properties. Biomacromolecules 14(8), 2433-2462.

Barbosa, O., Torres, R., Ortiz, C., Fernandez-Lafuente, R., 2012. Versatility of glutaraldehyde to immobilize lipases: Effect of the immobilization protocol on the properties of lipase B from Candida antarctica. Process Biochemistry 47(8), 1220-1227.

Begara-Morales, J.C., López-Jaramillo, F.J., Sánchez-Calvo, B., Carreras, A., Ortega-Muñoz, M., Santoyo-González, F., Corpas, F.J., Barroso, J.B., 2013. Vinyl sulfone silica: application of an open preactivated support to the study of transnitrosylation of plant proteins by S-nitrosoglutathione. BMC Plant Biology 13(1), 61.

Blanco, R.M., Calvete, J.J., Guisán, J., 1989. Immobilization-stabilization of enzymes; variables that control the intensity of the trypsin (amine)-agarose (aldehyde) multipoint attachment. Enzyme and Microbial Technology 11(6), 353-359.

Blanco, R.M., Guisán, J., 1989. Stabilization of enzymes by multipoint covalent attachment to agarose-aldehyde gels. Borohydride reduction of trypsin-agarose derivatives. Enzyme and Microbial Technology 11(6), 360-366.

Bolivar, J.M., Mateo, C., Grazu, V., Carrascosa, A.V., Pessela, B.C., Guisan, J.M., 2010. Heterofunctional supports for the one-step purification, immobilization and stabilization of large multimeric enzymes: Amino-glyoxyl versus amino-epoxy supports. Process Biochemistry 45(10), 1692-1698.

Boller, T., Meier, C., Menzler, S., 2002. EUPERGIT Oxirane Acrylic Beads: How to Make Enzymes Fit for Biocatalysis. Organic Process Research & Development 6(4), 509-519.

Bonomi, P., Bavaro, T., Serra, I., Tagliani, A., Terreni, M., Ubiali, D., 2013. Modulation of the Microenvironment Surrounding the Active Site of Penicillin G Acylase Immobilized on Acrylic Carriers Improves the Enzymatic Synthesis of Cephalosporins. Molecules 18(11), 14349.

Brady, D., Jordaan, J., 2009. Advances in enzyme immobilisation. Biotechnology Letters 31(11), 1639.

Bryjak, J., Liesiene, J., Kolarz, B.N., 2008. Application and properties of butyl acrylate/pentaerythrite triacrylate copolymers and cellulose-based Granocel as carriers for trypsin immobilization. Colloids and Surfaces B: Biointerfaces 61(1), 66-74.

Cao, L., 2011. 2.34 - Immobilized Enzymes A2 - Moo-Young, Murray. Comprehensive Biotechnology (Second Edition), pp. 461-476. Academic Press, Burlington.

Chibata, I., Tosa, T., Sato, T., 1986. Biocatalysis: Immobilized cells and enzymes. Journal of Molecular Catalysis 37(1), 1-24.

DeLano, W., 2002. CCP4 Newsletter on Protein Crystallography.

Fernandez-Lafuente, R., 2009. Stabilization of multimeric enzymes: Strategies to prevent subunit dissociation. Enzyme and Microbial Technology 45(6–7), 405-418.

Garcia-Galan, C., Berenguer-Murcia, Á., Fernandez-Lafuente, R., Rodrigues, R.C., 2011. Potential of Different Enzyme Immobilization Strategies to Improve Enzyme Performance. Advanced Synthesis & Catalysis 353(16), 2885-2904.

Gianfreda, L., Scarfi, M.R., 1991. Enzyme stabilization: state of the art. Molecular and Cellular Biochemistry 100(2), 97-128.

Gilis, D., Rooman, M., 1996. Stability Changes upon Mutation of Solvent- accessible Residues in Proteins Evaluated by Database-derived Potentials. Journal of Molecular Biology 257(5), 1112-1126.

Gilis, D., Rooman, M., 1997. Predicting protein stability changes upon mutation using database-derived potentials: solvent accessibility determines the importance of local versus non-local interactions along the sequence1. Journal of Molecular Biology 272(2), 276-290.

Grazú, V., López-Gallego, F., Montes, T., Abian, O., González, R., Hermoso, J.A., García, J.L., Mateo, C., Guisán, J.M., 2010. Promotion of multipoint covalent immobilization through different regions of genetically modified penicillin G acylase from E. coli. Process Biochemistry 45(3), 390-398.

Guisán, J.M., Bastida, A., Cuesta, C., Fernandez-Lufuente, R., Rosell, C.M., 1991. Immobilization-stabilization of α-chymotrypsin by covalent attachment to aldehyde-agarose gels. Biotechnology and Bioengineering 38(10), 1144-1152.

Guzik, U., Hupert-Kocurek, K., Wojcieszyńska, D., 2014. Immobilization as a Strategy for Improving Enzyme Properties-Application to Oxidoreductases. Molecules 19(7), 8995.

Hartmeier, W., 1985. Immobilized biocatalysts — From simple to complex systems. Trends in Biotechnology 3(6), 149-153.

Hernandez, K., Fernandez-Lafuente, R., 2011. Control of protein immobilization: Coupling immobilization and site-directed mutagenesis to improve biocatalyst or biosensor performance. Enzyme and Microbial Technology 48(2), 107-122.

Hernandez, K., Berenguer-Murcia, A., C. Rodrigues, R., Fernandez-Lafuente, R., 2012. Hydrogen Peroxide in Biocatalysis. A Dangerous Liaison. Current Organic Chemistry 16(22), 2652-2672.

Hilterhaus, L., Minow, B., Müller, J., Berheide, M., Quitmann, H., Katzer, M., Thum, O., Antranikian, G., Zeng, A.P., Liese, A., 2008. Practical application of different enzymes immobilized on sepabeads. Bioprocess and Biosystems Engineering 31(3), 163-171.

Ilan, E., Morton, P.G., Chang, T.M.S., 1993. The anaerobic reaction of bovine hemoglobin with divinyl sulfone: structural changes and functional consequences. Biochimica et Biophysica Acta (BBA) - Protein Structure and Molecular Enzymology 1163(3), 257-265.

Illanes, A., 2011. 1.04 - Immobilized Biocatalysts A2 - Moo-Young, Murray. Comprehensive Biotechnology (Second Edition), pp. 25-39. Academic Press, Burlington.

Katchalski-Katzir, E., Kraemer, D.M., 2000. Eupergit® C, a carrier for immobilization of enzymes of industrial potential. Journal of Molecular Catalysis B: Enzymatic 10(1–3), 157-176.

Katchalski-Katzir, E., 1993. Immobilized enzymes — learning from past successes and failures. Trends in Biotechnology 11(11), 471-478.

Kennedy, J.F., Melo, E.H.M., Jumel, K., 1990. Immobilized enzymes and cells. Chemical Engineering Progress 86(7), 81-89.

Klibanov, A.M., 1979. Enzyme stabilization by immobilization. Analytical Biochemistry 93, 1-25.

Klibanov, A.M., 1983. Immobolized enzymes and cells as practical catalysts. Science 219(4585), 722-727.

Labus, K., Turek, A., Liesiene, J., Bryjak, J., 2011. Efficient Agaricus bisporus tyrosinase immobilization on cellulose-based carriers. Biochemical Engineering Journal 56(3), 232-240.

Lopez-Jaramillo, F.J., Ortega-Muñoz, M., Megia-Fernandez, A., Hernandez-Mateo, F., Santoyo-Gonzalez, F., 2012. Vinyl Sulfone Functionalization: A Feasible Approach for the Study of the Lectin–Carbohydrate Interactions. Bioconjugate Chemistry 23(4), 846-855.

Mansfeld, J., Ulbrich-Hofmann, R., 2000. Site-specific and random immobilization of thermolysin-like proteases reflected in the thermal inactivation kinetics. Biotechnology and Applied Biochemistry 32(3), 189-195.

Mansfeld, J., Vriend, G., Van den Burg, B., Eijsink, V.G.H., Ulbrich-Hofmann, R., 1999. Probing the Unfolding Region in a Thermolysin-like Protease by Site-Specific Immobilization. Biochemistry 38(26), 8240-8245.

Mateo, C., Abian, O., Bernedo, M., Cuenca, E., Fuentes, M., Fernandez-Lorente, G., Palomo, J.M., Grazu, V., Pessela, B.C.C., Giacomini, C., Irazoqui, G., Villarino, A., Ovsejevi, K., Batista-Viera, F., Fernandez-Lafuente, R., Guisán, J.M., 2005. Some special features of glyoxyl supports to immobilize proteins. Enzyme and Microbial Technology 37(4), 456-462.

Mateo, C., Abian, O., Fernández-Lorente, G., Pedroche, J., Fernández-Lafuente, R., Guisan, J.M., 2002. Epoxy Sepabeads: A Novel Epoxy Support for Stabilization of Industrial Enzymes via Very Intense Multipoint Covalent Attachment. Biotechnology Progress 18(3), 629-634.

Mateo, C., Fernandes, B., van Rantwijk, F., Stolz, A., Sheldon, R.A., 2006a. Stabilisation of oxygen-labile nitrilases via co-aggregation with poly(ethyleneimine). Journal of Molecular Catalysis B: Enzymatic 38(3–6), 154-157.

Mateo, C., Palomo, J.M., Fernandez-Lorente, G., Guisan, J.M., Fernandez-Lafuente, R., 2007. Improvement of enzyme activity, stability and selectivity via immobilization techniques. Enzyme and Microbial Technology 40(6), 1451-1463.

Mateo, C., Palomo, J.M., Fuentes, M., Betancor, L., Grazu, V., López-Gallego, F., Pessela, B.C.C., Hidalgo, A., Fernández-Lorente, G., Fernández-Lafuente, R., Guisán, J.M., 2006b. Glyoxyl agarose: A fully inert and hydrophilic support for immobilization and high stabilization of proteins. Enzyme and Microbial Technology 39(2), 274-280.

Medina-Castillo, A.L., Morales-Sanfrutos, J., Megia-Fernandez, A., Fernandez-Sanchez, J.F., Santoyo-Gonzalez, F., Fernandez-Gutierrez, A., 2012. Novel synthetic route for covalent coupling of biomolecules on super-paramagnetic hybrid nanoparticles. Journal of Polymer Science Part A: Polymer Chemistry 50(19), 3944-3953.

Melander, W.R., Corradini, D., Horváth, C., 1984. Salt-mediated retention of proteins in hydrophobic-interaction chromatography : Application of solvophobic theory. Journal of Chromatography A 317, 67-85.

Morales-Sanfrutos, J., Lopez-Jaramillo, J., Ortega-Munoz, M., Megia-Fernandez, A., Perez-Balderas, F., Hernandez-Mateo, F., Santoyo-Gonzalez, F., 2010. Vinyl sulfone: a versatile function for simple bioconjugation and immobilization. Organic & Biomolecular Chemistry 8(3), 667-675.

Nevell, T., Whistler, R., 1963. Methods in Carbohydrate Chemistry Vol. III. Academic Press, New York.

Ortega-Munoz, M., Morales-Sanfrutos, J., Megia-Fernandez, A., Lopez-Jaramillo, F.J., Hernandez-Mateo, F., Santoyo-Gonzalez, F., 2010. Vinyl sulfone functionalized silica: a "ready to use" pre-activated material for immobilization of biomolecules. Journal of Materials Chemistry 20(34), 7189-7196.

Pedroche, J., del Mar Yust, M., Mateo, C., Fernández-Lafuente, R., Girón-Calle, J., Alaiz, M., Vioque, J., Guisán, J.M., Millán, F., 2007. Effect of the support and experimental conditions in the intensity of the multipoint covalent attachment of proteins on glyoxyl-agarose supports: Correlation between enzyme–support linkages and thermal stability. Enzyme and Microbial Technology 40(5), 1160-1166.

Petkar, M., Lali, A., Caimi, P., Daminati, M., 2006. Immobilization of lipases for non-aqueous synthesis. Journal of Molecular Catalysis B: Enzymatic 39(1–4), 83-90.

Porath, J., Axén, R., 1976. [3] Immobilization of enzymes to agar, agarose, and sephadex support. Methods in Enzymology, pp. 19-45. Academic Press.

Prikryl, P., Lenfeld, J., Horak, D., Ticha, M., Kucerova, Z., 2012. Magnetic Bead Cellulose as a Suitable Support for Immobilization of α-Chymotrypsin. Applied Biochemistry and Biotechnology 168(2), 295-305.

Rodrigues, R.C., Berenguer-Murcia, Á., Fernandez-Lafuente, R., 2011. Coupling Chemical Modification and Immobilization to Improve the Catalytic Performance of Enzymes. Advanced Synthesis & Catalysis 353(13), 2216-2238.

Rodrigues, R.C., Ortiz, C., Berenguer-Murcia, A., Torres, R., Fernandez-Lafuente, R., 2013. Modifying enzyme activity and selectivity by immobilization. Chemical Society Reviews 42(15), 6290-6307.

Singh, R., Tiwari, M., Singh, R., Lee, J.-K., 2013. From Protein Engineering to Immobilization: Promising Strategies for the Upgrade of Industrial Enzymes. International Journal of Molecular Sciences 14(1), 1232.

Smalla, K., Turkova, J., Coupek, J., Hermann, P., 1988. Influence of Salts on the Covalent Immobilization of Proteins to Modified Copolymers of 2-Hydroxyethyl Methacrylate with Ethylene Dimethacrylate. Biotechnology and Applied Biochemistry 10(1), 21-31.

Srere, P.A., Uyeda, K., 1976. [2] Functional groups on enzymes suitable for binding to matrices. Methods in Enzymology, pp. 11-19. Academic Press.

Turková, J., Bláha, K., Malaníková, M., Vančurová, D., Švec, F., Kálal, J., 1978. Methacrylate gels with epoxide groups as supports for immobilization of enzymes in pH range 3–12. Biochimica et Biophysica Acta (BBA) - Enzymology 524(1), 162-169.

Wheatley, J.B., Schmidt, D.E., 1993. Salt-induced immobilization of proteins on a high-performance liquid chromatographic epoxide affinity support. Journal of Chromatography A 644(1), 11-16.

Wheatley, J.B., Schmidt Jr, D.E., 1999. Salt-induced immobilization of affinity ligands onto epoxide-activated supports. Journal of Chromatography A 849(1), 1-12.

Bloque II

El diseño y desarrollo de nuevas fases sensoras ópticas basadas en materiales nanoestructurados constituye una de las muchas aplicaciones de la nanotecnología. Así, la producción de nanofibras poliméricas mediante la técnica de electrospinning y su utilización como soportes donde llevar a cabo la retención de biomoléculas es una estrategia con enormes posibilidades en el campo de los biosensores.

En general, las nanofibras poliméricas producidas por electrospinning se caracterizan por poseer una elevada área superficial y unas excelentes propiedades mecánicas, y, además, pueden ser fabricadas con una enorme variedad de dimensiones, porosidades y espesores, y con propiedades de biocompatibilidad y biodegradabilidad, lo que las convierte en excelentes soportes con un enorme potencial para la obtención de fases sensoras.

Los capítulos que conforman este bloque muestran dos ejemplos de la aplicabilidad de los tejidos de nanofibras poliméricas producidos por electrospinning para realizar la determinación óptica y directa de analitos presentes en muestras reales con matrices más o menos complejas.

Capítulo 3

Novel optical sensing film based on a functional nonwoven nanofibre mat for an easy, fast and highly selective and sensitive detection of tryptamine in beer

Teresa Ramon-Marquez[a], *Antonio L. Medina-Castillo*[b], *Alberto Fernandez-Gutierrez*[a], *Jorge F. Fernandez-Sanchez*[a]

[a] Department of Analytical Chemistry, University of Granada, Avd. Fuentenueva s/n, 18071 Granada, Spain

[b] NanoMyP®, Nanomateriales y Polimeros S.L., Spin-Off company of the UGR, BIC Building, Avd. Innovacion 1, E-18016, Granada, Spain

Published in *Biosensors and Bioelectronics*, 2016, **79**, 600–607

ABSTRACT

In this paper, the combination of Solid Surface-Room Temperature Phosphorescence (SS-RTP) and nanotechnology has led to a new approach in the detection of biogenic amines in complex matrices. This novel approach allows, for the first time, the direct determination of the concentration of tryptamine in beers. The novelty of the proposed optical sensor resides in its simplicity, rapidity, absence of complex chromatographic separation, sample clean-up, preconcentration, and derivatization protocols. Therefore, this novel methodology simplifies and reduces considerably the time and cost of the analysis, resolving the two major problems of the determination of tryptamine in beer up to now: low sensitivity and matrix effects.

The proposed sensor is based on a novel white, uncharged, and non-luminescent functional nonwoven nanofibre mat (Tiss®-Link) formed by hydrophilic nanofibres of 300 nm of diameter functionalized with a high concentration of active vinyl groups (330 μmol g^{-1}). It is used to carry out a kinetically controlled covalent immobilization of tryptamine via Michael type-reaction. The transduction of the sensor is phosphorescence; the covalently immobilized tryptamine is quantified by SS-RTP, obtaining a detection limit of 6 ng mL^{-1} with short response times (15 min). The applicability of the sensor was demonstrated by analysing tryptamine in 10 different varieties of beers, obtaining recovery percentages close to 100%.

Keywords: Optical sensor; Nanotechnology; SS-RTP; Nanofibre mat; Tryptamine; Beer.

1. Introduction

Biogenic amines (BAs) are a very important group of organic compounds formed by decarboxylation of amino acids or by amination and transamination of aldehydes and ketones (Izquierdo Cañas et al. 2008; Kalač et al. 1997; Silla Santos 1996) during metabolic processes in animals, plants and many microorganisms. Therefore, BAs are commonly found in a wide variety of foods and beverages such as cheese, wine, beer, fishery products and meat, and they are food quality marker associated to the degree of degradation and fermentation in foods (Anderson 2008; Lorenzo et al. 2007; Loret et al. 2005; Ntzimani et al. 2008).

High concentrations of BAs can induce in sensitive humans several health disorders such as respiratory discomfort, cold sweat, hot flushes, headaches, red rash, hypo- or hyper-tension, nausea, cardiac palpitations, and renal intoxication among others (Giuliano and Rampin 2004; Pérez-Serradilla and de Castro 2008). Histamine, putrescine, cadaverine, tyramine, agmatine, tryptamine, β-phenylethylamine, spermine, and spermidine are accepted to be the most important BAs occurring in foods (Shalaby 1996).

Beer has been commonly reported to be a health risk for some consumers due to its content in BAs (Önal et al. 2013; Simó et al. 2008). The types and levels of BAs in beers are affected mainly by raw materials, brewing techniques and hygienic conditions. Generally, putrescine, spermine, and spermidine are naturally present because malt is a source of these substances, while tryptamine, tyramine, histamine, and cadaverine are formed during fermentation (Cortacero-Ramírez et al. 2007; Kalač et al. 1997).

The more used and accepted methods to carry out the analysis of BAs in complex matrices are chromatographic ones coupled with fluorimetry and mass spectrometry (Moriarty et al. 2012). Beer is a quite complex matrix containing sugars, proteins, vitamins, minerals, polysaccharides, polyphenols, etc. Thus, the presence of these compounds can often cause ion suppression when liquid chromatography–mass spectrometry methods are used (Moriarty et al. 2012). Tandem mass spectrometry (MS/MS) coupled to chromatographic techniques is a recognized technique capable to minimize matrix interference in complex matrices (Moriarty et al. 2012).

Anyway, the chromatographic determination of BAs shows significant drawbacks, such as (1) it is necessary to carry out a clean-up of the matrices by different techniques, i.e. conventional solid phase extraction (SPE) (Casella et al. 2008; Mazzucco et al. 2010; Molins-Legua and Campins-Falcó 2005; Tang et al. 2011), protein precipitation (Ma et al. 2007; Miller et al. 2010),

liquid–liquid extraction (Almeida et al. 2012; Ramos et al. 2014), online SPE (de Jong et al. 2008; Monaghan et al. 2009; Tang et al. 2011), etc.; (2) in most of the cases pre-column derivatization reactions are also necessary (Almeida et al. 2012; Hu et al. 2014; Naccarato et al. 2014; Ramos et al. 2014; Tang et al. 2011; Tang et al. 2009); (3) many of these methods involve the use of relatively large amounts of solvents, long preparation times and incomplete removal of matrix components (Moriarty et al. 2012); and (4) expensive equipment and highly qualified technicians are needed (Sun et al. 2011a).

In order to avoid these drawbacks, several sensors have been developed as alternative to the expensive instrumentation of chromatographic methods (Bedia Erim 2013). However, they are mainly focused in the analysis of fish (Azab et al. 2011; Chow et al. 2011; Nakamura et al. 2011) and meat (Bóka et al. 2012) and only one for analysing beers (Di Fusco et al. 2011). In addition, this sensor is based on the use of a biomolecule (diamine oxidase) and an electrochemical transduction, with the consequent difficulties and disadvantages of the amperometric biosensors (Wang and Wolfbeis 2014); high cost of the biomolecule, poor long-term stability, long response times, etc.

Phosphorescence sensors have been proposed to solve some of the main drawbacks of the electrochemical ones (Wang and Wolfbeis 2014), but only a few molecules exhibit intrinsic phosphorescence (de Ribamar et al. 1995). The amino acid tryptophan (TRYPH), tryptamine (TRYP) and serotonin show intrinsic phosphorescence, however serotonin is not present in the composition of the beers but TRYPH and TRYP are present in beer. The determination of TRYP in beers is very important because it is one of the main BAs which is in the composition of the beers (Anderson 2008; Izquierdo Cañas et al. 2008; Kalač et al. 1997; Lorenzo et al. 2007; Loret et al. 2005; Ntzimani et al. 2008; Shalaby 1996; Silla Santos 1996), several health disorders have been correlated with high content of TRYP (Giuliano and Rampin 2004; Pérez-Serradilla and de Castro 2008), and the presence of TRYP can be correlated with other important BA as tyramine (Izquierdo-Pulido et al. 1994). Therefore it could be very interesting to develop simple analytical methods for determining TRYP directly in beers (Cañabate-Díaz et al. 2003).

In this paper, we have combined the capacity of the nanostructured functional material Tiss®-Link (Medina-Castillo et al. 2011a; Medina-Castillo et al. 2011b) for covalent immobilization of amines, with the sensitivity of the intrinsic phosphorescence of TRYP to allow the development of an optical sensing film for the direct determination of TRYP in beer.

Tiss®-Link is a nonwoven nanofibre mat made by electrospinning and formed by 150 microns thick of nanofibres (300 nm of diameter) functionalized with a high amount of activated vinyl groups (330 µmol g^{-1}), which allows a fast and efficient covalent immobilization of small amines such as TRYP via solid phase Michael type-reaction (Medina-Castillo et al. 2012).

The use of Tiss®-Link combined with Solid Surface-Room Temperature Phosphorescence (SS-RTP), has allowed for the first time the development of an optical sensing film which allows the quick and easy determination of the concentration of TRYP directly in beer, reducing considerably the time and cost of the analysis.

2. Experimental

2.1. Reagents and Materials

Tiss®-Link support was kindly supplied by NanoMyP® (http://www.nanomyp.com), Tween 20, Potassium iodide (KI), Sodium carbonate (Na_2CO_3), Potassium phosphate (K_2HPO_4), Tryptamine (TRYP) and Tryptophan (TRYPH) were all purchased from Sigma Aldrich and used without further purification.

Tiss®-Link is a non-woven nanofibre mat made by electrospinning. It has a preactivated surface for direct covalent immobilization of primary and secondary amines. It is non-luminescent, uncharged and highly hydrophilic but insoluble in aqueous media as well as in apolar solvents (oil, toluene…). It shows a high robustness and stability in a wide range of pH (at least between pH 5 and 10 up to 24 hours) as well as excellent mechanical properties: high mechanical strength, high consistency, high flexibility and temperature resistance (up to 100 º C). It has been previously used for covalent immobilization of large molecules such as proteins and enzymes, but this is the first time that it is used in the fast covalent immobilization of small amines for a subsequent luminescent detection on solid phase.

2.2. Instrumentation

The SS-RTP of TRYP immobilised onto Tiss®-Link was measured on a Varian Cary-Eclipse luminescence spectrophotometer equipped with flow-through cell which allows the use of a gas stream in order to allow the measurement in an inert-gas atmosphere. Supplementary Material (SM) shows the setup used for measuring SS-RTP (see SM, Fig. SM-3.1). The flow-through cell

is made of black polytetrafluoroethylene (PTFE) to prevent stray reflections and to ensure that the system was chemically inert.

The gas stream was controlled with a mass-flow controller (MFC) (EL-FLOW Select F-201CV, Bronkhorst High-Tech, www.bronkhorst.com, Ruurlo, Netherlands) connected with the flow cell using copper and stainless steel tubing and a PC via a RS-232 serial port by a Flow-Bus Interface (Bronkhorst High-Tech).

All the measurements were performed at room temperature (21 ºC). The temperature was continuously monitored using a commercial temperature sensor (MicroLite, Fourtec-Fourier Technologies, www.fouriersystems.com) placed at a point close to the flow cell.

2.3. General procedure

The determination of TRYP by using the proposed sensing film requires two steps: the covalent immobilization of TRYP onto Tiss®-Link and the SS-RTP measurement.

The covalent immobilization of TRYP onto Tiss®-Link was carried out by incubating 3 mg (≈ 0.8 cm^2) of nanofibre mat in 4 mL of sample at pH = 10 (20 mM carbonate buffer) for 15 min at room temperature (RT) in a rotating shaker. Then, it was washed (3 x 5 min in a rotating shaker) with 4 mL of a solution containing 8.5 g/L of NaCl and 0.5 g/L of Tween 20 (washing solution) to remove all the no covalently bounded molecules and dried with a nitrogen flow.

The SS-RTP intensity was measured at excitation and emission slits of 10 nm wide, excitation wavelength of 290 nm, emission wavelength of 443 nm, delay time (t_d) 120 µs, gate time (t_g) 5 ms, detector voltage of 800 V, using 20 µL of 1 M KI which acts as heavy atom and flowing a current flow of 300 mL min^{-1} nitrogen which acts as oxygen scavenger.

Heavy atom was applied by dropping 20 µL of 1 M KI over the nanofibre mat after the covalent immobilization of TRYP.

The sensing response is the difference between the phosphorescence emission of the TRYP immobilised on Tiss®-Link and the noise (RTP emission of Tiss®-Link in absence of TRYP).

All the experiments were replicated four times in order to evaluate the error $\left({}^{st}/_{\sqrt{n}}\right)$ where s is the standard deviation, t the Student t and n the number of replicas.

2.4. Beer sample procedure

To demonstrate the predictive ability of the proposed sensing film for analysing TRYP in beers, a total of 10 varieties of Spanish and international beer (Alhambra, Amstel, Budweiser, Carlsberg, Cruzcampo, free-alcohol Cruzcampo, Heineken, Mahou, free-alcohol Mahou and San Miguel Especial) were purchased from local markets, stored at room temperature, opened immediately prior to analysis and degassed by ultrasonication for 2 min.

2 mL of degassed beer was mixed with 2 mL of 20 mM carbonate buffer at pH = 10 (1:1 dilution) and it was treated as indicated under the general procedure.

3. Results

3.1. Characterization of Tiss®-Link

Tiss®-Link was morphologically characterized. Fig. 3.1a shows a picture of the nanofibre mat just after its production by electrospinning and the Fig. 3.1b shows its microstructure by SEM.

The ability of Tiss®-Link for covalent immobilization of small amines via Michael type-reaction was evaluated using dansylcadaverine (DC) as a model because it is a highly fluorescent amine. The first experiment was focused on the effect of the incubation time over the covalent immobilization. To develop this experiment, 3 mg of Tiss®-Link were incubated at RT in 4 mL of 280 μg mL^{-1} DC solution containing 100 mM phosphate buffer solution at pH = 8.5 for different times (0, 30, 60, 120, 180, 240, 300, 375, 420 and 1000 min), and the concentration of DC in the supernatants were measured by fluorescence (see Fig. 3.1c). The binding kinetic of DC on Tiss®-Link was very fast, decreasing the concentration of DC in the supernatants from 280 μg mL^{-1} to 240 μg mL^{-1} in only 30 min and from 240 μg mL^{-1} to 80 μg mL^{-1} for the next 16 hours. Fig. 3.1d shows the picture of Tiss®-Link incubated with DC for several reaction times in a UV transiluminator. It can be concluded that the amount of DC immobilized at 10 min was already enough to have a quite intense luminescent signal.

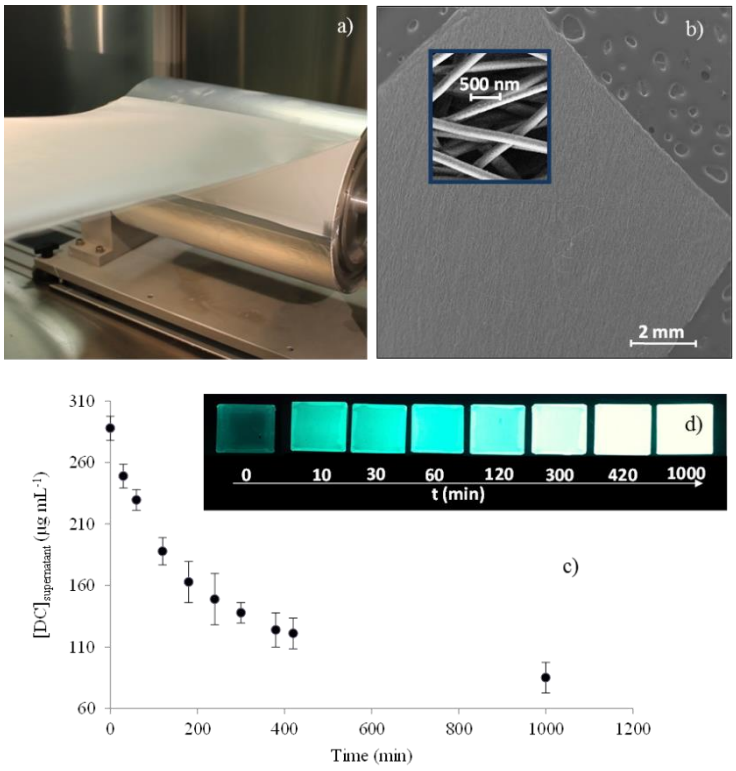

Fig. 3.1. Characterization of Tiss®-Link: a) picture of the nanofibre mat just after its production by electrospinning; b) SEM pictures of its microstructure; c) binding kinetics of DC on it; d) pictures of Tiss®-Link incubated with DC at different times in a UV transiluminator.

The stability of active vinyl groups of Tiss®-Link *versus* pH and time was also evaluated. Tiss®-Link was immersed in 50 mM buffer solutions at several pHs (citrate buffer at pH = 5, phosphate buffer at pH = 7, and carbonate buffer at pHs = 9 and 10) for 2, 8 and 24 h. Then the fibre mats were washed three times with the washing solution described in the general procedure and incubated in 4 mL of 280 µg mL^{-1} DC solution containing 100 mM phosphate buffer solution at pH=8.5 for 24 h at RT. After that, the fibre mats were washed three times with washing solution, dried and the fluorescence of the immobilized DC was measured ($\lambda_{exc/em}$ = 330/480 nm, slit $widths_{exc/em}$ = 5/5 nm, and detector voltage of 500 V). A freshly prepared Tiss®-Link incubated at room temperature for 24 h with the same DC solution, was used as control. The results are shown in SM (see Fig. SM-3.2a). It is possible to conclude that the active vinyl groups of Tiss®-Link are stable in a wide range of pH for at least 24 h.

In order to estimate the stability of activated vinyl groups of Tiss®-Link *versus* temperature and time, Tiss®-Link was stored at RT and 36ºC for 6 and 62 days. Then, the mats were incubated in 4 mL of 280 µg mL^{-1} DC solution containing 100 mM phosphate buffer solution at

pH = 8.5 for 24 h at RT, washed three times with the washing solution and the fluorescence of immobilised DC was measured ($\lambda_{exc/em}$ = 330/480 nm, slit $widths_{exc/em}$ = 5/5 nm, and detector voltage of 500 V). A freshly prepared Tiss®-Link incubated at room temperature for 24 h with the same DC solution, was used as control. The results are shown in SM (see Fig. SM-3.2b). It is possible to conclude that the active vinyl groups of Tiss®-Link are stable at RT and 36 ºC for more than 2 months.

3.2. Optical characterisation of TRYP immobilised on Tiss®-Link

Fig. 3.2 shows the luminescence spectra (fluorescence and phosphorescence) of TRYP immobilised on Tiss®-Link, as well as the luminescence spectra of Tiss®-Link (fluorescence and phosphorescence backgrounds).

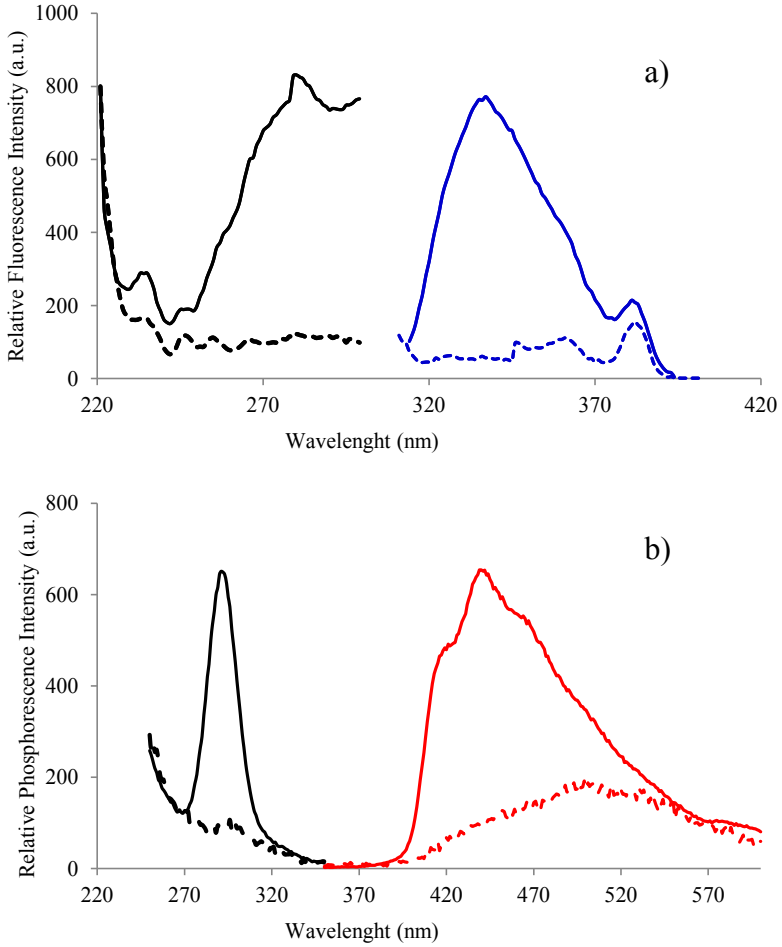

Fig. 3.2. Luminescence properties of TRYP covalently immobilised on Tiss®-Link: a) fluorescence excitation (black lines) and emission (blue lines) of TRYP immobilised on Tiss®-Link (solid lines) and the nanofibre mat free of TRYP (dashed lines); b) phosphorescence excitation (black lines) and emission (red lines) of TRYP immobilised on Tiss®-Link (solid lines) and the nanofibre mat free of TRYP (dashed lines). [TRYP] = 500 ng mL^{-1}.

For obtaining the SS-RTP emission of TRYP on Tiss®-Link it is necessary to use a heavy atom perturber and an oxygen scavenger; SM (see Fig. SM-3.3) shows that phosphorescence is not detected when the heavy atom solution is not spotted on Tiss®-Link, and it also evidences that the SS-RTP signal is quenched in the presence of oxygen. Thus a solution of KI must be dropped to the nanofibre mat and oxygen must be removed from the measuring cell before the RTP measurement.

SM (Fig. SM-3.3) also shows that a decrease in the oxygen concentration provides an increase in the luminescence signal. Thus, in order to exclude a possible underestimation of TRYP concentration, oxygen has to be completely removed from the measurement cell, i.e. pure N_2 must be flowed before the RTP measurement.

In order to check the reproducibility of the sensing film, the SS-RTP of TRYP immobilised onto Tiss®-Link was measured in several section of the mat as well as in both sides (upper and lower) at several TRYP concentration levels. SM (see Fig. SM-3.4) shows the experimental results. All the sections and sides provide very similar phosphorescence emissions for all the concentrations tested, thus it is possible to conclude that the solid support is reproducible and it is not necessary to distinguish between section and side for carrying out the measurement.

3.3. Optimization of covalent immobilization of TRYP on Tiss®-Link

The covalent immobilization of TRYP on Tiss®-Link was studied at pH = 8 (20 mM phosphate buffer) and pH = 10 (20 mM carbonate buffer) for several times (1, 2, 3, and 4 h).

Tiss®-Link was immersed in a solution of 1 µg mL^{-1} TRYP at the selected pHs and times. Then, the mats were washed three times with the washing solution, dried, and the luminescence of TRYP immobilised on Tiss®-Link was measured. Fig. 3.3a shows the results.

TRYP was not immobilised at pH 8 but it was efficiently immobilized at pH = 10. It could be due to the pKa of TRYP. It is 10.2, and therefore at pH = 8 the primary amino group is mostly protonated, and thus it loses its nucleophilic character, whereby the immobilization reaction does not occur, whereas at pH = 10 the primary amine groups of TRYP are mostly in its neutral form preserving its nucleophilic character, and therefore the immobilization reaction can occur. The maximum amount of immobilized TRYP was reached at pH = 10 and 3 hours of reaction.

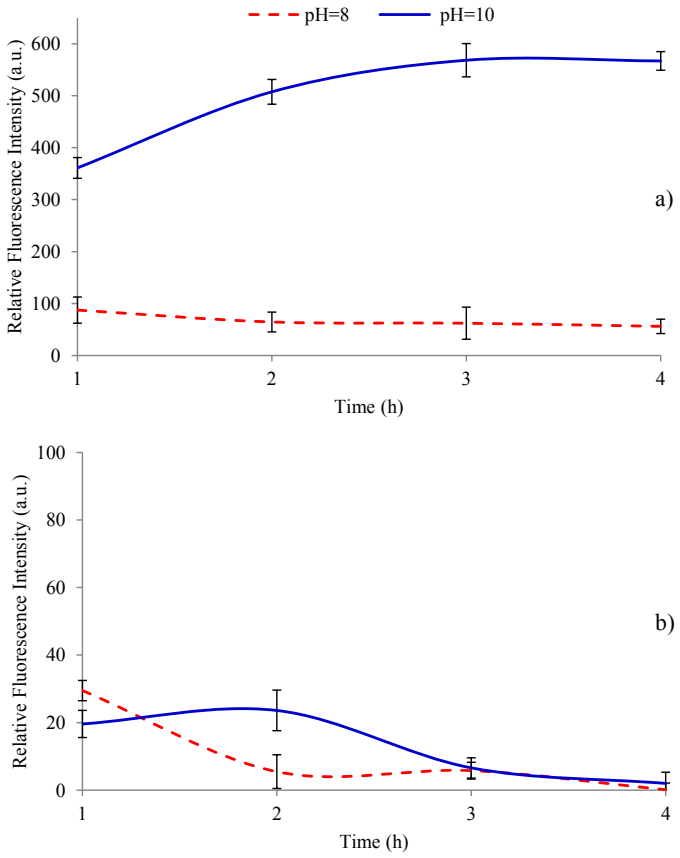

Fig. 3.3. Binding kinetics of a) TRYP and b) TRYPH on Tiss®-Link at pH = 8 (red dashed line) and pH = 10 (solid blue line). [TRYP] = [TRYPH] = 1 μg mL^{-1}, $\lambda_{exc/em}$ = 280/337 nm**,** monochromator slits $width_{exc/em}$ = 5/5 nm, detector voltage of 500 V.

The effect of the ionic strength over the covalent immobilization of TRYP on Tiss-Link® was also studied. Tiss®-Link was immersed in a solution of 1 μg mL^{-1} TRYP at pH = 10 for 1 and 4 h in the presence of NaCl (0, 30, 50, 80, 100, 150 and 200 mM). Then, the mats were washed three times with the washing solution, dried, and the luminescence of TRYP immobilised on Tiss®-Link was measured. SM (Fig. SM-3.5) shows the experimental results. It is possible to conclude that the ionic strength does not affect the immobilisation of TRYP on the nanofibre mat.

3.4. Interference study

The interferent species of the proposed methods may be classified in two types: (1) amines affecting the phosphorescence determination of TRYP (phosphorescence amines which are present in beer); and (2) those components of the beer affecting the covalent immobilisation of TRYP on the nanofibre mat.

The literature published over the past few years shows that the BAs which are present in beer can be classified according to their chemical structure into: aliphatic (agmatine, putrescine, cadaverine, spermine, spermidine), aromatic (tyramine and β-phenylethylamine) and heterocyclic (histamine and tryptamine) (Izquierdo-Pulido et al. 1996; Jastrzębska et al. 2013). In addition, several amino acids such as glutamine, leucine, glutamic acid, aspartic acid, lysine, histidine, tryptophan and valine can be also found in beer (Jia et al. 2011). Several of these amines and amino acids show weak fluorescence, but only two of them (tryptamine and tryptophan) show native phosphorescence (Bruxvoort et al. 1993). Consequently, the use of SS-RTP decreases the number of interferent species and therefore, improves the selectivity of the sensing film. Moreover, the long triplet excited state lifetime of the luminophore allows the use of an appropriate delay time, so that any fluorescence emission and scattering light can be easily eliminated. Thus, the use of RTP also increases the sensitivity.

To evaluate the potential interference of tryptophan (TRYPH), the immobilization of this amino acid on Tiss®-Link at pH = 8 (20 mM phosphate buffer) and pH = 10 (20 mM carbonate buffer) was also studied. Fig. 3.3b shows that when the concentration of TRYPH is 1 μg mL^{-1}, it is not covalently bonded to Tiss®-Link in any of the tested conditions. The inefficiency of the immobilization at pH = 8 can be explained by the same reasons than in the case of TRYP. The inefficiency of the immobilization at pH = 10 could be mainly due to the combination of two causes: (1) the primary amino group of TRYPH is sterically hindered because it is very close to the carboxyl group; and (2) Tiss®-Link is an uncharged material at pH = 10 while the carboxyl group of TRYPH at this pH is fully deprotonated, and therefore it has a higher affinity for the aqueous medium than for Tiss®-Link, and this fact could hinder a fast diffusion of TRYPH from water to Tiss®-Link.

On the other hand, one of the most relevant events on the determination of TRYP with the proposed sensing film is the extraction of the TRYP from the sample to the nanofibre mat. Thus, the determination is highly influenced by the binding kinetic of TRYP on Tiss®-Link. As it was demonstrated previously, the covalent immobilisation of TRYP on Tiss®-Link at pH = 10 is highly effective, but the matrix (beer) can modify this binding kinetic and therefore, the conditions must be set according with this effect.

For this experiment, the Spanish beer San Miguel Especial was selected as model. The first step consisted on the determination of the concentration of TRYP (see Section 3.6). The concentration of TRYP in this sample was estimated in 387 ng mL^{-1}.

To study the matrix effect, the binding kinetics of TRYP on Tiss®-Link was evaluated in buffer and beer at the same initial concentration of TRYP (387 ng mL^{-1}) and chemical conditions (20 mM carbonate buffer at pH = 10). In addition, to determine if the dilution of the sample may affect the binding kinetic, two dilutions (1:1 and 1:3) of the buffer solution and beer, both containing 387 ng mL^{-1} TRYP, were also tested. SM (see Fig. SM-3.6) shows all the results and Fig. 3.4 summarises the binding kinetics of TRYP for times shorter than 30 min.

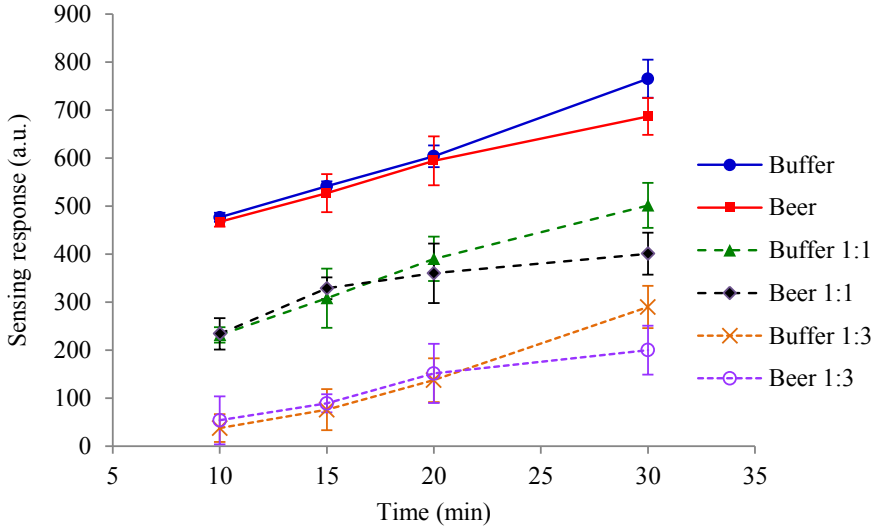

Fig. 3.4. Binding kinetics of TRYP on Tiss®-Link for times shorter than 30 min in 20 mM carbonate buffer at pH = 10 (—●—) and San Miguel Especial beer sample at pH = 10 (—■—), as well as their 1:1 dilutions (dashed line) and 1:3 dilutions (dotted line) with 20 mM carbonate buffer at pH = 10. $[TRYP]_0$ = 387 ng mL^{-1}, [KI] = 1 M, $\lambda_{exc/em}$ = 290/443 nm, t_d = 120 µs, t_g = 5 ms, monochromator slits $width_{exc/em}$ = 10/10 nm, detector voltage of 750 V in a current flow of 300 mL min^{-1} nitrogen.

The amount of immobilized TRYP increases, in all the cases, with the time. For reaction times higher than 30 min, the reaction rates in buffer and its dilutions are higher than in beer and its dilutions. Therefore, the matrix affects the binding kinetic of TRYP on Tiss®-Link for reaction times over 20 min, but for shorter reaction times (between 0 and 20 min) the effect of matrix to the binding kinetic of TRYP is completely negligible (see Fig. 3.4).

To simplify the analytical procedure and allow a standard calibration, it is necessary to set experimental conditions in which the reaction rates in buffer and beer are similar. It can be reached at reaction times lower than 20 min.

The negligible matrix effect at short reaction times can be due to the high number of active vinyl groups of Tiss®-Link (330 µmol g^{-1}). At short reaction times (between 0 and 15 min), all the

amine compounds of the beer (including BAs, macromolecules such as proteins, and some polysaccharides) can find free active vinyl groups in the material, and thus they do not interfere each other: 3 mg of Tiss®-Link have enough functional groups to immobilise all the amines of 4 mL of 200 µg mL^{-1} solution while the total concentration of BAs in beer is between 5 and 25 µg mL^{-1} (Almeida et al. 2012; Izquierdo-Pulido et al. 1996; Jia et al. 2011). When the reaction time increases (above 20 min) the number of free active vinyl groups in the material decreases, and a competition between the amine components of the beer (including macromolecules with amine groups) by the active vinyl groups of the material begins, changing the immobilization rate of each amine.

To sum up, TRYPH is the only phosphorescence specie that can interfere on the RTP signal of TRYP, but it is not immobilised on the nanofibre mat at pH = 10 (immobilization conditions of TRYP). On the other hand, 15 min of binding time was selected in order to eliminate the matrix effect and make possible the use of a standard calibration procedure in the determination of TRYP in beer.

3.5. Analytical Figures of merits

A standard linear calibration graph was drawn according to recommended procedures. The regression equation was $SR = 1.24 \cdot C - 32.67$, where SR is the sensing response and C is the concentration of TRYP in ng mL^{-1} (see Fig. SM-3.7).

The wide linear range (19-600 ng mL^{-1}), small standard errors, correlation coefficient (r = 0.9914) and good detection limit (6 ng mL^{-1}) and quantification limit (19 ng mL^{-1}) indicate very good calibration linearity. The detection and quantification limits were determined using the IUPAC method (LOD = $3s_b/m$; LOQ = $10s_b/m$) (IUPAC 1976).

3.6. Application and validation of the sensor

The good analytical figures of merits of the proposed method allow the determination of TRYP in beer. Table 3.1 shows the results.

Since there is no official method to determine the analyte under study, the estimation of the absolute TRYP concentration was not optimised and the validation of the proposed method was carried out with a Standard Addition Method, the evaluation of the similarity of the slopes, and the analysis of spiked real samples.

Table 3.1. Analytical application results and recovery percentages of spiked samples at two concentration levels (200 and 400 ng mL^{-1}) in 10 commercially available beer samples.

Sample	Analysis of beers	Recovery percentage study		
	Found, ng mL^{-1} (RSD, %, n = 4)	Added, ng mL^{-1}	Found, ng mL^{-1} (RSD, %)	Recovery percentage, % (RSD, %)
Alhambra	469.6 (4.7)	200	642.6 (1.8)	96.1 (5.0)
		400	776.8 (0.3)	89.4 (2.3)
Amstel	447.0 (6.1)	200	650.2 (2.9)	100.6 (3.4)
		400	783.7 (3.3)	92.6 (6.2)
Budweiser	697.6 (3.5)	200	884.5 (2.6)	98.6 (3.0)
		400	1092.6 (3.5)	99.6 (4.9)
Calsberg	655.6 (5.6)	200	744.6 (5.2)	87.0 (3.8)
		400	844.5 (1.0)	89.6 (4.4)
Cruzcampo	370.6 (4.5)	200	594.5 (3.9)	104.2 (4.0)
		400	828.2 (2.8)	107.5 (2.2)
Cruzcampo (free alcohol)	315.3 (1.8)	200	596.6 (3.4)	115.7 (2.6)
		400	717.5 (6.4)	100.3 (7.0)
Heineken	531.6 (5.2)	200	754.1 (1.1)	103.2 (4.7)
		400	918.5 (3.4)	98.6 (2.5)
Mahou	366.8 (5.7)	200	583.6 (7.0)	103.0 (6.4)
		400	773.2 (3.8)	100.9 (6.1)
Mahou (free alcohol)	405.5 (2.5)	200	536.0 (2.1)	88.5 (1.8)
		400	729.3 (5.8)	90.5 (5.5)
San Miguel Especial	387.6 (5.6)	200	557.0 (3.4)	94.9 (6.8)
		400	675.8 (3.8)	85.9 (5.5)

The method was validated with a standard addition method of calibration by San Miguel Especial beer (see SM, Fig. SM-3.7). The standard addition regression equation was $SR = 1.3882 \cdot C + 269.89$ (r = 0.9899), where *SR* is the sensing response and *C* is the added concentration of TRYP in ng mL^{-1}. The TRYP concentrations were 389.0 ng mL^{-1} (RSD = 1.8%) and 387.6 ng mL^{-1} (RSD = 5.6%) for the standard addition method and the standard calibration, respectively.

To check the similarity of the slopes, a Student's t-test was used (Cudros Rodriguez et al. 1995); the $t_{calculated}$ was 1.8622 while the $t_{tabulated}$ at 19º of freedom and $\alpha = 0.05$ is 2.093. Therefore, the slopes are essentially the same and we can conclude that the method is free of matrix effect.

On the other hand, the method was also validated by spiking all the beers and determining the recovery percentage (see Table 3.1). For this experiment, the 10 samples of beers were spiked with TRYP at two concentration levels (200 and 400 ng mL^{-1}), and the amount of TRYP was determined following the beer sample procedure previously described. The recovery percentage was calculated using the TRYP content of the beer previously determined and the TRYP added. All the recovery percentages were between 85.9 and 115.7% with relative standard deviations lower than 9.5% in all the cases.

Table 3.2 shows a comparison of the proposed method with the others proposed in the literature for the determination of TRYP in beer samples. It is possible to conclude that the use of Tiss®-Link for determining and quantifying TRYP in beer samples provides: (1) the best analytical figures of merits, i.e. the lowest LOD and LOQ; (2) the fastest method for analysing TRYP in beers; it only takes 17 min (15 min for incubation and 2 min for recording the luminescence signal) whilst the rest of the methods require complex sample procedures and longer measurement protocols; (3) the cheapest instrumentation for carrying out the measurement; it only uses a luminescent spectrometer which is considerably cheaper than chromatographic instruments; (4) the most environmental friendly method due to it is the only one that only uses water or aqueous solutions while all the other methods require organic solvents, most of them a high amount of organic solvents.

4. Conclusions

We have developed a novel optical sensor based in the combination of nanotechnology (nanofibre mat functionalised with active vinyl groups) with SS-RTP as transduction system which has resulted in a highly selective and sensitive method for detecting (LOD of 6 ng mL^{-1}) and quantifying (LOQ of 19 ng mL^{-1}) TRYP in a complex matrix such as beer.

Table 3.2. Comparison of the proposed method with others published in the literature for analysing TRYP in beer samples.

Analytical technique	Sample treatment	LOD, ng mL^{-1}	LOQ, ng mL^{-1}	Analysis time, min[a]	Reference
LC-Q-TOFMS	Dilution with 0.1M HCl 60 min incubation with Na_2CO_3 and dansyl chloride at 40ºC 30 min incubation with ammonia 3 min centrifugation	20	50	115	(Jia et al. 2011)
HPLC	Degassing Filtration Derivatization with ortho-phthalaldehyde	300	-	-	(Izquierdo-Pulido et al. 1996)
HPLC-DAD	Filtration 30 min incubation with 4-chloro-3,5-dinitrobenzotrifluoride at 60 ºC Addition of 2 M HCl Filtration	50	-	52	(Tang et al. 2009)
HPLC-UV	Degassing Filtration 40 min incubation with dansyl chloride in acetone and $NaHCO_3$ at 65 ºC 2 min centrifugation SPE with acetonitrile-methanol	14	45	90	(Mazzucco et al. 2010)
Ion-pair LC–CLND	Filtration	400	-	35	(Sun et al. 2011a)
HAI-RTP	Degassing SPE or liquid–liquid extraction with evaporation of the eluate/organic phase	28	94	30	(Cañabate-Díaz et al. 2003)
SS-RTP	Degassing Dilution with Na_2CO_3 buffer at pH = 10 15 min incubation with Tiss®-Link	6	19	17	This work

[a] For the calculation of the analysis time only the available times required for incubation, derivatization and separation procedures have been used.

The proposed method is the most sensitive, the fastest, the cheapest, and the most environmental friendly method published in the literature so far; it has a LOD which is the half of the most sensitive method hitherto published, it only takes the half of the time of the fastest one and it is the first time to our knowledge that TRYP has been analysed directly in beer, avoiding the clean-up, pre-concentration and derivatization protocols, it only uses a luminescence spectrometer which is considerably cheaper than chromatographic instruments, and it only requires the use of water or aqueous solutions.

The proposed sensor simplifies considerably the methodology to analyse TRYP, reducing time and cost of the analysis and therefore, it could be easily applied in a routine quality control lab during the production of beer for controlling the fermentation. On the other hand, similar protocols might be also used for the determination of TRYP in other foods and beverages such as cheese, wine, fishery products and meat, as well as to determine other important phosphorescent heterocyclic amines such as serotonin in biological samples.

Acknowledgments

The authors gratefully acknowledge the financial support of the Spanish Ministry of Economy and Competitiveness (Ramon-Marquez‘s grant reference AP2012-0944 and Medina-Castillo‘s Torres Quevedo contract reference PTQ-11-04904), the Regional Government of Andalucia (Orden de incentivos, Proyectos de I+D+I reference 451551) and the Corporación Tecnológica de Andalucía (project reference 11/557).

References

Almeida, C., Fernandes, J.O., Cunha, S.C., 2012. A novel dispersive liquid-liquid microextraction (DLLME) gas chromatography-mass spectrometry (GC-MS) method for the determination of eighteen biogenic amines in beer. Food Control 25(1), 380-388.

Anderson, A.K., 2008. Biogenic and volatile amine-related qualities of three popular fish species sold at Kuwait fish markets. Food Chemistry 107(2), 761-767.

Azab, H.A., El-Korashy, S.A., Anwar, Z.M., Khairy, G.M., Steiner, M.S., Duerkop, A., 2011. High-throughput sensing microtiter plate for determination of biogenic amines in seafood using fluorescence or eye-vision. Analyst 136(21), 4492-4499.

Bedia Erim, F., 2013. Recent analytical approaches to the analysis of biogenic amines in food samples. TrAC Trends in Analytical Chemistry 52(0), 239-247.

Bóka, B., Adányi, N., Virág, D., Sebela, M., Kiss, A., 2012. Spoilage Detection with Biogenic Amine Biosensors, Comparison of Different Enzyme Electrodes. Electroanalysis 24(1), 181-186.

Bruxvoort, C.B., Dawson, G.G., Francis, T.A., Reiter, W.S., Haustein, C.H., 1993. Room-Temperature Luminescence of Formaldehyde-Condensed Amines Adsorbed on Filter Paper. Microchemical Journal 47(1–2), 140-147.

Cañabate-Díaz, B., Segura Carretero, A., Cruces-Blanco, C., Fernández-Gutiérrez, A., 2003. Determination of the amino acid tryptophan and the biogenic amine tryptamine in foods by the heavy atom induced-room temperature phosphorescence methodology. Analyst 128(4), 411-415.

Casella, I.G., Palladino, G.A., Contursi, M., 2008. Determination of aliphatic amines by cation-exchange chromatography with suppressed conductivity detection after solid phase extraction. Journal of Separation Science 31(21), 3718-3726.

Cortacero-Ramírez, S., Arráez-Román, D., Segura-Carretero, A., Fernández-Gutiérrez, A., 2007. Determination of biogenic amines in beers and brewing-process samples by capillary electrophoresis coupled to laser-induced fluorescence detection. Food Chemistry 100(1), 383-389.

Cudros Rodriguez, L., Garcia Campana, A.M., Ales Barrero, F., Jimenez Linares, C., Roman Cera, M., 1995. Validation of an analytical instrumental method by standard addition methodology. Journal of AOAC International 78(2), 471-476.

Chow, C.F., Kong, H.K., Leung, S.W., Chiu, B.K.W., Koo, C.K., Lei, E.N.Y., Lam, M.H.W., Wong, W.T., Wong, W.Y., 2011. Heterobimetallic Ru(II)-Eu(III) complex as chemodosimeter for selective biogenic amine odorants detection in fish sample. Analytical Chemistry 83(1), 289-296.

de Jong, W.H.A., Graham, K.S., de Vries, E.G.E., Kema, I.P., 2008. Urinary 5-HIAA measurement using automated on-line solid-phase extraction-high-performance liquid chromatography-tandem mass spectrometry. Journal of Chromatography B 868(1-2), 28-33.

de Ribamar, J., Júnior, F., Campiglia, A.D., 1995. Solid-surface room-temperature phosphorescence detection of serotonin, tryptamine, and gramine enhanced by inorganic salts and sodium dodecyl sulfate. Talanta 42(10), 1505-1512.

Di Fusco, M., Federico, R., Boffi, A., MacOne, A., Favero, G., Mazzei, F., 2011. Characterization and application of a diamine oxidase from Lathyrus sativus as component of an electrochemical biosensor for the determination of biogenic amines in wine and beer. Analytical and Bioanalytical Chemistry 401(2), 707-716.

Giuliano, F.o., Rampin, O., 2004. Neural control of erection. Physiology & Behavior 83(2), 189-201.

Hu, Z., Li, L., Yuan, Y., Yue, T., 2014. Ultrasensitive and simultaneous determination of twenty-one amino acids and amines in culture media, red wine and beer. Food Chemistry 158(0), 56-65.

IUPAC, 1976. COMMISSION ON SPECTROCHEMICAL AND OTHER OPTICAL PROCEDURES FOR ANALYSIS - NOMENCLATURE, SYMBOLS, UNITS AND THEIR USAGE IN SPECTROCHEMICAL ANALYSIS .3. ANALYTICAL FLAME SPECTROSCOPY AND ASSOCIATED NON-FLAME PROCEDURES. Pure Appl. Chem. 45(2), 105-123.

Izquierdo-Pulido, M., Hernández-Jover, T., Mariné-Font, A., Vidal-Carou, M.C., 1996. Biogenic Amines in European Beers. Journal of Agricultural and Food Chemistry 44(10), 3159-3163.

Izquierdo-Pulido, M., Mariné-Font, A., Vidal-Carou, M.C., 1994. Biogenic Amines Formation during Malting and Brewing. Journal of Food Science 59(5), 1104-1107.

Izquierdo Cañas, P.M., García Romero, E., Gómez Alonso, S., Fernández González, M., Palop Herreros, M.L.L., 2008. Amino acids and biogenic amines during spontaneous malolactic fermentation in Tempranillo red wines. Journal of Food Composition and Analysis 21(8), 731-735.

Jastrzębska, A., Piasta, A., Szłyk, E., 2013. Simultaneous determination of selected biogenic amines in alcoholic beverage samples by isotachophoretic and chromatographic methods. Food Additives & Contaminants: Part A 31(1), 83-92.

Jia, S., Kang, Y.P., Park, J.H., Lee, J., Kwon, S.W., 2011. Simultaneous determination of 23 amino acids and 7 biogenic amines in fermented food samples by liquid chromatography/quadrupole time-of-flight mass spectrometry. Journal of Chromatography A 1218(51), 9174-9182.

Kalač, P., Hlavatá, V., Křížek, M., 1997. Concentrations of five biogenic amines in Czech beers and factors affecting their formation. Food Chemistry 58(3), 209-214.

Lorenzo, J.M., Martínez, S., Franco, I., Carballo, J., 2007. Biogenic amine content during the manufacture of dry-cured lacon, a Spanish traditional meat product: Effect of some additives. Meat Science 77(2), 287-293.

Loret, S., Deloyer, P., Dandrifosse, G., 2005. Levels of biogenic amines as a measure of the quality of the beer fermentation process: Data from Belgian samples. Food Chemistry 89(4), 519-525.

Ma, N., Tan, L.-w., Wang, Q., Li, Z.-x., Li, L.-j., 2007. Lower levels of whole blood serotonin in obsessive-compulsive disorder and in schizophrenia with obsessive-compulsive symptoms. Psychiatry Research 150(1), 61-69.

Mazzucco, E., Gosetti, F., Bobba, M., Marengo, E., Robotti, E., Gennaro, M.C., 2010. High-Performance Liquid Chromatography−Ultraviolet Detection Method for the Simultaneous Determination of Typical Biogenic Amines and Precursor Amino Acids. Applications in Food Chemistry. Journal of Agricultural and Food Chemistry 58(1), 127-134.

Medina-Castillo, A.L., Fernández-Sánchez, J.F., Fernández-Gutiérrez, A., 2011a. One-Step Fabrication of Multifunctional Core-Shell Fibres by Co-Electrospinning. Advanced Functional Materials 21(18), 3488-3495.

Medina-Castillo, A.L., Fernandez-Sanchez, J.F., Segura-Carretero, A., Fernandez-Gutierrez, A., 2011b. Design and synthesis by ATRP of novel, water-insoluble, lineal copolymers and their application in the development of fluorescent and pH-sensing nanofibres made by electrospinning. Journal of Materials Chemistry 21(18), 6742-6750.

Medina-Castillo, A.L., Morales-Sanfrutos, J., Megia-Fernandez, A., Fernandez-Sanchez, J.F., Santoyo-Gonzalez, F., Fernandez-Gutierrez, A., 2012. Novel synthetic route for covalent coupling of biomolecules on super-paramagnetic hybrid nanoparticles. Journal of Polymer Science Part A: Polymer Chemistry 50(19), 3944-3953.

Miller, A.G., Brown, H., Degg, T., Allen, K., Keevil, B.G., 2010. Measurement of plasma 5-hydroxyindole acetic acid by liquid chromatography tandem mass spectrometry-Comparison with HPLC methodology. Journal of Chromatography B 878(7-8), 695-699.

Molins-Legua, C., Campins-Falcó, P., 2005. Solid phase extraction of amines. Analytica Chimica Acta 546(2), 206-220.

Monaghan, P.J., Brown, H.A., Houghton, L.A., Keevil, B.G., 2009. Measurement of serotonin in platelet depleted plasma by liquid chromatography tandem mass spectrometry. Journal of Chromatography B 877(22), 2163-2167.

Moriarty, M., Lee, A., O'Connell, B., Lehane, M., Keeley, H., Furey, A., 2012. The Application and Validation of HybridSPE-Precipitation Cartridge Technology for the Rapid Clean-up of Serum Matrices (from Phospholipids) for the Clinical Analysis of Serotonin, Dopamine and Melatonin. Chromatographia 75(21-22), 1257-1269.

Naccarato, A., Gionfriddo, E., Sindona, G., Tagarelli, A., 2014. Development of a simple and rapid solid phase microextraction-gas chromatography-triple quadrupole mass spectrometry method for the analysis of dopamine, serotonin and norepinephrine in human urine. Analytica Chimica Acta 810(0), 17-24.

Nakamura, M., Sanji, T., Tanaka, M., 2011. Fluorometric sensing of biogenic amines with aggregation-induced emission-active tetraphenylethenes. Chemistry - A European Journal 17(19), 5344-5349.

Ntzimani, A.G., Paleologos, E.K., Savvaidis, I.N., Kontominas, M.G., 2008. Formation of biogenic amines and relation to microbial flora and sensory changes in smoked turkey breast fillets stored under various packaging conditions at 4°C. Food Microbiology 25(3), 509-517.

Önal, A., Tekkeli, S.E.K., Önal, C., 2013. A review of the liquid chromatographic methods for the determination of biogenic amines in foods. Food Chemistry 138(1), 509-515.

Pérez-Serradilla, J.A., de Castro, M.D.L., 2008. Role of lees in wine production: A review. Food Chemistry 111(2), 447-456.

Ramos, R.M., Valente, I.M., Rodrigues, J.A., 2014. Analysis of biogenic amines in wines by salting-out assisted liquid-liquid extraction and high-performance liquid chromatography with fluorimetric detection. Talanta 124(0), 146-151.

Shalaby, A.R., 1996. Significance of biogenic amines to food safety and human health. Food Research International 29(7), 675-690.

Silla Santos, M.H., 1996. Biogenic amines: their importance in foods. Int J Food Microbiol 29(2-3), 213-231.

Simó, C., Moreno-Arribas, M.V., Cifuentes, A., 2008. Ion-trap versus time-of-flight mass spectrometry coupled to capillary electrophoresis to analyze biogenic amines in wine. Journal of Chromatography A 1195, 150-156.

Sun, J., Guo, H.-X., Semin, D., Cheetham, J., 2011. Direct separation and detection of biogenic amines by ion-pair liquid chromatography with chemiluminescent nitrogen detector. Journal of Chromatography A 1218(29), 4689-4697.

Tang, T., Qian, K., Shi, T., Wang, F., Li, J., Cao, Y., Hu, Q., 2011. Monitoring the contents of biogenic amines in sufu by HPLC with SPE and pre-column derivatization. Food Control 22(8), 1203-1208.

Tang, T., Shi, T., Qian, K., Li, P., Li, J., Cao, Y., 2009. Determination of biogenic amines in beer with pre-column derivatization by high performance liquid chromatography. Journal of Chromatography B 877(5-6), 507-512.

Wang, X.-d., Wolfbeis, O.S., 2014. Optical methods for sensing and imaging oxygen: materials, spectroscopies and applications. Chemical Society Reviews 43(10), 3666-3761.

Appendix. Supplementary Material (SM)

Content:

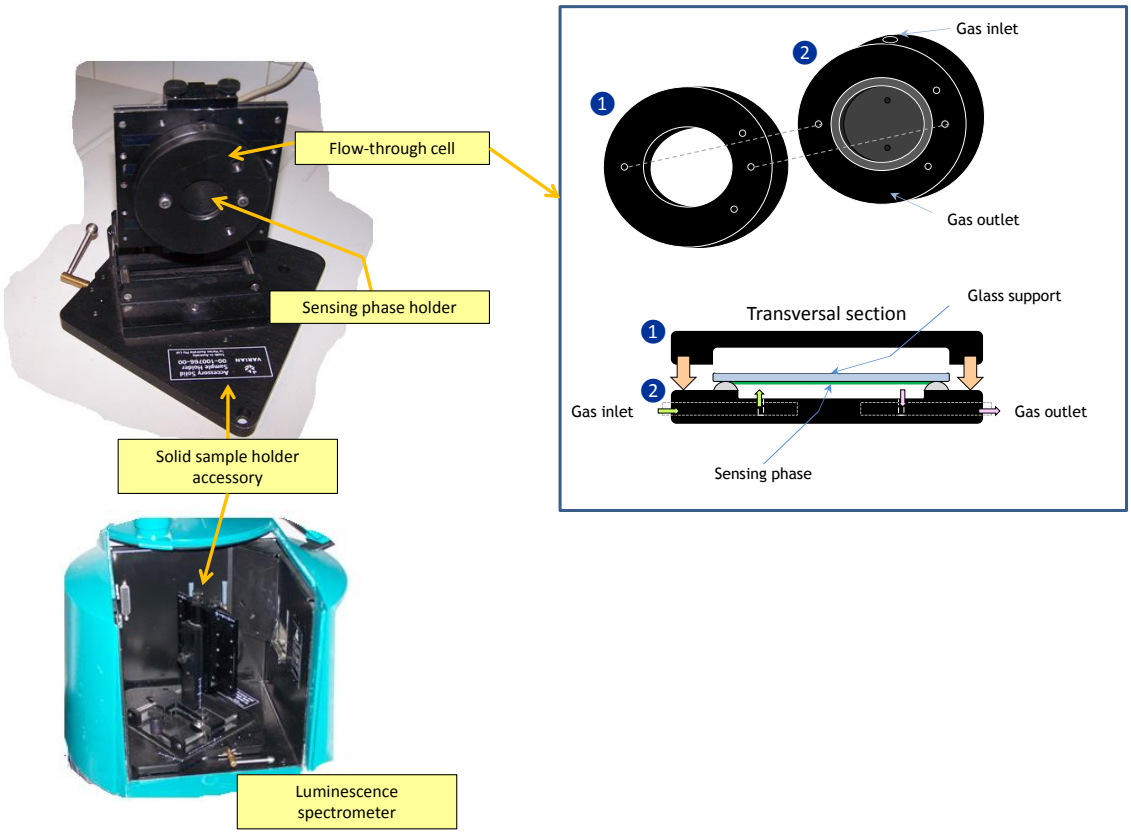

Figure SM-3.1. Measuring setup.

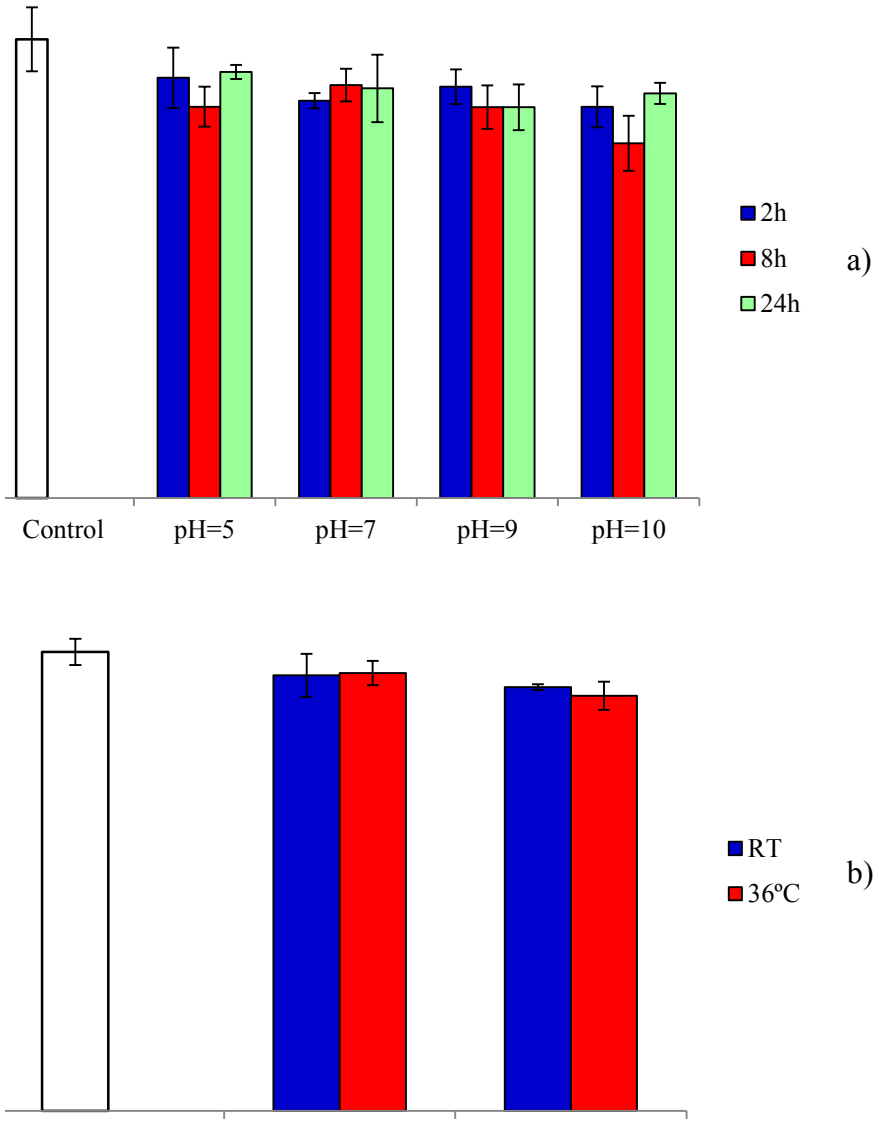

Fig. SM-3.2. Stability of the active vinyl groups of Tiss®-Link *versus* a) pH, and b) temperature. For the fluorescence measurement the fibre mats were incubated in 4 mL of 280 µg mL^{-1} DC solution containing 100 mM phosphate buffer solution at pH = 8.5 for 24 h at RT, and the fluorescence was measured at $\lambda_{exc/em}$ = 330/480 nm, slit widths $_{exc/em}$ = 5/5 nm, and detector voltage of 500 V.

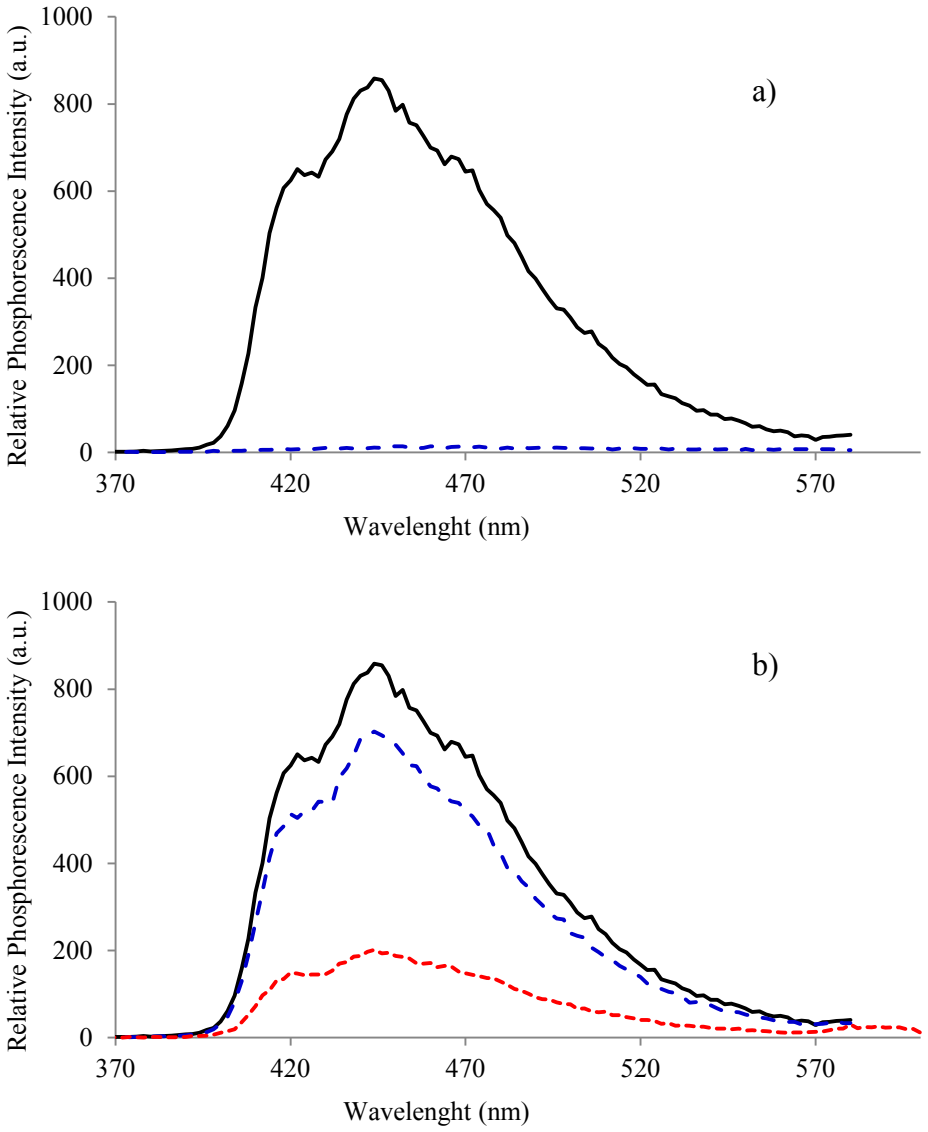

Fig. SM-3.3. Luminescence properties of TRYP covalently immobilised on Tiss®-Link. a) Effect of the KI: in the presence of KI and 100% N_2 (solid black line) and in the absence of KI and 100% N_2 (dashed blue line). b) Effect of the oxygen concentration: in the presence of KI and 0% O_2 (solid black line), in the presence of KI and air, 21% O_2, (dashed blue line), and in the presence of KI and 100% O_2.

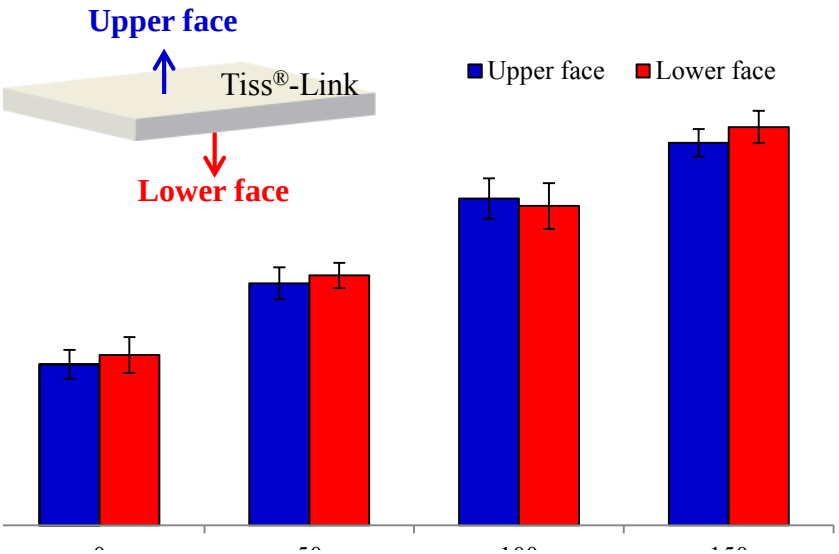

Fig. SM-3.4. Phosphorescence intensity of several sections and sides of the sensing films after immobilization of TRYP.

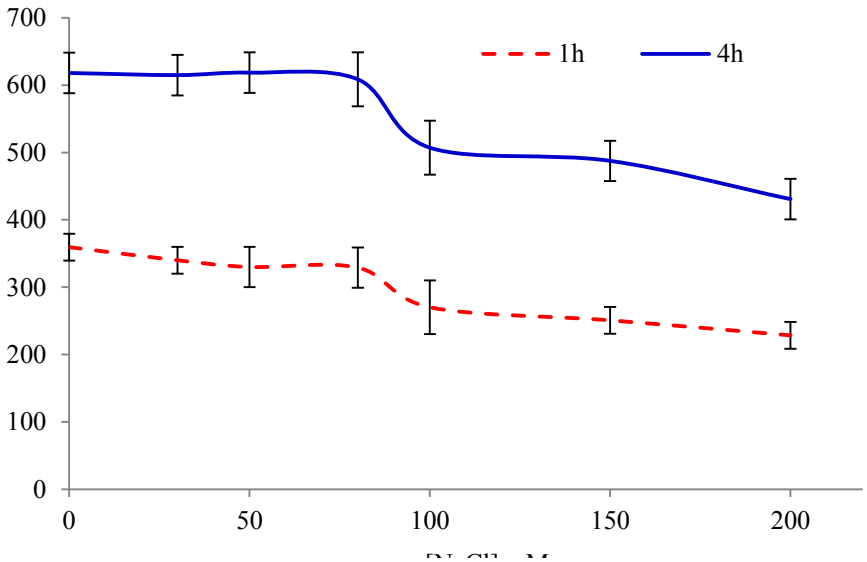

Fig. SM-3.5. Effect of the ionic strength on the covalent immobilization of 1 µg mL^{-1} TRYP on Tiss®-Link at two different incubation times.

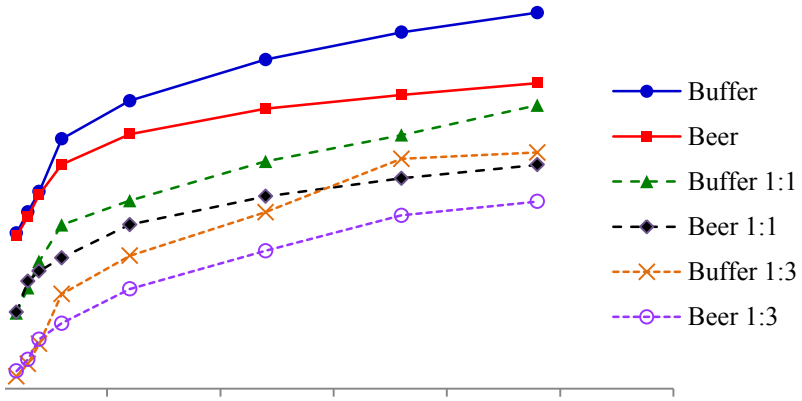

Fig. SM-3.6. Binding kinetics of TRYP on Tiss®-Link in 20 mM carbonate buffer at pH = 10 (—●—) and San Miguel Especial beer sample at pH = 10 (—■—), as well as their 1:1 dilutions (dashed line) and 1:3 dilutions (dotted line) with 20 mM carbonate buffer at pH = 10. [TRYP] = 387 ng mL^{-1}, [KI] = 1 M, $\lambda_{exc/em}$ = 290/443 nm**,** t_d = 120 µs, t_g = 5 ms, monochromator slits $width_{exc/em}$ = 10/10 nm, detector voltage of 750 V in a current flow of 300 mL min^{-1} nitrogen.

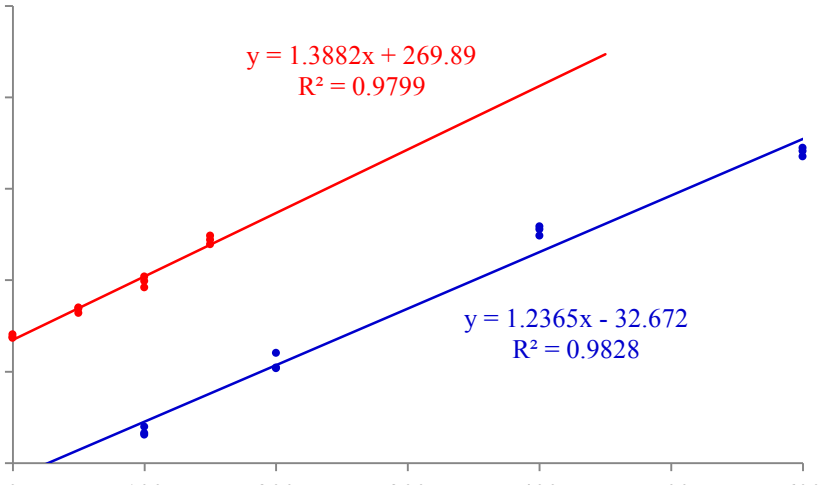

Fig. SM-3.7. Analytical evaluation of the proposed method: standard calibration (blue curve) and standard addition calibration using San Miguel Especial sample (red curve).

Capítulo 4

A novel optical biosensor for direct and selective determination of serotonin in serum by Solid Surface-Room Temperature Phosphorescence

Teresa Ramon-Marquez[a], *Antonio L. Medina-Castillo*[b], *Alberto Fernandez-Gutierrez*[a], *Jorge F. Fernandez-Sanchez*[a]

[a] Department of Analytical Chemistry, University of Granada, Avd. Fuentenueva s/n, 18071 Granada, Spain

[b] NanoMyP®, Nanomateriales y Polimeros S.L., Spin-Off company of the UGR, BIC Building, Avd. Innovacion 1, E-18016, Granada, Spain

Published in *Biosensors and Bioelectronics*, 2016, **82**, 217-223

ABSTRACT

This paper describes a novel biosensor which combines the use of nanotechnology (non-woven nanofibre mat) with Solid Surface-Room Temperature Phosphorescence (SS-RTP) measurement for the determination of serotonin in human serum. The developed biosensor is simple and can be directly applied in serum; only requires a simple clean-up protocol. Therefore it is the first time that serotonin is analysed directly in serum with a non-enzymatic technique. This new approach is based on the covalent immobilisation of serotonin directly from serum on a functional nanofibre material (Tiss®-Link) with a preactivated surface for direct covalent immobilisation of primary and secondary amines, and the subsequent measurement of serotonin phosphorescent emission from the solid surface. The phosphorescent detection allows avoiding the interference from any fluorescence emission or scattering light from any molecule present in the serum sample which can be also immobilised on the nanofibre material. The determination of serotonin with this SS-RTP sensor overcomes some limitations, such as large interference from the matrix and high cost and complexity of many of the methods widely used for serotonin analysis.

The potential applicability of the sensor in the clinical diagnosis was demonstrated by analysing serum samples from seven healthy volunteers. The method was validated with an external reference laboratory, obtaining a correlation coefficient of 0.997 which indicates excellent correlation between the two methods.

Keywords: Nanotechnology; Tiss®-Link; SS-RTP; Nanofibre mat; Serum; Phosphorescence; Serotonin; Protein clean-up.

1. Introduction

Serotonin or 5-hydroxytryptamine (5-HT) is a biogenic amine that acts as a neurotransmitter in the central and peripheral nervous systems (Berger et al. 2009; Jacobs and Azmitia 1992). It controls a wide variety of physiological and behavioural processes, including depression, mood, sleep, anxiety, addiction, sexual activity, aggression and cognition as well as memory or perception (Berger et al. 2009; Deemyad et al. 2013; Hoyer et al. 2002; Julius 1998; Makris et al. 2016; Meneses and Liy-Salmeron 2012; Piszczek et al. 2015; Ramboz et al. 1998; Udupa and Chen 2015).

Atypical concentrations of 5-HT in physiological fluids (serum and plasma) and body tissues have been related as a critical factor to several mental disorders such as Alzheimer‘s disease, schizophrenia, depression, infantile autism and obsessive compulsive disorder (Berger et al. 2009; Hoyer et al. 2002; Tecott et al. 1995). Other studies have also shown that high levels of 5-HT can affect the cardiovascular and gastrointestinal systems, and can be related with the carcinoid syndrome (Berger et al. 2009; Brand and Anderson 2011; Kema et al. 2001; Meijer et al. 2000; Pussard et al. 1996).

Due to the multiple roles played by the serotonergic systems, it is important for pathological investigations and clinical diagnostics to establish sensitive, highly selective, rapid and simple methods for determining 5-HT levels in biological samples, mainly in serum.

Many methodologies have been developed for the determination of 5-HT in biological samples, including enzyme immunoassays (Chauveau et al. 1991; Lee et al. 2014; Nichkova et al. 2012), chromatographic (Danaceau et al. 2003; de Jong et al. 2010; Kema et al. 2001; Pussard et al. 1996; Yi et al. 1994; Yoshitake et al. 2004; Yubero-Lahoz et al. 2014), capillary electrophoresis (Peterson et al. 2004; Román et al. 2004), electrochemical (Goyal and Agrawal 2012; Gupta and Goyal 2014; Hasanzadeh et al. 2013; Mazloum-Ardakani and Khoshroo 2014; Wang et al. 2013; Xue et al. 2014a) and spectrofluorometric (Bracamonte and Veglia 2011; Peng and Jiang 2007) methods.

Both enzyme immunoassay (Darwish 2006; Wu 2006) (EIA) and enzyme-linked immunosorbent assay (Comley 2012; Gan and Patel 2013; Grange et al. 2014) (ELISA) methods are widely used as diagnostic tools in medicine and biomedical researches to analyse 5-HT, among other analytes, in serum samples (Chauveau et al. 1991). These assays require the immobilization of antigens, haptens, or antibodies on a solid surface, involving some

disadvantages such as: 1) the presence of natural inhibitors in the samples which can provide wrong results, 2) nonspecific binding of the antibody or antigen to the solid support which leads to false-positive results, and 3) the enzyme reactions are very sensitive to temperature (Berg 2002; Coolbear et al. 1992; Hedstrom 2001; Iyer and Ananthanarayan 2008). Moreover, these assays need of many steps of reaction (Chauveau et al. 1991; Darwish 2006), incubation processes (Li and Cassone 2015; Nichkova et al. 2012) and washing steps (Huisman et al. 2010; Kim et al. 2009) which increase the analysis time and cost (Kim et al. 2008; Nichkova et al. 2013) as well as require experimented technicians.

Separative methods, in special HPLC with fluorescence detection, are also commonly used for routine clinical analysis of 5-HT in serum. However, chromatographic determination of 5-HT shows significant drawbacks: they usually require previous solid phase, liquid-liquid extractions or protein precipitations (de Jong et al. 2010; Golubchik et al. 2009; Zhen et al. 2011), pre or post-column derivatization reactions (Hirowatari et al. 2004; Mao et al. 2009; Ohkawa et al. 2005), use of relatively large amounts of solvents (Mao et al. 2009; Sa et al. 2012), long preparation times (Hirowatari et al. 2004; Mao et al. 2009; Teradaira et al. 2007) and expensive equipments.

Electrochemical methods are sensitive enough to estimate the concentration of 5-HT in biological samples, but they are not available in clinical laboratories due to problems of maintenance, limited life time of the electrodes and variability on sensitivity (Babaei et al. 2013; Hasanzadeh et al. 2013; Li and Lin 2007; Myers and Lee 2008).

Spectrofluorometric methods have also been developed to determine 5-HT in serum, but optical measurements are not selective enough to develop a good routine method in this field. One of the main problem of the analysis of 5-HT in serum samples by spectrofluorometric methods is the complexity of the matrix, which contains potential interfering compounds such as proteins, antibodies, antigens, hormones, etc. Many of these compounds show weak natural fluorescence and, therefore can affect the reliability of the results. In fact, many proteins show intrinsic fluorescence emission due to the excitation of tryptophan residues (Gorinstein et al. 2000; Kowalska-Baron et al. 2015).

On the other hand, there are only few components of the serum that show intrinsic phosphorescence emission, where 5-HT, tryptamine (TRYP) and tryptophan (TRYPH) are included (Bruxvoort et al. 1993; de Ribamar et al. 1995). They are structurally and metabolically

related (D'Andrea et al. 2015). Therefore, phosphorescence could be a good alternative to much more complex methods to determine 5-HT in human serum. Phosphorescence sensors have been successfully used for the direct, quick and easy (in one step) determination of different molecules in complex matrices, solving the main drawbacks of the enzymatic and separative techniques previously discussed (Bi et al. 2014; Ramon-Marquez et al. 2016; Wu et al. 2010).

Since 5-HT has native phosphorescence, in this paper, we have developed a novel biosensor for the direct determination of 5-HT in human serum samples with satisfactory results, by taking advantage of the benefit of the functional material Tiss®-Link (Medina-Castillo et al. 2011a; Medina-Castillo et al. 2011b; Ramon-Marquez et al. 2016), and the high sensitivity and selectivity of Solid Surface-Room Temperature Phosphorescence (SS-RTP). Tiss®-Link is a non-woven nanofibre mat made by electrospinning which has been demonstrated to be useful for covalent immobilization of amines from complex matrices (Medina-Castillo et al. 2011a; Medina-Castillo et al. 2011b; Ramon-Marquez et al. 2016). The use of Tiss®-Link combined with SS-RTP simplifies the procedure to analyse 5-HT directly in serum samples (it only requires minimal clean-up of the samples), reducing considerably the time and cost of the analysis. In addition, the developed biosensor is highly selective and sensitive in the determination and quantification of 5-HT and therefore, it is a good candidate to be used as routine tool in diagnosis and clinical labs.

2. Experimental

2.1. Reactives and Materials

Tiss®-Link, and PolymP®-Pyridine were kindly supplied by NanoMyP® (http://www.nanomyp.com), Tween 20, potassium iodide (KI), sodium carbonate (Na_2CO_3), potassium phosphate (K_2HPO_4), tryptamine (TRYP), serotonin (5-HT), tryptophan (TRYPH) and human serum albumin (HSA) were all purchased from Sigma Aldrich and used without further purification. Human serum samples were obtained from seven healthy volunteers and stored frozen until assay.

Tiss®-Link is a non-woven nanofibre mat manufactured by electrospinning using PolymBlend® (http://nanomyp.com/es/page.cfm?id=212&title=polymblend%C2%AE) as raw material. PolymBlend® is a polymeric blend formulated with an optimum mixture of two high

molecular weight statistic copolymers, containing a high percentage of hydroxyl groups in their structure (40%). Therefore, the nanofibre mats produced with PolymBlend® have high hydrophilicity. During the fabrication process of Tiss®-Link, part of its hydroxyl groups have been functionalized with active vinyl groups, thus the final material has two functionalities: the non-functionalized hydroxyl groups which provide a high hydrophilicity, and the active vinyl groups (330 µmol/g) which can be used for covalent immobilization of primary and secondary amines.

The hydrophilicity of Tiss®-Link was determined by calculating the ω parameter (amount of absorbed water per mass of material) (Stathopoulos et al. 2010). The obtained ω parameter was 2.0, indicating that Tiss®-Link can absorb 2 g of water per gram of material. On the other hand, the pKa of the primary hydroxyl groups of the material (which are the only one which can provide ionic charge) is 15, thus, at pH = 10 the material is uncharged. Therefore, the properties are kept at pH = 10.

Tiss®-Link has excellent mechanical properties (high mechanical strength, high consistency and high flexibility). It is non-luminescent, uncharged, insoluble in aqueous media as well as in apolar solvents (oil, toluene, etc.), showing a high robustness and stability in a wide range of pHs (at least between pH 5 and 10 up to 24 hours), and temperature resistance (up to 100 ° C).

PolymP®-Pyridine is a cationic ion exchange material with format of monodisperse and spherical polymeric particles of 2.5 µm of diameter. They have a high surface density of accessible pyridine groups (250 µmol g^{-1}) with a pKa of 6. These particles are suitable for protein immobilization in a pH range between 3 and 6.

Supporting Material (SM) (see Fig. SM-4.1) shows images of scanning electron microscopy (SEM) in which the microstructure and morphology of Tiss®-Link and PolymP®-Pyridine are shown.

2.2. Apparatus and measurements

All SS-RTP measurements were performed on a Varian Cary-Eclipse luminescence spectrophotometer equipped with a homemade flow cell. A general description of the equipment for SS-RTP measurements has previously been specified (Ramon-Marquez et al. 2016). Since gaseous oxygen is well known to be a quenching agent, it has to be completely removed from the

sample before carrying out the measurements. This was achieved by the application of a gaseous nitrogen stream through the flow cell.

The gas stream was controlled with a mass-flow controller (MFC) (EL-FLOW Select F-201CV, Bronkhorst High-Tech, www.bronkhorst.com, Ruurlo, Netherlands) connected with the flow cell using copper and stainless steel tubing and a PC via a RS-232 serial port by a Flow-Bus Interface (Bronkhorst High-Tech).

All the measurements were carried out at room temperature (21 ºC). The temperature was continuously monitored using a commercial temperature sensor (MicroLite, Fourtec-Fourier Technologies, www.fouriersystems.com) placed at a point close to the flow cell.

The pH of the samples was controlled using a digital pH meter (Crison micropH 2000) calibrated at 20 ± 2 ºC.

2.3. General procedure

For the determination of 5-HT by SS-RTP, three steps are necessary: elimination of serum proteins, covalent immobilization of 5-HT on Tiss®-Link, and SS-RTP measurements.

The elimination of the proteins of serum was carried out following the protocol developed and recommended by the supplier of PolymP®-Pyridine. Briefly, 0.75 mL of serum were incubated with 20 mg of PolymP®-Pyridine at pH = 5 (adjusted with 1 M HCl) for 30 min at room temperature (RT) in a rotating shaker. After incubation, the samples were centrifuged, the particles with the immobilized proteins were discarded and the pH of the supernatant (free-protein samples) was adjusted to 10 with a solution of 1 M NaOH. Finally, it was diluted with carbonate buffer at pH = 10 (1:3 v/v, sample:carbonate buffer 20 mM; pH = 10).

The covalent immobilization of 5-HT on Tiss®-Link was carried out by incubating 3 mg (≈ 0.8 cm^2) of nanofibre mat with 3 mL of sample at pH = 10 for 15 min at RT in a rotating shaker. Then, the mat was washed (3x5 min) with 4 mL of a solution containing 8.5 g/L of NaCl and 0.5 g/L of Tween 20 (washing solution) to remove all the no covalently bounded molecules and dried with a nitrogen flow.

The SS-RTP signal was measured at excitation wavelength of 315 nm, emission wavelength of 449 nm, delay time (t_d) 10 ms, gate time (t_g) 5 ms, excitation and emission slits of 10 nm wide and detector voltage of 850 V. All the measurements were carried out adding 20 µL of 1 M KI as

heavy atom and under a current flow of 300 mL min^{-1} nitrogen to avoid possible quenching effects from oxygen.

The sensing response was established as the difference between the phosphorescence emission of the 5-HT immobilised on Tiss®-Link and the background (RTP emission of Tiss®-Link in the absence of 5-HT).

All the experiments were replicated six times in order to evaluate the error $\left(st/\sqrt{n}\right)$ where *s* is the standard deviation, *t* the Student t and *n* the number of replicas.

2.4. Analysis of 5-HT in serum samples

Seven serum samples were obtained from seven healthy volunteers. The seven samples were analysed with both the proposed biosensor and an external reference laboratory (http://reference-laboratory.es/) located in Barcelona (Spain), which determined the amount of 5-HT by an official enzyme immunoassay method.

The analysis of 5-HT in serum samples by the proposed biosensor requires a standard addition calibration method. It was obtained from the SS-RTP emission of Tiss®-Link (0.8 cm^2) incubated for 15 min at RT directly in the serum samples after the protein clean-up protocol. The calibration was developed diluting the sample with 20 mM carbonate buffer at pH = 10 (dilution 1:3 v/v, serum:carbonate buffer) and adding four concentrations of 5-HT (0, 50, 100 and 200 ng mL^{-1}). The SS-RTP emission was measured at the following conditions: $\lambda_{exc/em}$ = 315/449 nm, t_d = 10 ms, t_g = 5 ms, slit $widths_{exc/em}$ = 10/10 nm, and detector voltage of 850 V.

Three replicas at each concentration level (n = 12) were used for obtaining all the standard addition calibrations. The errors of the 5-HT concentrations were determined by using the following equations (Bruce and Gill 1999):

$$S_x = \frac{S_y}{|b|}\sqrt{\frac{1}{n} + \frac{\bar{y}^2}{b^2 \sum(x_i - \bar{x})^2}}$$

$$S_y = \sqrt{\frac{\sum(y_i - bx_i - a)^2}{n-2}}$$

where S_y is the standard deviation in the residuals, b is the slope, a is the y-intercept of the line, n is the number of replicas, $\bar{y}$ is the average measurement of the standards, x_i are the concentrations of the standards, and $\bar{x}$ is the average concentration of the standards. The error is expresses as $\pm S_x \cdot t$, where t is the Student t at 95 % probability and n-2 freedom degrees.

3. Results

3.1. Luminescence properties of 5-HT immobilized on Tiss®-Link

To characterize the luminescent spectra of 5-HT immobilized on Tiss®-Link, a solution of 1 µg mL^{-1} of 5-HT (pH = 10) was prepared and the covalent immobilization of 5-HT on Tiss®-Link was carried out by incubating 3 mg (≈ 0.8 cm^2) of nanofibre mat in 3 mL of solution for 30 min at RT in a rotating shaker. Then the material was washed, and the luminescence emission and excitation spectra of 5-HT covalently attached to Tiss®-Link were characterized (see Fig. 4.1). It shows that 5-HT immobilized on Tiss®- Link emits fluorescence at 337 nm when it is excited at 280 nm and emits phosphorescence at 440 nm when it is excited at 305 nm. SM (see Fig. SM-4.2) shows that a heavy atom perturber (KI) and an oxygen scavenger (N_2) have to be used to obtain the phosphorescence emission of 5-HT.

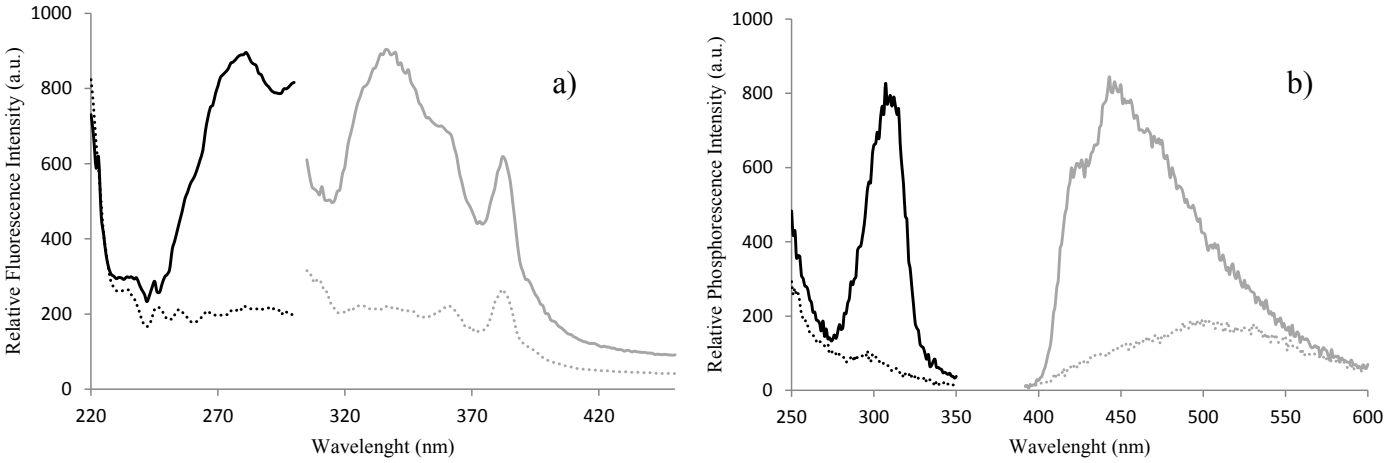

Fig. 4.1. Fluorescence a) and Phosphorescence b) excitation (black lines) and emission (grey lines) spectra of 5-HT immobilised on Tiss®-Link (solid lines) and the nanofibre mat free of 5-HT (dotted lines). [5-HT] = 1 µg mL^{-1}.

3.2. Determination of the optimal conditions for the immobilization of 5-HT on Tiss®-Link

The covalent immobilization of 5-HT on Tiss®-Link occurs through a Michael type-reaction between the primary amino of 5-HT and the activated vinyl groups of Tiss®-Link (Medina-Castillo et al. 2012; Ramon-Marquez et al. 2016). In order to determinate the optimum pH for the covalent immobilization of 5-HT, 3 mg of nanofibre mat were incubated at RT with 4 mL of 1 µg mL^{-1} 5-HT solution at pH = 8 (20 mM phosphate buffer) and pH = 10 (20 mM carbonate buffer) for different times (1, 2, 3 and 4 h). Then, the 5-HT immobilised on Tiss®-Link was measured by fluorescence. Fig. 4.2 shows that the immobilization of 5-HT on Tiss®-Link only occurs at pH = 10, whereas at pH = 8 negligible immobilization is detected. This phenomenon could be attributed to the pKa of 5-HT. The primary amino of 5-HT has a pKa = 9.97 (Pratuangdejkul et al. 2006), and therefore at pH = 8 it is protonated and has not enough nucleophilic character to react with the vinyl groups of the material. However, at pH = 10 it is mostly in its neutral form, which has sufficient nucleophilic character to react. This result was similar than others previously published by using the same material (Ramon-Marquez et al. 2016).

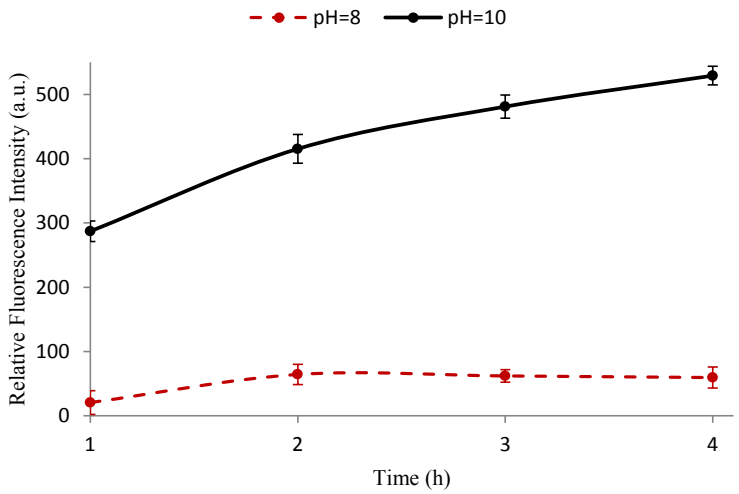

Fig. 4.2. Binding kinetics of 5-HT on Tiss®-Link at pH = 8 (red dashed line) and pH = 10 (solid black line). $[5\text{-HT}]_0$ = 1 µg mL^{-1}, $\lambda_{exc/em}$ = 280/337 nm**,** monochromator slits $width_{exc/em}$ = 5/5 nm, detector voltage of 500 V.

Fig. 4.2 also shows that the amount of 5-HT immobilized on Tiss®-Link increases when the time also increases. Anyway, to decrease the analysis time, 15 min was chosen as immobilization time. At this time the amount of 5-HT immobilized on the solid support is enough to obtain a

good sensitivity (as it will be showed in Section 3.3) and the amount of potential interfering species (mainly proteins) is not so high (as it will be showed in Section 3.4).

Therefore, the incubation of 5-HT with Tiss®-Link was carried out, for the rest of the experiments, in 20 mM carbonate buffer pH 10 for 15 min at RT.

3.3. Effect of coexisting compounds

Since the proposed methodology is based on a kinetic method, the interfering species might be classified in two types: 1) Phosphorescent amines present in serum which can interfere the SS-RTP measurements; 2) Components of serum which can affect the binding kinetic of 5-HT on Tiss®-Link.

3.3.1. Phosphorescent amines present in serum which can interfere the SS-RTP measurements

Serum is a very complex matrix which contains a lot of molecules and macromolecules such as proteins, vitamins, free amino acid, hormones, etc. Many of these molecules have weak natural fluorescence, but only three of them (5-HT, tryptamine (TRYP) and the amino acid tryptophan (TRYPH)) show phosphorescent emission (Bruxvoort et al. 1993; de Ribamar et al. 1995). Therefore, most of the luminescent interferences of serum matrix can be avoided by SS-RTP measurements, but TRYP and TRYPH have to be evaluated as potential interference species.

In a previous publication (Ramon-Marquez et al. 2016) we have demonstrated that TRYP is efficiently immobilized on Tiss®-Link at pH = 10 (the same condition of the 5-HT immobilization). However, the interference of TRYP in the phosphorescent detection of 5-HT can be eliminated using the appropriate phosphorescence parameters because they have different excitation wavelengths and lifetimes. SM (see Fig. SM-4.3) shows the effect of the t_d on the excitation spectra of 500 ng mL^{-1} 5-HT and 500 ng mL^{-1} TRYP covalently immobilised on Tiss®-Link at λ_{em} = 449 nm. It can be concluded that when the λ_{em} = 449 nm, an increase on the t_d provides a decrease on the phosphorescence emission of both 5-HT and TRYP, but it is more pronounced in TRYP. In fact, when λ_{em} = 449 nm, [5-HT] = [TRYP] = 500 ng mL^{-1} and t_d is equal or higher than 10 ms, TRYP is not excited between 310 and 330 nm whereas 5-HT can be excited. Therefore, a t_d of 10 ms has to be used in order to eliminate the phosphorescence interference of TRYP.

In addition, to evaluate more deeply the TRYP interference in the detection of 5-HT, several mixtures with a wide range of TRYP:5-HT ratios (1:3, 1:1, 3:1, 5:1, 10:1, 20:1, 50:1) were

prepared in 20 mM carbonate buffer at pH = 10. Then, they were incubated with Tiss®-Link (0.8 cm^2) for 15 min at RT. Finally, the concentrations of 5-HT in these mixtures were calculated by using standard calibrations carried out at $\lambda_{exc/em}$ = 315/449 nm and $\lambda_{exc/em}$ = 320/449 nm (see SM, Fig. SM-4.4 shows the calibrations). The results of the 5-HT concentrations and the recovery percentages found in these mixtures are shown in SM (see Table SM-4.1). Table SM-4.1 shows that exciting at 315 nm, the interference of TRYP does not affect to the 5-HT determination when the concentration of TRYP is equal or lower than 10 times the 5-HT concentration; whereas when 320 nm is used as excitation wavelength, the interference of TRYP occurs for TRYP:5-HT ratios higher than 20:1. The concentration range of TRYP and 5-HT in serum is practically the same (0.1-1 mg L^{-1}), therefore bearing in mind the recovery percentages indicated in Table SM-4.1, it can be concluded that the TRYP interference can be eliminated by using excitation wavelengths equal or higher than 315 nm and delay times equal o higher than 10 ms.

Although we have also demonstrated that TRYPH is not immobilized on Tiss®-Link at low concentrations (1 µg mL^{-1}) (Ramon-Marquez et al. 2016), the concentration of TRYPH in serum is highly variable (depending on the amount of proteins consumed in the diet), and much higher than 1 µg mL^{-1}. The normal concentration of free TRYPH in serum is usually between 40 and 50 µg mL^{-1}. In addition, TRYPH can be found as an amino acid of the serum proteins, principally human serum albumin (HSA) and human serum globulin (HSG) (Gorinstein et al. 2000; Kowalska-Baron et al. 2015). The concentration of proteins in serum is very high, and proteins can be covalently attached to Tiss®-Link (by their amine or thiol groups). Therefore, the interference of TRYPH (free and as a component of the proteins) has to be also carefully evaluated.

In order to study the interference produced by high concentrations of TRYPH (free and as a component of the proteins), 4 mL of 48 µg mL^{-1} TRYPH and 4 mL of 1500 µg mL^{-1} HSA solutions were prepared in 20 mM carbonate buffer at pH = 10. Tiss®-Link (3 mg) was incubated in both solutions for 15 min at RT. After incubation the materials were washed 3 times with the washing solution, and the SS-RTP spectra of immobilized TRYPH and HSA were characterized (see Fig. 4.3).

Fig 4.3 shows that free TRYPH is poorly immobilised on Tiss®-Link at the tested conditions even when the concentration of the free TRYPH is 480 times higher than the concentration of 5-HT. In addition, free TRYPH is excited at a shorter wavelength than 5-HT. Therefore, it can be concluded that the interference of free TRYPH can be eliminated by using the same conditions

than for eliminating the interference of TRYP ($\lambda_{exc} \geq 315$ nm and $t_d \geq 10$ ms). But the interference produced by the TRYPH of the proteins cannot be spectroscopically eliminated and, therefore, a protocol for protein clean-up is required. In this case, we have used a cationic ion exchange material (PolymP®-Pyridine) for protein clean-up.

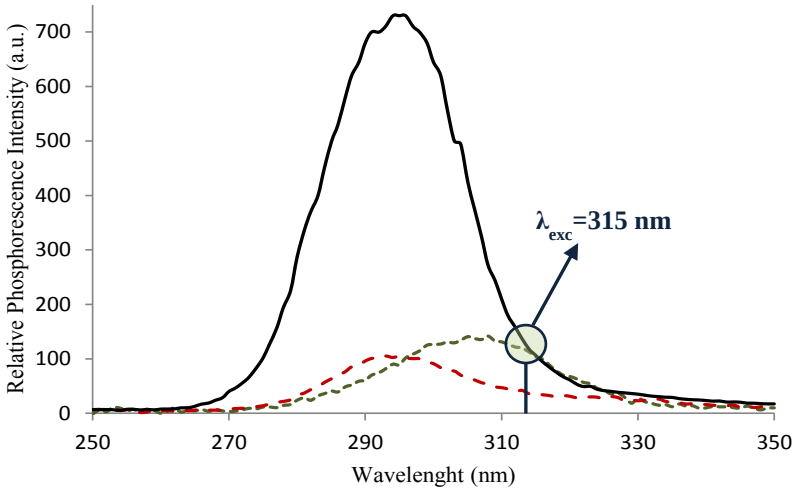

Fig. 4.3. Excitation spectra of 5-HT (green dotted line), TRYPH (red dashed line) and HSA (black solid line) immobilized on Tiss®-Link. [5-HT] = 0.1 µg mL^{-1}, [TRYPH] = 48 µg mL^{-1}, [HSA] = 1500 µg mL^{-1}, λ_{em} = 449 nm, slits width$_{exc/em}$ = 10/10 nm, t_d = 10 ms, t_g = 5 ms, detector voltage of 800 V, 20 µL of 1 M KI, in a current flow of 300 mL min^{-1} nitrogen.

We evaluated the binding capacity of PolymP®-Pyridine using HSA as protein model. For this, 40 mg of PolymP®-Pyridine were added to 2 mL of solutions containing different concentrations of HSA (100, 200, 400, 800, 1500 y 2000 mg L^{-1}) at pH = 5 (adjusted with HCl). Then, the suspensions were sonicated for 30 s and incubated for 30 min under shaking at RT. After incubation, the samples were centrifuged and the HSA concentrations in the supernatants were calculated by fluorescence. The amount of adsorbed HSA onto PolymP®-Pyridine was calculated as the difference between the initial concentration of HSA and those found in the supernatants. Adsorption isotherm (see SM, Fig. SM-4.5) was fitted to the Langmuir-Freundlich model by using a non-linear regression method (Yoon et al. 1999), and the obtained setting parameters: adsorption constant (K = 0.56), maximum amount of adsorption (C_m = 83.92 mg g^{-1}), and exponential factor (n = 0.78), showed that PolymP®-Pyridine exhibits a high affinity for serum proteins by electrostatic interactions (Yoon et al. 1999).

3.3.2. Components of serum which can affect the binding kinetic of 5-HT on Tiss®-Link

There are lot of molecules and macromolecules in the serum which can originate different rheological properties in serum, regarding to buffer media. Besides, these molecules can be adsorbed on Tiss®-Link surface during covalent immobilization of 5-HT. These facts can affect the diffusion rate of 5-HT from serum to the active sites of Tiss®-Link. Therefore, the reaction rate of covalent immobilization of 5-HT on Tiss®-Link in serum could be different than the covalent immobilization in a buffer solution.

In order to study the reaction rates in serum, serum sample C was selected, and the binding kinetic of 5-HT on Tiss®-Link in 20 mM carbonate buffer at pH = 10 was compared with the binding kinetics of 5-HT performed directly in serum (dilution 1:3 v/v, serum:carbonate buffer) before and after the protein clean-up protocol described in Section 2.3. The initial concentration of 5-HT was the same in the three cases ($[5\text{-HT}]_0$ = 75 ng mL^{-1}; concentration of 5-HT after serum dilution).

Fig. 4.4 shows that the binding kinetics of 5-HT on Tiss®-Link in buffer, serum before clean-up, and serum after clean-up are different. The binding kinetic in free-protein serum is closer to the binding kinetic in buffer, but they are not equal. Therefore the diffusion rate of 5-HT to Tiss®-Link is affected by the media, and this matrix effect cannot be eliminated. Thus, a standard calibration method cannot be used and the proposed biosensor requires a standard addition method for the calibration.

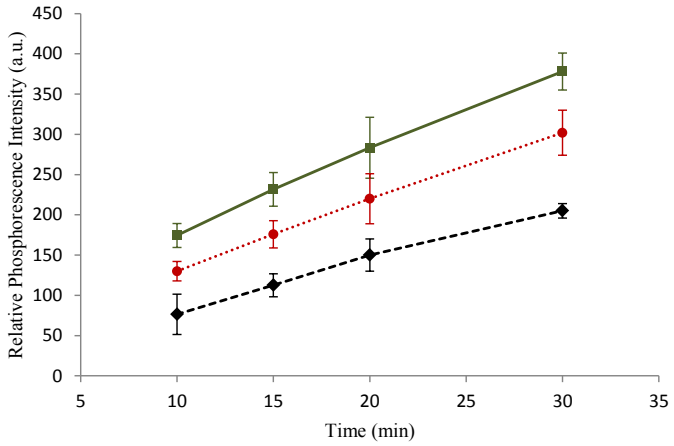

Fig. 4.4. Binding kinetics of 5-HT on Tiss®-Link in 20 mM carbonate buffer at pH = 10 (green solid line), serum C after protein clean-up (dilution 1:3 v/v, serum:carbonate buffer) at pH = 10 (red dotted line), and serum C before protein clean-up (dilution 1:3 v/v, serum:carbonate buffer) at pH = 10 (black dashed line). $[5\text{-HT}]_0$ = 75 ng mL^{-1}, [KI] = 1 M, $\lambda_{exc/em}$ = 315/449 nm, t_d = 10 ms, t_g = 5 ms, slit $widths_{exc/em}$ = 10/10 nm, and detector voltage of 850 V in a current flow of 300 mL min^{-1} nitrogen.

3.4. Application and sensor validation

Firstly, in order to evaluate the necessity of carrying out both the protein clean-up protocol and the standard addition method, two of the serum samples (samples A and B) were analysed by the proposed method before and after protein clean-up protocol and the results were compared with those provided by the reference laboratory. The protein clean-up protocol is described in Section 2.3 and the analysis of these samples were carried out following the procedure described in Section 2.4 (Analysis of 5-HT in Serum Samples). The results obtained for samples A and B before the protein clean-up protocol were 315 ± 20 ng mL^{-1} and 128 ± 15 ng mL^{-1}, after the protein clean-up protocol were 137 ± 16 ng mL^{-1} and 75 ± 15 ng mL^{-1}, and by an external reference laboratory were 122 ng mL^{-1} and 62 ng mL^{-1}, respectively. It is possible to conclude that both the protein clean-up protocol and the standard addition method have to be used in order to obtain reliable results.

In order to evaluate the practical applications, the 7 samples of serum were analysed by both the proposed assay protocol and an external reference laboratory following the procedure described in Section 2.4 (Analysis of 5-HT in Serum Samples). Table 4.1 summarises the results. A correlation coefficient of 0.997 was calculated by comparing the concentrations of 5-HT obtained with the proposed biosensor (by using SS-RTP), with those obtained by the external reference laboratory (by using enzyme immunoassay), which indicates excellent correlation between the two methods; SM (see Fig. SM-4.6) shows the calculation of this correlation coefficient.

In comparison with other methods previously published in the literature for determining 5-HT in serum samples, the use of Tiss®-Link combined with a protein clean-up protocol and a SS-RTP measurement offers several advantages such as: 1) it is one of the most simple methods, requiring only a protein clean-up and the incubation with the material, while the rest of the methods require more complicated sample treatment, *e.g.* solid phase extractions, preconcentration techniques, derivatization reactions, the use of immunogenic conjugates and antibodies specific for serotonin, etc.; 2) it is the most environmentally friendly method using only aqueous solutions, whilst the other methods require organic solvents and hazardous reagents.

Table 4.1. Results of the 5-HT determination by the proposed biosensor and an external reference laboratory.

Sample	[5-HT] (ng mL^{-1}) Proposed biosensor	[5-HT] (ng mL^{-1}) External reference laboratory
A	122 ± 16	122
B	75 ± 12	62
C	304 ± 6	303
D	114 ± 8	104
E	226 ± 12	209
F	449 ± 13	463
G	197 ± 9	202

4. Conclusions

In this paper, a novel optical biosensor for analysing 5-HT by SS-RTP has been developed. The developed biosensor combines the nanotechnology (non-woven nanofibre mat made by electrospinning) with the detection by solid surface-RTP, which has led to a significant improvement in the selectivity and sensitivity of the detection and quantification of 5-HT. It is the first time to our knowledge that 5-HT has been quantified directly in a complex matrix such as human serum by using a non-enzymatic technique. This novel method is very simple and solves the two major problems of the methods proposed to date for the analysis of 5-HT in serum: 1) the large interference in the measurements of 5-HT produced by coexisting species, such as proteins, hormones, amino acid, vitamins, etc.; 2) the low sensitivity that hinders the determination of 5-HT due to it can be found at very low concentrations in serum (between 40 and 450 ng mL^{-1}). In addition, the proposed biosensor simplifies the methodology to determine 5-HT in complex matrices, avoiding pre-concentration and derivatization steps, and allowing the direct analysis in serum samples.

In conclusion, the proposed sensor has proved to be valid for the detection of 5-HT in serum with good accuracy and short analysis time (55 min), which make it a good candidate to be applied in routine clinical analysis.

Acknowledgments

The authors gratefully acknowledge the financial support of the Spanish Ministry of Economy, Competitiveness (Ramon-Marquez's Grant reference AP2012-0944, Medina-Castillo's Torres Quevedo contract reference PTQ-11-04904 and project CTQ2014-53442-P), and the Technological Corporation of Andalusia (CTA) (project reference 11/557).

References

Babaei, A., Taheri, A.R., Aminikhah, M., 2013. Nanomolar simultaneous determination of levodopa and serotonin at a novel carbon ionic liquid electrode modified with Co(OH)2 nanoparticles and multi-walled carbon nanotubes. Electrochimica Acta 90, 317-325.

Berg, J.M.T., J.L.; Stryer L., 2002. Enzymes Can Be Inhibited by Specific Molecules., Biochemistry. 5th edition., New York.

Berger, M., Gray, J.A., Roth, B.L., 2009. The Expanded Biology of Serotonin. Annual Review of Medicine 60(1), 355-366.

Bi, L., Dong, X.-t., Yu, Y.-h., 2014. Room-temperature phosphorescence sensor based on manganese doped zinc sulfide quantum dots for detection of urea. Journal of Luminescence 153, 356-360.

Bracamonte, A.G., Veglia, A.V., 2011. Spectrofluorimetric determination of serotonin and 5-hydroxyindoleacetic acid in urine with different cyclodextrin media. Talanta 83(3), 1006-1013.

Brand, T., Anderson, G.M., 2011. The measurement of platelet-poor plasma serotonin: a systematic review of prior reports and recommendations for improved analysis. Clinical chemistry 57(10), 1376-1386.

Bruce, G.R., Gill, P.S., 1999. Estimates of Precision in a Standard Additions Analysis. Journal of Chemical Education 76(6), 805.

Bruxvoort, C.B., Dawson, G.G., Francis, T.A., Reiter, W.S., Haustein, C.H., 1993. Room-Temperature Luminescence of Formaldehyde-Condensed Amines Adsorbed on Filter Paper. Microchemical Journal 47(1–2), 140-147.

Comley, J., 2012. ELISA assays: Recent innovations take analyte detection to new levels. Drug Discovery World 13(4), 23-45.

Coolbear, T., Daniel, R.M., Morgan, H.W., 1992. The enzymes from extreme thermophiles: Bacterial sources, thermostabilities and industrial relevance. Enzymes and Products from Bacteria Fungi and Plant Cells, pp. 57-98. Springer Berlin Heidelberg.

Chauveau, J., Fert, V., Morel, A.M., Delaage, M.A., 1991. Rapid and specific enzyme immunoassay of serotonin. Clinical chemistry 37(7), 1178-1184.

D'Andrea, G., Cevoli, S., Colavito, D., Leon, A., 2015. Biochemistry of primary headaches: role of tyrosine and tryptophan metabolism. Neurological Sciences 36, 17-22.

Danaceau, J.P., Anderson, G.M., McMahon, W.M., Crouch, D.J., 2003. A Liquid Chromatographic-Tandem Mass Spectrometric Method for the Analysis of Serotonin and Related Indoles in Human Whole Blood. Journal of Analytical Toxicology 27(7), 440-444.

Darwish, I.A., 2006. Immunoassay Methods and their Applications in Pharmaceutical Analysis: Basic Methodology and Recent Advances. International Journal of Biomedical Science : IJBS 2(3), 217-235.

de Jong, W.H., Wilkens, M.H., de Vries, E.G., Kema, I.P., 2010. Automated mass spectrometric analysis of urinary and plasma serotonin. Analytical and bioanalytical chemistry 396(7), 2609-2616.

de Ribamar, J., Júnior, F., Campiglia, A.D., 1995. Solid-surface room-temperature phosphorescence detection of serotonin, tryptamine, and gramine enhanced by inorganic salts and sodium dodecyl sulfate. Talanta 42(10), 1505-1512.

Deemyad, T., Metzen, M.G., Pan, Y., Chacron, M.J., 2013. Serotonin selectively enhances perception and sensory neural responses to stimuli generated by same-sex conspecifics. Proceedings of the National Academy of Sciences 110(48), 19609-19614.

Gan, S.D., Patel, K.R., 2013. Enzyme Immunoassay and Enzyme-Linked Immunosorbent Assay. J Invest Dermatol 133(9), e12.

Golubchik, P., Mozes, T., Vered, Y., Weizman, A., 2009. Platelet poor plasma serotonin level in delinquent adolescents diagnosed with conduct disorder. Progress in Neuro-Psychopharmacology and Biological Psychiatry 33(7), 1223-1225.

Gorinstein, S., Goshev, I., Moncheva, S., Zemser, M., Weisz, M., Caspi, A., Libman, I., Lerner, H., Trakhtenberg, S., Martín-Belloso, O., 2000. Intrinsic Tryptophan Fluorescence of Human Serum Proteins and Related Conformational Changes. J Protein Chem 19(8), 637-642.

Goyal, R.N., Agrawal, B., 2012. Ag ion irradiated based sensor for the electrochemical determination of epinephrine and 5-hydroxytryptamine in human biological fluids. Analytica Chimica Acta 743, 33-40.

Grange, R.D., Thompson, J.P., Lambert, D.G., 2014. Radioimmunoassay, enzyme and non-enzyme-based immunoassays. British Journal of Anaesthesia 112(2), 213-216.

Gupta, P., Goyal, R.N., 2014. Polymelamine modified edge plane pyrolytic graphite sensor for the electrochemical assay of serotonin. Talanta 120, 17-22.

Hasanzadeh, M., Shadjou, N., Omidinia, E., 2013. A novel electroanalytical method for simultaneous detection of two neurotransmitter dopamine and serotonin in human serum. Journal of Neuroscience Methods 219(1), 52-60.

Hedstrom, L., 2001. Enzyme Specificity and Selectivity. eLS. John Wiley & Sons, Ltd.

Hirowatari, Y., Hara, K., Kamihata, H., Iwasaka, T., Takahashi, H., 2004. High-performance liquid chromatographic method with column-switching and post-column reaction for determination of serotonin levels in platelet-poor plasma. Clinical Biochemistry 37(3), 191-197.

Hoyer, D., Hannon, J.P., Martin, G.R., 2002. Molecular, pharmacological and functional diversity of 5-HT receptors. Pharmacology Biochemistry and Behavior 71(4), 533-554.

Huisman, H., Wynveen, P., Setter, P.W., 2010. Studies on the immune response and preparation of antibodies against a large panel of conjugated neurotransmitters and biogenic amines: specific polyclonal antibody response and tolerance. Journal of Neurochemistry 112(3), 829-841.

Iyer, P.V., Ananthanarayan, L., 2008. Enzyme stability and stabilization—Aqueous and non-aqueous environment. Process Biochemistry 43(10), 1019-1032.

Jacobs, B.L., Azmitia, E.C., 1992. Structure and function of the brain serotonin system. Physiological Reviews 72(1), 165-229.

Julius, D., 1998. Serotonin receptor knockouts: A moody subject. Proceedings of the National Academy of Sciences of the United States of America 95(26), 15153-15154.

Kema, I.P., Meijer, W.G., Meiborg, G., Ooms, B., Willemse, P.H., de Vries, E.G., 2001. Profiling of tryptophan-related plasma indoles in patients with carcinoid tumors by automated, on-line, solid-phase extraction and HPLC with fluorescence detection. Clinical chemistry 47(10), 1811-1820.

Kim, J., Jeon, M., Paeng, K.-J., Paeng, I.R., 2008. Competitive enzyme-linked immunosorbent assay for the determination of catecholamine, dopamine in serum. Analytica Chimica Acta 619(1), 87-93.

Kim, J., Park, H., Ryu, J., Jeon, O., Paeng, I.R., 2009. Competitive enzyme-linked immunosorbent assay for a selective and sensitive determination of dopamine in the presence of ascorbic acid and uric acid. Journal of Immunoassay and Immunochemistry 31(1), 33-44.

Kowalska-Baron, A., Gałęcki, K., Wysocki, S., 2015. Room temperature phosphorescence study on the structural flexibility of single tryptophan containing proteins. Spectrochimica Acta Part A: Molecular and Biomolecular Spectroscopy 134, 380-387.

Lee, G.S., Simpson, C., Sun, B.-H., Yao, C., Foer, D., Sullivan, B., Matthes, S., Alenina, N., Belsky, J., Bader, M., Insogna, K.L., 2014. Measurement of Plasma, Serum, and Platelet Serotonin in Individuals With High Bone Mass and Mutations in LRP5. Journal of Bone and Mineral Research 29(4), 976-981.

Li, J., Lin, X., 2007. Simultaneous determination of dopamine and serotonin on gold nanocluster/overoxidized-polypyrrole composite modified glassy carbon electrode. Sensors and Actuators B: Chemical 124(2), 486-493.

Li, Y., Cassone, V.M., 2015. A simple, specific high-throughput enzyme-linked immunosorbent assay (ELISA) for quantitative determination of melatonin in cell culture medium. International Immunopharmacology 28(1), 230-234.

Makris, G.D., Reutfors, J., Larsson, R., Isacsson, G., Ösby, U., Ekbom, A., Ekselius, L., Papadopoulos, F.C., 2016. Serotonergic medication enhances the association between suicide and sunshine. Journal of Affective Disorders 189, 276-281.

Mao, H.-m., Chen, B.-g., Qian, X.-m., Liu, Z., 2009. Simultaneous determination of twelve biogenic amines in serum by high performance liquid chromatography. Microchemical Journal 91(2), 176-180.

Mazloum-Ardakani, M., Khoshroo, A., 2014. Electrocatalytic properties of functionalized carbon nanotubes with titanium dioxide and benzofuran derivative/ionic liquid for simultaneous determination of isoproterenol and serotonin. Electrochimica Acta 130, 634-641.

Medina-Castillo, A.L., Fernández-Sánchez, J.F., Fernández-Gutiérrez, A., 2011a. One-Step Fabrication of Multifunctional Core-Shell Fibres by Co-Electrospinning. Advanced Functional Materials 21(18), 3488-3495.

Medina-Castillo, A.L., Fernandez-Sanchez, J.F., Segura-Carretero, A., Fernandez-Gutierrez, A., 2011b. Design and synthesis by ATRP of novel, water-insoluble, lineal copolymers and their application in the development of fluorescent and pH-sensing nanofibres made by electrospinning. Journal of Materials Chemistry 21(18), 6742-6750.

Medina-Castillo, A.L., Morales-Sanfrutos, J., Megia-Fernandez, A., Fernandez-Sanchez, J.F., Santoyo-Gonzalez, F., Fernandez-Gutierrez, A., 2012. Novel synthetic route for covalent coupling of biomolecules on super-paramagnetic hybrid nanoparticles. Journal of Polymer Science Part A: Polymer Chemistry 50(19), 3944-3953.

Meijer, W.G., Kema, I.P., Volmer, M., Willemse, P.H., de Vries, E.G., 2000. Discriminating capacity of indole markers in the diagnosis of carcinoid tumors. Clinical chemistry 46(10), 1588-1596.

Meneses, A., Liy-Salmeron, G., 2012. Serotonin and emotion, learning and memory. Reviews in the Neurosciences 23(5-6), 543-553.

Myers, F.B., Lee, L.P., 2008. Innovations in optical microfluidic technologies for point-of-care diagnostics. Lab on a Chip 8(12), 2015-2031.

Nichkova, M., Wynveen, P.M., Marc, D.T., Huisman, H., Kellermann, G.H., 2013. Validation of an ELISA for urinary dopamine: applications in monitoring treatment of dopamine-related disorders. Journal of Neurochemistry 125(5), 724-735.

Nichkova, M.I., Huisman, H., Wynveen, P.M., Marc, D.T., Olson, K.L., Kellermann, G.H., 2012. Evaluation of a novel ELISA for serotonin: Urinary serotonin as a potential biomarker for depression. Analytical and bioanalytical chemistry 402(4), 1593-1600.

Ohkawa, R., Hirowatari, Y., Nakamura, K., Ohkubo, S., Ikeda, H., Okada, M., Tozuka, M., Nakahara, K., Yatomi, Y., 2005. Platelet release of β-thromboglobulin and platelet factor 4 and serotonin in plasma samples. Clinical Biochemistry 38(11), 1023-1026.

Peng, Q., Jiang, C., 2007. A New Spectrofluorimetric Method for Determination of Trace Amounts 5-Hydroxytryptamine in Human Urine and Serum. J Fluoresc 17(3), 339-343.

Peterson, Z.D., Lee, M.L., Graves, S.W., 2004. Determination of serotonin and its precursors in human plasma by capillary electrophoresis–electrospray ionization–time-of-flight mass spectrometry. Journal of Chromatography B 810(1), 101-110.

Piszczek, L., Piszczek, A., Kuczmanska, J., Audero, E., Gross, C.T., 2015. Modulation of anxiety by cortical serotonin 1A receptors. Frontiers in Behavioral Neuroscience 9, 48.

Pratuangdejkul, J., Nosoongnoen, W., Guérin, G.-A., Loric, S., Conti, M., Launay, J.-M., Manivet, P., 2006. Conformational dependence of serotonin theoretical pKa prediction. Chemical Physics Letters 420(4-6), 538-544.

Pussard, E., Guigueno, N., Adam, O., Giudicelli, J.F., 1996. Validation of HPLC-amperometric detection to measure serotonin in plasma, platelets, whole blood, and urine. Clinical chemistry 42(7), 1086-1091.

Ramboz, S., Oosting, R., Amara, D.A., Kung, H.F., Blier, P., Mendelsohn, M., Mann, J.J., Brunner, D., Hen, R., 1998. Serotonin receptor 1A knockout: An animal model of anxiety-related disorder. Proceedings of the National Academy of Sciences 95(24), 14476-14481.

Ramon-Marquez, T., Medina-Castillo, A.L., Fernandez-Gutierrez, A., Fernandez-Sanchez, J.F., 2016. Novel optical sensing film based on a functional nonwoven nanofibre mat for an easy, fast and highly selective and sensitive detection of tryptamine in beer. Biosensors and Bioelectronics 79, 600-607.

Román, D.A., Carretero, A.S., Blanco, C.C., Gutiérrez, A.F., 2004. Subminute and sensitive determination of the neurotransmitter serotonin in urine by capillary electrophoresis with laser-induced fluorescence detection. Biomedical Chromatography 18(7), 422-426.

Sa, M., Ying, L., Tang, A.-G., Xiao, L.-D., Ren, Y.-P., 2012. Simultaneous determination of tyrosine, tryptophan and 5-hydroxytryptamine in serum of MDD patients by high performance liquid chromatography with fluorescence detection. Clinica Chimica Acta 413(11–12), 973-977.

Stathopoulos, A., Klonos, P., Kyritsis, A., Pissis, P., Christodoulides, C., Rodriguez Hernández, J.C., Monleón Pradas, M., Gómez Ribelles, J.L., 2010. Water sorption and polymer dynamics in hybrid poly(2-hydroxyethyl-co-ethyl acrylate)/silica hydrogels. European Polymer Journal 46(1), 101-111.

Tecott, L.H., Sun, L.M., Akana, S.F., Strack, A.M., Lowenstein, D.H., Dallman, M.F., Julius, D., 1995. Eating disorder and epilepsy in mice lacking 5-HT2C serotonin receptors. Nature 374(6522), 542-546.

Teradaira, R., Itoh, Y., Kawai, K., Ishikawa, H., Ohashi, K., Nagamura, Y., 2007. Mental stress-induced changes in plasma serotonin, tryptophan, kynurenine concentrations in healthy participants. International Congress Series 1304, 175-179.

Udupa, K., Chen, R., 2015. The mechanisms of action of deep brain stimulation and ideas for the future development. Progress in Neurobiology 133, 27-49.

Wang, F., Wu, Y., Lu, K., Ye, B., 2013. A simple but highly sensitive and selective calixarene-based voltammetric sensor for serotonin. Electrochimica Acta 87, 756-762.

Wu, A.H.B., 2006. A selected history and future of immunoassay development and applications in clinical chemistry. Clinica Chimica Acta 369(2), 119-124.

Wu, P., He, Y., Wang, H.-F., Yan, X.-P., 2010. Conjugation of Glucose Oxidase onto Mn-Doped ZnS Quantum Dots for Phosphorescent Sensing of Glucose in Biological Fluids. Analytical Chemistry 82(4), 1427-1433.

Xue, C., Wang, X., Zhu, W., Han, Q., Zhu, C., Hong, J., Zhou, X., Jiang, H., 2014a. Electrochemical serotonin sensing interface based on double-layered membrane of reduced graphene oxide/polyaniline nanocomposites and molecularly imprinted polymers embedded with gold nanoparticles. Sensors and Actuators B: Chemical 196, 57-63.

Yi, Y.-H., Liao, W.-P., Lu, X., 1994. Simultaneous determination of tryptophan, 5-hydroxytryptophan, 5-hydroxytryptamine, 5-hydroxyindoleacetic acid, 4-hydroxy-3-methoxyphenylacetic acid and 3-methoxy-4-hydroxyphenylglycol in human cerebrospinal fluid. Journal of Chromatography B: Biomedical Sciences and Applications 661(1), 143-148.

Yoon, J.-Y., Kim, J.-H., Kim, W.-S., 1999. The relationship of interaction forces in the protein adsorption onto polymeric microspheres1. Colloids and Surfaces A: Physicochemical and Engineering Aspects 153(1–3), 413-419.

Yoshitake, T., Iizuka, R., Fujino, K., Inoue, O., Yamagata, K., Nohta, H., Yamaguchi, M., 2004. Simultaneous Determination of Serotonin and 5-Hydroxyindole-3-acetic Acid in Human Urine by Automated Precolumn Derivatization and Semi-microbore Column Liquid Chromatography with Fluorescence Detection. Analytical Sciences 20(12), 1687-1690.

Yubero-Lahoz, S., Rodríguez, J., Faura, A., Pascual, J., Oliveras, A., Cao, H., Farré, M., de la Torre, R., 2014. Determination of free serotonin and its metabolite 5-HIAA in blood human samples with consideration to pre-analytical factors. Biomedical Chromatography 28(12), 1641-1646.

Zhen, Q., Xu, B., Ma, L., Tian, G., Tang, X., Ding, M., 2011. Simultaneous determination of tryptophan, kynurenine and 5-hydroxytryptamine by HPLC: Application in uremic patients undergoing hemodialysis. Clinical Biochemistry 44(2–3), 226-230.

Appendix. Supplementary Material (SM)

Content:

Figures:

Tables:

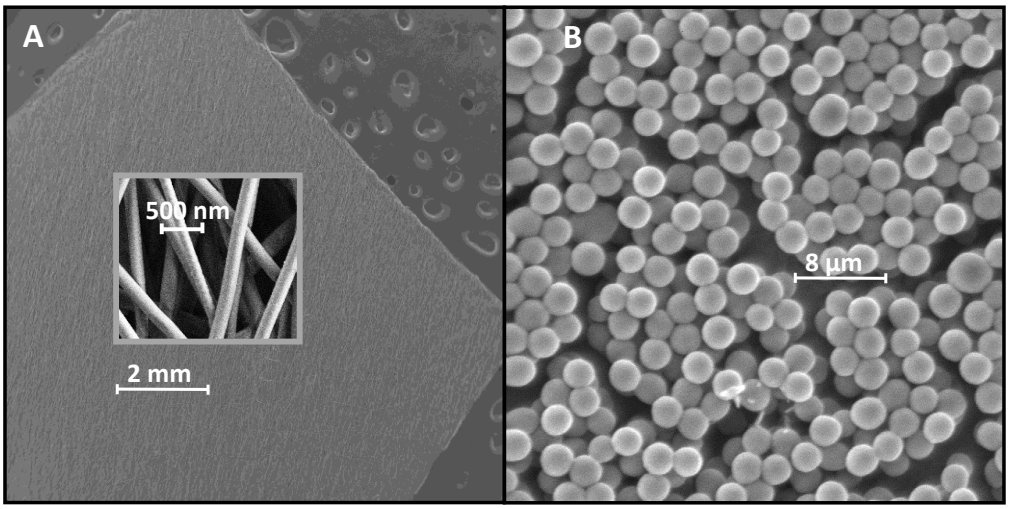

Fig. SM-4.1. Scanning electron microscopy (SEM) of A)Tiss®-Link and B) PolymP®-Pyridine.

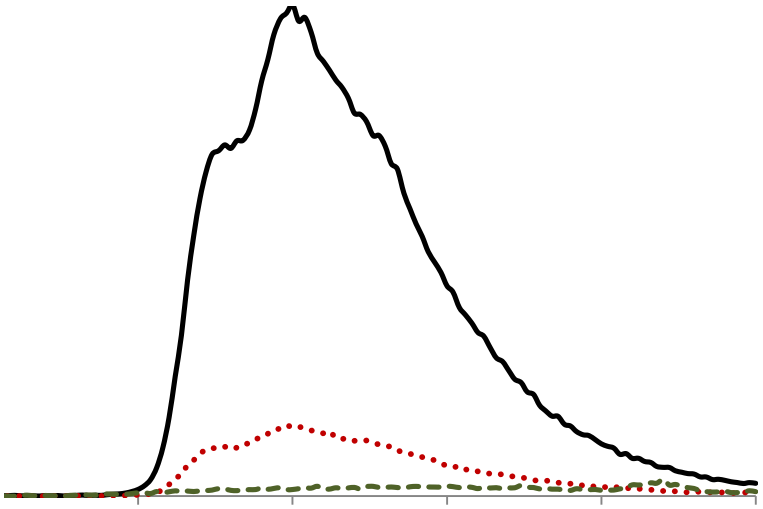

Fig. SM-4.2. Luminescence properties of 5-HT covalently immobilized on Tiss®-Link in the presence of KI and 100% N_2 (black solid line), in the presence of KI and 100% O_2 (red dotted line), and in the absence of KI (green dashed line).

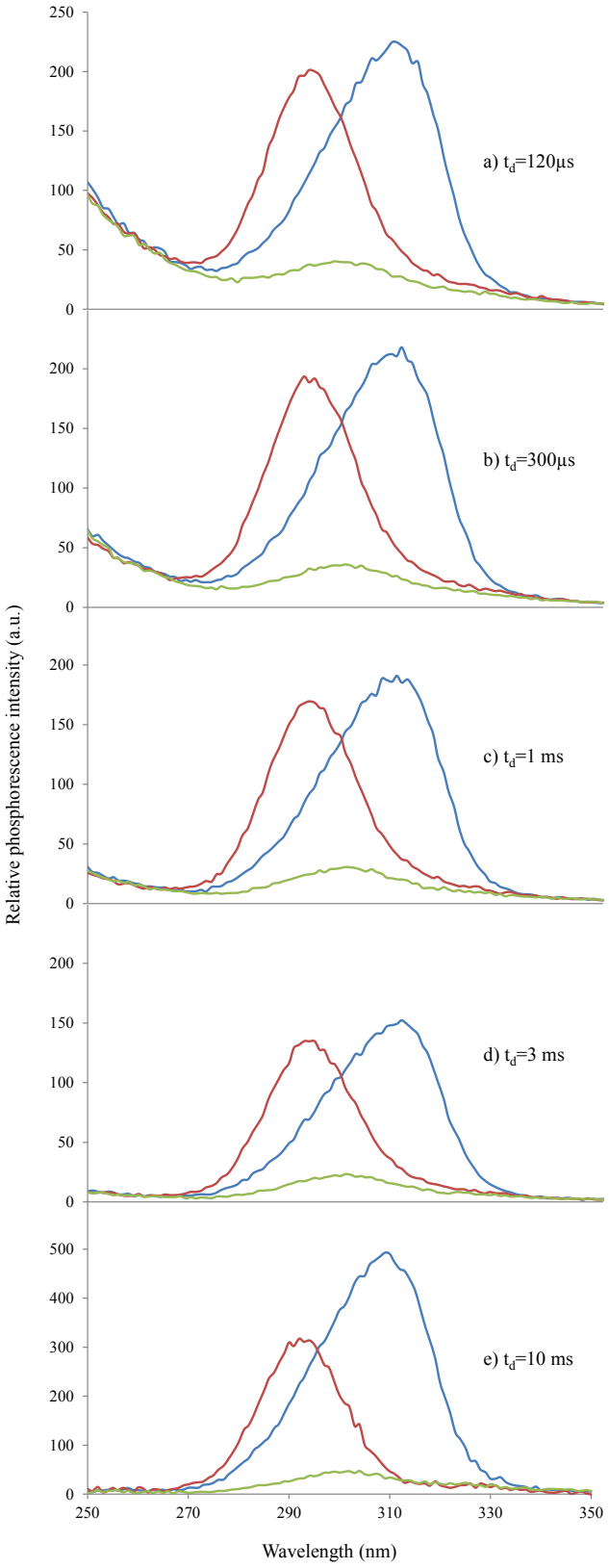

Fig. SM-4.3. Excitation spectra of 5-HT immobilized on Tiss®-Link (blue line), TRYP immobilized on Tiss®-Link (red line) and Tiss®-Link (green line) at different delay times. [5-HT] = 500 ng mL^{-1}, [TRYP] = 500 ng mL^{-1}, λ_{em} = 449 nm, slits $width_{exc/em}$ = 10/10 nm, t_g = 5 ms, detector voltage of 600 V except for e) which is 800 V, 20 µL of 1 M KI, in a current flow of 300 mL min^{-1} nitrogen.

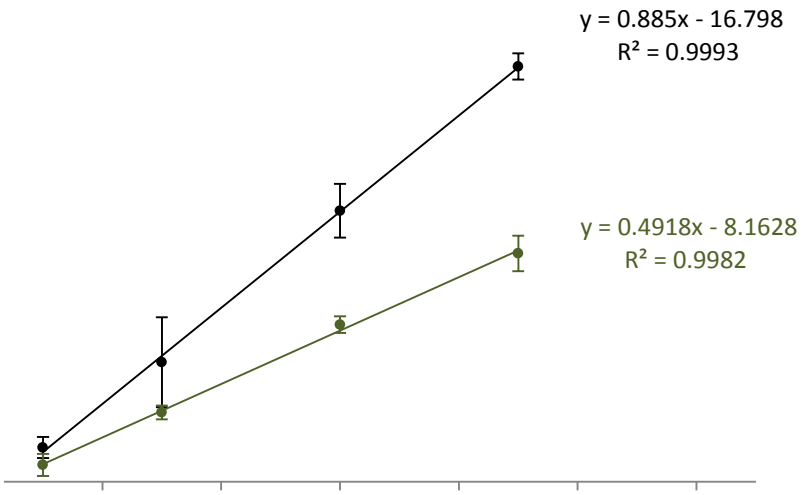

Fig. SM-4.4. Standard calibrations curves carried out at $\lambda_{exc/em}$ = 315/449 nm (black line) and $\lambda_{exc/em}$ = 320/449 nm (green line). The rest of the instrumental parameters are: t_d = 10 ms, t_g = 5 ms, excitation and emission slits of 10 nm wide and detector voltage of 850 V.

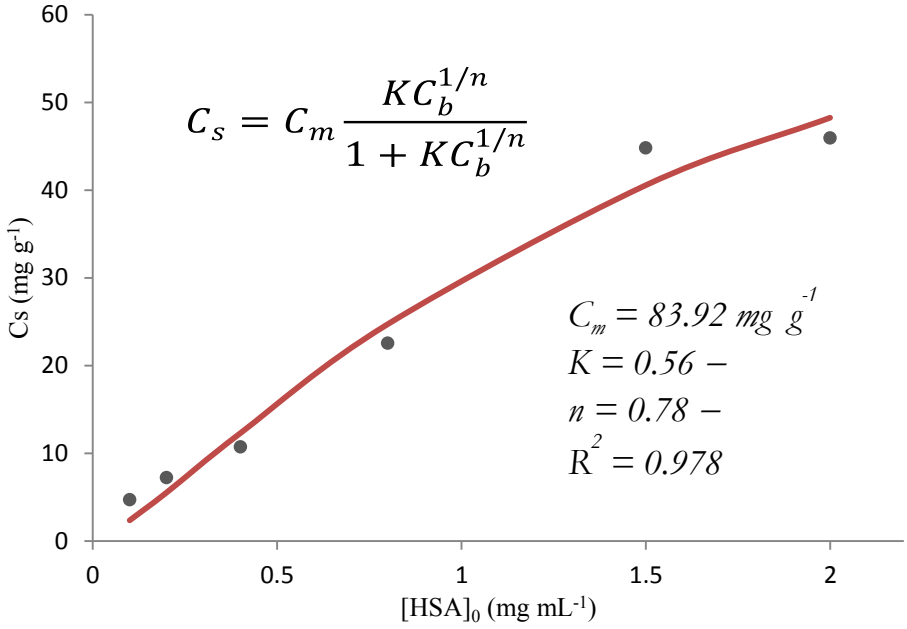

Fig. SM-4.5. Fit of the experimental data to Langmuir-Freundlich model.

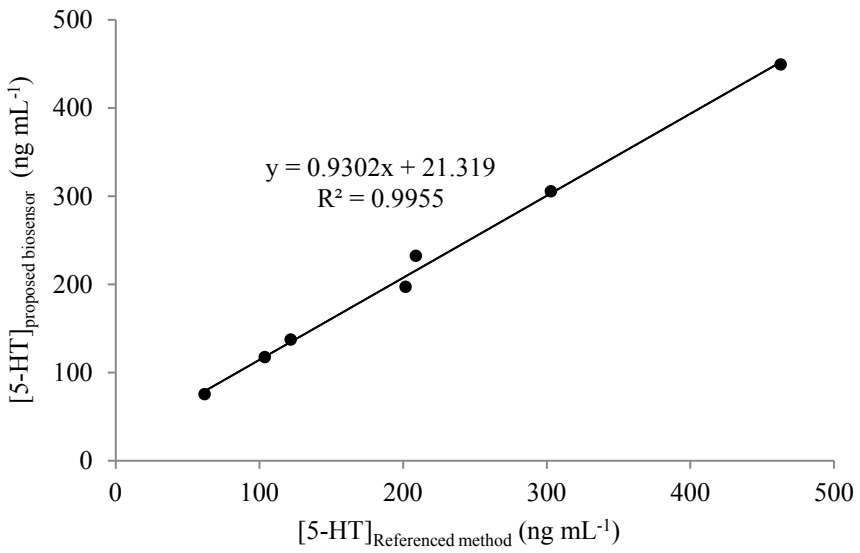

Fig. SM-4.6. Correlation between 5-HT values determined in serum by the standard enzyme immunoassay method (x axis) and the proposed biosensor (y axis).

Table SM-4.1. Concentrations of 5-HT and recovery percentages found in the mixtures TRYP:5-HT by using standard calibration curves exciting at 315 and 320 nm.

[TRYP] (ng mL^{-1})	[5-HT] (ng mL^{-1})	TRYP:5-HT ratio	$\lambda_{exc/em}$ = 315/449nm		$\lambda_{exc/em}$ = 320/449nm	
			[5-HT] (ng mL^{-1})	Recovery percentage (%)	[5-HT] (ng mL^{-1})	Recovery percentage (%)
100	300	1:3	288.3 ± 9.4	96.1	328.0 ± 14.3	109.3
200	200	1:1	183.4 ± 10.2	91.7	185.2 ± 0.6	92.6
300	100	3:1	108.1 ± 4.2	108.1	101.5 ± 10.9	101.5
500	100	5:1	114.2 ± 10.6	114.2	107.4 ± 14.7	107.4
1000	100	10:1	112.1 ± 3.5	112.1	102.4 ± 12.4	102.4
2000	100	20:1	133.5 ± 2.4	133.5	113.3 ± 4.6	113.3
5000	100	50:1	172.4 ± 7.3	172.4	140.3 ± 5.6	140.3

Bloque III

La fabricación de biosensores con transducción óptica de oxígeno requiere, en la mayoría de los casos, de la incorporación esencial de un elemento de transducción con propiedades espectroscópicas. Algunos de los compuestos más ampliamente utilizados con características ópticas excepcionales son los complejos organometálicos (OMCs) basados en metales de transición como platino, paladio, rutenio, iridio y europio. El diseño y obtención de nuevos OMCs con mejores propiedades ópticas (tiempos de vida más largos, altos rendimientos cuánticos y mayores desplazamientos de Stokes), físico-químicas (reactividad, solubilidad y carga más adecuadas, elevada estabilidad y compatibilidad con disolventes) y analíticas (sensibilidad y selectividad elevadas, y tiempos de respuesta cortos) constituye uno de los retos actuales en el ámbito de los sensores ópticos.

Así, el trabajo recogido en este bloque consiste en una revisión bibliográfica de los complejos basados en iridio(III) utilizados en el diseño de sensores ópticos, considerando tanto aquellos casos en los que los complejos de iridio han sido retenidos en soportes sólidos como aquellos en los que se encuentran sin inmovilizar. Asimismo, también se detallan las características estructurales y morfológicas de varios de los compuestos más representativos y los mecanismos de detección de una gran parte de ellos.

Capítulo 5

Iridium Complexes in the Development of Optical Sensors

Teresa Ramón-Márquez, Marta Marín-Suárez, Alberto Fernández-Gutiérrez and J.F. Fernández-Sánchez

Department of Analytical Chemistry, Faculty of Science. University of Granada
Granada, Spain

Published as chapter of the book:
Iridium(III) in Optoelectronic and Photonics Applications (*2 Volume Set)*
First Edition
Edited by Eli Zysman-Colman

1. Generalities of Optical Sensors

IUPAC (Hulanicki et al. 1991) defines a chemical sensor as *a device that transforms chemical information into an analytically useful signal. The chemical information may originate from a chemical reaction of the analyte or from a physical property of the system investigated*.

This definition is rather general. Thus, many pragmatic descriptions exist in the literature, for example, that proposed by Prof. Wolfbeis in 1990 (Wolfbeis 1990) who defined a chemical sensor as *a small-sized device comprising a recognition element, a transduction element, and a signal processor capable of continuously and reversibly reporting a chemical concentration*.

This definition showed that the functions of a chemical sensor can be considered to be tasks of different units that were expressed by the IUPAC (Hulanicki et al. 1991). *Chemical sensors usually contain two basic components connected in series: a chemical (molecular) recognition system (receptor) and a physicochemical transducer*. Figure 5.1 shows a scheme of the components of a chemical sensor.

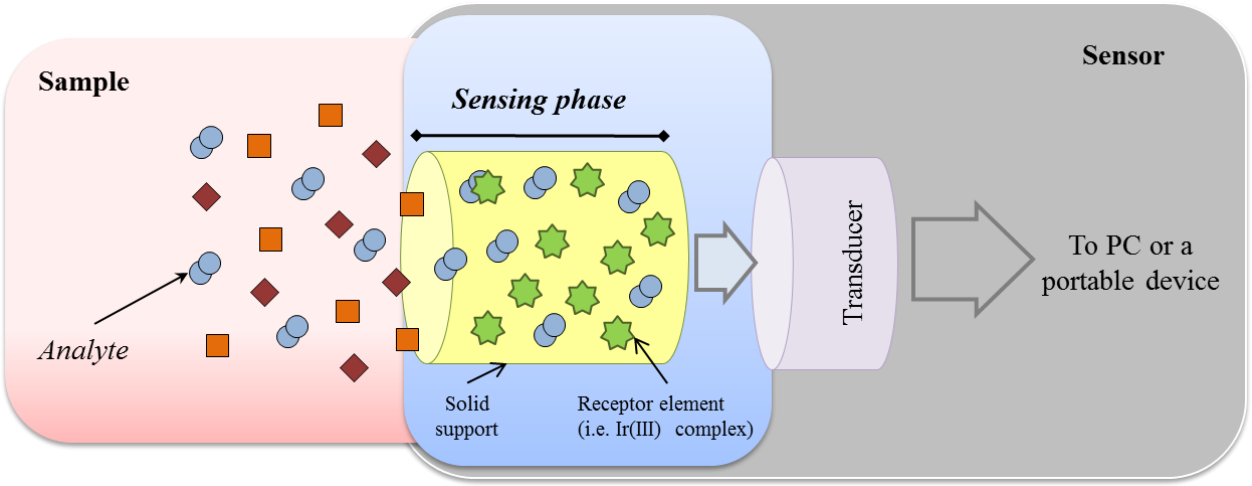

Figure 5.1. Schematic diagram of a chemical sensor.

The ***receptor*** or ***sensing layer*** is the component in which both sample and sensor interact; receptor layers can respond selectively to particular substances or to a group of substances. This interaction provides a change in any of its physicochemical properties whose magnitude is related to the concentration of the target analyte. Thus, the receptor may use two different principles:

- Physical principles: when no chemical reaction occurs between the analyte and the receptor, for example, changes in absorbance, luminescence, conductivity, mass, and so on.

- Chemical principles: when a chemical reaction between the analyte and the sensing layer is responsible for the analytical signal.

The ***transducer*** is responsible for transforming these physicochemical changes of the sensing layers into an useful analytical signal (optical or electrical signal).

The ***electronic*** (computing) element is responsible for the amplification, treatment, calculation, and transformation of the analytical signal into a useful result.

The chemical sensors may be classified following different ways, but the prevalent one is the classification following the principles of signal transduction proposed by IUPAC in 1991 (Hulanicki et al. 1991). Thus, chemical sensors can be classified as:

- ***Optical sensors***, following absorbance, reflectance, luminescence (fluorescence or phosphorescence), refractive index, optothermal effect, and light scattering principles.

- ***Electrochemical sensors***, voltammetric and potentiometric devices, chemically sensitized field effect transistor (CHEMFET), and potentiometric solid electrolyte gas sensors, among others.

- ***Electrical sensors,*** including those with metal oxide and organic semiconductors as well as electrolytic conductivity sensors.

- ***Mass sensitive sensors***, that is, piezoelectric devices and those based on surface acoustic waves.

- ***Magnetic sensors*** (mainly for oxygen) based on paramagnetic gas properties.

- ***Thermometric sensors*** based on the measurement of the heat effect of a specific chemical reaction or adsorption, which involves the analyte.

- ***Other sensors***, mainly based on X, β or Γ radiation.

The most relevant chemical sensors were the electrochemical ones, but their use is limited by the stability of the electrode surface and by instabilities in the analyte diffusion barrier, because they usually measure the rate of diffusion of the analyte to the cathode or the anode. In addition, they are not welcome for ~~–*in* *vivo*~~" investigations due to the probability of electroshock. For these reasons, optical sensors have been widely developed in the last decades. IUPAC defines an optical sensor as *a device that transforms changes of optical phenomena, which are the results of an interaction of the analyte with the receptor part* (Hulanicki et al. 1991).

Many of the optical sensors contain organic dyes or organometallic compounds (OMCs) as sensing elements immobilized in analyte permeable supports. The interaction between the sample (analyte) and the immobilized dye provides a change on an optical property of the sensing layer, which can be transduced and related with the concentration of the analyte in the sample.

Therefore, to improve the sensitivity and selectivity of optical receptors, numerous research efforts have been made in parallel on three main aspects: (i) molecular design of better luminophores and/or more selective dyes, (ii) engineering of advanced substrates, and (iii) development of improved detection apparatus.

Consequently, new organic, inorganic, and hybrid labels have been developed to prevent photobleaching of luminescent dyes while allowing the measurements of multiple fluorophores with a single excitation source at very low concentration levels (Bailey et al. 2004; Dubertret et al. 2001; McFarland and Van Duyne 2003; Sonnichsen et al. 2005; Taton et al. 2000; Zimmer 2002), and more selective OMCs have been designed in order to increase the selectivity of the sensing layers (Fernández-Sánchez et al. 2006; Fernández-Sánchez et al. 2007).

Immobilization of the sensing compound onto the matrix of the support is a critical step in the fabrication of optical sensors. The properties of the sensing compounds strongly depend on the properties of the supportive matrices because the organic dyes interact directly with the surface of the solid matrix. In addition, the reproducibility of the chemical composition of the surface and the reactivity of the surface matrices have been proved to be crucial in sensor applications. This is particularly critical in the case of gas sensors where the surface reactions are the origin of the gas detection mechanism. Ideally, a matrix should be structurally stable enough to withstand mechanical stress. It has to prevent leaching and migration of chemical compounds by insulating the compounds within its structure. The latter feature is assumed to stop aggregation, to increase

photostability and to prevent a reaction chain being set off. The aggregation of sensing dyes within polymer films is one of the most relevant problems to be solved.

In addition, advanced confocal optics and more reliable miniaturized detection devices were developed in order to increase the detection sensitivity (Medina-Rodríguez et al. 2014; Medina-Rodríguez et al. 2013b; Wang et al. 2005).

From the definition of an optical sensor, it is possible to conclude that a sensor has to contain a receptor part. This receptor part or sensing phase is composed, at least, of a sensing dye (or optical probe) and a matrix that acts as a host or support. It has become clear that it constitutes a key element in an optical sensor and, therefore, this chapter will be focused on the use of Ir(III) complexes as part of the optical sensitive component in the receptor part. Anyway, it is well known that several authors name the optical sensing dyes as ―sensors" or ―chemodosimeters" and, therefore, there are many optical probes that can be very useful for sensing but they have not been yet immobilized on a solid support (Wang and Wolfbeis 2014). For this reason, we have divided this chapter into two sections: Ir(III) optical probes and Ir(III) optical sensing layers.

2. Ir(III) Used as Optical Probes

2.1. Optical probes for the detection of gaseous species

Certain gaseous molecules, such as oxygen (O_2), carbon dioxide (CO_2) and carbon monoxide (CO), play crucial roles in biological and environmental science. In the past few years, many luminescent Ir(III) complexes have been developed with different sensing mechanisms for the detection of these and other gases. The changes of the optical properties of these sensors upon absorption of the gaseous analyte can be due to: (i) the modification of non-covalent interactions in the crystal packing of the complex (for example, hydrogen bonding, π-π interactions); (ii) the change of the coordination environment of the metal centre (for example, through the direct coordination of the analyte to the metal); and (iii) the quenching of the sensor luminescence (for example, by O_2).

2.2.1. Oxygen

The utility of the chemistry of Ir(III) has been exploited for developing oxygen optical probes, for example, to synthesize iridium(III)–octaethylporphyrins and benzoporphyrin, which present

strong phosphorescence (Koren et al. 2011). Other authors synthesized $[Ir(npy)_2(bpy\text{-}pyr)]PF_6$, an iridium complex containing a pyrene moiety (Denisov et al. 2014). The reversible electronic energy transfer between two chromophores, that is, Ir(III) complex and pyr, leads to an extraordinarily long lifetime (225 μs) compared to 8.3 μs for the model complex $[Ir(npy)_2(tBubpy)]PF_6$ (Denisov et al. 2014). These results are promising for lifetime-based sensing methods and low oxygen determination. Other Ir(III) luminophores (see Table 5.1) were specifically synthesized with pendent vinyl or allyl groups for its polymer attachment using hydrosilylation reactions (DeRosa et al. 2004).

Table 5.1. Ir(III) complexes used as optical probes for detecting O_2.

Complex[a]	λ_{exc} (nm)	λ_{em} (nm)	τ_{em} (μs)	Reference
$[Ir(ppy)_2(vacac)]$	257,400,448	520	0.4	(DeRosa et al. 2004)
[*fac*-$Ir(ppy)_2(vppy)$]	287,384,440	514,542,580	0.1	(DeRosa et al. 2004)
[*mer*-$Ir(ppy)_2(vppy)$]	274,390,445	535,572	0.2	(DeRosa et al. 2004)
[Ir(OEP)(CO)(Cl)]	404,518,550	672	97	(Koren et al. 2011)
$[Ir(OEP)(Py)_2]Cl$	389,509,539	655	40	(Koren et al. 2011)
$[Ir(OEP)(n\text{-}ButIm)_2]Cl$	390,508,541	655	27	(Koren et al. 2011)
$[Ir(OEP)(CarbIm)_2]Cl$	388,507,538	652	37	(Koren et al. 2011)
$[Ir(npy)_2(tBubpy)]PF_6$	-	590,625	8.3	(Denisov et al. 2014)
$[Ir(npy)_2(bpy\text{-}pyr)]PF_6$	-	590,625	225	(Denisov et al. 2014)
$[Ir(btp)_2(acac)]$	-	-	5.8	(Zhang et al. 2012)
	486	615	5.7	(Yoshihara et al. 2015)
$[Ir(btp)_2(phen\text{-}NH_2)]$	441	593	8.6	(Yoshihara et al. 2015)
$[Ir(btp)_2(phen\text{-}DMA)]$	440	594	7.5	(Yoshihara et al. 2015)
$[Ir(btp)_2(phen\text{-}DEA)]$	440	594	7.9	(Yoshihara et al. 2015)
$[Ir(btq)_2(acac)]$	543	672	3.1	(Yoshihara et al. 2015)
$[Ir(btq)_2(phen\text{-}NH_2)]$	505	655	5.7	(Yoshihara et al. 2015)
$[Ir(btq)_2(phen\text{-}DMA)]$	504	656	5.6	(Yoshihara et al. 2015)
$[Ir(btq)_2(phen\text{-}DEA)]$	505	657	5.8	(Yoshihara et al. 2015)
$[Ir(ttph)_2(acac)]$	516	693	3.1	(Yoshihara et al. 2015)
$[Ir(ttph)_2(phen\text{-}NH_2)]$	516	686	6.2	(Yoshihara et al. 2015)
$[Ir(ttph)_2(phen\text{-}DMA)]$	515	688	6.0	(Yoshihara et al. 2015)
$[Ir(btph)_2(acac)]$	529	718	1.9	(Yoshihara et al. 2015)
$[Ir(btph)_2(phen\text{-}NH_2)]$	532	710	2.3	(Yoshihara et al. 2015)
$[Ir(btph)_2(phen\text{-}DMA)]$	533	711	2.3	(Yoshihara et al. 2015)

Notes: [a] See Section 5.

The use of organometallic complexes as oxygen probes in biologic tissues and fluids is also common. This type of molecular probe needs to meet some requirements, such as solubility and long emission wavelength to avoid interferences with the surrounding media and to allow the penetration of light in deeper tissues. In this sense, the utility of the chemistry of Ir(III) allows to shift the emission of $[Ir(btp)_2(acac)]$, which has been used for tumour hypoxia, by including extended π-electronic phenyl rings, while grafting COOH groups improves its aqueous solubility (Zhang et al. 2012). In fact, other derivatives from $[Ir(btp)_2(acac)]$ have been used as mitochondrial oxygen probes following the same concept; 5-amino-1,10-phenanthroline ligand has been used to give a cationic charge to the complex to enhance the cellular penetration, and extended π-conjugated systems have been included to shift the emission to the NIR region (Yoshihara et al. 2015). Figure 5.2 shows the structures of the most relevant Ir(III) complex used as oxygen probes.

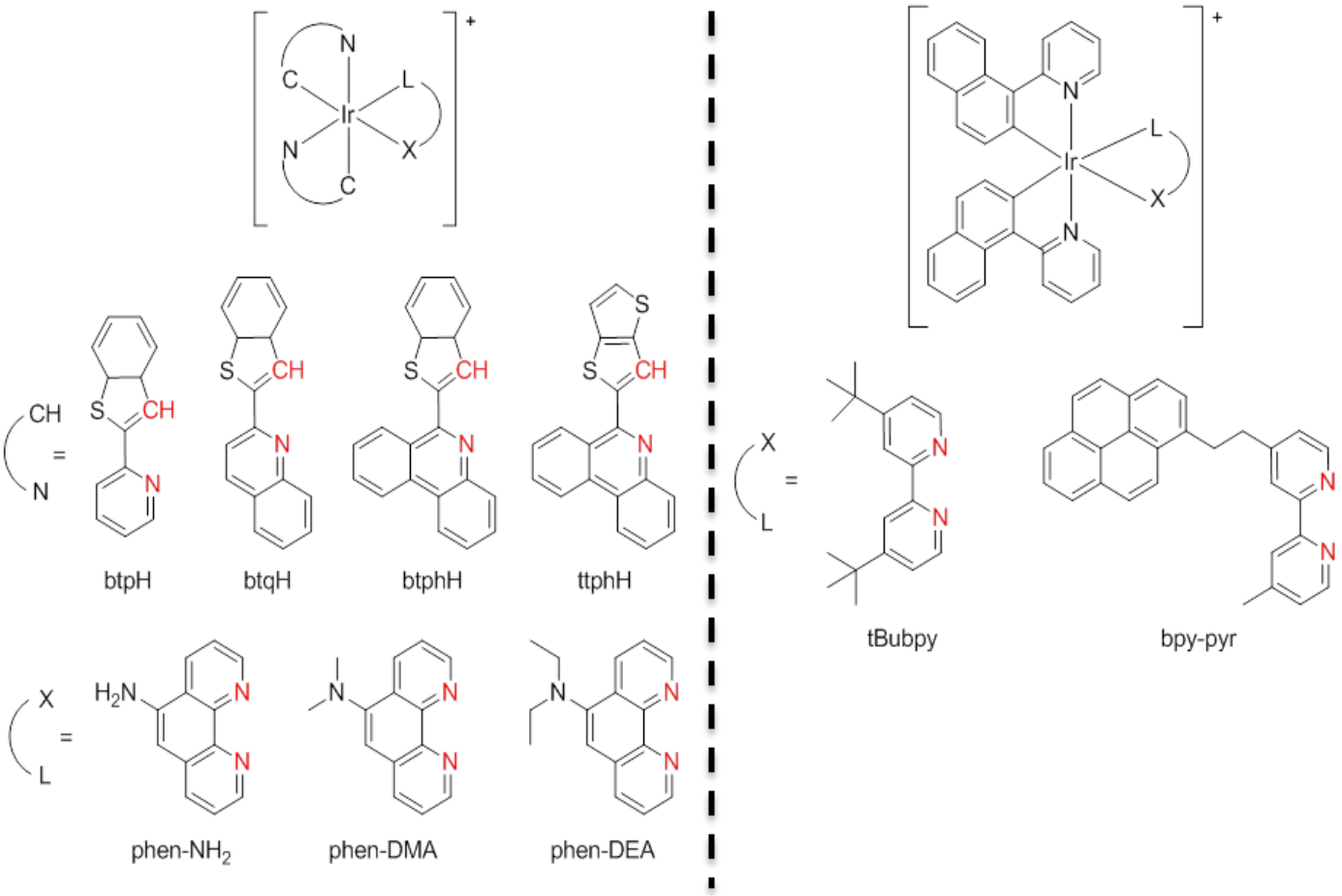

Figure 5.2. Most relevant Ir(III) complexes used as oxygen probes.

2.2.2. Other gaseous species

Table 5.2 summarizes the Ir(III) complexes used as optical probes for detecting gas species different than molecular oxygen.

Schwartz and Mann prepared the Ir(III) complex $[Ir(ppy)_2(N_2H_4)_2]^+$ for the direct optical detection of CO_2 based on the hydrazine/carbazate conversion, and demonstrated the utility of ligated N_2H_4 as a site for CO_2 binding (Schwartz and Mann 2011). The sensing mechanism involves the initial rapid binding of CO_2 by the Ir(III) complex to form a monodentate carbazate intermediate and the slower replacement of the second hydrazino ligand to form the final bidentate carbazate species.

The bimetallic complex [(Cl)$(CO)_3$Re(dmiphen)–Ir(1,5-cyclooctadiene)(Cl)], was synthesized and used for the optical recognition of CO (Park et al. 2014). This complex has the ability to react with CO producing appreciable changes in its spectroscopic properties, which indicates that the electronic communication between the two metal centres through the bis-chelating ligand R may occur. This interaction is accompanied by an enhancement of the emission intensity that can be used to quantify CO.

The detection of volatile organic compounds (VOCs) by vapochromic and vapoluminescent materials has attracted increasing attention due to the ability of these materials to detect gases via reversible changes in color and/or luminescence with fast response times. Liu *et al.* synthesized the complex $[Ir(ppy)_2(qnx)]$ that can act as a selective sensor for acetonitrile and propionitrile vapours (Liu et al. 2008). This complex exists as both black and red (visible to the naked eye) forms in the solid state: weak luminescence with a broadband centred at 692 nm and a decay lifetime of 43 ns for the black form, and intense luminescence with a peak centred at 654 nm and a decay lifetime of 130 ns for the red form. The black form can immediately translate into the red form after its exposure to acetonitrile, or it can change into the red form and lose its crystallinity over a period of only one minute when it is exposed to acetonitrile or propionitrile vapour, whereas no response is observed when it is exposed to other VOCs.

Table 5.2. Ir(III) complexes used as optical probes for detecting CO_2, CO and VOCs.

Analyte	Complex[a]	Detection[b]	Response[c]	λ_{exc} (nm)	λ_{em} (nm)	τ_{em} (µs)	Stoichiometry (complex:analyte)	Reference
Dissolved CO_2	$[Ir(ppy)_2(N_2H_4)_2]OTf$	L	Toff-R	405	501	1.56	1:1	(Schwartz and Mann 2011)
CO	$[(Cl)(CO)_3Re$ (dmiphen) –Ir(1,5-cyclooctadiene)(Cl)]	L	Ton	414	562	0.045	1:2	(Park et al. 2014)
Acetonitrile and propionitrile	$[Ir(ppy)_2(qnx)]$	L	Ton-B	365	692, 654	0.043, 0.130	-	(Liu et al. 2008)

Notes: [a] See Section 5.

[b] L is Luminescence, it is used when the authors did not clarify if fluorescence (F) or phosphorescence (P) occurred.

[c] Ton is Turn-on; Toff-R is Turn-off and red shift; Ton-B is Turn-on and blue shift.

2.2. Optical probes for the detection of ionic species

2.2.1. Cations

Traditional analytical techniques for the detection of metal cations include inductively coupled plasma mass spectroscopy, cold vapour atomic absorption spectrometry, and gas chromatography. Cold vapour atomic absorption spectrometry, with a very low detection limit, is one of the most selective, sensitive, and popular techniques for determining cations in a wide variety of samples due to its advantages, such as simplicity, high sensitivity, and selectivity. However, these methods need long analysis times and sophisticated instrumentation. Therefore, faster and simpler methods are currently receiving considerable attention. Among other, optical methods are a suitable alternative to the on-site analysis of cations with cheaper instrumentation. In fact, the application of transition metal complexes as luminescent probes presents important advantages as their simplicity, easy visualization and high sensitivity.

The incorporation of a Lewis base as a cation receptor on the ancillary ligands of the luminescent Ir(III) complexes is a very used strategy for the recognition of cations. Among other cations, Hg^{2+} is one of the most studied cations mainly due to its toxicity.

One of the most common mechanisms for Hg^{2+} sensing is based on the decomposition of Ir(III) complex. This decomposition is produced by the interaction between Hg^{2+} and a heteroatom of the complex with lone-pair electrons, usually sulfur, and it is the responsible for the significant changes in the emission properties of the complex. These changes can be used to determine Hg^{2+} in solution.

Tong *et al.* developed a series of cyclometalated Ir(III) complexes with different S^S ancillary ligands (dithiocarbamate (Tong et al. 2012), phosphonodithioate (Tong et al. 2013b), bis(diphenylthiophosphoryl)amide (Tong et al. 2013c) and *N*-carbazolylcarbodithioate (Tong et al. 2013a)) for the detection of Hg^{2+} by the dissociation of the S^S ligand from the complex. Mei *et al.* designed another Ir(III) complex with dithiocarbamate as the ligand that is based on the same sensing mechanism (Mei et al. 2012) (see Figure 5.3).

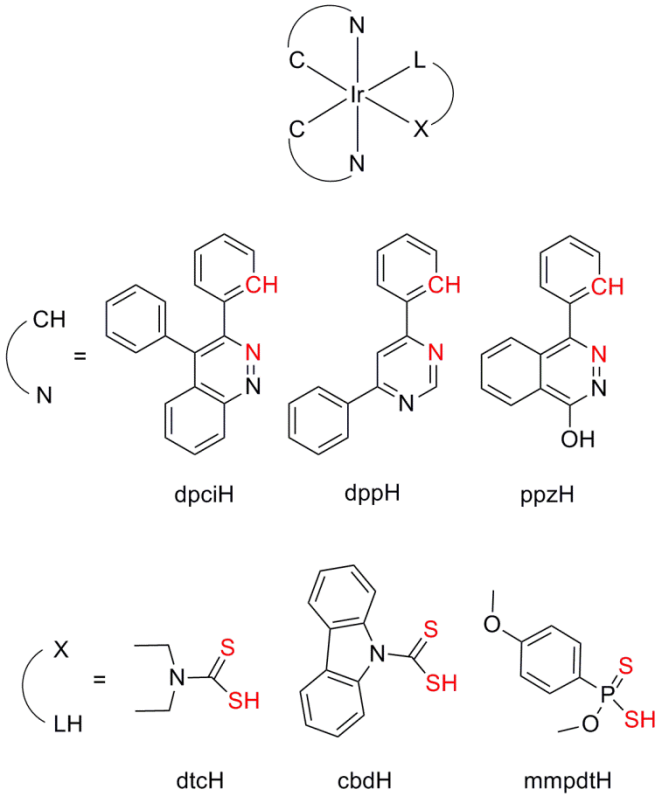

Figure 5.3. Most relevant Ir(III) complexes containing S^S ancillary ligands, which have been used as optical probes for determining Hg(II).

Yan *et al.* described the Ir(III) complex $[Ir(TBT)_2(acac)]$ with acetylacetonate (acac) as O^O ligand, wherein the interaction between Hg^{2+} and a sulfur atom also takes place (Yan et al. 2012). Wu *et al.* (Wu et al. 2011) synthesized the complex $[Ir(bt)_2(acac)]$, which also suffers the exit of the O^O ligand after the coordination between the Hg^{2+} and the sulfur atoms of the C^N ligands.

Another Ir(III) complex that undergoes the departure of the O^O ligand induced by Hg^{2+} ions was designed by Zeng *et al.* (Zeng et al. 2012). This sulfur-free complex, $[Ir(pbi)_2(acac)]$, has no heteroatom capable of providing binding sites with Hg^{2+} ions, since the lone-pair electrons of the nitrogen atom should participate predominantly in the benzimidazole conjugation system. However, it also possesses high specificity and sensitivity toward Hg^{2+} ions, suggesting that a pre-coordination step between the lone-pair electrons on the ligand and Hg^{2+} is not absolutely necessary in the probing mechanism (see Figure 5.4).

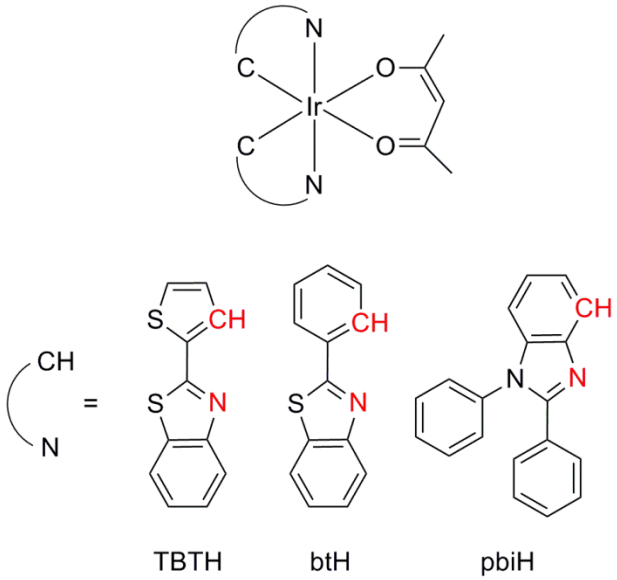

Figure 5.4. Most relevant Ir(III) complexes containing O^O ancillary ligands that have been used as optical probes for determining Hg(II).

Liu *et al.* synthesized the Ir(III) complex $[Ir(ppy)_2(PBT)]$, containing a sulfur atom in the N^O ligand. This complex can also serve as a selective chemodosimeter for Hg^{2+} due to the changes in the luminescence emission produced by the dissociation of the N^O ligand PBT from the complex (Liu et al. 2011b).

In another study, the Ir(III) phosphine complex $[Ir(dfppy)_2(PPh_2CH_2CH_2PPh_2)(Cl)]$, with lone-pair electrons on the phosphorous atom, was used as a chemodosimeter for the detection of Hg^{2+} (Alam et al. 2014). In this case, the free lone-pair on the non-coordinated phosphorous atom can easily interact with Hg^{2+} ions, which is the origin for the decomposition of the phosphine complex and the formation of the bis-aqua complex $[Ir(dfppy)_2(H_2O)_2]^+$, resulting in the quenching of the luminescence intensity.

Another mechanism used for the determination of Hg^{2+} is based on a chemical reaction between Hg^{2+} and sulfur atoms of the Ir(III) complex, but without decomposition of the complex. The Ir(III) complex $[Ir(ppy\text{-}1,3\text{-}dithiane)_2(bpy)]PF_6$ developed by Lu *et al.* is an example of this mechanism (Lu et al. 2013a). In another study, Yang *et al.* synthesized the Ir(III) complex $[Ir(dfppy)_2(NCS)_2]TBA$ (Yang et al. 2010). Herein, the selective reaction between Hg^{2+} and the sulfur atom of the thiocyanate group in CH_3CN solution induces the formation of $[Ir(dfppy)_2(NCCH_3)_2]^+$ species which are the responsible for the significant changes of the optical properties. Other examples of this mechanism are summarized in Table 5.3, while the use of other

mechanisms can be found in (Chan et al. 2013; Jee-Hye et al. 2012; Zhao et al. 2007a; Zhao et al. 2008b).

Table 5.3. Ir(III) complexes used as optical probes for detecting cations.

Analyte	Complex[a]	Detection[b]	Response[c]	λ_{exc} (nm)	λ_{em} (nm)	τ_{em} (µs)	LOD[d] (µM)	Stoichiometry (complex:analyte)	Reference
Hg^{2+}	$[Ir(dpci)_2(dtc)]$	UV–Vis, P	Ton-B (P)	373	686	0.077	1.6	1:1	(Piao et al. 2015)
	$[Ir(ppz)_2(mmpdt)]$	UV–Vis, P	R	385	465, 599	-	< 1	1:1	(Tong et al. 2012)
	$[Ir(ppa)(dmppa)((Ph_2PS)_2N)]$	UV–Vis, P	R	385	441, 598	-	1.2	1:1	(Tong et al. 2013b)
	$[Ir(dpci)_2(cbd)]$	UV–Vis, P	Ton	385	580, 645	-	0.16	1:1	(Tong et al. 2013c)
	$[Ir(dpp)_2(dtc)]$	UV–Vis, P	R	305	568	-	0.067	-	(Tong et al. 2013a)
	$[Ir(TBT)_2(acac)]$	UV–Vis, P	R	340	608	-	2.14	2:1	(Mei et al. 2012)
	$[Ir(bt)_2(acac)]$	UV-Vis, P	R	365	560	-	-	1:1	(Yan et al. 2012)
	$[Ir(pbi)_2(acac)]$	UV–Vis, P	R	384	520	-	0.24	1:1	(Wu et al. 2011)
	$[Ir(ppy)_2(PBT)]$	UV–Vis, P	R	360	607	0.98	0.1	1:1	(Zeng et al. 2012)
	$[Ir(dfppy)_2(PPh_2CH_2CH_2PPh_2)(Cl)]$	P	Toff	380	463	-	0.170	1:1	(Liu et al. 2011b)
	$[Ir(ppy\text{-}1,3\text{-}dithiane)_2(bpy)]PF_6$	UV–Vis, P	R	420	590	-	0.041	-	(Alam et al. 2014)
	$[Ir(dfppy)_2(NCS)_2]$ TBA	UV–Vis, P	Toff (P)	370	475	-	-	-	(Lu et al. 2013a)

Hg^{2+}	[Ir(ppy-oxime)$_2$(phen)]PF_6	UV–Vis, P	Toff (UV) Ton (P)	280	505, 541, 578	-	-	-	(Yang et al. 2010)
	[Ir(ppy)$_2$(bpy-(aza)$_2$)]Cl	P	Toff-R	370	588	-	-	-	(Chen et al. 2013)
	[Ir(dfppy)$_2$(dnbpy)]PF_6	P	Ton	310	490	4.53	2.8	-	(Jee-Hye et al. 2012)
	[Ir(btp)$_2$(acac)]	UV–Vis, P	R	440	610, 660	0.138	< 0.1	1:1	(Chan et al. 2013)
	[Ir(thq)$_2$(acac)]	UV–Vis, P	Toff	375	620	-	< 0.1	1:1	(Zhao et al. 2007a)
Cu^{2+}	[Ir(pq)$_2$(sa2p)]	UV–Vis, L	Ton (UV) Toff (L)	355	560	4.8	0.023	1:1	(Zhao et al. 2008b)
	[Ir(ppy)$_2$(bpy-CH_2CH_2-bpy)]PF_6	P	Toff	400	593	-	-	1:1	(Ma et al. 2014a)
	[Ir(DBQ)$_2$(bpy-(DPA)$_2$)]PF_6	P	Toff	360	560	0.486	-	1:2	(Lu et al. 2013b)
	[Ir(ppy)$_2$(btp-DPA)]	P	R	342	648	4.16	< 0.55 (I) < 1.46 (τ)	2:1	(Li et al. 2012)
	[Ir(ppy)$_2$(bpy-(DPA)$_2$)]PF_6	P	Toff	365	589	-	-	-	(You et al. 2011)
	[Ir(ppy)$_2$(phen-R1)]PF_6	P	Toff	365	600	-	-	1:1	(Kim et al. 2013)

	$[Ir(ppy)_2(bpy\text{-}acylhydrazone\text{-}Ph)]^+$	P	Ton	365	625	0.265	-	-	(Yang et al. 2012)
Cu^{2+}	$[Ir(ppy)_2(R2)]^+$	P	Ton	365	625	0.172	-	-	(Zhao et al. 2013a)
	$[Ir(ppy)_2(bpy\text{-}C\equiv C\text{-}C_6H_4\text{-}R3)]PF_6$	P	Ton	365	617	-	-	2:1	(Zhao et al. 2013a)
	$[Ir(ppy)_2(bpy\text{-}C\equiv C\text{-}C_6H_4\text{-}R4)]PF_6$	L	Ton	360	618	-	-	2:1	(Zhao et al. 2009)
	$[Ir(dCF3ppy)_2(phen\text{-}4\text{-}DPA)]^+$	P	Ton	393	499	5.13	0.66	-	(Zhao et al. 2009)
	$[Ir(dfppy)_2(phen\text{-}4\text{-}DPA)]^+$	P	Ton	359	518	1.92	-	-	(You et al. 2013)
Zn^{2+}	$[Ir(fppy)_2(phen\text{-}4\text{-}DPA)]^+$	P	Ton	362	548	1.32	-	-	(You et al. 2013)
	$[Ir(ppy)_2(phen\text{-}5\text{-}DPA)]PF_6$	L	Ton	-	575	7.97	-	1:1	(You et al. 2013)
	$[Ir(mppy)_2(phen\text{-}5\text{-}DPA)]PF_6$	L	Ton	-	584	5.19	-	1:1	(Lee et al. 2011)
	$[Ir(pq)_2(phen\text{-}5\text{-}DPA)]PF_6$	L	Ton	-	559	3.82	-	1:1	(Lee et al. 2011)
	$[Ir(pba)_2(phen\text{-}5\text{-}DPA)]PF_6$	L	Ton	-	536	29.92	-	1:1	(Lee et al. 2011)
	$[Ir(pp)_2(phen\text{-}TPA)]$	L	R	320	495	4.38	0.036	1:1	(Lee et al. 2011)

Zn^{2+}	[Ir(4-Me-ppy)$_2$(bpy-CH=CH–C$_6$H$_4$-DPA)]PF_6	UV–Vis, L	Toff-B	385	640	67	-	1:2	(Ma et al. 2014b)
Ag^{+}	[Ir (dfppy)$_2$(Py)(Cl)]	UV–Vis, P	Toff	365	476	-	-	-	(Araya et al. 2010)
Pb^{2+}	[Ir(pdpz)$_2$(py$_2$pz)]	P	Toff-R	340	485	2.6	-	-	(Xue et al. 2014b)
Cr^{3+}	[Ir(dfppy)$_2$(phen-BTTA)]$^{+}$	P	Ton-R	315	515, 557	-	73.1	1:1	(Ho et al. 2007)
Ca^{2+}	[Ir(pdpz)$_2$(azppz)]	P	Ton-B	295	560	0.038	-	-	(Han et al. 2012)
Mg^{2+}	[Ir(az-ppy)$_2$(bpy)]ClO_4	P	Ton	380	475, 507	2.45	-	-	(Ho et al. 2006)
Hg^{2+} and Ag^{+}	[Ir(ppy)$_2$(phen-2-aza-15-dithia-dioxa-crown ether)]$^{+}$	L	Ton-R (Ag^{+}) Toff-R (Hg^{2+})	375	527, 559	-	-	-	(Brandel et al. 2010)
Ba^{2+}	[Ir(ppy)$_2$(phen-2-aza-18-tetraoxa-crown ether)]$^{+}$	L	Ton-R	374	519, 547	-	-	-	(Schmittel and Lin 2007)

Notes: [a] See Section 5.

[b] UV-Vis is UV-Vis absorption; L is Luminescence, it is used when the authors did not clarify if fluorescence (F) or phosphorescence (P) occurred.

[c] Ton is Turn-on; Toff is Turn-off; Ton-R is Turn-on and red shift; Toff-R is Turn-off and red shift; Ton-B is Turn-on and blue shift ; Toff-B is Turn-off and blue shift; R is Ratiometric.

[d] I = Intensity; τ = Lifetime measurements.

Cu^{2+} has also been detected by Ir(III) complex-based sensors. The Cu^{2+} cation plays a significant role in many fundamental physiological processes and it is also an important environmental pollutant. The coordination interaction of the Cu^{2+} with an ion-recognition group on the Ir(III) complex causes variations in the luminescence intensity that may be used to detect Cu^{2+} (Kim et al. 2013; Li et al. 2012; Lu et al. 2013b; Ma et al. 2014a; Yang et al. 2012; You et al. 2011; Zhao et al. 2013a; Zhao et al. 2009). Ma *et al.* synthesized the complex $[Ir(pq)_2(sa2p)]$ containing a tetradentate Schiff base receptor, which was used as a Cu^{2+}-sensitive probe (Ma et al. 2014a). In other study, a free bipyridine of the biscyclometalated Ir(III) complex was used for Cu^{2+} recognition (Lu et al. 2013b). In this case, the Cu^{2+}-quenched emission was reversibly recovered by the addition of I^-. Other three Ir(III) complexes based on the connection of DPA to a ligand of the complex were used as copper ion receptors (Kim et al. 2013; Li et al. 2012; You et al. 2011). These complexes have a 1:2 stoichiometry (complex:Cu^{2+}) that was demonstrated by the binding titration data. Yang *et al.* designed the Ir(III) complex $[Ir(ppy)_2(phen\text{-}NHCOCH_2NHCH_2\text{-}Py)]PF_6$, wherein the coordination sites of the complex for Cu^{2+} are the N and O atoms on the amide group and the N atom on the pyridine unit (Yang et al. 2012). Two cationic cyclometalated iridium(III) complexes with 2,2‘-bipyridine-acylhydrazone were synthesized by Zhao *et al.* (Zhao et al. 2013a). These complexes behave as highly sensitive and selective Cu^{2+} probes based on the removal of the rapid isomerization of C=N bond in 2,2‘-bipyridine-acylhydrazone ligand. The excess of Cu^{2+} works as both catalyser and oxidant to promote C=N disruption and oxidative cyclization of the acylhydrazone, resulting in hydrolysis and cyclization products, which are highly emissive. Previously, they developed another Ir(III) complex with a 2,2‘-bipyridyl ligand containing a thiophene moiety as a binding receptor for the Cu^{2+} ion (Zhao et al. 2009). In this study, they also designed another Ir(III) complex with one 2,2‘-bipyridyl ligand, but containing a pyridyl moiety, which acts as receptor for Zn^{2+} ions.

In addition, Ir(III) complexes have also been employed for the determination of other metal cations such as Zn^{2+}, Ag^{+}, Pb^{2+}, Cr^{3+}, Ca^{2+}, Mg^{2+} and Ba^{2+} (Araya et al. 2010; Brandel et al. 2010; Han et al. 2012; Ho et al. 2007; Ho et al. 2006; Lee et al. 2011; Lin et al. 2010; Ma et al. 2014b; Schmittel and Lin 2007; Xue et al. 2014b; You et al. 2013) (see Table 5.3 and Figure 5.5).

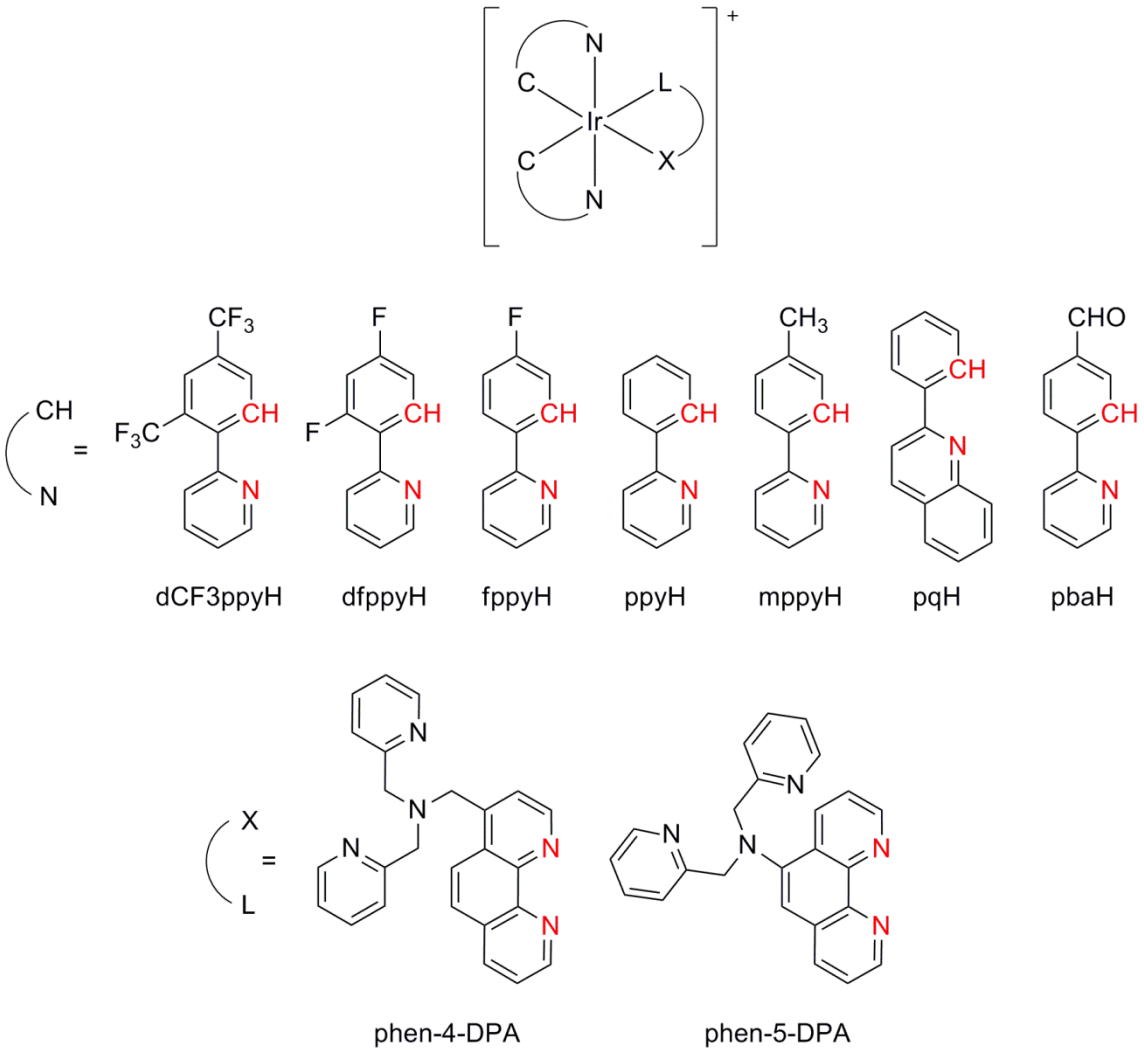

Figure 5.5. Most relevant Ir(III) complexes containing DPA, which have been used as optical probes for determining Zn(II).

The metal chelator DPA is frequently chosen as Zn^{2+} receptor because it has a strong affinity to divalent transition-metal ions over biologically abundant alkali and alkaline-earth-metal ions. For example, a series of luminescent Ir(III) complexes with different C^N ligands and containing a DPA moiety linked to a phenanthroline ligand have been synthesized as probes for Zn^{2+} ions (Lee et al. 2011; You et al. 2013). These particular complexes show phosphorescence turn-on responses in the presence of Zn^{2+}. The TPA is another metal chelator that specifically interacts with Zn^{2+} ions. In fact, $[Ir(pp)_2(phen\text{-}TPA)]$, a complex containing two phenylpyrazole ligands and a TPA moiety attached to a phenanthroline ligand, has also been used as a selective probe for analysing Zn^{2+} (Ma et al. 2014b).

In another study, the attachment of two DPA moieties to an Ir-coordinated bipyridine ligand allowed the modulation of the electronic structure upon coordination of metal cations at the DPA

amine nitrogen (Araya et al. 2010). In this complex, the addition of Ni^{2+} ions quenches completely the emission, whereas Cd^{2+} only leads to a partial quenching. In contrast, the coordination of Zn^{2+} ions induces a significant blue shift in the emission wavelength and a change in the luminescence lifetime.

Xue *et al.* designed the Ir(III) complex $[Ir(dfppy)_2(Py)(Cl)]$, wherein chloride is replaced by acetonitrile due to the strong interaction between Ag^+ and chloride, which probably combine to precipitate AgCl (Xue et al. 2014b). This reaction is responsible for the significant change of absorption and luminescence spectra and can be used for detecting Ag^+.

Ho *et al.* presented a phosphorescence sensor for Pb^{2+}, in which one py_2pz moiety is attached to the heteroleptic Ir(III) complex (Ho et al. 2007). The nitrogen atoms of py_2pz act as an effective donor site, allowing the direct recognition of the Pb^{2+} ions. This interaction with the metal produces a quenching of the emission intensity.

A BTTA has been used as Cr^{3+} receptor by Han *et al.* (Han et al. 2012). In this study, the interaction between Cr^{3+} and BTTA produces a sequential double ratiometric response that is specific to Cr^{3+}.

The incorporation of a crown ether as cation receptor is another approach used for the recognition of metal cations. The Ir(III) complex $[Ir(pdpz)_2(azppz)]$ synthesized by Ho *et al.* contains an 1-aza-15-crown-5-ether appended to one pyridyl pyrazolate ligand that acts as chelating agent. The interaction between the azacrown ether and Ca^{2+} ions alters the spectral properties of the Ir(III) complex, producing an increase of the emission intensity, which can be used to detect Ca^{2+} (Ho et al. 2006). In other study, two 1-aza-15-crown-5-ethers were attached to two phenylpyridine ligands of the Ir(III) complex, which showed selectivity to Mg^{2+} (Brandel et al. 2010).

Schmittel and Lin prepared an Ir(III) complex with two aza-dithia-dioxa crown ethers appended to one phenanthroline ligand (Schmittel and Lin 2007). This complex exhibits selective binding properties toward Ag^+ and Hg^{2+} ions in aqueous media by characteristic luminescence responses, which are attributed to the complexation between these ions and the aza-dithia-dioxa crown ethers. These authors synthesized another cyclometalated Ir(III) complexes containing two 1-aza-18-crown-6-ethers moieties attached to one phenanthroline ligand, which can be used for the detection of Ba^{2+} (Lin et al. 2010).

2.2.2. pH

Table 5.4 summarizes the Ir(III) complexes used as optical probes for detecting pH and Figure 5.6 shows the chemical structure of some of them.

The luminescent Ir(III) complexes incorporating terpyridine ligands with protonatable (pyridyl) or deprotonatable (phenolic) groups, constitute potential new sensing systems for pH. The protonation of the pyridyl nitrogen, as well as the deprotonation of the phenolic hydroxyl, can promote changes in the luminescence properties (*e.g.*, intensity, wavelength, or lifetime), which offer sensitivity over different pH regions. For example, Licini and Williams reported Ir(III) bis-terpyridine complexes, wherein the luminescence emission of the phenol-appended complexes was quenched over the pH range 6–10 due to the deprotonation of the phenol, whereas the intensity of the emission and the lifetime of the pyridyl-substituted complexes were reduced when pH decreases from 7 to 2 due to the protonation effect (Licini and A. Gareth Williams 1999).

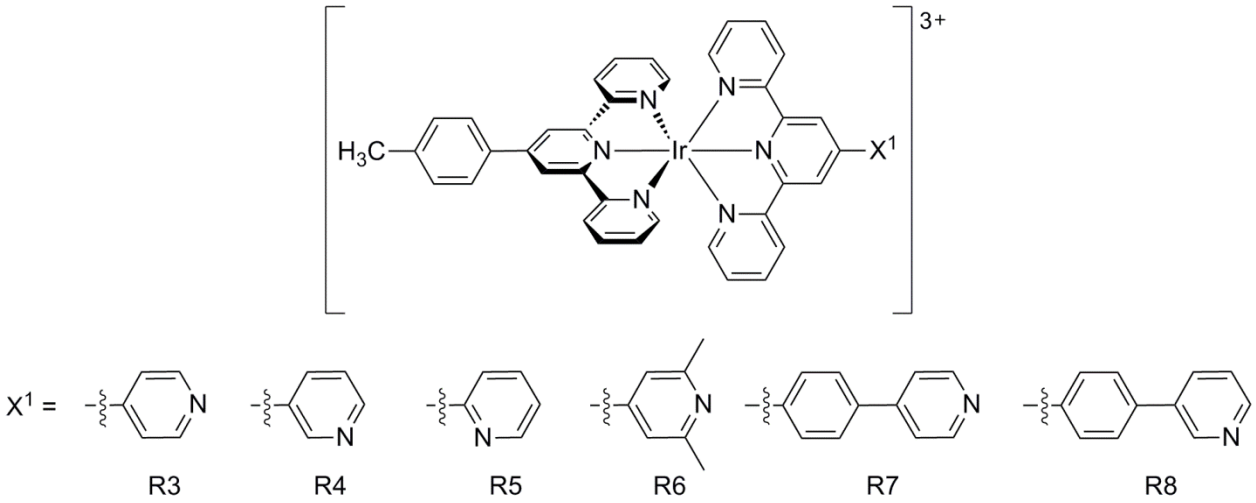

Figure 5.6. Most relevant Ir(III) complexes for optical determination of pH.

In another study, structural modifications of the pendent pyridyl groups were done to determine the influence of the ligand on the magnitude of the response and on the pH region wherein the luminescence changes occur (Arm et al. 2006). For this purpose, a series of Ir(III) bis-terpyridine complexes incorporating pendent pyridyl groups were prepared, including three mutually isomeric homoleptic complexes, in which the nitrogen atom of the pendent pyridyl is *para*, *meta* or *ortho* to the C–C bond to the terpyridine; their heteroleptic analogues, in which the second ligand is 4‘-tolyl-terpyridine (ttpy); analogous complexes of the new ligand, 4‘-(2,6-dimethylpyrid-4-yl)-terpyridine; and related complexes incorporating an additional phenyl ring

interposed between the terpyridine and the pendent pyridyl group. Both the emission intensity and lifetimes of all these heteroleptic complexes, except the *meta*-substituted system, were sensitive to the protonation state of the pendent pyridyl group.

Most recently, the incorporation of indole rings on the ligands of the cyclometalated iridium(III) complexes has allowed to obtain other phosphorescent complexes with pH-responsive characteristics (He et al. 2014).

Table 5.4. Ir(III) complexes used as optical probes for detecting pH.

Complex[a]	Detection[b]	Response[c]	λ_{exc} (nm)	λ_{em} (nm)	τ_{em} (μs)	Reference
$[Ir(tpy\text{-}R5)(tpy\text{-}R5)]^{3+}$	L (*I*&*τ*)	Toff pH 6→10	364	460-540	-	(Licini and A. Gareth Williams 1999)
$[Ir(tpy\text{-}R5)(tpy\text{-}R6)]^{3+}$	L (*I*&*τ*)	Toff pH 6→10	364	460-540	-	(Licini and A. Gareth Williams 1999)
$[Ir(tpy\text{-}R7)(tpy\text{-}R7)]^{3+}$	L (*I*&*τ*)	Toff pH 7→2	364	460-540	1.1	(Licini and A. Gareth Williams 1999)
$[Ir(tpy\text{-}R7)(tpy\text{-}R6)]^{3+}$	L (*I*&*τ*)	Toff pH 7→2	364	460-540	4.7	(Licini and A. Gareth Williams 1999)
$[Ir(tpy\text{-}R7)(tpy\text{-}R6)]^{3+}$	L (*I*&*τ*)	Toff	360	510-550	4.7	(Arm et al. 2006)
$[Ir(tpy\text{-}R8)(tpy\text{-}R6)]^{3+}$	L (*I*&*τ*)	Toff	360	510-550	6.2	(Arm et al. 2006)
$[Ir(tpy\text{-}R9)(tpy\text{-}R6)]^{3+}$	L (*I*&*τ*)	Toff	360	510-550	6.0	(Arm et al. 2006)
$[Ir(tpy\text{-}R10)(tpy\text{-}R6)]^{3+}$	L (*I*&*τ*)	Toff	360	510-550	5.8	(Arm et al. 2006)
$[Ir(tpy\text{-}R11)(tpy\text{-}R6)]^{3+}$	L (*I*&*τ*)	Toff	360	510-550	4.6	(Arm et al. 2006)
$[Ir(tpy\text{-}R12)(tpy\text{-}R6)]^{3+}$	L (*I*&*τ*)	Ton-B	360	510-550	4.0	(Arm et al. 2006)
$[Ir(ppy)_2(bpy\text{-}ind)]PF_6$	P	Ton pH 8.2→3.0	420	600	0.111	(He et al. 2014)
$[Ir(ppy)_2(pyq\text{-}ind)]PF_6$	P	Ton pH 8.2→3.0	420	645	0.140	(He et al. 2014)

Notes: [a] See Section 5.

[b] L is Luminescence, it is used when the authors did not clarify if fluorescence (F) or phosphorescence (P) occurred; *I* = Intensity; *τ* = Lifetime measurements.

[c] Ton is Turn-on; Toff is Turn-off; Ton-B is Turn-on and blue shift.

2.2.3. Anions

The determination of anions using optical probes is more difficult than the determination of cations due to the variable size, shape, and strong solvation of the anionic species. There are several approaches to design phosphorescent Ir(III) complexes for anion analysis: (i) to incorporate Lewis acids, such as boron or tin atoms, on the ligands of the Ir(III) complexes, which act as anion receptor through Lewis acid–base interactions; (ii) to introduce an acidic hydrogen group on the ligands, such as pyrrole, imidazole, amide, thioamide, urea or thiourea, which can be deprotonated or allows for hydrogen bonds with basic anions; (iii) to include a reactive functional group on the Ir(III) complex, which can react with anions. Table 5.5 summarizes the Ir(III) complexes used as optical probes for detecting anions.

In the field of anion sensing, the detection of fluoride ion is of particular importance because it plays an essential role in biological, chemical, and medical processes. Recently, the specific Lewis acid-base interactions between boron atoms and F^- ions, which can induce changes in the optical properties of heavy-metal complexes, have been adopted as an efficient method for fluoride detection. Concretely, sterically bulky boryl moieties, such as dimesitylboryl, are generally employed as receptors of fluoride ion due to its role for governing the selectivity for F^- (Xu et al. 2010; Xu et al. 2013; Xu et al. 2011a; Xu et al. 2011b; Zhao et al. 2008a) (see Figure 5.7).

Yinan and Myung-Ho reported the synthesis of a phosphorescent Ir(III) complex with two dimesitylboryl-phenylpyridine (Bppy) as C^N ligands and one picolinate as O^N ligand, and its application to the selective phosphorescent detection of fluoride anion (Yinan and Myung-Ho 2011), and Yang *et al.* designed two isomeric Ir(III) complexes containing two Bppy units as C^N ligands and one acetylacetonate (acac) as O^O ligand (Yang et al. 2013).

Most recently, Sharma *et al.* synthesized two Ir(III) complexes with the $B(Mes)_2$ moiety appended to an O^N ancillary ligand (phenyl-picolinate) (Sharma et al. 2014). These complexes show a turn-on phosphorescence response toward F^- ions, unlike the complexes with the borane moieties linked to a C^N ligand, where the interaction between the Ir(III)-borane conjugate and F^- ions usually results in a turn-off response.

Table 5.5. Ir(III) complexes used as optical probes for detecting anions.

Analyte	Complex[a]	Detection[b]	Response[c]	λ_{exc} (nm)	λ_{em} (nm)	τ_{em} (μs)	LOD (μM)	Stoichiometry (complex:analyte)	Reference
F^-	$[Ir(Bpq)_2(bpy)]PF_6$	P	Toff	379	592	2.67	-	1:2	(Lin et al. 2010)
	$[Ir(Bpq)_2(quqo)]PF_6$	P	Toff	613	680	0.2	-	1:2	(Zhao et al. 2008a)
	$[Ir(Bpq)_2(CzbpyCz)]PF_6$	P	Toff-B	430	584	1.96	-	1:2	(Xu et al. 2011b)
	$[Ir(Bpq)_2(CzfpbiCz)]PF_6$	P	R	383	584	2.81	-	-	(Xu et al. 2010)
	$[(Ir(Bpq)_2(Cz\text{-}bpy\text{-}C\equiv C))_2\text{-}R13](PF_6)_2$	P	Toff	442	606	0.63	-	-	(Xu et al. 2011a)
	$[Ir(Bppy)_2(pic)]$	P	Toff-R	392	580	-	-	1:2	(Xu et al. 2013)
	$[Ir(R14)_2(acac)]$	P	R	370	604, 556, 505	0.63, 0.14, 0.80	1.9	-	(Yinan and Myung-Ho 2011)
	$[Ir(R15)_2(acac)]$	P	R	370	602, 543	1.80, 0.26	3.2	-	(Yang et al. 2013)
	$[Ir(dfppy)_2(Bpic)]$	P	R	380	533, 501, 471	-	-	-	(Yang et al. 2013)
	$[Ir(ppy)_2(Bpic)]$	P	R	400	599, 509	-	-	-	(Sharma et al. 2014)

CN^-	$[Ir(ppy)_2(dmpp)]PF_6$	UV–Vis, L	Toff (UV) Ton (L)	396	518	-	< 40 (L)	-	(Sharma et al. 2014)
	$[Ir(pq)_2(Cl)]_2$	L	Ton	338	579	-	-	1:4	(Lou et al. 2010)
	$[Ir(pq)_2$(Fc-C≡C-phen-C≡C-Fc)$]PF_6$	L	Ton	330	580	-	10	-	(Schmittel and Qinghai 2012)
NO_2^-	$[Ir(pq)_2(Cl)]_2$	UV–Vis, L	Ton (UV) Ton (L)	430	567	-	50 (UV) 10 (L)	1:2	(Qinghai et al. 2012)
	$[Ir(ppy)_2(Cl)]_2$	UV–Vis, L	Ton (UV) Toff (L)	430	567	-	50 (UV)	1:4	(Qinghai et al. 2011)
Cl^-	[Ir(ttpy)(4'-*meta*-*N*-methylpyridyl-tpy)]$^{4+}$	L	Toff	366	510	5.8	-	-	(Qinghai et al. 2011)
	[Ir(ttpy)(4'-*para*-*N*-methylpyridyl-tpy)]$^{4+}$	L	Toff	366	510	1.7	-	-	(Goodall and Williams 2000)
ClO^-	$[Ir(ppy)_2(R16)]PF_6$	P	Ton	346	578	0.15	< 19.4	-	(Goodall and Williams 2000)
	$[Ir(ppy\text{-}oxime)_2(phen)]PF_6$	L	Ton	280	589	-	-	-	(Zhao et al. 2011)
	$[Ir(R17)_2(bpy\text{-}dmn)]Cl$	P	Ton	405	534-598	-	-	-	(Chen et al. 2013)

MoO_4^{2-}	$[Ir(R18)_2(H_2\text{-phencat})]PF_6$	L	Toff	326	596	-	-	-	(Li et al. 2014b)
	$[Ir(R19)_2(H_2\text{-phencat})]PF_6$	L	Toff	330	610	-	-	-	(Castillo et al. 2012)
	$[Ir(R20)_2(H_2\text{-phencat})]PF_6$	L	Toff	400	588	-	-	-	(Castillo et al. 2012)
$H_2PO_4^-$	$[Ir(ppy)_2(bpy\text{-}(CH_2\text{-}3\text{-}butylurea)_2)]Cl$	P ($I\&\tau$)	Ton	372	560	0.34	-	-	(Castillo et al. 2012)
	$[Ir(ppy)_2(bpy\text{-}(Zn\text{-}DPA)_2)]PF_6$	P ($I\&\tau$)	Ton	365	580-590	0.080	-	-	(Li et al. 2014c)
OAc^-, F^- and $H_2PO_4^-$	$[Ir(R21)_2(R22)]PF_6$	L	Toff	252-274	561-593	0.34-2.58	-	1:1	(Kim et al. 2014)
	$[Ir(ppy)_2(R23)]PF_6$	UV–Vis, L	Toff	360	587	0.704	-	-	(Lo et al. 2006b)
	$[Ir(ppy)_2(R24)]PF_6$	UV–Vis, L	Toff	360	593	0.469	-	-	(Zhao et al. 2007b)
	$[Ir(ppy)_2(R25)]PF_6$	UV–Vis, L	Toff	360	580	0.593	-	-	(Zhao et al. 2007b)
	$[Ir(ppy)_2(fppi)]PF_6$	UV–Vis, L	Toff	282	572	0.82	-	-	(Zhao et al. 2007b)

OAc^-, F^- and $H_2PO_4^-$	$[Ir(ppy)_2(dfppi)]PF_6$	UV–Vis, L	Toff	282	589	0.71	-	-	(Jayabharathi et al. 2014)
	$[Ir(ppy)_2(tfppi)]PF_6$	UV–Vis, L	Toff	282	598	0.69	-	-	(Jayabharathi et al. 2014)
	$[Ir(ppy)_2(tfmppi)]PF_6$	UV–Vis, L	Toff	282	594	0.70	-	-	(Jayabharathi et al. 2014)
SO_3^{2-} and HSO_3^-	$[Ir(ppy)_2(azobpy)Ir(ppy)_2](PF_6)_2$	P	Ton	405	600	-	0.24 (SO_3^{2-}) 0.14 (HSO_3^-)	-	(Jayabharathi et al. 2014)

Notes: [a] See Section 5.

[b] UV-Vis is UV-Vis absorption; L is Luminescence, it is used when the authors did not clarify if fluorescence (F) or phosphorescence (P) occurred; I = Intensity; τ = Lifetime measurements.

[c] Ton is Turn-on; Toff is Turn-off; Toff-R is Turn-off and red shift; R is Ratiometric.

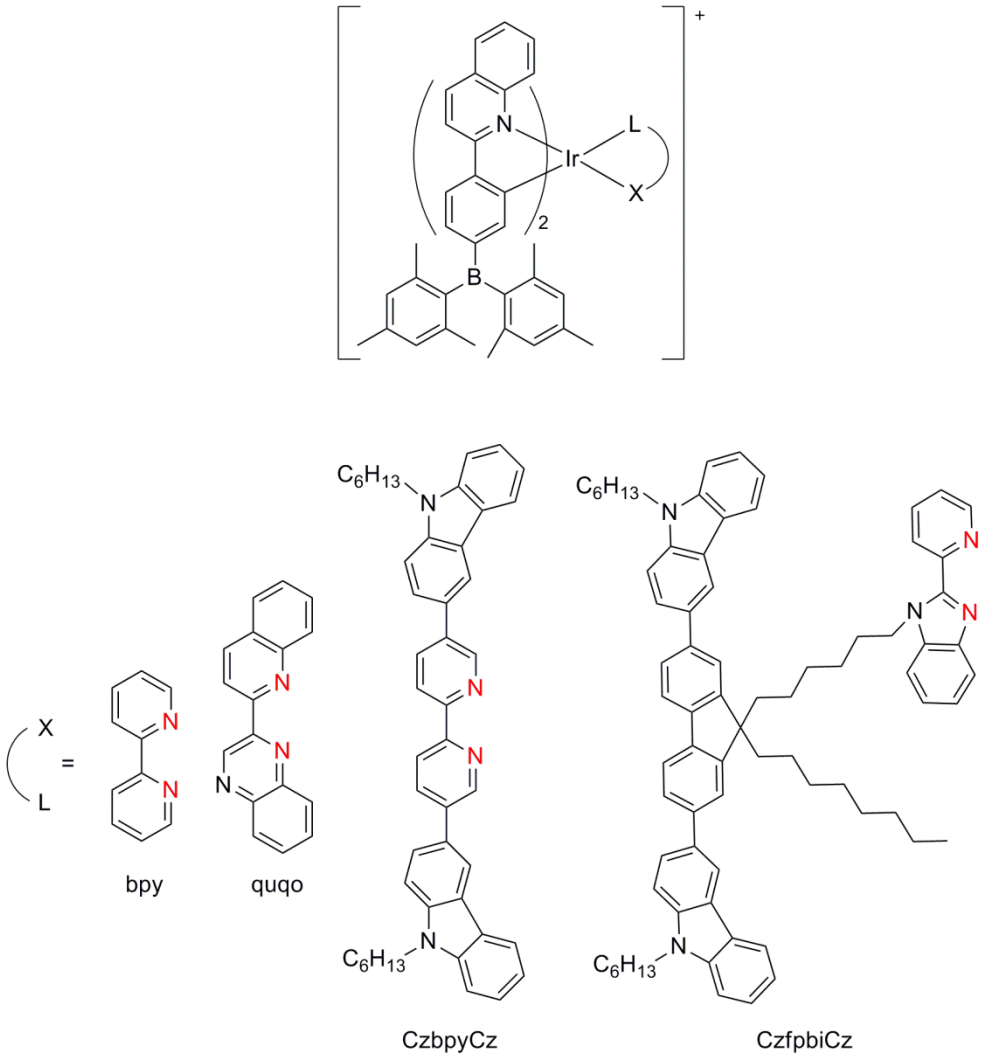

Figure 5.7. Most relevant Ir(III) complexes for optical determination of F^-.

Due to the high toxicity of cyanide anions, there is a growing interest in the development of new cyanide sensing probes. In the last few years, the use of phosphorescent Ir(III) complex-based chemosensors has been a novel approach for the detection of cyanide (Lou et al. 2010; Qinghai et al. 2011; Qinghai et al. 2012; Schmittel and Qinghai 2012). For example, Lou *et al.* developed the Ir(III) complex $[Ir(ppy)_2(dmpp)]PF_6$, (Lou et al. 2010), which changes its optical properties in the presence of cyanide due to the chemical reaction between the cyanide and the α,β-unsaturated carbonyl compound of the dmpp ligand (pyridine-pyrazole derivative). In another study, Schmittel and Qinghai synthesized the dimeric Ir(III) complex $[Ir(pq)_2(Cl)]_2$, which acts as another chemodosimeter for the detection of cyanide (Schmittel and Qinghai 2012). In this case, the variations in the optical properties depend on a standard nucleophilic substitution, wherein the chloride ions are displaced by cyanide originating the luminescent monomeric Ir(III) complex $[Ir(pq)_2(CN)_2]^-$. This dimeric complex had been previously used as chemodosimeter for nitrite

detection. Herein, the nitrite produces the nucleophilic shift of the chloride ions, generating the monomeric Ir(III) complex $[Ir(pq)_2(NO_2)]$, which shows a luminescent emission enhancement (Qinghai et al. 2011). On the other hand, the related dimeric Ir(III) complex $[Ir(ppy)_2(Cl)]_2$ can also act as chemodosimeter for nitrite because of its luminescent emission is quenched by this analyte. The recognition mechanism is based on the nucleophilic substitution of the chloride ions by nitrite, which leads to the complex $[Ir(ppy)_2(NO_2)_2]^-$. The different coordination and stoichiometry result in the extinction of the luminescence. Later, Qinghai *et al.* prepared the Ir(III) complex $[Ir(pq)_2(Fc\text{-}C\equiv C\text{-}phen\text{-}C\equiv C\text{-}Fc)]^+$ that exhibits off-on luminescence response with the addition of cyanide (Qinghai et al. 2012). This complex is non-luminescent due to photoinduced electron transfer (PET) quenching of the excited Ir(III) phenylquinoline unit by the electron-rich ferrocenyl units. In this case, the sensing mechanism involves the nucleophilic displacement of the phenanthroline ligand by cyanide to furnish the same luminescent dicyano Ir(III) complex $[Ir(pq)_2(CN)_2]^-$.

In addition, other anions, such as Cl^-, ClO^-, MoO_4^{2-}, $H_2PO_4^-$, OAc^-, SO_3^{2-} and HSO_3^- have also been detected by luminescent Ir(III) complexes (Castillo et al. 2012; Chen et al. 2013; Goodall and Williams 2000; Jayabharathi et al. 2014; Kim et al. 2014; Li et al. 2013; Li et al. 2014b; Li et al. 2014c; Lo et al. 2006b; Zhao et al. 2011; Zhao et al. 2007b).

Goodall and Williams described two isomeric bis-terpyridine Ir(III) complexes that incorporate a *meta*- or *para*-*N*-methylpyridyl substituent at the terpyridine 4'-position as site of anion interaction, and whose luminescence is quenched by chloride ions (Goodall and Williams 2000). The *para*-*N*-methylpyridyl substituted isomer shows lower intensity and shorter lifetimes due to the direct conjugation of the alkylated pyridine nitrogen with the terpyridine. On the other hand, in the *meta*-*N*-methylpyridyl substituted isomer, the pyridine nitrogen is not in conjugation with the terpyridine, which improves the sensing properties of the complex, causing both the intensity and the lifetime are perturbed by chloride.

The most useful methodology for detecting hypochlorite is based on the use of a reactive oxime group as a ligand. For example, Zhao *et al.* synthesized the Ir(III) complex $[Ir(ppy)_2(R16)]PF_6$, where R16 is a 4'-methyl-2,2'-bipyridyl-4-carbaldehyde oxime (Zhao et al. 2011). This complex is almost non-emissive in solution due to the rapid isomerization of oxime group as an effective non-radiative decay process. However, the addition of ClO^- provides the oxidation of the oxime group to a carboxylic acid; it provides an increase in the phosphorescence emission, which can be used for the selective detection of ClO^-. Other example of this

methodology is the Ir(III) complex [Ir(ppy-oxime)$_2$(phen)]PF_6 designed by Chen *et al.*, which responds to ClO^- by an oxidative hydrolysis in alkaline aqueous solution (Chen et al. 2013). This complex is also non-emissive due to the isomerization of the oxime group, and its luminescence emission is also enhanced after the reaction with ClO^- because of the formation of the dicarboxylate in alkaline solution. Recently, a series of cyclometalated Ir(III) complexes with a diaminomaleonitrile moiety have been reported as probes for ClO^- (Li et al. 2014b). All these complexes are weakly emissive in solution due to the non-radiative decay process of the C=N bond. However, its phosphorescence intensities increase significantly with increasing concentrations of ClO^-, indicating the destruction of the C=N bond and the formation of the carboxylate products. In addition, these complexes show selectivity for ClO^- over other biologically relevant reactive oxygen species, such as H_2O_2, $^1O_2$, $O_2^{\cdot-}$, NO, ROO^-, $^{\cdot}OH$, and $ONOO^-$.

For molybdate detection, Castillo *et al.* developed a series of luminescent Ir(III) complexes, [Ir(C^N)$_2$(H_2-phencat)]$^+$, containing a catecholamide appended to a phenanthroline ligand, and whose emission intensity decreases proportionally with the concentration of molybdate (Castillo et al. 2012). The catecholamide acts as receptor unit and is able to distinguish biologically relevant oxometalates, such as molybdate (MoO_4^{2-}) from structurally related oxoanions, such as SO_4^{2-} or HPO_4^{2-}, as well as potentially competing cations such as Cu^{2+} and Fe^{3+}. Also, these cationic complexes show an increase in intensity when the pH is also increased due to the deprotonation of the catechol unit and the formation of the neutral complexes. Thus, these Ir(III) complexes can be used as luminescent probes for molybdate and pH.

The development of probes for phosphate anions is an active research goal. For example, two phosphorescent Ir(III) complexes with the general formula [Ir(ppy)$_2$(N^N)]$^+$ were reported as selective turn-on probes for $H_2PO_4^-$. The first one contains two pre-organized urea groups as recognition pocket of $H_2PO_4^-$ through the formation of hydrogen bonds (Li et al. 2014c), whereas the second one consists in two Zn-DPA units acting as binding site for $H_2PO_4^-$ by Lewis acid–base interactions (Kim et al. 2014). Lo *et al.* synthesized a series of luminescent cyclometalated Ir(III) complexes with a thiourea moiety attached to a phenanthroline ligand, which can act as receptor for dihydrogen phosphate, fluoride and acetate ions (Lo et al. 2006b). The emission intensities of all the complexes are reduced in the presence of these three anions. However, the binding affinity of the complexes for OAc^- is higher than those for F^- and $H_2PO_4^-$. In another study, Zhao *et al.* described three cationic Ir(III) complexes based on different imidazo[4,5-*f*]-

[1,10]phenanthroline derivatives, whose emission is completely quenched by F^-, OAc^- and $H_2PO_4^-$ (Zhao et al. 2007b). In this case, the NH of the imidazolyl group is responsible for the recognition of these anions. Moreover, from the binding constant values, it can be deduced that these complexes prefer to bind F^- and OAc^- over $H_2PO_4^-$. Most recently, Jayabharathi *et al.* have reported the synthesis of four cationic Ir(III) complexes, which are also based on phenanthroline derivatives, but contain highly electron-withdrawing fluoro- and trifluoromethyl substituents (Jayabharathi et al. 2014). The emission of these complexes is also completely quenched in the presence of F^-, OAc^- and $H_2PO_4^-$, whereas the binding constants indicate a higher tendency for binding F^- over OAc^- and $H_2PO_4^-$.

For selective sulphite (SO_3^{2-}) and bisulphite (HSO_3^-) detection, a non-emissive dinuclear Ir(III) complex linked via an azo group have been designed (Li et al. 2013). This complex shows a turn-on phosphorescent response toward SO_3^{2-} and HSO_3^- because the conjugation between these anions and the azo group produces the destruction of the azo group, which is responsible for the quenching of the luminescent.

2.3. Optical probes for the detection of biomolecules

Chromatographic methods are the most commonly used procedures for the detection of biomolecules. However, they are generally laborious and expensive for routine detection in a biochemistry laboratory. For this reason, as well as for the excellent spectroscopic and luminescent properties of the transition-metal complexes, the design of luminescent complexes has experienced an important progress in recent years. Table 5.6 summarizes the Ir(III) complexes used as optical probes for detecting biomolecules.

2.3.1. Amino acids and proteins

Thiol-containing amino acids and peptides. The development of optical probes for the selective detection of small thiol-containing biomolecules, such as cysteine (Cys), homocysteine (Hcy) and glutathione (GSH), has received considerable attention due to the crucial roles in physiological processes that these biological compounds play. Recently, several luminescent Ir(III) complexes have been utilized for recognition of these thiols. For example, Zhao *et al.* synthesized a cyclometalated Ir(III) complex containing an α,β-unsaturated ketone moiety as selective phosphorescent probe for thiol detection (Zhao et al. 2010). The sensing mechanism is based on the 1,4-addition of thiols to the α,β-unsaturated ketone, which produces the formation of the complex-thiol adduct accompanied by the significant increase in the emission intensity.

The Ir(III) complex $[Ir(bq)_2(phen\text{-}M)]^+$, with a maleimide group attached to the phenanthroline ligand, is another example of thiols probe that uses an α,β-unsaturated ketone as thiol receptor (Huang et al. 2012).

There are other more selective complexes that only respond to Cys and Hcy in the presence of various amino acids and GSH, for example, a series of Ir(III) complexes with a vinyl sulfide linkage as thiols receptor (Shiu et al. 2011), an ―off-on" luminescent probe (Tang et al. 2013), and a lab-on-a-molecule probe based on an Ir(III) complex (Chen and Schmittel 2013).

In addition, there are other complexes that only recognize Hcy over other amino acids (including Cys) and thiol-related peptides (including GSH) (Chen et al. 2007). In this case, the enhancement of the luminescent emission is also attributed to the formation of a thiazinane group by the reaction of the aldehyde group with the thiol.

Most recently, a structurally related Ir(III) complex with the same C^N ligands (pba) and therefore with aldehyde groups as recognition site, has also been synthesized as probe for Hcy and Cys, but with different responses to them (Xiong et al. 2010). In this case, the formation of thiazinane or thiazolidine derived from the reaction of the aldehyde with Hcy or Cys also takes place. However, a turn-off response and a red shift in the emission are observed. This behaviour is attributed to the change of the excited states from C^N ligand to N^N ligand, which does not occur in the previous example.

The Ir(III) complex $[Ir(pba)_2(pto)]PF_6$ is another example of probe for Cys and Hcy with a turn-on response (Ma et al. 2011). The aldehyde group of the complex reacts with Cys and Hcy to form the corresponding heterocyclic derivatives, which leads to the disappearance of the electron-withdrawing effect of the aldehyde group, with the consequent enhancement in the phosphorescent emission intensity.

Histidine and histidine-rich proteins. A series of cyclometalated Ir(III) solvato complexes $[Ir(C^N)_2(solv)_2]^+$ (solv = H_2O or CH_3CN), which contain weakly bound solvent ligands, was synthesized for the detection of histidine/histidine-rich proteins (Ma et al. 2008; Ma et al. 2013a). These complexes can bind covalently to histidine or proteins with a relatively high abundance of histidine residues through a substitution reaction of the labile solvent ligands, which induces a significant increase in the luminescent emission of the complexes. The specific sensing mechanism is based on the recognition of histidine through the covalent attachment to its imidazole moiety rather than to the carboxylate group of other natural amino acids. This binding

reduces the solvent mediated non-radiative decay of the excited state and therefore increases the emission of the complex.

Amino acid derivatives. α-Amino acid derivatives have been used for a wide range of chemical transformations, including synthesis of many kinds of bioactive compounds, such as β-lactam antibiotics and glycopeptides. Recently, an Ir(III) complex bearing two thiourea groups as binding sites and two acetyl-β-D-glucopyranosyl groups as chiral barriers, was reported as phosphorescent probe for the chiral recognition of α-amino acid derivatives (Li et al. 2014c). This complex shows an increase of phosphorescent emission upon addition of tetrabutyl ammonium salts of *t*-Boc-amino acids, while displays a decrease in the phosphorescent emission with 3,5-dinitrobenzoyl (DNB)-amino acids. This different behaviour is attributed to the emission quenching effects produced by the nitro groups of DNB.

Phosphorylated peptides. Optical probes for the detection of phosphorylated proteins have a great utility in the study of biological events. Kang *et al.* reported a phosphorylated peptides probe based on an Ir(III) complex coupled to a bis(Zn^{2+}–dipicolylamine) (Zn-DPA) unit (Kang et al. 2014). These Zn-DPA moieties act as an anion-binding site by the coordination to the two metal ions and the formation of a phenoxo-bridged dinuclear metal complex. Upon binding to several phosphorylated peptides, this complex shows an increase in the luminescence intensity. This turn-on response is the result of both the higher hydrophobicity of the surrounding environment of the complex upon binding to phosphorylated peptides and the reduction of the electrostatic repulsion between Zn^{2+} ions in the Zn-DPA unit. This complex can distinguish between phosphorylated peptides and non-phosphorylated peptides, anions, such as CO_3^{2-}, NO_3^- and SO_4^{2-}, and nucleotides including ATP.

Avidin. In the last few years, many transition-metal biotin complexes have been reported as luminescent probes for avidin. Moreover, in view of the interesting luminescent properties of Ir(III) complexes, several series of cyclometalated Ir(III) complexes with different C^N and N^N ligands, and containing one or two biotin moieties have been designed for avidin detection (Baschieri et al. 2014; Lo et al. 2004; Lo et al. 2006a; Lo and Lau 2007; Lo et al. 2005) (see Figure 5.8). In almost all cases, these Ir(III) complexes show a relevant emission intensity enhancement accompanied by emission lifetime elongation upon their binding to avidin. These effects are attributed to the specific binding of the biotin moiety to the hydrophobic binding sites of the protein.

In another study, a neutral Ir(III) complex with an energy acceptor, an energy donor, and biotin, showed a higher increase in luminescent intensity due to the intramolecular energy transfer between the donor and the acceptor, as well as the increased hydrophobicity after binding to avidin (Kwon et al. 2008b).

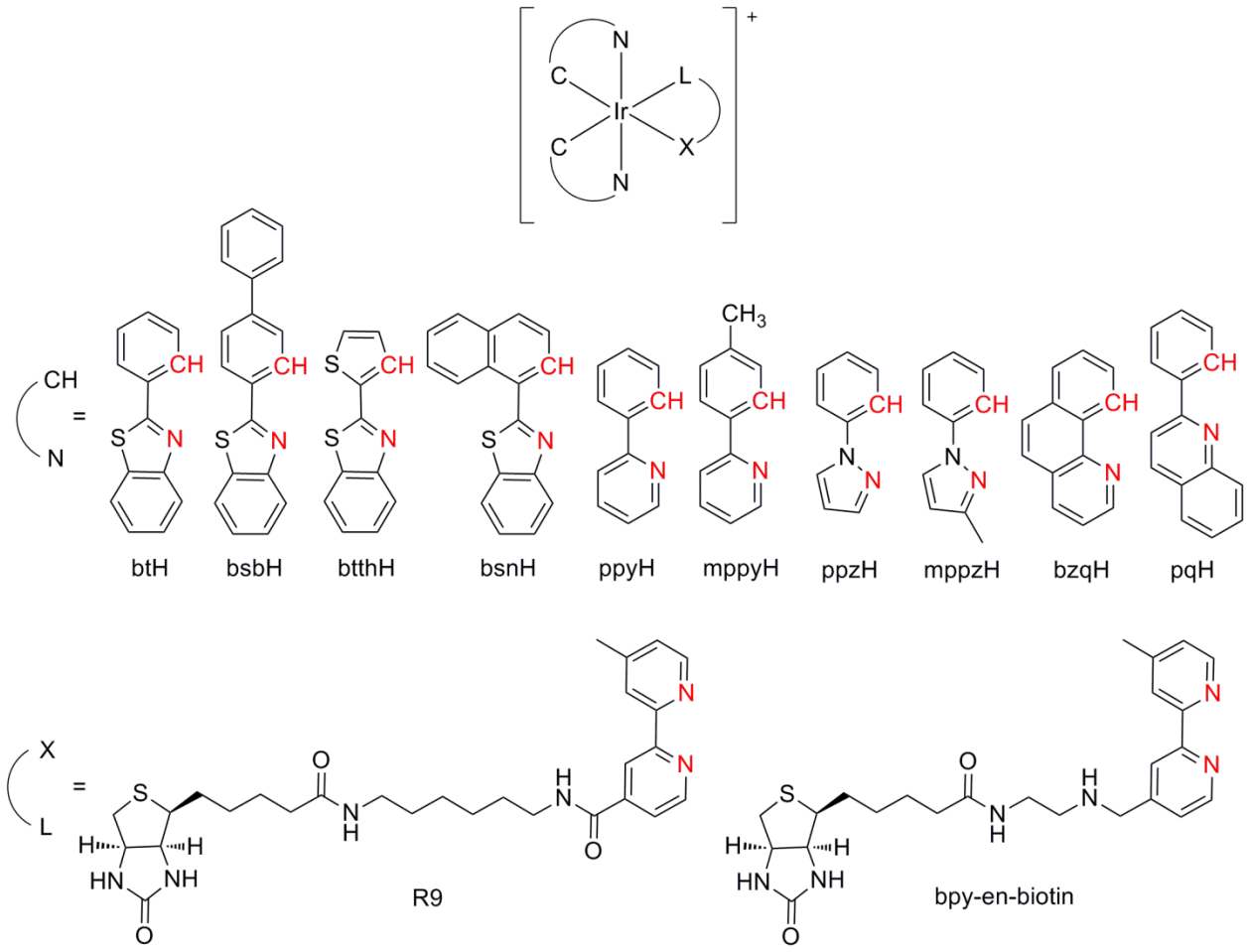

Figure 5.8. Cyclometalated Ir(III) complexes containing one biotin moiety for optical determination of avidin.

In contrast to this avidin-induced emission enhancement, Lo *et al.* synthesized an Ir(III)–biotin complex with dual-emissive properties, that shows a decrease in its high-energy (HE) emission intensity upon binding to avidin, while a new low-energy (LE) shoulder appears, thereby resulting in an isoemissive point (Lo et al. 2008). This complex is one of the few examples of luminescent Ir(III) complex with turn-off response toward avidin.

Estrogen receptors. Due to the important roles of estradiol and its receptor in female physiology, the design of new probes capable of binding to this receptor has attracted much attention. For example, various series of luminescent Ir(III) complexes containing bipyridine-estradiol

conjugates have been synthesized as probes for estrogen receptor alpha (ERα) (Lo et al. 2007; Lo et al. 2008) (see Figure 5.9). Upon addition of ERα, the emission intensities of all these complexes are increased about 1.3 to 4.8 times, the emission wavelengths do not change substantially, and the emission lifetimes are extended about 2.4 to 7.0 times. The emission enhancement and the lifetime elongation are attributed to the increase in hydrophobicity and rigidity of the local environment of the complexes after binding to ERα.

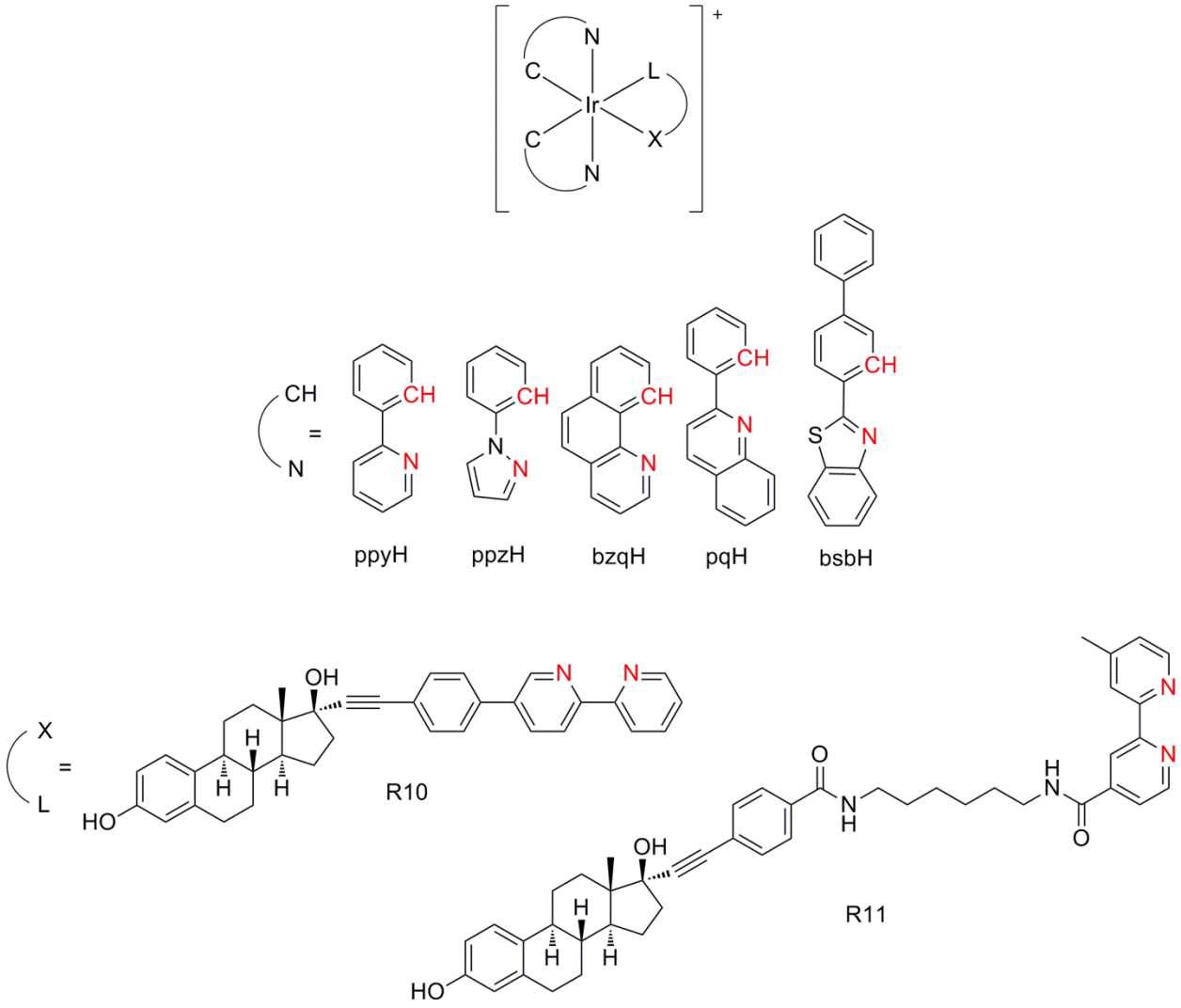

Figure 5.9. Ir(III) complexes containing bipyridine-estradiol conjugates for optical determination of estrogen receptors.

Lectins. The growing interest on studying the vital carbohydrate–protein interactions has triggered much attention in developing optical probes for lectins detection. Currently, several lectins probes have been designed by using sugar-substituted luminescent metal complexes (Li et al. 2011; Mandal et al. 2012).

BSA. In the past few years, a variety of luminescent Ir(III) complexes have been reported as probes for BSA, for example, luminescent cyclometalated iridium(III) complexes containing polypyridine indole moieties with different spacers (Lau et al. 2009) and with dpq or dpqa moieties (Zhang et al. 2010).

HSA. The precise detection and quantification of HSA have a high demand in clinical and biochemical applications. The attractive advantages of luminescence detection as well as the specific biomolecule-binding selectivity and spectroscopic properties of luminescent metal complexes have stimulated the development of optical probes for HSA based on these complexes.

Lo *et al.* synthesized a cyclometalated Ir(III)–polypyridine complex as HSA probe, which displays a dual emission wherein the intensity of LE emission band is higher than that of the HE band (Lo et al. 2008).

More recently, another Ir(III) complex has been reported as luminescent probe for selective detection of HSA in aqueous solution (Lu et al. 2014). This complex is weakly emissive and shows a great enhancement in its luminescence intensity with the addition of HSA. This turn-on response is attributed to the formation of effective Van der Waals interactions between the aromatic C^N and N^N ligands of the complex and the hydrophobic side chains of the binding pocket of the protein.

2.3.2. Nucleotides and nucleic acids

DNA. Interactions between transition-metal complexes and nucleic acid molecules have been the focus of many studies for years. The intercalation characteristics of Ir(III) complexes into DNA have attracted much attention due to the interesting photophysical and photochemical properties of luminescent Ir(III) complexes, which make it excellent luminescent intercalators for DNA.

For example, several cyclometalated Ir(III) dipyridoquinoxaline (dpq) and dipyridophenazine (dppz) complexes $[Ir(C^N)_2(N^N)]PF_6$, with different C^N ligands (2-phenylpyridine (Lo et al. 2006a), 1-phenylpyrazole, 7,8-benzoquinoline, and 2-phenylquinoline (Zhang et al. 2010)), were designed as luminescent intercalators for DNA. These complexes display emission enhancement in the presence of double-stranded calf thymus DNA (ct-DNA), which is attributed to the non-covalent intercalation of the complexes to the base pairs of the DNA molecules. In general, the intercalation of the complexes to the double-stranded DNA results in an increase in the hydrophobicity and the rigidity of the local surroundings of the complexes, as well as in the

protection of the ligands of the complexes from interacting with the water molecules. These factors lead to the enhancement of the emission intensity, which can be used to determine DNA.

In another study, a cyclometalated Ir(III) complex with a dithiocarbamate ligand was also used as a luminescent intercalator for DNA (Mukherjee et al. 2014). The interaction of this complex with DNA was evaluated using absorption and fluorescence measurements. In this case, the absorption band of the complex shows an increase with the binding of the complex to the DNA helix, whereas the fluorescence intensity exhibits a decreasing trend.

Previously, Herebian and Sheldrick designed a series of cationic complexes of the type $[Ir(\eta^5\text{-}C_5Me_5)(Aa)(dppz)]^{n+}$ (n = 1-3) containing S-coordinated amino acids (methionine or cysteine), and determined its DNA binding capacity by UV-Vis absorption (Herebian and Sheldrick 2002). Upon addition of ct-DNA, a decrease in absorbance and a bathochromic shift of the absorption maxima are observed, which is consistent with stable intercalative DNA binding for these complexes.

Thymidine 5'-triphosphate. Luminescent Ir(III) complexes have been also developed for the direct detection of nucleotides. Kwon *et al.* synthesized an ensemble sensor system, which shows a high sensitivity and selectivity for thymidine 5'-triphosphate among the nucleotides and other various anions (Kwon et al. 2008a). This system consists of an energy acceptor derived from an Ir(III) complex with a Zn^{2+}-DPA moiety and an energy donor derived from the *N*,*N*'-dicarbazolyl-3,5-benzene (mCP) attached to a Zn^{2+}-cyclen unit. The Zn-DPA moiety acts as binding site for the triphosphate unit of the nucleotide (due to its stronger binding affinity), whereas the Zn-cyclen group interacts mainly with the nucleobase unit.

Table 5.6. Ir(III) complexes used as optical probes for detecting biomolecules.

Analyte	Complex[a]	Detection[b]	Response[c]	λ_{exc} (nm)	λ_{em} (nm)	τ_{em} (μs)	LOD (μM)	Reference
Thiol-containing amino acids and peptides	$[Ir(ppy)_2(bpy\text{-}R26)]PF_6$	P	Ton	358	587	0.109	-	(Li et al. 2013)
	$[Ir(bq)_2(R27)]^+$	L	Ton	370	590	-	0.0143 (Hcy) 0.0164 (Cys) 0.0186 (GSH)	(Zhao et al. 2010)
	$[Ir(ppy)_2(phen\text{-}R28)]^+$	L	Ton	360	590	-	130 (Hcy) 150 (Cys)	(Huang et al. 2012)
	$[Ir(ppy)_2(phen\text{-}R29)]^+$	L	Ton	360	590	-	120 (Hcy) 150 (Cys)	(Shiu et al. 2011)
	[Ir(2-(thiophen-2-yl) quinoline)$_2$(pic-DNBS)]	P	Ton	-	603	-	-	(Shiu et al. 2011)
	$[Ir(ppy)_2(R30)]PF_6$	L	Ton	323	606	-	-	(Tang et al. 2013)
	$[Ir(pba)_2(acac)]$	P	Ton-B	360	615	0.106	-	(Chen and Schmittel 2013)
	$[Ir(pba)_2(bpy)]PF_6$	P	Toff-R	360	547	0.691	-	(Chen et al. 2007)
	$[Ir(pba)_2(pto)]PF_6$	P	Ton	-	565	-	-	(Xiong et al. 2010)
Histidine and histidine-rich proteins	$[Ir(pq)_2(H_2O)_2]OTf$	P	Ton	365	598	-	-	(Ma et al. 2011)
	$[Ir(ppy)_2(solv)_2]OTf$	L	Ton	-	505	-	-	(Ma et al. 2013a)

Amino acid derivatives	$[Ir(ppy)_2(bpy\text{-}(CH_2\text{-thiourea-acetylglucopyranosyl})_2)]Cl$	P	Ton (AMA) Toff (DNB)	372	560	-	-	(Ma et al. 2008)
Phosphorylated peptides	$[Ir(dfppy)_2(pic\text{-}ZnDPA)]$	P	Ton	380	475	-	-	(Li et al. 2014c)
Avidin	$[Ir(ppy)_2(R31)]PF_6$	L	Ton	-	606	0.09	-	(Kang et al. 2014)
	$[Ir(ppy)_2(R32)]PF_6$	L	Ton	-	520	1.40	-	(Lo et al. 2006a)
	$[Ir(ppy\text{-}4\text{-}CH_2NHC_2NH\text{-biotin})_2(Me_4\text{-phen})]PF_6$	L	Ton	-	545	1.94	-	(Lo et al. 2006a)
	$[Ir(ppy\text{-}4\text{-}CH_2NHC_6NH\text{-biotin})_2(Me_4\text{-phen})]PF_6$	L	Ton	-	546	1.63	-	(Lo and Lau 2007)
	$[Ir(ppy\text{-}4\text{-}CH_2NHC_2NH\text{-biotin})_2(Ph_2\text{-phen})]PF_6$	L	Ton	-	598	0.71	-	(Lo and Lau 2007)
	$[Ir(ppy\text{-}4\text{-}CH_2NHC_6NH\text{-biotin})_2(Ph_2\text{-phen})]PF_6$	L	Ton	-	600	0.54	-	(Lo and Lau 2007)
	$[Ir(ppy)_2(R33\text{-}C_{11}H_{22}\text{-NH-CO-biotin})]Cl$	L	Ton	380	476, 508	0.14	-	(Lo and Lau 2007)
	$[Ir(ppy)_2(R33\text{-}C_{11}H_{22}\text{-O-CO-biotin})]Cl$	L	Ton	380	476, 508	0.15	-	(Baschieri et al. 2014)
	$[Ir(ppy)_2(R33\text{-}C_6H_4\text{-NH-CO-biotin})]Cl$	L	Ton	380	478, 506	0.13	-	(Baschieri et al. 2014)
	$[Ir(ppy)_2(R33\text{-}C_6H_4\text{-O-CO-biotin})]Cl$	L	Ton	380	476, 508	0.13	-	(Baschieri et al. 2014)

Avidin	$[Ir(ppy)_2(R33\text{-}(C_6H_4)_2\text{-}NH\text{-}CO\text{-}biotin)]Cl$	L	Ton	380	476, 508	0.23	-	(Baschieri et al. 2014)
	$[Ir(ppy)_2(R33\text{-}(C_6H_4)_2\text{-}O\text{-}CO\text{-}biotin)]Cl$	L	Ton	380	476, 506	0.13	-	(Baschieri et al. 2014)
	$[Ir(bt)_2(R34)]PF_6$	L	Ton	-	570	1.31	-	(Baschieri et al. 2014)
	$[Ir(bsb)_2(R34)]PF_6$	L	Ton	-	556	5.84	-	(Lo et al. 2005)
	$[Ir(btth)_2(R34)]PF_6$	L	Ton	-	580	8.53	-	(Lo et al. 2005)
	$[Ir(bsn)_2(R34)]PF_6$	L	Ton	-	598	3.92	-	(Lo et al. 2005)
	$[Ir(ppy)_2(bpy\text{-}en\text{-}biotin)]PF_6$	L	Ton	-	576 (1)	0.48	-	(Lo et al. 2005)
	$[Ir(mppy)_2(bpy\text{-}en\text{-}biotin)]PF_6$	L	Ton	-	587	0.35	-	(Lo et al. 2004)
	$[Ir(ppz)_2(bpy\text{-}en\text{-}biotin)]PF_6$	L	Ton	-	560	0.92	-	(Lo et al. 2004)
	$[Ir(mppz)_2(bpy\text{-}en\text{-}biotin)]PF_6$	L	Ton	-	574	0.39	-	(Lo et al. 2004)
	$[Ir(bzq)_2(bpy\text{-}en\text{-}biotin)]PF_6$	L	Ton	-	577	0.47	-	(Lo et al. 2004)
	$[Ir(pq)_2(bpy\text{-}en\text{-}biotin)]PF_6$	L	Ton	-	554	2.95	-	(Lo et al. 2004)
	$[Ir(dfppy)_2(pic\text{-}OCH_2\text{-}Ph\text{-}OCH_2\text{-}mCP\text{-}CONHC_2H_4NH\text{-}biotin)]$	L	Ton	310	473, 498	0.49	$3.2\cdot10^{-5}$	(Lo et al. 2004)
	$[Ir(ppy\text{-}CH_2NH\text{-}C_4H_9)_2(bpy\text{-}CONH\text{-}C6\text{-}NH\text{-}biotin)]PF_6$	L	R	350	492	2.06	-	(Kwon et al. 2008b)

Estrogen receptor α (ERα)	[Ir(ppy-CH_2NH-C_4H_9)$_2$(bpy-CONH-C6-Ph-estradiol)]PF_6	L (I&τ)	Ton	350	490, 520, 598	1.13	-	(Lo et al. 2008)
	[Ir(ppy)$_2$(R35)]PF_6	L (I&τ)	Ton	257-334	605	0.39	-	(Lo et al. 2008)
	[Ir(ppz)$_2$(R35)]PF_6	L (I&τ)	Ton	257-334	577	0.68	-	(Lo et al. 2007)
	[Ir(bzq)$_2$(R35)]PF_6	L (I&τ)	Ton	257-334	608	0.33	-	(Lo et al. 2007)
	[Ir(pq)$_2$(R35)]PF_6	L (I&τ)	Ton	257-334	564	1.40	-	(Lo et al. 2007)
	[Ir(bsb)$_2$(R35)]PF_6	L (I&τ)	Ton	257-334	554	4.93	-	(Lo et al. 2007)
	[Ir(ppy)$_2$(R36)]PF_6	L (I&τ)	Ton	257-334	604	0.24	-	(Lo et al. 2007)
	[Ir(ppz)$_2$(R36)]PF_6	L (I&τ)	Ton	257-334	588	0.31	-	(Lo et al. 2007)
	[Ir(bzq)$_2$(R36)]PF_6	L (I&τ)	Ton	257-334	606	0.18	-	(Lo et al. 2007)
	[Ir(pq)$_2$(R36)]PF_6	L (I&τ)	Ton	257-334	582	0.56	-	(Lo et al. 2007)
	[Ir(bsb)$_2$(R36)]PF_6	L (I&τ)	Ton	257-334	554	4.02	-	(Lo et al. 2007)

Lectins	$[Ir(ppy)_2(bpy\text{-}(methoxymethyl\text{-}triazol\text{-}mannose)_2)]Cl$	F	Ton	390	600	78.32	-	(Lo et al. 2007)
	$[Ir(pq)_2(bpy\text{-}(methylthio\text{-}glucose)_2)]Cl$	L	Ton	430	557	1.02	-	(Mandal et al. 2012)
BSA	$[Ir(ppy)_2(bpy\text{-}ind)]PF_6$	L	Ton	350	614	0.28	-	(Li et al. 2011)
	$[Ir(ppy)_2(bpy\text{-}C6\text{-}ind)]PF_6$	L	Ton	350	615	0.24	-	(Lau et al. 2009)
	$[Ir(bzq)_2(bpy\text{-}ind)]PF_6$	L	Ton	350	613	0.21	-	(Lau et al. 2009)
	$[Ir(bzq)_2(bpy\text{-}C6\text{-}ind)]PF_6$	L	Ton	350	616	0.17	-	(Lau et al. 2009)
	$[Ir(pq)_2(bpy\text{-}ind)]PF_6$	L	Ton	350	580	0.51	-	(Lau et al. 2009)
	$[Ir(pq)_2(bpy\text{-}C6\text{-}ind)]PF_6$	L	Ton	350	596	0.46	-	(Lau et al. 2009)
	$[Ir(ppz)_2(dpq)]PF_6$	L	Ton	350	576	0.35	-	(Lau et al. 2009)
	$[Ir(ppz)_2(dpqa)]PF_6$	L	Ton	350	589	0.05	-	(Zhang et al. 2010)
	$[Ir(bzq)_2(dpq)]PF_6$	L	Ton	350	600	0.26	-	(Zhang et al. 2010)
	$[Ir(bzq)_2(dpqa)]PF_6$	L	Ton	350	606	0.03	-	(Zhang et al. 2010)
	$[Ir(pq)_2(dpq)]PF_6$	L	Ton	350	577	1.24	-	(Zhang et al. 2010)
	$[Ir(pq)_2(dpqa)]PF_6$	L	Ton	350	564	0.22	-	(Zhang et al. 2010)
	$[Ir(ppy)_2(Morphcdt)]$	UV–Vis, F	Toff	280	340	-	-	(Zhang et al. 2010)
HSA	$[Ir(ppy\text{-}CH_2NH\text{-}C_4H_9)_2(bpy\text{-}CONH\text{-}C_{18}H_{37})]PF_6$	L	Ton	350	491, 521, 610	1.98	-	(Mukherjee et al. 2014)
	$[Ir(ppy)_2(R37)]PF_6$	L	Ton	310	575, 550	4.618	0.05	(Lo et al. 2008)

DNA	$[Ir(ppy)_2(dpq)]PF_6$	UV–Vis, L	Ton (L)	-	601	0.34	-	(Lu et al. 2014)
	$[Ir(ppy)_2(dpqa)]PF_6$	UV–Vis, L	Ton (L)	-	608	0.13	-	(Lo et al. 2006a)
	$[Ir(ppy)_2(dppz)]PF_6$	UV–Vis, L	Ton (L)	-	630	0.077	-	(Lo et al. 2006a)
	$[Ir(ppy)_2(dppn)]PF_6$	UV–Vis, L	Ton (L)	-	588	0.36	-	(Lo et al. 2006a)
	$[Ir(ppz)_2(dpq)]PF_6$	L	Ton	350	576	0.35	-	(Lo et al. 2006a)
	$[Ir(bzq)_2(dpq)]PF_6$	L	Ton	350	600	0.26	-	(Zhang et al. 2010)
	$[Ir(pq)_2(dpq)]PF_6$	L	Ton	350	577	1.24	-	(Zhang et al. 2010)
	$[Ir(bzq)_2(dpqa)]PF_6$	L	Ton	350	606	0.028	-	(Zhang et al. 2010)
	$[Ir(ppy)_2(Morphcdt)]$	UV–Vis, F	Ton (UV) Toff (F)	522	612	-	-	(Zhang et al. 2010)
Nucleotides	$[Ir(dfppy)_2(pic\text{-}OCH_2\text{-}CONHC_2H_4\text{-}Ph\text{-}(Zn\text{-}DPA)_2)]$	P	Ton	310	475, 527	-	-	(Mukherjee et al. 2014)

Notes: [a] See Section 5.

[b] UV-Vis is UV-Vis absorption; L is Luminescence, it is used when the authors did not clarify if fluorescence (F) or phosphorescence (P) occurred; I = Intensity; τ = Lifetime measurements.

[c] Ton is Turn-on; Toff is Turn-off; R is Ratiometric.

2.4. Optical probes for the detection of other small molecules

Table 5.7 summarizes the Ir(III) complexes used as optical probes for detecting other small molecules.

2.4.1. Explosives

The nitro-explosives, TNP (2,4,6-trinitrophenol) and TNT (2,4,6-trinitroluene) are by far the most studied. Recently, the use of phosphorescent Ir(III) complexes as explosive chemosensors has gained increasing attention due to their strong luminescent properties.

Fei *et al.* reported the highly efficient red phosphorescent Ir(III) complex [Ir(SBFIQ)$_2$(acac)] for TNT sensing, based on the quenching of its luminescent emission by TNT (Fei et al. 2014). The long excited-state lifetime of the complex and the suitable matching of its lowest unoccupied molecular orbital (LUMO) with TNT benefit the electron transfer from the complex to the TNT molecules, which enhances the luminescence quenching and the sensory capacity.

Hou *et al.* synthesized a cationic Ir(III) complex with AIE (aggregation-induced emission) characteristics, which exhibits highly sensitive and selective detection of TNP by emission quenching (Hou et al. 2014). In this case, the strong interaction between this complex and TNP facilitates the electron transfer and the energy transfer from the complex to TNP, and thus enhances the quenching response.

2.4.2. Free radicals

In the past few years, new photoluminescence-based sensors have been developed to directly monitor free radicals. Yoshikawa *et al.* developed a photofunctional Ir(III) complex containing a radical ligand (iminonitroxide bipyridine), which can act as a preluminescent probe for carbon-centred free radicals (Yoshikawa et al. 2010). Although the luminescent emission of this complex is nearly completely quenched by the nitronyl radical on the ligand moiety, it suffers a strong enhancement after the reaction with the carbon-centred free radicals, generated from azobisisobutyronitrile (AIBN) by UV irradiation. This increase in luminescence is due to the trapping of the free radical at the nitronyl-radical moiety and the consequent elimination of the radical in the complex.

Table 5.7. Ir(III) complexes used as optical probes for detecting others small molecules.

Analyte	Complex[a]	Detection[b]	Response[c]	λ_{exc} (nm)	λ_{em} (nm)	τ_{em} (µs)	LOD (µM)	Reference
TNT	$[Ir(SBFIQ)_2(acac)]$	P	Toff	560	652	0.309	< 1.86	(Kwon et al. 2008a)
TNP	$[Ir(ppy)_2(R38)]PF_6$	P	Toff	365	560	0.20	-	(Fei et al. 2014)
Free radicals	$[Ir(ppy)_2(MebpyIN)]Cl$	L	Ton	362	620	-	$1.2 \cdot 10^5$	(Hou et al. 2014)
H_2O_2	$[Ir(Bthc–bpe)_2(acac)]$	P	Toff	460	560	-	-	(Yoshikawa et al. 2010)
n-butylamine	$[Ir(ppy)_2(bpy\text{-}dicarboxylate)]PF_6$	UV–Vis	Blue shift	352	431	-	-	(Li et al. 2014a)
AgOTf	$cis\text{-}[Ir(ppy)_2(4\text{-}PyNH_2)_2]NO_3$	L	Ton	258	496	0.300	-	(Mothajit et al. 2014)
HOCl	$[Ir(ptpy)_2(R39)]PF_6$	P	Ton	400	620	-	0.016	(Sie et al. 2008)

Notes: [a] See Section 5.

[b] UV-Vis is UV-Vis absorption; L is Luminescence, it is used when the authors did not clarify if fluorescence (F) or phosphorescence (P) occurred.

[c] Ton is Turn-on; Toff is Turn-off.

2.4.3. H_2O_2

Recently, the use of heavy-metal complexes with long emission lifetimes as H_2O_2-sensitive probes has attracted great interest because these complexes overcome the main drawback of the amply used organic dye-based indicators, in which the signal could be significantly interfered by autofluorescence from complicated biological samples. For example, a neutral Ir(III) complex that incorporates a benzeneboronic acid pinacol ester moiety as a specific recognition site into a cyclometalated ligand has been employed as phosphorescent probe for H_2O_2 (Li et al. 2014a). This boronic ester is efficiently removed upon reaction with H_2O_2 to release the phenol group, causing changes in the emission intensity of the complex that is correlated to the H_2O_2 concentration.

2.4.4. Amines

Recently, phosphorescent iridium(III) complexes have also been reported as probes for detection of amines. For example, an Ir(III) complex with two methyl carboxylate groups connected to a bipyridine ligand was synthesized as amine probe (Mothajit et al. 2014). The ester moieties can act as amine recognition groups in the presence of an acid catalyst.

2.4.5. Silver salts

The silver trifluoromethanesulfonate (AgOTf) is one of the most used silver salts as reagents in many chemical reactions, such as the glycosylation of glycosyl halides, the deprotection of protected thiols, or the substitution of halides by triflate. Among the few methods for the determination of silver salts, the iridium(III) complex *cis*-$[Ir(ppy)_2(4\text{-}pyNH_2)_2]NO_3$, with two 4-aminopyridine ligands, showed a sensing response toward AgOTf in methanol (Sie et al. 2008). Upon the addition of AgOTf in methanol, an increase in the emission intensity of the complex is observed, which is attributed to the interaction between the Ag^+ (Lewis acid) and the amine nitrogen atom of the coordinated ligands (Lewis base).

2.4.6. Hypochlorous acid (HOCl)

Hypochlorous acid is a normal by-product of cellular metabolism. Therefore, the design of new optical receptors for its sensitive and selective determination has experienced important advances in the last few years. Recently, Lu *et al.* have designed an Ir(III) complex substituted with an *o*-nitroanilino group (4-amino-3-nitrophenyl) as probe for HOCl (Lu and Nabeshima 2014). This complex exhibits a very weak luminescent emission due to the PET effect imposed

by the electron-rich *o*-nitroanilino moiety. However, upon the addition of HOCl, the *o*-nitroanilino is oxidized, followed by the cleavage of the 4-amino-3-nitrophenyloxy moiety and the generation of a hydroxymethyl group appended to the complex, which, without the PET effect, exhibits strong luminescence. This turn-on emission response is highly specific to HOCl among several reactive oxygen and nitrogen species.

3. Ir(III) Used in the Development of Sensing Phases

3.1. Sensing phases for the detection of gases

3.1.1. Oxygen

The main optical mechanism used in optical oxygen detection is the luminescence quenching. The first characterization of oxygen sensing materials using an Ir(III) complex ([$Ir(ppy)_3$]) immobilized in polystyrene (PS) is found in 1994 (Vander Donckt et al. 1994). Later on, four Ir(III) complexes synthesized in previous works were also characterized as oxygen optical sensor in solid phase by their immobilization in poly(ethyleneglycol) ethyl ether methacrylate (pPEGMA) (Di Marco et al. 1998). These four Ir(III) cyclometalated complexes, which are shown in Table 5.8, showed intense luminescence spectra when they are immobilized, with maximums in the range 500−650 nm and lifetimes between 1 and 2 μs, which agree with data in solution. Monoexponential decay times and linear Stern-Volmer (SV) fits suggested good compatibility between the pPEGMA and the dyes (Di Marco et al. 1998). These results confirmed that Ir(III) cyclometalated complexes could be used as a valid alternative to the commonly used Ru(II) for optical sensors (Di Marco et al. 1998).

Another example that many phosphorescent emitters in organic light-emitting devices (OLEDs) can be used for oxygen sensing is the work developed by Huynh *et al*. (Huynh et al. 2005). They also observed that the excited states generated during the electroluminescence of some Ir(III) complexes exhibited long lifetimes (in the microsecond regime) and therefore could be a promising alternative for optical oxygen sensing. Based on previous procedures (Nazeeruddin et al. 2003; Sprouse et al. 1984; Tamayo et al. 2003), the complexes $[Ir(ppy)_2(CN)_2]Bu_4N$ and $[Ir(ppy)_2(acac)]$, and the polymer poly((*n*-butylamino) thionylphosphazene (*n*BuPTP) (Liang and Manners 1991; Ni et al. 1996) were synthesized. The *n*BuPTP was used for the immobilization of the complexes since it had previously shown good

results for oxygen sensing with other types of complexes (Huynh et al. 2005). The results showed a linear Stern-Volmer (SV) plot, where the sensitivity of complex $[Ir(ppy)_2(acac)]$ was about two times higher than those provides by $[Ir(ppy)_2(CN)_2]Bu_4N$. It can be explained by its longer lifetime (4.78 vs. 1.40 µs), and their good photostability (Huynh et al. 2005). The complex $[Ir(ppy)_2(acac)]$ was especially susceptible to quenching, even compared to other dyes with longer lifetime, such as Pt(II) porphyrin immobilized in the same polymer (102 µs).

In another work, $[Ir(ppy\text{-}NPh_2)_3]$ in ethyl cellulose (EC) was characterized for oxygen sensing and compared to $[Ir(ppy)_3]$. The main difference is a red shift on the emission of $[Ir(ppy\text{-}NPh_2)_3]$, due to the electron-donating properties of the diphenylamino substitutions. It results in smaller MLCT character and in a longer emission decay time (Mak et al. 2009).

Table 5.8 summarises the oxygen optical sensing phases that contain an Ir(III) complex, and Figure 5.10 shows the chemical structures of the most relevant Ir(III) complexes used in the development of optical oxygen sensing phases.

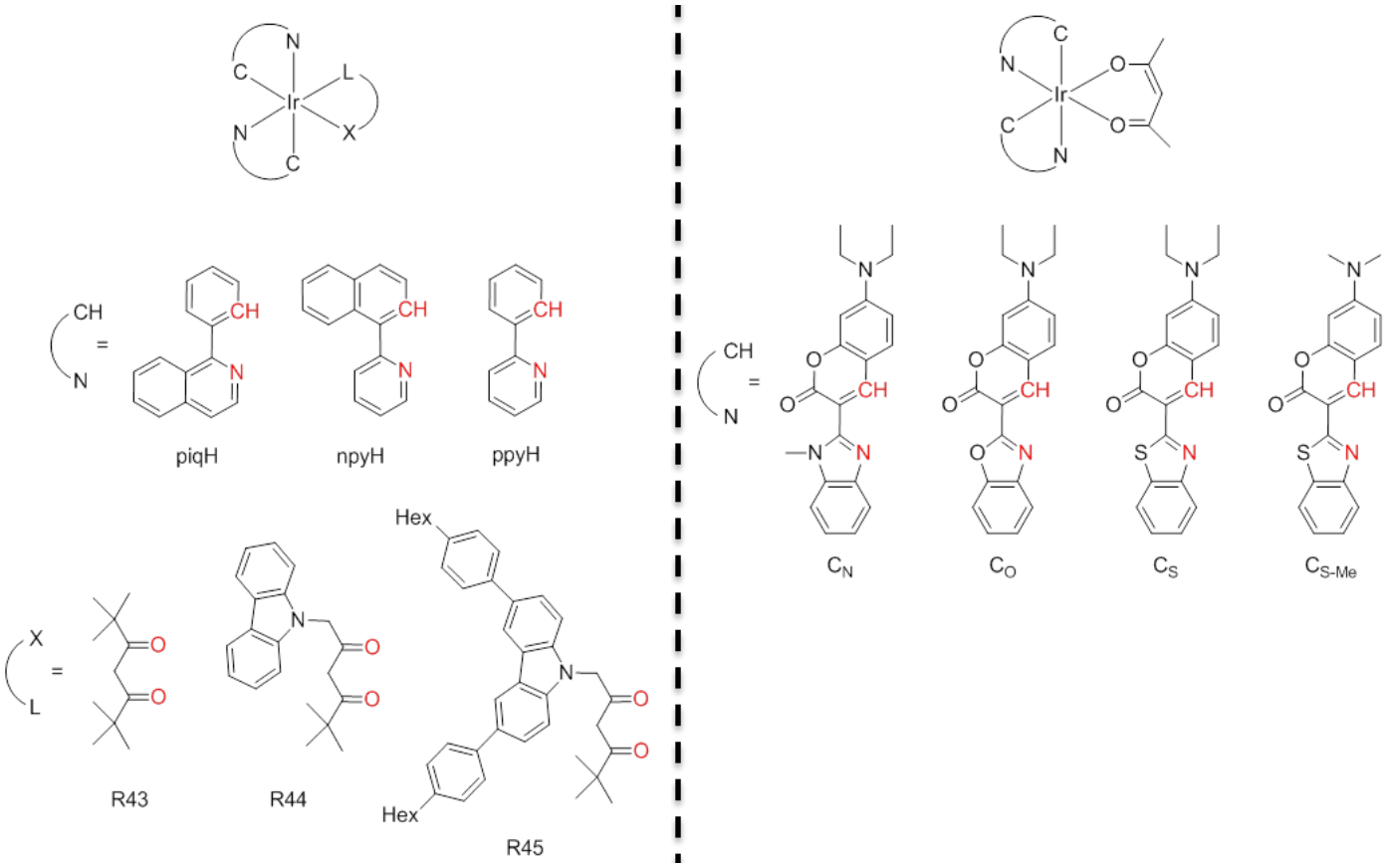

Figure 5.10. Chemical structure of the most relevant Ir(III) complexes used in the development of optical oxygen sensing films.

Table 5.8. Optical sensing layers based on Ir(III) complexes for analysing oxygen.

Complex[a]	Solid support[b]	λ_{ex} (nm)	λ_{em} (nm)	τ_0 (µs)[c]	I_0/I	k_{SV} (bar^{-1})	Reference
$[Ir(ppy)_3]$	PS	-	-	-	-	-	(Vander Donckt et al. 1994)
	nBuPTP	370	510	1.40	3.36	-	(Huynh et al. 2005)
	Ps-*co*-TFEM	346	511	-	15.3	15.02	(Amao et al. 2001a)
	PDMS(C) + PS	440	510	1.0	-	1.89	(Köse et al. 2005)
	PS	-	-	1.2 (A)	-	0.05	(Tian et al. 2010)
$[Ir(ppy)_2(vpy)(Cl)]$	PDMS (C)	265, 396	509, 537	0.190	-	-	(DeRosa et al. 2003b)
$[Ir(ppy)_2(dpt\text{-}NH_2)]PF_6$	pPEGMA	-	610	2.10	-	1.45	(Di Marco et al. 1998)
$[Ir(R40)(R41)](PF_6)_2$	pPEGMA	-	620	1.40	-	1.54	(Di Marco et al. 1998)
$[Ir(R41)_2]PF_6$	pPEGMA	-	525	1.13	-	1.58	(Di Marco et al. 1998)
$[(ppy)_2Ir(dpt\text{-}cy\text{-}dpt)Ir(ppy)_2](PF_6)_2$	pPEGMA	-	-	1.30	-	1.58	(Di Marco et al. 1998)
$[Ir(ppy)_2(CN)_2]Bu_4N$	nBuPTP	340	470	4.78	6.04	-	(Huynh et al. 2005)
$[Ir(ppy)_2(bpy\text{-}(DMA)_2)]Cl$	PS	400	526	-	2.4	1.20	(Fernández-Sánchez et al. 2007)
	AlOOH	460	530	-	-	191.90	(Fernández-Sánchez et al. 2006)
$[Ir(ppy)_2(NCS)_2]TBA$	PS	402	529	-	1.3	0.34	(Fernández-Sánchez et al. 2007)
	AlOOH	402	530	-	-	34.90	(Fernández-Sánchez et al. 2006)
$[Ir(ppy)_2(CN)_2]TBA$	PS	398	528	-	1.8	0.70	(Fernández-Sánchez et al. 2007)
	AlOOH	398	530	-	-	87.10	(Fernández-Sánchez et al. 2006)

$[Ir(ppy)_2(bpy\text{-}(R42)_2)]Cl$	PS	494	665	102	-	19.40	(Medina-Castillo et al. 2007)
	AlOOH	494	665	22	-	52.10	(Medina-Castillo et al. 2007)
$[Ir(C_S)_2(acac)]$	PS	448, 477	566	9.1	-	4.30	(Borisov and Klimant 2007)
	EC+UPNP	980	566	-	-	-	(Achatz et al. 2011)
$[Ir(C_O)_2(acac)]$	PS	444, 472	554	7.7	-	4.31	(Borisov and Klimant 2007)
$[Ir(C_{S\text{-}Me})_2(acac)]$	PS	446, 475	566	10.4	-	5.18	(Borisov and Klimant 2007)
$[Ir(C_N)_2(acac)]$	PS	421, 455	544	7.5	-	3.95	(Borisov and Klimant 2007)
$[(C_S)_2Ir(\mu\text{-}Cl)_2Ir(C_S)_2]$	PS	457, 484	588	12.6	-	7.01	(Borisov and Klimant 2007)
$[(C_N)_2Ir(\mu\text{-}Cl)_2Ir(C_N)_2]$	PS	432, 463	567	8.8	-	5.73	(Borisov and Klimant 2007)
$[Ir(btpy)_3]$	PS	-	-	6.6 (A)	-	0.22	(Tian et al. 2010)
$[Ir(ppy\text{-}NPh_2)_3]$	EC	-	-	-	-	5.20	(Mak et al. 2009)
$[Ir(3\text{-}(2\text{-}pyridyl)benzoate)_3]$	Zn-CP (C)	385	538	-	-	-	(Xie et al. 2009)
$Ir(4\text{-}(2\text{-}pyridyl)benzoate)_3]$	Zn-CP (C)	400	565	-	-	-	(Xie et al. 2009)
	Zn-CP (C)	385	538	-	-	-	(Xie et al. 2009)
$[Ir(mebtp)_3]$	FIB	296	595	9.2	-	-	(Carlson et al. 2010)
$[Ir(piq)_2(R43)]$	PS	293, 344, 419, 484	630	1.1 (A)	-	0.06	(Tian et al. 2010)
$[Ir(npy)_2(R43)]$	PS	240, 300, 458, 497	600	3.6 (A)	-	0.13	(Tian et al. 2010)
$[Ir(ppy)_2(R43)]$	PS	260, 341, 412	522	1.2 (A)	-	0.07	(Tian et al. 2010)

$[Ir(piq)_2(R44)]$	PS	247, 291, 341, 478	624	-	-	-	(Tian et al. 2010)
$[Ir(npy)_2(R44)]$	PS	242, 296, 346, 490	597	3.4 (A)	-	0.15	(Tian et al. 2010)
$[Ir(ppy)_2(R44)]$	PS	240, 262, 345, 462	521	1.3 (A)	-	0.06	(Tian et al. 2010)
$[Ir(piq)_2(R45)]$	PS	264, 299, 359, 481	625	-	-	-	(Tian et al. 2010)
$[Ir(npy)_2(R45)]$	PS	262, 296, 356, 490	595	3.3 (A)	-	0.13	(Tian et al. 2010)
$[Ir(ppy)_2(R45)]$	PS	235, 262, 291, 466	522	1.1 (A)	-	0.06	(Tian et al. 2010)
$[Ir(fppy)_3]$	PS	-	-	1.0 (A)	-	0.04	(Tian et al. 2010)
$[Ir(dfppy)_2(bpy\text{-}(DMA)_2)]PF_6$	PS	385	585	-	5.0	358	(Marin-Suarezdel Toro et al. 2010)
	AlOOH	350	490	3.74	47.6	1231	(Marin-Suarezdel Toro et al. 2010; Medina-Rodríguez et al. 2013b)
$[Ir(phen\text{-}Ph_2)(ppy)_2]PF_6$	PS	300	530	-	7.3	164	(Marin-Suarezdel Toro et al. 2010)
	AlOOH	330	549	-	4.3	2848	(Marin-Suarezdel Toro et al. 2010)

[Ir(phen-Ph_2)(dfppy)$_2$]PF_6	PS	305	510	-	8.2	72	(Marin-Suarezdel Toro et al. 2010)
	AlOOH	340	512	8.40	13.5	222	(Marin-Suarezdel Toro et al. 2010; Medina-Rodríguez et al. 2013b)
[Ir(ppy)$_2$(bpy-Br)]PF_6	PS	300	520	-	2.0	313	(Marin-Suarezdel Toro et al. 2010)
	AlOOH	330	545	-	1.2	561	(Marin-Suarezdel Toro et al. 2010)
[Ir(fppy)$_2$(*t*-Bu-iCN)$_2$]CF_3SO_3	Silamine D208-EDA (C) + MC	239, 263, 317	461	20.6	-	0.502[d]	(Habibagahi et al. 2009)
[Ir(ptpy)$_2$(*t*-Bu-iCN)$_2$]CF_3SO_3	Silamine D208-EDA + MC	260	458	35.6	-	0.299[d]	(Habibagahi et al. 2009)
[Ir(dfppy-COOMe)$_2$(pic-DMA)]	PS	303	470	-	-	134.65	(Marín-Suárez et al. 2012)
	AlOOH	335	479	-	-	780.77	(Marín-Suárez et al. 2012)
[Ir(dfppy-COOMe)$_2$(pic)]	PS	300	470	-	-	150.30	(Marín-Suárez et al. 2012)
	AlOOH	335	467	-	-	667.06	(Marín-Suárez et al. 2012)
[Ir(dfppy-$COCF_3$)$_2$(pic)]	PS	300	465	-	-	178.41	(Marín-Suárez et al. 2012)
	AlOOH	340	465	1.88	-	748.66	(Marín-Suárez et al. 2012; Medina-Rodríguez et al. 2013b)

$[Ir(ppy)_2(H_2dcbpy)]PF_6$	Zn-CP (C)	406	613	-	-	0.83	(Ho et al. 2012)
	Zn-CP (C)	-	596	-	-	3.55	(Cheng et al. 2014)
	Cd-CP (C)	406	595	-	-	2.82	(Ho et al. 2012)
	Co-CP (C)	406	587	-	-	1.33	(Ho et al. 2012)
	Ni-CP (C)	406	600	-	-	1.11	(Ho et al. 2012)
$[Ir(dpq)_2(Cl)]_2$	P(phen-TFEMA) (C)	405	650	1.15	2.5	-	(Jin et al. 2013)
$[Ir(npy)_2(bpy\text{-}pyr)]PF_6$	PS	336	585	-	-	294	(Denisov et al. 2014)
	AlOOH	340	585	-	-	1103	(Denisov et al. 2014)

Notes: The response of all of these sensing layers is luminescence quenching.

[a] See Section 5.

[b] Zn-CP: Zn Coordination polymer; Cd-CP: Cd Coordination polymer; Co-CP: Co Coordination polymer; Ni-CP: Ni Coordination polymer.

[c] A = At 50 mbar air pressure.

[d] Stern-Volmer constants determined as a function of Silamine:MC ratio and therefore the value is a non-dimensional number.

Versatility of the Ir(III) chemistry. Several authors have exploited the versatility of Ir(III) to fulfil three main objectives: (i) tune the color emission to simplify the measurement setup to allow the development of dual measurements (see Section 3.4 Sensing phases for multiparametric sensing); (ii) attach covalently the iridium complex to solid supports to avoid aggregation and leaching of the dye and to improve sensor performance; and (iii) improve the compatibility between the complex and the solid support to decrease dye aggregation effects.

Cyclometalated Ir(III) complexes with coumarins ligand were developed by Borisov *et al*. (Borisov and Klimant 2007) and DeRosa *et al* (DeRosa et al. 2004) to be used as oxygen probes. Because of the effect of the substituent of coumarins in the spectral properties, Borisov *et. al* synthesized and investigated the influence of three different ligands (C_N as the shortest waved, C_O and C_S as the long-waved ligand) and derivatives in the development of oxygen probes (Borisov and Klimant 2007). These Ir(III) coumarins showed excellent brightness properties compared with traditional Ru(II) oxygen complexes. In addition, they show good phosphorescence decay times (10 µs), relatively high quantum yield (0.34-0.54), and their photophysical characteristics can be tuned by changing the dyes, thus they are also excellent candidates for dual sensing. The use of these new type of dyes was investigated as oxygen probes by immobilizing them in PS and comparing to Ru-dpp and PtTFPP (platinum(II)-5,10,-15,20-tetrakis-(2,3,4,5,6-pentafluorphenyl)-porphyrin). As it is common when immobilized on solid support, the coumarins dyes showed a red shift in their emission spectra compared to solution but maintained their adequate properties to act as oxygen probe: high brightness, good oxygen sensitivity, and low temperature cross-sensitivity. However, the main drawback of these types of complexes was the photostability, making them not suitable for long measurement or for high power excitation such as microscopy or microsensors, but, due to their high brightness, they are specially recommended when rapid response or high signal-to-noise ratios are required.

The most photostable coumarin complex was $[Ir(C_S)_2(acac)]$ applied as a smart approach for ratiometric oxygen sensing. Due to the absorbance at 468 nm and maximum emission at 568 nm, this complex supported in ethylcellulose was excited with upconversion nanoparticles (UCNPs) made of $NaYF_4$:Yb,Tm, whose emission acts as light source for the Ir coumarins. The emission of UCNPs, upon excitation in the NIR, at 455, 475 and 630 nm, overlaps absorption but not emission spectra of $[Ir(C_S)_2(acac)]$, making this approach suitable to obtain a NIR-excited oxygen sensor and avoid background signals, which are especially strong in samples such as serum, produced when exciting in the blue of UV region of the spectra (Achatz et al. 2011).

The properties of Ir(III) complexes were also exploited for the covalent attachment of iridium luminophores to a silicone polymer, and their properties were compared to sensors in which the luminophore is dispersed within the polymer matrix (DeRosa et al. 2003a). The same authors utilized the nonionic complex $[Ir(ppy)_2(vpy)(Cl)]$ for its covalent attachment to a given silicone matrix, in this case poly(dimethylsiloxane) (PDMS) (DeRosa et al. 2003b). The selected strategy was a transition-metal-catalysed hydrosilation for creating carbon−silicon bonds between the silicone and the dye possessing a pendent vinyl group.

In fact, the use of linkable polymers and dyes is common to avoid aggregation and leaching of the dye and to improve sensor performance. In another example, linear PDMS was end-functionalized with $[Ir(ppy)_3]$ (Köse et al. 2005). Because the Ir-containing polymers are not cross-linked, they were blended with polystyrene (PS) in order to improve their mechanical stability. The heterogeneity of blends with different composition was studied based on oxygen quenching, demonstrating its applicability to study the gas permeability with high spatial resolution.

Cross-linking advantages to avoid phase separation and high permeability were combined in the synthesis of P(Ir-TFEMA) copolymer (Jin et al. 2013). The feed molar ratio of the copolymerization between TFEMA and cyclometalated iridium(III) complex had minimal influence on oxygen sensing behaviour, and the material was applied to analyse oxygen demand (DO) during cephalosporin C fermentation process. Instead of using spin coating to produce the oxygen sensing films, the authors employed the screen-printing technique, which is expected to make industrial-scale production possible. The obtained films remained photostable after irradiation every 10 s for 4 h. Because of the covalent attachment, no leaching was observed either under water or ambient air, confirming the utility of the films for long-time monitoring in fermentation process.

Other authors have exploited the versatility of Ir(III) to decrease dye aggregation effects by improving the compatibility between the matrix materials and the complex. It was already shown that lipophilic complexes, such as $[Ir(ppy)_2(bpy\text{-}(R42)_2)]Cl$ (Medina-Castillo et al. 2007), have shown improved quantum yield in polymeric complex. Therefore, it is possible to increase dye solubility by tuning the counter ion in the neutral Ir(III) complex. To investigate this, $[Ir(mebtp)_3]$ was immobilized in poly(1,1,1,3,3,3-hexafluoroisopropylmethacrylate-co-1*H*,1*H*-dihydroperfluorobutyl-methacrylate) (FIB) and compared with other complexes. They also

carried out DFT calculations in order to understand the variances in the relative quenching rate observed between them (Carlson et al. 2010).

In a most in-depth study, a series of heterocyclic Ir(III) complexes that emit from green to red were synthesized and compared with three commercially available iridium complexes. They were synthesized with different decorations in order to gradually increase the unsymmetrical architecture and try to identify structure–property relationships respect its oxygen sensitivity (Tian et al. 2010). The dyes were not very efficiently quenched by oxygen, except those based on the npy ligand. These red-emitting npy complexes showed much higher oxygen sensitivity than the green complexes with ppy ligands, as it is expected for complexes possessing longer lifetimes.

Effect of the solid support. The permeability of the support where oxygen dyes are immobilized is important in order to achieve better sensitivity and improved response times. Amao *et al.* specially remarked the oxygen permeability of the matrix as a key property for the development of improved optical sensing film. They reported the use of $[Ir(ppy)_3]$ immobilized in poly(styrene-2,2,2-trifluoroethyl methacrylate) copolymer (poly(styrene-*co*-TFEM)) for optical sensing (Amao et al. 2001a). In fact, the use of a fluoropolymer increased the sensitivity (expressed as I_0/I_{100}) to oxygen of $[Ir(ppy)_3]$ when compared with the same dye immobilized in polystyrene (15 times higher) and with other sensing films based on Ir(III) complexes previously reported (around 6 times higher) (Di Marco et al. 1998). The main reason for the high permeability to oxygen of this fluoropolymer is the affinity induced by the high electronegativity of fluorine, which, together with its large electron-withdrawing character, makes the polymer stable forward photooxidation and a good choice for sensing support (Amao et al. 2001a). This fact should be considered with care as excessive oxygen permeability could lead to a poor selectivity if other quenchers enter the matrix.

The importance and role of the support material is clearly highlighted in the research carried out by Fernández *et al.* (Fernández-Sánchez et al. 2006; Fernández-Sánchez et al. 2007). The Ir(III) complexes $[Ir(ppy)_2(bpy\text{-}(DMA)_2)]Cl$, $[Ir(ppy)_2(NCS)_2]TBA$ and $[Ir(ppy)_2(CN)_2]TBA$, that were synthesized by Nazeerudin *et al.* (Nazeeruddin et al. 2003), were immobilized in PS with and without the plasticizer *o*-nitrophenyl octyl ether (*o*-NPOE) and *o*-cyanophenyl octyl ether (*o*-CPOE) for their evaluation as oxygen sensing layers (Fernández-Sánchez et al. 2007). The effect of plasticizer is important in this type of sensing, since it improves the oxygen permeability of the polymer, although, as was demonstrated by these authors, it does not always improve the

sensitivity, probably due to charge incompatibility with dyes that lead to aggregation effects (Fernández-Sánchez et al. 2007; Marín-Suárez et al. 2012; Marin-Suarezdel Toro et al. 2010; Medina-Castillo et al. 2007). However, although heterogeneity effects are important, the forces driving oxygen inside the matrix seems to have a predominant role in oxygen sensing, as demonstrated when nanostructured films are used (Fernández-Sánchez et al. 2006).

The same matrix (AlOOH) was used for the physical immobilization of Ir(III) complex $[Ir(ppy)_2(bpy\text{-}(R42)_2)]Cl$ (Medina-Castillo et al. 2007). However, in this case, the higher lipophilicity of this complex was likely to improve its solubility in PS, leading to improved quantum yield (0.57) compared to AlOOH (0.20) and, as expected, longer lifetimes (102 µs for PS and 22 for AlOOH based films). However, regarding the oxygen sensitivity properties of the sensing phases, AlOOH showed better results than PS, with Stern-Volmer constants of 52 and 19.4 bar^{-1}, respectively. This result emphasizes the importance of both the support structure and nature. On the one hand, nanostructure seems to be responsible for the increase in the capillary forces that lead oxygen through the nanostructured matrix, allowing its interaction with the excited state of the dye. On the other hand, due to the larger structure and lipophilicity of $[Ir(ppy)_2(bpy\text{-}(R42)_2)]Cl$ compared with other complexes, it is likely to avoid adequate penetration of the day into the positively charge AlOOH, hindering the isolating properties of the nanopores, which results in both a decreased lifetime due to self-quenching and improved oxygen sensitivity due to an easier oxygen-complex interaction (Medina-Castillo et al. 2007).

The capacity of AlOOH to improve oxygen sensing performance was further studied using different emission tuned Ir complexes (Marín-Suárez et al. 2012; Marin-Suarezdel Toro et al. 2010; Medina-Rodríguez et al. 2013b). Regardless of the charge of the dye and excitation/emission wavelengths, all the sensing phases studied showed improved performance when immobilized in AlOOH for low oxygen concentration. The heterogeneity of the support and different nature of the complexes make difficult to observe a general trend between the oxygen sensing and dyes properties, which would be of great interest for the design of improved sensing Ir(III) complexes. However, it is especially remarkable for the complex $[Ir(dfppy)_2(bpy\text{-}(DMA)_2)]PF_6$, which showed improved behaviour for low oxygen concentration than other complexes more commonly used for oxygen trace sensing when it was incorporated in AlOOH solid support (Medina-Rodríguez et al. 2013b).

Another way for creating highly porous supports that allows a rapid diffusion of oxygen inside the matrix is to build crystalline coordination polymer from Ir(III) as the binding ligands.

For example, [Ir(ppy)$_3$] derivates such as [Ir(3-(2-pyridyl)benzoate)$_3$] and [Ir(4-(2-pyridyl)benzoate)$_3$] were used to develop different crystalline Zn-based coordination polymer, although only the one obtained from [Ir(3-(2-pyridyl)benzoate)$_3$] was found to be porous enough to allow adequate oxygen quenching (Xie et al. 2009).

[Ir(ppy)$_2$(H$_2$dcbpy)]PF$_6$ was also used as ligand to build coordination polymers based on different cations, such as Zn^{2+}, Cd^{2+}, Co^{2+}, and Ni^{2+} (Ho et al. 2012). As it is shown in Table 5.8, the use of different cations lead to longer emission wavelength for the tetrahedrally coordinated Zn^{2+}, which is expected to have larger relaxation than octahedrally coordinated Co^{2+} and Ni^{2+}. When compared with the free ligand, [Ir(ppy)$_2$(H$_2$dcbpy)]PF$_6$, the coordination polymer obtained with Zn and Cd showed an increased quantum yield, probably due to rigidity introduced by the metal ion with d^{10} configuration, which reduce the non-radiative deactivation pathways. However, the oxygen sensitivity properties does not improve in the polymers compare to the free ligand (except for the Cd-based polymer), although in all the cases they can be considered as suitable candidates for oxygen quenchable sensors. Their values of K_{sv}, larger than other reported Ir complexes in polymeric matrixes, did not follow the same trend than quantum yield values, which highlights the role of the different geometries associated to crystal packing in the oxygen sensing properties (Ho et al. 2012).

3.1.2. Other gases

The Langmuir-Blodgett (LB) technique enables the fabrication and characterization of single molecule thick films with control over the packing density of molecules. These films can be transferred to solid surfaces with preserved density, thickness, and homogeneity of the sample. This technique also gives the possibility to create organized multilayer structures with varying layer compositions.

Sato *et al.* used this technique to prepare luminescent LB films of amphiphilic Ir(III) complexes with gas sensing properties (Sato et al. 2010). For this, a film of *fac*-[Ir(ppy)$_n$(R46)$_{3-n}$] (R46 = 2-(3-octadecyloxyphenyl)pyridine and n = 0–3) floating at an air–water interface was transferred horizontally onto a hydrophobic glass plate as a single-layered LB film, whose emission ($\lambda_{exc}/\lambda_{em}$ = 430/560 nm) was monitored under the atmosphere of various kinds of gases. As a result, molecules with functional groups such as hydroxyl, carbonyl, and amino quenched efficiently the excited iridium complexes incorporated into the film, while molecules with no specific functional groups such as benzene, diethyl ether, and cyclohexane increased the emission

intensity instead of acting as a quencher. So, these LB films of cyclometalated Ir(III) complexes can be used for gas sensing.

3.2. Sensing phases for the detection of ions

In the last few years, a variety of conjugated polymers that contain phosphorescent Ir(III) complexes have been reported as chemosensors for different ions. These polymers allow a faster and more efficient intra- and interchain energy transfer, which results in an amplified signal output and, therefore, in an increasing sensitivity. For example, Shi *et al.* introduced the phosphorescent Ir(III) complex [Ir(thq)$_2$(dbm)] (as energy guest and receptor for Hg^{2+}) into polyfluorene (PFO) backbones (as energy hosts), obtaining a series of conjugated polymer-based chemodosimeters for Hg^{2+} analysis (Shi et al. 2010). The sensing mechanism is based on the decomposition of the Ir(III) complex and the formation of the copolymer PFO-dbm when Hg^{2+} is added. In this copolymer, the fluorene moieties can act as electron donors and the β-diketone ligands (dbm) as electron acceptors. Thus, an intrachain charge-transfer state from fluorene to dbm can be formed, resulting in a significantly enhanced and red shifted emission relative to PFO, while the emission peak from the Ir(III) complex decreases until it is completely quenched. In other study, the introduction of this iridium complex in a conjugated polyelectrolyte (CPE) also allowed the ratiometric detection of Hg^{2+} (Shi et al. 2013a).

Table 5.9 summarises the optical sensing layers using Ir(III) complexes for the determination of ions.

As was mentioned earlier (see Section 2.2.3), the Bppy ligands of the Ir(III) complexes can be used for the selective detection of fluoride anions. However, there are few examples of these complexes that are immobilized onto solid supports. You and Park detected selectively aqueous fluoride ions using spin-coated poly(methyl methacrylate) films doped with [Ir(Bppy)$_2$(acac)] (You and Park 2008). The addition of an aqueous solution of tetrabutylammonium fluoride (TBAF) on these films and the subsequent evaporation of the water solvent provides a red shift and a decrease in the emission intensity. It is attributed to an intermolecular energy transfer. However, they observed that these films do not respond to NaF or KF due to the absence of phase transfer activity in these analytes.

Li *et al.* combined upconversion oleic acid-$NaYF_4$ nanocrystals with a cyanide anion responsive chromophoric Ir(III) complex (Liu et al. 2011a). These nanocrystals can be used as ratiometric upconversion luminescence (UCL) probes for selective detection of cyanide anions

through the inhibition of the energy transfer process from the UCL emission of the nanocrystals to the absorbance of the chromophoric iridium complex. The high selectivity of this probe is attributed to the unique reaction of CN^- with the α,β-unsaturated carbonyl moiety of the ligand, leading to the disruption of the π-conjugation system. However, this probe does not work in purely aqueous media. Most recently, in order to obtain a probe to detect cyanide in pure water, these authors fabricated a nanosized amphiphilic structure, composed of a hydrophobic layer of carbon chains from oleic acid molecules and a hydrophilic layer of PEG moieties attached to UCNPs, and with a CN^--reactive Ir(III) complex inside the hydrophobic layer (Yao et al. 2012). This hybrid upconversion material can serve as an optical probe in pure water to detect CN^- based on a luminescent resonance energy transfer process with UCNPs as energy donor and the Ir(III) complex as energy acceptor.

Table 5.9. Optical sensing layers based on Ir(III) complexes for analysing ions.

Analyte	Complex[a]	Solid support[b]	Detection[c]	λ_{exc} (nm)	λ_{em} (nm)	τ_{em} (μs)	LOD (μM)	Reference
Hg^{2+}	$[Ir(thq)_2(dbm)]$	Polyfluorene (C)	UV–Vis, L	380	618	-	< 0.002 (L)	(Shi et al. 2010)
	$[Ir(thq)_2(dbm)]$	Polyfluorene (C)	UV–Vis, P	380	635	0.170	< 0.2	(Shi et al. 2013a)
F^-	$[Ir(Bppy)_2(acac)]$	PMMA	P	345	512	0.56	-	(You and Park 2008)
CN^-	$[Ir(bpy\text{-}2\text{-}COO^-)(dmphp)_2]$	OA-$NaYF_4$: 20%Yb, 1.6%Er, 0.4%Tm nanocrystals	UV–Vis, UCL	980	540 (UCL)	-	0.18 (UCL)	(Liu et al. 2011a)
	$[Ir(ppy)_2(dmpp)]PF_6$	PEG-OA-$NaYF_4$: 20%Yb, 2%Ho	UV–Vis, UCL	980	545 (UCL)	-	62.6 (UCL)	(Yao et al. 2012)

Notes: The response of all of these sensing layers is ratiometric.

[a] See Section 5.

[b] OA = oleic acid; C indicated a covalent attachment.

[c] UV-Vis is UV-Vis absorption; L is Luminescence, it is used when the authors did not clarify if fluorescence (F) or phosphorescence (P) occurred; UCL is upconversion luminescence.

3.3. Sensing phases for the detection of biomolecules

Table 5.10 summarises the optical sensing layers using Ir(III) complexes for the determination of biomolecules.

3.3.1. Glucose

When a biological recognition element, such as an enzyme, is included within the oxygen-sensitive matrix, it is possible to develop an optical biosensor based in oxygen transduction.

Luminescent transition-metal complexes have been widely used for fabricating optical oxygen and glucose biosensors based on the high oxygen quenching efficiency. Recently, iridium complexes with stronger photostability and higher quantum efficiency than those of other transition metals have gained much attention as glucose sensors. For example, Zhou *et al.* designed an electrospun optical fibrous (EOF) membrane doped with the Ir(III) complex $[Ir(bt)_2(acac)]$, and covalently functionalized with glucose oxidase (GOx) (Zhou et al. 2013). The oxygen molecules that quenched the luminescence of the iridium complex are consumed by GOx when glucose is added to the media. It results in a significantly enhancement of the luminescent emission, which can be used to detect glucose.

In other study, a layer-by-layer structure was used as a photoluminescence sensor for glucose. In this case, a sol–gel matrix was used as a solid support for the immobilization of an Ir–Cd coordination polymer as the first layer, fresh eggshell membrane was overlaid as the second layer, and GOx was encapsulated in a calcium alginate hydrogel sphere as the third layer (Ho et al. 2014). This system can be used as a sensitive and reversible glucose sensor with a detection mechanism based on the oxygen depletion after exposure to a glucose solution and the subsequent increase in the phosphorescence emission. The same approach but using Zn coordination polymers obtained by electrochemical methods was also used (Cheng et al. 2014).

3.3.2. BSA

The covalent attachment of metal complexes to gold is attractive as a platform to develop sensing systems. So, Adams *et al.* assembled a cyclometalated Ir(III) complex on gold surfaces that showed a sensitive response to BSA (Adams et al. 2014). This complex has a bipyridine ligand with a long spacer chain to reduce the luminescence quenching from the gold surface, resulting not only in the quenching decrease but also in the luminescence lifetime enhancement.

Table 5.10. Optical sensing layers based on Ir(III) complexes for analysing biomolecules.

Analyte	Complex[a]	Solid support[b]	Detection[c]	Response[d]	λ_{exc} (nm)	λ_{em} (nm)	τ_{em} (μs)	LOD (μM)	Reference
Glucose	$[Ir(bt)_2(acac)]$	Electrospun PS	L	Ton	405	562	-	$1 \cdot 10^{-4}$	(Lu and Nabeshima 2014)
	$[Cd([Ir(ppy)_2(dcbpy)]PF_6)_2(H_2O)_2] \cdot 3DMF \cdot 6H_2O$	Octyl-triEOS/TEOS	P	Ton	405	609	-	10	(Zhou et al. 2013)
	$[Zn([Ir(ppy)_2(dcbpy)]PF_6)_2] \cdot 3DMF \cdot 5H_2O$	Octyl-triEOS/TEOS	P	Toff	-	596	-	50	(Ho et al. 2014)
BSA	$[Ir(ppy)_2(bpySS)]$	Planar gold film (C)	L	Ton	360	532	0.130	-	(Cheng et al. 2014)
Hcy and Cys	$[Ir(pba)_2(phen)]PF_6$	Gel	L	R	356	430	-	-	(Adams et al. 2014)
	$[Ir(pba)_2(pic\text{-}O\text{-}CONH\text{-}C_3H_6\text{-}TES]$	Si-NP (C)	UV–Vis, P	Ton-B	365	545	-	-	(Cao et al. 2012)
	$[Ir(pba)_2(paa)]PF_6$	PNIPAM (C)	P	Ton	-	564	0.366	-	(Liu et al. 2012)
	$[Ir(pba)_2(pic)]$	PNIPAM (C)	P	Ton-B	365	567	-	1.2 (Hcy) 2.4 (Cys)	(Ma et al. 2013b)
Heparin	$[Ir(thq)_2(dbm)]$	Polyfluorene (C)	P	R	379	632	0.223	< 0.020	(Liu et al. 2013)
Histone	$[Ir(ppy)_2(FlPy)]$	Polyfluorene (C)	P	R	380	605	-	0.06	(Shi et al. 2013b)

Notes: [a] See Section 5.

[b] PS = Polystyrene; Si-NP = Silica nanoparticles; C indicated a covalent attachment.

[c] UV-Vis is UV-Vis absorption; L is Luminescence, it is used when the authors did not clarify if fluorescence (F) or phosphorescence (P) occurred.

[d] Ton is Turn-on; Toff is Turn-off; Ton-B is Turn-on and blue shift; R is Ratiometric.

3.3.3. Cysteine and homocysteine

Organogels formed by specific non-covalent interactions have been extensively studied due to the possibility of tuning their morphology and their emission properties. These gels are ideal constituents for the design of supramolecular light-harvesting materials, and when they are functionalized with the adequate components, they can be used for the determination of analytes. For example, a two-component gel with a phenol substituted 1,8-naphthalimide derivative acting as donor and an Ir(III) complex acting as acceptor was used to determine cysteine with an obvious change in luminescence that is visible to the naked eye (Cao et al. 2012).

There are others solid supports containing luminescent Ir(III) complexes that have demonstrated to be useful for the detection of Cys and Hcy. The sensing mechanism is based on the reaction between the thiol of Cys/Hcy and the aldehyde group of the iridium complex, resulting in the formation of thiazolidine or thiazinane units that avoid the quenching of the excited-state complex through electron transfer, and the subsequent luminescent enhancement.

Liu *et al.* developed an aqueous-based phosphorescent probe for the detection of Cys and Hcy with mesoporous silica nanoparticles as solid supports and an Ir(III) complex as signalling unit (Liu et al. 2012). These nanoparticles are often selected as carriers due to their simple preparation and surface functionalization, and their excellent biocompatibility and stability. The binding to Hcy/Cys provides a double-signal response: a turn-on phosphorescence emission and a color change, which can be observed by the naked eye.

Conjugated polymers with Ir(III) complexes introduced into the polymer backbone have also been reported as sensing layers for Cys and Hcy. For example, the water-soluble poly(*N*-isopropylacrylamide) (PNIPAM) containing iridium(III) complexes with aldehyde groups that could selectively react with thiol groups has been successfully applied for detecting Cys and Hcy (Liu et al. 2013; Ma et al. 2013b). The PNIPAM backbone improves the water solubility and the biocompatibility of the probe, whereas the Ir(III) complex acts as a phosphorescent signalling unit. PNIPAM is a thermal sensitive polymer, thus these sensing layers are also sensitive to temperature.

3.3.4. Heparin

Conjugated polyelectrolytes (CPEs) are a class of conjugated polymers with ionic side groups, which combine the optoelectronic properties of the conjugated backbone with solubility in polar

solvents. They often suffer interference from background, such as autofluorescence, which complicate their measurements. However, the incorporation of phosphorescent heavy-metal complexes with long emission lifetimes, such as Ir(III) complexes, is an alternative to eliminate this undesirable background. So, CPEs containing Ir(III) complexes and polyfluorene units have been employed by Shi *et al.* to develop a probe for heparin (Shi et al. 2013b). The electrostatic interaction between the CPEs and heparin improves the energy transfer from the polyfluorene units to the iridium complexes, which produces an increase in the emission intensity of the complexes and a decrease in the emission of the polyfluorene, allowing the ratiometric detection and quantification of heparin in solution.

3.3.5. Histone

CPEs containing a phosphorescent Ir(III) complex [$Ir(ppy)_2(FlPy)$] as the energy acceptor and polyfluorene units as donor have also been used for the sensitive detection of histone (Sun et al. 2011b). These CPEs display an efficient intrinsic fluorescence resonance energy transfer (FRET) in aqueous solution due to the polymer aggregation induced by its poor water solubility. The addition of histone provides a gradually increase in the donor emission intensity, whereas the acceptor emission intensity decreases. It corresponds with a weakened FRET process induced by histone that is selective for histone over other proteins. As a result, the emission color of the polymer solution changes from red to lilac, while it remains red for other proteins, enabling its visual discrimination.

3.4. Sensing phases for multiparametric sensing

The use of spectrally independent sensing systems is a common approach to develop multiple-analyte sensors. One example is a quadruple sensor for oxygen, carbon dioxide, pH and temperature, based on [$Ir(C_S)_2(acac)$] as both the oxygen sensing and reference dye for the CO_2 sensing scheme (Borisov et al. 2011). In this case, the oxygen indicator was physically immobilized in PS-DVB microparticles, both to improve stability of the dye and avoid damage of the CO_2 indicator due to single oxygen production during emission from [$Ir(C_S)_2(acac)$]. These microbeads were subsequently incorporated in an EC layer with the $HPTS(TOA)_3$ ion pair, prepared from pH fluorescent 8-hydroxy-pyrene-1,3,6-trisulfonate (HPTS) and tetraoctylammonium chloride (TOA). With appropriate selection of LED sources and filters (both short pass and band pass for excitation and emission) and materials to isolate the different optical indicator, it was possible to monitor these four chemical parameters. In addition, the higher

volume fraction of oxygen-sensitive bead leads to increase oxygen sensitivity compared to the same dye in a planar PS film (Borisov et al. 2011).

One of the most common problems of pressure sensitive paint (PSP) measurements is the inherent temperature dependence. It makes difficult the accurate determination of oxygen concentration and consequently the local air pressure. Temperature dependence is caused by several physical processes such as temperature-dependent oxygen permeability in the paint and thermal quenching of the luminescent probe. Thus, for precise measurement of pressure, it is also necessary to measure the temperature. One of the simplest ways to do it consists in the incorporation into the film of two luminophores that allow spectrally resolved measurement of oxygen pressure and temperature. Fischer *et al.* designed a water-based dual sensitive paint for lifetime imaging of barometric pressure and temperature (Fischer et al. 2010). It is formed by combining core–shell particles composed by a polystyrene core and a poly(vinyl pyrrolidone) shell dyed with a luminescent platinum(II) porphyrin probe for oxygen (pressure), and microparticles of poly(acrylonitrile) with the luminescent iridium(III) complex $[Ir(ppy)_2(carbac)]$ acting as a probe for temperature.

In another study, a dual luminescent sensitive paint for barometric pressure and temperature based exclusively on the use of Ir(III) complexes as luminescent indicators was reported (Fischer et al. 2009). It consists of the green-emitting Ir(III) complex $[Ir(ppy)_2(carbac)]$ as probe for temperature and the red-emitting complex $[Ir(btpy)_3]$, which functions as a barometric (oxygen-sensitive) probe. These complexes are incorporated into two different polymer matrices; $[Ir(ppy)_2(carbac)]$ is dispersed in gas-blocking poly(acrylonitrile) microparticles in order to suppress any quenching of its luminescence by oxygen, and $[Ir(btpy)_3]$ is incorporated in a cellulose acetate butyrate film, which exhibits good permeability to oxygen. The difference between their emissions allows the separation of the signals and therefore the determination of barometric pressure and temperature, at the same time.

There are other kinds of temperature sensors based on conjugated polymers that contain Ir(III) complexes (Liu et al. 2013; Ma et al. 2013b), all of these are summarised in Table 5.11.

Table 5.11. Optical sensing layers based on Ir(III) complexes for multiparametric sensing.

Parameters	Analyte detected with Ir(III)	Complex[a]	Solid support[b]	Detection[c]	Response[d]	λ_{exc} (nm)	λ_{em} (nm)	τ_{em} (µs)	Reference
Cys/Hcy and temperature	T	$[Ir(pba)_2(paa)]PF_6$	PNIPAM (C)	P	Ton	-	564	0.366	(Sun et al. 2011b)
	T	$[Ir(pba)_2(pic)]$	PNIPAM (C)	P	Ton	365	567	-	(Ma et al. 2013b)
Temperature and barometric pressure	T	$[Ir(ppy)_2(carbac)]$	PAN (MP)	L	Toff	405	519	2.3	(Liu et al. 2013)
	O_2	$[Ir(btpy)_3]$	CAB	L	Toff	405	596, 645	8.60	(Fischer et al. 2010; Fischer et al. 2009)
O_2, CO_2, pH and temperature	O_2	$[Ir(C_S)_2(acac)]$	PS-DVB (1)	L	Ton	470	566	-	(Fischer et al. 2009)

Notes: [a] See Section 5.

[b] MP = microparticles; CAB = Cellulose acetate butyrate; C indicated a covalent attachment; 1 indicates cross-linked beads dispersed in EC.

[c] L is Luminescence, it is used when the authors did not clarify if fluorescence (F) or phosphorescence (P) occurred.

[d] Ton is Turn-on; Toff is Turn-off.

4. Conclusion and Future Challenges

The use of cyclometalated Ir(III) complexes for optical sensing is taking special attention due to their good spectroscopic properties: they are usually excellent triplet emitters with remarkable quantum yield and absorption coefficients. In addition, the chemistry and reactivity of these complexes allow not only to tune wavelengths, but also to introduce moieties that actively participate in the sensing mechanism, to anchor the complex into a solid support, or to simply improve its solubility in the surrounding media.

Therefore, the progress experimented on the Ir(III) chemistry, driven by the design of new organic LEDs emitters, has allowed the development of Ir(III)-based sensors for a variety of analytes, offering a new alternative to develop both probes and sensing phases. Some of them, the so-called probes, lack of a solid support, while the immobilization of the Ir(III) complex into a solid material to develop a sensing phase leads to a better mechanical stability and, usually, improves optical properties of the complex with an ease of handling. Both probes and sensing phases find application for various gaseous (O_2, CO_2, etc.) and ionic species (anions and cations, including pH), as well as for the detection of biomolecules (glucose, BSA, cysteine, etc.), although probes seem to be more suited for the detection of small molecules (such as explosives, amines, silver salts, etc.) and small biomolecules (proteins, amino acids, nucleotides, etc.).

In general, Ir(III) complexes have a range of advantages that make them an excellent choice as luminescent sensors:

- Rich photophysical properties and emission behaviour highly sensitive to changes in the environment or in the structure.
- Extensive diversity of ligand structures that allow obtaining varied selectivity and sensitivity toward many different analytes.
- High luminescence quantum yields and long phosphorescence lifetimes that allow them to function in the presence of a high fluorescent background.

The detection scheme for many of these molecules and ions is therefore based on the change on the emission properties of Ir(III), with or without decomposition of the complex, upon analyte binding or interaction, which in any case required the proper receptor to be introduced in the complex ligands. For example, a Schiff base can be used as a receptor for Cu detection, and Lewis bases or acids for both cations and anions, such as Hg^{+} and F^{-}. Similarly, the addition of specific ligands with protanable (pyridyl) and deprotonable (phenolic) groups can be used for pH

sensing. In the same line, and depending on the functional group of the analyte to be sensed, that is, thiols for some small biomolecules, specific ligand can be introduced as receptors within the Ir(III) complex.

On the other hand, the sensing mechanism for gas sensing is normally based on the quenching of the luminescence by the gaseous analyte. Due to the importance of oxygen, special attention is given to its detection through the quenching of the luminescence, and different Ir(III) complexes have been synthesized in order to increase the sensitivity, stability, and response time of the sensing layers for this gas, which find many applications in life sciences.

The best Ir(III) complex for optical sensing, however, cannot be defined, and the properties that the complex should fulfill have to be defined for each specific application. Therefore, it is expected that this field continue growing towards the design of Ir(III) complexes with specific characteristics, bearing in mind the considerations stated along this chapter: more efficient luminophores, with tuned wavelengths and solubility, and improved selectivity as well as stability under both irradiation and storage. For actual applications of phosphorescent probes, the water solubility is very important. However, the number of reported phosphorescent Ir(III) complexes which can be used in aqueous solution with minimal organic solvent maintaining their detection performance are very few. Therefore, the new challenges are focused on the design and synthesis of water-compatible Ir(III) complexes for the determination of ions in the environment. Another important challenge is to increase the selectivity of ion-sensitive phosphorescent probes. For example, while most of the reported anion-sensitive probes have achieved excellent discrimination between strongly and weakly basic anions, the selectivity exhibited between two strongly basic anions such as fluoride and acetate have been relatively modest.

Concerning with oxygen detection, optical oxygen sensors benefit from the good spectroscopic properties of Ir(III) complex, which gently allow to use smaller, simpler, and cheaper electroelectronic devices. Nowadays, the use of optical oxygen sensors has great applicability in the field of imaging, specifically for pressure sensitive paints and oxygen surface distribution monitoring in water systems and biological fluids, besides others. For real time measurements and to avoid interferences from other substances present in the media, this type of sensing requires a fast response time, and, more specifically, an emission in the NIR region of the spectra where the chemistry of Ir(III) can be very useful. In addition, because the human eye is not able to differentiate a change of luminescence as good as the change of color, it would be of great interest to exploit the chemistry of Ir(III) to develop materials with a reversible change of

color upon changes on the oxygen concentration, which could be used as reversible test strips for certain applications. Furthermore, actual market urgently demands optical oxygen sensors for detecting high concentrations of oxygen, in order to compete with the commercial Clark electrode.

In conclusion, we anticipate that the interesting structural and emissive properties of Ir(III) complexes will continue to contribute to the development of sensitive and selective sensing probes and phases. This, together with the engineering of supporting materials and advances in spectroscopy, will allow to improve the performance of current sensors as well as to develop optical sensors for analytes that lack of this sensing technology and that can benefit from the Ir(III) chemistry.

5. Acronyms Used in the Names of the Complexes

acac	acetylacetonate
azaH	3,9-dithia-6-azaundecane
azobpy	4,4''-azobis(2,2'-bipyridine)
az-ppyH	aza-15-crown-5 ether phenylpyridine
azppzH	3-(4-aza-15-crown-5-phenyl) pyridyl pyrazole
bpe	4-methyl- benzeneboronic acid pinacol ester
BpicH	5-(4-(dimesitylboryl)phenyl)picolinic acid
BppyH	2-(4-(dimesitylboryl)phenyl)pyridine
Bpq	2-(4-(dimesitylboryl)phenyl)quinoline
bpy	2,2‘-bipyridine
bpy-dmn	4-methyl-2,2'-bipyridine-4'-diaminomaleonitrile
bpy-en-biotin	4-(*N*-((2-biotinamido)ethyl)-aminomethyl)-4‘-methyl-2,2‘-bipyridine
bpySS	4,4‘-di(5-lipoamido-1-pentoxy)-2,2‘-bipyridine
bq	benzo[*h*]quinoline
bsbH	2-((1,1'-biphenyl)-4-yl)benzothiazole
bsnH	2-(1-naphthyl)benzothiazole
btH	2-phenylbenzothiazole
Bthc	3-(benzothiazol-2-yl)-7-hydroxy-coumarin
btp	2-(benzo[*b*]thiophen-2-yl)pyridine

btph	benzothienylphenanthridine
btpy	(benzo[*b*]thiophene-2-yl)pyridinato
btq	benzothienylquinoline
BTTA	bis(2-(2-(methylthio)ethylthio)ethyl)amino
btthH	2-(2-thienyl)benzothiazole
ButIm	*N*-(*n*-butyl)imidazole
bzqH	7,8-benzoquinoline
carbac	1-(9*H*-carbazol-9-yl)-5,5-dimethylhexane-2,4-dione
CarbIm	carboxyimidazole
cbd	*N*-carbazolylcarbodithioate
C_N	3-(1-methylbenzoimidazol-2-yl)-7-(diethylamino)-coumarin
C_O	3-(5-chlorobenzooxazol-2-yl)-7-(diethylamino)-coumarin
C_S	3-(benzothiazol-2-yl)-7-(diethylamino)-coumarin
$C_{S\text{-}Me}$	3-(benzothiazol-2-yl)-7-(dimethylamino)-coumarin
cyH_2	cyclohexane-1,4-dicarboxamide
CzH	9-hexyl-9*H*-carbazole
dbm	dibenzoylmethanate
DBQ	dibenzo[*f*,*h*]quinoxaline
dCF3ppyH	4,6-bis(trifluoromethyl)phenyl pyridine
DEA	diethyl amine
dfppi	2-(2,4-difluorophenyl)-1-phenyl-1*H*-imidazo[4,5-*f*][1,10]phenanthroline
dfppyH	4,6-difluorophenyl pyridine
DMA	dimethyl amine
dmiphen	1,3-dimethyl-2,3-dihydro-1*H*-imidazo[4,5-*f*][1,10]phenanthroline-2-yl
dmphp	4-(4-(dimethylamino)benzylidene)-3-methyl-1-phenyl-1*H*-pyrazol-5(4*H*)-one
dmpp	4-(4-(dimethylamino)benzylidene)-3-methyl-1-(pyridin-2-yl)-1*H*-pyrazol-5(4*H*)-one
dmppa	1-(2,6-dimethylphenoxy)-4-phenylphthalazine
dnbpy	4,4'-dinonyl-2,2'-bipyridine
DNBS	2,4-dinitrobenzenesulfonyl
DPA	di(2-picolyl)-amine
dpciH	3,4-diphenylcinnoline
dppH	4,6-diphenylpyrimidine
dppn	benzo[*i*]dipyrido[3,2-*a*:2‘,3‘-*c*]phenazine

dppz	dipyrido[3,2-*a*:2‘,3‘-*c*]phenazine
dpq	dipyrido[3,2-*f*:2‘,3‘-*h*]quinoxaline
dpqa	2-*n*-butylamidodipyrido[3,2-*f*:2‘,3‘-*h*]quinoxaline
dpt	3,5-di-2-pyridyl-4*H*-1,2,4-triazole
dtcH	diethyl dithiocarbamic acid
Fc	ferrocene
$FlPyH_2$	2-(9,9-dioctyl-9*H*-fluoren-2-yl)pyridine
fpbi	1-(8-(9-octyl-9*H*-fluoren-9-yl)octyl)-2-(pyridin-2-yl)-3*a*,7*a*-dihydro-1*H*-benzo[*d*]imidazole
fppi	2-(4-fluorophenyl)-1-phenyl-1*H*-imidazo[4,5-*f*][1,10]phenanthroline
fppyH	4,6-difluorophenyl pyridine
H_2dcbpy	4,4′-dicarboxy-2,2′-bipyridine
ind	indole ring
mCP	*N,N’*-dicarbazolyl-3,5-benzene
MebpyIN	4-methyl-4‘-(1-oxyl-4,4,5,5-tetramethylimidazolin-2-yl)-2,2‘-bypyridine
mebtp	2-benzo[*b*]thiophene-2-yl-4-methyl-pyridine
mmpdt	(4-methoxyphenyl)-*O*-methyl phosphonodithioate
Morphcdt	morpholine-4-carbodithioic acid
mppyH	2-(4-methylphenyl)pyridine
mppzH	3-methyl-1-phenylpyrazole
npyH	2-(naphthalen-1-yl)pyridine
OEP	octaethyl porphyrins
paa	*N*-(1,10-phenanthrolin-5-yl)acrylamide
pbaH	4-(2-pyridyl)benzaldehyde
pbiH	1,2-diphenyl-1*H*-benzo[*d*]imidazole
PBT	2-(2-hydroxyphenyl)-benzothiazole
pdpzH	1-phenyl-3,5-dimethyl pyrazole
phen	1,10-phenanthroline
$phencatH_2$	2,3-dihydroxy-*N*-(1,10-phenanthrolin-5-yl)benzamide
picH	picolinic acid
piq	1-phenylisoquinoline
pp	3-phenyl-1*H*-pyrazole
ppa	4-phenylphthalazin-1-ol
ppyH	2-phenylpyridine

ppzH	4-phenylphthalazinone
pqH	2-phenylquinoline
pto	2-((1,10-phenanthrolin-5-yl)amino)-*N*,*N*,*N*-triethyl-2-oxo-ethanaminium chloride
ptpy	2-(*p*-tolyl)pyridine
Py	pyridine
py_2pzH	3,5-di(2-pyridyl) pyrazole
pyq	2-(pyridin-2-yl)quinoline
pyr	pyrene
qnx	quinoxaline-2-carboxylate
quqo	2-(quinolin-2-yl)quinoxaline
R1	$NHCOCH_2NHCH_2$-Py
R10	4-pyridyl-3,5-dimethyl
R11	4-(4-pyridyl)phenyl
R12	4-(3-pyridyl)phenyl
R13	9,9-dioctyl-9*H*-fluorene
R14	5-(dimesitylboryl)-2-phenylpyridine
R15	2-(4-(dimesitylboryl)phenyl)pyridine
R16	4‘-methyl-2,2‘-bipyridyl-4-carbaldehyde oxime
R17	dfppy, 2-pq, bzq, dpq
R18	2-phenylpyrazole
R19	2-(3-*H*-phenylpyridine)
R2	bpy-acylhydrazone-thiophene
R20	2-(3-Br-phenylpyridine)
R21	ppy, bzq, pq
R22	*N*-ethyl-*N’*-1,10-phenanthrolin-5-yl thiourea, *N*-(1-adamantanemethyl)-*N’*-1,10-phenanthrolin-5-yl thiourea, *N*-phenyl-*N’*-1,10-phenanthrolin-5-yl thiourea
R23	2-phenyl-1*H*-imidazo[4,5-*f*][1,10]phenanthroline
R24	2-(1*H*-imidazo[4,5-*f*][1,10]phenanthrolin-2-yl)phenol
R25	2-(9-ethyl-9*H*-carbazol-2-yl)-1*H*-imidazo[4,5-*f*][1,10]phenanthroline
R26	1-(4-(diethylamino)phenyl)prop-2-en-1-one
R27	1,10-phenanthroline-5-maleimide
R28	oxohexylbenzamide-diarylazo quencher
R29	oxopentyl-triazol-benzamide-diarylazo quencher
R3	thiophen-2-ylmethylamine

R30	4-(1*H*-imidazo[4,5-*f*][1,10]phenanthrolin-2-yl)benzaldehyde
R31	2-((2-biotinamido)ethyl) amidodipyrido[3,2-*f*:2‘,3‘-*h*]quinoxaline
R32	11-((2-biotinamido)ethyl)amidodipyrido [3,2-*a*:2‘,3‘-*c*]phenazine
R33	(2-pyridyl)-1,2,3-triazole
R34	4-(*N*-((6-biotinamido) hexyl)amido)-4‘-methyl-2,2‘-bipyridine
R35	5-(4-(17α-ethynylestradiolyl)phenyl)-2,2‘-bipyridine
R36	4-(*N*-(6-(4-(17α-ethynylestradiolyl)benzoylamino)hexyl)aminocarbonyl)-4‘-methyl-2,2‘-bipyridine
R37	2-(3,4-dimethoxy-phenyl)-1*H*-imidazo[4,5-*f*][1,10]phenanthroline
R38	10-(4-(3-phenyl-5-(pyridin-2-yl)-1*H*-1,2,4-triazol-1-yl)butyl)-10*H*-phenothiazine
R39	4-[(4-amino-3-nitrophenoxy)-methylene]-4‘-methyl-2,2‘-bipyridine
R4	pyridin-2-ylmethylamine
R40	2,6-bis(7_-methyl-4_-phenyl-2_-quinolyl)pyridine
R41	monoanion of R40
R42	*N*-hexyl-*N*-methyl-4-vinylaniline
R43	2,2,6,6-tetramethylheptane-3,5-dione
R44	1-(9*H*-carbazol-9-yl)-5,5-dimethylhexane-2,4-dione
R45	1-(3-(4-heptylphenyl)-6-(4-hexylphenyl)-9*H*-carbazol-9-yl)-5,5-dimethylhexane-2,4-dione
R46	2-(3-octadecyloxyphenyl)pyridine
R5	4-hydroxyphenyl
R6	4-tolyl
R7	4-pyridyl
R8	3-pyridyl
R9	2-pyridyl
sa2p	5,6-bis(salicylideneimino)-1,10-phenanthroline
SBFIQ	1-(9,9‘-spirobi[fluorene]-7-yl)isoquinoline
solv	H_2O, CH_3CN
TBTH	2-thiophen-2-yl-benzothiazole
tBubpy	4,4′-di-*tert*-butyl-2,2′-bipyridine
t-Bu-iCN	*tert*-butyl-isocyanate
TES	triethoxysilane
tfmppi	1-phenyl-2-(4-(trifluoromethyl)phenyl)-1*H*-imidazo[4,5-*f*][1,10]phenanthroline
tfppi	1-phenyl-2-(2,4,6-trifluorophenyl)-1*H*-imidazo[4,5-*f*][1,10]phenanthroline

thq	2-(thiophen-2-yl)quinoline
TPA	tris(2-pyridylmethyl)amine
tpy	terpyridine
ttph	thienothiophenylphenanthridine
ttpy	4'-(4-methylphenyl)-2,2':6',2"-terpyridine
vacac	allylacetoacetate
vppyH	2-(4-vinylphenyl)pyridine
vpy	4-vinylpyridine

References

Achatz, D.E., Meier, R.J., Fischer, L.H., Wolfbeis, O.S., 2011. Luminescent Sensing of Oxygen Using a Quenchable Probe and Upconverting Nanoparticles. Angewandte Chemie International Edition 50(1), 260-263.

Adams, S.J., Lewis, D.J., Preece, J.A., Pikramenou, Z., 2014. Luminescent Gold Surfaces for Sensing and Imaging: Patterning of Transition Metal Probes. ACS Applied Materials & Interfaces 6(14), 11598-11608.

Alam, P., Kaur, G., Climent, C., Pasha, S., Casanova, D., Alemany, P., Roy Choudhury, A., Laskar, I.R., 2014. New 'aggregation induced emission (AIE)' active cyclometalated iridium(III) based phosphorescent sensors: high sensitivity for mercury(II) ions. Dalton Transactions 43(43), 16431-16440.

Amao, Y., Ishikawa, Y., Okura, I., 2001a. Green luminescent iridium(III) complex immobilized in fluoropolymer film as optical oxygen-sensing material. Analytica Chimica Acta 445(2), 177-182.

Araya, J.C., Gajardo, J., Moya, S.A., Aguirre, P., Toupet, L., Williams, J.A.G., Escadeillas, M., Le Bozec, H., Guerchais, V., 2010. Modulating the luminescence of an iridium(iii) complex incorporating a di(2-picolyl)anilino-appended bipyridine ligand with Zn^{2+} cations. New Journal of Chemistry 34(1), 21-24.

Arm, K.J., Leslie, W., Williams, J.A.G., 2006. Synthesis and pH-sensitive luminescence of bis-terpyridyl iridium(III) complexes incorporating pendent pyridyl groups. Inorganica Chimica Acta 359(4), 1222-1232.

Bailey, R.E., Smith, A.M., Nie, S., 2004. Quantum dots in biology and medicine. Physica E: Low-dimensional Systems and Nanostructures 25(1), 1-12.

Baschieri, A., Muzzioli, S., Fiorini, V., Matteucci, E., Massi, M., Sambri, L., Stagni, S., 2014. Introducing a New Family of Biotinylated Ir(III)-Pyridyltriazole Lumophores: Synthesis, Photophysics, and Preliminary Study of Avidin-Binding Properties. Organometallics 33(21), 6154-6164.

Borisov, S.M., Klimant, I., 2007. Ultrabright oxygen optodes based on cyclometalated iridium(III) coumarin complexes. Analytical Chemistry 79(19), 7501-7509.

Borisov, S.M., Seifner, R., Klimant, I., 2011. A novel planar optical sensor for simultaneous monitoring of oxygen, carbon dioxide, pH and temperature. Analytical and Bioanalytical Chemistry 400(8), 2463-2474.

Brandel, J., Sairenji, M., Ichikawa, K., Nabeshima, T., 2010. Remarkable Mg^{2+}-selective emission of an azacrown receptor based on Ir(III) complex. Chemical Communications 46(22), 3958-3960.

Cao, X., Wu, Y., Liu, K., Yu, X., Wu, B., Wu, H., Gong, Z., Yi, T., 2012. Iridium complex triggered white-light-emitting gel and its response to cysteine. Journal of Materials Chemistry 22(6), 2650-2657.

Carlson, B., Eichinger, B.E., Kaminsky, W., Phelan, G.D., 2010. Organometallic osmium and iridium complexes as phosphorescent dye in barometric sensitive coatings. Sensors and Actuators, B: Chemical 145(1), 278-284.

Castillo, C.E., Davies, D.L., Klair, A.-K.D., Singh, K., Singh, S., 2012. Luminescent iridium complexes for detection of molybdate. Dalton Transactions 41(2), 628-635.

Chan, D.S.-H., Fu, W.-C., Wang, M., Liu, L.-J., Leung, C.-H., Ma, D.-L., 2013. A Highly Selective and Non-Reaction Based Chemosensor for the Detection of Hg^{2+} Ions Using a Luminescent Iridium(III) Complex. PLoS ONE 8(3), e60114.

Chen, H., Zhao, Q., Wu, Y., Li, F., Yang, H., Yi, T., Huang, C., 2007. Selective Phosphorescence Chemosensor for Homocysteine Based on an Iridium(III) Complex. Inorganic Chemistry 46(26), 11075-11081.

Chen, K., Bats, J.W., Schmittel, M., 2013. Iridium-Based Lab-on-a-Molecule for Hg^{2+} and ClO^- with Two Distinct Light-Up Emissions. Inorganic Chemistry 52(22), 12863-12865.

Chen, K., Schmittel, M., 2013. An iridium(III)-based lab-on-a-molecule for cysteine/homocysteine and tryptophan using triple-channel interrogation. Analyst 138(22), 6742-6745.

Cheng, K.Y., Wang, J.C., Lin, C.Y., Lin, W.R., Chen, Y.A., Tsai, F.J., Chuang, Y.C., Lin, G.Y., Ni, C.W., Zeng, Y.T., Ho, M.L., 2014. Electrochemical synthesis, characterization of Ir-Zn containing coordination polymer, and application in oxygen and glucose sensing. Dalton Transactions 43(17), 6536-6547.

Denisov, S.A., Cudré, Y., Verwilst, P., Jonusauskas, G., Marín-Suárez, M., Fernández-Sánchez, J.F., Baranoff, E., McClenaghan, N.D., 2014. Direct observation of reversible electronic energy transfer involving an iridium center. Inorganic Chemistry 53(5), 2677-2682.

DeRosa, M.C., Hodgson, D.J., Enright, G.D., Dawson, B., Evans, C.E.B., Crutchley, R.J., 2004. Iridium Luminophore Complexes for Unimolecular Oxygen Sensors. Journal of the American Chemical Society 126(24), 7619-7626.

DeRosa, M.C., Mosher, P.J., Evans, C.E.B., Crutchley, R.J., 2003a. Iridium(III) complexes as polymer bound oxygen sensors. Macromolecular Symposia 196(1), 235-248.

DeRosa, M.C., Mosher, P.J., Yap, G.P.A., Focsaneanu, K.S., Crutchley, R.J., Evans, C.E.B., 2003b. Synthesis, Characterization, and Evaluation of [Ir(ppy)2(vpy)Cl] as a Polymer-Bound Oxygen Sensor. Inorganic Chemistry 42(16), 4864-4872.

Di Marco, G., Lanza, M., Mamo, A., Stefio, I., Di Pietro, C., Romeo, G., Campagna, S., 1998. Luminescent Mononuclear and Dinuclear Iridium(III) Cyclometalated Complexes Immobilized in a Polymeric Matrix as Solid-State Oxygen Sensors. Analytical Chemistry 70(23), 5019-5023.

Dubertret, B., Calame, M., Libchaber, A.J., 2001. Single-mismatch detection using gold-quenched fluorescent oligonucleotides. Nat Biotech 19(4), 365-370.

Fei, T., Jiang, K., Zhang, T., 2014. Highly sensitive TNT photoluminescent sensing by a phosphorescent complex. Sensors and Actuators B: Chemical 199(0), 148-153.

Fernández-Sánchez, J.F., Cannas, R., Spichiger, S., Steiger, R., Spichiger-Keller, U.E., 2006. Novel nanostructured materials to develop oxygen-sensitive films for optical sensors. Analytica Chimica Acta 566(2), 271-282.

Fernández-Sánchez, J.F., Roth, T., Cannas, R., Nazeeruddin, M.K., Spichiger, S., Graetzel, M., Spichiger-Keller, U.E., 2007. Novel oxygen sensitive complexes for optical oxygen sensing. Talanta 71(1), 242-250.

Fischer, L.H., Borisov, S.M., Schaeferling, M., Klimant, I., Wolfbeis, O.S., 2010. Dual sensing of pO_2 and temperature using a water-based and sprayable fluorescent paint. Analyst 135(6), 1224-1229.

Fischer, L.H., Stich, M.I.J., Wolfbeis, O.S., Tian, N., Holder, E., Schäferling, M., 2009. Red- and Green-Emitting Iridium(III) Complexes for a Dual Barometric and Temperature-Sensitive Paint. Chemistry – A European Journal 15(41), 10857-10863.

Goodall, W., Williams, J.A.G., 2000. Iridium(III) bis-terpyridine complexes incorporating pendent N-methylpyridinium groups: luminescent sensors for chloride ions. Journal of the Chemical Society, Dalton Transactions(17), 2893-2895.

Habibagahi, A., Mébarki, Y., Sultan, Y., Yap, G.P.A., Crutchley, R.J., 2009. Water-Based Oxygen-Sensor Films. ACS Applied Materials & Interfaces 1(8), 1785-1792.

Han, Y., You, Y., Lee, Y.-M., Nam, W., 2012. Double Action: Toward Phosphorescence Ratiometric Sensing of Chromium Ion. Advanced Materials 24(20), 2748-2754.

He, L., Tan, C.-P., Ye, R.-R., Zhao, Y.-Z., Liu, Y.-H., Zhao, Q., Ji, L.-N., Mao, Z.-W., 2014. Theranostic Iridium(III) Complexes as One- and Two-Photon Phosphorescent Trackers to Monitor Autophagic Lysosomes. Angewandte Chemie International Edition 53(45), 12137-12141.

Herebian, D., Sheldrick, W.S., 2002. Synthesis and DNA binding properties of bioorganometallic (η^5-pentamethylcyclopentadienyl)iridium(III) complexes of the type $[(\eta^5\text{-}C_5Me_5)Ir(Aa)(dppz)]^{n+}$ (dppz = dipyrido[3,2-*a*:2',3'-*c*]-phenazine, *n* = 1-3), with S-coordinated amino acids (Aa) or peptides. Journal of the Chemical Society, Dalton Transactions(6), 966-974.

Ho, M.-L., Chen, Y.-A., Chen, T.-C., Chang, P.-J., Yu, Y.-P., Cheng, K.-Y., Shih, C.-H., Lee, G.-H., Sheu, H.-S., 2012. Synthesis, structure and oxygen-sensing properties of Iridium(iii)-containing coordination polymers with different cations. Dalton Transactions 41(9), 2592-2600.

Ho, M.-L., Cheng, Y.-M., Wu, L.-C., Chou, P.-T., Lee, G.-H., Hsu, F.-C., Chi, Y., 2007. Probing Pb^{2+} cation via the iridium based phosphorescent dye. Polyhedron 26(17), 4886-4892.

Ho, M.-L., Hwang, F.-M., Chen, P.-N., Hu, Y.-H., Cheng, Y.-M., Chen, K.-S., Lee, G.-H., Chi, Y., Chou, P.-T., 2006. Design and synthesis of iridium(III) azacrown complex: application as a highly sensitive metal cation phosphorescence sensor. Organic & Biomolecular Chemistry 4(1), 98-103.

Ho, M.L., Wang, J.C., Wang, T.Y., Lin, C.Y., Zhu, J.F., Chen, Y.A., Chen, T.C., 2014. The construction of glucose biosensor based on crystalline iridium(III)-containing coordination polymers with fiber-optic detection. Sensors and Actuators, B: Chemical 190, 479-485.

Hou, X.-G., Wu, Y., Cao, H.-T., Sun, H.-Z., Li, H.-B., Shan, G.-G., Su, Z.-M., 2014. A cationic iridium(III) complex with aggregation-induced emission (AIE) properties for highly selective detection of explosives. Chemical Communications 50(45), 6031-6034.

Huang, K., Bulik, I.W., Marti, A.A., 2012. Time-resolved photoluminescence spectroscopy for the detection of cysteine and other thiol containing amino acids in complex strongly autofluorescent media. Chemical Communications 48(96), 11760-11762.

Hulanicki, A., Glab, S., Ingman, F., 1991. Chemical sensors definitions and classification. Pure & Appl. Chem. 63(9), 1247-1250.

Huynh, L., Wang, Z., Yang, J., Stoeva, V., Lough, A., Manners, I., Winnik, M.A., 2005. Evaluation of Phosphorescent Rhenium and Iridium Complexes in Polythionylphosphazene Films for Oxygen Sensor Applications. Chemistry of Materials 17(19), 4765-4773.

Jayabharathi, J., Sathishkumar, R., Thanikachalam, V., Jayamoorthy, K., 2014. Tuning Photophysical and Electrochemical Properties of Phosphorescent Heteroleptic Iridium Complex Salts-as Chemosensors. Journal of Fluorescence 24(2), 445-453.

Jee-Hye, A., Yinan, L., Myung-Ho, H., 2012. 3,9-Dithia-6-azaundecane-appended Iridium (III) Complex for the Selective Detection of Hg2+ in Aqueous Acetonitrile. Bulletin of the Korean Chemical Society 33(10), 3465-3468.

Jin, P., Guo, Z., Chu, J., Tan, J., Zhang, S., Zhu, W., 2013. Screen-printed red luminescent copolymer film containing cyclometalated iridium(III) complex as a high-permeability dissolved-oxygen sensor for fermentation bioprocess. Industrial and Engineering Chemistry Research 52(11), 3980-3987.

Kang, J.H., Kim, H.J., Kwon, T.-H., Hong, J.-I., 2014. Phosphorescent Sensor for Phosphorylated Peptides Based on an Iridium Complex. The Journal of Organic Chemistry 79(13), 6000-6005.

Kim, H.-B., Li, Y., Hyun, M.H., 2013. Phosphorescent Chemosensor Based on Iridium(III) Complex for the Selective Detection of Cu(II) Ion in Aqueous Acetonitrile. Bulletin of the Korean Chemical Society 34(2), 653-656.

Kim, H.-b., Liu, Y., Nam, D., Li, Y., Park, S., Yoon, J., Hyun, M.H., 2014. A new phosphorescent chemosensor bearing Zn-DPA sites for $H_2PO_4^-$. Dyes and Pigments 106(0), 20-24.

Koren, K., Borisov, S.M., Saf, R., Klimant, I., 2011. Strongly phosphorescent iridium(III)-porphyrins - New oxygen indicators with tuneable photophysical properties and functionalities. European Journal of Inorganic Chemistry(10), 1531-1534.

Köse, M.E., Crutchley, R.J., DeRosa, M.C., Ananthakrishnan, N., Reynolds, J.R., Schanze, K.S., 2005. Morphology and Oxygen Sensor Response of Luminescent Ir-Labeled Poly(dimethylsiloxane)/Polystyrene Polymer Blend Films. Langmuir 21(18), 8255-8262.

Kwon, T.-H., Kim, H.J., Hong, J.-I., 2008a. Phosphorescent Thymidine Triphosphate Sensor Based on a Donor–Acceptor Ensemble System using Intermolecular Energy Transfer. Chemistry – A European Journal 14(31), 9613-9619.

Kwon, T.-H., Kwon, J., Hong, J.-I., 2008b. Signal Amplification via Intramolecular Energy Transfer Using Tripodal Neutral Iridium(III) Complexes upon Binding to Avidin. Journal of the American Chemical Society 130(12), 3726-3727.

Lau, J.S.-Y., Lee, P.-K., Tsang, K.H.-K., Ng, C.H.-C., Lam, Y.-W., Cheng, S.-H., Lo, K.K.-W., 2009. Luminescent Cyclometalated Iridium(III) Polypyridine Indole Complexes-Synthesis, Photophysics, Electrochemistry, Protein-Binding Properties, Cytotoxicity, and Cellular Uptake. Inorganic Chemistry 48(2), 708-718.

Lee, P.-K., Law, W.H.-T., Liu, H.-W., Lo, K.K.-W., 2011. Luminescent Cyclometalated Iridium(III) Polypyridine Di-2-picolylamine Complexes: Synthesis, Photophysics, Electrochemistry, Cation Binding, Cellular Internalization, and Cytotoxic Activity. Inorganic Chemistry 50(17), 8570-8579.

Li, C., Wang, S., Huang, Y., Wen, Q., Wang, L., Kan, Y., 2014a. Photoluminescence properties of a novel cyclometalated iridium(III) complex with coumarin-boronate and its recognition of hydrogen peroxide. Dalton Transactions 43(14), 5595-5602.

Li, G., Chen, Y., Wang, J., Lin, Q., Zhao, J., Ji, L., Chao, H., 2013. A dinuclear iridium(III) complex as a visual specific phosphorescent probe for endogenous sulphite and bisulphite in living cells. Chemical Science 4(12), 4426-4433.

Li, G., Lin, Q., Ji, L., Chao, H., 2014b. Phosphorescent iridium(III) complexes as multicolour probes for imaging of hypochlorite ions in mitochondria. Journal of Materials Chemistry B 2(45), 7918-7926.

Li, M.-J., Jiao, P., He, W., Yi, C., Li, C.-W., Chen, X., Chen, G.-N., Yang, M., 2011. Water-Soluble and Biocompatible Cyclometalated Iridium(III) Complexes: Synthesis, Luminescence and Sensing Application. European Journal of Inorganic Chemistry 2011(2), 197-200.

Li, X., Lan, H., Chen, Y., Lv, K., Zhang, A., Huang, T., 2012. A dipicolylamine-appended cyclometalated iridium(III) complex: Synthesis, characterization and metal ions recognition. Inorganica Chimica Acta 390(0), 41-46.

Li, Y., Liu, Y., Nam, D., Park, S., Yoon, J., Hyun, M.H., 2014c. New iridium complexes with two pre-organized urea groups and thiourea groups as phosphorescent chemosensors for $H_2PO_4^-$ and chiral carboxylates. Dyes and Pigments 100(0), 241-246.

Liang, M., Manners, I., 1991. Poly(thionylphosphazenes): a new class of inorganic polymers with skeletal phosphorus, nitrogen, and sulfur(VI) atoms. Journal of the American Chemical Society 113(10), 4044-4045.

Licini, M., A. Gareth Williams, J., 1999. Iridium(III) bis-terpyridine complexes displaying long-lived pH sensitive luminescence. Chemical Communications(19), 1943-1944.

Lin, H., Cinar, M.E., Schmittel, M., 2010. Comparison of ruthenium(ii) and cyclometalated iridium(iii) azacrown ether phenanthroline hybrids for the detection of metal cations by electrochemiluminescence. Dalton Transactions 39(21), 5130-5138.

Liu, J., Liu, Y., Liu, Q., Li, C., Sun, L., Li, F., 2011a. Iridium(III) Complex-Coated Nanosystem for Ratiometric Upconversion Luminescence Bioimaging of Cyanide Anions. Journal of the American Chemical Society 133(39), 15276-15279.

Liu, S., Qiao, W., Cao, G., Chen, Y., Ma, Y., Huang, Y., Liu, X., Xu, W., Zhao, Q., Huang, W., 2013. Smart Poly(N-isopropylacrylamide) Containing Iridium(III) Complexes as Water-Soluble Phosphorescent Probe for Sensing and Bioimaging of Homocysteine and Cysteine. Macromolecular Rapid Communications 34(1), 81-86.

Liu, X., Xi, N., Liu, S., Ma, Y., Yang, H., Li, H., He, J., Zhao, Q., Li, F., Huang, W., 2012. Highly selective phosphorescent nanoprobes for sensing and bioimaging of homocysteine and cysteine. Journal of Materials Chemistry 22(16), 7894-7901.

Liu, Y., Li, M., Zhao, Q., Wu, H., Huang, K., Li, F., 2011b. Phosphorescent Iridium(III) Complex with an N^O Ligand as a Hg^{2+}-Selective Chemodosimeter and Logic Gate. Inorganic Chemistry 50(13), 5969-5977.

Liu, Z., Bian, Z., Bian, J., Li, Z., Nie, D., Huang, C., 2008. Acetonitrile-Vapor-Induced Color and Luminescence Changes in a Cyclometalated Heteroleptic Iridium Complex. Inorganic Chemistry 47(18), 8025-8030.

Lo, K.K.-W., Chan, J.S.-W., Lui, L.-H., Chung, C.-K., 2004. Novel Luminescent Cyclometalated Iridium(III) Diimine Complexes That Contain a Biotin Moiety. Organometallics 23(13), 3108-3116.

Lo, K.K.-W., Chung, C.-K., Zhu, N., 2006a. Nucleic Acid Intercalators and Avidin Probes Derived from Luminescent Cyclometalated Iridium(III)–Dipyridoquinoxaline and –Dipyridophenazine Complexes. Chemistry – A European Journal 12(5), 1500-1512.

Lo, K.K.-W., Lau, J.S.-Y., 2007. Cyclometalated Iridium(III) Diimine Bis(biotin) Complexes as the First Luminescent Biotin-Based Cross-Linkers for Avidin. Inorganic Chemistry 46(3), 700-709.

Lo, K.K.-W., Lau, J.S.-Y., Lo, D.K.-K., Lo, L.T.-L., 2006b. Luminescent Cyclometalated Iridium(III) Polypyridine Complexes Containing a Thiourea Moiety: Synthesis, Characterization, Photophysics,

Electrochemistry and Anion-Binding Properties. European Journal of Inorganic Chemistry 2006(20), 4054-4062.

Lo, K.K.-W., Li, C.-K., Lau, J.S.-Y., 2005. Luminescent Cyclometalated Iridium(III) Arylbenzothiazole Biotin Complexes. Organometallics 24(19), 4594-4601.

Lo, K.K.-W., Zhang, K.Y., Chung, C.-K., Kwok, K.Y., 2007. Synthesis, Photophysical and Electrochemical Properties, and Protein-Binding Studies of Luminescent Cyclometalated Iridium(III) Bipyridine Estradiol Conjugates. Chemistry – A European Journal 13(25), 7110-7120.

Lo, K.K.-W., Zhang, K.Y., Leung, S.-K., Tang, M.-C., 2008. Exploitation of the Dual-emissive Properties of Cyclometalated Iridium(III)–Polypyridine Complexes in the Development of Luminescent Biological Probes. Angewandte Chemie International Edition 47(12), 2213-2216.

Lou, B., Chen, Z.-Q., Bian, Z.-Q., Huang, C.-H., 2010. Multisignaling detection of cyanide anions based on an iridium(III) complex: remarkable enhancement of sensitivity by coordination effect. New Journal of Chemistry 34(1), 132-136.

Lu, F., Nabeshima, T., 2014. A highly selective and sensitive turn-on chemodosimeter for hypochlorous acid based on an iridium(III) complex and its application to bioimaging. Dalton Transactions 43(25), 9529-9536.

Lu, F., Yamamura, M., Nabeshima, T., 2013a. A highly selective and sensitive ratiometric chemodosimeter for Hg2+ ions based on an iridium(iii) complex via thioacetal deprotection reaction. Dalton Transactions 42(34), 12093-12100.

Lu, F., Yamamura, M., Nabeshima, T., 2013b. Luminescent biscyclometalated iridium(III) complex for selective and switchable Cu^{2+} ion binding in aqueous media. Tetrahedron Letters 54(8), 779-782.

Lu, L., He, H.-Z., Zhong, H.-J., Liu, L.-J., Chan, D.S.-H., Leung, C.-H., Ma, D.-L., 2014. Luminescent detection of human serum albumin in aqueous solution using a cyclometallated iridium(III) complex. Sensors and Actuators B: Chemical 201(0), 177-184.

Ma, D.-L., He, H.-Z., Chan, D.S.-H., Wong, C.-Y., Leung, C.-H., 2014a. A Colorimetric and Luminescent Dual-Modal Assay for Cu(II) Ion Detection Using an Iridium(III) Complex. PLoS ONE 9(6), e99930.

Ma, D.-L., He, H.-Z., Zhong, H.-J., Lin, S., Chan, D.S.-H., Wang, L., Lee, S.M.-Y., Leung, C.-H., Wong, C.-Y., 2014b. Visualization of Zn^{2+} Ions in Live Zebrafish Using a Luminescent Iridium(III) Chemosensor. ACS Applied Materials & Interfaces 6(16), 14008-14015.

Ma, D.-L., Wong, W.-L., Chung, W.-H., Chan, F.-Y., So, P.-K., Lai, T.-S., Zhou, Z.-Y., Leung, Y.-C., Wong, K.-Y., 2008. A Highly Selective Luminescent Switch-On Probe for Histidine/Histidine-Rich Proteins and Its Application in Protein Staining. Angewandte Chemie International Edition 47(20), 3735-3739.

Ma, D.-L., Zhong, H.-J., Fu, W.-C., Chan, D.S.-H., Kwan, H.-Y., Fong, W.-F., Chung, L.-H., Wong, C.-Y., Leung, C.-H., 2013a. Phosphorescent Imaging of Living Cells Using a Cyclometalated Iridium(III) Complex. PLoS ONE 8(2), e55751.

Ma, Y., Liu, S., Yang, H., Wu, Y., Sun, H., Wang, J., Zhao, Q., Li, F., Huang, W., 2013b. A water-soluble phosphorescent polymer for time-resolved assay and bioimaging of cysteine/homocysteine. Journal of Materials Chemistry B 1(3), 319-329.

Ma, Y., Liu, S., Yang, H., Wu, Y., Yang, C., Liu, X., Zhao, Q., Wu, H., Liang, J., Li, F., Huang, W., 2011. Water-soluble phosphorescent iridium(III) complexes as multicolor probes for imaging of homocysteine and cysteine in living cells. Journal of Materials Chemistry 21(47), 18974-18982.

Mak, C.S.K., Penflehner, D., Stich, M., Wolfbeis, O.S., Chan, W.K., Yersin, H., 2009. Exceptional oxygen sensing capabilities and triplet state properties of Ir(ppy-NPh2)3. Chemistry of Materials 21(11), 2173-2175.

Mandal, S., Das, R., Gupta, P., Mukhopadhyay, B., 2012. Synthesis of a sugar-functionalized iridium complex and its application as a fluorescent lectin sensor. Tetrahedron Letters 53(30), 3915-3918.

Marín-Suárez, M., Curchod, B.F.E., Tavernelli, I., Rothlisberger, U., Scopelliti, R., Jung, I., Di Censo, D., Grätzel, M., Fernández-Sánchez, J.F., Fernández-Gutiérrez, A., Nazeeruddin, M.K., Baranoff, E., 2012. Nanocomposites Containing Neutral Blue Emitting Cyclometalated Iridium(III) Emitters for Oxygen Sensing. Chemistry of Materials 24(12), 2330-2338.

Marin-Suarezdel Toro, M., Fernandez-Sanchez, J.F., Baranoff, E., Nazeeruddin, M.K., Graetzel, M., Fernandez-Gutierrez, A., 2010. Novel luminescent Ir(III) dyes for developing highly sensitive oxygen sensing films. Talanta 82(2), 620-626.

McFarland, A.D., Van Duyne, R.P., 2003. Single Silver Nanoparticles as Real-Time Optical Sensors with Zeptomole Sensitivity. Nano Letters 3(8), 1057-1062.

Medina-Castillo, A.L., Fernández-Sánchez, J.F., Klein, C., Nazeeruddin, M.K., Segura-Carretero, A., Fernández-Gutiérrez, A., Graetzel, M., Spichiger-Keller, U.E., 2007. Engineering of efficient phosphorescent iridium cationic complex for developing oxygen-sensitive polymeric and nanostructured films. The Analyst 132(9), 929-936.

Medina-Rodríguez, S., de la Torre-Vega, Á., Sainz-Gonzalo, F.J., Marín-Suárez, M., Elosúa, C., Arregui, F.J., Matias, I.R., Fernández-Sánchez, J.F., Fernández-Gutiérrez, A., 2014. Improved Multifrequency Phase-Modulation Method That Uses Rectangular-Wave Signals to Increase Accuracy in Luminescence Spectroscopy. Analytical Chemistry 86(11), 5245-5256.

Medina-Rodríguez, S., Marín-Suárez, M., Fernández-Sánchez, J.F., Torre-Vega, Á.D.L., Baranoff, E., Fernández-Gutiérrez, A., 2013b. High performance optical sensing nanocomposites for low and ultra-low oxygen concentrations using phase-shift measurements. Analyst 138(16), 4607-4617.

Mei, Q.-b., Guo, Y.-h., Tong, B.-h., Weng, J.-N., Zhang, B., Huang, W., 2012. Phosphorescent chemosensor for Hg2+ and acetonitrile based on iridium(iii) complex. Analyst 137(22), 5398-5402.

Mothajit, K., Wongkhan, K., Jitchati, R., 2014. A Novel charged iridium(III) complex for amine sensor application. Advanced Materials Research(893), 91-94.

Mukherjee, T., Mukherjee, M., Sen, B., Banerjee, S., Hundal, G., Chattopadhyay, P., 2014. Synthesis, characterization, interactions with DNA and bovine serum albumin (BSA), and antibacterial activity

of cyclometalated iridium(III) complexes containing dithiocarbamate derivatives. Journal of Coordination Chemistry 67(15), 2643-2660.

Nazeeruddin, M.K., Humphry-Baker, R., Berner, D., Rivier, S., Zuppiroli, L., Graetzel, M., 2003. Highly Phosphorescence Iridium Complexes and Their Application in Organic Light-Emitting Devices. Journal of the American Chemical Society 125(29), 8790-8797.

Ni, Y., Park, P., Liang, M., Massey, J., Waddling, C., Manners, I., 1996. Polymers with Sulfur(VI-Nitrogen-Phosphorus Backbones: Synthesis, Characterization, and Properties of Atactic Poly[(amino)thionylphosphazenes]. Macromolecules 29(10), 3401-3408.

Park, H.-J., Kim, K., Chung, Y.K., 2014. Re^{I}-Ir^{I} bimetallic complexes based on a bis(chelating) ligand composed of 1,10-phenanthroline and N-heterocyclic carbene: Coordination chemistry and their application for optical indicator of CO gas. Inorganica Chimica Acta 410(0), 214-220.

Qinghai, S., Bats, J.W., Schmittel, M., 2011. Two Closely Related Iridium(III) Complexes as Colorimetric and Fluorometric Chemodosimeters for Nitrite in Aqueous Solution Operating along Different Modes of Action. Inorganic Chemistry 50(21), 10531-10533.

Qinghai, S., Birlenbach, L., Schmittel, M., 2012. A Bis(ferrocenyl)phenanthroline Iridium(III) Complex as a Lab-on-a-Molecule for Cyanide and Fluoride in Aqueous Solution. Inorganic Chemistry 51(24), 13123-13127.

Sato, H., Tamura, K., Taniguchi, M., Yamagishi, A., 2010. Highly luminescent Langmuir-Blodgett films of amphiphilic Ir(III) complexes for application in gas sensing. New Journal of Chemistry 34(4), 617-622.

Schmittel, M., Lin, H., 2007. Luminescent Iridium Phenanthroline Crown Ether Complex for the Detection of Silver(I) Ions in Aqueous Media. Inorganic Chemistry 46(22), 9139-9145.

Schmittel, M., Qinghai, S., 2012. A lab-on-a-molecule for anions in aqueous solution: using Kolbe electrolysis and radical methylation at iridium for sensing. Chemical Communications 48(21), 2707-2709.

Schwartz, K.R., Mann, K.R., 2011. Optical Response of a Cyclometalated Iridium(III) Hydrazino Complex to Carbon Dioxide: Generation of a Strongly Luminescent Iridium(III) Carbazate. Inorganic Chemistry 50(24), 12477-12485.

Sharma, S., Kim, H., Lee, Y.H., Kim, T., Lee, Y.S., Lee, M.H., 2014. Heteroleptic Cyclometalated Iridium(III) Complexes Supported by Triarylborylpicolinate Ligand: Ratiometric Turn-On Phosphorescence Response upon Fluoride Binding. Inorganic Chemistry 53(16), 8672-8680.

Shi, H.-F., Liu, S.-J., Sun, H.-B., Xu, W.-J., An, Z.-F., Chen, J., Sun, S., Lu, X.-M., Zhao, Q., Huang, W., 2010. Simple Conjugated Polymers with On-Chain Phosphorescent Iridium(III) Complexes: Toward Ratiometric Chemodosimeters for Detecting Trace Amounts of Mercury(II). Chemistry – A European Journal 16(40), 12158-12167.

Shi, H., Liu, S., An, Z., Yang, H., Geng, J., Zhao, Q., Liu, B., Huang, W., 2013a. A Ratiometric Probe Composed of an Anionic Conjugated Polyelectrolyte and a Cationic Phosphorescent Iridium(III)

Complex for Time-Resolved Detection of Hg(II) in Aqueous Media. Macromolecular Bioscience 13(10), 1339-1346.

Shi, H., Sun, H., Yang, H., Liu, S., Jenkins, G., Feng, W., Li, F., Zhao, Q., Liu, B., Huang, W., 2013b. Cationic Polyfluorenes with Phosphorescent Iridium(III) Complexes for Time-Resolved Luminescent Biosensing and Fluorescence Lifetime Imaging. Advanced Functional Materials 23(26), 3268-3276.

Shiu, H.-Y., Wong, M.-K., Che, C.-M., 2011. "Turn-on" FRET-based luminescent iridium(III) probes for the detection of cysteine and homocysteine. Chemical Communications 47(15), 4367-4369.

Sie, W.-S., Lee, G.-H., Tsai, K.Y.-D., Chang, I.J., Shiu, K.-B., 2008. Synthesis, structures, properties, and chemical-sensor application of iridium(III) bis-cyclometallated complexes with two pyridine-derived ligands. Journal of Molecular Structure 890(1-3), 198-202.

Sonnichsen, C., Reinhard, B.M., Liphardt, J., Alivisatos, A.P., 2005. A molecular ruler based on plasmon coupling of single gold and silver nanoparticles. Nat Biotech 23(6), 741-745.

Sprouse, S., King, K.A., Spellane, P.J., Watts, R.J., 1984. Photophysical effects of metal-carbon .sigma. bonds in ortho-metalated complexes of iridium(III) and rhodium(III). Journal of the American Chemical Society 106(22), 6647-6653.

Sun, P., Lu, X., Fan, Q., Zhang, Z., Song, W., Li, B., Huang, L., Peng, J., Huang, W., 2011b. Water-Soluble Iridium(III)-Containing Conjugated Polyelectrolytes with Weakened Energy Transfer Properties for Multicolor Protein Sensing Applications. Macromolecules 44(22), 8763-8770.

Tamayo, A.B., Alleyne, B.D., Djurovich, P.I., Lamansky, S., Tsyba, I., Ho, N.N., Bau, R., Thompson, M.E., 2003. Synthesis and Characterization of Facial and Meridional Tris-cyclometalated Iridium(III) Complexes. Journal of the American Chemical Society 125(24), 7377-7387.

Tang, Y., Yang, H.-R., Sun, H.-B., Liu, S.-J., Wang, J.-X., Zhao, Q., Liu, X.-M., Xu, W.-J., Li, S.-B., Huang, W., 2013. Rational Design of an ―OF–ON" Phosphorescent Chemodosimeter Based on an Iridium(III) Complex and Its Application for Time-Resolved Luminescent Detection and Bioimaging of Cysteine and Homocysteine. Chemistry – A European Journal 19(4), 1311-1319.

Taton, T.A., Mirkin, C.A., Letsinger, R.L., 2000. Scanometric DNA Array Detection with Nanoparticle Probes. Science 289(5485), 1757-1760.

Tian, N., Lenkeit, D., Pelz, S., Fischer, L.H., Escudero, D., Schiewek, R., Klink, D., Schmitz, O.J., González, L., Schäferling, M., Holder, E., 2010. Structure–Property Relationship of Red- and Green-Emitting Iridium(III) Complexes with Respect to Their Temperature and Oxygen Sensitivity. European Journal of Inorganic Chemistry 2010(30), 4875-4885.

Tong, B., Ma, P., Zhang, M., Liu, Y., Mei, Q., Zhang, Q.-F., 2013a. Phosphorescent iridium(III) carbodithioate complex for the detection of Hg^{2+} and acetonitrile. Inorganic Chemistry Communications 37(0), 121-126.

Tong, B., Mei, Q., Lu, M., 2012. A highly selective chemosensor for mercury(II) cations based on cyclometalated iridium(III) complex. Inorganica Chimica Acta 391(0), 15-19.

Tong, B., Zhang, M., Han, Z., Mei, Q., Zhang, Q., 2013b. Novel colorimetric phosphorescent chemodosimeter for Hg^{2+} based iridium(III) complex with phosphonodithioate auxiliary ligand. Journal of Organometallic Chemistry 724(0), 180-185.

Tong, B., Zhang, Y., Han, Z., Chen, D., Zhang, Q.-F., 2013c. Highly sensitive colorimetric phosphorescent chemodosimeter for Hg^{2+} based iridium(III) complex with $(Ph_2PS)_2N$ auxiliary ligand. Inorganic Chemistry Communications 28(0), 31-36.

Vander Donckt, E., Camerman, B., Hendrick, F., Heme, R., Vandeloise, R., 1994. Polystyrene Immobilized Ir(III) Complex as a new Material for Optical Oxygen Sensing. Bulletin des Sociétés Chimiques Belges 103(5-6), 207-211.

Wang, T.-H., Peng, Y., Zhang, C., Wong, P.K., Ho, C.-M., 2005. Single-Molecule Tracing on a Fluidic Microchip for Quantitative Detection of Low-Abundance Nucleic Acids. Journal of the American Chemical Society 127(15), 5354-5359.

Wang, X.-d., Wolfbeis, O.S., 2014. Optical methods for sensing and imaging oxygen: materials, spectroscopies and applications. Chemical Society Reviews 43(10), 3666-3761.

Wolfbeis, O., 1990. Chemical sensors — survey and trends. Fresenius J Anal Chem 337(5), 522-527.

Wu, Y., Jing, H., Dong, Z., Zhao, Q., Wu, H., Li, F., 2011. Ratiometric Phosphorescence Imaging of Hg(II) in Living Cells Based on a Neutral Iridium(III) Complex. Inorganic Chemistry 50(16), 7412-7420.

Xie, Z., Ma, L., deKrafft, K.E., Jin, A., Lin, W., 2009. Porous Phosphorescent Coordination Polymers for Oxygen Sensing. Journal of the American Chemical Society 132(3), 922-923.

Xiong, L., Zhao, Q., Chen, H., Wu, Y., Dong, Z., Zhou, Z., Li, F., 2010. Phosphorescence Imaging of Homocysteine and Cysteine in Living Cells Based on a Cationic Iridium(III) Complex. Inorganic Chemistry 49(14), 6402-6408.

Xu, W.-J., Liu, S.-J., Zhao, X.-Y., Sun, S., Cheng, S., Ma, T.-C., Sun, H.-B., Zhao, Q., Huang, W., 2010. Cationic Iridium(III) Complex Containing both Triarylboron and Carbazole Moieties as a Ratiometric Fluoride Probe That Utilizes a Switchable Triplet–Singlet Emission. Chemistry – A European Journal 16(24), 7125-7133.

Xu, W.-J., Liu, S.-J., Zhao, X., Zhao, N., Liu, Z.-Q., Xu, H., Liang, H., Zhao, Q., Yu, X.-Q., Huang, W., 2013. Synthesis, One- and Two-Photon Photophysical and Excited-State Properties, and Sensing Application of a New Phosphorescent Dinuclear Cationic Iridium(III) Complex. Chemistry – A European Journal 19(2), 621-629.

Xu, W., Liu, S., Sun, H., Zhao, X., Zhao, Q., Sun, S., Cheng, S., Ma, T., Zhou, L., Huang, W., 2011a. FRET-based probe for fluoride based on a phosphorescent iridium(III) complex containing triarylboron groups. Journal of Materials Chemistry 21(21), 7572-7581.

Xu, W., Liu, S., Zhao, Q., Ma, T., Sun, S., Zhao, X., Huang, W., 2011b. A near-infrared phosphorescent probe for F^- based on a cationic iridium(III) complex with triarylboron moieties. Science China Chemistry 54(11), 1750-1758.

Xue, F., Lu, Y., Zhou, Z., Zhang, C., Fang, S., Yang, H., Yang, S., 2014b. Synthesis, crystal structure, and application as a Ag^{+} chemodosimeter of phosphorescent iridium complexes. Journal of Coordination Chemistry 67(8), 1353-1360.

Yan, F., Mei, Q., Wang, L., Tong, B., Xu, Z., Weng, J., Wang, L., Huang, W., 2012. A highly selective and ratiometric sensor for Hg2+ based on a phosphorescent iridium (III) complex. Inorganic Chemistry Communications 22(0), 178-181.

Yang, H., Qian, J., Li, L., Zhou, Z., Li, D., Wu, H., Yang, S., 2010. A selective phosphorescent chemodosimeter for mercury ion. Inorganica Chimica Acta 363(8), 1755-1759.

Yang, H., Zhu, Y., Li, L., Zhou, Z., Yang, S., 2012. A phosphorescent chemosensor for Cu^{2+} based on cationic iridium(III) complexes. Inorganic Chemistry Communications 16(0), 1-3.

Yang, X., Huang, Z., Ho, C.-L., Zhou, G., Whang, D.R., Yao, C., Xu, X., Park, S.Y., Chui, C.-H., Wong, W.-Y., 2013. Dynamic dual stage phosphorescence chromatic change in a diborylated iridium phosphor for fluoride ion sensing with concentration discriminating capability. RSC Advances 3(18), 6553-6563.

Yao, L., Zhou, J., Liu, J., Feng, W., Li, F., 2012. Iridium-Complex-Modified Upconversion Nanophosphors for Effective LRET Detection of Cyanide Anions in Pure Water. Advanced Functional Materials 22(13), 2667-2672.

Yinan, L., Myung-Ho, H., 2011. Phosphorescent Dimesitylboryl-Appended Iridium(III) Complex for Fluoride Anion Sensing. Bulletin of the Korean Chemical Society 32(11), 4125-4128.

Yoshihara, T., Murayama, S., Masuda, T., Kikuchi, T., Yoshida, K., Hosaka, M., Tobita, S., 2015. Mitochondria-targeted oxygen probes based on cationic iridium complexes with a 5-amino-1, 10-phenanthroline ligand. Journal of Photochemistry and Photobiology A: Chemistry 299, 172-182.

Yoshikawa, H., Kobayashi, M., Takahashi, T., Awaga, K., 2010. A Novel Free Radical Probe Based on a Preluminescent Iridium Complex Bearing a Nitronyl Radical Moiety. Bulletin of the Chemical Society of Japan 83(7), 762-766.

You, Y., Cho, S., Nam, W., 2013. Cyclometalated Iridium(III) Complexes for Phosphorescence Sensing of Biological Metal Ions. Inorganic Chemistry 53(4), 1804-1815.

You, Y., Han, Y., Lee, Y.-M., Park, S.Y., Nam, W., Lippard, S.J., 2011. Phosphorescent Sensor for Robust Quantification of Copper(II) Ion. Journal of the American Chemical Society 133(30), 11488-11491.

You, Y., Park, S.Y., 2008. A Phosphorescent Ir(III) Complex for Selective Fluoride Ion Sensing with a High Signal-to-Noise Ratio. Advanced Materials 20(20), 3820-3826.

Zeng, H., Yu, F., Dai, J., Sun, H., Lu, Z., Li, M., Jiang, Q., Huang, Y., 2012. A highly selective sulfur-free iridium(iii)-complex-based phosphorescent chemidosimeter for detection of mercury(ii) ions. Dalton Transactions 41(16), 4878-4883.

Zhang, K.Y., Li, S.P.-Y., Zhu, N., Or, I.W.-S., Cheung, M.S.-H., Lam, Y.-W., Lo, K.K.-W., 2010. Structure, Photophysical and Electrochemical Properties, Biomolecular Interactions, and Intracellular

Uptake of Luminescent Cyclometalated Iridium(III) Dipyridoquinoxaline Complexes. Inorganic Chemistry 49(5), 2530-2540.

Zhang, S., Hosaka, M., Yoshihara, T., Negishi, K., Iida, Y., Tobita, S., Takeuchi, T., 2012. Phosphorescent Light-Emitting Iridium Complexes Serve as a Hypoxia-Sensing Probe for Tumor Imaging in Living Animals. Cancer Research 70(11), 4490-4498.

Zhao, N., Wu, Y.-H., Luo, J., Shi, L.-X., Chen, Z.-N., 2013. Aggregation-induced phosphorescence of iridium(iii) complexes with 2,2'-bipyridine-acylhydrazone and their highly selective recognition to Cu^{2+}. Analyst 138(3), 894-900.

Zhao, N., Wu, Y.-H., Shi, L.-X., Lin, Q.-P., Chen, Z.-N., 2010. A sensitive phosphorescent thiol chemosensor based on an iridium(III) complex with α,β-unsaturated ketone functionalized 2,2'-bipyridyl ligand. Dalton Transactions 39(35), 8288-8295.

Zhao, N., Wu, Y.-H., Wang, R.-M., Shi, L.-X., Chen, Z.-N., 2011. An iridium(iii) complex of oximated 2,2'-bipyridine as a sensitive phosphorescent sensor for hypochlorite. Analyst 136(11), 2277-2282.

Zhao, N., Wu, Y.-H., Wen, H.-M., Zhang, X., Chen, Z.-N., 2009. Conversion from ILCT to LLCT/MLCT Excited State by Heavy Metal Ion Binding in Iridium(III) Complexes with Functionalized 2,2'-Bipyridyl Ligands. Organometallics 28(19), 5603-5611.

Zhao, Q., Cao, T., Li, F., Li, X., Jing, H., Yi, T., Huang, C., 2007a. A Highly Selective and Multisignaling Optical-Electrochemical Sensor for Hg^{2+} Based on a Phosphorescent Iridium(III) Complex. Organometallics 26(8), 2077-2081.

Zhao, Q., Li, F., Liu, S., Yu, M., Liu, Z., Yi, T., Huang, C., 2008a. Highly Selective Phosphorescent Chemosensor for Fluoride Based on an Iridium(III) Complex Containing Arylborane Units. Inorganic Chemistry 47(20), 9256-9264.

Zhao, Q., Liu, S., Li, F., Yi, T., Huang, C., 2008b. Multisignaling detection of Hg2+ based on a phosphorescent iridium(iii) complex. Dalton Transactions(29), 3836-3840.

Zhao, Q., Liu, S., Shi, M., Li, F., Jing, H., Yi, T., Huang, C., 2007b. Tuning Photophysical and Electrochemical Properties of Cationic Iridium(III) Complex Salts with Imidazolyl Substituents by Proton and Anions. Organometallics 26(24), 5922-5930.

Zhou, C., Shi, Y., Ding, X., Li, M., Luo, J., Lu, Z., Xiao, D., 2013. Development of a Fast and Sensitive Glucose Biosensor Using Iridium Complex-Doped Electrospun Optical Fibrous Membrane. Analytical Chemistry 85(2), 1171-1176.

Zimmer, M., 2002. Green Fluorescent Protein (GFP): Applications, Structure, and Related Photophysical Behavior. Chemical Reviews 102(3), 759-782.

Bloque IV

Uno de los factores altamente influyentes en el proceso de fabricación de un biosensor es el procedimiento de inmovilización del componente biológico sobre el soporte sólido seleccionado. Esta influencia viene determinada por el hecho de que los mecanismos que conducen a la inmovilización del componente biológico o biomolécula implican la participación de grupos reactivos de la biomolécula que normalmente pueden estar involucrados en el desarrollo de su actividad biológica. Es por ello que, para llevar a cabo con éxito y de manera eficiente un procedimiento de inmovilización, deben tenerse en cuenta la estructura de la biomolécula, su conformación espacial y los grupos funcionales de la misma que participan en la reacción de reconocimiento biológico necesaria para su correcto funcionamiento.

Teniendo en mente estas consideraciones fundamentales, en este bloque, dividido en dos capítulos, se incluyen los estudios de inmovilización realizados mediante la aplicación de diferentes metodologías de inmovilización (sobre un mismo soporte y utilizando una misma biomolécula), con el fin de obtener una fase sensora con las mejores características analíticas posibles, y con capacidad para ser aplicada satisfactoriamente en el análisis y la determinación de un determinado analito en muestras reales.

Capítulo 6

A multifunctional material based on co-electrospinning for developing biosensors with optical oxygen transduction

Teresa Ramon-Marquez[a], *Antonio L. Medina-Castillo*[b], *Naveen Nagiah*[b], *Alberto Fernandez-Gutierrez*[a], *Jorge F. Fernandez-Sanchez*[a]

[a] Department of Analytical Chemistry, University of Granada, Avd. Fuentenueva s/n, 18071 Granada, Spain

[b] NanoMyP®, Nanomateriales y Polimeros S.L., Spin-Off company of the UGR, BIC Building, Avd. Innovacion 1, E-18016, Granada, Spain

Submitted to *Biosensors and Bioelectronics*

ABSTRACT

A multifunctional material based on co-electrospinning has been developed as a basic material for the development of biosensors with optical oxygen transduction. It is based on coaxial nanofibres: an inner fibre containing an oxygen sensitive dye and an outer fibre containing aldehyde groups to allow the formation of Schiff bases with the amino groups of the enzyme. The resulting material preserves the oxygen sensing properties of the inner optical transducer as well as exhibits a high capacity for immobilizing molecules on its surface.

Uricase has been selected as model enzyme and several parameters (temperature, pH, reaction time, buffer, and enzyme concentration) have been optimised to demonstrate the versatility of this novel multifunctional material in the development of a biosensor with optical oxygen transduction for determining uric acid in serum samples. It suggests that the proposed multifunctional material can provide a promising multifunctional platform for biosensing applications.

Keywords: Multifunctional material; Nanotechnology; Oxygen transduction; Optical biosensor; Uric acid.

1. Introduction

The development of advanced multifunctional platforms with sensing properties based on new nanomaterials has attracted great interest in the past few years due to their tuneable physical, chemical, optical, mechanical and electronic properties, versatility, applicability in many different fields and, in some cases, biocompatibility and biodegradability (Agrawal et al. 2012; Liu and An 2014; Su et al. 2014; Wang et al. 2012).

Advances in nanotechnology in recent years have stimulated the fast development of new nanomaterials with multiple functions and shapes (nanotubes (Dai 2002; Iijima 1991; Mehra et al. 2014), nanofibres (Ouyang et al. 2013; Yang et al. 2007), nanoparticles (Rao and Geckeler 2011), nanocages (Ghanbari et al. 2011), etc.), and made with a variety of materials (carbon (Saifuddin et al. 2013), silicon (Boukai et al. 2008; Ohtani et al. 1998; Wu et al. 2015), metals (Xu et al. 2012), polymers (Camli et al. 2010; Cui et al. 2007; Zhang et al. 2004)). Furthermore, the high capacity of modification of these nanomaterials allows functionalizing their surface with multiple chemical groups that improve their ability to attach (bio)molecules. This modification results in huge number of applications in catalysis, biosensing, bioimaging, drug delivery and biomedicine (Kruss et al. 2013; Liu et al. 2010; Oliveros et al. 2013; Willander et al. 2014).

Among the wide diversity of novel functional nanomaterials, nanofibres membranes prepared by electrospinning technique offer several advantages such as high surface-to-volume ratio, controllable morphology, pore size, porosity and flexibility, and they can be fabricated as long or short fibres with modifiable orientation to provide a wide variety of sizes and shapes, which can lead to the fabrication of smart membranes (Ahmed et al. 2015; Bhardwaj and Kundu 2010). Because of these improved properties, nanofibres membranes could be very promising materials for designing biosensors (Baranowska-Korczyc et al. 2015; Chen et al. 2015; Mahmoudifard et al. 2016; Xue et al. 2015; Zhou et al. 2013). In addition, co-electrospinning technique allows one-step fabrication of multifunctional coaxial micro- and nano- fibre membranes which generates two different chemical environments that increase the functionality of these nanofibres (Bi et al. 2015; Kye et al. 2015; Liu et al. 2016; Yan et al. 2016) as well as their applicability (Medina-Castillo et al. 2011; Sun et al. 2003), including sensing applications (Medina-Castillo et al. 2011).

On the other hand, the use of optical oxygen transduction has been widely applied on the development of biosensors because it is simple, rapid and high sensitive and there is available a huge number of systems to do it (Chang et al. 2010; Schrenkhammer and Wolfbeis 2008; Steiner

et al. 2011; Wang et al. 2008). The monitoring of an enzymatic reaction by using oxygen transduction requires an increase or a decrease in the oxygen concentration, which has to be produced during the catalytic activity of the enzyme. These changes in the oxygen concentration can be used to determine indirectly other substrates which are also implicated in the enzymatic reaction. For example, glucose is widely determined by measuring changes in oxygen concentration produced during the catalytic activity of glucose oxidase (Chang et al. 2010; Steiner et al. 2011; Wang et al. 2008) as well as other oxidases such as cholesterol oxidase, lactate oxidase, tyramine oxidase or urate oxidase (uricase) (Duong and Rhee 2007; Schrenkhammer and Wolfbeis 2008; Valencia-Gonzalez and Diaz-Garcia 1994; Wang et al. 2004; Wu and Choi 2003).

To develop biosensor membranes using optical oxygen transduction, a multifunctional material is required because it is necessary: 1) to immobilize a biomolecule which catalyses the oxidation of the analyte and 2) to incorporate an oxygen sensitive dye to measure the consumption of oxygen during this oxidation. Most biomolecules are hydrophilic compounds and require to be immobilized on hydrophilic supports in order to enhance its enzymatic activity (Talbert and Goddard 2012). On the other hand, oxygen sensitive dyes are hydrophobic compounds and need to be incorporated into hydrophobic supports in order to avoid aggregations and because water can quench their luminescence, resulting in a decrease in sensitivity. Thus, the incorporation of both compounds in the same matrix maintaining their best analytical figures of merits is not trivial at all. Anyway, co-electrospinning technique allows the production of membranes with two different chemical environments; one hydrophobic to incorporate the oxygen sensitive dye and other hydrophilic to immobilize the biomolecule. In addition, this technique provides well-organized materials. It is important because the biomolecule must be located on the surface of the membrane to be accessible to the analyte while the oxygen sensitive dye can be incorporated into the membrane to avoid contact with water. Lastly, co-electrospinning also allows the production of this complex material in only one step, simplifying its scaling-up and therefore, its ability to be marketed.

In this work, we have developed and characterized a multifunctional coaxial material prepared from two different polymeric solutions by using co-electrospinning, which originates nonwoven nanofibre membranes with very large surface area, excellent mechanical properties (resistance to abrasion, high tensile strength, flexibility, easy handling) and high chemical resistance. It is based on an inner fibre containing an oxygen sensitive dye (Pd^{2+}-based porphyrin) and an outer fibre

containing an appropriate chemical functionalization for immobilizing oxidase enzymes. After the immobilization of the enzyme, the sensing material preserves the oxygen sensing properties of the embedded dye and can specifically react with the substrate of the enzyme.

In order to demonstrate its applicability, uricase has been selected as model enzyme and it has been used for determining uric acid in serum samples, obtaining similar results than those obtained with a reference method (developed by an external laboratory). The good correlation obtained between both methods, makes these nanofibre membranes a potential material for sensing applications.

2. Experimental

2.1. Reagents and Materials

For the fabrication of the coaxial nanofibre membranes, PolymBlend®, (NanoMyP®, Granada, Spain, http://www.nanomyp.com), was used in the outer fibre and poly(methyl methacrylate), (PMMA) (Sigma Aldrich, Madrid, Spain) was used for the inner fibre. In addition, several oxygen sensitive dyes were also tested: Pt(II) meso-tetra(pentafluorophenyl)porphine (PtTFPP) (Frontier Scientific, Logan, UT, USA), Pd(II) meso-tetra(pentafluorophenyl)porphine (PdTFPP) (Frontier Scientific, Logan, UT, USA), Pt(II)-5-(4-bromophenyl)-10,15,20-tri(phenyl)-tetrabenzoporhyrin (PtTPTBPBr), which was synthesized following the procedure described by (Hutter et al. 2014), and $[Ir(npy)_2(bpy\text{-}pyr_2)]PF_6$ (npyH = 2-(naphthalen-1-yl)pyridine; bpy = 2,2‘-bipyridine; pyr = pyrene) (IrBPY), which was synthesized following the procedure described by (Medina-Rodriguez et al. 2016). Finally, N,N-dimethylformamide (DMF) (Sigma Aldrich, Madrid, Spain) was used as solvent for the outer and inner polymeric mixtures.

For the immobilization of uricase, ethylenediamine (EDA), glutaraldehyde (GA), potassium dihydrogen phosphate (KH_2PO_4), boric acid (H_3BO_3), glycine, uricase from *Candida* sp. (EC 1.7.3.3) and Tween 20 were all purchased from Sigma Aldrich, Madrid, Spain and used without further purification. All the solutions were prepared using doubly distilled water.

To assay the activity of uricase, 4-aminoantipyrine (4-AAP) and peroxidase (HRP) from horseradish (EC 1.11.1.7) were purchased from Sigma Aldrich, Madrid, Spain, and uric acid and sodium 3,5-dichloro-2-hydroxybenzenesulfonate (DCHBS) were purchased from Alfa Aesar, Karlsruhe, Germany.

Human serum samples were obtained from a clinical analysis laboratory and stored frozen until assay.

2.2. Instrumentation

The UV-Visible absorption spectra were recorded on a Varian Cary 50 UV-Vis spectrophotometer. The luminescence measurements were carried out on a Varian Cary-Eclipse luminescence spectrophotometer.

To characterize the optical properties of the materials, a flow cell which allows the use of a gas stream was used in order to perform the measurements in a controlled atmosphere. The gas stream was controlled with a mass-flow controller (MFC) (EL-FLOW Select F-201CV, Bronkhorst High-Tech, Ruurlo, Netherlands) connected with the flow cell using copper and stainless steel tubing and a PC via a RS-232 serial port by a Flow-Bus Interface (Bronkhorst High-Tech Ruurlo, Netherlands).

All the luminescence measurements were carried out by controlling the temperature, which was continuously regulated by a commercial Peltier cell holder connected to a temperature control module (Agilent Technologies, Madrid, Spain).

The pH of the buffer solutions was controlled using a digital pH meter (Crison micropH 2000) calibrated at 20 ± 2 ºC.

2.3. Fabrication of multifunctional coaxial fibre membranes

To make the coaxial fibres by co-electrospinning two different solutions were used: a solution of PolymBlend® (10% w/w) in DMF was used for the outer fibre and PMMA (6% w/w) with the oxygen-sensitive dye (1% w/w) in DMF was prepared and utilized for the inner fibre.

The liquid flow rates formed by outer and inner solutions were independently driven by two syringe pumps (Cole Parmer 74900 Series) using a flow-rate of 1.3 and 0.3 mL h^{-1} for the outer and inner solutions, respectively. The syringes used are Teflon Becton & Dickinson with 12.45 mm diameter. The outer and inner solutions were passed through a Teflon capillary tube until reaching a concentric couple of stainless-steel capillary tubes (injector). The outer and inner diameters of stainless-steel capillary tubes were: external tube Φ_{ext}/Φ_{int} = 1.7/1.4 mm, internal tube Φ_{ext}/Φ_{int} = 1/0.7 mm. To apply the electric field, two high-voltage power supplies were used (Gamma High Voltage ES30P and Bertan 205B-10R) to establish a potential difference between

the injector and the collector, which was a rotator drum (30 cm length and 20 cm diameter rotating at 400 rpm) located 25 cm apart from the injector. One of the power supplies was connected to the injector in positive polarity (8.9 kV) with respect to ground, while the second power supply was hooked to the collector and run in negative polarity (-1.3 kV) with respect to ground. The selected flow rates and voltages within this configuration allowed the collection of dry fibre mats. The process was run for 8 h to collect membranes with thickness about 150 µm.

The obtained membrane is hydrophobic, but when it is introduced in warm water at 40ºC (thermal wetting) the hydration is produced and the material is transformed in a very high hydrophilic membrane; during the thermal wetting the membrane must be keep stretched in order to prevent a shrink. It happens because during the thermal wetting the polymeric chains suffer a rearrangement and the hydrophilic domains of the polymeric chains are exposed to water while the hydrophobic domains are hidden to water (Kyritsis et al. 2011; Stathopoulos et al. 2010). Therefore at the end of the thermal wetting the surface of the mat reaches a high concentration of hydroxyl groups transforming the membrane in a very hydrophilic material without producing any change in diameter and fibre morphology (Campillo-Fernández et al. 2008). After thermal wetting the water absorption capacity was calculated by calculating the ω parameter (amount of absorbed water per mass of material) (Stathopoulos et al. 2010). It was 2.0 for the membrane with thermal wetting and 0.0 for the membrane without the thermal wetting.

The resulting coaxial-nanofibre membranes after the thermal wetting were attached to adhesive sheets (Lohmann Technologies Corp.) to facilitate their handling.

2.4. Characterization of multifunctional coaxial fibre mats

The morphological characterization of coaxial fibre membranes was done by TEM (Zeiss DSM 950) and SEM (LEO, Carl Zeiss, GEMINI-1530).

The oxygen sensing properties of the coaxial membranes were evaluated by applying different O_2 partial pressures, which were obtained by mixing O_2 and N_2 with different flow ratios, assuming a constant environmental pressure of 1000 mbar. The standard settings for the luminescence intensity measurements were: excitation and emission slits of 10 nm wide, delay time (t_d) 200 µs, gate time (t_g) 5 ms, and a current flow of 150 mL min^{-1}. Different emission and excitation wavelengths were selected for each oxygen-sensitive dye: $\lambda_{exc/em}$(PtTFPP) = 390/648 nm, $\lambda_{exc/em}$(PdTFPP) = 402/669 nm; $\lambda_{exc/em}$(PtTPTBPBr) = 614/767 nm and $\lambda_{exc/em}$(IrBPY) = 334/577 nm.

Luminescence quenching methods of analysis can be described by the Stern–Volmer equation (see Eq. (1)), which was used to fit the calibration curves for the oxygen sensing membranes.

$$\frac{I_0}{I} = 1 + K_{SV} pO_2 \qquad (1)$$

where I_0 and I are the luminescence emission intensities from the membranes exposed to 100% N_2 concentration and to different O_2 concentrations, respectively, K_{SV} is the Stern-Volmer constant and pO_2 is the oxygen partial pressure.

2.5. Immobilization of uricase

The surface of the coaxial material was first functionalized with a vinyl active group (Medina-Castillo et al. 2012) and then with amino groups by using 0.9 M EDA in phosphate buffer (100 mM, pH 8.4) for 20 min at room temperature (RT) (Goddard and Hotchkiss 2007). After this, 1.9 cm^2 of material were incubated with 5 mL of GA (Goddard and Hotchkiss 2007) solution 3 % v/v in phosphate buffer (100 mM, pH 7.4) for 40 min at RT in a rotating shaker. Then, it was washed with 5 mL of doubly distilled water (3x10 min in a rotating shaker).

The covalent immobilization of uricase on the material was carried out by incubating 1.9 cm^2 of activated material with 4 mL uricase solution (25 µg mL^{-1}) in phosphate buffer (50 mM, pH 7.4) at 4 ºC for 20 h. Unbound enzyme was removed by washing the material with 4 mL phosphate buffer (3x10 min in a rotating shaker). The washing solutions and the reaction supernatant were reserved for further testing. The material with immobilized uricase was stored in phosphate buffer (pH 7.4) at 4 ºC.

The amount of enzyme immobilized on the material was calculated from the difference between the initial free enzyme amount and the total amount of enzyme present in the reaction supernatant and washing solutions after immobilization, assuming that the loss of enzyme in each experiment is negligible. The enzyme concentrations in the supernatant and washing solutions were measured by the spectrofluorometric method at 334 nm (Caves et al. 2013).

The relative activity (%) of the immobilized uricase was determined by a colorimetric method based on two enzymatic reactions (Ramon-Marquez et al. 2015). First, uricase catalyses the oxidation of uric acid to allantoin, carbon dioxide and hydrogen peroxide. Next, HRP catalyses the oxidation of DCHBS in the presence of hydrogen peroxide, which originates a phenoxyl radical that reacts with 4-AAP, producing a red quinoneimine dye with an absorption maximum

at 515 nm. The relative activity of uricase was calculated as a percentage of the immobilized uricase referred to free uricase activities.

In detail, to assay the activity of the immobilized uricase, 3 mL glycine buffer (50 mM, pH 8.8) containing 0.1 µmol uric acid were incubated with 1.9 cm^2 of coaxial membrane with immobilized uricase for 20 min at 40 ºC. Next, 0.5 mL 4-AAP (10 mM), 0.5 mL DCHBS (50 mM) and 0.5 mL HRP (20 U mL^{-1}) in phosphate buffer (50 mM, pH 7.4) were added and kept at 40 ºC for 5 min to develop the colour. All the solutions were freshly prepared daily.

2.6. Analytical characterization and application

The luminescence signal of the oxygen sensitive dye incorporated into the inner fibre increases with the concentration of uric acid due to the consumption of oxygen during the oxidation reaction. Supporting Material (SM) shows the typical format of the evolution of the luminescence versus time (see SM, Fig. SM-6.1). As shown in SM, Fig. SM-6.1, it does not provide a plateau at least in a short period of time. In order to avoid large analysis times, the slope of this signal was used as sensing response.

The slope of the signal can be calculated with the following equation (see Eq. (2)):

$$Sensing\ response = \frac{S_i - S_0}{t_i - t_0} \qquad (2)$$

where S_i and S_0 are the luminescence signal recorded at time t_i and t_0, respectively, and t_0 must be equal o higher than the time in which the uric acid is added.

The calibration curve was done by immersing the coaxial membranes in 600 µL of glycine buffer (50 mM, pH = 8.8) and then 100 µL of uric acid solutions were added to reach final acid uric concentrations from 20 to 500 µM, maintaining the temperature at 40 ºC during the measurement time. The luminescence intensity was measured at excitation wavelength of 402 nm, emission wavelength of 669 nm, delay time (t_d) 200 µs, gate time (t_g) 5 ms, detector voltage of 680 V and excitation and emission slits of 10 nm wide.

In order to demonstrate the capacity of the developed sensing membrane for determining uric acid, 4 real serum samples were analysed. The concentration of uric acid in the serum samples was also determined by an accredited external laboratory.

The measurement was carried out by immersing the coaxial membranes in 600 µL of glycine buffer (50 mM, pH = 8.8) and then 100 µL of serum sample were added. The temperature was maintained at 40 ºC during the measurement time. The luminescence intensity was measured at excitation wavelength of 402 nm, emission wavelength of 669 nm, delay time (t_d) 200 µs, gate time (t_g) 5 ms, detector voltage of 680 V and excitation and emission slits of 10 nm wide.

3. Results

3.1. Fabrication of the multifunctional coaxial membrane

To develop biosensor membranes using optical oxygen transduction, it is necessary to develop a material with 2 functionalities: 1) it must allow the immobilization of a biomolecule on its surface to catalyse the oxidation of the analyte and 2) it must contain an oxygen sensitive dye to measure the consumption of oxygen during this oxidation. In addition, due to the different character of the biomolecule (hydrophilic) and the oxygen sensitive dye (hydrophobic), these bi-functional materials have to contain two different chemical environments: a hydrophilic environment for the enzyme and a hydrophobic environment for the oxygen-sensitive dye.

In order to obtain the hydrophilic environment, PolymBlend® was selected for the outer polymer solution because it is hydrophilic and oxygen permeable, it contains OH groups that can be easily functionalized to allow the covalent immobilization of the enzyme, and it has been formulated with an optimum mixture of two high molecular weight statistic copolymers to provides excellent mechanical and chemical properties of non-woven mats produced by electrospinning (Ramon-Marquez et al. 2016a, b).

For the hydrophobic environment to incorporate the oxygen-sensitive dye, PMMA was selected because it is hydrophobic, compatible with the oxygen sensitive dyes, oxygen permeable, it has a good transparency to allow the luminescence measurement and it was proved that it is a good polymer to develop oxygen sensing membranes by electrospinning (Medina-Castillo et al. 2011).

Concerning the oxygen sensitive dye, there is a huge variety of optical indicators with different structures and chemical nature to determine oxygen (Amao 2003; Quaranta et al. 2012; Stich et al. 2010) and most of them are based on the measurement of the luminescence quenching produced by oxygen (Medina-Rodríguez et al. 2014; Wang and Wolfbeis 2014; Wolfbeis 2015).

Organometallic complexes containing Ru^{2+}, Re^{+}, Os^{3+}, Ir^{3+}, Pt^{2+} and Pd^{2+} as well as with polypyridyl and porphyrin structures are the most usually compounds used as oxygen-sensitive dyes in optical sensing. There are a vast number of these complexes with different physicochemical properties, emission and excitation wavelengths, lifetimes, Stokes' shifts, quantum yields, photostability, etc. (Amao 2003; Quaranta et al. 2012; Wang and Wolfbeis 2014). Thus, the selection of the most adequate oxygen dye would mainly depend on the application of the sensor, taking into account factors like sensitivity to oxygen and stability.

Platinum and palladium-based metalloporphyrins are the most widely used indicators in optical oxygen sensing due to their photostability, optimal oxygen sensitivity, compatibility with common polymers and solvents, long lifetimes, and large Stokes' shift (Borisov et al. 2011; Chu 2013; Papkovsky and O'Riordan 2005). Moreover, structural modifications of these metalloporphyrins can originate changes in their photophysical and chemical properties, which can improve their stability and their oxygen sensitivity (Hutter et al. 2014; Koren et al. 2012). In addition, iridium(III) complexes have also used as oxygen probes due to their excellent optical properties such as high quantum yields, long decay times, large Stokes' shift, fast response time and high Stern-Volmer constant (Marin-Suarezdel Toro et al. 2010; Medina-Castillo et al. 2007; Medina-Rodriguez et al. 2016; Medina-Rodriguez et al. 2013).

In this work, we have selected two commercially available metalloporphyrins (PtTFPP and PdTFPP), one modified Pt(II)–benzoporphyrin (PtTPTBPBr), and one cyclometalated Ir(III) complex ($[Ir(npy)_2(bpy\text{-}pyr_2)]PF_6$), as oxygen-sensitive dyes, due to their exceptional luminescence properties and their compatibility with the polymeric solution (PMMA in DMF) used to obtain the inner fibre of the coaxial membranes.

To produce a stable and continuous co-electrospinning procedure, we tested two different concentrations (13 and 10% w/w) of PolymBlend® in the outer fluid and three concentrations (13, 9 and 6% w/w) of PMMA in the inner fluid. We selected 10% w/w of PolymBlend® and 6% w/w of PMMA as optimum concentrations because they allow obtaining a stable and definite cone and helping to solidify the electrified jet near its point of generation (see SM, Fig. SM-6.2). The percentage of the polymer in the outer solution is higher because a sufficiently high viscosity of the outer fluid is essential to develop a compound cone in the steady state and it helps to increase the polymeric chain entanglements and thus to prevent various instabilities (break up of the jet into droplets).

Apart from the requirements regarding the physical properties of fluids, for a given setup and fluid pair, there exists a parametrical range of operation in which the compound cone, and thus the compound fibres, are produced. In this work, to develop a compound cone in the steady state, we studied different outer/inner flow rates (1/0.2, 1.3/0.1, 1.3/0.3, 1.3/0.5, and 2.5/0.5 mL h^{-1}, respectively), and different injector/collector voltages (10.3/-0.6, 9.5/-1.7, 8.9/-1.3, 8.8/-2.6, and 10.0/-1.7 kV, respectively). The selected voltages were injector voltage of 8.9 kV and collector voltage of -1.3 kV, and the optimal outer and inner flow rates were 1.3 and 0.3 mL h^{-1} (see SM, Fig. SM-6.3), respectively, because these conditions provided the most homogeneous compound cone in the steady state for long time.

Fig. 6.1 and SM (see Fig. SM-6.2) shows SEM and TEM pictures of the optimal coaxial nanofibre mat. They show a regular and homogeneous formation of the fibres, during the co-electrospinning procedure. The addition of 1% w/w of the O_2 indicator into the inner suspension did not affect the co-electrospinning process, and thus the morphology of the coaxial fibres did not change. No leaching of the dyes from the membrane was observed and all the coaxial mats showed similar mechanical properties. SM (see Fig. SM-6.4) shows the luminescence emission before and after the thermal wetting of the mat, due to the luminescence emission is the same before and after the treatment we can assume that the dye was not leached during this procedure.

The fibre diameters of the obtained coaxial fibres are 680 and 530 nm for outer and inner fibres, respectively. These values were calculated by 20 measurements made in five different SEM pictures (total of 100 measurements).

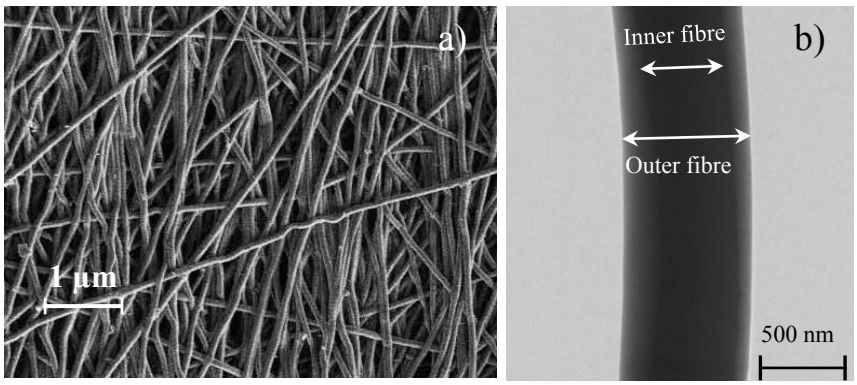

Fig. 6.1. Images of a) SEM and b) TEM of the multifunctional coaxial membrane formed by PMMA-PdTFPP as inner fibre and PolymBlend® as outer fibre.

3.2. Optical characterization and oxygen sensing properties

In order to study the effect of the incorporation of the dye into the fibre material, a simple polymeric nanofibre membranes obtained by electrospinning containing 1% w/w of PtTFPP (selected as a model oxygen sensitive dye) was produced. SM (see Fig SM-6.5) shows its luminescent properties $\lambda_{exc/em}$(PtTFPP-simple fibre) = 395/650 nm, which are the same to the obtained in a classical PS membrane ($\lambda_{exc/em}$(PtTFPP-PS) = 395/650 nm (Medina-Rodriguez et al. 2013)), thus the incorporation of the dye into a nanofibre mat produced by electrospinning does not affect its optical properties. It also shows that the luminescence emission of the dye incorporated into the fibre was quenched when it was exposed to oxygen.

After that, a coaxial membrane was produced containing several dyes in order to evaluate the effect of the incorporation of a dye into the inner fibre of the material. The emission and excitation spectra of the coaxial materials based on the different oxygen dyes (1 % w/w) and under different oxygen concentrations are shown in Fig. 6.2 and Table 6.1. The luminescence properties of the dyes incorporated into the inner fibre of the coaxial material are very similar to those obtained in a classical PS membrane ($\lambda_{exc/em}$(PtTFPP-PS) = 395/650 nm (Medina-Rodriguez et al. 2013), $\lambda_{exc/em}$(PdTFPP-PS) = 406/671 nm (Borisov and Klimant 2008); $\lambda_{exc/em}$(PtTPTBPBr-PS) = 614/770 nm (Hutter et al. 2014) and $\lambda_{exc/em}$(IrBPY-PS) = 334/577 nm (Medina-Rodriguez et al. 2016)), thus the incorporation of the dye into a nanofibre mat produced by co-electrospinning does not affect its optical properties.

Table 6.1. Maxima luminescence excitation and emission wavelengths ($\lambda_{exc/em}$) and oxygen sensitivity of the dyes (K_{SV}) incorporated into the coaxial nanofibre membrane. [Dye concentration] = 1% w/w, t_d = 200 µs, t_g = 5 ms and monochromator slitwidth$_{exc/em}$ = 10/10 nm.

Oxygen dye	**$\lambda_{exc/em}$ (nm)**	**K_{SV} (bar^{-1})**
PtTFPP	390/648	5.41
PdTFPP	402/669	20.84
PtTPTBPBr	614/767	5.26
IrBPY	334/577	13.60

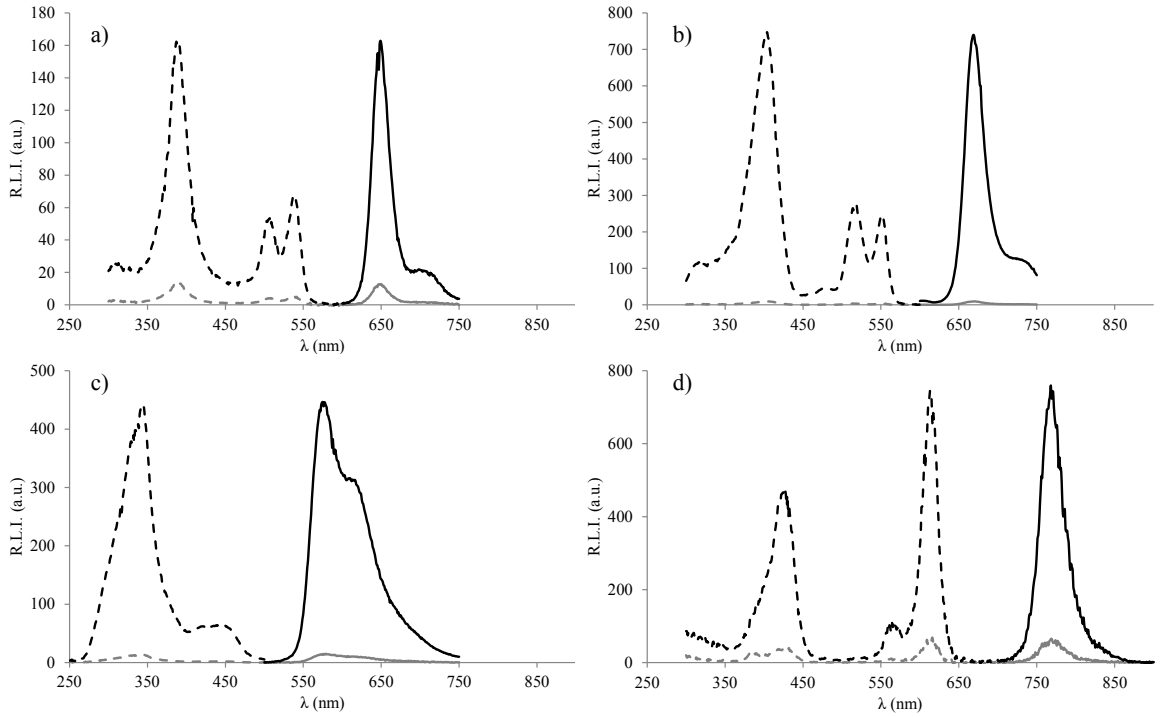

Fig. 6.2. Excitation (dashed line) and emission (solid line) spectra in the presence of 100% O_2 (grey line) and 100% N_2 (black line) of the coaxial membrane when a) PtTFPP, b) PdTFPP, c) IrBPY and d) PtTPTBPBr were used as oxygen sensitive dyes. [Dye concentration] = 1% w/w, t_d = 200µs, t_g = 5 ms and monochromator slitwidth$_{exc/em}$ = 10/10 nm.

Concerning the sensitivity to oxygen, all the obtained Stern-Volmer plots (see SM, Fig. SM-6.6) showed linearity up to 10% of oxygen concentration so all of them might be used as optical oxygen sensing. Table 6.1 also shows the sensitivity (K_{SV}) of the coaxial membranes. The K_{SV} of PtTFPP incorporated into the coaxial membrane (5.41 bar^{-1}) is higher than the K_{SV} of the dye incorporated into the simple one (3.3 bar^{-1}), thus the entrapment of the dye into the inner fibre of the coaxial membrane originates an improvement of the sensitivity of the oxygen-sensitive dye compared to the membrane without coaxial structure. This can be explained by the size of the fibres in which the dye is incorporated. In the coaxial material, the dye is entrapped inside fibres with nanometric diameter, which decreases the probability of aggregation, resulting in higher Stern-Volmer constant.

Comparing the sensitivity to oxygen of the different dyes incorporated into the coaxial membranes and in a classical membrane (PS membrane), it is possible to conclude that the K_{SV} of the coaxial fibre mats based on Pt(II) complexes (see Table 6.1) are smaller than those of the classical membranes (K_{SV}(PtTFPP-PS) = 41.42 bar^{-1} (Medina-Rodriguez et al. 2013), and K_{SV}

(PtTPTBPBr-PS) = 22.8 bar^{-1} (Hutter et al. 2014)). On the other hand, the K_{SV} of the coaxial fibre mats based on Pd(II) and Ir(III) complexes (see Table 6.1) are higher than the those of the classical membranes (K_{SV} (PdTFPP-PS) = 9.60 bar^{-1} (Borisov and Klimant 2008) and K_{SV} (IrBPY-PS) = 8.79 bar^{-1} (Medina-Rodriguez et al. 2016)). It can be due to aggregation of Pt(II) dyes during the electrospinning process while PdTFPP and IrBPY are more soluble in PMMA than in PS. Anyway, the obtained sensitivity is enough for the requested application and it might be improved, if necessary, by using advanced photoluminescent measurements such as the use of rectangular-wave signals (Medina-Rodríguez et al. 2014).

Analysing the results summarized in Table 6.1, PdTFPP showed the highest sensitivity to oxygen thus it was selected as the oxygen-sensitive dye on the fabrication of the multifunctional material.

3.3. Optimization of covalent immobilization of the enzyme on coaxial membrane

The immobilization of enzymes whose catalytic activity involves the consumption or the production of oxygen, such as oxidases, on oxygen-sensitive membranes can be used to develop biosensors that determine the substrates of the enzymatic reactions. To demonstrate the versatility of the proposed material, uricase was selected as model enzyme and the resulting membrane was used to analyse uric acid by oxygen transduction.

Uricase was covalently immobilized on the outer surface of the coaxial material through the formation of Schiff bases between the amino groups of the enzyme and the free aldehyde groups of GA on the material. Therefore, the OH groups of the outer polymer fibres was first functionalized with vinyl active groups, then with amino groups by using EDA and finally with GA (Goddard and Hotchkiss 2007).

The optimum GA concentration was assayed by incubating the material with solutions containing 1, 3, 5, 10 and 15 % v/v GA in phosphate buffer (100 mM, pH 6.5 and 7.4) for 40 min at RT, and then immobilizing uricase in phosphate buffer (50 mM, pH 7.4) at 4 ºC for 20 h. Fig. 6.3 shows that an increase of the GA concentration from 3 to 15 % v/v provides an increase of the immobilised enzyme but also a considerable decrease of the activity. It is because an increase of the GA concentration provides an increase of the amount of aldehyde groups that can react with the enzyme and therefore an increase of the amount of enzyme which has been covalently immobilized on the material. But, at the same time, an increase of the amount of aldehyde groups also provides that the multipoint attachment of the enzyme occurs more extensively and,

therefore, the rigidity of the enzyme is increased, changing its conformation and therefore reducing its activity (Cao 2006; dos Santos et al. 2015).

The reaction time with GA was also tested. Fig. 6.3 shows that the incubation time has a similar effect over the enzyme immobilization than the GA concentration; an increase in the reaction time from 40 min to 2 h provides an increase in the immobilised enzyme but the activity is decreased. Thus, the best relationship between activity and amount of immobilized enzyme was obtained at 3 % v/v GA and 40 min reaction time, which were selected as optimum GA concentration and incubation time, respectively. These conditions provide an immobilization yield of 7.4 µg cm^{-2} and an enzymatic activity of 18 % of the native enzymatic activity (activity of the free enzyme).

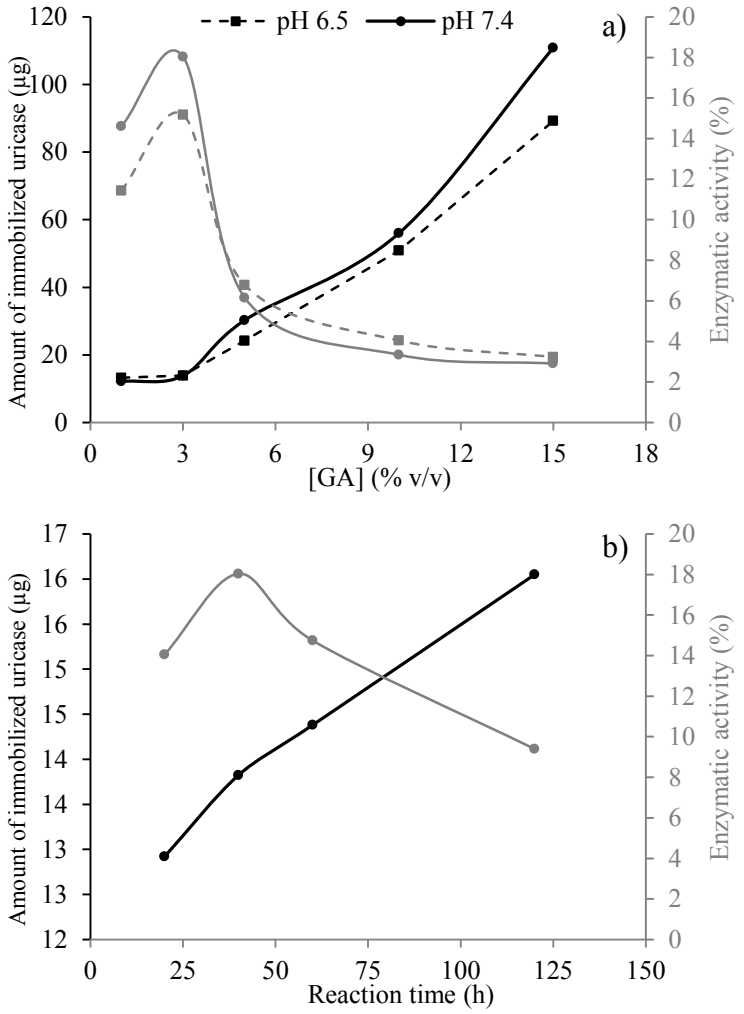

Fig. 6.3. a) Effect of the concentration of GA on the amount (black line) and enzymatic activity (grey line) of immobilised uricase at pH 7.4 (experimental data indicated with a solid circle); b) Effect of the reaction time with GA on the amount (black line) and enzymatic activity (grey line) of immobilised uricase at pH 7.4.

The effects of the reaction time and the temperature on the enzyme immobilization were also studied. The GA activated material was immersed in 4 mL uricase solution (25 μg mL^{-1}) in phosphate buffer (50 mM, pH 7.4) at 4 and 25 ºC for different reaction times. Then the amount of immobilized enzyme and its activity were evaluated. SM (see Fig. SM-6.7) shows the experimental results. The maximum amount of immobilized enzyme was reached at 25 ºC, but at this temperature the activity of the immobilised enzyme practically disappears. Thus, 4ºC was selected as optimum temperature for enzyme incubation. On the other hand, and increase of the incubation time at 4ºC provides an increase of the amount of the immobilised enzyme but a decrease in its activity. However, 20 h was selected in order to have a good amount of immobilised enzyme to increase the precision of the analytical determination.

To determine the influence of the pH, the immobilization of uricase on the activated material was carried out at pH = 6.5 (50 mM phosphate buffer), pH = 7.4 (50 mM phosphate buffer), pH = 8.8 (50 mM borate buffer) and pH = 8.8 (50 mM glycine buffer) at 4 ºC for 20 h. As can be seen in SM (see Fig. SM-6.8), the pH significantly affects both the amount and activity of the immobilized enzyme. The amount of immobilized enzyme increases with the pH, but the activity decreases considerably. It can be due to the change of the spatial conformation of the enzyme with the pH. The highest activity of the free enzyme is reached at pH 8.5 (Jianguo et al. 1994), and at this pH the active sites of the enzyme are more accessible so it is easier that at this pH the active site can interact with the aldehyde groups of GA and can be modified. Therefore, pHs close to 8.5 are not adequate to carry out the covalent immobilization on the material.

When the pH is between 6.5 and 7.4, the amount and the activity of the immobilised enzyme is practically the same, so phosphate buffer at pH 7.4 was selected as the optimum medium for developing the immobilization of uricase.

Finally, the effect of the enzyme concentration was also investigated. 4 mL uricase solutions with four different concentrations (25, 50, 100 and 150 μg mL^{-1}) in phosphate buffer (50 mM, pH 7.4) were incubated with the GA activated material at 4 ºC for 20 h. SM (see Fig. SM-6.9) shows the experimental results. An increase of the initial enzyme concentration increases the amount of the immobilized enzyme and decreases the activity. It could be due to the formation of aggregates when the enzyme concentration increases; an increase of the enzyme concentration increases the probability of the aggregation of the enzyme on the surface of the material, which might originate the blockage of their active sites. Thus, 25 μg mL^{-1} was selected as optimum uricase

concentration providing an immobilization yield of 7.4 µg cm^{-2} and an enzymatic activity of the 18 % of the native enzymatic activity (activity of the free enzyme).

3.4. Analytical figures of merits

For the analytical characterization of uric acid, the coaxial membrane was immersed in glycine buffer (50 mM, pH = 8.8) because, as it was commented before, this is the best medium to obtain the maximum activity of the enzyme (Jianguo et al. 1994) and then different concentrations of uric acid were added. The luminescence responses obtained for different uric acid concentrations in buffer solutions increase with the time and do not provide a plateau at least in a short period of time (see Fig. SM-6.1). In order to avoid large analysis times, the slope of this signal was used as sensing response following the procedure described in Section 2.6.

A linear relationship between the sensing response and the uric acid concentration was obtained in the range from 61 to 500 µM (see SM, Fig. SM-6.10), which covers the normal range in human serum (150-460 µM). Table 6.2 summarizes the analytical figures of merits of the biosensing membrane produced. The detection and quantification limits were calculated by using the IUPAC method (LOD = $3s_b/m$; LOQ = $10s_b/m$).

Table 6.2. Analytical figures of merits of the coaxial nanofibre membrane based on an inner fibre composed by PdTFPP/PMMA and an outer fibre composed by PolymBlend® functionalised with uricase (25 µg mL), $\lambda_{exc/em}$ = 402/669 nm, t_d = 200 µs, t_g = 5 ms, detector voltage of 680 V and monochromator slitwidth$_{exc/em}$ = 10/10 nm.

	Estimated value
Linearity (%)	99.25
Slope (μM^{-1})	0.1133
Intercept	19.404
Linear range (µM)	61-500
Limit of detection (µM)	18
Limit of quantification (µM)	61

In spite of the low relative activity of the immobilized uricase (18 %) and the smaller K_{SV} (20.84 bar^{-1}) of the dye incorporated on the coaxial membrane, they are enough to determine uric acid in real serum samples. Anyway, further optimisation of the sensing material can be done in order to increase the sensitivity on those applications that need it. For example, the amount of dye

can be reduced in order to avoid agglomeration and it must increase significantly the sensitivity to oxygen.

3.5. Application

In order to determine the applicability of the designed multifunctional material in complex matrices, the uric acid concentration was measured in 4 serum samples from healthy adults using 3 different coaxial membranes per sample following the procedure described in Section 2.6.

To test the accuracy of the results, the values of uric acid concentration in the serum samples obtained with the developed biosensor were compared with those obtained by using a reference method (external laboratory). Table 6.3 summarizes the results. A good correlation coefficient (0.996) and the regression equation ($y = 1.063x - 14.164$) were calculated by comparing the concentrations of uric acid obtained by both methods (see SM, Fig. SM-6.11).

Table 6.3. Results of the acid uric determination by the proposed biosensor and an external reference laboratory.

Sample	[uric acid] (μM) external reference laboratory	[uric acid] (μM) proposed biosensor[a]
1	220.1	219.8 ± 13.8
2	190.4	192.5 ± 13.4
3	148.7	142.1 ± 14.2
4	220.1	217.3 ± 17.6

[a] 3 different membranes per sample were used to determine the uric acid concentration

4. Conclusions

In this study, we have successfully designed a multifunctional material with sensing properties. It is constituted by nanofibres with a coaxial morphology, which originates two different chemical environments: an inner hydrophobic environment and an outer hydrophilic environment. The high capacity of the outer fibre for immobilizing biomolecules combined with the ability of the inner fibre to entrap optical indicators, result in a material with a high versatility and applicability in many fields.

In order to demonstrate the usefulness of this material, uricase and PdTFPP were selected as biomolecule and optical indicator, respectively. Several chemical parameters have been optimized in order to achieve the best analytical figures. The obtained biosensing membrane provides a detection limit of 18 µM and a linear range of 61-500 µM, which allow determining uric acid in serum samples. The obtained results showed a good correlation (0.996) with those obtained by an external laboratory, which indicates that this material can be used as a promising sensing membrane. Moreover, it could also be used for the immobilization of other enzymes and for hosting other dyes, which could originate interesting applications in the field of biosensing.

Acknowledgments

This work has received funding from the People Programme (Marie Curie Actions, Multi-ITN) of the European Union‘s Seventh Framework Programme for research, technological development and demonstration under grant agreement n° 608104 (EUROMBR) and the Spanish Ministry of Economy and Competitiveness (Ramon-Marquez‘s grant reference AP2012-0944, Medina-Castillo‘s Torres Quevedo contract reference PTQ-11-04904 and project CTQ2014-53442-P). The authors also thank the research groups of E. Baranoff and I. Klimant for providing the IrBPY and PtTPTBPBr complexes, respectively, for this work.

References

Agrawal, U., Gupta, M., Jadon, R.S., Sharma, R., Vyas, S.P., 2012. Multifunctional nanomedicines: potentials and prospects. Drug Delivery and Translational Research 3(5), 479-497.

Ahmed, F.E., Lalia, B.S., Hashaikeh, R., 2015. A review on electrospinning for membrane fabrication: Challenges and applications. Desalination 356, 15-30.

Amao, Y., 2003. Probes and Polymers for Optical Sensing of Oxygen. Microchimica Acta 143(1), 1-12.

Baranowska-Korczyc, A., Sobczak, K., Dluzewski, P., Reszka, A., Kowalski, B.J., Klopotowski, L., Elbaum, D., Fronc, K., 2015. Facile synthesis of core/shell ZnO/ZnS nanofibers by electrospinning and gas-phase sulfidation for biosensor applications. Physical Chemistry Chemical Physics 17(37), 24029-24037.

Bhardwaj, N., Kundu, S.C., 2010. Electrospinning: A fascinating fiber fabrication technique. Biotechnology Advances 28(3), 325-347.

Bi, F., Dong, X., Wang, J., Liu, G., 2015. Tunable and enhanced simultaneous magnetism-luminescence bifunctionality assembled into a coaxial nanofiber. New Journal of Chemistry 39(5), 3444-3451.

Borisov, S.M., Klimant, I., 2008. Luminescent nanobeads for optical sensing and imaging of dissolved oxygen. Microchimica Acta 164(1), 7.

Borisov, S.M., Lehner, P., Klimant, I., 2011. Novel optical trace oxygen sensors based on platinum(II) and palladium(II) complexes with 5,10,15,20-meso-tetrakis-(2,3,4,5,6-pentafluorphenyl)-porphyrin covalently immobilized on silica-gel particles. Analytica Chimica Acta 690(1), 108-115.

Boukai, A.I., Bunimovich, Y., Tahir-Kheli, J., Yu, J.-K., Goddard Iii, W.A., Heath, J.R., 2008. Silicon nanowires as efficient thermoelectric materials. Nature 451(7175), 168-171.

Camli, S.T., Buyukserin, F., Balci, O., Budak, G.G., 2010. Size controlled synthesis of sub-100 nm monodisperse poly(methylmethacrylate) nanoparticles using surfactant-free emulsion polymerization. Journal of Colloid and Interface Science 344(2), 528-532.

Campillo-Fernández, A.J., Salmerón Sánchez, M., Sabater i Serra, R., Meseguer Dueñas, J.M., Monleón Pradas, M., Gómez Ribelles, J.L., 2008. Water-induced (nano) organization in poly(ethyl acrylate-co-hydroxyethyl acrylate) networks. European Polymer Journal 44(7), 1996-2004.

Cao, L., 2006. Covalent Enzyme Immobilization. Carrier-bound Immobilized Enzymes, pp. 169-316. Wiley-VCH Verlag GmbH & Co. KGaA.

Caves, M.S., Derham, B.K., Jezek, J., Freedman, R.B., 2013. Thermal Inactivation of Uricase (Urate Oxidase): Mechanism and Effects of Additives. Biochemistry 52(3), 497-507.

Cui, X., Zhong, S., Wang, H., 2007. Emulsifier-free core-shell polyacrylate latex nanoparticles containing fluorine and silicon in shell. Polymer 48(25), 7241-7248.

Chang, G., Tatsu, Y., Goto, T., Imaishi, H., Morigaki, K., 2010. Glucose concentration determination based on silica sol–gel encapsulated glucose oxidase optical biosensor arrays. Talanta 83(1), 61-65.

Chen, X., Li, D., Li, G., Luo, L., Ullah, N., Wei, Q., Huang, F., 2015. Facile fabrication of gold nanoparticle on zein ultrafine fibers and their application for catechol biosensor. Applied Surface Science 328, 444-452.

Chu, C.-S., 2013. Optical fiber oxygen sensor based on Pd(II) complex embedded in sol–gel matrix. Journal of Luminescence 135, 5-9.

Dai, H., 2002. Carbon Nanotubes: Synthesis, Integration, and Properties. Accounts of Chemical Research 35(12), 1035-1044.

dos Santos, J.C.S., Rueda, N., Torres, R., Barbosa, O., Gonçalves, L.R.B., Fernandez-Lafuente, R., 2015. Evaluation of divinylsulfone activated agarose to immobilize lipases and to tune their catalytic properties. Process Biochemistry 50(6), 918-927.

Duong, H.D., Rhee, J.I., 2007. Preparation and characterization of sensing membranes for the detection of glucose, lactate and tyramine in microtiter plates. Talanta 72(4), 1275-1282.

Ghanbari, H., Cousins, B.G., Seifalian, A.M., 2011. A Nanocage for Nanomedicine: Polyhedral Oligomeric Silsesquioxane (POSS). Macromolecular Rapid Communications 32(14), 1032-1046.

Goddard, J.M., Hotchkiss, J.H., 2007. Polymer surface modification for the attachment of bioactive compounds. Progress in Polymer Science 32(7), 698-725.

Hutter, L.H., Muller, B.J., Koren, K., Borisov, S.M., Klimant, I., 2014. Robust optical oxygen sensors based on polymer-bound NIR-emitting platinum(ii)-benzoporphyrins. Journal of Materials Chemistry C 2(36), 7589-7598.

Iijima, S., 1991. Helical microtubules of graphitic carbon. Nature 354(6348), 56-58.

Jianguo, L., Gaoxiang, L., Hong, L., Xiukai, Z., 1994. Purification and properties of uricase fromCandida sp. and its application in uric acid analysis in serum. Applied biochemistry and biotechnology 47(1), 57-63.

Koren, K., Borisov, S.M., Klimant, I., 2012. Stable optical oxygen sensing materials based on click-coupling of fluorinated platinum(II) and palladium(II) porphyrins—A convenient way to eliminate dye migration and leaching. Sensors and Actuators B: Chemical 169, 173-181.

Kruss, S., Hilmer, A.J., Zhang, J., Reuel, N.F., Mu, B., Strano, M.S., 2013. Carbon nanotubes as optical biomedical sensors. Advanced Drug Delivery Reviews 65(15), 1933-1950.

Kye, Y., Kim, C., Lagerwall, J., 2015. Multifunctional responsive fibers produced by dual liquid crystal core electrospinning. Journal of Materials Chemistry C 3(34), 8979-8985.

Kyritsis, A., Spanoudaki, A., Pandis, C., Hartmann, L., Pelster, R., Shinyashiki, N., Rodríguez Hernández, J.C., Gómez Ribelles, J.L., Monleón Pradas, M., Pissis, P., 2011. Water and polymer dynamics in poly(hydroxyl ethyl acrylate-co-ethyl acrylate) copolymer hydrogels. European Polymer Journal 47(12), 2391-2402.

Liu, G., An, Z., 2014. Frontiers in the design and synthesis of advanced nanogels for nanomedicine. Polymer Chemistry 5(5), 1559-1565.

Liu, Y., Ma, Q., Yang, M., Dong, X., Yang, Y., Wang, J., Yu, W., Liu, G., 2016. Flexible hollow nanofibers: Novel one-pot electrospinning construction, structure and tunable luminescence–electricity–magnetism trifunctionality. Chemical Engineering Journal 284, 831-840.

Liu, Z., Tabakman, S., Welsher, K., Dai, H., 2010. Carbon nanotubes in biology and medicine: In vitro and in vivo detection, imaging and drug delivery. Nano Research 2(2), 85-120.

Mahmoudifard, M., Soudi, S., Soleimani, M., Hosseinzadeh, S., Esmaeili, E., Vossoughi, M., 2016. Efficient protein immobilization on polyethersolfone electrospun nanofibrous membrane via covalent binding for biosensing applications. Materials Science and Engineering: C 58, 586-594.

Marin-Suarezdel Toro, M., Fernandez-Sanchez, J.F., Baranoff, E., Nazeeruddin, M.K., Graetzel, M., Fernandez-Gutierrez, A., 2010. Novel luminescent Ir(III) dyes for developing highly sensitive oxygen sensing films. Talanta 82(2), 620-626.

Medina-Castillo, A.L., Fernández-Sánchez, J.F., Fernández-Gutiérrez, A., 2011. One-Step Fabrication of Multifunctional Core-Shell Fibres by Co-Electrospinning. Advanced Functional Materials 21(18), 3488-3495.

Medina-Castillo, A.L., Fernandez-Sanchez, J.F., Klein, C., Nazeeruddin, M.K., Segura-Carretero, A., Fernandez-Gutierrez, A., Graetzel, M., Spichiger-Keller, U.E., 2007. Engineering of efficient phosphorescent iridium cationic complex for developing oxygen-sensitive polymeric and nanostructured films. Analyst 132(9), 929-936.

Medina-Castillo, A.L., Morales-Sanfrutos, J., Megia-Fernandez, A., Fernandez-Sanchez, J.F., Santoyo-Gonzalez, F., Fernandez-Gutierrez, A., 2012. Novel synthetic route for covalent coupling of biomolecules on super-paramagnetic hybrid nanoparticles. Journal of Polymer Science Part A: Polymer Chemistry 50(19), 3944-3953.

Medina-Rodríguez, S., de la Torre-Vega, Á., Sainz-Gonzalo, F.J., Marín-Suárez, M., Elosúa, C., Arregui, F.J., Matias, I.R., Fernández-Sánchez, J.F., Fernández-Gutiérrez, A., 2014. Improved Multifrequency Phase-Modulation Method That Uses Rectangular-Wave Signals to Increase Accuracy in Luminescence Spectroscopy. Analytical Chemistry 86(11), 5245-5256.

Medina-Rodriguez, S., Denisov, S.A., Cudre, Y., Male, L., Marin-Suarez, M., Fernandez-Gutierrez, A., Fernandez-Sanchez, J.F., Tron, A., Jonusauskas, G., McClenaghan, N.D., Baranoff, E., 2016. High performance optical oxygen sensors based on iridium complexes exhibiting interchromophore energy shuttling. Analyst 141(10), 3090-3097.

Medina-Rodriguez, S., Marin-Suarez, M., Fernandez-Sanchez, J.F., Torre-Vega, A.d.l., Baranoff, E., Fernandez-Gutierrez, A., 2013. High performance optical sensing nanocomposites for low and ultra-low oxygen concentrations using phase-shift measurements. Analyst 138(16), 4607-4617.

Mehra, N.K., Mishra, V., Jain, N.K., 2014. A review of ligand tethered surface engineered carbon nanotubes. Biomaterials 35(4), 1267-1283.

Ohtani, N., Takahashi, J., Katsuno, M., Yashiro, H., Kanaya, M., 1998. Development of large single-crystal SiC substrates. Electronics and Communications in Japan (Part II: Electronics) 81(6), 8-19.

Oliveros, A., Guiseppi-Elie, A., Saddow, S.E., 2013. Silicon carbide: a versatile material for biosensor applications. Biomedical Microdevices 15(2), 353-368.

Ouyang, Z., Li, J., Wang, J., Li, Q., Ni, T., Zhang, X., Wang, H., Li, Q., Su, Z., Wei, G., 2013. Fabrication, characterization and sensor application of electrospun polyurethane nanofibers filled with carbon nanotubes and silver nanoparticles. Journal of Materials Chemistry B 1(18), 2415-2424.

Papkovsky, D.B., O'Riordan, T.C., 2005. Emerging applications of phosphorescent metalloporphyrins. Journal of fluorescence 15(4), 569-584.

Quaranta, M., Borisov, S.M., Klimant, I., 2012. Indicators for optical oxygen sensors. Bioanalytical Reviews 4(2), 115-157.

Ramon-Marquez, T., Medina-Castillo, A.L., Fernandez-Gutierrez, A., Fernandez-Sanchez, J.F., 2016a. A novel optical biosensor for direct and selective determination of serotonin in serum by Solid Surface-Room Temperature Phosphorescence. Biosensors and Bioelectronics 82, 217-223.

Ramon-Marquez, T., Medina-Castillo, A.L., Fernandez-Gutierrez, A., Fernandez-Sanchez, J.F., 2016b. Novel optical sensing film based on a functional nonwoven nanofibre mat for an easy, fast and highly selective and sensitive detection of tryptamine in beer. Biosensors and Bioelectronics 79, 600-607.

Ramon-Marquez, T., Medina-Castillo, A.L., Fernandez-Sanchez, J.F., Fernandez-Gutierrez, A., 2015. Evaluation of different functional groups for covalent immobilization of enzymes in the development of biosensors with oxygen optical transduction. Analytical Methods 7(7), 2943-2949.

Rao, J.P., Geckeler, K.E., 2011. Polymer nanoparticles: Preparation techniques and size-control parameters. Progress in Polymer Science 36(7), 887-913.

Saifuddin, N., Raziah, A.Z., Junizah, A.R., 2013. Carbon Nanotubes: A Review on Structure and Their Interaction with Proteins. Journal of Chemistry 2013, 18.

Schrenkhammer, P., Wolfbeis, O.S., 2008. Fully reversible optical biosensors for uric acid using oxygen transduction. Biosensors and Bioelectronics 24(4), 994-999.

Stathopoulos, A., Klonos, P., Kyritsis, A., Pissis, P., Christodoulides, C., Rodriguez Hernández, J.C., Monleón Pradas, M., Gómez Ribelles, J.L., 2010. Water sorption and polymer dynamics in hybrid poly(2-hydroxyethyl-co-ethyl acrylate)/silica hydrogels. European Polymer Journal 46(1), 101-111.

Steiner, M.-S., Duerkop, A., Wolfbeis, O.S., 2011. Optical methods for sensing glucose. Chemical Society Reviews 40(9), 4805-4839.

Stich, M.I.J., Fischer, L.H., Wolfbeis, O.S., 2010. Multiple fluorescent chemical sensing and imaging. Chemical Society Reviews 39(8), 3102-3114.

Su, Z., Ding, J., Wei, G., 2014. Electrospinning: a facile technique for fabricating polymeric nanofibers doped with carbon nanotubes and metallic nanoparticles for sensor applications. RSC Advances 4(94), 52598-52610.

Sun, Z., Zussman, E., Yarin, A.L., Wendorff, J.H., Greiner, A., 2003. Compound Core–Shell Polymer Nanofibers by Co-Electrospinning. Advanced Materials 15(22), 1929-1932.

Talbert, J.N., Goddard, J.M., 2012. Enzymes on material surfaces. Colloids and Surfaces B: Biointerfaces 93, 8-19.

Valencia-Gonzalez, M.J., Diaz-Garcia, M.E., 1994. Enzymic Reactor/Room-Temperature Phosphorescence Sensor System for Cholesterol Determination in Organic Solvents. Analytical Chemistry 66(17), 2726-2731.

Wang, S., Li, S., Yu, Y., 2004. Immobilization of Cholesterol Oxidase on Cellulose Acetate Membrane for Free Cholesterol Biosensor Development. Artificial Cells, Blood Substitutes, and Biotechnology 32(3), 413-425.

Wang, X.-d., Wolfbeis, O.S., 2014. Optical methods for sensing and imaging oxygen: materials, spectroscopies and applications. Chemical Society Reviews 43(10), 3666-3761.

Wang, X.-D., Zhou, T.-Y., Chen, X., Wong, K.-Y., Wang, X.-R., 2008. An optical biosensor for the rapid determination of glucose in human serum. Sensors and Actuators B: Chemical 129(2), 866-873.

Wang, Y., Chen, L., Liu, P., 2012. Biocompatible Triplex Ag@SiO2@mTiO2 Core–Shell Nanoparticles for Simultaneous Fluorescence-SERS Bimodal Imaging and Drug Delivery. Chemistry – A European Journal 18(19), 5935-5943.

Willander, M., Khun, K., Ibupoto, Z., 2014. Metal Oxide Nanosensors Using Polymeric Membranes, Enzymes and Antibody Receptors as Ion and Molecular Recognition Elements. Sensors 14(5), 8605.

Wolfbeis, O.S., 2015. Luminescent sensing and imaging of oxygen: Fierce competition to the Clark electrode. BioEssays 37(8), 921-928.

Wu, R., Zhou, K., Yue, C.Y., Wei, J., Pan, Y., 2015. Recent progress in synthesis, properties and potential applications of SiC nanomaterials. Progress in Materials Science 72, 1-60.

Wu, X.J., Choi, M.M.F., 2003. Hydrogel Network Entrapping Cholesterol Oxidase and Octadecylsilica for Optical Biosensing in Hydrophobic Organic or Aqueous Micelle Solvents. Analytical Chemistry 75(16), 4019-4027.

Xu, B., Song, R.G., Wang, C., 2012. Preparation and characterization of Ag, Au and Ti metal nanoparticles colloids by pulsed laser ablation in liquids. Advanced Materials Research, pp. 648-651.

Xue, R., Ge, C., Richardson, K., Palmer, A., Viapiano, M., Lannutti, J.J., 2015. Microscale Sensing of Oxygen via Encapsulated Porphyrin Nanofibers: Effect of Indicator and Polymer —Core Permeability. ACS Applied Materials & Interfaces 7(16), 8606-8614.

Yan, E., Cao, M., Wang, Y., Yuan, M., Zheng, H., Hao, X., Yu, Z., Ba, X., Gu, X., Zhang, D., 2016. Degradable polyvinyl alcohol/poly(butylene carbonate) core–shell nanofibers for chemotherapy and tissue engineering. Materials Letters 167, 13-17.

Yang, D.-J., Zhang, L.-F., Xu, L., Xiong, C.-D., Ding, J., Wang, Y.-Z., 2007. Fabrication and characterization of hydrophilic electrospun membranes made from the block copolymer of poly(ethylene glycol-co-lactide). Journal of Biomedical Materials Research Part A 82A(3), 680-688.

Zhang, J., Cao, Y., He, Y., 2004. Ultrasonically irradiated emulsion polymerization of styrene in the presence of a polymeric surfactant. Journal of Applied Polymer Science 94(2), 763-768.

Zhou, C., Shi, Y., Ding, X., Li, M., Luo, J., Lu, Z., Xiao, D., 2013. Development of a Fast and Sensitive Glucose Biosensor Using Iridium Complex-Doped Electrospun Optical Fibrous Membrane. Analytical Chemistry 85(2), 1171-1176.

Appendix. Supplementary Material (SM)

Content:

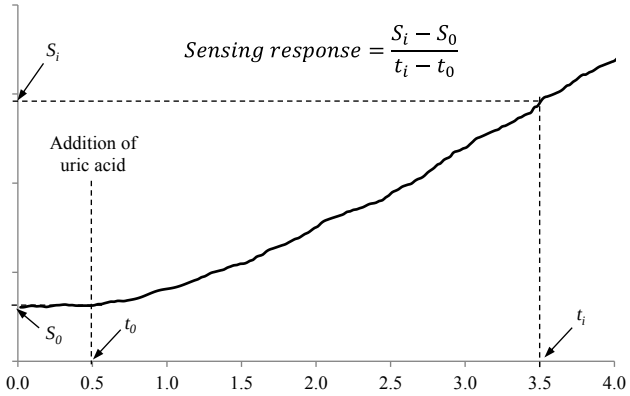

Fig. SM-6.1. Luminescence response of the biosensor when it is exposed to acid uric and example of determination of the sensing response.

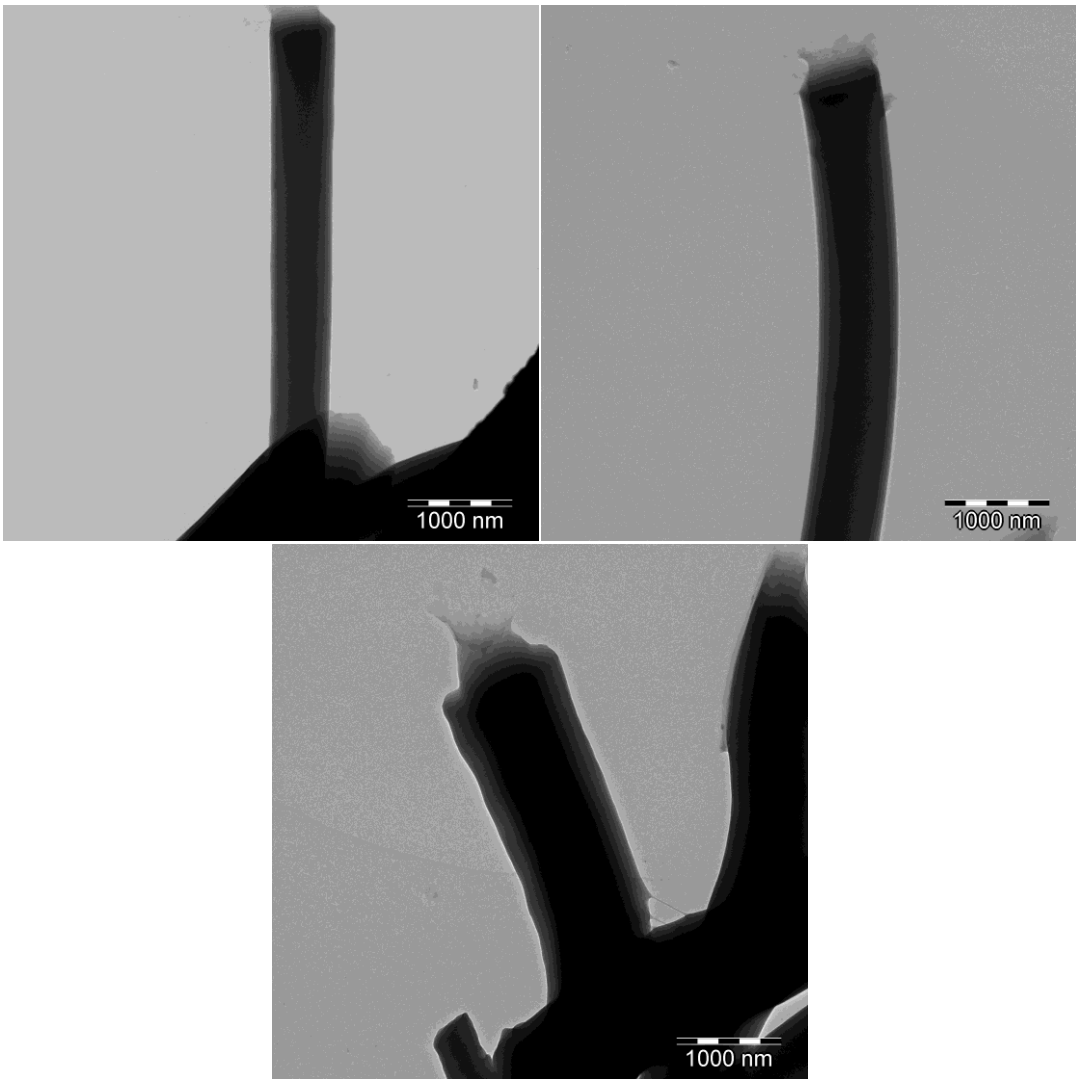

Fig. SM-6.2. TEM pictures of the nanofibre mats obtained at the optimal, selected conditions.

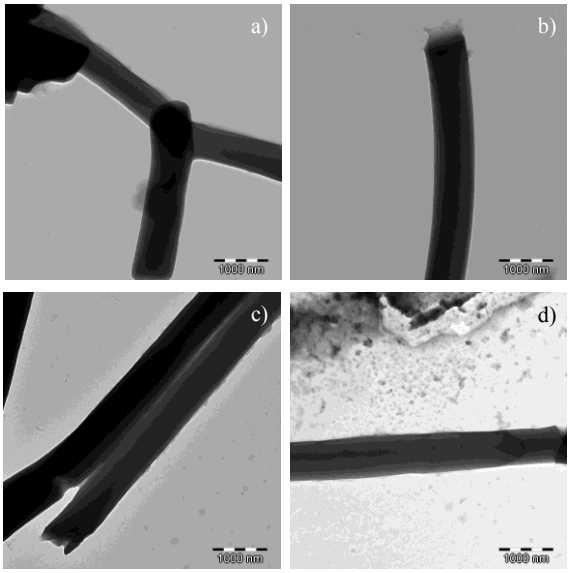

	Outer/inner flow rates (mL h^{-1})	Difference between inner and outer diameters (nm)
a)	1.3/0.1	190
b)	1.3/0.3	150
c)	1.3/0.5	100
d)	2.5/0.5	60

Fig. SM-6.3. TEM pictures of the coaxial nanofibre mats obtained at different outer/inner flow rates. The Table shows the conditions and the differences between the inner and outer diameter for each condition.

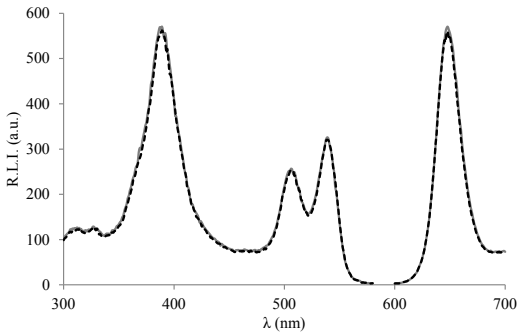

Fig. SM-6.4. Luminescence excitation and emission spectra of the coaxial nanofibre mat before (grey solid line) and after (black dashed line) the thermal wetting. $\lambda_{exc/em}$ = 390/648, t_d = 200µs, t_g = 5 ms, detector voltage of 500 V and monochromator slitwidth$_{exc/em}$ = 10/10 nm.

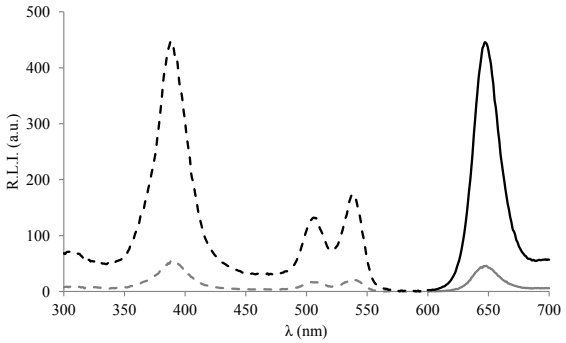

Fig. SM-6.5. Excitation (dashed line) and emission (solid line) spectra in the presence of 100% O_2 (grey line) and 100% N_2 (black line) of the simple fibre membrane produced by electrospinning using PtTFPP. $\lambda_{exc/em}$ = 390/648, [dye concentration] = 1% w/w, t_d = 200µs, t_g = 5 ms, and monochromator slitwidth$_{exc/em}$ = 10/10 nm.

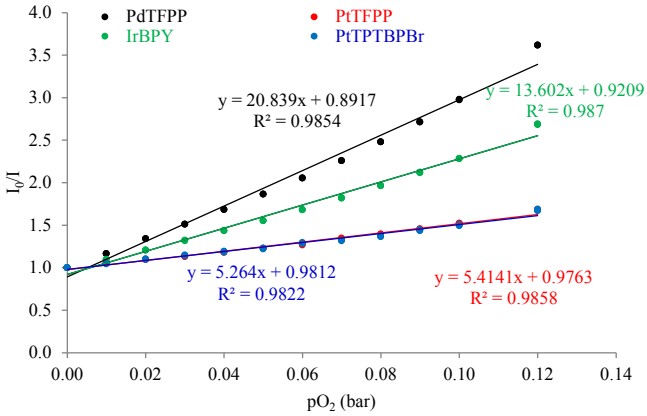

Fig. SM-6.6. Stern-Volmer plots of data for PtTFPP, PdTFPP, PtTPTBPBr and IrBPY incorporated into the inner fibre of the developed coaxial membranes.

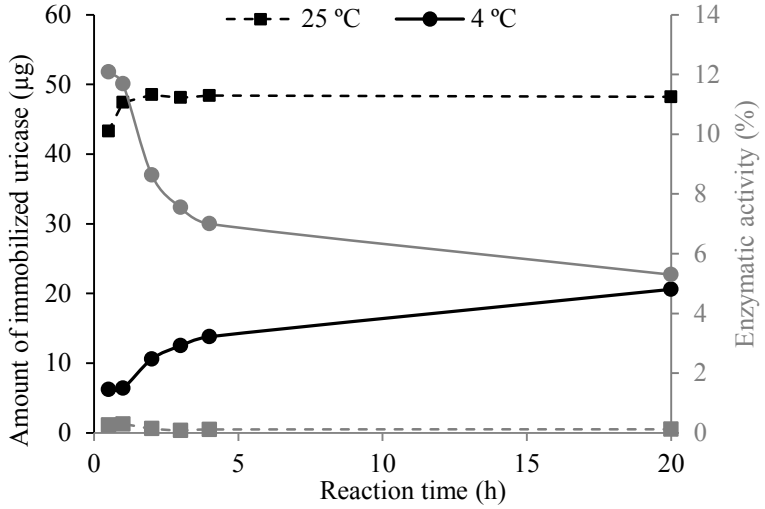

Fig. SM-6.7. Effect of the temperature and reaction time on the amount (black line) and enzymatic activity (grey line) of immobilized uricase at 25 ºC (dashed line; experimental data indicated with a solid square) and 4 ºC (solid line; experimental data indicated with a solid circle).

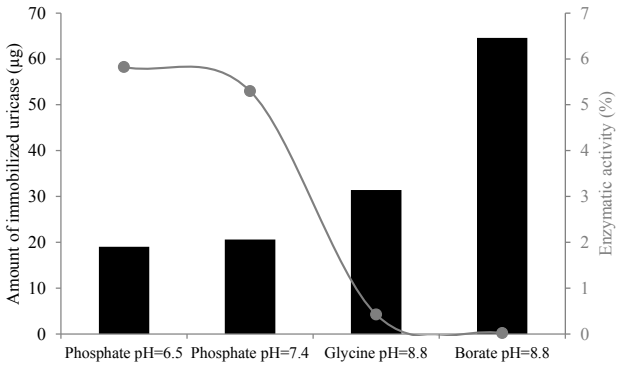

Fig. SM-6.8. Effect of the pH on the amount (black barrels) and enzymatic activity (grey line, experimental data indicated with a solid circle) of immobilized uricase.

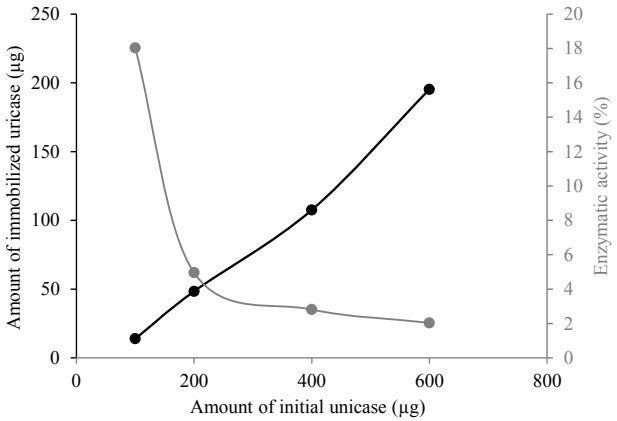

Fig. SM-6.9. Effect of the initial concentration of uricase on the amount (black line; experimental data indicated with a solid circle) and enzymatic activity (grey line, experimental data indicated with a solid circle) of immobilized uricase.

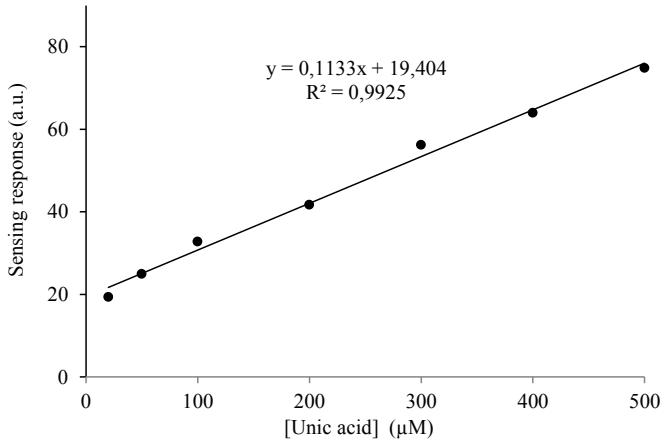

Fig. SM-6.10. Analytical calibration curve.

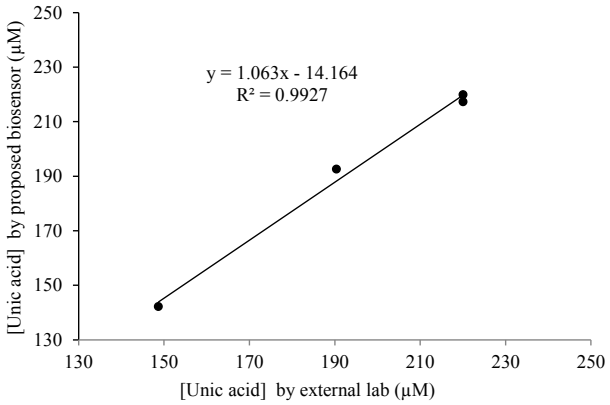

Fig. SM-6.11. Correlation between uric acid values determined in serum by a reference method developed in an external laboratory (x axis) and the proposed biosensor (y axis).

Capítulo 7

Evaluation of two sterically directed attachments of biomolecules on a coaxial nanofibre membrane to improve the development of optical biosensors

Teresa Ramon-Marquez[a], *Antonio L. Medina-Castillo*[b], *Alberto Fernandez-Gutierrez*[a], *Jorge F. Fernandez-Sanchez*[a]

[a] Department of Analytical Chemistry, University of Granada, Avd. Fuentenueva s/n, 18071 Granada, Spain

[b] NanoMyP®, Nanomateriales y Polimeros S.L., Spin-Off company of the UGR, BIC Building, Avd. Innovacion 1, E-18016, Granada, Spain

In progress

ABSTRACT

In this study, we have optimised the sterically directed attachment of biomolecules on the surface of coaxial membranes prepared by co-electrospinning which have been proved to be a material with very high performance for the development of biosensors with optical oxygen transduction.

Two sterically directed strategies: a) covalent attachment via maleimide, and b) affinity bonding via biotin-streptavidin interaction, have been tested in order to preserve the enzymatic activity of uricase and to improve the analytical figures of merits on the determination of uric acid. The best results were obtained with biotin-streptavidin affinity interaction and using a biotinylation reagent containing a polyethylene glycol chain. The developed biosensor showed high sensitivity towards uric acid with a detection limit of 0.5 µM, a quantification limit of 1.8 µM and linear range from 1.8 to 250 µM. The applicability of the membrane as biosensor with optical oxygen transduction was proved by determining uric acid in serum samples. The obtained results showed a good correlation (0.999) with those obtained by an external reference laboratory.

Keywords: Optical biosensor; Oxygen transduction; Multifunctional material; Biotin; Streptavidin; Uric acid.

1. Introduction

To develop biosensor membranes using optical oxygen transduction, a multifunctional material is required because it is necessary: 1) to immobilize a biomolecule which catalyses the oxidation of the analyte and 2) to incorporate an oxygen sensitive dye to measure the consumption of oxygen during this oxidation (Ramon-Marquez et al. 2017). In our previous work (Ramon-Marquez et al. 2017), we developed a multifunctional material based on co-electrospinning as a basic material for the development of biosensors with optical oxygen transduction (using uricase as model enzyme). It is based on coaxial nanofibres: an inner fibre containing an oxygen sensitive dye and an outer fibre containing aldehyde groups to allow the formation of Schiff bases with the amino groups of the uricase. However, the covalent attachment of uricase to the coaxial nanofibre membrane by aldehyde groups caused a high decrease in the relative activity of the enzyme and therefore, the sensitivity and the response time can be improved.

It is well-known that the method used for the immobilization of a biomolecule is a key factor that must be taken into consideration when a biosensor is developed (Ahuja et al. 2007; Gao and Kyratzis 2008; Hall et al. 2016; Sassolas et al. 2012; Tereshchenko et al. 2016). Immobilization methods range broadly from physical methods, which include adsorption (Samanta and Sarkar 2011), encapsulation (Edwards et al. 2006) and entrapment within a membrane (Monton et al. 2012), to more advanced chemical attachment procedures using chemically activated supports, which include covalent binding (Sassolas et al. 2012), crosslinking (Talekar et al. 2013), and affinity interactions (Prieto-Simon et al. 2008) between a functional group of the support (e.g. avidin, lectin, metal chelates) and a specific group (e.g. biotin, carbohydrate, histidine) of the biomolecule.

Covalent binding of biomolecules is a widely used immobilization method due to it allows achieving strong and efficient bonding between the biomolecules and the solid supports. This immobilization strategy is generally carried out by initial activation of the solid support, followed by biomolecule coupling. In order to obtain good biological performance the linking of the biomolecule to the support has to be made through functional groups not essential for its biological activity. Thus, in this work, to improve the enzymatic performance of uricase, we have modified the previously described covalent attachment of uricase to the coaxial nanofibre membrane (based on the interaction of aldehyde groups of the support with amino groups of the

biomolecule) (Ramon-Marquez et al. 2017), selecting reagents (maleimide) that can react with functional groups of the enzyme which are not implicated in its active site (thiol).

On the other hand, among the large variety of possible strategies for the immobilization of biomolecules on different supports, the specific biotin-(strept)avidin affinity interaction shows interesting advantages.

The strong and specific non-covalent interaction between biotin and avidin or streptavidin, leads to the formation of a high-affinity complex ($K_d \approx 10^{-15}$ M) with a strong association similar to the formation of a covalent bond. This interaction occurs very quickly and is highly resistant to wide ranges of pH, detergents, denaturing agents, organic solvents and high temperatures (Diamandis and Christopoulos 1991; Sakahara and Saga 1999; Savage 1996). Furthermore, several studies have demonstrated that the immobilization based on the biotin-(strept)avidin affinity reaction results in the preservation of the biological activity of the immobilized molecules in a higher degree than other methods (Amounas et al. 2000; Limoges et al. 2003; Schetters 1999).

In addition, biotin can be easily covalently coupled to a large number of molecules by the carboxyl group of the valeric acid side chain. This group can be derivatized to incorporate several reactive groups that can be used to attach biotin to other biomolecules such as proteins, antibodies, polysaccharides, nucleic acids, etc. (Elia 2001; Hermanson 2013b; Kay et al. 2009). Thus, the small size of biotin makes it a perfect tag for biomolecules because biotinylation does not significantly alter their biological activity, and also the attaching to the valeric acid side chain does not usually interfere with the binding to streptavidin or avidin (Elia 2008; Hermanson 2013b). Therefore, the immobilization of biomolecules on solid supports through the biotin-(strept)avidin interaction is an exceptional tool for the different disciplines of biosciences, biomedicine and biotechnology (Lin et al. 2002; Liu et al. 2013; Liu et al. 2010; Orth et al. 2003; Yang et al. 2013).

In this study, we have carefully selected the reagents in order to preserve the enzymatic activity of the uricase by using these strategies. Moreover, the best strategy has been used to determine acid uric in serum samples and the results have been compared with the previous one obtained by immobilizing uricase via aldehyde interaction (Ramon-Marquez et al. 2017).

2. Experimental

2.1. Reagents and Materials

For the fabrication of the coaxial materials, PolymBlend® was kindly supplied by NanoMyp® (http://www.nanomyp.com); poly(methyl methacrylate) (PMMA) and N,N-dimethylformamide (DMF) were purchased from Sigma Aldrich; Pd(II) meso-tetra(pentafluorophenyl)porphine (PdTFPP) was obtained from Frontier Scientific.

For the immobilization of uricase, potassium dihydrogen phosphate (KH_2PO_4), ethylenediamine (EDA), glutaraldehyde (GA), poly(ethylene glycol) [*N*-(2-maleimidoethyl)carbamoyl]methyl ether 2-(biotinylamino)ethane (biotin-PEG), maleimide-PEG_6-succinimidyl ester, *N*-biotinoyl-*N*′-(6-maleimidohexanoyl)hydrazide (biotin-maleimide), ethanolamine, uricase from *Candida* sp. (EC 1.7.3.3), and Tween 20 were all purchased from Sigma Aldrich; streptavidin (SAv) from *Streptomyces avidinii* (expressed in *Escherichia coli*) was obtained from Nuptec (China). All the solutions were prepared using doubly distilled water and used without further purification.

For the purification of biotinylated uricase, Zeba™ Spin Desalting Columns with a 7K molecular-weight cutoff were purchased from Thermo Fisher Scientific (http://www.thermofisher.com), and Amicon® Ultra-4 centrifugal filters with a membrane NMWL of 10 kDa were obtained from Merck Millipore (http://www.merckmillipore.com). To quantify the biotin label incorporation, 4´-hydroxyazobenzene-2-carboxylic acid (HABA) was purchased from Sigma Aldrich.

To assay the activity of uricase, glycine, 4-aminoantipyrine (4-AAP), and peroxidase (HRP) from horseradish (EC 1.11.1.7) were purchased from Sigma Aldrich, and uric acid and sodium 3,5-dichloro-2-hydroxybenzenesulfonate (DCHBS) were purchased from Alfa Aesar.

Human serum samples were obtained from a clinical analysis laboratory and stored frozen until assay.

2.2. Instrumentation

The UV-Visible absorption spectra were recorded on a Varian Cary 50 UV-Vis spectrophotometer. The luminescence measurements were carried out on a Varian Cary-Eclipse luminescence spectrophotometer.

All the luminescence measurements were carried out by controlling the temperature, which was continuously regulated by a commercial peltier cell holder connected to a temperature control module (Agilent Technologies, www.agilent.com).

The pH of the buffer solutions was controlled using a digital pH meter (Crison micropH 2000) calibrated at 20 ± 2 ºC.

2.3. Fabrication of coaxial membranes

The fabrication of the coaxial nanofibre membranes was done by co-electrospinning following the procedure previously described by our research group (Ramon-Marquez et al. 2017). Briefly, two different polymeric solutions (10% w/w PolymBlend® in DMF and 6% w/w PMMA containing 1% w/w PdTFPP in DMF) were independently driven by two syringe pumps towards a single coaxial needle using a flow-rate of 1.3 and 0.3 mL h^{-1} for the outer (PolymBlend®) and inner (PMMA with PdTFPP) solutions, respectively, until reaching a concentric couple of stainless-steel capillary tubes (injector). Then, a potential difference between the injector and the collector (30 cm length and 20 cm diameter rotator drum located 25 cm apart from the injector and rotating at 400 rpm) was applied and the process was run for 8 h to collect membranes with thickness about 150 µm. After that, the obtained coaxial nanofibre membranes were submitted to a thermal wetting in distilled water in order to increase their hydrophilicity. Finally, the treated membranes were attached to adhesive sheets (Lohmann Technologies Corp.) to facilitate their handling.

2.4. Immobilization of uricase on the coaxial nanofibre membrane

The immobilization of uricase on the coaxial nanofibre membrane was carried out by two different strategies, one by covalent immobilization and the other by biotin-streptavidin interaction:

1) For the covalent immobilization strategy: 20 cm^2 of material was first functionalized with vinyl active groups (Medina-Castillo et al. 2012) and then with amino groups by using 0.9 M EDA in phosphate buffer (100 mM, pH 8.4) for 2.5 h at room temperature (RT) (Goddard and Hotchkiss 2007). After this, amino groups were reacted with maleimide-PEG_6-succinimidyl ester by incubating 1.875 cm^2 of material with 4 mL of a solution of 0.75 mg mL^{-1} maleimide-PEG_6-succinimidyl ester in phosphate buffer (50 mM, pH 7.4) for different times (10, 20, 30,

60, 120 and 180 min) at RT in a rotating shaker. Then, it was washed with 5 mL of doubly distilled water (2x5 min).

The covalent immobilization of uricase on this material was carried out by incubating 1.875 cm^2 of maleimide activated material with 4 mL uricase solution (20 µg mL^{-1}) in phosphate buffer (50 mM, pH 7.0) at 4 ºC for 20 h.

2) For the biotin-streptavidin interaction strategy: 20 cm^2 of material functionalized with vinyl active groups was reacted with 0.9 M EDA in phosphate buffer (100 mM, pH 8.4) for 45 min at RT. Then, amino groups were reacted with GA (Goddard and Hotchkiss 2007) by incubating 1.875 cm^2 of material with 5 mL of 15 % v/v GA solution in phosphate buffer (100 mM, pH 7.4) for 1 h at RT in a rotating shaker. After washing with doubly distilled water (3x10 min), the material was incubated with 2 mL of a solution of 125 µg mL^{-1} SAv in phosphate buffer (100 mM, pH 7.4) at 30 ºC for 24 h. Then, it was washed (3x10 min) with a solution containing 8.5 g L^{-1} of NaCl and 0.5 g L^{-1} of Tween 20 to remove all the no covalently bounded SAv.

   The free aldehyde groups of the material that had not reacted with SAv were blocked with a solution of 0.9 M ethanolamine in phosphate buffer (100 mM, pH 8) for 1 h at RT. Then the material was incubated with 4 mL of biotinylated uricase (5, 10, 15, 20, 40 and 80 µg mL^{-1}) in phosphate buffer (50 mM, pH 7.0) at 4 ºC for 20 h.

In both cases, after the incubation with uricase, the materials were washed with 4 mL phosphate buffer (15 min in a rotating shaker), and these washing solutions and the reaction supernatants were reserved for further testing. After washing with phosphate buffer, the materials were also washed (3x10 min) with the NaCl-Tween 20 solution. The materials with immobilized uricase were stored in phosphate buffer (pH 7.4) at 4 ºC.

The amounts of SAv and uricase immobilized on the coaxial membrane were determined from the difference between the initial free amount and the total amount in the reaction supernatant and washing solutions after immobilization, assuming that the loss of biomolecule in each experiment is negligible. The biomolecule concentrations in the supernatant and washing solutions were measured by a spectrofluorometric method at 334 nm (Ramon-Marquez et al. 2017).

2.5. Biotinylation of uricase

The incorporation of a biotin label to the uricase was carried out by using two different biotinylation reagents following the next procedure: 1.5 mL of a solution of 1.375 mg mL^{-1} uricase in phosphate buffer (50 mM, pH 7.0) was incubated with 0.5 mL of a solution of 12 mg mL^{-1} biotin-PEG or 2 mg mL^{-1} biotin-maleimide, in the same buffer at 4 ºC for 24 h.

The level of biotin label incorporation was measured by a spectrophotometric method based on the strong biotin-SAv interaction (Green 1970). The assay uses the ability of the dye HABA to bind to SAv originating a complex with an absorption peak at 500 nm. Since the affinity between HABA and SAv is relatively weak ($K_d \approx 10^{-4}$ M) compared to the affinity between biotin and SAv ($K_d \approx 10^{-15}$ M), biotin and biotinylated molecules can displace HABA from the HABA/SAv complex, resulting in a decrease in the absorption at 500 nm that can be related to the amount of biotin or biotinylated molecule in the sample.

Briefly, 500 µL of a solution containing SAv (0.2 mg mL^{-1}) and HABA (4 µg mL^{-1}) in phosphate buffer (100 mM, pH 7.4) were mixed with 12 µL of biotin solutions with different concentrations (0, 50, 100, 150, and 200 µg mL^{-1}) or 12 µL of unknown biotin concentration samples at RT for 5 min, and then the absorbance at 500 nm was measured.

2.6. Assay of the immobilized uricase activity

The relative activity (%) of the immobilized uricase was determined by a colorimetric method based on two enzymatic reactions (Ramon-Marquez et al. 2017). The oxidation of uric acid catalysed by the action of uricase produces hydrogen peroxide, which reacts with DCHBS and 4-AAP in the presence of HRP to form a red quinoneimine dye with an absorption maximum at 513 nm. Based on this, the relative activity of uricase was calculated as a percentage of the immobilized uricase and free uricase absorbances.

In detail, to assay the activity of the immobilized uricase, 3 mL glycine buffer (50 mM, pH 8.8) containing 0.1 µmol uric acid were incubated with 1.875 cm^2 of coaxial with immobilized uricase for 20 min at 40 ºC. Then, 0.5 mL 4-AAP (10 mM), 0.5 mL DCHBS (50 mM) and 0.5 mL HRP (20 U mL^{-1}) in phosphate buffer (50 mM, pH 7.4) were added and kept at 40 ºC for 5 min to develop the colour. All the solutions were freshly prepared every day.

2.7. Evaluation of the analytical features of the membrane and application

The determination of uric acid with the membrane was carried out by measuring the luminescence signal of the oxygen sensitive dye incorporated into the inner fibre. The luminescence intensity of the dye increases with the concentration of uric acid due to the decrease in the dissolved oxygen concentration during the selective oxidation of uric acid by uricase. Supporting Material (SM) shows the typical evolution of the luminescence response versus time when the membrane is exposed to acid uric (see SM, Fig. SM-7.1).

The luminescence intensity was measured at excitation wavelength of 402 nm, emission wavelength of 669 nm, delay time (t_d) 200 µs, gate time (t_g) 5 ms, detector voltage of 650 V and excitation and emission slits of 10 nm wide.

In order to study the applicability of the developed sensing membrane, the concentration of uric acid in four serum samples was determined, and the obtained results were compared with those determined by an accredited external laboratory.

All the measurements were carried out by immersing the functionalised coaxial membranes in glycine buffer (50 mM, pH = 8.8) and adding 40 µL of serum sample (final dilution 1:9, serum:buffer) or different volumes of 1 mM uric acid solution. The temperature was maintained at 40 ºC during the measurements.

The sensing response was calculated as the increase in the luminescence intensity when the membrane is exposed to uric acid or serum samples:

$$Sensing\ response = S_i - S_0$$

where S_i is the luminescence intensity at the plateau and S_0 is the luminescence signal before adding uric acid or serum sample (see SM, Fig, SM-7.1).

3. Results

3.1. Selection of the biotinylation reagents and the reagent for the covalent immobilization

In order to preserve the enzymatic activity of the uricase, the binding of the biotinylation reagent to the enzyme has to be carried out through amino acid residues of the enzyme that are not in its active site.

The active site of the uricase is delimited by arginine and glutamine residues that hold the substrate (uric acid) by H-bond, a phenylalanine residue that maintains a close π-stacking with the substrate, and asparagine and threonine residues that build a peroxo hole for dioxygen, water, and hydrogen peroxide molecules (Gabison et al. 2011; Gabison et al. 2008). Therefore, the thiol side chain of cysteine residues is not implicated in the enzymatic activity of uricase and could be used to bind a biotin label. We selected biotin-PEG and biotin-maleimide as biotinylation reagents because their maleimido functional groups can react specifically with free sulfhydryls at pH 6.5-7.5 to form stable thioether bonds (Hermanson 2013a), which do not affect the enzymatic activity of the uricase.

On the other hand, the reagent used to attach the uricase by covalent immobilization was also selected to preserve the enzymatic activity of the enzyme. Thus, we choose maleimide-PEG_6-succinimidyl ester, which contains a maleimido functional group to react with free sulfhydryls of the uricase.

3.2. Optimization of the immobilization of the enzyme on the coaxial nanofibre membrane

Two different strategies for the sterically directed immobilization of uricase on the coaxial membrane were evaluated to obtain the best sensing properties: 1) covalent attachment through a maleimide-PEG_6-succinimidyl ester linker; 2) biotin-streptavidin interaction by using biotin-maleimide or biotin-PEG as linkers.

For the covalent immobilization of the uricase to the membrane, a heterobifunctional crosslinker (maleimide-PEG_6-succinimidyl ester) with an ethylene oxide spacer (length = 31.7 Å) was used. The succinimidyl ester group of the crosslinker was first reacted with the amino groups of the material, whereas its maleimide functional group was subsequently used to form thioether directed bonds with free sulfhydryls of the uricase. The effect of the reaction time of crosslinker with the material (10, 20, 30, 60, 120 and 180 min) versus uricase immobilization was studied. The amount of immobilized enzyme and its relative activity versus reaction time are shown in Fig. 7.1. The relative activity of the enzyme decreases when the immobilized amount increases, obtaining the highest relative activity (36.5 %) at 10 min of reaction time. This relative activity is higher than those obtained in our previous work (Ramon-Marquez et al. 2017) by using the aldehyde interaction (18 %). This increase can be due to the selective reaction between the maleimide group of the crosslinker and the sulfhydryls of the uricase belonging to cysteine residues which are not implicated in the enzymatic activity, whereas the aldehyde groups react mainly with amino groups which could be part of the active site of the enzyme.

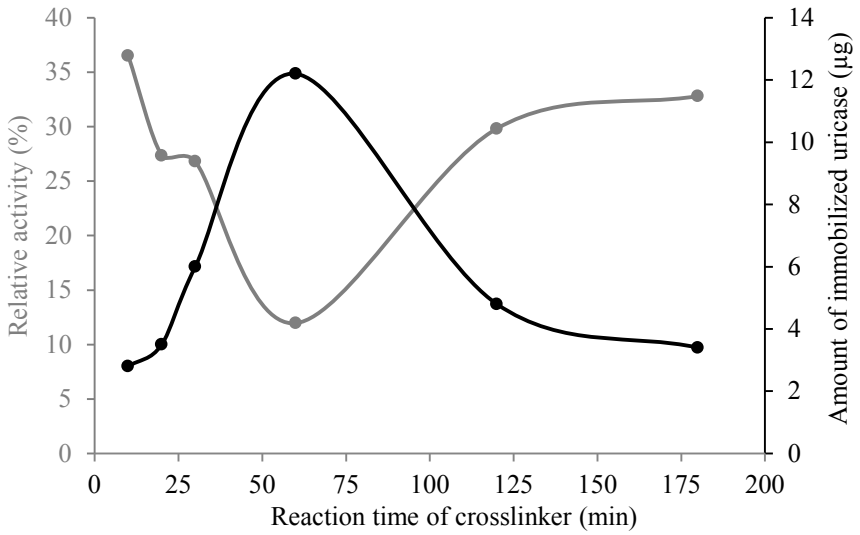

Fig. 7.1. Effect of the reaction time of maleimide-PEG_6-succinimidyl ester on the amount (black line) and relative enzymatic activity (grey line) of immobilised uricase (experimental data indicated with solid circles).

For the biotin-streptavidin immobilization of the uricase to the membrane, the membrane has to be functionalized with streptavidin (SAv) and uricase must be labelled with biotin.

The functionalization of the coaxial nanofibre membrane was done following the procedure described in Section 2.4.

Two different biotinylation reagents (biotin-maleimide and biotin-PEG) with the same terminal functional groups but different spacer arm lengths (13 and 341 atoms from the biotin to the maleimide groups, respectively) were used to incorporate the biotin label to the uricase. The reactions to incorporate the biotin labels to the enzyme are described in Section 2.5. In both cases the amount of enzyme was the same but different amounts of biotinylation reagents were used because they have different solubility in phosphate buffer. The hydrophilic character of PEG spacer arm increases the solubility of the biotin-PEG reagent in the aqueous reaction media which allowed the use of a more concentrated solution of this reagent.

Two different devices (spin desalting columns and centrifugal filters) were tested for purification. The biotinylation level was quantified by the HABA method (Green 1970). The highest biotinylation level was obtained with the biotin-PEG reagent. The biotinylation level was calculated by taking into account the efficiency of the spin columns to purify the reaction solutions. Thus, solutions of both biotinylation reagents without enzyme were passed through the

columns to determine their retention degree. The highest purification degree was obtained with the spin desalting column based on size exclusion for the biotin-maleimide reagent (80 % retention of reagent) and with the centrifugal filter for the biotin-PEG reagent (73 **%** retention of reagent).

The effect of the purification step through the spin columns was also studied by measuring the activity of the enzyme in solution before and after the purification step. Fig. SM-7.2 shows that both, the use of the spin desalting column as well as the centrifugal filter, decreased the enzymatic activity (36 and 28 %, respectively). Therefore, in order to avoid this decrease in the activity of the enzyme, the incubation of the uricase, the biotinylation reagent and the streptavidin-functionalized membrane was performed in a single step.

The uricase biotinylated with the two biotinylation reagents were then incubated with the streptavidin-functionalized membrane following the procedure described in Section 2.4, and the amount of immobilized enzyme and its activity were evaluated (see Fig. 7.2). The maximum amount of immobilized uricase was achieved with the biotin-maleimide reagent, but the highest relative activity of the enzyme was obtained with the biotin-PEG reagent for all the tested concentrations.

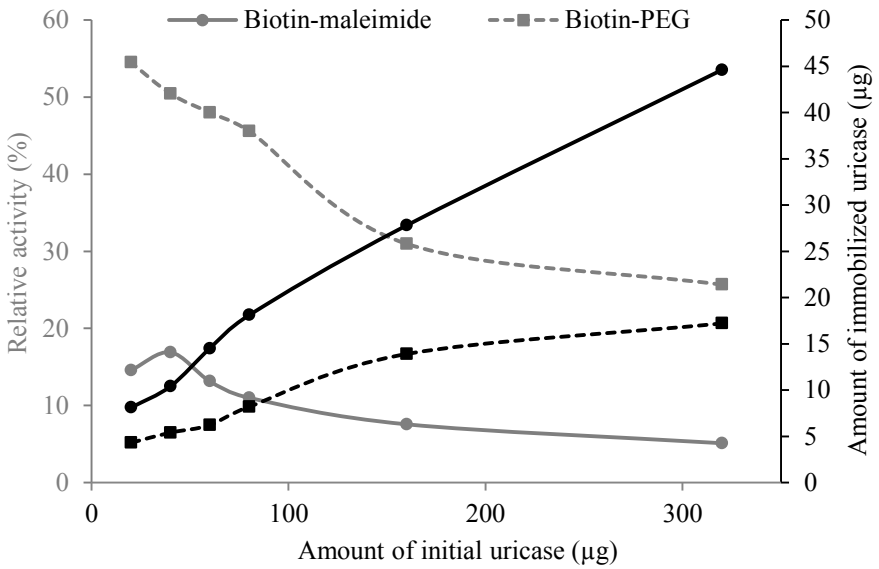

Fig. 7.2. Effect of the initial amount of uricase and the biotinylation reagent on the amount (black line) and enzymatic activity (grey line) of immobilised uricase with biotin-maleimide (solid line; experimental data indicated with solid circles) and biotin-PEG (dashed line; experimental data indicated with solid squares).

These results indicate that the introduction of a longer spacer during the immobilization of uricase produces an improvement in the relative activity of the enzyme. Therefore, the distance from the surface of the membrane to the immobilized enzyme is a key factor to ensure a high enzymatic activity. This effect of the spacer on the enzyme activity can be due to the higher mobility of the enzyme in the presence of a longer spacer between the enzyme and the solid support (Cao 2006; Talbert and Goddard 2012); the increase in the mobility of the immobilized enzyme can favour the accessibility of the substrate to the enzyme, allowing a better interaction between them, and can reduce the influence of the solid surface on the enzyme and the alteration of the enzyme microenvironment. Thus, biotin-PEG with a poly(ethylene glycol) long linker was selected as the most adequate biotinylation reagent.

To determine the influence of the amount of immobilized streptavidin on the immobilization of biotinylated uricase, several SAv concentrations were tested (5, 25, 37.5, 50, 87.5, 125, 250 and 375 μg mL^{-1}) in phosphate buffer (100 mM, pH 7.4) at 30 ºC for 24 h. SM (see Fig. SM-7.3) shows that the amount of immobilized SAv increases linearly with the initial amount, maintaining an immobilization percentage between 76 and 89 % for all the tested concentrations.

Then the material was blocked for 1 h with a solution of 0.9 M ethanolamine, and subsequently it was incubated with 4 mL of biotin-PEG (60 μg mL^{-1}) and uricase (20 μg mL^{-1}) in phosphate buffer (50 mM, pH 7.4) at 4 ºC for 20 h. The variation of the amount of immobilized uricase and its activity with the amount of immobilized SAv were also studied (see SM, Fig. SM-7.4). This study shows that the amount of immobilized uricase is not practically affected by the amount of SAv on the membrane. This is probably because the amount of available SAv molecules is higher than the amount of biotinylated uricase. However, the relative activity of the uricase increases with the amount of SAv up to 36.0 % when the membrane contains 200 μg of immobilized SAv and then decreases. This variation could be due to the density of the affinity binding sites (Cao 2006). The increase in the amount of SAv molecules might lead to an increase in unspecific interactions that does not lead to an increase in the activity of the immobilized uricase, thus the control over the density of the affinity binding sites is essential to favour the specific binding. 200 μg of immobilised SAv (initial concentration of 125 μg mL^{-1} SAv) was selected as optimum to achieve the highest uricase relative activity.

The obtained results indicated that the immobilized SAv retained its capacity to bind biotinylated conjugates and the incorporation of the biotin label to the uricase did not affect its activity or the ability of biotin to interact with SAv.

To optimise the concentration of uricase, the coaxial membrane functionalised with 125 µg mL^{-1} of SAv was incubated with 5 µg mL^{-1} biotin-PEG and different concentrations of uricase in phosphate buffer (50 mM, pH 7.0), resulting in different biotin-PEG:uricase molar ratios (1:0.25, 1:0.5, 1:1, 1:2, 1:3, 1:4, 1:5, 1:6, 1:7 and 1:8). Fig. 7.3 shows the variation of the amount of immobilised uricase and the absorbance of the red quinoneimine dye produced during the catalytic process (see Section 2.6) which is related with the specific activity of the enzyme.

Fig. 7.3. Effect of the initial amount of uricase on the amount of immobilised uricase (black line; experimental data indicated with solid squares) and the absorbance of the red quinoneimine dye at 513 nm (grey line; experimental data indicated with solid circles).

The amount of immobilized uricase increases with the initial amount of uricase, maintaining an immobilization percentage between 6.2 and 11.4 % for all the tested concentrations. However, the absorbance produced by catalytic action of immobilized uricase increases with the initial amount of uricase up to 260 µg and then it reaches a plateau. Therefore, an increase in the amount of immobilised uricase does not provide an increase of the compound produced by the catalytic action of immobilized uricase. It can be explained considering an unspecific adsorption of the uricase at concentrations higher than 65 µg mL^{-1} (initial amount of uricase of 260 µg); at low initial concentrations of uricase the immobilization is mostly produced by an affinity interaction due to the high amount of available streptavidin molecules and, on the other hand, at high initial concentrations of uricase the steric hindrance produced by the immobilized uricase

hinders the access to the rest of streptavidin molecules, causing an unspecific adsorption. Thus, the optimal initial concentration of uricase was set at 65 μg mL^{-1} (which corresponds with a biotin-PEG:uricase molar ratio of 1:2) in order to obtain low unspecific adsorption of the enzyme; at this molar ratio, the immobilization yield was 9.1 μg cm^{-2} and the relative enzymatic activity was 31.5 %.

The influence of the biotin-PEG concentration on the extent of uricase immobilization and the retention of its enzymatic activity was studied by maintaining the 1:2 biotin-PEG:uricase molar ratio and varying the concentration of biotin-PEG (from 1.3 to 25.6 μg mL^{-1}) during the incubation on the coaxial nanofibre membrane functionalised with 125 μg mL^{-1} SAv in phosphate buffer (50 mM, pH 7.0). The results of this experiment are shown in Fig. 7.4.

This figure shows that when the biotin-PEG concentration is smaller than 8 μg mL^{-1} the amount of immobilized uricase is practically constant (from 9.5 to 14.1 μg) and the relative activity is high (from 35.2 to 41.4 %). At higher concentrations, the immobilization yield increases to reach a maximum at 43 μg cm^{-2} (80.8 μg of immobilized uricase), but the relative activity decreases considerably to 7.3 %. In this case (see Fig. 7.4b) the obtained absorbance signals also increase to reach a plateau, suggesting that at biotin-PEG concentrations lower than 8 μg mL^{-1}, the unspecific adsorptions are relatively low, but at higher concentrations the immobilization of the enzyme is mostly unspecific, leading to a significant decrease in the relative activity. Thus, an initial biotin-PEG concentration of 8 μg mL^{-1} (corresponding with a SAv:biotin-PEG molar ratio 1:1.5) was selected. It provides a material with a relative enzymatic activity of 41.2 % and an immobilization yield of 8.1 μg cm^{-2}.

Therefore, the resulting membrane using the sterically directed strategy based on affinity bonding via biotin-streptavidin interaction (relative activity of 41.2 %) is a more active membrane than those obtained by covalent attachment via maleimide (36.5 % relative activity) or by non sterically directed strategy via aldehyde interaction (18 % relative activity; (Ramon-Marquez et al. 2017)). In addition, the selection of adequate molar ratios of biotin-PEG:uricase and SAv:biotin-PEG allows controlling the unspecific adsorption level, achieving a higher relative activity of the immobilized uricase.

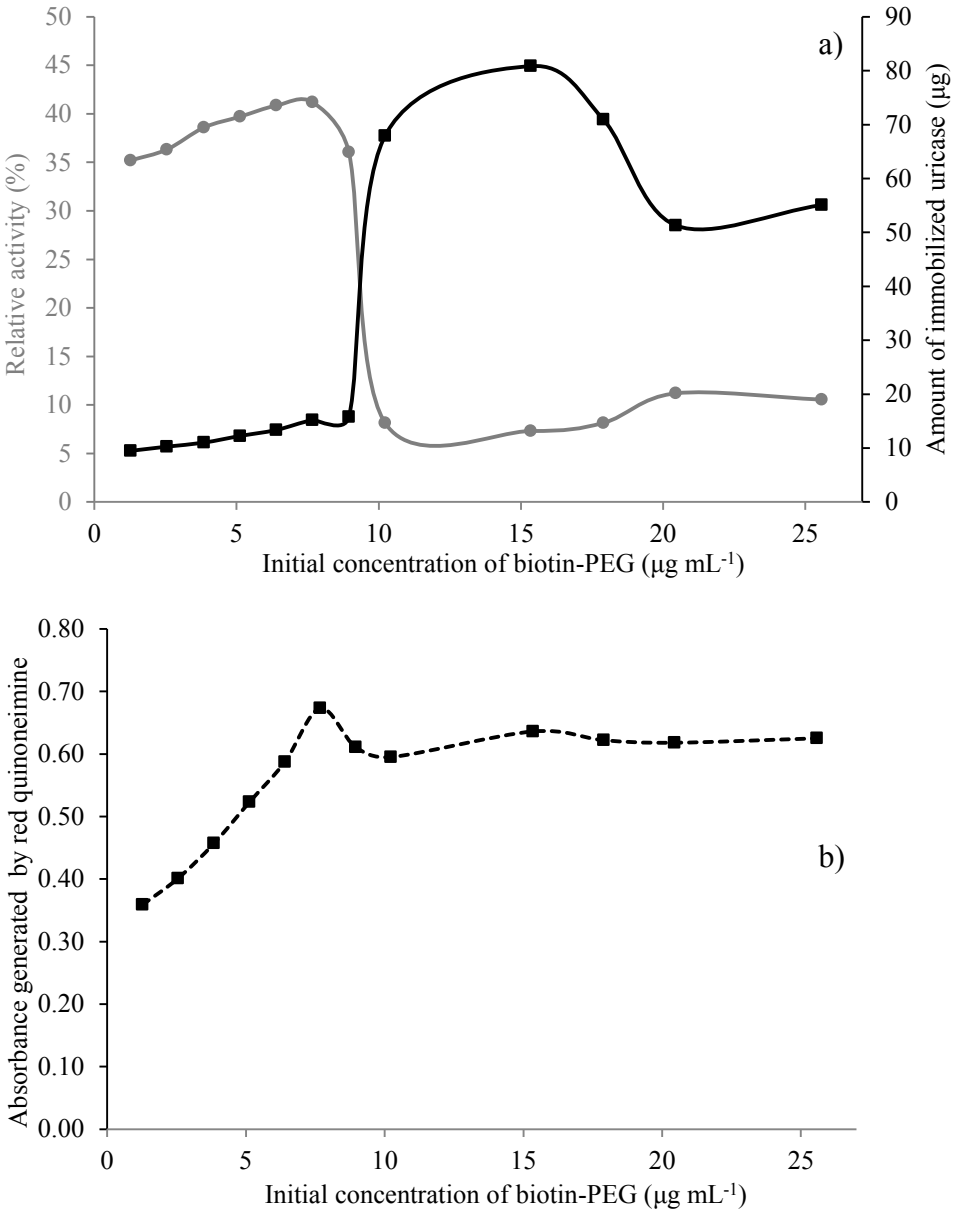

Fig. 7.4. Effect of the initial concentration of biotin-PEG on a) the relative enzymatic activity (grey solid line; experimental data indicated with solid circles) and the amount (black solid line; experimental data indicated with solid squares) of immobilized uricase; b) the absorbance of the red quinoneimine dye at 513 nm (black dashed line; experimental data indicated with solid squares).

3.3. Analytical figures of merits

In order to determine the response of the developed biosensor toward uric acid, the selected membranes were submerged in glycine buffer with different concentrations of uric acid and the evolution of the luminescence intensity with the time was registered (see SM, Fig. SM-7.1). The luminescence intensity of the membranes increases when the concentration of uric acid in glycine buffer also increases until to reach a plateau. The difference between the luminescence intensity

after reaching the plateau and before adding the uric acid was used as sensing response to plot the calibration curve. The calibration curve was determined by measuring twice seven different concentrations of uric acid within three different membranes. The response time, determined as the time required for reaching the plateau from the addition of uric acid, was established as 5 min for all the membranes and all the tested concentrations. A linear relationship between the sensing response and the uric acid concentration was obtained in the range from 1.8 to 250 µM (see SM, Fig. SM-7.5). Table 7.1 summarizes the analytical figures of merits of the developed sensing membrane. The detection and quantification limits were calculated using the IUPAC method (LOD = $3s_b/m$; LOQ = $10s_b/m$); where s_b is the standard deviation of 10 blanks and m is the slope of the calibration curve.

Comparing the analytical figures of merits of this new biosensor based on a biotin-SAv interaction with the previous one (Ramon-Marquez et al. 2017) based on an aldehyde interaction, it is possible to conclude that the biotin-SAv interaction improves considerably the sensitivity of the biosensing films; the slope of the calibration curve is increased from 0.11 to 3.77 μM^{-1} and the detection limit is reduced more than 30 times (from 18 to 0.5 µM).

Table 7.1. Analytical figures of merits of the developed sensing membrane functionalized with uricase by biotin-streptavidin affinity interaction, $\lambda_{exc/em}$ = 402/669 nm, t_d = 200 µs, t_g = 5 ms, detector voltage of 650 V and monochromator slitwidth$_{exc/em}$ = 10/10 nm.

	This paper (biotin-SAv interaction)	**Previous material (aldehyde interaction) (Ramon-Marquez et al. 2017)**
Linearity (%)	99.97	99.25
Slope (μM^{-1})	3.7716	0.1133
Intercept	9.7467	19.404
Linear range (µM)	1.8-250	61-500
Limit of detection (µM)	0.5	18
Limit of quantification (µM)	1.8	61

3.4. Application

The developed membranes were employed for the determination of uric acid in four serum samples from healthy adults. Each serum sample was analysed with four different coaxial

membranes following the procedure described in Section 2.7. The accuracy of the obtained results was tested by comparing the concentrations of uric acid in the serum samples calculated by the developed biosensor with those obtained by an external laboratory (reference method). Table 7.2 shows a comparison of the concentrations in serum samples determined by both methods. The values obtained by both methods showed a good correlation coefficient (0.999) with regression equation $y = 0.9107x + 17.03$ (Fig. SM-7.6). These results indicate that the developed membrane is an excellent biosensor for the accurate determination of uric acid in human serum, by using a small volume of serum (40 µL) and without any sample treatment.

Table 7.2. Results of the acid uric determination by the proposed biosensor and an external reference laboratory.

Sample	[uric acid] (µM) External reference laboratory	[uric acid] (µM) Proposed biosensor[a]
1	220.1	218.5 ± 12.6
2	190.4	191.6 ± 3.9
3	148.7	152.0 ± 5.5
4	220.1	215.7 ± 6.9

[a] Four different coaxial membranes per sample were used to determine the uric acid concentration

4. Conclusions

In this study, we have demonstrated that biotin-SAv affinity interaction can be used to produce a sterically directed immobilization of uricase on the surface of coaxial fibers improving the analytical figures of merits of the coaxial nanofibre membrane with optical oxygen transduction developed by our research group.

The presence of molecules of SAv as binding points on the surface of the membrane enhanced the immobilization of uricase, and the use of biotin-PEG as biotinylation reagent allowed keep the immobilized enzyme at an adequate distance from the surface of the membrane. In addition, the incubation of uricase and biotin-PEG with the streptavidin-functionalized membrane can be done in one single step, avoiding purification steps and reducing loss of enzymatic activity.

In order to achieve the best enzymatic activity, the immobilization of uricase on the coaxial membrane was optimized selecting adequate biotin-PEG:uricase (1:2) and SAv:biotin-PEG

(1:1.5) molar ratios, which allowed obtain a relative enzymatic activity of 41.2 %, higher than those obtained via maleimide (36.5 %) and aldehyde (18 %) interactions.

The developed sensing membrane provides good analytical figures (detection limit of 0.5 µM, quantification limit of 1.8 µM, and linear range from 1.8 to 250 µM) and can be used to determine the uric acid concentration in serum samples without any sample treatment. The obtained results analysing serum samples with the developed membrane were compared with those obtained by an external reference laboratory, achieving a good correlation (0.999) which demonstrates its applicability as biosensor with optical oxygen transduction.

Acknowledgments

This work has received funding from the People Programme (Marie Curie Actions, Multi-ITN) of the European Union‘s Seventh Framework Programme for research, technological development and demonstration under grant agreement n° 608104 (EUROMBR) and the Spanish Ministry of Economy and Competitiveness (Ramon-Marquez‘s grant reference AP2012-0944, Medina-Castillo‘s Torres Quevedo contract reference PTQ-11-04904 and project CTQ2014-53442-P).

References

Ahuja, T., Mir, I.A., Kumar, D., Rajesh, 2007. Biomolecular immobilization on conducting polymers for biosensing applications. Biomaterials 28(5), 791-805.

Amounas, M., Innocent, C., Cosnier, S., Seta, P., 2000. A membrane based reactor with an enzyme immobilized by an avidin–biotin molecular recognition in a polymer matrix. Journal of Membrane Science 176(2), 169-176.

Cao, L., 2006. Covalent Enzyme Immobilization. Carrier-bound Immobilized Enzymes, pp. 169-316. Wiley-VCH Verlag GmbH & Co. KGaA.

Diamandis, E.P., Christopoulos, T.K., 1991. The biotin-(strept)avidin system: principles and applications in biotechnology. Clinical Chemistry 37(5), 625-636.

Edwards, K., Kato, M., Utsunomiya-Tate, N., Toyo'oka, T., 2006. Encapsulated Biomolecules Using Sol-Gel Reaction for High-Throughput Screening. Frontiers in Drug Design & Discovery, 273-294.

Elia, G., 2001. Protein Biotinylation. Current Protocols in Protein Science. John Wiley & Sons, Inc.

Elia, G., 2008. Biotinylation reagents for the study of cell surface proteins. PROTEOMICS 8(19), 4012-4024.

Gabison, L., Chopard, C., Colloc'h, N., Peyrot, F., Castro, B., Hajji, M.E., Altarsha, M., Monard, G., Chiadmi, M., Prangé, T., 2011. X-ray, ESR, and quantum mechanics studies unravel a spin well in the cofactor-less urate oxidase. Proteins: Structure, Function, and Bioinformatics 79(6), 1964-1976.

Gabison, L., Prangé, T., Colloc'h, N., El Hajji, M., Castro, B., Chiadmi, M., 2008. Structural analysis of urate oxidase in complex with its natural substrate inhibited by cyanide: Mechanistic implications. BMC Structural Biology 8(1), 32.

Gao, Y., Kyratzis, I., 2008. Covalent Immobilization of Proteins on Carbon Nanotubes Using the Cross-Linker 1-Ethyl-3-(3-dimethylaminopropyl)carbodiimide—a Critical Assessment. Bioconjugate Chemistry 19(10), 1945-1950.

Goddard, J.M., Hotchkiss, J.H., 2007. Polymer surface modification for the attachment of bioactive compounds. Progress in Polymer Science 32(7), 698-725.

Green, N.M., 1970. [74] Spectrophotometric determination of avidin and biotin. Methods in Enzymology, pp. 418-424. Academic Press.

Hall, E.A.H., Chen, S., Chun, J., Du, Y., Zhao, Z., 2016. A molecular biology approach to protein coupling at a biosensor interface. TrAC Trends in Analytical Chemistry 79, 247-256.

Hermanson, G.T., 2013a. Chapter 6 - Heterobifunctional Crosslinkers. Bioconjugate Techniques (Third edition), pp. 299-339. Academic Press, Boston.

Hermanson, G.T., 2013b. Chapter 11 - (Strept)avidin–Biotin Systems. Bioconjugate Techniques (Third edition), pp. 465-505. Academic Press, Boston.

Kay, B.K., Thai, S., Volgina, V.V., 2009. High-throughput Biotinylation of Proteins. Methods in molecular biology (Clifton, N.J.) 498, 185-196.

Limoges, B., Savéant, J.-M., Yazidi, D., 2003. Quantitative Analysis of Catalysis and Inhibition at Horseradish Peroxidase Monolayers Immobilized on an Electrode Surface. Journal of the American Chemical Society 125(30), 9192-9203.

Lin, B., Qiu, J., Gerstenmeier, J., Li, P., Pien, H., Pepper, J., Cunningham, B., 2002. A label-free optical technique for detecting small molecule interactions. Biosensors and Bioelectronics 17(9), 827-834.

Liu, J., Ye, Y., Hu, Z., Zou, Y., Chen, G., Yu, L., 2013. A hypersensitive biotin-avidin-TRFIA for quantitative detection of ANA-Ig(GAM) and its clinical application. Journal of Immunoassay and Immunochemistry 34(2), 197-207.

Liu, Z., Jiang, L., Galli, F., Nederlof, I., Olsthoorn, R.C.L., Lamers, G.E.M., Oosterkamp, T.H., Abrahams, J.P., 2010. A Graphene Oxide˙Streptavidin Complex for Biorecognition – Towards Affinity Purification. Advanced Functional Materials 20(17), 2857-2865.

Medina-Castillo, A.L., Morales-Sanfrutos, J., Megia-Fernandez, A., Fernandez-Sanchez, J.F., Santoyo-Gonzalez, F., Fernandez-Gutierrez, A., 2012. Novel synthetic route for covalent coupling of biomolecules on super-paramagnetic hybrid nanoparticles. Journal of Polymer Science Part A: Polymer Chemistry 50(19), 3944-3953.

Monton, M.R.N., Forsberg, E.M., Brennan, J.D., 2012. Tailoring Sol–Gel-Derived Silica Materials for Optical Biosensing. Chemistry of Materials 24(5), 796-811.

Orth, R.N., Clark, T.G., Craighead, H.G., 2003. Avidin-Biotin Micropatterning Methods for Biosensor Applications. Biomedical Microdevices 5(1), 29-34.

Prieto-Simon, B., Campas, M., Marty, J.L., 2008. Biomolecule Immobilization in Biosensor Development: Tailored Strategies Based on Affinity Interactions. Protein and Peptide Letters 15(8), 757-763.

Ramon-Marquez, T., Medina-Castillo, A.L., Nagiah, N., Fernandez-Gutierrez, A., Fernandez-Sanchez, J.F., 2017. A multifunctional material based on co-electrospinning for developing biosensors with optical oxygen transduction. Biosensors and Bioelectronics (submitted).

Sakahara, H., Saga, T., 1999. Avidin–biotin system for delivery of diagnostic agents. Advanced Drug Delivery Reviews 37(1–3), 89-101.

Samanta, D., Sarkar, A., 2011. Immobilization of bio-macromolecules on self-assembled monolayers: methods and sensor applications. Chemical Society Reviews 40(5), 2567-2592.

Sassolas, A., Blum, L.J., Leca-Bouvier, B.D., 2012. Immobilization strategies to develop enzymatic biosensors. Biotechnology Advances 30(3), 489-511.

Savage, M.D., 1996. An Introduction to Avidin-Biotin Technology and Options for Biotinylation. In: Meier, T., Fahrenholz, F. (Eds.), A Laboratory Guide to Biotin-Labeling in Biomolecule Analysis, pp. 1-29. Birkhäuser Basel, Basel.

Schetters, H., 1999. Avidin and streptavidin in clinical diagnostics. Biomolecular Engineering 16(1–4), 73-78.

Talbert, J.N., Goddard, J.M., 2012. Enzymes on material surfaces. Colloids and Surfaces B: Biointerfaces 93, 8-19.

Talekar, S., Joshi, A., Joshi, G., Kamat, P., Haripurkar, R., Kambale, S., 2013. Parameters in preparation and characterization of cross linked enzyme aggregates (CLEAs). RSC Advances 3(31), 12485-12511.

Tereshchenko, A., Bechelany, M., Viter, R., Khranovskyy, V., Smyntyna, V., Starodub, N., Yakimova, R., 2016. Optical biosensors based on ZnO nanostructures: advantages and perspectives. A review. Sensors and Actuators B: Chemical 229, 664-677.

Yang, Z., Shen, J., Li, J., Zhu, J., Hu, X., 2013. An ultrasensitive streptavidin-functionalized carbon nanotubes platform for chemiluminescent immunoassay. Analytica Chimica Acta 774, 85-91.

Appendix. Supplementary Material (SM)

Content:

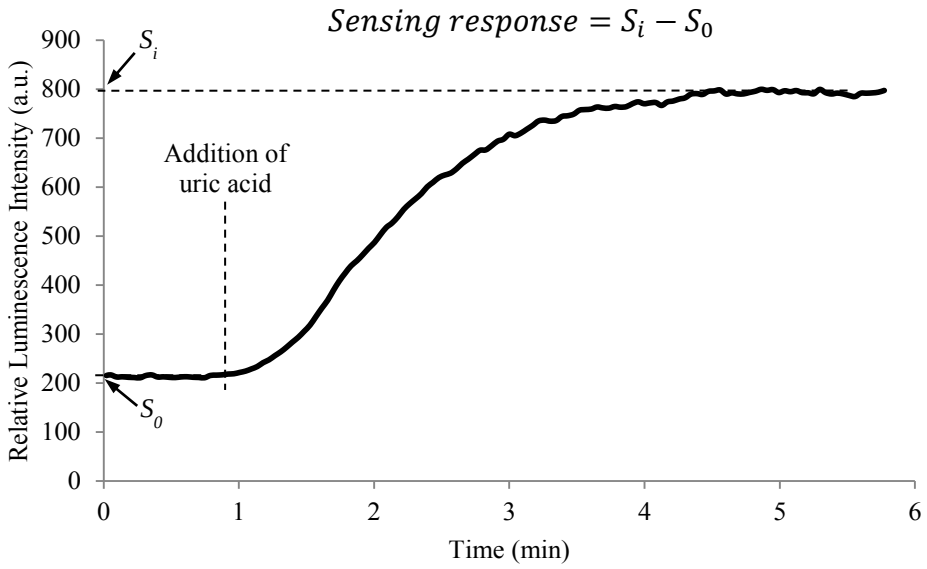

Fig. SM-7.1. Luminescence response of the biosensor membrane when it is exposed to acid uric and example of determination of the sensing response.

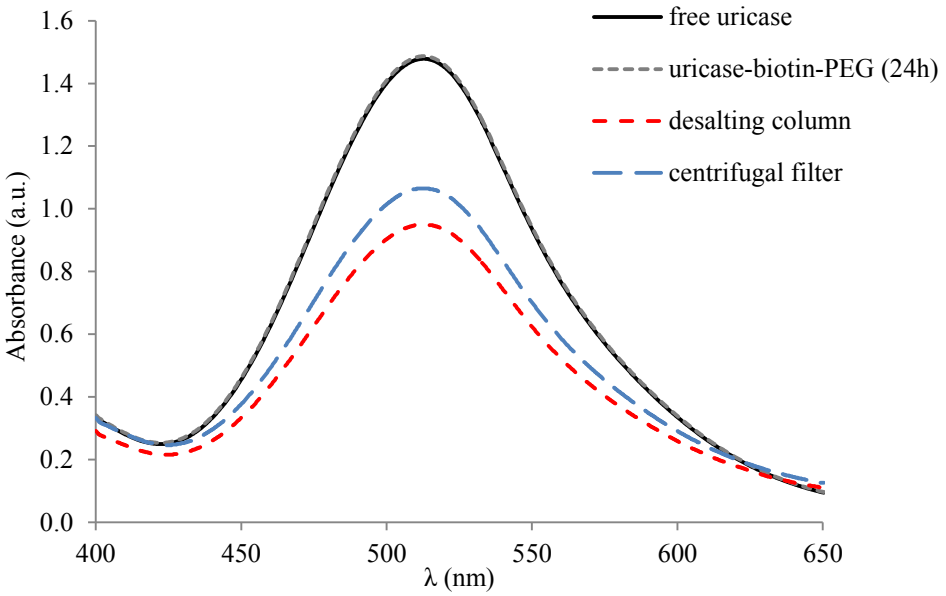

Fig. SM-7.2. Effect of the purification step through the spin desalting column (red dashed line) and the centrifugal filter (blue dashed line) on the enzymatic activity of free uricase (black solid line) measured as absorbance (Section 2.7). The effect of the incubation with biotin-PEG for 24 h is also shown (grey dotted line).

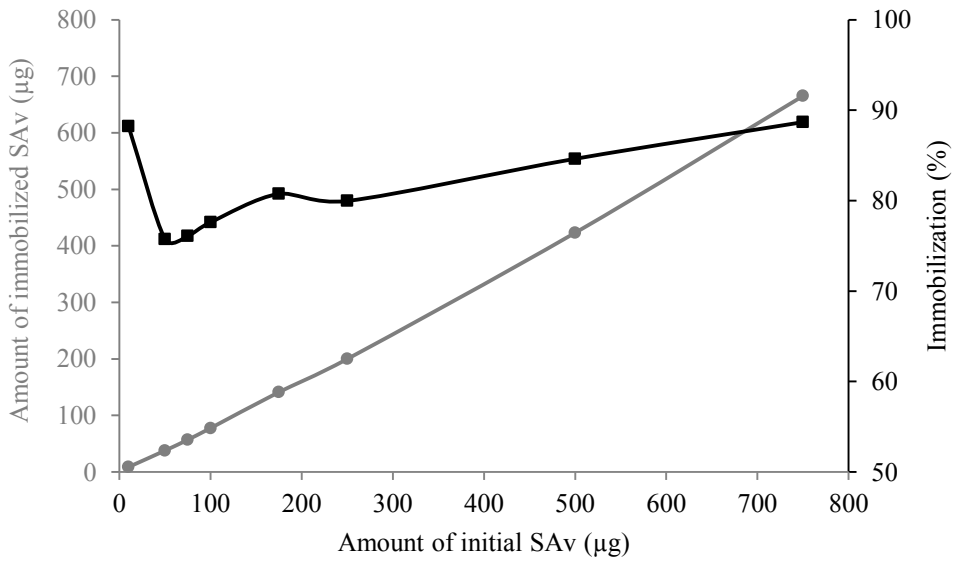

Fig. SM-7.3. Effect of the initial amount of SAv on the amount (grey line; experimental data indicated with a solid circle) and immobilization percentage (black line; experimental data indicated with a solid square) of immobilised SAv.

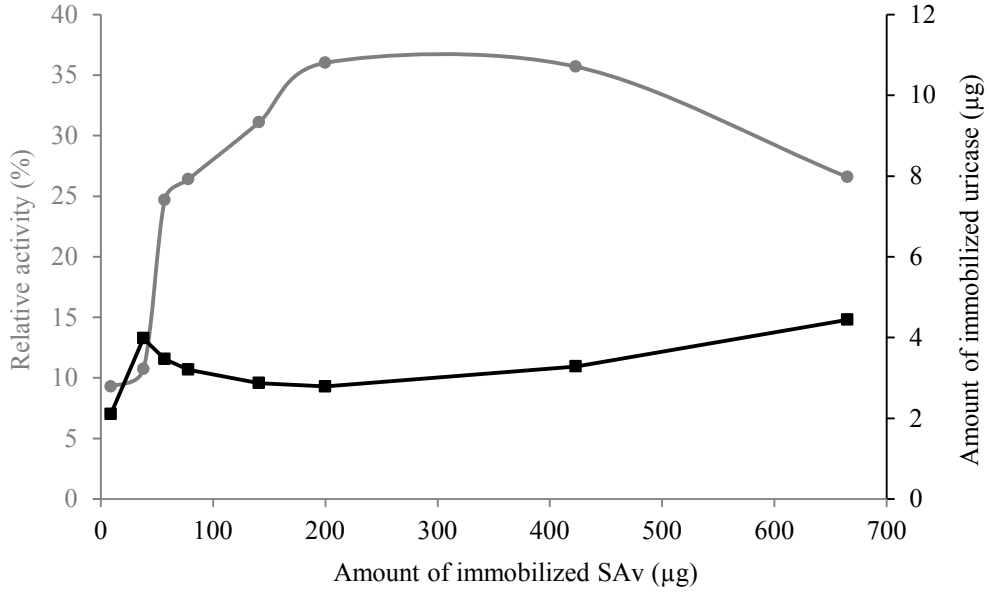

Fig. SM-7.4. Effect of the initial amount of SAv on the relative enzymatic activity (grey line; experimental data indicated with a solid circle) and amount (black line; experimental data indicated with a solid square) of immobilised uricase.

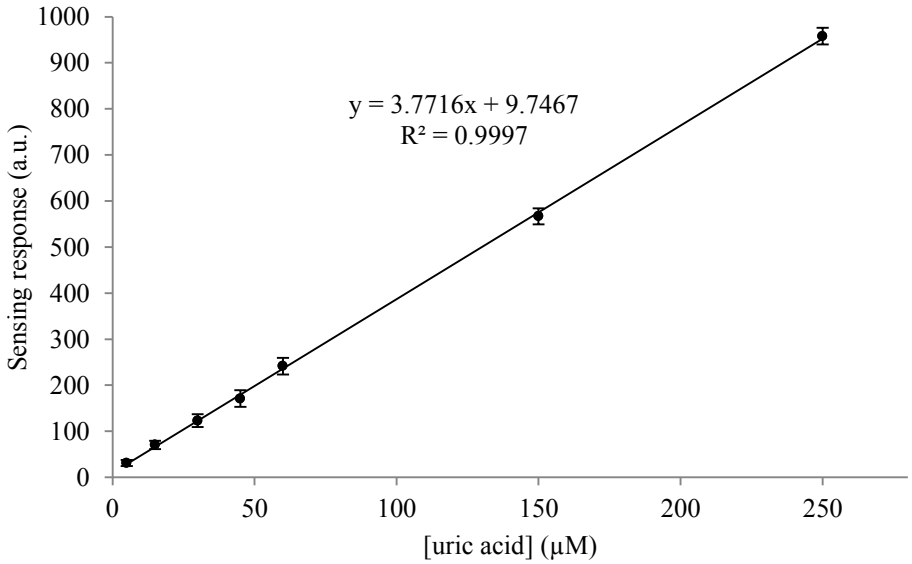

Fig. SM-7.5. Analytical calibration curve.

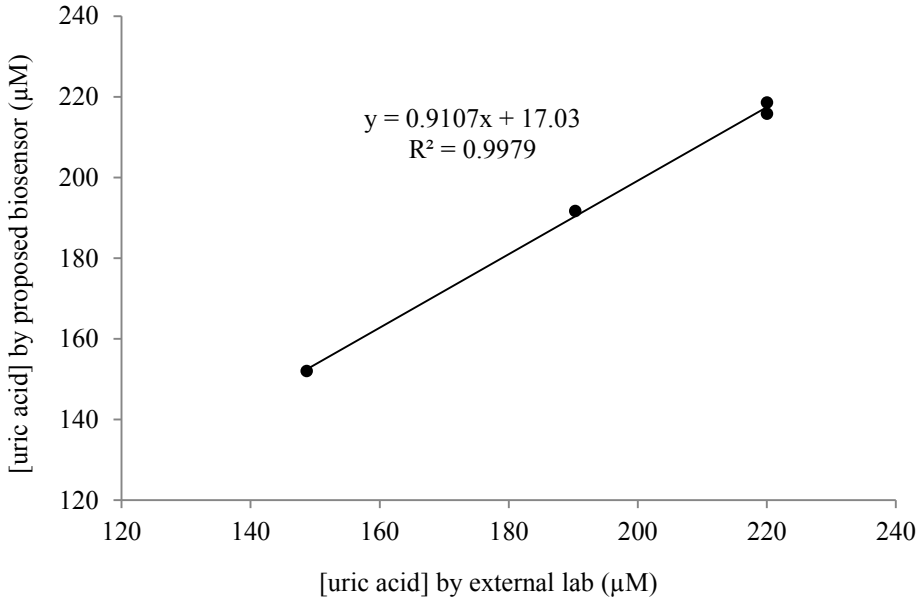

Fig. SM-7.6. Correlation between uric acid values determined in serum by an external laboratory (x axis) and the proposed biosensor (y axis).

Bloque V

La combinación de, por un lado, fases sensoras nanoestructuradas y multifuncionales fabricadas a través de procesos nanotecnológicos, y, por otro lado, sistemas integrados que permiten el fácil manejo de muestras y reactivos, minimizando las dificultades de muchos procedimientos de análisis y permitiendo la miniaturización y la automatización de dichos procedimientos, ha conducido hacia la fabricación de novedosos dispositivos con una elevada versatilidad y aplicabilidad en el campo de los biosensores.

Así, este bloque se centra en el procedimiento de obtención de nuevos dispositivos de determinación óptica mediante la integración de fases sensoras formadas por nanofibras poliméricas en chips de microfluídica, y en el estudio de las propiedades analíticas, tales como límites de detección y cuantificación e intervalo de calibración, de dichos dispositivos.

Capítulo 8

A microfluidic device with integrated coaxial nanofibre membranes for optical determination of glucose

Teresa Ramon-Marquez[a], Adama M. Sesay[b], Peter Panjan[b], Antonio L. Medina-Castillo[c], Alberto Fernandez-Gutierrez[a], Jorge F. Fernandez-Sanchez[a]

[a] Department of Analytical Chemistry, University of Granada, Avd. Fuentenueva s/n, 18071 Granada, Spain

[b] CEMIS-Oulu Measurement Technology Unit (MITY), Kajaani University Consortium, University of Oulu, 87400 Kajaani, Finland

[c] NanoMyP®, Nanomateriales y Polimeros S.L., Spin-Off company of the UGR, BIC Building, Avd. Innovacion 1, E-18016, Granada, Spain

Published in *Sensors & Actuators: B. Chemical*, 2017, **250**, 156-161

ABSTRACT

In this work, a multifunctional material with a core-shell structure containing an inner optical oxygen transducer (PdTFPP) has been successfully used for the immobilization of glucose oxidase on its outer surface and the subsequent determination of glucose. The material was fabricated by co-electrospinning and immobilizing the enzyme by physical adsorption. The sensing mechanism is based on glucose oxidase oxidation of glucose that creates a localized decrease in the dissolved oxygen amount and consequently produces a measurable increase in the luminescence intensity of the inner oxygen transducer. The material was applied to detect glucose at room temperature, and exhibited a good luminescent response.

Furthermore, this coaxial material was integrated into a microfluidic chip and its sensitivity to glucose was tested (LOD of 35 µM and LOQ of 105 µM), obtaining higher sensing properties than using the membrane alone under ambient conditions. This improvement in the sensing response can be explained by considering that the chip limits the oxygen transfer from the ambient air to the coaxial membrane, creating a more controlled environment in where to carry out the measurements. Therefore, the combination of this core-shell material with microfluidic devices could have great potential in the fabrication of oxygen dependent optical biosensors.

Keywords: Multifunctional material; Microfluidic; Optical biosensor; Glucose; Oxygen transduction.

1. Introduction

Microfluidic devices have shown their high potential as micro- and nano-scale platforms with applications in many areas such as biology, physics, chemistry and biomedicine (Chin et al. 2011; Gerami et al. 2016; Kirstine 2016; Li et al. 2015; Liu et al. 2016b; Raub et al. 2015; Warren et al. 2014). The use of these devices often allows a decrease in sample and reagent volumes and faster analyte detection, and provides a well-controlled microenvironment, automation and high portability (Araci and Brisk 2014; Hansen and Quake 2003; Wu et al. 2005). Moreover, the integration of different detection techniques into microfluidic devices can create device systems for multiplexed sensing and detection, and makes it possible to achieve higher sensitivity using very small sample volumes (Ali et al. 2016; Pollock et al. 2012; Ren and Leung 2016; Soares et al. 2017).

The fast development of nanotechnology has provided a wide variety of possibilities in the design and fabrication of new nanomaterials with different and tuneable properties, which generally exhibit enhanced performance compared to their large scale counterparts (Biju 2014; Farahani et al. 2016; Limongi et al. 2016; Tinkle et al. 2014). More precisely, the use of new nanomaterials in the field of sensing and biosensing has meant a high boost for the development of new multifunctional devices with improved features such as high sensitivity and selectivity, improved resolution, fast response, biocompatibility, and reusability (Ding et al. 2015; Goryacheva et al. 2015; Yin et al. 2016). In addition, these new sensors can take an assortment of forms depending on the particular application, from carbon nanotubes used for the detection of DNA or the delivery of small drug molecules (Kruss et al. 2013; Li and Lee 2017; Liu et al. 2016a; Liu et al. 2009; Wong et al. 2013), to nanoparticles and nanofibres employed in bioimaging and for the enzymatic or non-enzymatic determination of a high variety of biomolecules (Cobley et al. 2011; de Dios and Díaz-García 2010; Li et al. 2016; Ma et al. 2017; Mahmoudifard et al. 2016; Ramon-Marquez et al. 2017; Zhao et al. 2013).

The integration of nanomaterials into microfluidic devices has allowed the combination of the excellent advantages and properties of both the nanomaterials with the unique and distinctive characteristics of microfluidic technology (Han and Koh 2016; Mu et al. 2011; Tavares et al. 2016; Zhang et al. 2015; Zhang et al. 2011).

Among the materials used in the fabrication of microfluidic chips, silicon, glass and polymers are the most popular (de Mello 2002; Ning et al. 2016; Piruska et al. 2005; Quake and Scherer

2000; Ren et al. 2013). The selection of the material is a key step for the performance and function of the chips, and has to be based on the requirements and features of the specific application. Thus, properties of the materials such as stability, compatibility with solvents, chemical inertness, non-toxicity, biocompatibility, optical transparency, and high-pressure resistance are often taken into account for the fabrication of microfluidic chips (Goyal et al. 2016; Hung et al. 2008; Su et al. 2016; Taberham et al. 2008).

In this study, we have used a core-shell nanofibre membrane with an inner optical oxygen dye as a support and transducer material for the immobilization of glucose oxidase which has been successfully used for the optical determination of glucose. We have previously demonstrated the capability of this nanofibre membrane in the development of an optical oxygen transduction biosensor for the analysis of uric acid in serum (Ramon-Marquez et al. 2017). Here we demonstrate that the nanofibre based biosensor can be implemented into a microfluidic chip for the detection and quantification of glucose as well as that this implementation provides an improvement in its sensitivity and range.

2. Experimental

2.1. Instrumentation

A Varioskan® Flash spectral scanning multimode reader with temperature control was used in all the luminescence measurements. The luminescence intensity was measured at an excitation wavelength of 405 nm, emission wavelength of 668 nm, bandwidth of 5 nm, delay time of 200 µs, and a measurement time of 100 ms.

2.2. Fabrication of coaxial membranes

The preparation of the coaxial membrane was made following the procedure previously described by our research group (Ramon-Marquez et al. 2017). Briefly, two different solutions were used: a solution of PolymBlend® (10%, w/w) in DMF was used for the outer fibre and PMMA (6%, w/w) with PdTFPP (1%, w/w) in DMF was used for the inner fibre. These solutions were independently driven by two syringe pumps (Cole Parmer 74900 Series) using flow-rates of 1.3 and 0.3 mL h^{-1} for the outer and inner solutions, respectively, establishing a potential difference between the injector and the collector, of 8.9 kV and -1.3 kV with respect to ground, respectively. The process was run for 8 h to obtain membranes with thickness about 150 µm.

2.3. Preparation of the microfluidic chip

The microfluidic chip was made out of optically clear chemically inert poly(methyl methacrylate) (PMMA) substrate (2 mm). 8 parallel channels were accommodated in a geometry mimicking 96-well microtiter plates in order to fit the Varioskan® instrument, allowing easy readout of the coaxial membrane. Sensing cell chambers (diameter = 7 mm, depth = 0.2 mm) were positioned 10 mm from one another. Each chamber had an inlet and outlet channel (overall length = 30 mm, depth = 0.1 mm, width = 2.5 mm). Channels and chambers have been CO_2-laser cut out of the double sided medical grade adhesive substrate (125 µm) (LG, South Korea) and secured between two 2 mm thick PMMA plates (one plate had CO_2-laser cut inlet and outlet holes). The chip was assembled from bottom up – first securing the double sided adhesive onto the bottom PMMA plate, followed by the insertion of the coaxial membrane into the dedicated chamber and closing the chip with the top PMMA plate. Finally, pressure was applied to the assembly in order to ensure a tight fit and prevent any slippage or leakages. Fig. 8.1 shows a schematic representation of the microfluidic chip.

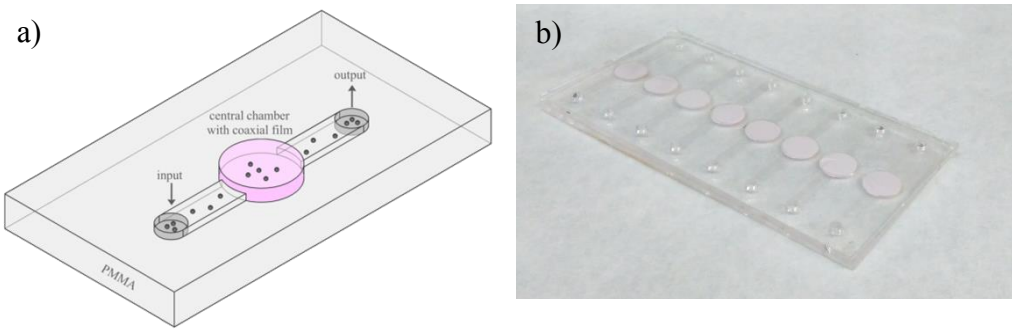

Fig. 8.1. Microfluidic developed chip: a) schematic diagram and b) real picture.

2.4. Immobilization of glucose oxidase

The immobilization of glucose oxidase on to the coaxial membrane was carried out by incubating directly membrane disks (6 mm dia.) with 10 µL of a glucose oxidase solution (1 mg mL^{-1}) in PBS (100 mM, pH = 7.4) for 15 min at room temperature. After this time, the excess solution was rinsed with 10 mL water.

The amount of immobilized GOx onto the coaxial material was determined from the difference between the initial free enzyme amount and the total enzyme amount which is in the

washing solution after immobilization. The enzyme concentration in the washing solution was measured by a spectrofluorometric method at 348 nm (Ramon-Marquez et al. 2015).

The relative activity (%) of the immobilized GOx was calculated by a colorimetric method based on two enzymatic reactions (Ramon-Marquez et al. 2015). First, GOx catalyses the oxidation of D-glucose to gluconic acid and hydrogen peroxide. Next, in the presence of peroxidase (HRP), the released hydrogen peroxide reacts with sodium 3,5-dichloro-2-hydroxybenzenesulfonate (DCHBS) and 4-aminoantipyrine (4-AAP), producing a red quinoneimine dye with an absorption maximum at 515 nm. The relative activity of GOx was calculated as a percentage of the immobilized GOx referred to free GOx activities.

In detail, to determine the relative activity of the immobilized GOx, 3 mL PBS (100 mM, pH 7.4) containing 5 µmol D-glucose was incubated with the membrane disks with immobilized GOx for 15 min at 37 ºC. Next, 0.5 mL 4-AAP (10 mM), 0.5 mL DCHBS (50 mM) and 0.1 mL HRP (20 U mL^{-1}) in PBS (100 mM, pH 7.4) were added and kept at 37 ºC for 5 min to develop the colour.

2.5. Measurements

Two kinds of experiments were carried out. First, the coaxial membrane with the immobilized glucose oxidase was attached to a black vinyl support substrate and then the luminescence measurements were carried out after adding 20 µL of glucose solution in PBS (100 mM, pH = 7.4) to the coaxial membrane. Second, the membrane with the immobilized enzyme was integrated into the microfluidic chip and the measurements were carried out after flowing 50 µL of glucose solution in PBS (100 mM, pH = 7.4) through the channel of the chip. Experimental temperature was maintained at 25 ºC during all the measurements.

The detection mechanism for glucose is based on the increased measurement of the luminescence intensity of the embedded oxygen dye due to the decrease in the localized dissolved oxygen concentration as a result of the selective oxidation of glucose catalyzed by GOx. Therefore, an increase in the concentration of glucose produces an increase in the luminescence intensity which is proportionally related with the glucose concentration. To avoid large analysis times, the slope of this signal was used instead of the equilibrium final luminescence signal. Thus, the sensing response was calculated as the increase in the slope (see Eq. (1)) once the glucose solution was added,

$$Sensing\ response = \frac{S_x - S_0}{t_x} \qquad (1)$$

where S_0 is the luminescence intensity of the material before the addition of glucose, S_x is the signal after the addition of glucose and t_x is the time in which S_x was obtained; t_x = 60 s was used in this study. Although, the sensing response increases when the concentration of glucose increases (due to the oxygen concentration decreasing), this increase is not linear. This is due to the measurement of glucose being made indirectly by measuring the concentration of O_2. It is well known that the luminescence decreasing with the O_2 concentration is not always linear and for this reason is not possible to use the Stern-Volmer equation and a more complex scenario such as Demas or Lehrer two-site models needs to be used (Wang and Wolfbeis 2014). The equation for the Demas model is:

$$\frac{I_0}{I} = \left[\frac{f_1}{1+k_{SV,1}pO_2} + \frac{f_2}{1+k_{SV,2}pO_2}\right]^{-1} \qquad (2)$$

where I is the luminescence intensity and the subscript "0" refers to the value in the absence of oxygen, f_i denotes the fractional contribution of the total luminescence emission from the luminophore located at site type i under unquenched conditions, which exhibit a discrete Stern–Volmer quenching constant given by K_{SVi}, and pO_2 is the partial pressure of oxygen.

In this case, the oxygen concentration decreases and hence this equation can be extrapolated to calibrate the sensing response of glucose by using the following equation:

$$\frac{Sensing\ response}{S_0} = \left[\frac{f_1}{1+k_1[glucose]} + \frac{f_2}{1+k_2[glucose]}\right]^{-1} \qquad (3)$$

where the sensing response is defined in Eq. (1); S_0 is the luminescence intensity in the absence of glucose; f_i denotes the fractional contribution of the total luminescence emission from the luminophore located at site type i under quenched conditions, which exhibit a discrete constant given by k_i. This constant is related to the sensitivity of the sensing membrane and *[glucose]* is the concentration of glucose.

The normalization of the sensing response (*Sensing response*/S_0) is not essential for calibrating the sensing membrane, but it is essential to compare the sensitivity (k_i) of different systems, which is the aim of this work.

All the measurements were carried out in triplicate to evaluate the error. The experimental results were expressed as the average of 3 replicas ± error ($s \cdot t/\sqrt{n}$), where s is the standard deviation, t the student t and n the number of replicas.

3. Results and discussion

The concentration of glucose oxidase (GOx) to be used for the incubation of the core-shell nanofibre membrane was firstly evaluated. In this study, the coaxial nanofibre membrane was incubated with different concentrations of GOx (0.25, 0.5, 1.0, 2.0 and 3.0 mg mL^{-1}) in PBS (100 mM, pH = 7.4) for 15 min at room temperature, and the sensing response was determined by adding 5 µL of glucose (50 mg mL^{-1}) in PBS (100 mM, pH = 7.4). Fig. 8.2 shows the experimental results.

Fig. 8.2 shows that an increase in GOx increases the sensing response up to 1 mg mL^{-1}. Higher GOx concentrations produce a decrease in the sensing response. Thus, 1 mg mL^{-1} was set as the optimum GOx for incubating the coaxial nanofibre membrane. At this concentration, the amount of immobilized GOx was 8.75 µg mg^{-1} and the enzymatic activity was 91 % of the native GOx activity (activity of the free enzyme). Therefore, the enzymatic activity of GOx was not significantly affected by physically adsorbing it on the outer fibre of the material.

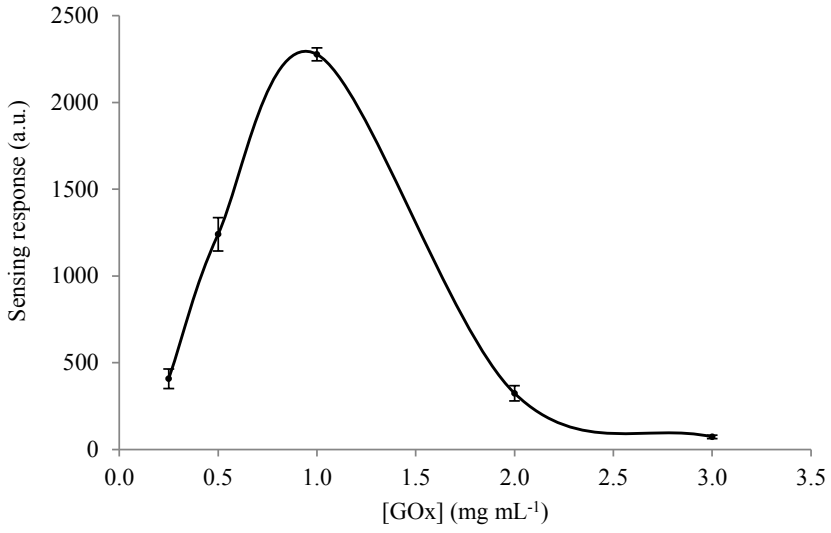

Fig. 8.2. Variation of the sensing response with the GOx concentration used for incubating the core-shell nanofibre membrane (n = 3).

The analytical characterization of the core-shell membrane after the GOx immobilization was made by adding different concentrations (from 0 to 25 mg mL^{-1}) of glucose in PBS. Each sample was measured three times under the same conditions and the average of the sensing response was used to obtain the calibration curve (see Fig. 8.3; grey line). As mentioned above, the correlation between the sensing response and the glucose concentration was calculated using Eq. (3) for calibrating the sensing membrane material (see Section 2.5).

In order to study the possibility of automating the assay, the coaxial material was incorporated into a microfluidic chip. The use of double sided tape for its construction is a facile and rapid prototyping technique for producing microfluidic devices. The integration of the nanofibre material with the immobilized enzyme into the microfluidic chip chamber was carried out before assembling the chip. This integrated chip not only allowed for easier handling of the coaxial material, but also control over the microenvironment of the material and the area where the enzymatic reaction occurs.

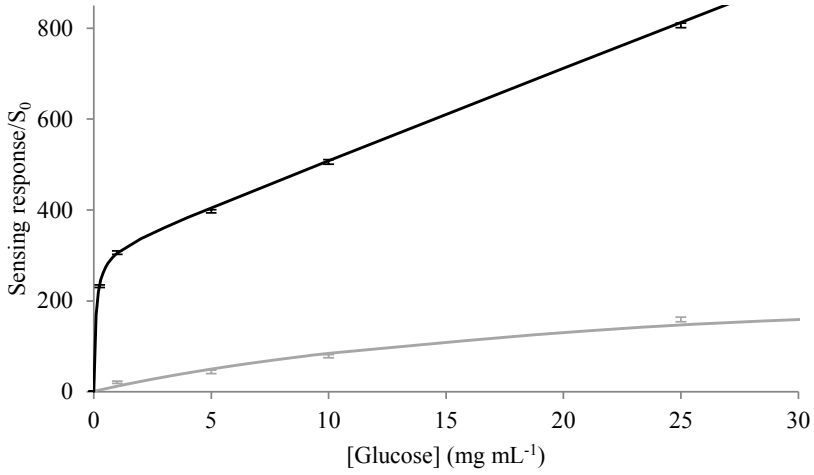

Fig. 8.3. Variation of the sensing response with the glucose concentration of the core-shell nanofibre membrane outside of the microfluidic chip (grey line) and incorporated into the microfluidic chip (black line). The error bars correspond to the experimental data (n = 3) and the lines correspond with the fitted equations according to Eq. (3).

The chip containing the GOx functionalized core-shell membrane was analytically characterized by flowing different concentrations (from 0 to 25 mg mL^{-1}) of glucose in PBS (see Fig. 8.3; black line). As can be seen, the experimental data can be properly fitted by using Eq. (3). Table 8.1 shows the fitting parameters.

Table 8.1. Parameters of the sensing-calibration curves obtained by adjusting the experimental sensing responses with Eq. (3).

	Coaxial membrane	**Microfluidic chip**
k_1 **(mg mL^{-1})$^{-1}$**	12 ± 2	3600 ± 800
f_1	0.9965 ± 0.0004	0.9968 ± 0.0004
k_2 **(mg mL^{-1})$^{-1}$**	0.0000 ± 0.0000	0.070 ± 0.004
f_2	0.0035 ± 0.0004	0.0032 ± 0.0004
R^2 **(%)**	98.76	99.98

It is possible to conclude that the microchip containing the GOx functionalized core-shell membrane luminescence signal is over 300 times more sensitive to glucose (k_1 = 3600 (mg mL^{-1})$^{-1}$) than the free membrane in ambient conditions (k_1 = 12 (mg mL^{-1})$^{-1}$). This phenomenon can be attributed to the limitation of ambient oxygen from the air being transferred to the coaxial membrane when the material is incorporated into the microfluidic chip. To demonstrate this claim, the oxygen sensitivity of the raw material (without any immobilized enzyme) placed outside and inside of the microfluidic chip was determined (see Fig. 8.4). The experimental results show that in both scenarios the material exhibits the same sensitivity to oxygen. Therefore, the increase in sensitivity to glucose inside of the microchip must be due to a lower localized concentration of oxygen after the enzymatic catalytic reaction occurs when integrated within than when outside of the chip. The enzyme activity of the immobilized enzyme is exactly the same weather inside or outside of the chip. Thus, the only reason to have a lower oxygen concentration inside of the chip is due to the decrease in the ambient gas diffusion from the surrounding air to the measurement material/solution interface due to the walls of the PMMA chip, i.e., the use of a closed chip provides a more controlled environment which contributes to a more precise measurement and determination of the glucose concentration.

Although it is true that the use of microfluidic devices usually allows for a decrease in the sample volumes, in this case, higher sample volumes are needed when the material is inside the microfluidic chip (50 µL were used for the microfluidic experiments and only 20 µL for the non-microfluidic measurements) because a part of the volume has to be used to fill the channel of the chip from the input/output of the sensing chamber in order for the material to be properly covered with sample. Further optimization of the design and dimensions of the microfluidic device is required when used as part of an automated system with continuous liquid flow through the

channels, allowing for faster analytes detection and smaller volumes. In addition, the use of a microfluidic system allows the development of multiplexed sensing and detection analytical systems.

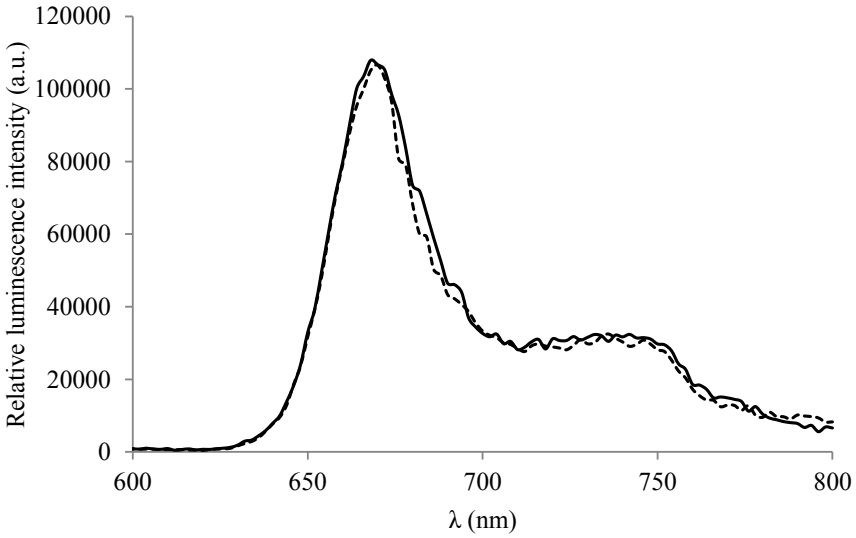

Fig. 8.4. Emission spectra of the coaxial material outside (dashed line) and inside (solid line) of the microfluidic chip. λ_{exc} = 405 nm, t_d = 200 µs.

The proposed microfluidic device provides an efficient integrated optical system for the detection and quantification of glucose by the variation in the luminescence intensity measurements of the oxygen-sensitive dye.

Table 8.2 shows a comparison of published GOx immobilized biosensors for the determination of glucose. It can be seen that although the proposed microfluidic biosensor device cannot detect very low concentration of glucose compared to others previously published (see Table 8.2). The LOD is good enough for a multitude of applications and as an analytical biosensing device it provides the widest calibration working range; thus, it can be used to determine higher concentrations of glucose without having to dilute the sample. This is especially useful for monitoring fermentation bio-reactions and process control.

Table 8.2. Comparison of published GOx immobilized biosensors for the determination of glucose.

Detection	Immobilization type	LOD (µM)	Calibration range (mM)	Reference
Amperometric	Covalent	110	1 – 10	(Dias et al. 2016)
Amperometric	Covalent	1.40	0.0025 – 0.075	(Cerdeira Ferreira et al. 2013)
Amperometric	Adsorption	20	0.05 – 5.00	(Xiong et al. 2013)
Amperometric	Entrapment	150	1 – 10	(Nien et al. 2011)
Colorimetric	Adsorption	23	0.1 – 1.0	(Gabriel et al. 2016)
Chemiluminescence	Adsorption	140	0.42 – 50.00	(Yu et al. 2011)
Fluorescence	Entrapment	6.64	0.02 – 3.00	(Piao et al. 2015)
Fluorescence imaging	Photochemical	0.2	0.0006 – 0.1280	(Nakajima et al. 2006)
Luminescence quenching	Adsorption	35	0.1 – 140.0	This work

4. Conclusions

A nanofibres material with a core-shell structure which contains an oxygen dye (PdTFPP) in its core was prepared by using coaxial electrospinning technique. The hydrophilic properties of the outer fibre allowed for the immobilization of glucose oxidase by physical adsorption on its surface. The coaxial material was introduced into a microfluidic chip and the determination of glucose was successfully carried out with higher sensitivity, detection limit of 35 µM (0.0063 mg mL^{-1}) and quantification limit of 105 µM (0.019 mg mL^{-1}), and a large calibration range, from 0.1 to 140 mM (0.02–25.00 mg mL^{-1}); the sensing response for the coaxial membrane inside the chip was over 300 times higher than the response for the coaxial material outside of the chip.

The results show that the combination of this coaxial material, that is formed by polymers with optical clarity/transparency, permeability to oxygen and oxygen-sensitive dyes with long luminescence lifetimes and high photostability and oxygen sensitivity, integrated into microfluidic chips can create promising optical biosensors with high sensing features.

This report describes a brief study about the possibilities of combining multifunctional materials and bio-sensing principles with microfluidic devices; we believe that the proposed system can be adapted with other types of enzymes, therefore, allow for easy analytical automation and a high portability. Further work is currently in progress in our laboratory.

Acknowledgments

This work has received funding from the People Programme (Marie Curie Actions, Multi-ITN) of the European Union‘s Seventh Framework Programme for research, technological development and demonstration under grant agreement n° 608104 (EUROMBR), the Spanish Ministry of Economy and Competitiveness (Ramon-Marquez‘s grant reference AP2012-0944, Medina-Castillo‘s Torres Quevedo contract reference PTQ-11-04904 and project CTQ2014-53442-P) and The University of Granada (PhD international mobility program of UGR-CEI-BioTic Granada).

References

Ali, M.A., Mondal, K., Jiao, Y., Oren, S., Xu, Z., Sharma, A., Dong, L., 2016. Microfluidic Immuno-Biochip for Detection of Breast Cancer Biomarkers Using Hierarchical Composite of Porous Graphene and Titanium Dioxide Nanofibers. ACS Applied Materials & Interfaces 8(32), 20570-20582.

Araci, I.E., Brisk, P., 2014. Recent developments in microfluidic large scale integration. Current Opinion in Biotechnology 25, 60-68.

Biju, V., 2014. Chemical modifications and bioconjugate reactions of nanomaterials for sensing, imaging, drug delivery and therapy. Chemical Society Reviews 43(3), 744-764.

Cerdeira Ferreira, L.M., da Costa, E.T., do Lago, C.L., Angnes, L., 2013. Miniaturized flow system based on enzyme modified PMMA microreactor for amperometric determination of glucose. Biosensors and Bioelectronics 47, 539-544.

Cobley, C.M., Chen, J., Cho, E.C., Wang, L.V., Xia, Y., 2011. Gold nanostructures: a class of multifunctional materials for biomedical applications. Chemical Society Reviews 40(1), 44-56.

Chin, C.D., Laksanasopin, T., Cheung, Y.K., Steinmiller, D., Linder, V., Parsa, H., Wang, J., Moore, H., Rouse, R., Umviligihozo, G., Karita, E., Mwambarangwe, L., Braunstein, S.L., van de Wijgert, J., Sahabo, R., Justman, J.E., El-Sadr, W., Sia, S.K., 2011. Microfluidics-based diagnostics of infectious diseases in the developing world. Nat Med 17(8), 1015-1019.

de Dios, A.S., Díaz-García, M.E., 2010. Multifunctional nanoparticles: Analytical prospects. Analytica Chimica Acta 666(1–2), 1-22.

de Mello, A., 2002. Focus: Plastic fantastic? Lab on a Chip 2(2), 31N-36N.

Dias, A.A., Cardoso, T.M.G., Cardoso, R.M., Duarte, L.C., Muñoz, R.A.A., Richter, E.M., Coltro, W.K.T., 2016. Paper-based enzymatic reactors for batch injection analysis of glucose on 3D printed cell coupled with amperometric detection. Sensors and Actuators B: Chemical 226, 196-203.

Ding, H., Yang, D., Zhao, C., Song, Z., Liu, P., Wang, Y., Chen, Z., Shen, J., 2015. Protein–Gold Hybrid Nanocubes for Cell Imaging and Drug Delivery. ACS Applied Materials & Interfaces 7(8), 4713-4719.

Farahani, R.D., Dubé, M., Therriault, D., 2016. Three-Dimensional Printing of Multifunctional Nanocomposites: Manufacturing Techniques and Applications. Advanced Materials 28(28), 5794-5821.

Gabriel, E.F.M., Garcia, P.T., Cardoso, T.M.G., Lopes, F.M., Martins, F.T., Coltro, W.K.T., 2016. Highly sensitive colorimetric detection of glucose and uric acid in biological fluids using chitosan-modified paper microfluidic devices. Analyst 141(15), 4749-4756.

Gerami, A., Mostaghimi, P., Armstrong, R.T., Zamani, A., Warkiani, M.E., 2016. A microfluidic framework for studying relative permeability in coal. International Journal of Coal Geology 159, 183-193.

Goryacheva, I.Y., Speranskaya, E.S., Goftman, V.V., Tang, D., De Saeger, S., 2015. Synthesis and bioanalytical applications of nanostructures multiloaded with quantum dots. TrAC Trends in Analytical Chemistry 66, 53-62.

Goyal, S., Economou, A.E., Papadopoulos, T., Horstman, E.M., Zhang, G.G.Z., Gong, Y., Kenis, P.J.A., 2016. Solvent compatible microfluidic platforms for pharmaceutical solid form screening. RSC Advances 6(16), 13286-13296.

Han, S.W., Koh, W.-G., 2016. Hydrogel-Framed Nanofiber Matrix Integrated with a Microfluidic Device for Fluorescence Detection of Matrix Metalloproteinases-9. Analytical Chemistry 88(12), 6247-6253.

Hansen, C., Quake, S.R., 2003. Microfluidics in structural biology: smaller, faster… better. Current Opinion in Structural Biology 13(5), 538-544.

Hung, L.-H., Lin, R., Lee, A.P., 2008. Rapid microfabrication of solvent-resistant biocompatible microfluidic devices. Lab on a Chip 8(6), 983-987.

Kirstine, B.-S., 2016. Optical two-beam traps in microfluidic systems. Japanese Journal of Applied Physics 55(8S3), 08RA01.

Kruss, S., Hilmer, A.J., Zhang, J., Reuel, N.F., Mu, B., Strano, M.S., 2013. Carbon nanotubes as optical biomedical sensors. Advanced Drug Delivery Reviews 65(15), 1933-1950.

Li, D., Ao, K., Wang, Q., Lv, P., Wei, Q., 2016. Preparation of Pd/Bacterial Cellulose Hybrid Nanofibers for Dopamine Detection. Molecules 21(5), 618.

Li, J., Lee, E.-C., 2017. Functionalized multi-wall carbon nanotubes as an efficient additive for electrochemical DNA sensor. Sensors and Actuators B: Chemical 239, 652-659.

Li, Y., Xuan, J., Song, Y., Wang, P., Qin, L., 2015. A microfluidic platform with digital readout and ultra-low detection limit for quantitative point-of-care diagnostics. Lab on a Chip 15(16), 3300-3306.

Limongi, T., Tirinato, L., Pagliari, F., Giugni, A., Allione, M., Perozziello, G., Candeloro, P., Di Fabrizio, E., 2016. Fabrication and Applications of Micro/Nanostructured Devices for Tissue Engineering. Nano-Micro Letters 9(1), 1.

Liu, X., Shuai, H.-L., Liu, Y.-J., Huang, K.-J., 2016a. An electrochemical biosensor for DNA detection based on tungsten disulfide/multi-walled carbon nanotube composites and hybridization chain reaction amplification. Sensors and Actuators B: Chemical 235, 603-613.

Liu, Z., Han, X., Qin, L., 2016b. Recent Progress of Microfluidics in Translational Applications. Advanced Healthcare Materials 5(8), 871-888.

Liu, Z., Tabakman, S., Welsher, K., Dai, H., 2009. Carbon nanotubes in biology and medicine: In vitro and in vivo detection, imaging and drug delivery. Nano Research 2(2), 85-120.

Ma, L., Liu, F., Lei, Z., Wang, Z., 2017. A novel upconversion@polydopamine core@shell nanoparticle based aptameric biosensor for biosensing and imaging of cytochrome c inside living cells. Biosensors and Bioelectronics 87, 638-645.

Mahmoudifard, M., Soudi, S., Soleimani, M., Hosseinzadeh, S., Esmaeili, E., Vossoughi, M., 2016. Efficient protein immobilization on polyethersolfone electrospun nanofibrous membrane via covalent binding for biosensing applications. Materials Science and Engineering: C 58, 586-594.

Mu, Q., Li, Y., Zhang, Q., Wang, H., 2011. TiO2 nanofibers fixed in a microfluidic device for rapid determination of chemical oxygen demand via photoelectrocatalysis. Sensors and Actuators B: Chemical 155(2), 804-809.

Nakajima, H., Ishino, S., Masuda, H., Nakagama, T., Shimosaka, T., Uchiyama, K., 2006. Photochemical immobilization of protein on the inner wall of a microchannel and Its application in a glucose sensor. Analytica Chimica Acta 562(1), 103-109.

Nien, P.-C., Chen, P.-Y., Hsu, C.-Y., Ho, K.-C., 2011. On-chip glucose biosensor based on enzyme entrapment with pre-reaction to lower interference in a flow injection system. Sensors and Actuators B: Chemical 157(1), 64-71.

Ning, R., Wang, F., Lin, L., 2016. Biomaterial-based microfluidics for cell culture and analysis. TrAC Trends in Analytical Chemistry 80, 255-265.

Piao, Y., Han, D.J., Azad, M.R., Park, M., Seo, T.S., 2015. Enzyme incorporated microfluidic device for in-situ glucose detection in water-in-air microdroplets. Biosensors and Bioelectronics 65, 220-225.

Piruska, A., Nikcevic, I., Lee, S.H., Ahn, C., Heineman, W.R., Limbach, P.A., Seliskar, C.J., 2005. The autofluorescence of plastic materials and chips measured under laser irradiation. Lab on a Chip 5(12), 1348-1354.

Pollock, N.R., Rolland, J.P., Kumar, S., Beattie, P.D., Jain, S., Noubary, F., Wong, V.L., Pohlmann, R.A., Ryan, U.S., Whitesides, G.M., 2012. A Paper-Based Multiplexed Transaminase Test for Low-Cost, Point-of-Care Liver Function Testing. Science Translational Medicine 4(152), 152ra129-152ra129.

Quake, S.R., Scherer, A., 2000. From Micro- to Nanofabrication with Soft Materials. Science 290(5496), 1536-1540.

Ramon-Marquez, T., Medina-Castillo, A.L., Fernandez-Sanchez, J.F., Fernandez-Gutierrez, A., 2015. Evaluation of different functional groups for covalent immobilization of enzymes in the development of biosensors with oxygen optical transduction. Analytical Methods 7(7), 2943-2949.

Ramon-Marquez, T., Medina-Castillo, A.L., Nagiah, N., Fernández-Gutierrez, A., Fernandez-Sanchez, J.F., 2017. A multifunctional material based on co-electrospinning for developing biosensors with optical oxygen transduction. Biosensors and Bioelectronics (submitted).

Raub, C.B., Lee, C., Kartalov, E., 2015. Sequestration of bacteria from whole blood by optimized microfluidic cross-flow filtration for Rapid Antimicrobial Susceptibility Testing. Sensors and Actuators B: Chemical 210, 120-123.

Ren, K., Zhou, J., Wu, H., 2013. Materials for Microfluidic Chip Fabrication. Accounts of Chemical Research 46(11), 2396-2406.

Ren, Y., Leung, W., 2016. Numerical Investigation of Cell Encapsulation for Multiplexing Diagnostic Assays Using Novel Centrifugal Microfluidic Emulsification and Separation Platform. Micromachines 7(2), 17.

Soares, R.R.G., Santos, D.R., Chu, V., Azevedo, A.M., Aires-Barros, M.R., Conde, J.P., 2017. A point-of-use microfluidic device with integrated photodetector array for immunoassay multiplexing: Detection of a panel of mycotoxins in multiple samples. Biosensors and Bioelectronics 87, 823-831.

Su, W., Cook, B.S., Fang, Y., Tentzeris, M.M., 2016. Fully inkjet-printed microfluidics: a solution to low-cost rapid three-dimensional microfluidics fabrication with numerous electrical and sensing applications. Scientific Reports 6, 35111.

Taberham, A., Kraft, M., Mowlem, M., Morgan, H., 2008. The fabrication of lab-on-chip devices from fluoropolymers. Journal of Micromechanics and Microengineering 18(6), 064011.

Tavares, M.R., de Menezes, L.R., do Nascimento, D.F., Souza, D.H.S., Reynaud, F., Marques, M.F.V., Tavares, M.I.B., 2016. Polymeric nanoparticles assembled with microfluidics for drug delivery across the blood-brain barrier. The European Physical Journal Special Topics 225(4), 779-795.

Tinkle, S., McNeil, S.E., Mühlebach, S., Bawa, R., Borchard, G., Barenholz, Y.C., Tamarkin, L., Desai, N., 2014. Nanomedicines: Addressing the scientific and regulatory gap. Annals of the New York Academy of Sciences, pp. 35-56.

Wang, X.-d., Wolfbeis, O.S., 2014. Optical methods for sensing and imaging oxygen: materials, spectroscopies and applications. Chemical Society Reviews 43(10), 3666-3761.

Warren, A.D., Kwong, G.A., Wood, D.K., Lin, K.Y., Bhatia, S.N., 2014. Point-of-care diagnostics for noncommunicable diseases using synthetic urinary biomarkers and paper microfluidics. Proceedings of the National Academy of Sciences 111(10), 3671-3676.

Wong, B.S., Yoong, S.L., Jagusiak, A., Panczyk, T., Ho, H.K., Ang, W.H., Pastorin, G., 2013. Carbon nanotubes for delivery of small molecule drugs. Advanced Drug Delivery Reviews 65(15), 1964-2015.

Wu, M.-H., Cai, H., Xu, X., Urban, J.P.G., Cui, Z.-F., Cui, Z., 2005. A SU-8/PDMS Hybrid Microfluidic Device with Integrated Optical Fibers for Online Monitoring of Lactate. Biomedical Microdevices 7(4), 323-329.

Xiong, M., Gu, B., Zhang, J.-D., Xu, J.-J., Chen, H.-Y., Zhong, H., 2013. Glucose microfluidic biosensors based on reversible enzyme immobilization on photopatterned stimuli-responsive polymer. Biosensors and Bioelectronics 50, 229-234.

Yin, Y., Qin, X., Wang, Q., Yin, Y., 2016. A novel electrochemical aptasensor for sensitive detection of streptomycin based on gold nanoparticle-functionalized magnetic multi-walled carbon nanotubes and nanoporous PtTi alloy. RSC Advances 6(45), 39401-39408.

Yu, J., Ge, L., Huang, J., Wang, S., Ge, S., 2011. Microfluidic paper-based chemiluminescence biosensor for simultaneous determination of glucose and uric acid. Lab on a Chip 11(7), 1286-1291.

Zhang, L., Yu, X., You, S., Liu, H., Zhang, C., Cai, B., Xiao, L., Liu, W., Guo, S., Zhao, X., 2015. Highly sensitive microfluidic flow sensor based on aligned piezoelectric poly(vinylidene fluoride-trifluoroethylene) nanofibers. Applied Physics Letters 107(24), 242901.

Zhang, Y., Sinha-Ray, S., Yarin, A.L., 2011. Mechanoresponsive polymer nanoparticles, nanofibers and coatings as drug carriers and components of microfluidic devices. Journal of Materials Chemistry 21(23), 8269-8281.

Zhao, Y., He, Z., Yan, Z., 2013. Copper@carbon coaxial nanowires synthesized by hydrothermal carbonization process from electroplating wastewater and their use as an enzyme-free glucose sensor. Analyst 138(2), 559-568.

CONCLUSIONES

Cuando el objetivo te parezca difícil, no cambies de objetivo;

busca un nuevo camino para llegar a él.

Confucio

En la presente memoria de Tesis Doctoral se han desarrollado nuevas fases sensoras para la determinación de diferentes analitos, presentes tanto en muestras biológicas como en muestras alimentarias, mediante la utilización de diferentes aproximaciones de inmovilización, distintos soportes y una variedad de biomoléculas, incluyendo aminoácidos, enzimas y aminas biógenas. Las principales conclusiones derivadas de este trabajo son las siguientes:

1. Se ha evaluado y determinado la capacidad de inmovilización de biomoléculas de cuatro grupos funcionales diferentes presentes en la superficie de micropartículas poliméricas con la misma naturaleza pero distinta química superficial. Para ello se utilizó la enzima glucosa oxidasa como biomolécula modelo y los grupos químicos cloruro, epóxido, ácido carboxílico y vinil sulfona como funcionalización superficial de las micropartículas utilizadas como soporte sólido. La funcionalización con grupos carboxílicos fue tomada como referencia debido a que es el grupo funcional más ampliamente utilizado para realizar la inmovilización de biomoléculas.

   Los resultados permitieron llegar a dos conclusiones concretas: por un lado, el procedimiento de inmovilización de la enzima se ve altamente afectado por las condiciones en las que se lleva a cabo, incluyendo temperatura, pH, concentración de enzima, tiempo de reacción y grupo funcional del soporte. Por otro lado, la inmovilización a través del grupo funcional vinil sulfona origina una mayor retención de la actividad catalítica de la enzima, permitiendo obtener una mayor actividad con cantidades menores de enzima inmovilizada.

2. Se han estudiado las características de un soporte formado por agarosa activada con divinil sulfona, su utilidad en la inmovilización y estabilización de biomoléculas, así como las ventajas e inconvenientes aportados por la presencia de dicho grupo funcional.

   Se ha demostrado que dicho soporte presenta dos características fundamentales y necesarias para la inmovilización de biomoléculas: por una parte es muy estable, siendo capaz de mantener su reactividad durante meses incluso en condiciones de humedad a 36 ºC, y tras incubaciones en un amplio rango de pHs (entre 4.0 y 10.5) a 25 ºC; y por otra parte es altamente reactivo, permitiendo inmovilizar enzimas sin etapas previas de adsorción o activación, en un intervalo de pHs mayor que otros grupos funcionales tales como epóxido o aldehído, y conduciendo además a la formación de enlaces directamente estables entre las biomoléculas y el soporte. Sin embargo, esta elevada reactividad puede a su vez ser también

un inconveniente si se requiere un control de la cantidad de biomolécula inmovilizada, siendo necesario en esos casos realizar un bloqueo de parte de los grupos vinil sulfona reactivos.

3. Se ha investigado el potencial de los tejidos de nanofibras poliméricas producidos por electrospinning para la fabricación de fases sensoras con transducción óptica. Para ello se aplicó el conocimiento adquirido en procedimientos de inmovilización de biomoléculas y se realizó la combinación de nanotecnología y técnicas de medida de fosforescencia a temperatura ambiente en fase sólida. Esta investigación condujo a la obtención de membranas sensoras altamente selectivas y sensibles a los analitos de interés presentes en muestras con matrices complejas.

   Así, ha sido posible desarrollar dos tipos de métodos novedosos para la determinación de aminas biógenas en muestras reales. En primer lugar, la detección y análisis de triptamina en muestras de cerveza mediante un método simple y directo que no requiere etapas de tratamiento de muestra, y que permite reducir los costes y el tiempo de análisis, manteniendo una elevada sensibilidad y selectividad. En segundo lugar, la determinación de serotonina en muestras de suero haciendo uso de una metodología sencilla, con una única etapa de pretratamiento de las muestras y sin necesidad de utilizar enzimas u otro tipo de biomoléculas. Los resultados de este segundo método mostraron tener una elevada correlación con los obtenidos por un laboratorio certificado externo, lo que demuestra la aplicabilidad de estas fases sensoras en el diseño de biosensores para el análisis de muestras reales complejas.

4. Se ha establecido y detallado una clasificación de los complejos de iridio(III) empleados en el diseño y desarrollo de sensores ópticos para la determinación de una variedad de analitos y parámetros bioquímicos, incluyendo una descripción de los mecanismos en los que se basa el funcionamiento de una gran parte de ellos, así como sus características estructurales principales y más representativas.

   Este estudio ha permitido demostrar que los complejos luminiscentes de iridio(III), con unas excelentes propiedades espectroscópicas, constituyen una seria alternativa a los

ampliamente utilizados complejos de platino(II) y rutenio(II) en la fabricación de fases sensoras ópticas para el análisis de especies gaseosas, iónicas, pequeñas moléculas y diversidad de biomoléculas.

5. Se ha diseñado mediante la técnica de co-electrospinning un soporte de nanofibras poliméricas con una estructura coaxial, que lo convierte en un material altamente multifuncional con dos ambientes diferentes contiguos: uno interno hidrofóbico que permite la retención de moléculas, tales como complejos organometálicos luminiscentes sensibles a oxígeno, preservando sus propiedades ópticas; y otro externo hidrofílico y con capacidad para ser funcionalizado con multitud de grupos químicos que permitan y faciliten la inmovilización de biomoléculas en el soporte.

   Este nuevo soporte de nanofibras ha sido empleado para la inmovilización de uricasa con el fin de llevar a cabo la determinación de ácido úrico en muestras reales de orina mediante transducción óptica de oxígeno. Dicha inmovilización se realizó a través de diferentes metodologías y los resultados obtenidos con cada una de ellas fueron comparados, concluyendo que el procedimiento de inmovilización mediante el empleo de la interacción de afinidad que tiene lugar entre las moléculas de estreptavidina y biotina conduce a una mayor retención de actividad biológica tras la inmovilización de la biomolécula en el soporte.

   Asimismo, también se ha estudiado y optimizado el proceso de incorporación de varios complejos luminiscentes sensibles a oxígeno en la fibra interna del material coaxial. Esta investigación reveló, por una parte, que las propiedades ópticas de los indicadores estudiados prácticamente no se ven afectadas cuando son incorporados en el material, y, por otra parte, que el complejo de paladio(II) examinado (PdTFPP) presenta la mayor sensibilidad a oxígeno de entre los complejos estudiados.

   Finalmente, se ha podido concluir que este soporte de nanofibras, con uricasa inmovilizada en su superficie y PdTFPP como indicador de oxígeno recluido en el interior de las fibras, constituye un novedoso material con aplicaciones en el ámbito de los biosensores.

6. Se ha realizado la incorporación de los tejidos de nanofibras poliméricas y coaxiales en el interior de dispositivos de microfluídica, obteniendo sistemas con un entorno altamente controlado donde es posible realizar la detección y el análisis de variedad de analitos.

   La aplicabilidad de estos sistemas ha sido demostrada llevando a cabo la determinación de glucosa mediante transducción óptica de oxígeno, la cual fue posible al realizar la inmovilización de glucosa oxidasa en la superficie de las fibras y la retención de PdTFPP en el interior del material.

   Los resultados obtenidos tras los análisis realizados han permitido concluir que la combinación de las nanofibras poliméricas con los chips de microfluídica aporta una mejora significativa en la sensibilidad de la determinación óptica de glucosa.

CONCLUSIONS

In this thesis, new sensing phases for the determination of different analytes present in biological and alimentary samples have been developed. In order to design these sensing phases, different immobilization approaches, different supports and a variety of biomolecules, including amino acids, enzymes and biogenic amines, have been studied. Thus, the following conclusions have been derived:

1. The capacity of four different functional groups of polymeric particles to immobilize biomolecules has been evaluated and determined. For this, GOx was selected as a model enzyme, and chloride, epoxy, carboxylic acid and vinyl sulfone were selected as superficial functional groups of the polymeric particles. The carboxyl-functionalized particles were used as a reference material due to the carboxylic acid is the functional group most widely used for immobilizing biomolecules.

   Two important conclusions were obtained: on the one hand, the immobilization of the enzyme is highly influenced by the chemistry of the carrier, pH, temperature, enzyme concentration, and immobilization time. On the other hand, the particle containing vinyl sulfone groups provides higher activity with a smaller amount of immobilized enzyme than the other tested particles.

2. The characteristics of divinyl sulfone-activated agarose, its utility in the immobilization and stabilization of biomolecules, and the advantages and disadvantages provide by divinyl sulfone functional group have been studied.

   The divinyl sulfone-activated agarose has two essential features: it is very stable, maintaining its reactivity after storage for two months even at 36 ºC in wet condition, and after 24 h of incubation at pH 4.0 to 10.5 at 25 ºC. On the other hand, it is highly reactive, being able to covalently immobilize enzymes without requiring the previous adsorption of the enzyme or the activation of the functional group in a wider range of pHs. Moreover, divinyl sulfone can directly yield stable enzyme-support linkages, being no necessary any treatment to stabilize these bonds. However, this high reactivity could originate uncontrolled enzyme-support reaction, being necessary to block the support with different nucleophiles.

3. The potential of nanofibres membranes produced by electrospinning for the fabrication of sensing films with optical transduction has been investigated. For this, the combination of nanotechnology with solid surface-room temperature phosphorescence measurements was carried out. This investigation provided highly selective and sensitive membranes for detecting and quantifying different analytes in samples with complex matrices.

   Thus, two protocols for the determination of biogenic amines in real samples have been developed. Firstly, one simple and direct method to carry out the detection and analysis of tryptamine in beer samples without sample treatment steps, simplifying considerably the methodology to analyze tryptamine, reducing time and cost of the analysis, and providing a high sensitivity and selectivity. Secondly, a methodology for the determination of serotonin in serum samples with only one sample treatment step and by using a non-enzymatic technique. The obtained results showed a high correlation with those obtained by an external certified laboratory, which proves the applicability of these sensing membranes to design biosensors for analyzing real complex samples.

4. A classification of iridium(III) complexes used in the design and development of optical sensors for the determination of different analytes and biochemical parameters has been detailed and established, including a description of the action mechanisms of a large number of them, as well as their main and most representative structural features.

   This study has demonstrated that iridium(III) luminescent complexes, with excellent spectroscopic properties, are a serious alternative to widely used platinum(II) and ruthenium(II) complexes in the fabrication of optical sensing phases for determining gaseous and ionic species, small molecules, and variety of biomolecules.

5. A polymeric nanofibres support with a coaxial structure has been designed by using co-electrospinning technique. The use of this technology has allowed obtaining a highly multifunctional material with two different environments: an inner hydrophobic one that allows the retention of molecules, such as luminescent organometallic complexes sensitive to oxygen, preserving their optical properties; and another outer hydrophilic environment

which can be functionalized with variety of chemical groups, allowing the immobilization of biomolecules on the support.

This new nanofibre support has been used to carry out the immobilization of uricase in order to determine the uric acid concentration in serum by optical oxygen transduction. This immobilization was performed by different methodologies concluding that the immobilization procedure through biotin-streptavidin affinity interaction leads to a higher retention of biological activity after the immobilization of the biomolecule on the support.

Moreover, the process to incorporate several oxygen-sensitive luminescent complexes into the inner fibre of the coaxial material has also been studied and optimized. This research revealed, on the one hand, that the optical properties of the studied indicators are practically unaffected when they are incorporated into the material, and, on the other hand, that the studied palladium(II) complex (PdTFPP) is the most sensitive to oxygen of the tested ones.

Finally, it has been possible to conclude that this nanofibres support, with uricase immobilized on its surface, and PdTFPP as an oxygen indicator entrapped inside the fibres, is a novel material with applications in the field of biosensors.

6. The incorporation of the polymeric coaxial nanofibres membranes into microfluidic devices has been carried out, obtaining systems with a highly controlled environment where it is possible to realize the detection and analysis of a variety of analytes.

   The applicability of these systems has been demonstrated by determining the concentration of glucose by using optical oxygen transduction. This determination was realized after immobilizing glucose oxidase on the surface of the fibres, and retaining PdTFPP inside the material.

   The obtained results conclude that the combination of the polymeric nanofibres with the microfluidic chip provides a significant enhancement in the sensitivity of the optical determination of glucose.

ÍNDICE DE FIGURAS

Introducción

Experimental

Capítulo 1

Capítulo 2

Capítulo 3

Capítulo 4

Capítulo 5

Capítulo 6

Capítulo 7

Capítulo 8

ÍNDICE DE TABLAS

Introducción

Experimental

Capítulo 1

Capítulo 2

Capítulo 3

Capítulo 4

Capítulo 5

Capítulo 6

Capítulo 7

Capítulo 8